Transport properties and multi-species modelling of slag based concretes

Juan Manuel Rafael Lizarazo Marriaga

A thesis submitted in partial fulfilment of the University's requirements

For the degree of Doctor of Philosophy

December, 2009

Coventry University

ABSTRACT

In this work, the chloride transport related properties of slag concrete have been studied. For this, traditional experiments and an innovative computational method were applied to novel mixes with a low carbon footprint.

In part 1 combination of Ground Granulated Blast Furnace Slag and Steel Basic Oxygen Slag activated using ordinary Portland cement, waste cement industrial residues and recycled Plasterboard Gypsum were studied. In order to characterize these blended binders, the compressive strength, the volume stability, the mineralogical changes due to hydration and the setting times were measured.

In part 2 the chloride penetration was simulated to study the transport properties using a multi-species model. In this, the ionic species flow is given by the Nernst–Planck equation; however, due to ion–ion interactions there are ionic fields that affect the final flux producing an additional voltage known as the membrane potential. In order to calculate the inputs of the model a neural network methodology was developed to find the fundamental properties of concrete including the diffusion coefficients

In part 3 a range of traditional transport chloride related experimental tests were carried out on concrete mixtures developed in part 1. These tests were workability, compressive strength, open porosity, initial water absorption capacity (sorptivity), carbonation, chloride migration and self diffusion, electrical resistivity, water permeability, and corrosion. Additionally, the methods developed in part 2 were used to calculate the chloride transport related properties of those mixes.

PREFACE

This thesis was jointly funded by the *Programme Alßan* (the European Union programme of High Level Scholarships for Latin America, scholarship No. E06d101124CO), the *Universidad Nacional de Colombia – Departamento de Ingeniería Civil y Agrícola*, and *La Fundación para el Futuro de Colombia – COLFUTURO*.

The supervisory team was composed by Professor Peter Claisse as director of studies, and Dr. Esmail Gangian as second supervisor.

During the progress of the research many scientific topics were of great interest and were disseminate in various journal papers, conferences and workshops. A list of the most relevant contributions is listed below.

Papers marked with a "*" are presented in appendix 7.

*Lizarazo Marriaga, J., and Claisse, P. (2009) 'Effect of non-linear membrane potential on the migration of ionic species in concrete'. **Elecrochemica Act**a 54 (10) 2761-2769

*Lizarazo Marriaga, J., and Claisse, P. (2009) 'Determination of the concrete chloride diffusion coefficient based on an electrochemical test and an optimization model'. **Materials Chemistry and Physics** 117 (2-3) 536-543

*Lizarazo Marriaga, J., and Claisse, P. (2009) 'Determination of the transport properties of a blended concrete from its electrical properties measured during a migration test'. **Accepted for publication in Magazine of Concrete Research** 10th September 2009

*Lizarazo Marriaga, J., and Claisse, P. (2009) 'Compressive strength and rheology of environmentally-friendly binders'. **Ingeniería e Investigación** 29 (2) 5-9 (In Spanish)

Juan Lizarazo-Marriaga, Peter Claisse, Eshmaiel Ganjian, "Effect of steel slag and Portland cement in the rate of hydration and strength of blast furnace slag pastes". Submitted 2 July of 2009 to **Journal of Materials in Civil Engineering – ASCE**

*Lizarazo-Marriaga J., and Claisse P. (2009) 'Determination of the chloride transport properties of blended concretes from a new electric test', **Proc. Int. conf "Concrete in aggressive aqueous environments, performance, testing and modelling"** Ed. M. Alexander & A. Bertron, Toulouse, France 3-5 June 2009. RILEM, Pp 269-277, ISBN 978-2-35158-069-1 (Vol. 1)

Lizarazo Marriaga J., and Claisse P. (2008) 'Assessment and Simulation of the chloride penetration of a fly ash blended concrete' **"Decoupling growth from environmental impact"**, REKTN WARMNET join conference, 30 June – 1 July 2008

Poster: Lizarazo Marriaga J., and Claisse P. (2008) 'Effect of the non-linear membrane potential on the migration of ionic species in concrete' **Coventry University Research Symposium**, Tuesday 20th May 2008. Won first prize

ACKNOWLEDGMENTS

TABLE OF CONTENTS

PART 3

FINAL REMARKS

REFERENCES

APPENDICES

LIST OF FIGURES

LIST OF TABLES

1 INTRODUCTION

1.1 GENERAL BACKGROUND

The first major theme of this thesis is cement replacement in concrete. As Ordinary Portland Cement (OPC) production accounts for 9% of worldwide greenhouse gas emissions, there are international efforts to develop different binder materials for use in civil construction projects (Naik 2007). Government directives around the world are being employed to pro-actively encourage the use of non-hazardous waste materials and by-products, (which would otherwise go to landfill), in construction applications.

Waste slag from the iron and steel industry has been used for many years in concrete production, usually blended in some combination with OPC. Although iron slag has shown to be a good binder, its performance does depend on which activator is being used. A number of other waste materials, also obtained as by-products of various industrial processes, have proven to be adequate activators. A programme of experimental studies has been carried out previously by Coventry University to assess the suitability of such waste materials for engineering applications. Those tests indicated the potential for achieving increased strength using quite substantial proportions of waste materials, resulting in a range of blended cements having tangible environmental, economic and engineering benefits.

The second theme of this thesis is the transport of chlorides in concrete, particularly in tests which use an applied voltage to obtain rapid results. Naturally the strength and durability of concrete are of primary concern to the engineering community. However, increasingly in recent years the focus has turned towards trying to reduce the concrete infrastructure's huge maintenance and repair costs. In the majority of cases weakness and structural breakdown can be directly attributed to damage due to steel corrosion. As the presence of chloride ions heightens the level of metallic corrosion activity, the mechanisms by which such chlorides penetrate the concrete fabric are of great interest. Assisted by the ever-growing computational power available, increasingly sophisticated concrete service-life models have been developed. An emerging trend is for these to incorporate transport mechanisms related with diffusion of chloride ions and moisture. However, under specific conditions, chloride diffusion can be considered the main mechanism.

Despite the large amount of research and computer modelling that has taken place of recent years, simplified models for explaining chloride penetration in concrete are still commonly in use. Fick's Laws remain in widespread and popular use where a simple approach is thought desirable. Indeed most of the established concrete diffusion models are based around the analytical solution of Fick's Second Law. Great advances have been made in these models, and it is common to find models using time-dependent chloride diffusion coefficients or time-dependent chloride binding isotherms (Luping 2008). However, Fick's Laws do assume that chlorides are isolated particles. This assumption is not an entirely realistic one, because in the pore solution of concrete, chloride ions will typically be interacting with other ions according to their electrical charge.

One of the reasons why Fick's Laws have not been completely replaced by other more "appropriate" theories or models is because according to them, the chloride penetration depends entirely on a single parameter, the coefficient of diffusion. To define a complex phenomenon using a single coefficient is a situation that brings several advantages to engineers; however, scientists have known for some time, that the Nernst-Planck equation should be used accounting for possible ionic interactions.

The Nernst-Planck equation includes an electrical field in addition to a gradient of ionic concentration, so, it has been proposed as a tool to determine the chloride diffusion coefficient in experimental migration tests (NTBuild-492 1999). However, using those approaches the Nernst-Planck model continues to be used assuming the chloride ions are isolated from other species.

Multi-species models have been developed in recent years (Claisse and Beresford 1997, Truc, Olliviera and Nilsson 2000). These incorporate the presence of several free species in the pore solution (normally OH^-, Na^+, and K^+) along with the chlorides penetrating from the exterior. Although the Nernst-Planck equation governs the phenomenon, it does need to be coupled with the physical principle of charge neutrality, which must be preserved at any point. Even in a self diffusion test, the condition of charge neutrality generates an electric field (known as the membrane potential), affects the flow of each ion. For a multi-ionic system the major difficulty is the determination of those parameters that will define the transport, (principally the diffusion coefficients), of all the species involved.

The rapid chloride permeability test (RCPT) is an electrochemical-migration test used extensively in the concrete industry and is included in specification documents (ASTM C1202). It is quite widely used for assessing concrete quality, and measures the ability of concrete to protect embedded reinforcement from chloride salt.

A computer model of this test has been developed at Coventry University, incorporating the Nernst-Planck equation and including ionic interaction of the different species. Using this tool, initial simulations indicated that the inclusion of a voltage measurement in the centre of the sample during the RCPT test would provide additional information about the transport properties and features of the concrete and substantially improve the reliability of the results.

1.2   AIMS AND OBJECTIVES

The principal aim of this project was to investigate the chloride transport related properties of slag concrete mixtures both by traditional experimental methods and by computational methods. It is predicted that the insight obtained could contribute significantly to a more precise evaluation of the chloride transport in slag mixes and other types of concrete.

For this aim, a number of objectives were developed:

1. Develop new slag mix designs with a low carbon footprint. The focus of this objective was to investigate the potential use of slag based materials to create cementitious binders for cement replacement. Combinations of iron and steel slag activated with ordinary Portland cement and a range of mineral alkali (cement kiln dust) and sulphated wastes were explored. This objective is of particular interest to industrial concerns in Colombia.

2. Review the relevant literature about chloride electro-diffusion in concrete, particularly that related to chloride migration tests; and assess the potential of the electro-diffusion numerical model developed in the Construction Materials Applied Research Group at Coventry University.

3. Develop a theoretical explanation for the movements of chloride ions in concrete. Using that theory, calculate the evolution of the membrane potential during the ASTM C1202 test, and provide an experimental validation for this.

4. Develop a new, alternative computational method for calculating the transport chloride related properties of cement based materials, based on the electro-diffusion numerical model and using the experimental mid point membrane potential observations.

5. Carry out a range of experimental tests and numerical simulations to determine the chloride transport related properties and other key parameters of the new slag-based mixes.

1.3   STRUCTURE OF THE THESIS

The arrangement of this thesis is quite different from the traditional way of writing a standard dissertation, where the order of the main chapters is normally: literature review, experimental methods, tests programme, results, discussion, and conclusions. In this document all those elements are included; however, the whole thesis has been divided into three parts because of the necessity of presenting the results and discussion of each part independently. It is expected that this methodology will help the reader to understand the progression of the work, which involved an integration of many concepts of concrete science and technology.

In the first part of this dissertation a comprehensive experimental program is presented with the aim of developing suitable slag mixes with acceptable strength properties. In this initial phase, combinations of granulated blast furnace slag and steel slag were activated with ordinary Portland cement, recycled gypsum and industrial cement by-products, in order to produce concrete mixes suitable for structural applications. In chapter 1, the literature relating the candidate raw materials is reviewed. In chapter 2, the results of the experimental program are presented and discussed. In this, the compressive strength was optimized to obtain 5 final binders representing the most desirable combinations of the materials. In chapter 3 the hydration and setting mechanisms of these final binders were identified, measured and discussed.

In the second part of this research the theoretical basis and the experimental validation of the numerical models used to predict the chloride penetration in cementitious materials is presented. Additionally, a new methodology to obtain the chloride transport related properties was developed. In chapter 5 some of the principal aspects of chloride penetration in concrete are summarized, especially

those related theoretically with the electro-diffusion model applied in this research. Special attention was given to migration tests, binding capacity, diffusion coefficients, membrane potential, composition of the pore solution and electrical current during a migration test.

Chapter 6 introduces two physical ideal states named voltage control and current control that define the possible conditions under which chlorides move through concrete. Additionally, this chapter reports on all experimental methods used in this second part of the research. In chapter 7 an experimental program dedicated to measuring the membrane potential on a migration test is summarized. For this, a new electrochemical test was developed. In chapter 8, an optimization technique was developed to obtain the transport related properties of a concrete mix from the results of the tests of membrane potential and the results of the Coventry model. The technique used was an artificial neural network algorithm (ANN). In chapter 9, the ability of the Coventry University model to simulate a voltage control test was assessed numerically and experimentally, giving great importance to the effect of the numerical process, the evolution of the electrical properties and the ionic concentrations. Models to simulate other possible electrical conditions, e.g. current control, power control, and variable voltage control were also developed, and the results discussed.

In the final part of the dissertation, the transport properties of the slag mixes developed in the first part of the research and mixes of Portland cement and ground blast furnace slag with different proportions were investigated. For this, several transport related tests and numerical simulations were carried out.

In chapter 10 the complementary experimental tests that were not introduced in chapter 6 are presented. In chapter 11, the results of the experimental program are presented and discussed, including tests to measure workability, compressive strength, open porosity, initial water absorption capacity (sorptivity), carbonation, chloride migration and self diffusion, electrical resistivity, water permeability, and corrosion. In the same chapter, for 20 different mixes the chloride transport related properties were obtained from the experimental tests and the optimization model. Based on simulations, the intrinsic diffusion coefficients of chloride, hydroxide, sodium and potassium were obtained. Also, the initial hydroxide composition of the pore solution, the porosity, and the chloride binding capacity were determined. A

complete discussion of the results of chloride transport properties is given in chapter 12.

Although essential conclusions are provided at the end of each chapter, a final chapter 13 deals with the main key conclusions and findings of this research. In this, the limitations of the work carried out are stated and considerations about future work are presented.

PART 1: DEVELOPMENT OF NOVEL SLAG MIXES

This first part of the research sets out to develop a group of suitable slag mixes all offering same potential environmental and engineering benefits. In a first chapter the literature relating the candidate raw materials is reviewed. In a second chapter, the results of an experimental program are presented and discussed; here, compressive strength was optimized to obtain 5 final binders representing the most desirable combinations of these materials. In a third and last chapter, the hydration and setting mechanisms of these final binders are identified, measured and discussed.

2 SLAG MIXES – "A REVIEW"

This chapter summarises the literature review carried out about the materials to be used as binders in this research programme.

2.1 WORK DONE PREVIOUSLY AT COVENTRY UNIVERSITY

The utilization of agricultural and industrial waste as construction material is not new; in the last 20 years considerable research has been carried out internationally in order to increase the utilisation of by-products and recycling technologies. As part of this, the Construction Materials Applied Research Group at Coventry University (COMARG) has carried out many research projects, with the intention of reducing the amount of Portland cement used in concrete, thereby obtaining potential environmental, economic, and engineering benefits.

For example, in a recently completed PhD, Karami (2008) studied the use of by-product industrial materials to replace all Portland cement in construction products. In this, the possibility of 100% cement replacement in low strength concrete and lightweight blocks was investigated with mixes of gypsum waste, by-pass dust, basic oxygen slag and run-of-station ash. The experimental programme included physical and chemical tests using paste and concrete, and a theoretical programme, which included analysis of the data collected with the response surface method and artificial neural networks.

An industrial project which COMARG completed in February of 2007 studied the potential application of plasterboard and gypsum waste in road bases, sub-bases and stabilised sub-grades (Ganjian, Claisse and Pouya 2007). This project investigated several combinations of plasterboard gypsum with basic oxygen slag, cement kiln dust, cement by-pass dust, and run-of-station ash, and their potential use in stabilising soils, and producing roller-compacted concrete for road foundation.

Between 1998 and 2005 a separate industrial project developed in partnership with other universities was conducted to study and develop novel composites suitable for landfill liners (Atkinson *et al.* 1998-2005). Among many potential candidates several waste materials were investigated as potential binders, and laboratory

measurements of strength and permeability were conducted. In addition, an in-depth study into the reaction kinetics of those binders was undertaken.

An international project, funded by the European Union, conducted in association with 8 international partners, investigated efficient processes to recover materials from lead-acid batteries (Cann, Claisse and Lorimer 2007). Coventry University participated in this research project studying the possibility of treating battery acid to obtain gypsum of a suitable purity and particle size for it to be commercially acceptable.

Projects on slag concrete have been carried out worldwide for many years, so, many research topics can be consulted in Taylor (1990).

2.2   MATERIALS TO BE USED IN THIS RESEARCH

2.2.1 Slag

Slag is a by-product of the smelting process, it is a foundry residue. Depending on which metals are being produced, slags will have different mineralogical properties. Production of Iron, steel, copper, lead, and aluminium dominate the metallurgical industry, generating vast volumes of slag. Depending on its chemical and physical properties a slag could be used (a) in the construction industry as

- aggregate in granular bases,
- asphalt mixes,
- cement replacement,
- concrete mixes,

or (b) in bulk applications such as

- embankments or fillers.

The utilization of slags as cement raw material or as replacement in blended concretes has been extensively studied for reasons such as

- the environmental benefits,
- the potential cementitious or puzzolanic properties,
- the high cost of the Portland cement.

Worldwide, the most commonly used slag is Granulated Blast Furnace slag (GGBS) - from the iron industry. Efforts are being made however to use other types of slag that

are available in large quantities and in the same way as GGBS, could have some potential cementitious properties. As was pointed out by Shi and Qian (2000), GGBS, steel slag, granulated phosphorus slag, and copper slag are all potential cementing materials.

In this research GGBS and steel slag were used as the main materials. From a literature survey the features of both materials are summarized, showing their principal properties.

2.2.1.1   Ground Granulated Blast Furnace Slag - GGBS

According to ASTM C125 (2007) blast-furnace slag is defined as *"the glassy, granular material formed when molten blast-furnace slag is rapidly chilled, as by immersion in water"*. During the production of iron in a blast furnace the raw materials (iron ore or iron pellets, coke, and a flux of limestone or dolomite) are smelted forming the molten slag and the molten iron as is shown in figure 2.1. The slag is a non-metallic material resulting from the combination of the calcium and magnesium in the calcareous stone with the aluminates and silicates in the ore. Because of the high temperatures inside the furnace (around 1500 °C) the way the slag is cooled affects the properties of the material. Natural cooling, air and water cooling, expanding, pelletizing, and granulating are the most common methods for cooling molten slag.

Figure 2-1 Iron blast furnace

Granulated slag is rapidly cooled by large amounts of water, producing sand size fragments with a glassy internal structure. When this material is ground to very fine particles it is known as GGBS. According to the Cementitious Slag Makers Association each year in the UK two million tonnes of GGBS in the cement industry are used.

The pelletized slag process was developed in Canada in the 1970's. In this process the slag is cooled with water and shot into air or steam by a rotary drum (Shi and Qian 2000). Due to the lightweight material produced this type of slag is used frequently as lightweight aggregate or if finely ground, can be used as cement replacement. If the slag were left to cool under natural conditions, a crystalline structure will be formed and no cementitious properties would obtain. In this condition the slag can be only be used as an aggregate or as a raw material to be used in clinker production. According to the United States Geological Survey (Oss 2003) in 2003 in the United States 7.3 million metric tons of naturally-cooled slag were generated, around 16% was used as concrete aggregates and around 6% in clinker production. Another type of blast furnace slag is the expanded one which is cooled by controlled amounts of water in order to obtain a low density material.

Figure 2-2 Blast furnace slag; left: molten slag – right: granulated slag

The chemical and mineralogical composition of GGBS depends on the characteristics of the metallurgical process and materials; however, a typical oxide composition is shown in Table 2.1. The principal compounds are CaO, SiO, Al_2O, and MgO; these are present in most hydraulic binders. Compared to OPC, the slag has a higher silica and lower calcium content, and contains low quantities of ferric oxide. For a typical sample of GGBS the glass content is around 85-90%, and this, together with its basicity, are considered the primary factors governing its hydraulicity. According to Detwiler, Bhatty and Bhattacharja (1996), the more basic the slag, the greater its hydraulic reactivity in the presence of alkaline activators.

Chemical constituents	Range of composition % by mass
SiO_2	32-42
Al_2O_3	7-16
CaO	32-45
MgO	5-15
S	0.7-2.2
Fe_2O_3	0.1-1.5
MnO	0.2-1.0

Table 2-1 Chemical composition of GGBS (ACI 2003)

GGBS as a binder can be used in different ways. Blended cements of GGBS and ordinary Portland cement (OPC) have been used for more than 100 years and are covered by international standards (ASTM-C595 2008). The combination of GGBS with OPC and pozzolans is reported by the American Concrete Institute Committee 233 (2003). GGBS-alkali-activated binder systems are used extensively in Eastern Europe (Tailing and Krivenko 1997), and the activation of slags using sulphate minerals has been practiced for more than 50 years in Europe (Matschei, Bellmann and Stark 2005).

Hydration and physical properties of GGBS:

GGBS of itself has few hydraulic properties. It needs to be activated with an external material and is consequently known as a latent hydraulic material. When GGBS is mixed with OPC the resulting products of the hydration of the slag correspond to those that are obtained during the OPC hydration, except no calcium hydroxide is liberated. In addition, the initial hydration of the slag is much slower than with OPC. The hydration of GGBS depends on the dissolution of the glassy slag structure, by hydroxyls ions released during the hydration of OPC (ACI 2003), or by the addition of alkali activators. Roy and Ldorn (1982) showed that during the hydration of GGBS, in the first 24 hours there is a two step reaction. During early hydration the most important reaction is with the alkali hydroxide, and during the later reaction the most important reaction is with calcium hydroxide. Alkalis and $Ca(OH)_2$ act as slag activators producing calcium-silicate and calcium aluminate hydrates.

As in the case of calcium hydroxide or certain alkalis, GGBS can also be hydrated in the presence of sulphate compounds (Roy and Ldorn 1982). The sulphate in any form (gypsum or anhydrite) combines with the aluminates (Al_2O_3) contributed by the slag, in the presence of calcium hydroxide, to form ettringite ($C_3A.3CaSO_4.32H_2O$). In the same way, the remaining calcium hydroxide reacts with the silicates to form tobermorite gel (Gruskovnjak *et al.* 2008). According to Czernin (1980), because of the differences in the final hydration compounds, the sulphate activation does not have a direct comparison with that of alkali activation. In an alkali activated system the calcium hydroxide is necessary as an activator and no important combination happens. By contrast, in a sulphate activated system the gypsum is converted to calcium sulphoaluminate. In the United Kingdom, there is a commercial product (not currently available) known as Super Sulphated Cement (BSi 1974), composed of

around of 80-85 per cent of GGBS, activated with 10-15 per cent of calcium sulphate, and 5 per cent of OPC.

Normally, there is a longer setting time for GGBS-blended cements; depending on the amount of replacement, the temperature of mixing, the features of the mix, and the type of cement. The prolonged setting times of slag binders are explained by the fact that its mineralogical composition is similar to that of dicalcium silicate C_2S, unlike OPC that is controlled by tricalcium silicate C_3S. The fineness of GGBS should be always greater than the OPC to obtain more activity at early ages. In the same way, it has been reported that the workability of blended mixes is improved by using GGBS (ACI 2003). The bleeding properties of slag mixes are related to the fineness of the slag and the fineness of the cement. If the GGBS is finer than the OPC and the level of replacement is around 50%, bleeding is reduced. By contrast, if GGBS is coarser than OPC, an increase in bleeding can be expected.

Mechanical properties of GGBS:

Normal blended OPC-GGBS mixes have a reduction in their early compressive and bending strengths (1 and 3 days) with respect to OPC mixes, but an increase in their strength at later ages (more than 14 days) can be expected (Mehta and Monteiro 1992). The effect that GGBS has on the strength is dependant upon the activity of the slag and the ratio of replacement. For samples tested with different levels of replacement, the optimum replacement level that gives the highest 28 days compressive strength was between 40 and 50 per cent of GGBS (Meusel and Rose 1983). In the same way, the relationship between the water binder ratio and strength follows the same trend as when OPC is used: the compressive strength falls as the water-cement ratio increases. Hot curing at early ages has a positive effect on strength as was reported by Roy and Ldorn (1982). The compressive strength of concrete is a function of porosity, pore size distribution, and pore shape (Pandey and Sharma 2000). In GGBS concrete mixes a reduction in porosity is expected with the advancement of hydration, due to the gradual filling of the pores by the hydration compounds.

In research carried out by Singh and Garg (2002) mixes of blast furnace slag were sulphated activated with calcium sulphate hemihydrate ($CaSO_4$. $1/2H_2O$) and anhydrite in addition to Portland cement. The proportions of the materials used were 75% GGBS, 15% sulphate and 10% OPC. The compressive strength of all sulphate

mixes was similar to that of OPC, and the setting times were shorter. In a paper reported by Uomoto and Kobayashi (1983) the compressive strengths of concrete slag cements activated with gypsum were determined (85% slag, 13% gypsum, and 2% OPC). They found that the strength of this material has a maximum or optimum value of water binder ratio and showed a different trend from that of OPC, (figure 2.3). They argue that the reason for this is because for low water binder ratios the gypsum hydration is slow, and point out that the water binder ratio needs to be analyzed in conjunction with the cementitious content. During the literature review conducted for the present research, no further data was found about the relationship between the water binder ratio and the strength of gypsum activated slag mixes.
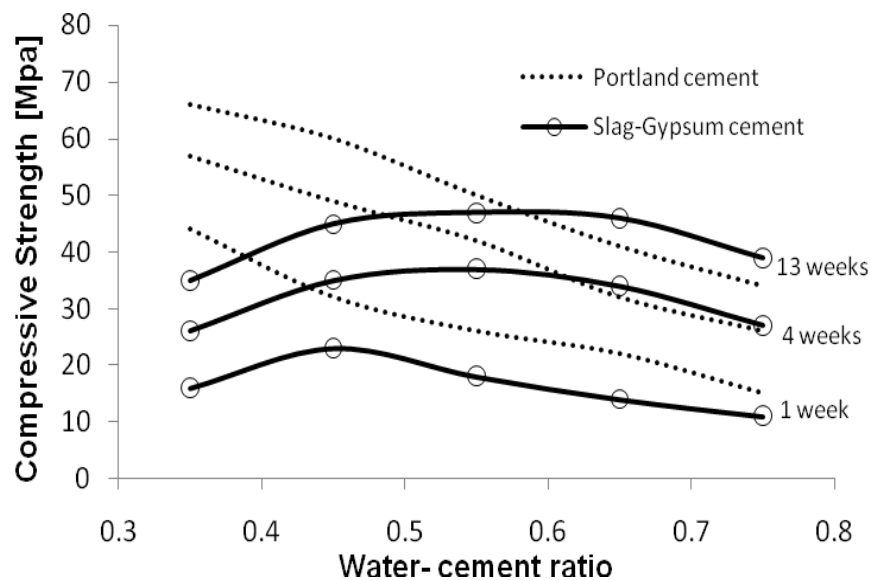
Figure 2-3 Relationship between compressive strength and water binder ratio of OPC and slag-gypsum concretes, Uomoto and Kobayashi (1983)

Durability of GGBS

Freezing and thawing, sulphate attack and expansion due to alkali-silica reaction (ARS) are common mechanisms of concrete deterioration; all are well documented in the technical literature. In general, it is reported that partial replacement of Portland cement with GGBS improves the sulphate resistance and reduces the potential for expansion due to alkali- silica reaction. In the same way, there is no evidence that the use of GGBS adversely affects the resistance of concrete to freezing and thawing (ACI 2003).

2.2.1.1.1 Transport-related properties

The main causes of corrosion in steel reinforcements are chloride ingress and carbonation. Both mechanisms are related in a direct way to the permeability of concrete, and this is reduced when GGBS is used as cement replacement (ACI 2003). As was mentioned above, like compressive strength, permeability depends upon porosity, pore size distribution, and the pore shape. Figure 2.4 shows the effect of pore distribution of an OPC and a blended OPC-GGBS cement with 40 per cent slag (Roy and Parker 1983). In the same way, it has been reported by Geiseler, Kollo and Lang (1992) that the capillary porosity, for pores with radius more than 30 nanometres, decreases proportionally to an increase in the amount of granulated blast furnace slag.
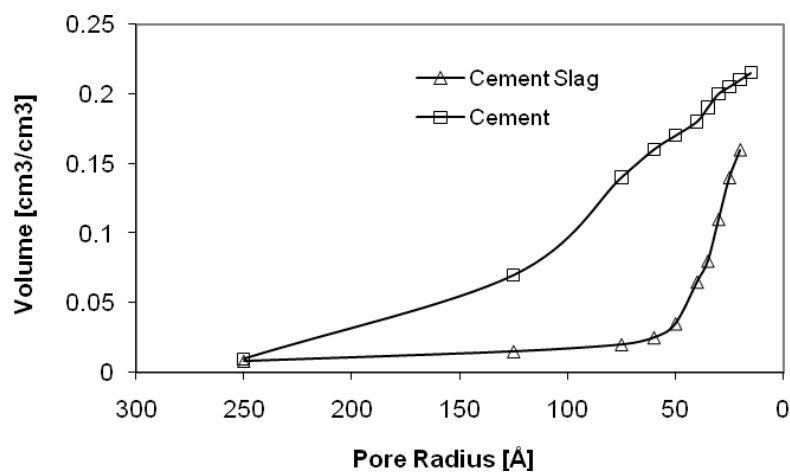
Figure 2-4 Comparison of pore size distribution of an OPC and a blended OPC-GGBS cement with 40 per cent slag replacement, Roy and Parker (1983)

In natural conditions carbonation is a low speed physiochemical process whereby carbon dioxide penetrates the porous matrix of hardened concrete and reacts with the cement hydration products, decreasing the pH and sometimes affecting the microstructure of the concrete. A reduction in the pH breaks down the natural protection provided by the alkaline environment of the reinforcement, permitting steel reinforcement corrosion.

Amongst the many reports and papers about the influence of the GGBS on carbonation penetration, there is no unanimity on the actual effect of GGBS on carbonation. According to the literature survey done for this research, there are a number of facts that can help explain the process of carbonation of GGBS concrete mixes:

(a) Carbon dioxide is reactive especially with calcium hydroxide and calcium silicate hydrate, and as a result, calcium carbonate, decalcified C-S-H and aluminosilicate gel are formed.

(b) In a blended cement, the replacement level of GGBS inversely affects the amount of calcium hydroxide content, the more GGBS the lower the calcium hydroxide content.

(c) Hydrated OPC with enough Ca forms calcium carbonate, which precipitates in the pores and forms a barrier for diffusion, decreasing the rate of carbonation (Bakharev, Sanjayan and Cheng 2001).

(d) Alkali-activated slag concretes are probably more vulnerable to carbonation than OPC because the decalcification of CSH increases concrete porosity (Bakharev, Sanjayan and Cheng 2001).

(e) In a mineral admixture-blended concrete, the calcium hydroxide content and the pore refinement are directly affected by the carbonation rate. For low fineness GGBS concrete, Sulapha *et al.* (2003) found higher rates of carbonation than for OPC. They state that the reduction of $Ca(OH)_2$ content has more influence than the pore refinement on carbonation. In addition, they show that for higher fineness GGBS concrete, the carbonation rates were lower than for OPC. They state that the pore refinement due to the GGBS is more dominant than the change in $Ca(OH)_2$.

(f) Concretes with low levels of GGBS replacement show similar carbonation rates to OPC samples (Geiseler, Kollo and Lang 1992).

Uomoto and Kobayashi (1983) reported that when supersulphated cement is used, any concrete surface in contact with the air suffers some deterioration due to the penetration of carbon dioxide. Using X-ray diffraction it was pointed out that in non-carbonated concrete the ettringite intensity was strong, while its intensity in calcium carbonate and gypsum was weak. By contrast, in carbonated concrete, calcium carbonate and gypsum had a strong X-ray intensity while that of ettringite was weak. The reaction of carbon dioxide with the hydration products in a supersulphated cement significantly increases porosity and thereby reduces the concrete's strength in the affected area.

2.2.1.1.2 Chloride penetration

It has been reported by Leng, Feng and Lu (2000) that blast furnace slag can improve resistance to chloride penetration. A reduction in the diffusion coefficient is expected because of the following factors:

1. In a GGBS concrete more calcium silicate hydration products are present in the concrete matrix and may therefore adsorb more chloride ions and block diffusion paths. Figure 2.5 shows the relationship between the diffusion coefficient and the water binder ratio in OPC and GGBS-blended concretes. The level of replacement was twenty five percent of cement. The diffusion coefficients were determined applying Fick's Second Law of diffusion to the results of the ponding test (D_p: ponding diffusion coefficient (see part two for definition)), and using the ACTM chloride migration test (D_n: non-steady diffusion coefficient (see part two for definition)) presented by Yang and Cho (2003).
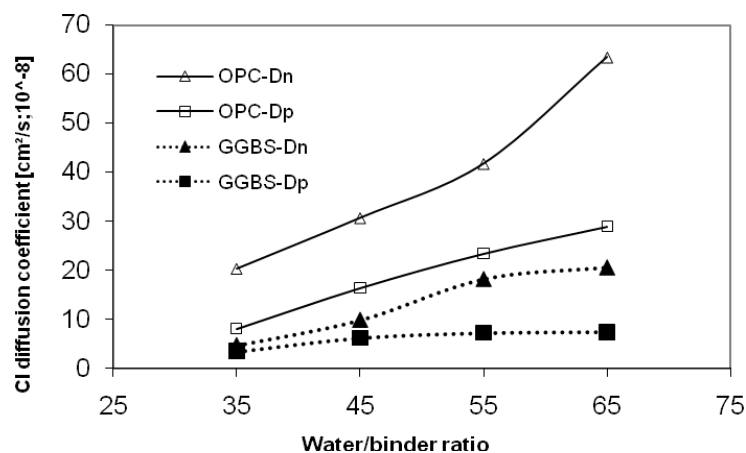
Figure 2-5 Diffusion coefficients and water to binder ratio relationships in OPC and GGBS-blended concretes obtained from ponding tests (Yang and Wang 2004)

2. The pore size and pore shape are improved due to the replacement with slag. Figure 2.6 shows the relationship between the chloride diffusion coefficient and the amount of GGBS used as replacement. The coefficients were obtained using the Nernst-Einstein equation (Leng, Feng and Lu 2000).
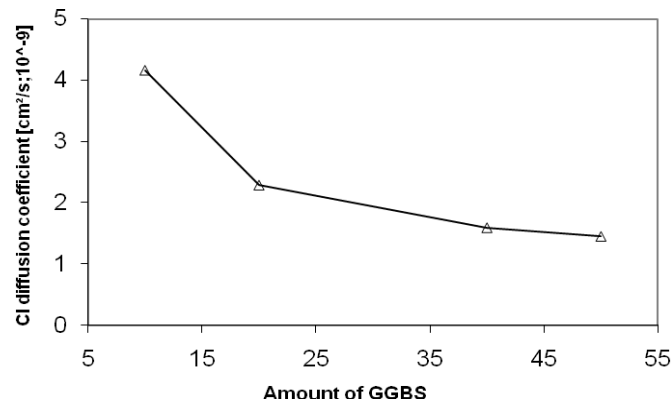
Figure 2-6 Chloride diffusivity for different amounts of GGBS used as OPC replacement (Leng, Feng and Lu 2000)

3. GGBS has more tricalcium aluminate which can adsorb more chlorides to form Friedel's salt (Leng, Feng and Lu 2000).

The ASTM C1202 Rapid Chloride Permeability Test has been used extensively to rank concrete mixes using the charge passed as a "permeability index". As the amount of replacement increases, so the charge passed in a GGBS blended concrete decreases. Taking mixes with different amounts of GGBS and GGBS fineness, but with the same water binder ratio of 0.5, Wee, Suryavanshi and Tin (2000) conducted ASTM C1202 tests at 28 days. Figure 2.7 shows the results of this research, which indicate that the addition of GGBS produces less charge passed. At low levels of replacement the total charge is dominated by the fineness of GGBS, but at higher levels of replacement the total charge is dominated by the amount of GGBS. This is discussed in detail in part 3 of this thesis.
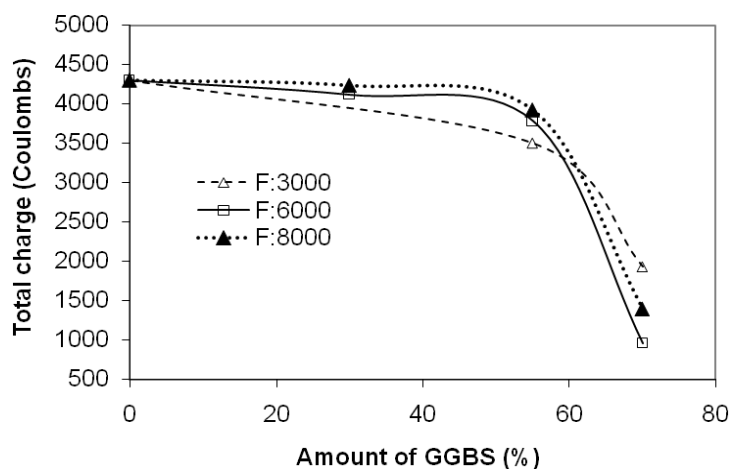
Figure 2-7 Charge passed for different amounts of GGBS replacement at 28 days (Wee, Suryavanshi and Tin 2000). F:3000 correspond to 3000 cm^2/g fineness

2.2.1.1.3 Corrosion of reinforcement

In OPC concrete structures the internal alkalinity of the hydration products together with the alkaline pore solution help prevent the steel reinforcement from damage caused by corrosion. When GGBS is used, it has been proved that the ingress of substances that can produce corrosion is delayed; however, the passive layer of the steel can be affected by the soluble sulphides in the GGBS. With the aim of investigating the effect of GGBS on steel corrosion in concrete, Pal, Mukherjee and Pathak (2002) carried out electrochemical tests and showed that as the amount of GGBS increases, so the corrosion resistance increases. They conclude that although there is an alteration in the passive layer due to the inclusion of some species (S^{2-}, HS^{-}, S_n^{2-}) from the slag, the improvement of pore structure and the increased resistivity causes a reduction in the rate of corrosion. In the same way, Hogan and Meusel (1981) showed that GGBS has no negative effect on the corrosion of steel. According to the American Concrete Institute Committee 233 (ACI 2003), the small reduction in the pH of pore solution has no detrimental effect on the steel reinforcement.

In the case of supersulphated cement, it was pointed out by O'rourke, Mcnally and Richardson (2009) that gypsum-rich cements should not be used in steel reinforced structures because they lack sufficient alkalinity to protect the steel from corrosion. Uomoto and Kobayashi (1983) pointed out that corrosion of steel in supersulphated concrete was detected at early stages (4 weeks), an effect not related directly with carbonation. The mix of slag and gypsum produces compounds that produce corrosion autonomously.

2.2.1.2 Steel Basic Oxygen Slag - BOS

Steel slag is a by-product of the transformation of iron into steel. The conversion is normally done in a basic oxygen furnace where iron from the blast furnace, molten scrap, oxygen, and fluxes (either lime or dolomite), are combined. In order to remove the impurities from the melting steel, high pressure oxygen is injected, producing carbon monoxide, silicon, manganese, phosphorus, and some iron residue. The impurities are combined with the lime and dolomite to form the BOS steel slag. After refining, the liquid steel is poured into a ladle to continue the metallurgical process, while the slag is collected using other process. Similarly, melting scrap can be used to make steel in an electric arc furnace (EAF), however hot iron is not commonly used, only steel scrap. The charged material is heated to a liquid condition with an

electric current; normally, three graphite electrodes are used to form an electric arc and melt the scrap. Once the steel is melted, oxygen and lime are added to the furnace to purify it, and the EAF slag is formed. Figure 2.8 shows these two types of furnace used in the production of steel. After the steel is poured from these furnaces, it is transported to a ladle for further refining or to form alloys. During this process a new slag is generated, called ladle slag.

After the metallurgical process the steel slag is cooled and the free metallics are magnetically removed. The remaining slag has many applications in the construction industry as was pointed out above, or as fertiliser or for use in other metallurgical applications.
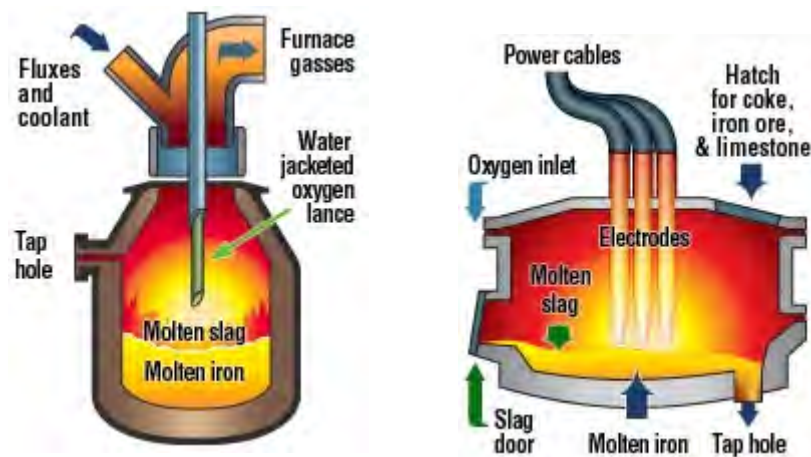
Figure 2-8 Oxygen furnace and electric arc furnace

Although in Western countries the volume of steel slag generated is as high as that of blast furnace slag, its usage is much lower. In 2006 in the United States the production of iron and steel slag was around 21.5 million tons, of which 40% was classified as steel slag. Three years earlier output of steel slag was estimated 8.8 million metric tons of which only 5% was used in the cement industry (Oss 2003). The principal reasons why steel slag is not used extensively in construction, especially in the cement and concrete industry as follows:

- Steel slag tends to have a highly variable composition. Depending of the grade and features of the steel produced, the resulting slag has different mineral composition; each slag needs to be treated separately.

- The steel slag has poor cementing properties. Due to the low content of reactive calcium silicate compounds it does not have the same binder potential that GGBS has.

- The high content of free calcium and magnesium oxides cause volume expansion problems. As was pointed out by Shi and Qian (2000), a long time ago the Ministry of Transportation of Ontario, Canada, banned the use of steel slag because of volume expansion problems. Nowadays there is still some fear about the use of slag because of its lack of volume stability, but great progress has been made in the last couple of years, for example, certain standards such as ASTM-D5106 (2008) becoming available.

- Steel slag has a higher density than other materials or rocks like basalt or limestone, and for some construction applications this is a disadvantage.

- The possibility of leaching of metals such as chromium and molybdenum has been an environmental obstacle; however, it has been reported by Geiseler (1996) that the leaching of chromium ions is low because of bonding with stable crystalline phases. In the same way, Tossavainen *et al.* (2007) concluded that the solubility of elements such as chromium, molybdenum and vanadium is very low.

In spite of the problems associated with steel slag, it has many possible uses in the cement and concrete industry. In China, for example, it has been commercialized for a long time in a cement that contains 35% Portland clinker, 5% gypsum, 30% steel furnace slag, and 30% blast furnace slag (Shi 2004b). In recent years, many investigations have been carried out into the possible use of steel slag as a binder or as a raw material in the cement production.

According to Shi (2004b) the chemical composition of BOS, EAF and ladle slag are shown in table 2.2. The quaternary system $CaO-MgO-SiO_2-FeO$ defines the principal components of steel slag, although variations can be found depending on the steel raw materials, type of steel produced, and type of furnace used. What mainly distinguishes them from OPC is their high FeO content. Depending on the flux material used during the metallurgical process, the MgO content of the slag could be high, in the case of dolomite, or low for a lime based flux.

Components	Basic oxygen slag	Electric arc furnace (carbon steel)	Electric arc furnace (alloy/stainless)	Ladle slag
SiO_2	8-20	9-20	24-32	2-35
Al_2O_3	1-6	2-9	3-7.5	5-35
FeO	10-35	15-30	1-6	0.1-15
CaO	30-55	35-60	39-45	30-60
MgO	5-15	5-15	8-15	1-10
MnO	2-8	3-8	0.4-2	0-5
TiO_2	0.4-2	***	***	***
S	0.05-0.15	0.08-0.2	0.1-0.3	0.1-1
P	0.2-2	0.01-0.25	0.01-0.07	0.1-0.4
Cr	0.1-0.5	0.1-1	0.1-20	0-0.5

Table 2-2 Chemical composition of steel slag (Shi 2004b)

According to the Chinese standard Yb/T022-92 (1992) steel slag can be classified, according to its basicity, into four groups: olivine, merwinite, dicalcium silicate, and tricalcium silicate. The basicity is determined according to the chemical composition of the principal bases and defines its potential hydraulic reactivity. Table 2.3 shows the classification presented by Shi (2004b). Although with a higher basicity more hydraulic reactivity can be expected, care must be taken because the free lime content may be higher.

Hydraulic reactivity	Types of steel slag	Basicity CaO/SiO_2	$CaO/(SiO_2+P_2O_5)$	Major mineral phases
Low	Olivine	0.9-1.5	0.9-1.4	Olivine, RO phase and merwinite
	Merwinite	1.5-2.7	1.4-1.6	Merwinite, C2S, and RO phase
Medium	Dicalcium silicate		1.6-2.4	C2S and RO phase
High	Tricalcium silicate	>2.7	>2.4	C3S, C2S, C4AF, C2F and RO phase

Table 2-3 Basicity, hydraulic reactivity and mineral phases of steel slag (Shi 2004b)

As the chemical composition of steel slag changes, so too can its mineralogical composition. The minerals normally present in air cooled steel slag are shown in table 2.4 (Shi 2004b). The existence of C_3S, C_2S, C_4AF, and C_2F in steel slag gives it some similarity to Portland cement; however, the reactivity of the slag is poor in relation to that of cement, although theoretically it can be expected that it reacts with water. Steel slag can be deployed in cement production in two different ways: it can be used as raw material in clinker production as was reported by Monshi and Asgarani (1999) and Tsivilis *et al.* (2008); or it can be blended with cement as a mineral admixture (Xuequan *et al.* 1999, Rai *et al.* 2002, Akin-Altun and Yilmaz 2002, Kourounis *et al.* 2007), aggregate, or just as filler (Qasrawi, Shalabi and Asi 2009, Sajkata, Ayano and Fujii 2007).

Mineral name	Chemical formula	Abbreviation
Merwinite	$2CaO.MgO.2SiO_2$	C_3MS_2
Tricalcium silicate	$3CaO.SiO_2$	C_3S
Dicalcium silicate	$2CaO.SiO_2$	$\beta C_2S, \gamma C_2S$
Rankinite	$3CaO.2SiO_2$	C_3S_2
Wollastonite	$CaO.SiO_2$	CS
Diopside	$CaO.MgO.2SiO_2$	CMS_2
Monticellite	$CaO.MgO.SiO_2$	CMS
Calcium aluminate	$CaO.Al_2O_3$	CA
Calcium ferrite	$CaO.Fe_2O_3$	CF
Magnesium silicate	$2MgO.SiO_2$	M_2S
Sulphide	CaS, MnS, FeS	---
RO phase	$FeO-MnO-CaO-MgO$	RO
Lime	CaO	---
Periclase	MgO	---
Wustite	$FeO,$	---

Table 2-4 Principal minerals in steel slag (Shi 2004b)

In contrast to GGBS, where the calcium and magnesium oxides combine and form non-expansive compounds, in the metallurgical process of steel slag calcium and magnesium oxides are left free. Free lime expansion occurs as an increase in volume caused by the hydration of lime, forming calcium hydroxide. On the subject of magnesium oxide expansion, it was reported by Geiseler (1996) that the important factor in an MgO rich steel slag is the content of magnesium-wustite, which can be greater than 70%. This mineral (FeO), which is one of the predominant phases in steel slag, does not have cementitious properties and is not present in Portland cement (Tsakiridis *et al.* 2008). When steel slag is used in road construction it is a common practice let it undergo a weathering process. This consists of leaving the slag in stockpiles exposed to the weather for a period sufficient to reduce its content of free lime (CaO).

As was mentioned earlier, steel slag has been used in a Portland cement-steel slag-GGBS cement (PSSBFC) produced in China. It has lower initial strength and longer setting times, but some benefits are reported by Shi (2004b), such as higher later strength (more than twice the 28 days strength at 10 years), low energy cost, good abrasion resistance, lower hydration heat, and good sulphate resistance. However, the deficiencies of early strength can apparently be rectified with the activation of the slag, although there is no reference made as to the kind of activator that might be required.

A steel slag - fly ash (FA) composite blended cement was reported by Xuequan *et al.* (1999) with a composition of 45% clinker, 3% gypsum, 22% Fly ash, and 30% steel slag. This blended cement showed similar strength to the Portland cement reference. Bin, Wu and Tang (1992) reported a GGBS-steel slag cement that had been alkali activated through the use of 5% of sodium silicate. The compressive strength for this blended cement is shown in figure 2.9. From the graph it is concluded that there is an optimum combination of both slags corresponding around 20% of steel slag, in addition, the mix with 100% steel slag is activated by the water glass reaching a considerable strength, although this strength is lower than 100% GGBS. In the same way, in a recent study Mahieux, Aubert and Escadeillas (2009) conclude that weathered BOS slag seems to have little hydraulic activity and apparently no pozzolanic properties; however, combining BOS slag with GGBS and small amounts of a catalyst (GGBS:52.5%, BOS:42.5%, catalyst:5%) gives very good results. The activation of GGBS is in part due to the total lime present in the BOS slag and in part due to the catalyst. In addition, it was found that the GGBS-BOS-catalyst cement did not presented expansion problems.
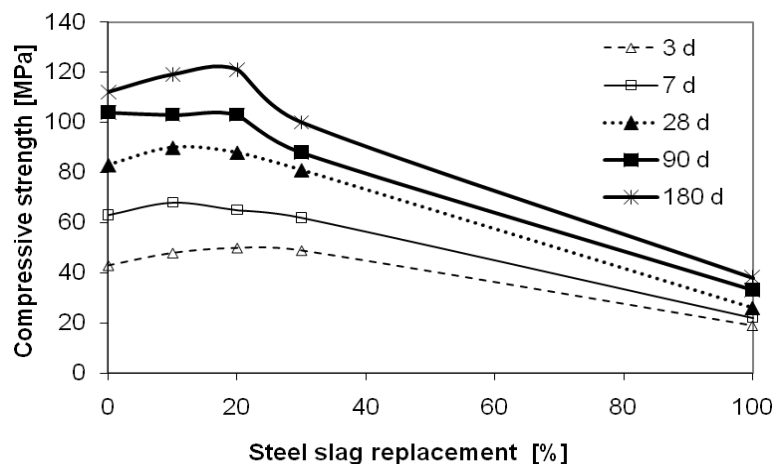
Figure 2-9 Strength development of GGBS-steel slag cement activated through the use of 5% of sodium silicate (Shi 2004b)

In different studies, Mahieux, Aubert and Escadeillas (2009) and Kourounis *et al.* (2007) investigate the influence of steel slag on the compressive strength of ordinary Portland cements at different levels of replacement. Figure 2.10 shows in the same graph the results of both investigations (note that although they are plotted together they were developed independently). It can be concluded from the figure that (a) the replacement of cement by BOS decreases the compressive strength, and (b) after 28 days any increase in strength is negligible.
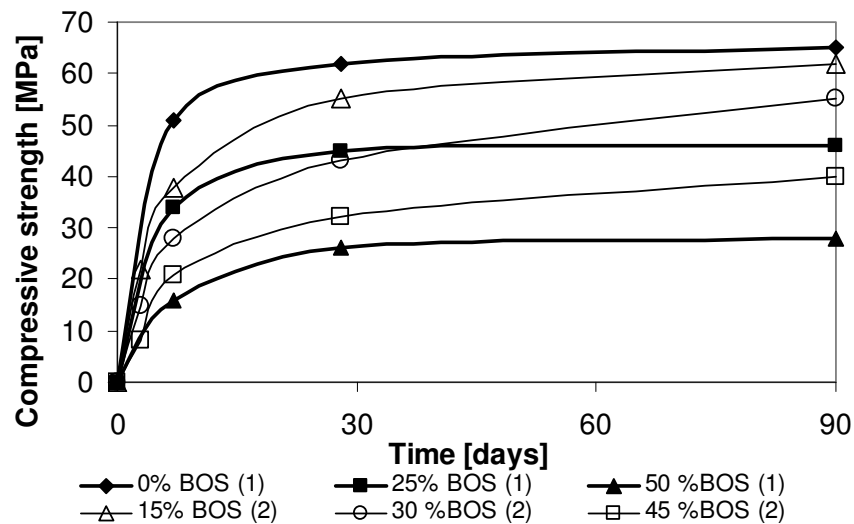
Figure 2-10 Compressive Strength development of OPC-Steel slag ((1):(Kourounis *et al.* 2007), (2):(Mahieux, Aubert and Escadeillas 2009))

Regarding the durability of the steel slag cement (blast furnace slag - steel slag – clinker - gypsum) Dongxue *et al.* (1997) carried out some experiments to determinate the chemical, carbonation, and alkali-aggregate resistance, and the pore structure. They conclude that the mixes tested had good chemical resistance in contact with sea water, sodium and magnesium sulphate. They reported that steel slag cement increases in strength after carbonation, and it reduces the alkali-aggregate reaction. The pore structure at 28 days is similar to ordinary Portland cement.

2.2.2 Cement Kiln Dust

Cement kiln dust (CKD) is a highly alkaline waste removed from the cement kiln by dust control procedures. Depending on its composition, it could be recycled directly into the cement production process or it may need to be treated prior to reuse. CKD that is totally unsuitable for recycling in cement production is typically disposed in landfills, and only a minor proportion can be used in other construction applications. The properties of CKD depend on the features of the kiln systems, the dust-collection point, and the maximum temperature reached. For example, some frequently found kiln dusts come from long wet rotary kilns, long dry rotary kilns, or alkali bypass precalciner systems (BPD). Todres, Mishulovich and Ahmed (1992) show average chemical compositions of different CKDs.

Constituent	Long wet kiln	Long dry kiln	Alkali bypass
SiO_2	15.02	9.64	15.23
Al_2O_3	3.85	3.39	3.07
Fe_2O_3	1.88	1.10	2.00
CaO	41.01	44.91	61.28
MgO	1.47	1.29	2.13
SO_3	6.27	6.74	8.67
Na_2O	0.74	0.27	0.34
K_2O	2.57	2.40	2.51
LOI	25.78	30.24	4.48
Free CaO	0.85	0.52	27.18

Table 2-5 Chemical composition of different CKD

As was mentioned above, one of the difficulties in the practical application of CKD is the variability of its chemical, mineralogical, and physical properties. The dust from each plant varies according to on the raw materials, type of plant operation, dust collection technology, and type of fuel used (Detwiler, Bhatty and Bhattacharja 1996). In research by Muller (1977), it is stated that the European CKDs are composed for four major components.

CKD component	Mineralogical compositions
Unreacted raw feed	Carbonates, Quartz, feldspar, clay minerals, Fe/Al oxides
Partially calcined feed and clinker dust	Decomposed raw feed Calcined clays Clinker minerals Intermediate phases
Free lime and alkali compounds	CaO, $Ca(OH)_2$
Alkali salts and other volatile compounds	KCl, $2NaCl$, $(K/Na)_2SO_4$, $CaSO_4$

Table 2-6 CKD mineral compositions (Muller 1977)

In a research carried out by Al-Harthy, Taha and Al-Maamary (2003) it has been reported that Increasing the CKD replacement has an adverse effect on compressive strength. The flexural strength and concrete toughness also decreases. However, it was reported that small amounts of replacement (5%) do not have an appreciable adverse effect on strength, especially at low water binder ratios. Similar results were found by Shoaib, Balaha and Abdel-Rahman (2000) who reported that the compression strength increases gradually with the curing time and with the reduction of the water binder ratio, but decreases with an increase in CKD.

Because of the high alkali and sulphate content of CKD, it can be used as an activator for ground granulated slag or pozzolanic materials. Konsta-Gdoutos and Shah (2003) studied the hydration of GGBS activated with CKD. They concluded that during curing the samples showed an increase in compressive strength, indicating slag activation. They stated that the principal products of the hydration of the slag were calcium silicate hydrates, and noted that in all cases observed, the strength of CKD-slag blends was lower compared with similar samples of OPC or OPC-Slag mixes. In the same study it was reported that the profile of the heat evolution in a CKD-slag mix is similar to those that can be obtained in a cement-slag mix. Similarly, an increase in the setting times of mixes blended with CKD-cement or CKD-slag was reported.

2.2.3 Plasterboard Gypsum - PG

In addition being found in its natural form, gypsum also exits as a by-product of a number of industrial processes. According to Roszczynialski, Gawlicki and Wczelik (1997) gypsum by-products can be divided in two groups: those that can be obtained by chemical or physical processing, and those obtained from flue gas desulphurization installations in power stations. Calcium sulphate dihydrate $CaSO_4.2H_2O$ is the principal component of chemical by-product gypsums, although other minerals may be found in lower proportions. Hemihydrate gypsum $CaSO_4.0.5H_2O$ and the products used during chemical processing are wastes in some industries and are know as phosphogypsum, fluorogypsum, titangypsum, borogypsum, citrogypsum, phenologypsum, sodagypsum, and saltgypsum.

Another possible source of gypsum is waste plasterboard (PG); a by-product of the building industry. Plasterboard is usually made from natural mined gypsum or gypsum obtained from flue gas desulphurization. The raw material is milled and calcined at around 120~130°C before use, to convert the dehydrate to hemihydrate.

$$CaSO_4.2H_2O + Heat \rightarrow CaSO_4.1/2H_2O + 3/2H_2O$$
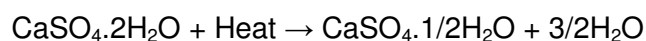
After drying, the gypsum is ground to a powder. Plasterboard is formed by combining the gypsum hemihydrate with some additives and water, so the gypsum is converted back to dihydrate gypsum, and the board is formed as a layer of gypsum sandwiched between layers of special facing paper.

2.3   CONCLUSIONS

1. A complete description about actual knowledge on blast furnace slag, steel slag, plasterboard gypsum and by-pass dust has shown the potential capabilities of those materials as hydraulic binders, which can be summarised in the following:

   - GGBS is a glassy material with potential hydraulic capabilities if is adequately activated. It can be activated under OPC mixes, under alkaline and under sulphate environments. It is reported that if the GGBS is mixed adequately its durability increases and its strength can be similar or higher than similar samples of OPC.

   - Steel Slag is reported as a material that contains principally CaO, MgO, SiO_2 and FeO. The first three oxides gives to the steel slag some mineralogical similarities than the OPC; however the cementitious properties are very poor because in the principal minerals are attached several impurities.

   - Cement kiln dust is a waste from the cement industry which is usually landfilled, used as a recycled raw material in cement production, or used as an admixture in blended concrete mixes. In construction applications, the use of this material is limited to small proportions because its chemical and mineralogical composition varies significantly from different sources.

   - The recycled plasterboard gypsum can be used as a sulphate material with an enough level of quality to be used in construction applications.

3 LABORATORY DEVELOPMENT OF SLAG BINDERS

In this chapter the combination of ground blast furnace slag and basic oxygen slag activated using ordinary Portland cement, cement by-past dust and plasterboard gypsum was investigated. The mixes were assessed in terms of compressive strength of paste mixtures to establish the optimum raw materials proportions.

3.1 INTRODUCTION

Different potential binders were developed from the raw materials selected for this research. All of them used GGBS or BOS as principal constituents and were activated in different ways. Three groups of mixes were established depending on the activator used: (I) binders activated with OPC, (II) alkali activated binders with BPD, and (III) sulphate activated binders with PG. From the combination of the raw materials five final mixes were proposed and optimized for compressive strength. Figure 3.1 shows the binary and ternary binders proposed in this research.
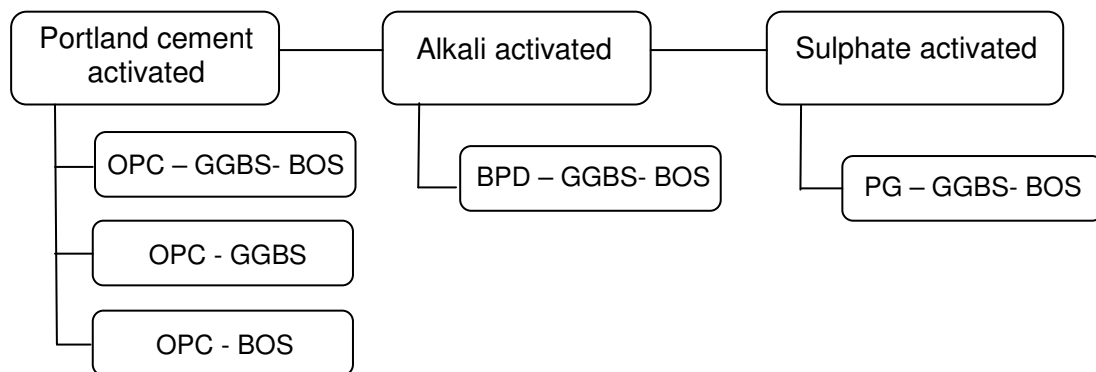
Figure 3-1 Groups of binary and ternary binders used

3.2 RAW MATERIALS USED

The materials used in this research were obtained from different sources. A summary of them is presented below.

- A commercial **Ordinary Portland cement (OPC)** classified as CEM-1 according BS EN 197-1 "*Composition, specifications and conformity criteria for common cements*" and composed of 95-100% clinker, free of admixtures except the gypsum acting as a retarder.

- The **Ground Granulated blast furnace slag (GGBS)** was obtained from Civil and Marine, a part of Hanson UK. The material was marketed under the standard BS 6699 "*Specification for ground granulated blast furnace slag for use with Portland cement*".

- The **Basic Oxygen slag (BOS)** used was obtained from Tarmac UK, from Corus Scunthorpe plant. It was prepared for use by being ground and passed through a 600 micron sieve. After a time lag of more than one year of storage, the slag was considered to be weathered.

- The Cement Kiln dust used in this research was obtained from Castle Cement, extracted from the kiln bypass. In this research this material is called alkali **by-pass dust (BPD)**.

- The **Plasterboard gypsum (PG)** was obtained from the Lafarge Plasterboard recycling plant in Bristol. After the initial collection from the demolition sites it was necessary to remove the pieces of paper and other contaminants by using various sieves. Finally the material was sieved at 600 micron and stored.

3.2.1 Characterization of raw materials

Different analytical techniques were applied to the raw materials in order to categorize them according to their chemical and mineralogical composition. In addition, the fineness and density of each powder was investigated.

3.2.1.1   Experimental Methods

- The chemical composition of the materials was analyzed by X–ray fluorescence analysis (XRF) using a Philips PW2400 instrument.

- The mineralogical composition was determined by X-ray diffraction Analysis (XRD) using a Philips 1820 diffractometer with a 20 position sample changer.

- The specific gravity of each powder was determined using a fully automatic gas displacement helium picnometer, a Micromeritics – Accupyc 1330.

- The particle size distribution was determined using a laser granulometer, a Malvern Mastersizer 2000 with a Hydro 2000MU pump attachment.

- The morphological appearance of the grains was determined using a scanning electron microscope (SEM), a Jeol JSM-6060 LV.

3.2.1.2 Results and discussion

3.2.1.2.1 Chemical composition

The results of the compositional analysis carried out for the different binders are presented in Table 3.1. Note that for OPC the values reported were taken from data supplied by the manufacturer and are well established in concrete technology and will not be discussed. For the GGBS the values measured for insoluble residue, magnesia, sulphur, and loss on ignition are within the limits specified in the Standard BS 6699. In addition, the requirements of the same standard for the composition of CaO, MgO, and SiO_2, including the chemical moduli, were met in full.

$$CaO + MgO + SiO_2 = 0.81 > 0.66 \quad (3.1)$$

$$(CaO + MgO) / SiO_2 = 1.34 > 1.0 \quad (3.2)$$

$$CaO / SiO_2 = 1.22 > 1.0 \quad (3.3)$$

Equation 3.2 defines the modulus of basicity of the slag as the ratio between the sums of basic oxides to the sum of acidic oxides, and Equation 3.3 defines the activity of the slag. The hydraulic activity of blast furnace slag trends to increase with increasing both moduli (Tailing and Krivenko 1997). The chemical composition of the GGBS is within the ranges shown in table 2.1 and is considered adequate to be used in this research.

	Chemical composition [%]											
Binder	**SiO₂**	**TiO₂**	**Al₂O₃**	**Fe₂O₃**	**MnO**	**MgO**	**CaO**	**Na₂O**	**K₂O**	**P₂O₅**	**SO₃**	**LOI**
OPC*	19.7	---	4.9	2.4	---	2.1	63.3	0.2	0.6	---	2.7	2.7
GGBS	34.5	0.55	13.16	0.74	0.45	7.75	38.7	0.29	0.55	0.02	1.75	0.7
BOS	11.45	0.37	2.32	27.32	3.65	9.32	37.44	0.03	0.01	1.26	0.28	3.12
BPD	15.67	---	4.04	2.08	---	2.40	46.52	1.12	3.88	---	3.01	---
PG	2.43	0.03	0.81	0.36	0.0	0.4	37.3	0.03	0.24	0.02	53.07	4.09

Table 3-1 Chemical oxide composition of the raw materials (*according to the producer)

The BOS slag consists mainly of CaO, MgO, SiO_2, and Fe_2O_3. The first three materials are just the 58.2% of the total sample, while the iron compounds are

27.3%. According to table 2.3 the basicity of this slag is expressed as equations 3.4 and 3.5, and is classified as a hydraulic reactivity BOS Slag (Shi 2004b), with some phases similar to those found in OPC. It is important to note that according to shy (2004b), equations 3.4 and 3.5 are just an indication of the basicity of the BOS, which is correlated with the major minerals phases expected (table 2.3). In addition, it is well known that the mineralogical phases of the BOS are contaminated with several impurities and the high values found indicate that hydration faces could be present. It does not necessarily represent high strength binders because impurities and size grain dependent factors.

$$CaO/(SiO_2 + P_2O_5) = 2.95 \quad (3.4)$$

$$CaO/SiO_2 = 3.27 \quad (3.5)$$

The chemical composition of BPD shows that the CaO and SiO$_2$ are 62.19% of the total sample; these oxides come from variables mixtures of calcined and uncalcined feed materials used during the cement production. In addition, the proportion of sodium, potassium, and sulphate salts present is 8%, which suggests that BPD can serve as an adequate alkali activator. Figure 3.2 shows the materials in a CaO+MgO-SiO$_2$-Fe$_2$O$_3$+Al2O3 System. Chemically BPD is similar to OPC, both materials are the product of the same industrial process, although one is a primary product while the other is a waste. It can be noticed as well that both slags are chemically different, due to the nature of their individual processes of production.
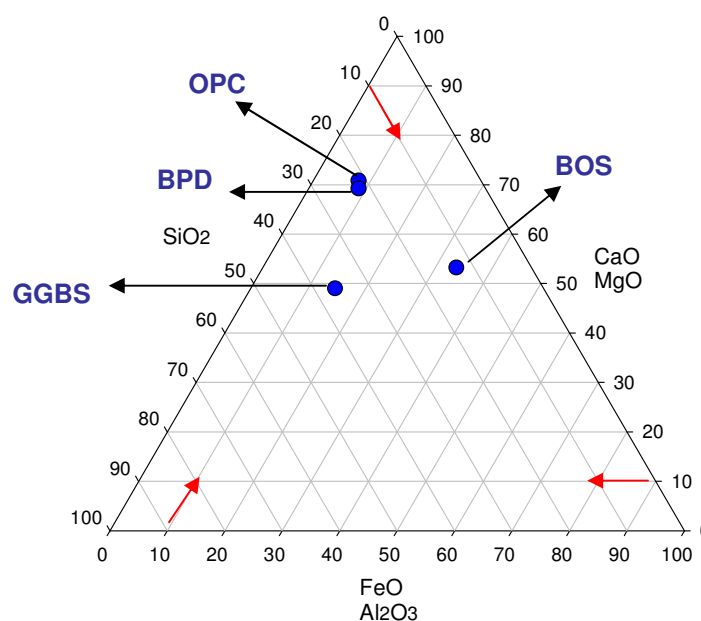
Figure 3-2 Raw materials ternary system CaO+MgO-SiO2-Fe2O3+Al2O3

The chemical analysis of plasterboard gypsum reveals that the principal oxides are sulphate and calcium with 90.4% of the total, compounds that theoretically form calcium sulphate dihydrate or anhydrite. According to that result, the collection, sieving, and grinding of recycled plasterboard yields a gypsum of sufficient purity to be used in the construction industry (Roszczynialski, Gawlicki and Wczelik 1997), without recourse any chemical treatment. The loss ignition reported is higher than for all the other raw materials probably due to the presence of paper impurities or other volatile materials that could not be removed by physical methods.

3.2.1.2.2 Mineralogy

X-ray diffraction was used as qualitative characterization of the raw materials used in this research. It is important to notice that each mineral phase produces an unique independent diffraction pattern, and the intensity of that pattern is proportional to its concentration (Stutzman 1996); however, it is stated in that reference that powder diffraction patterns are complex and the number of phases creates a composite pattern with many peaks overlapping. Because the strong peaks tend to coincide it is pertinent to identify the minerals using the weaker peaks. For normal OPC mineralogy, the principal phases have been widely studied and are well documented elsewhere (Chatterjee 2001). Figure 3.3 shows the phases C_3S, C_2S, C_3A, and C_4AF identified in the Portland cement used. In addition, there are some peaks that correspond to calcium carbonate (calcite).
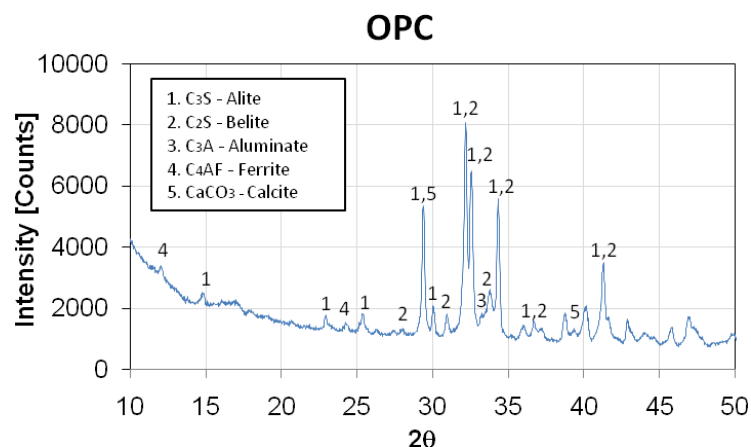
Figure 3-3 X-ray diffraction analysis of OPC

The mineral composition of the GGBS is shown in figure 3.4. As was reported by Taylor (1990), the XRD pattern for GGBS showed a diffuse band where merwinite and melilite were poorly differentiated.

GGBS

Intensity [Counts]

1. $Ca_3Mg(Si_2O_8)$ - Merwinite
2. $CaCO_3$ - Calcite
3. Melilite

2θ
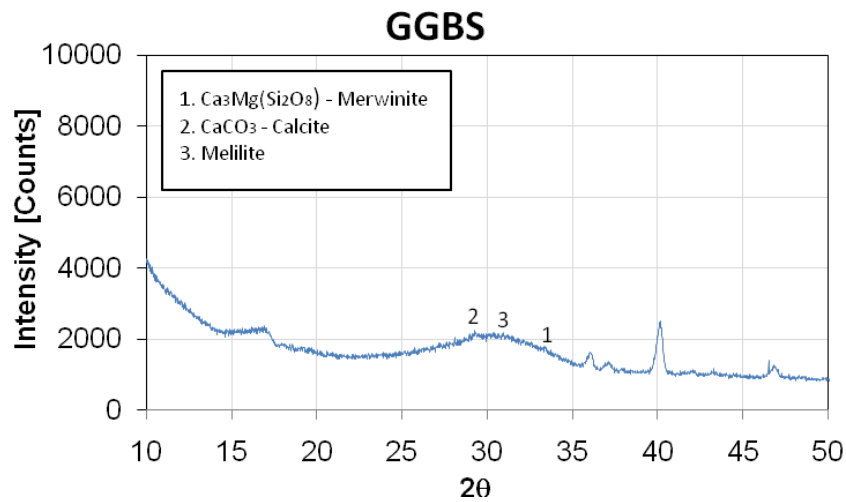
Figure 3-4 X-ray diffraction analysis of GGBS

The minerals associated with the basic oxygen slag are shown in figure 3.5. There is a significant similarity between the patterns of the Portland cement and the steel slag used in this research, however, according to Kourounis *et al.* (2007) it is expected that the calcium silicates of the BOS would have been stabilized in the presence of impurities, reducing its cementitious properties.

A common impurity found in the steel slag is the metallic Fe; it was present in different forms as Wustite and Magnetite, compounds that have a negligible cementing capacity. The Portlandite phase $(Ca(OH)_2)$ is clearly observed, its presence is probably due to the weathering of the slag. It is suggested that the contact of the BOS with the environmental conditions of the laboratory hydrated the free lime, producing calcium hydroxide.

BOS

Intensity [Counts]

1. C_2S - Belite
2. C_4AF - Ferrite
3. $Ca(OH)_2$ -Portlandite
4. C_3S- Alite
5. CaO - Lime
6. FeO - Wustite
7. Fe_3O_4 - Magnetite
8. SiO_2 - Quartz
9. MgO - Periclase
10. $CaCO_3$ - Calcita

2θ
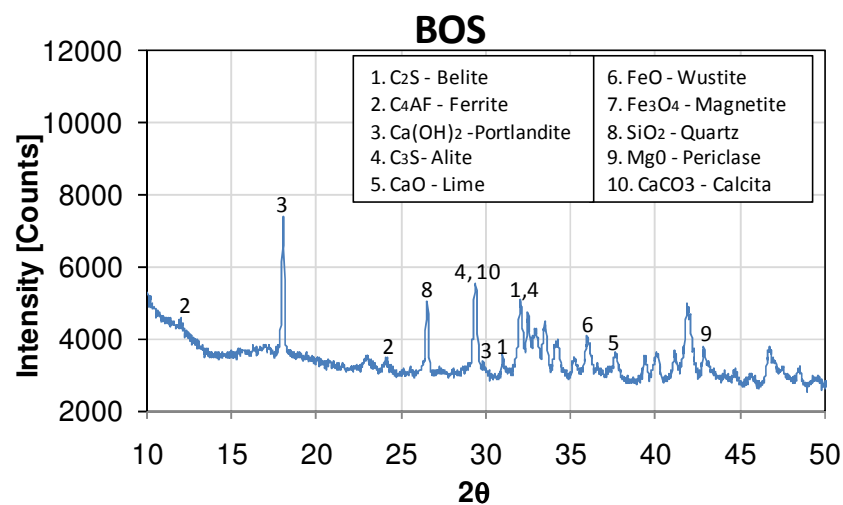
Figure 3-5 X-ray diffraction analysis of BOS

The X-ray pattern for the by-pass dust used is shown in figure 3.6, which shows the different minerals associated to the peaks detected. The difractogram is in close conformity with the one reported by Konsta-Gdoutos and Shah (2003) where calcite was identified as the predominant phase, in addition to free lime and quartz. The presence of sylvite as an independent phase confirms the possibility of BPD being considered as an alkaline activator.
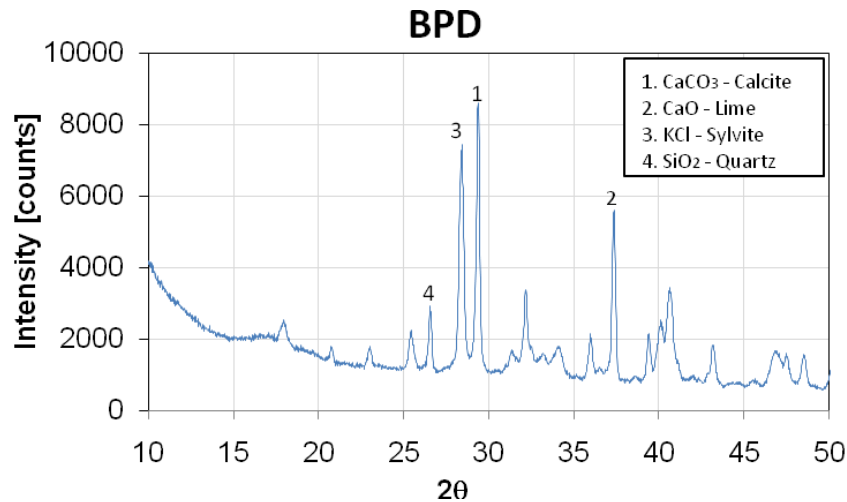
Figure 3-6 X-ray diffraction analysis of BPD

Figure 3.7 shows the X-ray patterns of the plasterboard used. It can be seen that the material is composed mainly of gypsum and anhydrite. The pattern obtained is very similar to that of a natural gypsum (Roszczynialski, Gawlicki and Wczelik 1997).
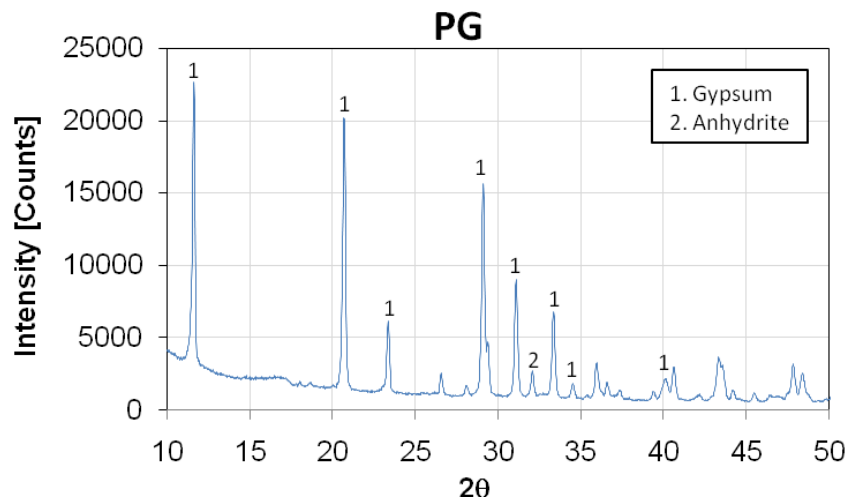
Figure 3-7 X-ray diffraction analysis of PG

3.2.1.2.3 Density

The densities of the raw materials are shown in figure 3.8, where the values measured are consistent with the ranges usually reported for similar materials. The high specific gravity of the BOS is due to its high concentration of iron impurities.
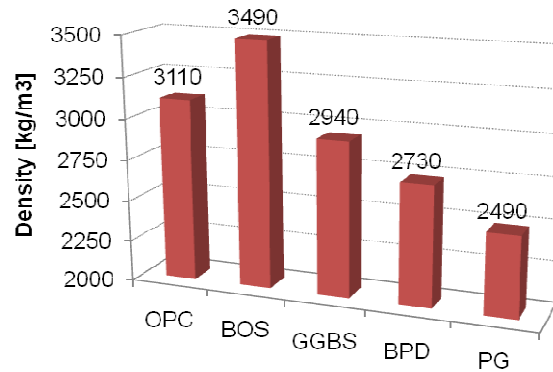
Figure 3-8 Densities of the raw materials

3.2.1.2.4 Fineness

In figure 3.9 it can be seen that the GGBS has the highest fineness of all the raw materials, followed by the OPC and the BPD. GGBS is normally ground to a very small size in order to increase its reactivity at initial ages avoiding prolonged setting times. The size distribution of the OPC and BPD is similar; although the fineness of the OPC is the result of the grinding of clinker, while the fineness of the BPD corresponds by itself to the fineness captured in the kiln. BOS and PG are the coarser materials, possibly because the grinding was not an industrial process.
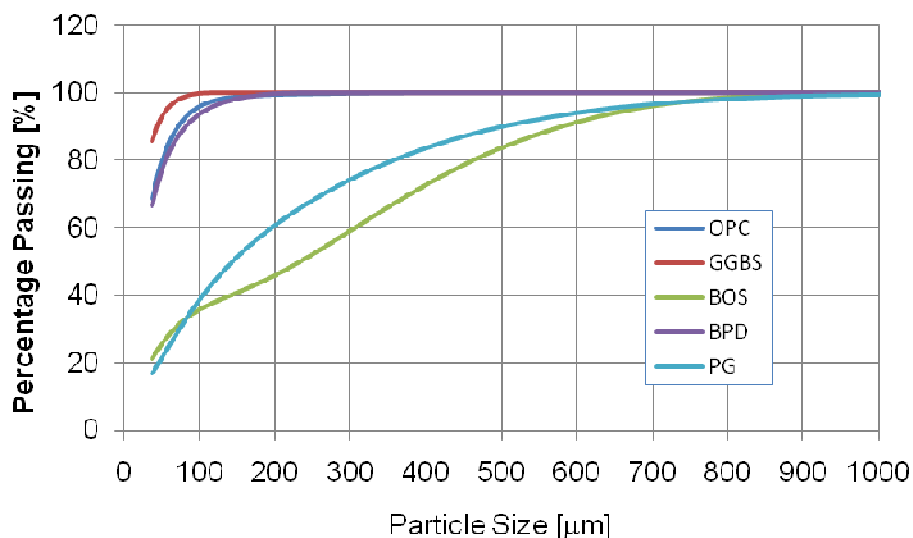
Figure 3-9 Raw materials size distribution

Photographs of the grain shapes are shown in figure 3.10 where the morphology of the grain powders can be seen. In the same figure the particle size analysis for all the raw materials is shown. OPC has grain sizes in the range between 0.3μm and 0.3mm and the average particle size is around 25μm. GGBS has grain sizes in the range between 0.3μm and 0.1mm, with an average particle size around 20μm. BOS presents a distribution with two predominant peaks, with grain sizes in the range between 1.5μm and 1mm. BPD has grain sizes in the range between 0.6μm and 0.2mm, with an average particle size around 20μm. Finally, PG has grain sizes in the range between 0.6μm and 1mm, with an average particle size around 250μm.
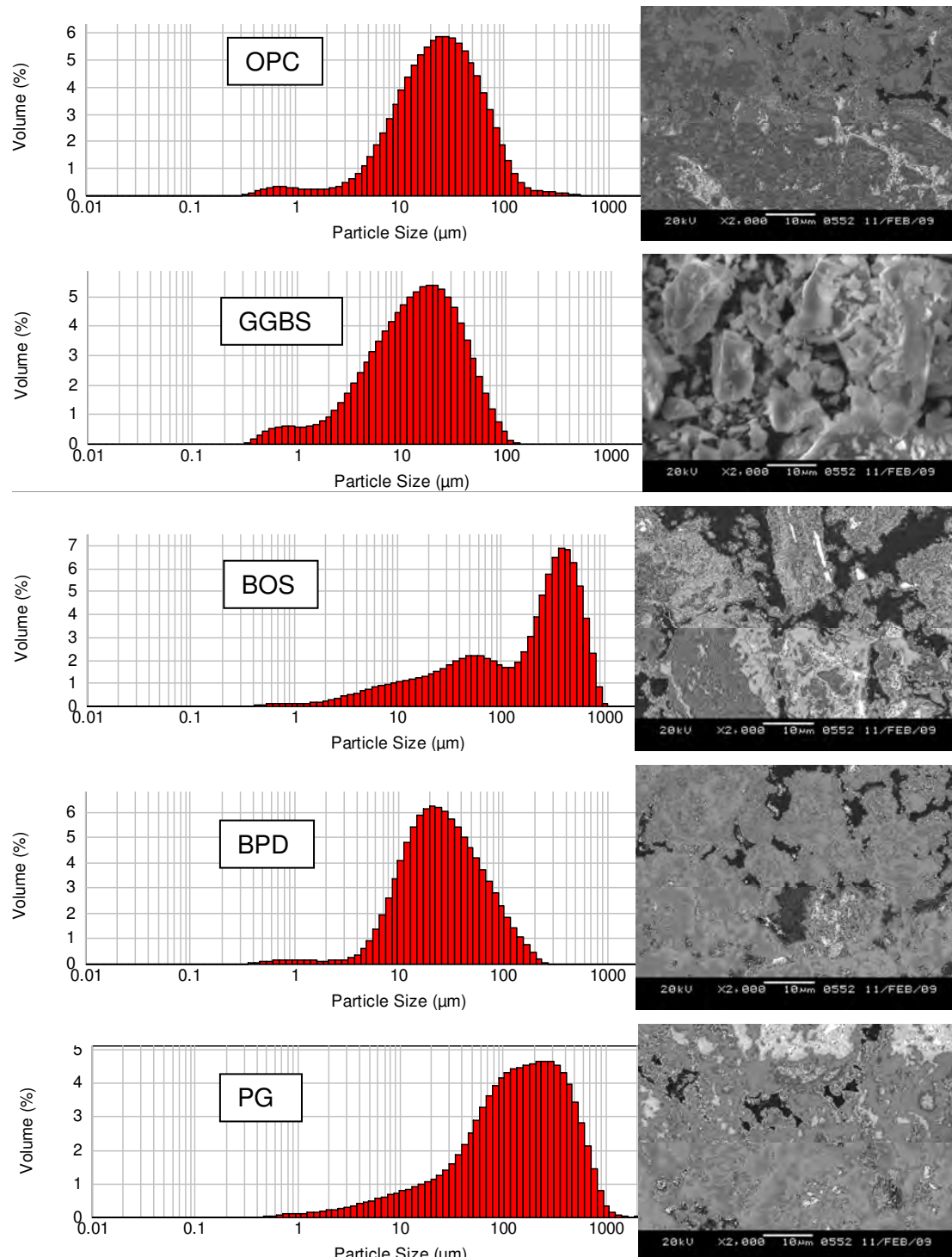
Figure 3-10 Particle size analysis and grain shape of the raw materials

3.3   OPTIMIZATION OF THE COMPRESSIVE STRENGTH: MIX SELECTION

In order to find the best combinations of materials and their relative proportions, an experimental laboratory programme was carried out. Mixes with different proportions of ground granulated blast furnace and basic oxygen slag activated with ordinary Portland cement, alkaline by-pass dust, and plasterboard gypsum were cast and

tested to optimize the mixture ingredients to achieve the highest compressive strength. In order to obtain the final proportion for each binary or ternary binder, a simple but effective experimental design was made. The compressive strength of several mixes with different proportions was evaluated to ascertain the influence of various proportions on the strength.

3.3.1 Experimental Design

For each group of raw materials an experimental design was developed with the objective of characterizing the influence of the proportions on the compressive strength. Samples of paste (mixtures of the combination of one or more binders and water with no aggregate) were cast, cured and tested under the same controlled conditions to make comparable results. The controlled variables were the following.

- The variable proportions of the materials that form each combination.

- The time of curing when the sample was tested: 7, 28 and 90 days.

- 3 replicate samples were made for each combination.

3.3.1.1 Combinations Mixes with OPC

The OPC-GGBS-BOS ternary diagram shown in figure 3.11 shows the blends investigated, with a total of 28 mixes. The location of each point represents the mixture proportions by weight, each corner point representing a single blend constituent. Points located on the perimeter are binary mixes, and points inside the triangle refer to ternary mixes. The selection of the mixes was made to include the broadest diversity of binary and ternary combinations available. In order to help the reader to understand the ternary diagrams and as a matter of example, the point "Y" was included in figure 3.11, which represents the combination 50%OPC, 40%BOS and 10%GGBS.

A complete list of the mixes investigated in this research is in appendix 1.
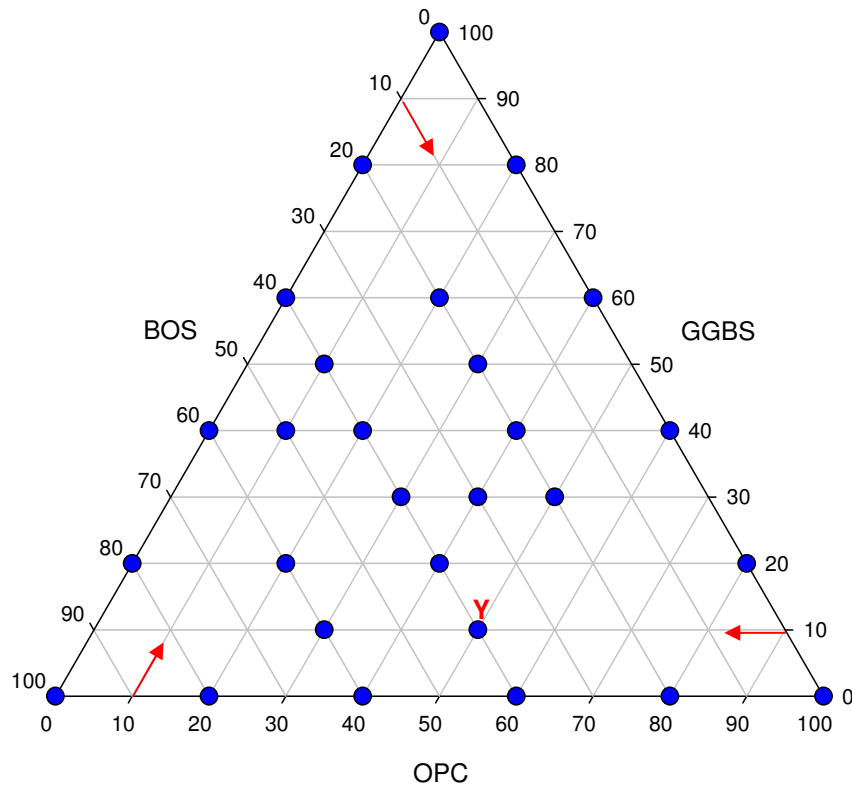
Figure 3-11 Proportions of the ternary OPC–GGBS–BOS paste mixes

3.3.1.2 Combinations alkali activated Mixes BPD – GGBS – BOS

Although BPD can be regarded as a very weak Portland cement and a good source of alkalinity, its chemical composition and properties vary significantly from source to source (Ganjian, Claisse and Pouya 2007). To minimize the effect of the variability of the BPD on the mixes, a low percentage of BPD has been used to activate the slag mixes. For this, the optimum percentage of GGBS and BOS for a binary mix composed with only these materials was activated with different percentages of BPD (5, 10 and 15%)

3.3.1.3 Combinations sulphated activated mixes PG – GGBS – BOS

Figure 3.12 shows the points representing the mixtures GGBS and BOS activated with PG, where 27 combinations were proposed. The amount of PG used in the mixtures was between 0 and 40% because it has been reported that any higher content does not have beneficial effect on the strength (Ganjian, Claisse and Pouya 2007). In addition, in the ternary mixes the percentage of GGBS was between 30 and 60%, because preliminary results obtained from section 3.3.1.1 showed that the maximum compressive strength is expected in that range.
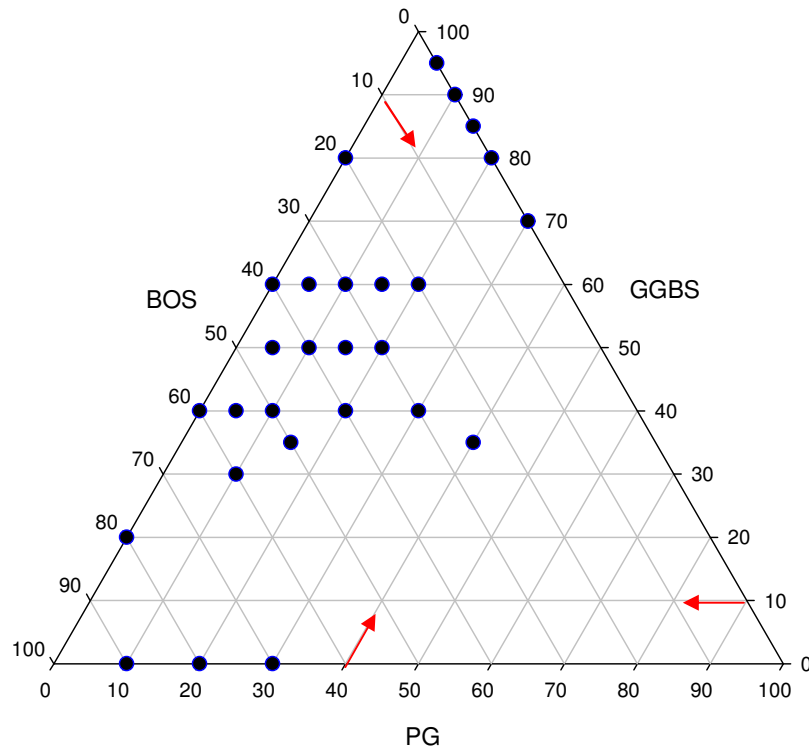
Figure 3-12 Proportions of the ternary PG–GGBS-BOS paste mixes

3.3.2 Experimental Methods

As was mentioned above, for this initial stage of the research, the principal aim was to assess the behaviour of the materials as binders. Therefore, a range of aggregate-free paste samples was tested, to identify mixes where the compression strength was at its greatest. A constant water binder ratio of 0.25 was maintained throughout.

3.3.2.1 Paste mixtures

In order to mix the raw materials a small mixer (2 litres) with both a planetary and a revolving motion was used. The materials for a batch were introduced into the bowl and mixed in the following manner:

- The raw materials were mixed dry until a homogenous distribution of the powders was obtained (usually 1 minute).
- Half of the mixing water was added to the bowl and mixed for 1 minute at medium speed.
- When necessary, the mixer was stopped and the mixture scraped off manually from the sides of the bowl and blades.
- The mixing was completed by adding the remaining water and mixing for two minutes at high speed.

3.3.2.2 Casting and curing

Samples were cast in pre-oiled 50 mm cubic moulds, covered with a polyethylene sheet and demoulded after 24 hours. Because of the differences among the raw materials and the proportions used, the mixes had different flow. In order to avoid affecting the strength because of the differences in the mix compaction, all the mixes were compacted mechanically using a vibrating table. The moulds were filled with paste in three layers and then compacted to remove the air and achieve maximum density. After demoulding specimens were cure in containers at 98% RH and 20±2 ℃.

3.3.2.3 Tests

The compressive strength was measured at 7, 28 and 90 days. A hydraulic testing machine was used in accordance with Chapter 5.9 of ASTM-C109 (2008): "*Compressive Strength of Hydraulic Cement Mortars*". The rate of loading was in the range of 1- 2 KN/s.

3.3.3 Results and discussion

In this chapter the influence of the combination of the raw materials on the compressive strength was analyzed. As each result corresponds to the average of three replicates, the variability of the experiments is shown with one standard deviation error bars in the figures.

3.3.3.1 Mixes using OPC

The average compressive strength of binary OPC - BOS mixes are presented in figure 3.13. It can be seen that an increase in the BOS replacement produces a decrease in the compressive strength. The reduction in strength is linearly proportional to the amount of BOS and the profile is similar for 7, 28 and 90 days. For mixes with BOS there is an increase in the compressive strength at 90 days with respect to that at 28 days. This can be attributed to the weak cementitious properties of the BOS developed at later stages (Shi 2004b). At 90 days replacement with 20% of slag shows no negative effect on the strength, and with a BOS replacement of 30%, a reduction of 7% was obtained.

The results of the average compressive strength of OPC - GGBS mixes are presented in figure 3.14. It can be seen that for all ages an increase up to 60% in the GGBS replacement produces a slight reduction in the strength, while greater

replacements have a more negative effect. At 90 days there was a maximum value of strength with a GGBS replacement of 40%; the reduction of strength for this level was of 6 percent.
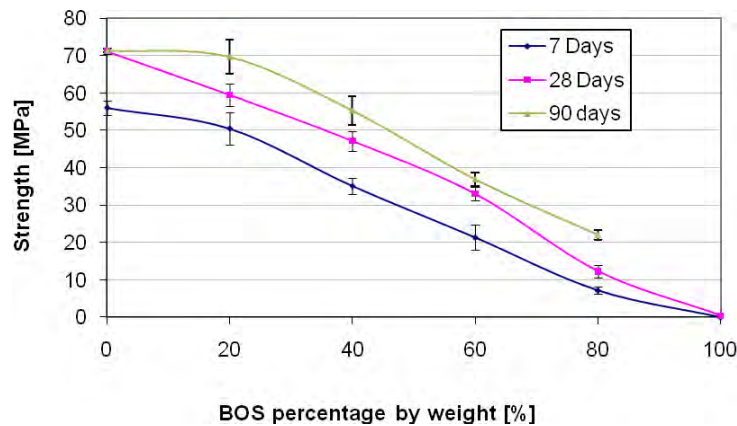
Figure 3-13 Compressive strength of OPC-BOS paste mixes

Although the mix 60% GGBS + 40% OPC showed a decrease of strength of 20% with respect to the reference, it was selected as final binder to be used through out the rest of experiments. This high volume GGBS mix can be considerate an environmentally friendly mix.
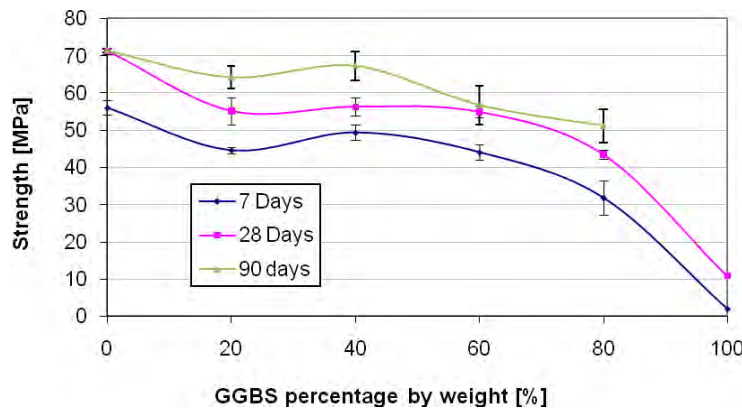
Figure 3-14 Compressive strength of OPC-GGBS paste mixes

The results of the average compressive strength at different ages for the combination of GGBS and BOS are presented in figure 3.15. It can be seen that the self - hydraulic properties of both materials are limited, especially for BOS, which practically did not develop strength by itself after being hydrated. In the same way, the results for the mix of 100% GGBS shows that at 7 days there was low strength development (2 MPa), while at 28 days there was a slight increase of the strength (10 MPa). The previous results confirm that both slags need to be activated to develop their full hydraulic cementitious capabilities.

The optimum amount of BOS in mixes with both slags is equal to 40%, the strength obtained at 7, 28 and 90 days with 40% of BOS were 10, 22, and 30 MPa respectively. That shows a continuous hydration that can presumably be explained either by the activation or by the reaction of the GGBS with the basicity of the steel slag.
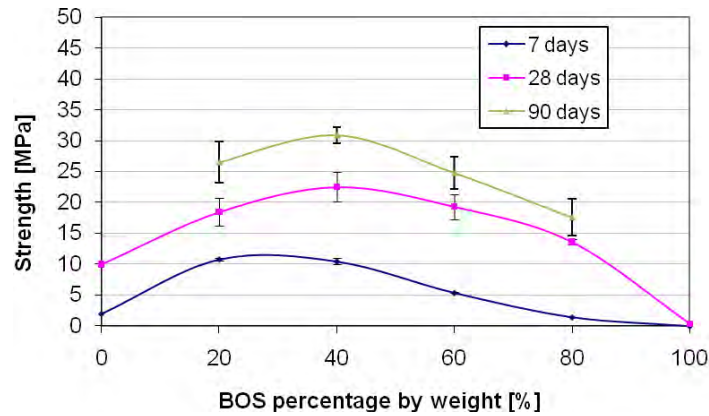
Figure 3-15 Compressive strength of BOS-GGBS paste mixes

The results of compressive strength for the ternary OPC - GGBS - BOS mixes are presented in figure 3.16 for 7, 28 and 90 days. The nomenclature used was given according to the proportional combinations of the materials. The mix O10G40B50 for example, comprises 10% of OPC, 40% of GGBS and 50% of BOS.
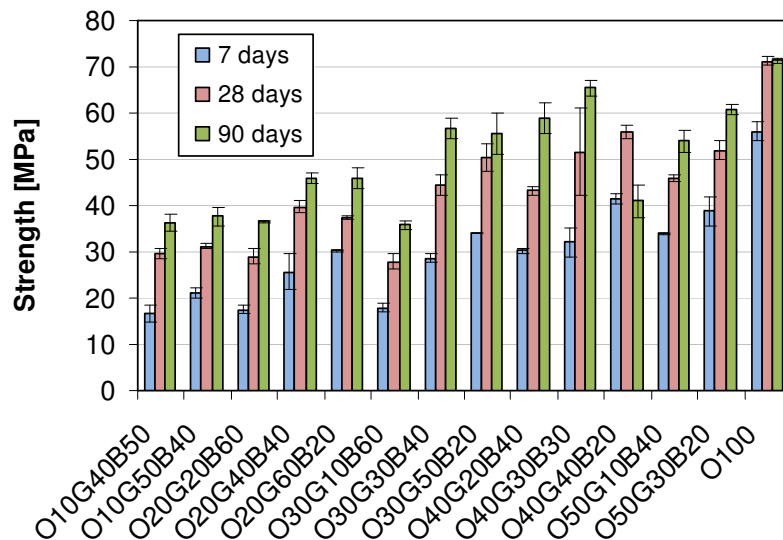
Figure 3-16 Compressive strength of ternary mixes OPC-GGBS-BOS. Mix O10G40B50 for example, comprises 10% of OPC, 40% of GGBS and 50% of BOS.

The compressive strength for any combination of OPC, GGBS, and BOS is shown in figures 3.17, 3.18, and 3.19 as iso-response or contour curves. In these figures, a new parameter called, in this research, slag index (I_s) was proposed. It was defined

as the amount of GGBS with respect the total amount of slag (3.6). The figures show the variation of the compressive strength for any combination of OPC as a percentage (vertical axis) and for any slag index (horizontal axis) at 7, 28, and 90 days. The contours were drawn with the commercial software Surfer® V8, which interpolated the experimental data.

$$I_s = \frac{GGBS}{GGBS + BOS} \qquad (3.6)$$

As was expected, the compressive strength increases as the percentage of OPC increases. In the same way, the behaviour of any compressive strength isoline at any age can be generalized by two lines. An initial "*line A*" defined by a straight line with a negative slope, where for the same strength a decrease in the amount of OPC corresponds to an increase in I_s, and a horizontal line "*line B*" where an increase of the slag index does not have any effect on the compressive strength. In the figures a schematic representation of lines *A* and *B* has been included as dashed lines. It is important to note that OPC is the most expensive of the materials, followed by the GGBS. The commercially optimal mix will be one that includes a minimum of those materials. For any specific strength, this optimum corresponds to the intersection between lines A and B (point C in the figures).
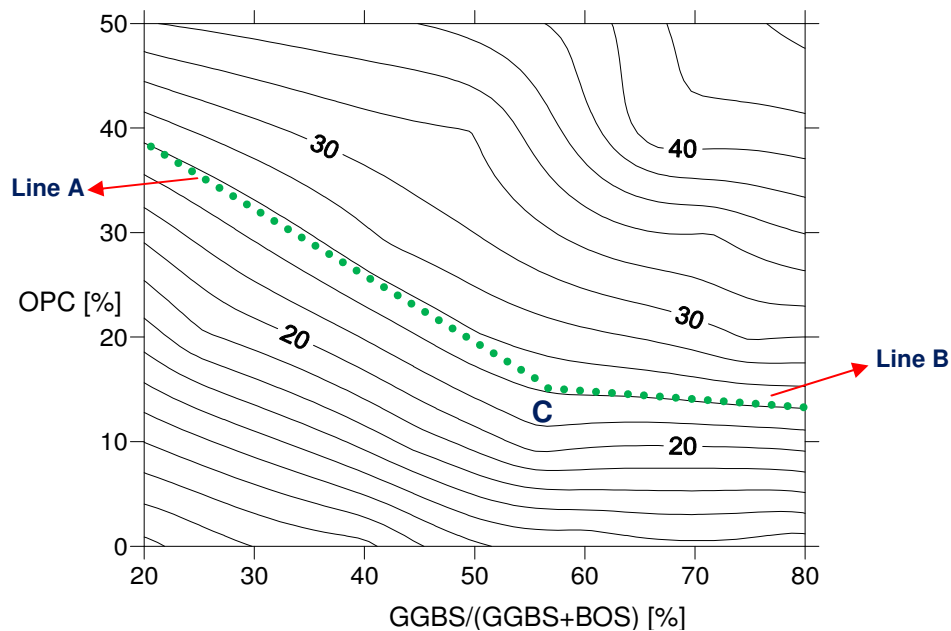
Figure 3-17 Compressive strength [MPa] contour of the ternary OPC-GGBS-BOS mix at 7 days

The point C changes its position depending on the iso-line value of strength selected and the time at which the compression test was conducted. It can be seen that the location of point C is between 40 and 60% of the slag index in most cases; an I_s of 50% is a good estimate. Figure 3.18 shows point C for three mixes. Figure 3.19 shows the optimized mix O40G30B30, composed of 40% of OPC, 30% of GGBS, and 30% BOS.
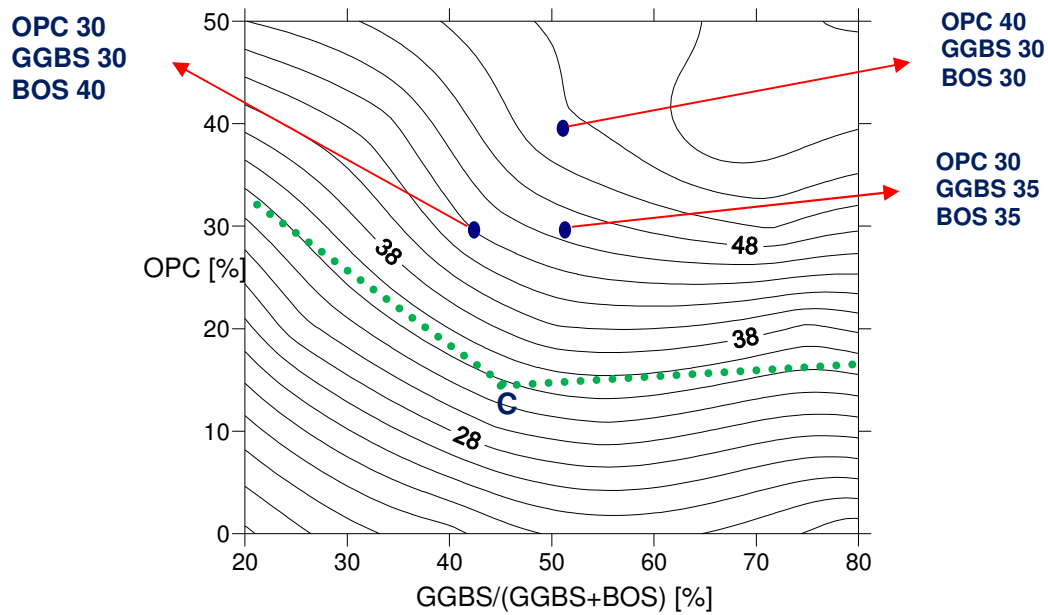
Figure 3-18 Compressive strength [MPa] contour of the ternary OPC-GGBS-BOS mix at 28 days
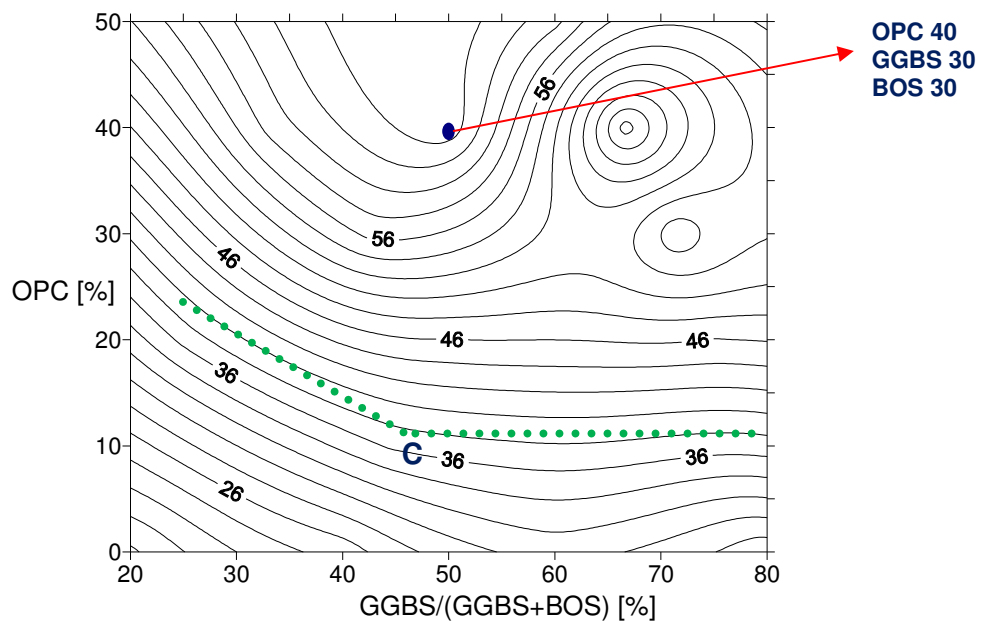
Figure 3-19 Compressive strength [MPa] contour of the ternary OPC-GGBS-BOS mix at 90 days

3.3.3.2 Alkali activated Mixes BPD – GGBS – BOS

From figure 3.15 it was observed that the highest compressive strength for the binary mix GGBS-BOS had a slag index of 0.6. Keeping this index constant, the strength results for the ternary BPD – GGBS – BOS are shown in figure 3.20. For samples tested at 7 days it can be seen that the addition of BPD up to 15% did not have any beneficial or detrimental effect, the graph is steady across the range. For 28 days, the profile of the strength is similar to that for 7 days, although some slight reductions were found. For 90 days there is a decrease of strength at 5% BPD replacement, followed by a local maximum at 10%, and a final slight reduction at 15%.

For 90 days, the optimum value of strength is at 10% BPD. This value is only 2% higher than the mix without BPD. The last finding might imply, taking into account the variability of the experiments and materials, that BPD does not react sufficiently to be included in the ternary mix. However, as will be explained later, the inclusion of BPD helps to shorten the settings times and increases the reactions at early stages.
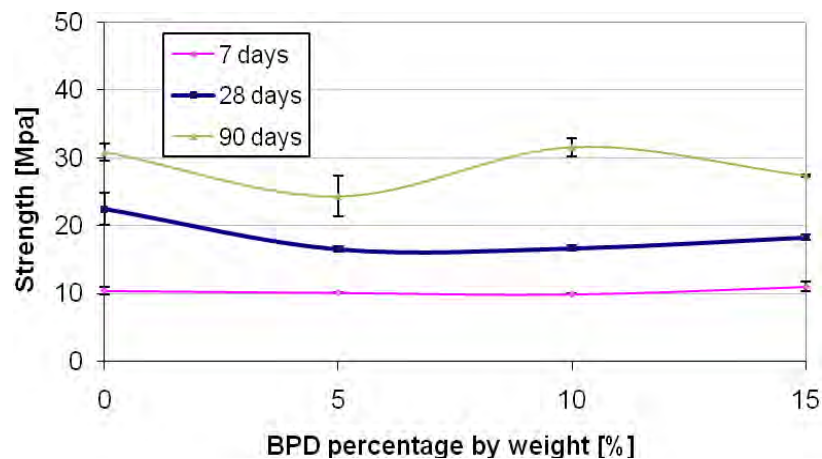
Figure 3-20 Compressive strength of BPD-GGBS-BOS mixes at different times

3.3.3.3 Sulphated activated mixes PG – GGBS – BOS

The results of strength for the binary PG-GGBS mixes are shown in figure 3.21. For seven days, regardless of the percentage of PG used, the GGBS did not develop any degree of activation. There was no evidence of reaction of GGBS due to the sulphate in less than one week because for all the levels of replacement the strength was below 0.2 MPa. In contrast, the mix of 100% GGBS at seven days obtained a strength of 2 MPa. After 7 days the mixes started to develop a sulphate reaction, giving acceptable results of strength. For 28 and 90 days there was an increase in

strength for all the percentages of PG. For both ages, a local maximum was found at 10% with compressive strengths of 32 and 48 MPa respectively. Although the GGBS was adequately activated through the gypsum, the compressive strength at early ages was too low, making it necessary to wait several days to demould the samples after casting.
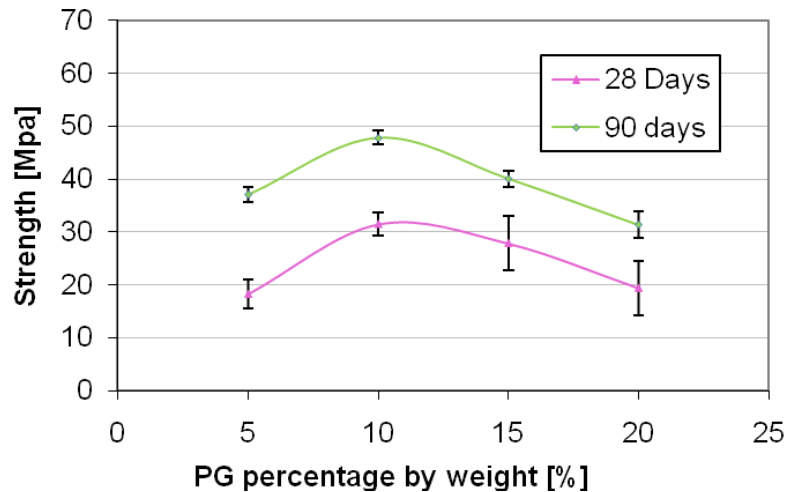
Figure 3-21 Compressive strength of PG-GGBS mixes at different times

Mixes of BOS and PG were cast with percentages of 10, 20 and 30% of gypsum. The effect of PG on the activation of the steel slag is shown in figure 3.22. For ages less than one week the mixes did not set completely and, at the time of the test, the strength was less than 0.1 MPa. At 28 days the compressive strength was lower than 1 MPa, and for 90 days it was between 3.5 and 4.5 MPa. From the compressive strength measurements there was no evidence that the BOS was adequately activated with the PG sulphate.
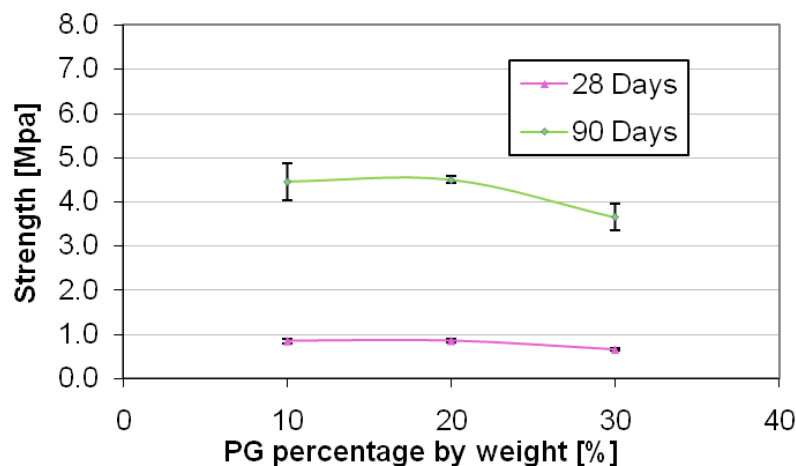
Figure 3-22 Compressive strength of PG-BOS mixes at different times

The results of compressive strength for ternary PG-GGBS-BOS mixes are presented in figure 3.23. The names of the mixes are given according to the replacement of the material. For example, the mix P05G40B55 has 5% PG, 40% GGBS and 55% BOS. For all samples strength always increases with age, indicating continuous hydration can be observed.
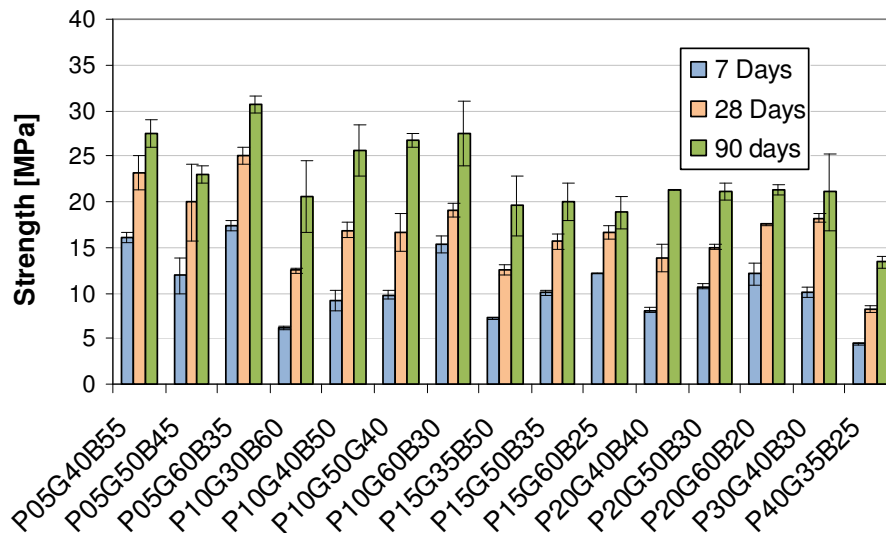
Figure 3-23 Compressive strength of PG-GGBS-BOS; The mix P05G40B55, for example, has 5% PG, 40% GGBS and 55% BOS

Figures 3.24, 3.25 and 3.26 show the contours of strength for 7, 28 and 90 days respectively. In the same way as for the contours for OPC, the graphs have the slag index on the horizontal axis and the percentage of PG in the vertical axis. The contours show the variation of the strength for a slag index in the range 20% to 80%; the results for 0 and 100% were shown in figures 3.21 and 3.22.

For all ages, the optimum mix was found at 5% of PG and has a slag index of 63%, corresponding to the mix with proportions: 5% PG + 60% GGBS + 35% BOS. In the same way as for the BPD mixes, it must be noticed that the binary mix BOS-GGBS with a slag index of 60 % had a similar strength to the optimum selected for PG ternary. However, the inclusion of PG accelerates the chemical reactions during the first 24 hours, as will be shown later.
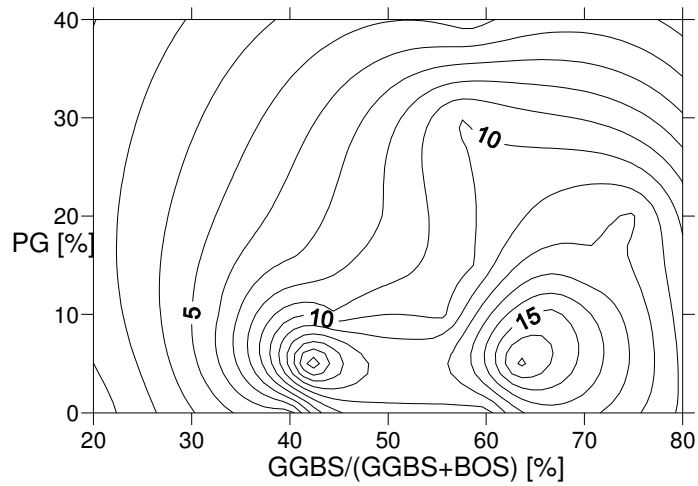
Figure 3-24 Compressive strength [MPa] contour of the ternary PG-GGBS-BOS mix at 7 days
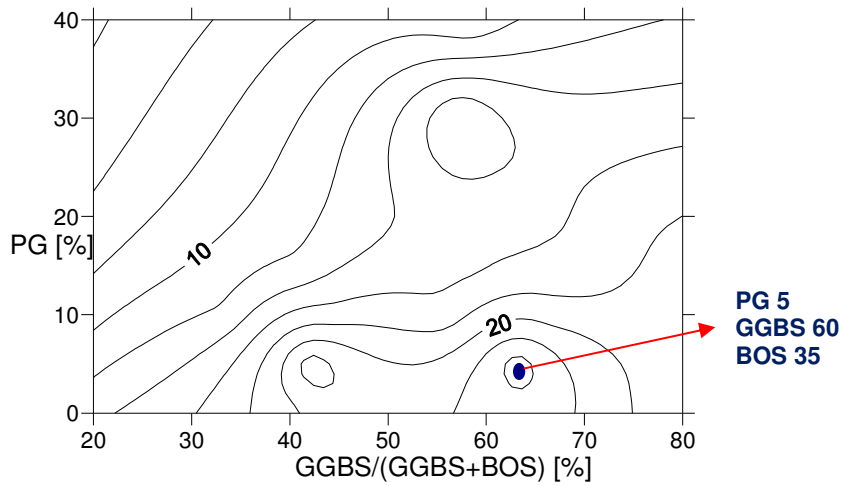
Figure 3-25 Compressive strength [MPa] contour of the ternary PG-GGBS-BOS mix at 28 days
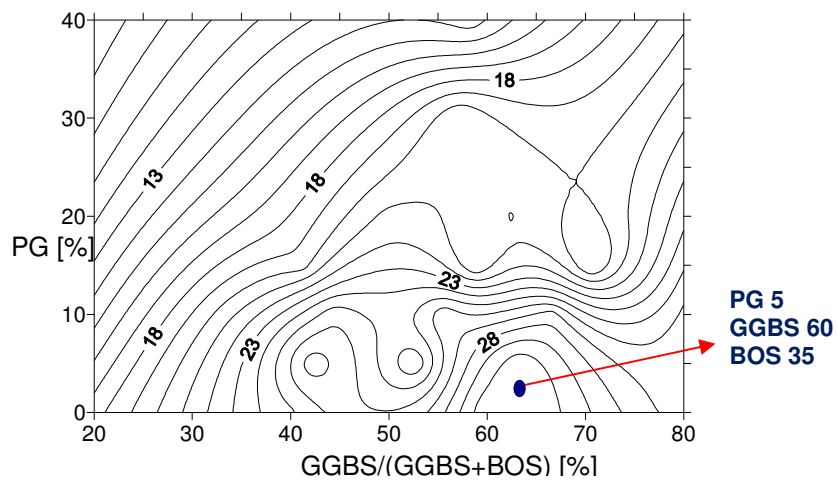
Figure 3-26 Compressive strength [MPa] contour of the ternary PG-GGBS-BOS mix at 90 days

67

3.3.4 Final binders

From results of the experimental programme, 5 slag binders activated in different ways were selected. As is shown in part 3 of this thesis, those were assessed for chloride penetration and their chloride transport-related properties were investigated. In addition, a commercial Portland cement was included as a reference material. A summary of the final binders selected in this first stage of the research is show in table 3.2. Binder 1 is the Portland cement reference. Binder 2 is a frequently used ground blast furnace slag mix activated with Portland cement. Binder 3 is Portland cement with a replacement of 30% by steel slag, not frequently used, but with some previous research carried out. Binder 4 is a ternary binder, with industrial applications in China, but with few references in the West. Finally, binders 5 and 6 are novel non-Portland cement blends not reported previously.

Binder	Materials	Binder name
1	100% OPC (reference)	OPC
2	40% OPC + 60% GGBS	OG
3	70% OPC + 30% BOS	OB
4	40% OPC + 30% GGBS + 30% BOS	OGB
5	10% BPD + 54% GGBS + 36% BOS	BGB
6	5%PG + 60% GGBS + 35% BOS	PGB

Table 3-2 Final slag mixes selected

3.4   CONCLUSIONS

2. Five sustainable and environmental binders were developed according to their optimum combination of different waste raw materials. Three of those include ordinary Portland cement and two are composed of one hundred percent wastes (without ordinary Portland cement replacement).

3. The physical, chemical and mineralogical properties of the raw materials used were measured. All of them were in the ranges expected and reported in the technical literature.

4. Incrementing the content of steel slag in the binary OPC-BOS mix causes a reduction in compressive strength for all ages. BOS replacement levels above 30% causes significant loss of strength. However, if the BOS replacement is restricted to less than 30%, the loss of strength does not exceed 10 percent.

5. In OPC-GGBS mixes for all ages an increase up to 60% in the slag replacement produces a slight reduction in the strength, while greater replacements have a more negative effect.

6. The hydraulic properties of GGBS and BOS are limited, particularly those for BOS, which in practice did not develop strength autonomously after being hydrated. GGBS showed a small increase of strength after 28 days (10 MPa).

7. GGBS was activated effectively with BOS; at 90 days the combination 60% GGBS + 40% BOS showed a compressive strength of 30 MPa.

8. The influence of the replacement level of OPC and BOS on the compressive strength of GGBS has been studied in detail. A proposed parameter called "slag index" has been introduced and its optimal value found was 0.5 in samples with OPC.

9. The mix 10% BPD + 54% GGBS + 36% BOS was determined as the optimum for this ternary combination.

10. The content of BPD used in ternary PG, GGBS and BOS mixes was lower than 15% because the variability of this material. Increasing the by-pass dust (BPD) content resulted in a negligible increase in the compressive strength. The combination 10% BPD + 54% GGBS + 36% BOS was selected as the optimum mixture.

11. Plasterboard gypsum showed to be a good activator of GGBS. The combination 10% PG and 90% GGBS had a compressive strength of 50 MPa at 90 days. However at three days the strength for this mix was negligible. In contrast, PG did not activate to any significant effect the BOS, the maximum compressive strength obtained at 90 days for this combination was only 4.5 MPa.

12. The mix 5%PG + 60% GGBS + 35% BOS was determined as the optimum for this ternary combination.

4 CHARACTERIZATION OF FINAL BINDERS

In this chapter are presented the results of a range of experiments carried out in order to characterize and investigate the hydration mechanisms of the final binders selected in the previous chapter.

4.1 INTRODUCTION

From the setting times and the early age temperature development, the intensity of the early reactions was determined. A mineralogical identification of the different hydration phases was made using X-ray diffraction at different ages. pH measurement of the extracted pore solution at early ages established the alkalinity of the binders, and the change in length measured at early and later ages determined the potential shrinkage or expansion of the binders.

4.2 EXPERIMENTAL METHODS

4.2.1 Normal consistency

Normal consistency corresponds to a specific amount of mixing water necessary to give the paste a standard condition. It was determined by ASTM C187 (2004) with the Vicat apparatus, figure 4.1, by trial and error. A binder paste with a known amount of mixing water is placed in a standard mould, below the Vicat apparatus. The needle C of 10 mm in diameter and 300 g is brought in contact with the surface of the paste and released, and then the penetration is measured. It is necessary to repeat this procedure until the normal consistency is obtained when the needle reaches a point of 10+1 mm below the surface of the paste in no more than 30 seconds. Normal consistency is expressed as the ratio of the weight of mixing water to binder.
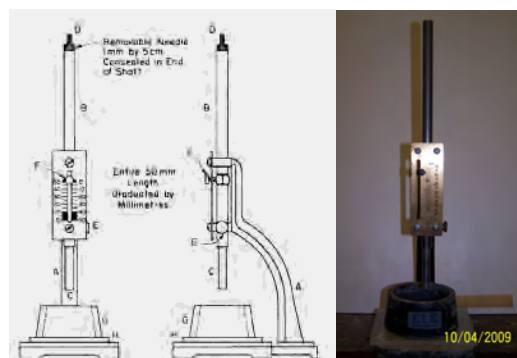
Figure 4-1 Vicat Apparatus used to measure the consistency and the setting times

4.2.2 Setting times

Some time after a hydraulic binder comes into contact with water it starts to lose its plasticity, progressively increasing in its stiffness. During this initial process, known as setting, the paste becomes brittle, but with no measurable increase in its strength. The hardening process is defined as starts once the paste begins to gain strength. Both processes are the result of complex hydration reactions of the binder and water. According to Popovics (1992) the initial setting is associated with the beginning of the stiffening and the final setting corresponds to the disappearance of plasticity. In this research the setting time was determined by measuring the changes in its resistance to penetration by a standard needle (ASTM-C191 2008).

The standard test procedure consists on the determination of the initial and final setting times using the Vicat apparatus. A needle of 1 mm in diameter was assembled in the end D. The initial set corresponds to the time when a paste of normal consistency allows the needle to penetrate a depth of 25 mm in 30 s and the final time corresponds to the time when the needle does not produce any mark on the surface of the sample.

4.2.3 Temperature at early age

The rate of early hydration of the mixtures proposed was monitored by measuring the temperature rise on fresh samples. The procedure to follow the evolution of the temperature consisted of introducing the sample into a semi-adiabatic container to quantify the temperature profile during the first 24 hours after mixing (figure 4.2). The temperature was recorded with an analogue/digital data-logger every minute, using a waterproof stainless-steel temperature probe with a high-level linear output of 10 mV per degree F. The room where the tests were carried out had a controlled temperature of (20±2) °C. The samples tested were mixed according to the procedure presented in 3.2.2.1 and were immediately placed inside the adiabatic chamber. The water binder ratio for all the mixes was 0.25 by weight.

4.2.4 pH measurement

A simple method was used to measure the pH of the raw materials. For each material 100 g of powder and 50 g of distilled water were intensely mixed for 3 minutes until the mixture was completely homogeneous. After mixing, 10 ml of suspension were poured into a test tube and the pH measured using a Hanna pH electrode with resolution of 0.01 pH. It is important to notice that the pH measured

does not correspond to the real pH developed for each final binder during the initial hydration. However, the pH comparison between all the raw materials can give some ideas about their potential alkalinity.
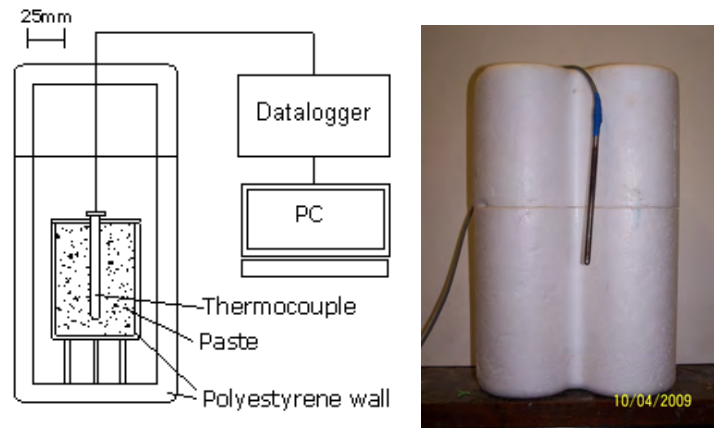
Figure 4-2 Temperature Apparatus (semi-adiabatic container)

The pH of the pore fluid held within the pore structure of the paste of the final binders was investigated a few hours after mixing, using an expression device similar to that described by Barneyback Jr and Diamond (1981). The cell used is shown in figure 4.3. Basically, a high tri-axial pressure (around 500 MPa) was applied to the paste in order to remould the pore distribution and express part of the pore solution. Small cylinders were cast for each paste mix using plastic bottles of 50 mm diameter and 60 mm length. For all mixes the water binder ratio was 0.25 and the tests were done 48 hours after casting. Around 10 ml of pore fluid was expressed from each sample and the pH was measured.
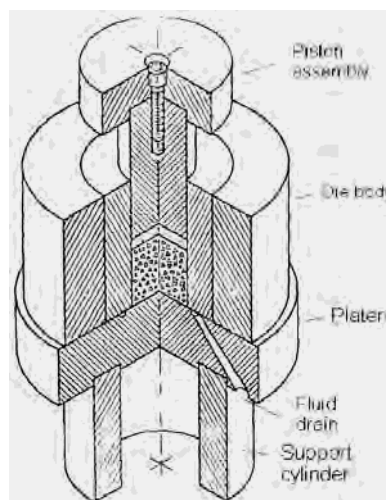
Figure 4-3 Pore fluid expression device (Barneyback Jr and Diamond 1981)

The procedure followed during the experiment was: (i) the cell was assembled clean with the sample inside. (ii) A low preload of 5 KN was applied for 5 minutes to push everything together and expel air from the system. (iii) The load was increased slowly to 200 KN in three stages of up to ten minutes each. Because of the early age of the paste samples, there was plenty water in the pores and it was expressed easily with this load. (iv) Finally, the collected sample was titrated for pH as soon as possible to avoid carbonation.

4.2.5 X-ray diffraction

The mineralogical composition for different stages of hydration was determined by X-ray diffraction analysis (XRD) deploying the same equipment as had been used to identify the cementitious powders in chapter 3.2.1.1. For this, samples with a water binder ratio of 0.25 were mixed and stored in small plastic bottles with airtight lids to protect them from carbonation. The bottles were kept under controlled conditions of temperature (20±2 °C) for 3, 28 and 90 days. For any desired age the sample was removed from the bottle, ground to a fineness of less than the 200 mesh, and tested.

4.2.6 Volume stability

The length change for all final mixes was measured at early and later ages, determining their potential expansion or shrinkage. Standard moulds, according to ASTM C490 (ASTM-C490 1997) were used to cast prisms 25×25×285 mm for paste mixes with a water binder ratio of 0.25. A steel frame with one adjustable and one fixed anvil was used to hold the samples while the length was measured using a digital length gauge with a 0.001 mm scale. Figure 4.4 shows the equipment used.

Figure 4-4 Shrinkage – expansion apparatus ASTM C490

4.3   RESULTS AND DISCUSSION

4.3.1 Consistency

 The results for the normal consistency measured following the procedure described in 4.2.1 are presented in figure 4.5. It can be seen that, for all binders, the consistency measured were in the range reported by Popovics (1992) as usual values for commercial cements (22 to 28%). For mixes without OPC, the values of consistency measured showed a lower water demand, influenced presumably by the coarser size of the steel slag.

Although the normal consistency is the amount of mixing water required to give the paste a standard wetness, it was stated by Popovics (1992) that it cannot be used as direct correlation of the slump of a mortar or concrete. In that way, the results of normal consistency were used principally to determine the setting times. The selection of a fixed value of wetness (consistency) and not binder content during the test was because the amount of water required in hydrating cement affects the setting time: pastes with more water require more time for setting.
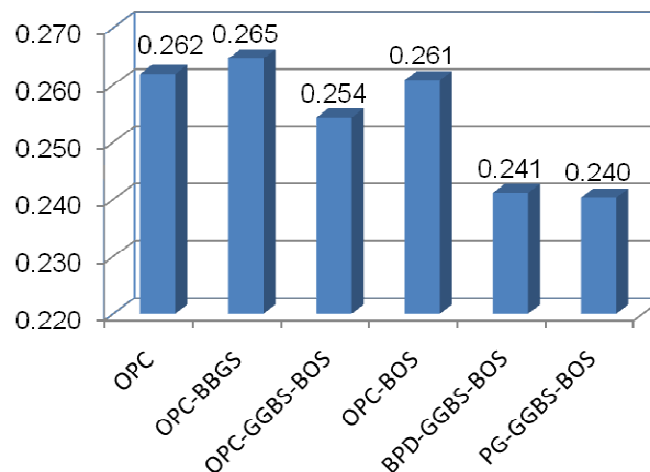
Figure 4-5 Normal consistency of final binders (water to binder ratio)

4.3.2 Setting times

The setting times were measured for the six final binders stated in the previous chapter. Additionally, the material composed of 60% of GGBS and 40% BOS, hereafter called GGBS-BOS was measured. The change in penetration depth during the first hours after mixing is shown in figure 4.6, where a period can be observed for all binders when virtually no penetration resistance and where the penetration

resistance increases linearly with time. Those two periods are shown schematically in the figure with lines "A" and "B" and it can be observed that the results are grouped in mixes with and without OPC. The rate of setting for those groups is different; in OPC mixes the addition of any slag produces a relatively short delay in the start of setting. In contrast, mixes with no OPC showed a prolonged "A" period, which is similar for the three non-Portland samples, but, with substantial differences in the period B. The inclusion of BPD and PG brings positive effects increasing the rate of setting, especially for the former.
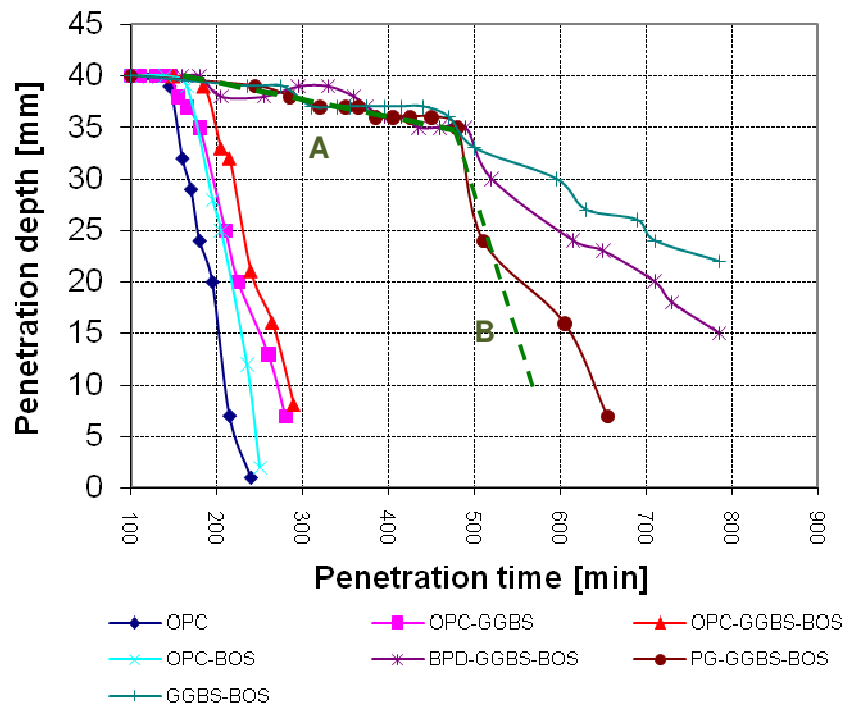
Figure 4-6 Needle penetration during the setting times experiments (ASTM C-191)

The standard setting times are presented in figure 4.7. As discussed in chapter 2, a delay was expected in all slag mixes; however, for mixes activated with OPC the values of initial time are in the range suggested by ASTM C150 (2007): >45 min and <375 min. Figure 4.7-A shows the times measured, and figure 4.7-B shows the increase in percentage of the time with respect to the OPC binder. There was a delay in the initial time for all slag binders which was higher than the delay in the final time. In the same way, the sulphate and alkali activated samples had shorter times than the binder composed just of GGBS and BOS. Some benefits were obtained using BPD and PG as activators. From the similarities of samples with no OPC presented in figures 4.6 and 4.7 it can be argued that the sulphate and the alkali help to increase the rate of setting of the GGBS-BOS binders. However, the main reactions, at least during the first 24 hours, are the result of the interaction of both slags.
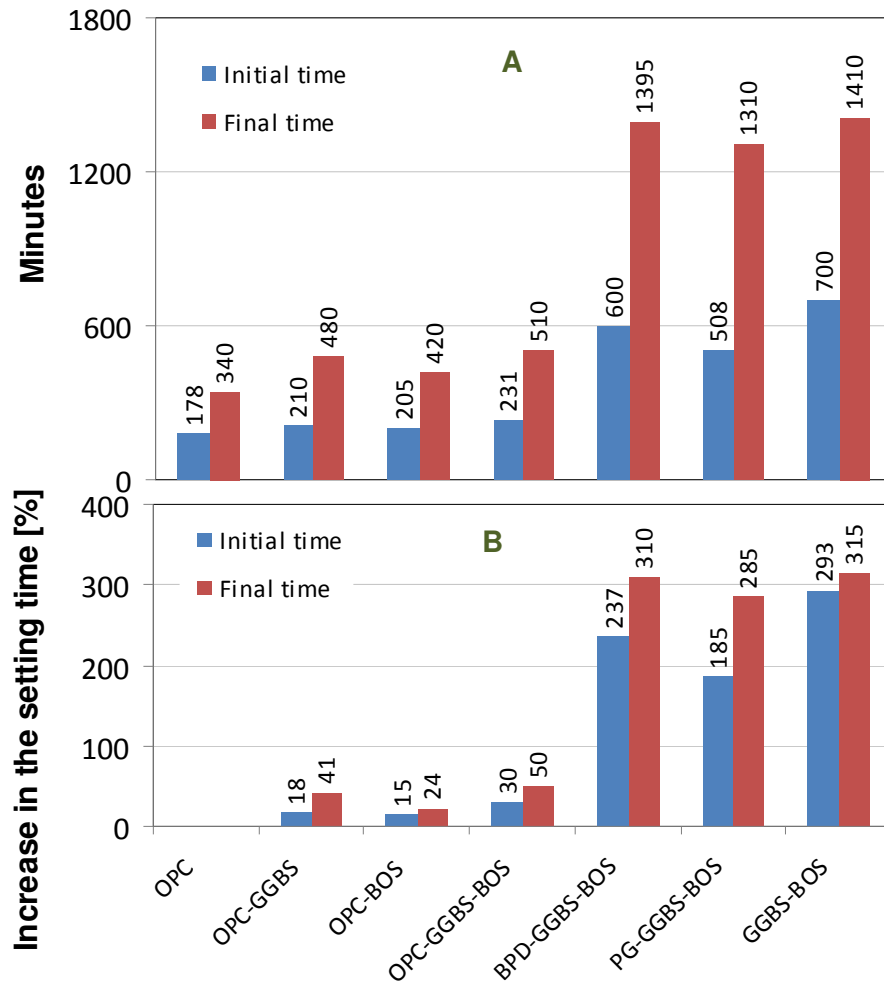
Figure 4-7 A: Setting times final binders. B: increase in percentage of the time with respect to the OPC binder

4.3.3 Temperature at early age

The early age development of temperature measured in an adiabatic cell during the first 24 hours of hydration is showed in figure 4.8 as increments from the initial value of temperature. Although the rate of temperature rise and the maximum temperatures were different for each binder, all samples had a similar profile: a sustained increase of the temperature until a maximum value was reached; followed by a sustained temperature decreasing. It is important to notice that some of the GGBS blended samples had a secondary local maximum that will be discussed later.

In the OPC reference sample the temperature increased rapidly during the first 7 hours and reached an increment of 25°C, after which the sample started to fall in temperature until the 22 hours point, when the temperature increase was negligible. The sample of OPC-BOS behaved in exactly the same way as the reference, but a

smaller and delayed maximum value was found; additionally, the temperature reduction had a lower rate. During the first 24 hours it was not expected that the steel slag would contribute significantly to the setting and hardening and it can be considered as an inert material, at least during the early ages. So, this sample can be seen as the same reference sample but with a replacement of 30% of cement with 30% of fine filler.

In the samples OPC-GGBS, OPC-GGBS-BOS, and BPD-GGBS-BOS in addition to the maximum peak, some locals or secondary maximum points were measured. These local maximum peaks appeared a couple hours before the maximum peak and were followed in all cases by an inflection point. This behaviour reported by Roy and Ldorn (1982) is characteristic of the early age hydration of GGBS, and Shi and Day (1995) state that the secondary peaks are the result of chemical reactions of the granulated slag and the alkalis used as activators. In the same way, De Schutter (1999) affirms that the presence of temperature multi-peaks can be explained by the fact that the hydration of slag cements is due of two independent reactions: a Portland reaction, and a slag-alkali reaction. For the clinker based ternary samples studied in this research, presumably there are three mechanisms of hydration: (i) the hydration of OPC can develop normal Portland hydration compounds, (ii) the lime, alkalis, and gypsum present in the OPC can activate or react with GGBS, and (iii) the lime of the steel slag can react with GGBS. In the same way, it is expected for the BPD and PG samples that only the last two mechanisms will be present.

The pattern of temperature rise for mixes OPC-GGBS and OPC-GGBS-BOS was very similar. The maximum point occurred at around 12°C. However, this occurred in the ternary binder with a delay of 2 hours approximately. At 24 hours for both samples there were remaining increments of temperature.

The non-Portland binders showed a very similar temperature rise during the first 8 hours consistent with the results of penetration measured during the setting times. After that time, the BPD activated binder showed a spontaneous peak, but thereafter quickly dissipated temperature, and after 17 hours it was very similar to the GGBS-BOS. After 8 hours, the sulphate activated binder began a steady increase in temperature, and presumably reached a maximum only beyond 24 hours. For the former mix, the late increments of temperature are the result of the sulphate reaction with GGBS, as was shown in figure 3.21 took long time. The profile of GGBS-BOS showed that by itself it is able to develop some exothermic reactions, the granulated

slag is activated by the steel slag, and although the values obtained do not show strong reactions, it can be considered by itself hydraulic binder.
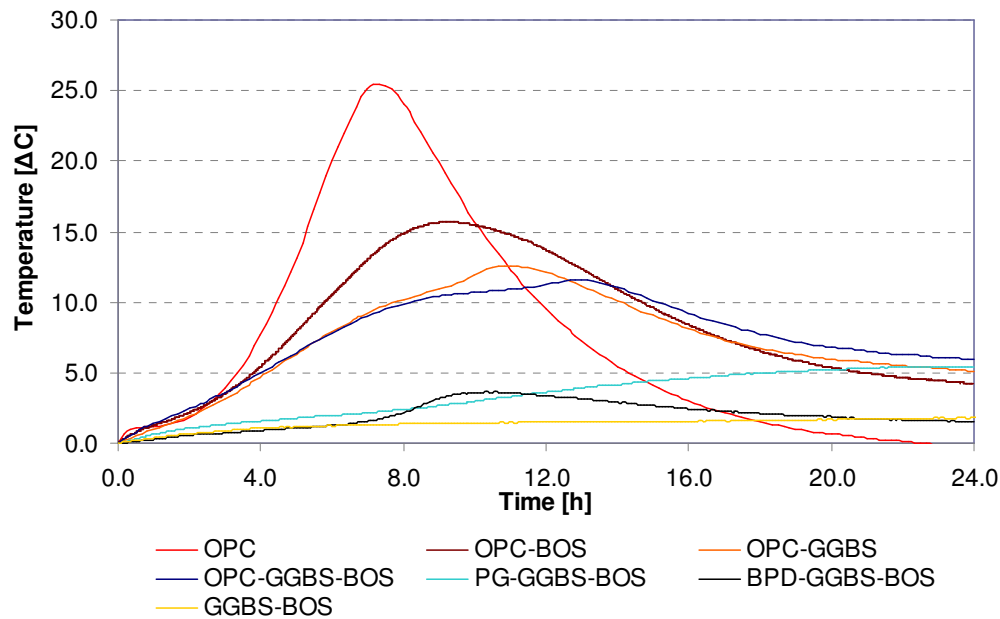
Figure 4-8 Increment of temperature of final mixes

4.3.4 pH measurement

The results of pH for the raw materials are shown in figure 4.9. Since the pH depends on the concentration, the powders were all hydrated with a water binder ratio of 0.5 in order to obtain the differences in alkalinity. The GGBS, for example, showed the lowest value of alkalinity. According to Taylor (1990), this result can explain why if granulated slag alone is mixed with water it can develop just a small degree of hydration. A protective film deficient in Ca^+ inhibits further reaction, but if the pH is kept sufficiently high the reaction continues. The lower basicity of GGBS compared with the Portland cement has been reported previously by Tailing and Krivenko (1997).

Research by Song and Jennings (1999) established that the pH of a mixing solution must be higher than 11.5 to activate GGBS. They state that in a pH lower that 11.5 the solubility of silica is low and GGBS does not dissolve and form silicate hydrates as principal compounds. The pH of the Portland cement, steel slag and by-pass dust is higher than the blast furnace slag, and presumably influenced their alkaline activation. The high pH of the BPD is due principally to the presence of soluble alkalis and lime content, while the high pH of the BOS is due principally to the high solubility of the lime content.
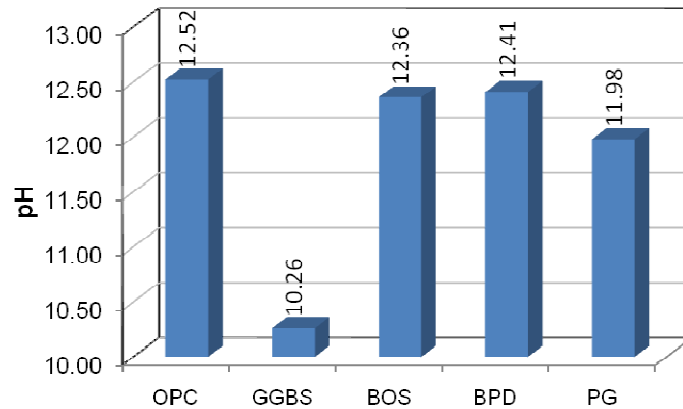
Figure 4-9 pH of the raw materials

Figure 4.10 shows the pH of the pore solution of the final binders, extracted after 48 hours of hydration using the procedure summarised in section 4.2.4. The pore solutions of the samples with BOS had a pH in all cases higher than 13.23. Although the lime and metal alkali content for OPC are considerable higher than for BOS (table 3.1), the pH of the extracted pore solution of the sample of OPC-BOS slightly exceeded that of the OPC binder. This was because most of the lime in the BOS remained into the pore solution.

According to Song and Jennings (1999), the solubility of the silica in the GGBS increases according to its level of alkalinity, affecting the nature and quality of the resulting calcium silicate hydrates. They conclude in their study that a C-S-H gel with low Ca/Si ratio and hydrotalcite is expected when the GGBS is activated under high alkali environments. The pH of the sulphate activated binder was the only one that was lower than 13; however, due to the presence of calcium sulphate the production of calcium silicate hydrates and ettringite as main hydration products is expected.
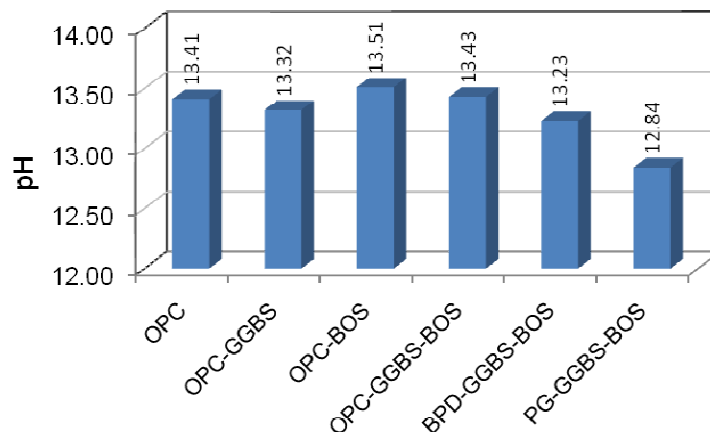
Figure 4-10 pH of the pore solutions of the final binders after 48 hours of hydration

4.3.5 Mineralogy - Hydration

The development with time of the final binders determined by XRD is shown in figures 4.11, 4.13, 4.14, 4.16 and 4.17 using the nomenclature given in table 3.2. They show the X-ray pattern obtained after 3, 28 and 90 days of curing under controlled conditions of temperature and humidity. The principal crystalline hydration products were determined, but it was not possible to determine the amorphous C-S-H gel by means of this technique.

The X-ray data for the 100% Portland cement reference (OPC), figure 4.11, shows a normal pattern which is discussed extensively in reference books (Taylor 1990, Hewlett 2004). Calcium hydroxide, known as portlandite (CH), was formed in significant quantity from early ages as the result of the hydration of calcium silicates. This compound remained stable throughout the period of investigation. Calcite or calcium carbonate (CC) was present, probably due to small amounts of limestone in the Portland cement. During the mixing and curing the exposure of the samples to carbon dioxide was limited (although during the X-ray preparation of the samples or during the X-ray scanning there could have been some minor carbonation). It is believed that any such carbonation was minimal, and was not significantly responsible for the presence of calcium carbonate. The peak found at 29.4° 2θ overlaps the calcite and the C_3S or alite (C3), however it decreases during curing meaning that some cement compounds had a hydration delay. At three days, there were still some un-hydrated calcium silicates (C3,C2). They decrease in intensity during curing, but at 90 day there were some calcium silicates remaining. As was expected, ettringite (E) was present as a stable compound.

The X-ray traces for the 40% Portland cement and 60% Blast furnace slag (OPC-GGBS) mix is shown in figure 4.11. The system had similar hydration products to Portland cement; however, the intensity of Portlandite was lower because a smaller amount of OPC was used. It can be noted that the amount of calcium hydroxide remains constant during all the period studied. From this observation it can be argued that during the hydration of GGBS in a Portland cement system the slag does not develop strong puzzolanic reactions and does not consume large quantities of the calcium hydroxide available. The alkalis released from Portland cement are responsible for activating the slag as is shown in the model of figure 4.12 (Roy and Ldorn 1982). Other minerals found in the pattern were calcite, anhydrous calcium silicates and ettringite.
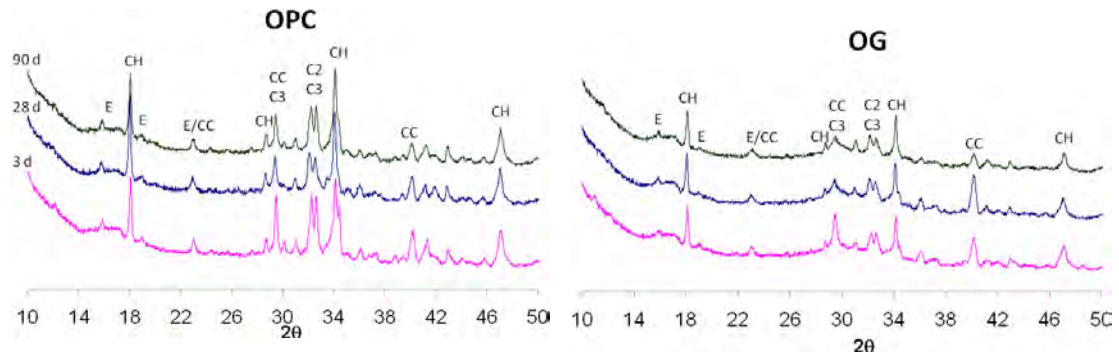
Figure 4-11 X-ray pattern of OPC and OPC-GGBS mixes
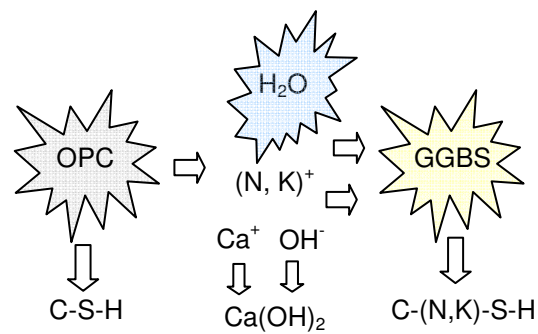
Figure 4-12 Hydration model for mix OPC-GGBS (Roy and Ldorn 1982)

Figure 4.13 shows the X-ray pattern of the binary mix 70%OPC+30%BOS (OB). The pattern was very similar to the one for OPC where ettringite, calcite, and non-hydrated calcium silicates were observed. The intensity of the porlandite peak was higher than the same peak for 100% OPC because in addition to the calcium hydroxide generated as product during the hydration of OPC, there is some portlandite provided by the steel slag.
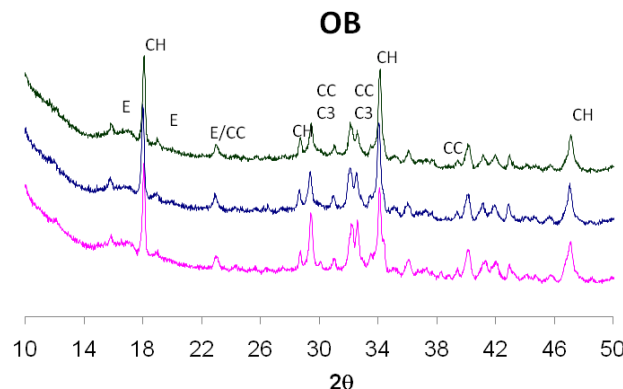
Figure 4-13 X-ray patern of the mix OPC-BOS

The X-ray pattern for the 60%GGBS+40%BOS mix is shown in figure 4.14. This mix does not include any Portland cement and is made up entirely of slag. It is important to notice from the pattern that there is no evidence to suggest the presence of calcium hydroxide; this was abundant in the non-hydrated steel slag, but it was not found in the hydrated binary slag mix. The absence of portlandite can be explained with the following mechanism: -the calcium hydroxide supplied by the BOS is consumed by pozzolanic reactions of GGBS before 3 days of hydration, producing some sort of calcium silicate hydrates (C-γ-S-H). Although this C-γ-S-H gel sets and develops some strength, it is much weaker than that obtained from the slag reaction with OPC. It is believed that this mechanism of hydration tends to occur principally in non-Portland mixes. For Portland cement slag mixes the mechanism of hydration is presented in figure 4.12. Figure 4.15 shows the proposed mechanism of hydration for the GGBS-BOS mix.
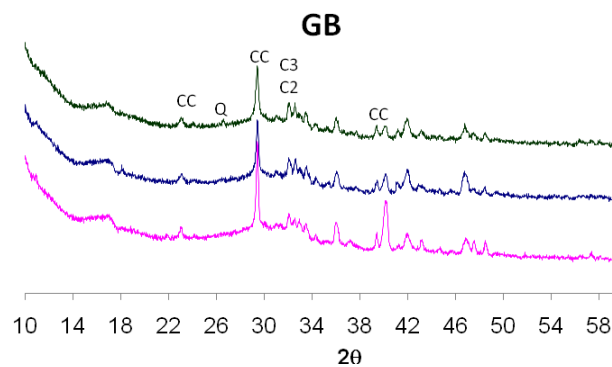
Figure 4-14 X-ray pattern of the GGBS-BOS mix
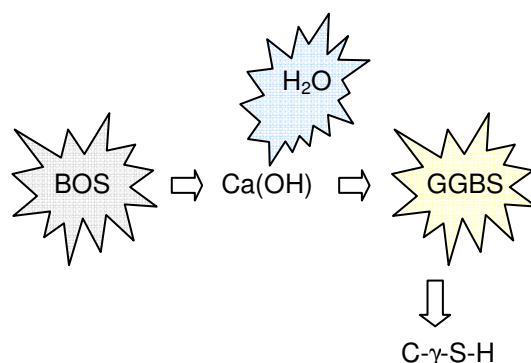
Figure 4-15 Hydration model proposed for BOS-GGBS mixes at early age

The pattern for the ternary mix 40%OPC+30%GGBS+30%BOS (OGB) is shown in figure 4.16. It can be seen that the peaks follow the pattern left by the cement hydration and similar minerals were obtained. For this mix, the mechanisms of hydration can be identified as three independent process; first, the hydration of the

OPC alone; second, the hydration of the slag through the alkalis available (figure 4.13): and a third mechanism in which the slag had weak pozzolanic reactions with the portlandite available from the steel slag.

OGB
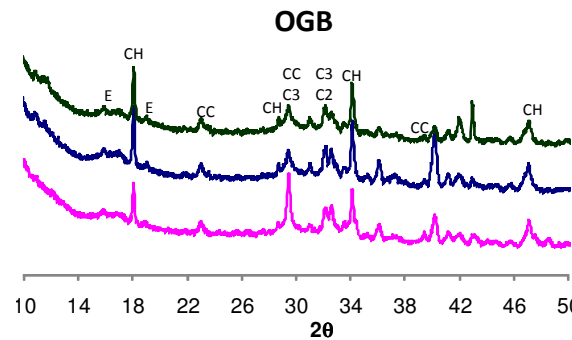
Figure 4-16 X-ray pattern of OPC-GGBS-BOS mixes

The X-ray patterns for the alkali and sulphated activated slag mixes are shown in figure 4.17. For both mixes, in the same way as in the steel slag blast furnace slag mixture there is not clear evidence of the presence of portlandite after three days of hydration. It is believed that the principal mechanism of hydration for these mixes is the result of the mixture of the two slags. However, the addition of BPD and gypsum produced an increase in the chemical reactions, as was shown in figure 4.8.

The difractogram for the 10%BPD+54%GGBS+36%BOS (BGB) mix shows that calcite (CC) and some calcium silicates phases (C2,C3) dominate the spectrum. However, those peaks remain constant for different ages, indicating that they are quite inert and do not participate strongly in any hydration reaction. It is believed that, in addition to the pozzolanic reaction of the GGBS induced by the BOS, the alkalis released from the slag activate the blast furnace slag. In the same way, from the diffractogram it can be seen that there is no evidence of the presence of ettringite. This can be explained because ettringite is a stable compound if there is a sufficient supply of sulphates, however if there is not enough the ettringite is converted to monosulphoaluminate (Konsta-Gdoutos and Shah 2003). Another mineral detected was calcium monochloroaluminate hydrate, known as Fried's salt, and although the chloride content was given in the chemical oxide composition shown in table 3.1, the presence of chloride is common in cement kiln dust by-products.

As was expected, the X-ray pattern for the 5%PG+60%GGBS+35BOS (PGB) mix shows the presence of stable ettringite peaks of high intensity. This mineral is related to the plasterboard gypsum used in the mixture. In the same way as in the BGB mix,

it is believed that the CSH gel is formed through two mechanisms, the pozzolanic reaction of BOS and GGBS and the sulphate reactions of GGBS.
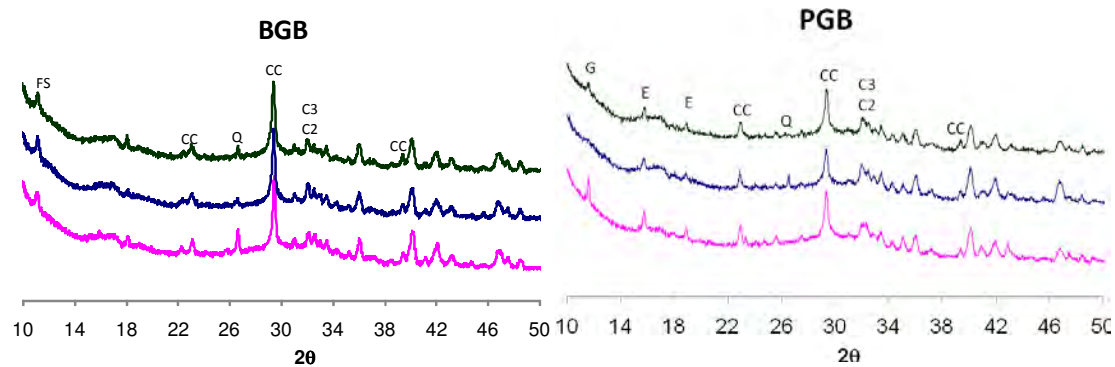
Figure 4-17 X-ray pattern of BPD-GGBS-BOS and PG-GGBS-BOS mixes

4.3.6 Volume stability - expansion

The volume stability for all mixes is reported as the linear expansion percentage at different ages in figure 4.19. No considerable expansion or shrinkage was measured for any of the mixes; all the values are smaller than 0.1% and are relatively stable over time. No expansion was measured in the mixes containing BOS, in contrast with the reported in some papers. The maximum acceptable value of expansion reported in the literature is dependant of the application of the binder as was stated by Ganjian, Claisse and Pouya (2007); in that way, for the potential alkali reactivity of cement-aggregate for example, the expansion is limited in the standards ASTM C1260 and ASTM C227 to 0.1%. The dimensional stability of the mix containing BOS is attributed to the weathered condition of the steel slag and the compensation due to the trend of the GGBS to have some shrinkage.
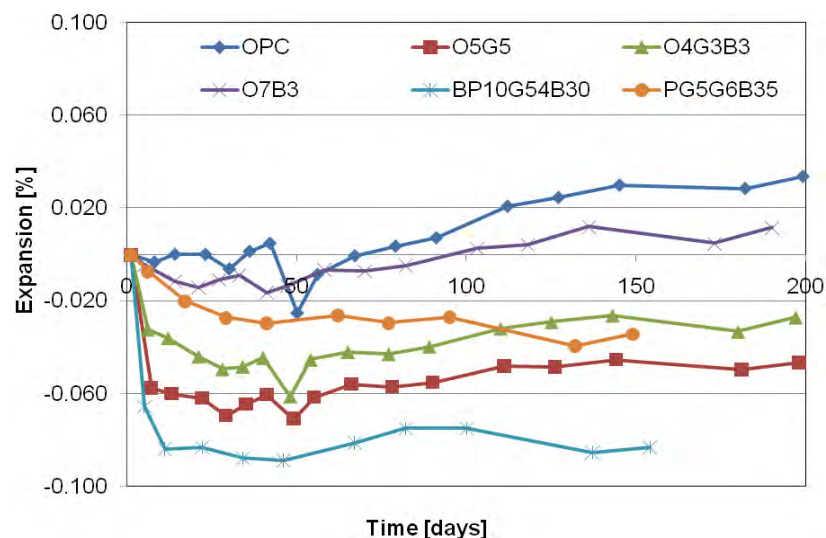
Figure 4-18 Measured expansion of final binders

4.4   CONCLUSIONS

The main conclusions to be drawn from the above findings are:

13. The most important physical properties have been measured for the binders selected in this research and with the mineralogy obtained with XRD some hydration mechanisms are proposed.

14. The setting times of all blended mixtures were extended. OPC blended mixes had a small increase of the initial setting time (between 10 and 30%). In contrast, non-OPC showed a prolonged initial time, which was around three times that measured for OPC samples.

15. The use of BPD or PG reduces the initial and final setting times on GGBS-BOS mixtures

16. The measurement of the temperature at early age showed that the use of waste as cement replacement produces a decrease in the heat of hydration generated. The compressive strength of the binary and ternary mixtures OPC-GGBS and OPC-GGBS-BOS was relatively similar to the OPC reference, however, the decrease in the maximum temperature measured was around 40%.

17. The mixtures with no Portland cement showed a minimal increase of temperature. However, the addition of BPD or PG to the binary GGBS-BOS mixture produces an increase in the hydration reactions, consistent with the results obtained from the setting times. Although BPD or PG do not produce large increases in the compressive strength, their inclusion in the mixtures helps to accelerate the initial hydration.

18. A model for GGBS in presence of BOS has been proposed. The calcium hydroxide supplied by the BOS is consumed by pozzolanic reactions of GGBS before 3 days of hydration, producing some calcium silicate hydrates (C-γ-S-H).

19. The steel slag as used in this research can be deployed as activator for GGBS. The material, weathered naturally under laboratory conditions, can be used effectively as a binder. The expansion problems reported in the

literature were not found in the measured mixes; it gives encouraging results for the potential use of blended mixes of weathered BOS and GGBS.

PART 2: CHLORIDE PENETRATION IN CEMENT BASED MATERIALS

This second part of the research deals with the entire theoretical basis necessary to apply the adopted computer model to a migration or diffusion test. Additionally, a methodology to obtain the chloride transport related properties was developed using the electro-diffusion model, a new electrochemical test (developed to measure the membrane potential experimentally), and an optimization technique.

5 CHLORIDE ELECTRO-MIGRATION IN CONCRETE – "A REVIEW"

This chapter presents the literature review carried out about the chloride diffusion-migration in concrete. Here, the theoretical and numerical aspects of the computer code adopted to simulate the ionic transport in a porous medium are presented and explained in detail.

5.1 INTRODUCTION

The traditional equations used to simulate chloride ingress into concrete are presented in this section (i.e. Fick's laws, the Nernst-Planck equation, and the Nernst-Einstein equation), as well as some aspects of the principal transport related properties and variables. Special attention is given to the binding capacity, the diffusion coefficient, the membrane potential, the composition of the pore solution and the electrical current during a migration test.

In order to define concrete properties, the most popular chloride experimental tests are reviewed. The pure diffusion tests are just named; however, the migration tests are summarized in detail. That interest in migration tests was motivated by the application of an electrochemical test to validate, understand, and improve the model used during the research. This model, developed previously at Coventry University, is presented in detail in the last part of this chapter.

5.2 CHLORIDE INGRESS IN CONCRETE

Corrosion of steel reinforcement is the major cause of deterioration in concrete structures, where carbon dioxide and especially chlorides are the main causes of damage. The rate at which chloride ions diffuse through concrete is a major determinant of the durability of structures. If chloride ions reach the vicinity of the rebar, the passive film around the steel can start to break down and the process of corrosion begins.

Different mechanisms of transport can lead the movement of ions inside porous media, including diffusion, migration, capillary suction and convective flow (Claisse 2005). Usually, in order to determine the ionic transport in concrete (when there is no applied pressure) only the diffusion is measured; however, some complications arise because of the nature of the material:

- Diffusion of ions in the pore solution of concrete occurs in long periods of time (months).

- Ions are not neutral particles. Because they are electrically charged, they interact with particles of the opposite charge. This interaction should be taken account of in order to understand the transport phenomena.

- Physical and chemical binding can occur between ions and the different cement compounds.

- Concrete is not an ideal solution. Ions moving inside a concrete sample cannot move freely - they have to describe a path defined by a) the development of the pore structure of hydrating cement compounds, and b) the aggregate-cement paste interface.

- Cement production includes supplementary mineral admixtures such as fly ash, blast furnace slag, silica fume and others, which can affect the diffusion of ions.

The classical approach of ion transport in solutions states that if there is a difference in the concentration of ions in different regions this gradient produces a flow of ions. Such a movement is called diffusion. In the same way, if there is a difference of electrical potential, this flow is called migration, electromigration or conduction. Figure 5.1.
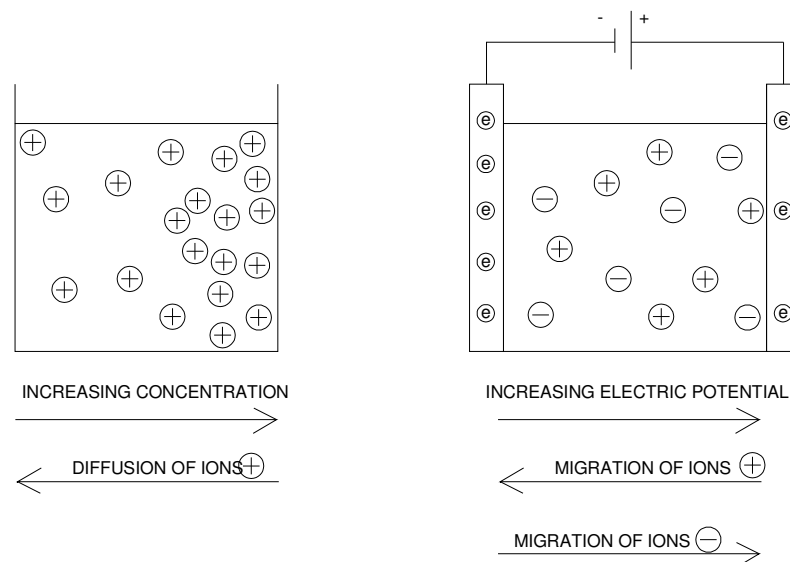
Figure 5-1 Schematic representation of the ionic diffusion and migration processes (Bockris and Reddy 1998)

In the evaluation of chloride penetration resistance pure diffusion tests take a long time; however, engineering and construction times are shorter. To overcome this problem, a pure diffusion can be accelerated by the application of an electrical potential gradient (migration tests). Under the influence of an electrical field ions experience a force directing them towards whichever has the opposite charge (Bockris and Reddy 1998). The time needed to perform a pure diffusion test may be months; by contrast, a migration test can be carried out in a matter of hours or perhaps a couple of days.

Usually, the movement of ions within a solution can be expressed as a flux *J*, "*the number of moles of a specie i* (any sort of ion) *crossing per second per unit area of a plane normal to the flow direction*" (Bockris and Reddy 1998). The flux *J* is initially time dependent but circumstances may cause it to become time independent. Thus two different conditions are found in a sample of concrete under an experimental test: steady and non-steady state conditions.

The relationship between the flux J_i and the concentration c_i in a solution has been known empirically since 1855 as Fick's First Law of steady state diffusion (Basheer 2001).

$$J_i = -D_i \frac{\partial C_i}{\partial x} \qquad (5.1)$$

where J_i is the flux of species *i* [mol/m^2/s], D_i is the diffusion coefficient of species *i* [m^2/s], C_i is the ionic concentration of species *i* in the pore fluid [mol/m^3], and *x* is the distance [m]. For non-steady state conditions when concentrations are changing with time, Fick's Second Law (5.2) can be used (Basheer 2001). The deduction of equation 5.2 is shown in appendix 2.

$$\frac{\partial C_i}{\partial t} = D_i \frac{\partial^2 C_i}{\partial x^2} \qquad (5.2)$$

Figure 5.2 shows how the concentration of chloride ions varies over time for a diffusion process. Before t_0 the diffusion of ions is in a non-steady state condition. After time t_0 the sample has reached a diffusion steady state, where $\partial C / \partial t$ has become constant.
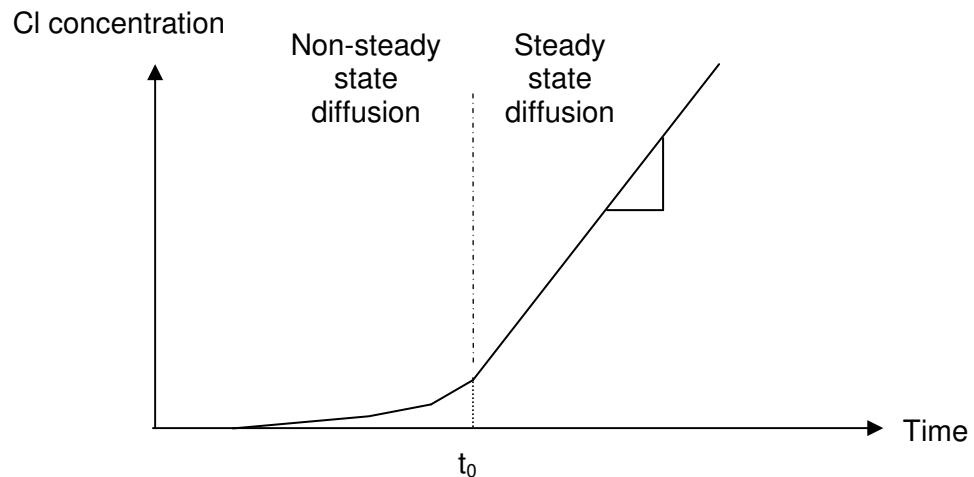
Figure 5-2 Non-steady and steady state conditions (Basheer 2001).

In the same way as for Fick's Laws, the expression known as the Nernst-Planck flux equation describes the flux of an ionic species under several possible driving forces. When there is a chemical potential or concentration gradient, an electrical field, and a difference of pressure, the flux for ionic transport can be expressed as equation 5.3.

$$J_i = -D_i \frac{\partial C_i}{\partial x} - \frac{z_i F}{RT} D_i C_i \frac{\partial E}{\partial x} - C_i V_i \quad (5.3)$$

where z_i is electrical charge of specie i, F is the Faraday constant [9.65 x10^4 Coulomb/mol], R is the gas constant [8.31 J/mol/$^\circ$K], T the absolute temperature [$^\circ$K], E the electrical voltage [V], and V the velocity of the flow due to pressure gradient [m/s].

If the material is fully saturated and does not have pressure gradients, the convection phenomena ($C_i V_i$) can be ignored (Andrade 1993). In the same way, according to Nilsson (1996), in some situations, if an external electrical potential difference applied exceeds 20 V/m, the diffusion term in equation 5.3 can be eliminated, leaving the pure electrical migration given by equation 5.4. In this equation, it is assumed that the voltage drop across the concrete is linear, the steady state conditions have been reached, the source chloride concentration is constant, and the heating of the solution and concrete is low (Stanish, Hooton and Thomas 2000).

$$J_i = \frac{z_i F}{RT} D_i c_i \frac{\partial E}{\partial x} \quad (5.4)$$

The Nernst-Planck equation 5.3 does not however take into account the chemical activity of the electrolytic solutions. From the electrochemistry, a term including a chemical activity coefficient (γ) could be added generating equation 5.5 (Yang, Cho and Huang 2002). For an infinitely (ideal) diluted solution the chemical activity coefficient has a value equal to 1, but when solutions have a high ionic strength as in cementitious materials this value could be different.

$$J_i = -D_i \frac{\partial c_i}{\partial x} - \frac{z_i F}{RT} D_i c_i \frac{\partial E}{\partial x} - c_i V_i - \frac{c_i}{\gamma_i} \frac{\partial \gamma_i}{\partial x} \qquad (5.5)$$

In another approach, Lu (1997) stated that if concrete is considered a solid electrolyte, the diffusivity of charged species i is related to its partial conductivity σ_i, and this relation is know as the Nernst-Einstein equation. If the partial conductivity and the concentration are known, the diffusivity of this particular species can be found from equation 5.6. For details see appendix 3.

$$D_i = \frac{RT\sigma_i}{z_i^2 F^2 c_i} \qquad (5.6)$$

As was mentioned, Fick's Laws, Nernst-Planck, and Nernst-Einstein equations are well known in the field of electrochemistry and can be used when there is an ideal electrolytic solution penetrating an inert porous medium. However, as concrete is by nature a complex porous material, to properly apply these equations it is important to define and understand the principal properties and variables that affect the transport mechanisms of chloride in concrete.

5.3 CONCRETE CHLORIDE TRANSPORT RELATED PROPERTIES AND VARIABLES

5.3.1 Binding capacity

Binding capacity is defined as the interaction of ionic species diffusing or migrating in saturated concrete with the cement matrix. Although the ionic transport takes place entirely through the pore system, the chemical and physical reactions of ions with the solid phases modify the rate of transport and should not be neglected. For chlorides, that interaction has been a matter of intense study and well-defined models are available. For other species such as alkalis and hydroxides, it is known that there are

strong mechanisms of binding, although there is a severe lack of studies or models currently available in the literature.

Chlorides can be present in concrete in two distinct forms - free chloride ions found in the concrete pore solution, and chloride ions bound physically or chemically to the solid concrete matrix. The total chloride concentration is the sum of these free and bound chlorides.

$$C_t = C_f + C_b \quad (5.7)$$

C_t, C_f and C_b are the total, free and bound chloride concentrations respectively. The experimental determination of the chloride concentration of a contaminated concrete can be made through standardized tests. The water-soluble procedure (ASTM-C1218 2008) can be used to quantify the free or weak bounded chloride concentration, which is responsible for the corrosion of steel reinforcement bars (Suryavanshi, Scantlebury and Lyon 1998), meanwhile the acid-soluble procedure ASTM-C1152 (2004) measures the total chloride concentrations. Although both types of chlorides can be measured by the standards given, in the process of evaluating the free chloride contents there are some difficulties (Mohammed and Hamada 2003). Specifically, the water-soluble chloride test is rather less accurate than the acid soluble test because some of the "bound" chlorides can be released during the test. For this reason the total concentration is usually experimentally determined.

Quantifying how many chloride ions are adsorbed by the concrete matrix is important because the bound ions do not participate in the ionic transport phenomena. Different experimental approaches can be found in the literature for measuring the binding capacity: the equilibrium method (Tang and Nilsson 1993), an immersion test under equilibrium (Larsen 1998), a local equilibrium approach (Khitab, Lorente and Ollivier 2005), a binding capacity factor (Atkinson and Nickerson 1984), a non-equilibrium approach (Rubin 1983), and binding isotherms for non-steady state migration experiments (Castellote, Andrade and Alonso 1999a).

Chloride binding can be explained either by chemical or physical interactions between chlorides and the hydration products of concrete. Chemical binding forms compounds like Frieldel's salt ($Ca_3Al_2O_6CaCl_210H_2O$), where an increase in the amount of C_3A and C_4AF in the cement paste determines an increase in its capacity of binding. Physically bound chlorides can be adsorbed by the amorphous calcium

silicate hydrates. Although both mechanisms can be present, the binding of chlorides in concrete is dominated by the chemical one. Mineral admixtures like fly ash and ground blast furnace slag increase the chloride binding due to the high content of aluminate hydrates in those materials. In contrast, silica fume tends to reduce the chloride binding. In presence of carbonation and sulphates the bound chlorides can be released (Yuan *et al.* 2009).

The binding of chloride ions has been extensively analysed in the literature, where it has been demonstrated that non-linear isotherms can be used to make good representations of the adsorption phenomena. An isotherm defines a relationship between free and bound ions over a range of concentrations at a given temperature. The most commonly used isotherms are the linear sorption isotherm (Yuan *et al.* 2009) equation 5.8, the Langmuir isotherm (Delagrave *et al* 1997) equation 5.9, and the Freundlich isotherm, equation 5.10 (Truc 2000). Usually the isotherms are shown in graphs with bound chlorides C_b along the ordinate axis [ads *ions/volume$_{solid}$*] and free chlorides C_l *as abscissa* [*free ions/volume$_{pores}$*].

$$C_b = \alpha C_f \qquad (5.8)$$

$$C_b = \frac{\alpha C_f}{(1 + \beta C_f)} \qquad (5.9)$$

$$C_b = \alpha C_f^{\beta} \qquad (5.10)$$

α and β are constants obtained experimentally. Figure 5.3 shows an example of the linear, Langmuir, and Freundlich isotherms for some α and β values.
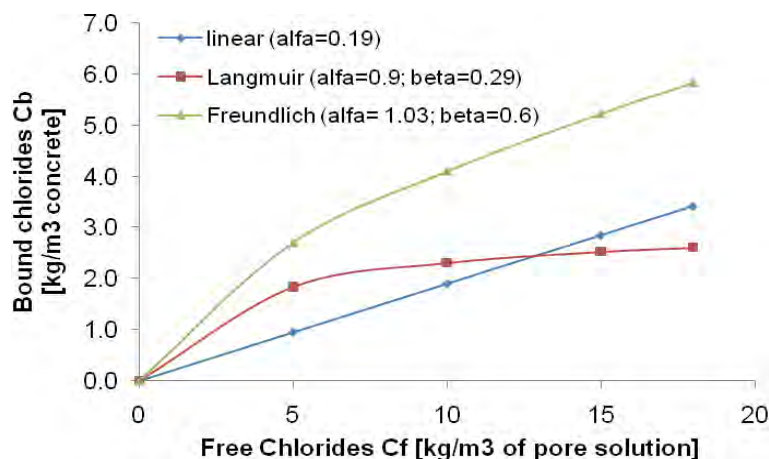
Figure 5-3 Chloride linear, Langmuir, and Freundlich isotherms

5.3.2 Diffusion coefficient

The diffusion coefficient represents the capacity of any specific concrete to resist ionic penetration, and is used to predict the service life of reinforced concrete structures. Following equation 5.1, the diffusion coefficient is defined as the flux of the diffusing substance divided by the space gradient of concentration at the section.

Concrete is not an ideal solution, due, in part, to its microstructure, but also to the binding reactions between ions and the cement matrix. The definition of the diffusion coefficient then varies according to the assumptions made in the case of modelling, or according to the test in the case of experimental determination. A complete definition of the diffusion coefficients used in the model applied in this research will be given in section 5.7.

The diffusion coefficient in Fick's First law can be expressed as the effective diffusion coefficient (often known as intrinsic). It relates to the diffusivity of the pore solution rather than the diffusivity of the porous medium. In its experimental determination, the microstructural properties are not accounted for (i.e. porosity, tortuosity, or binding capacity).

The apparent diffusion coefficient D_{app}, which does takes account of the porosity, tortuosity, and the binding capacity of the concrete matrix (Truc 2000), is calculated experimentally by the determination of the total or free chloride concentration profiles after a non-steady state diffusion test. For this, the so-called complementary error function $erfc$ is usually used, which corresponds to the solution of Fick's Second Law presented by Crank (1976). The apparent diffusion coefficient is determined by fitting profiles of chloride concentration to Fick's Second Law of diffusion (Nokken *et al.* 2006). Equation 5.11

$$C(x,t) - C_0 = (C_s - C_0)(erfc(\frac{x}{\sqrt{4tD_{app-Fick}}}))$$ (5.11)

C(x,t) is the concentration of chloride after a time *t* at a distance *x* from the surface of the sample, *ercf* is the complement of the error function *erf*, C_s is the steady chloride concentration at the surface, and C_0 is the initial chloride concentration of the concrete sample.

5.3.3 Membrane potential

The mechanism of chloride penetration into concrete is a topic that so far has not been clarified at all well. Different theories and methods have been proposed in the last 20 years; however, a long research path has to be covered. The differences that exist between the theoretical and experimental results indicate that there is something missing in the way that transport of chloride ion into the concrete is approached. Although the chloride ion penetration is a major concern due to the deterioration of the steel in reinforced concrete structures, its diffusion cannot be determined correctly without accounting for the interactions between the different ionic species present in the pores of the concrete, such as OH^-, Na^+, Ca^{2+} and K^+, (Truc 2000, Zhang and Gjorv 1996).

The mobility of any ion in concrete is related mainly to the chemical potential of the ion (concentration gradient), the electrical potential (if it exists), the charge of the ion, the concentration of each species in the pore solution, the tortuosity of the pore network, the porosity of concrete, and the reactions taking place between the ions present in the porous and the cement hydration products. These reactions can be of dissolution, of decalcification or of binding (Sugiyama, Ritthichauy and Tsuji 2003, Yang 2006).

For a fully saturated concrete sample with a difference in the concentration of ions in different regions and a constant difference of electrical potential, in the same way as the Rapid Chloride Penetrability Test ASTM-C1202 (2005) or NT 492 (1999), the total flux J_i for each species in the system must be the sum of the migration flux $(J_M)_i$ and the diffusion flux $(J_D)_i$.

$$J_i = (J_M)_i + (J_D)_i \qquad (5.12)$$

The flux due to a concentration gradient in a solution corresponds to equation 5.1. In an ideal solution the driving force for diffusion can be considered in terms of the chemical potential of the particular species *i*. In the same way, the electrical field is proportional to the driving force for migration. In an electrolytic system under a potential difference, in addition to the transport of charge that occurs as the current flows, there is also an accompanying ionic transport. The migration flux of species *i* is defined by equation 5.13 (Hamann, Hamnett and Vielstich 2007).

$$(J_M)_i = -u_i z_i F_i c_i \frac{\partial E}{\partial x} \qquad (5.13)$$

where u_i is mobility of species i in the pore fluid [m^2 s^{-1} volt^{-1}]. In the same way, the diffusion coefficient is proportional to the mobility of each ion (Bockris and Reddy 1998).

$$D_i = RTu_i \qquad (5.14)$$

As was stated before, the Nernst-Planck equation governs the ionic movements in concrete due to the chemical and electrical potential (Andrade 1993) (without a pressure gradient, and assuming that the influence of the activity coefficient is negligible).

$$J_i = -D_i \frac{\partial c_i}{\partial x} - \frac{z_i F}{RT} D_i c_i \frac{\partial E}{\partial x} \qquad (5.3)$$

The Nernst-Planck equation assumes that the flux of each ion is independent of any other ion. However, due to ion-ion interactions there will be ionic atmospheres that affect the final flux. The drift of a species i is affected by the flows of other species present. Physically, the law of electroneutrality ensures that no excess of charge can be introduced (Bockris and Reddy 1998). Under a concrete migration test, the current density into any concrete point will equal the current out of it, as is stated by Kirchoff's Law.

$$0 = F \sum_i z_i J_i \qquad (5.15)$$

Faraday's law states that the current density (i_i) is equivalent to the ionic flux.

$$i_i = -z_i F J_i \qquad (5.16)$$

In an electrolyte solution in which concentration gradients of the ionic species and an electrical field are present, the total current density (i_T) is equal to the sum of the current density produced by the diffusion and the migration conditions.

$$i_T = -\sum_i z_i F (J_D + J_M)_i \qquad (5.17)$$

The total current can be given by a combination of equations 5.1, 5.13 and 5.14.

$$i_T = \sum_i z_i F D_i \frac{\partial c_i}{\partial x} + \sum_i z_i^2 F^2 u_i c_i \frac{\partial E}{\partial x} \qquad (5.18)$$

The electric potential gradient is given by two terms: a linear or ohmic potential and a non-linear or membrane potential.

$$\frac{\partial E}{\partial x} = \underbrace{\frac{i_T}{\sum_i z_i^2 F^2 u_i c}}_{\text{Ohmic potential}} - \underbrace{\frac{\sum_i z_i F R T u_i \frac{\partial c_i}{\partial x}}{\sum_i z_i^2 F^2 u_i c}}_{\text{Membrane potential}} \qquad (5.19)$$

The first term is related to the ohmic potential when an external voltage is applied. Also, it is characteristic for charge transfer accounting exclusively the migration driving forces.

$$i_T = \sum_i i_i = -\sum_i z_i F (J_M)_i \approx -\sum_i z_i^2 F^2 u_i c_i \frac{\partial E}{\partial x} \qquad (5.20)$$

According to Ohm's law and by inspection, the conductivity can be defined as equation 5.21 and 5.22.

$$i_T = \kappa \frac{\partial E}{\partial x} \qquad (5.21)$$

$$\kappa \approx \sum_i z_i^2 F^2 u_i c_i \qquad (5.22)$$

The second term of Equation 5.19 is that for the membrane potential gradient $\partial E_p / \partial x$, formed when various charged species have different mobility. In a concrete migration test the non-linearity of the electrical field is due to the membrane potential gradient, and it is equivalent to the liquid junction potential (Lorente *et al.* 2007)

$$\frac{\partial E_p}{\partial x} = -\frac{RT}{F} \frac{\sum_i z_i D_i \frac{\partial c_i}{\partial x}}{\sum_i z_i^2 D_i c_i} \qquad (5.23)$$

Under migration, since the current density due to an ionic species i is related to the mobility of the ion and the mobility of each ion is different, it can be stated that all ions feel the externally applied electric force, but some will respond by migrating more than others. In a system with the same concentration for all ions, those with higher mobility contribute more to transporting the current through the sample. A quantitative measure of the current transported by each ion with respect to the total current is known as the transport number (t_i) (Castellote, Andrade and Alonso 1999b), which is defined as:

$$t_i = \frac{i_i}{i_T} = \frac{z_i^2 F^2 u_i c_i}{\sum_i z_i^2 F^2 u_i c_i} \qquad (5.24)$$

Likewise, the internal electrical field due to the diffusion potential can be expressed in terms of the transference number (Bockris and Reddy 1998).

$$\frac{\partial E_p}{\partial x} = -\frac{RT}{F} \sum_i \frac{t_i}{z_i} \frac{\partial \ln c_i}{\partial x} \qquad (5.25)$$

The non-linearity of the electric field in a migration test can be explained from a physical point of view. At the start of the test the field is uniform across the concrete; however, when the different ions start to migrate due to the external voltage applied, they cannot move freely, they are charged particles and thus interact with species of opposite signs. In a solution of sodium hydroxide, for example, the hydroxide ion will tend to move more quickly than the sodium ion due to its higher mobility, but, as they have different charge, an electrical field is developed between them in order to slow down the faster ions and accelerate the slower ions. This electrical field is the same diffusion or membrane potential gradient shown before and is also known as the liquid-junction potential (Revil 1999).

The membrane potential affects the external electrical field across the concrete, and its effect over the sample can be explained in term of resistances (Claisse 2006).

Each point within the concrete sample has a variable resistivity during a migration test due to the different mobility of the ions.
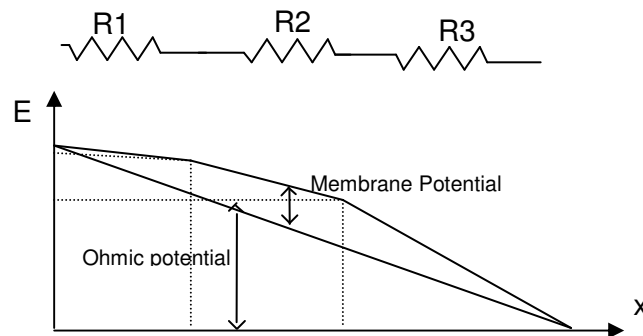
Figure 5-4 Voltage variation in a migration test (Claisse 2006)

5.3.4 Composition of the pore solution

The composition of the solution into the pores of hydrated concrete materials defines the conductivity of the material. In a fully saturated concrete sample the conductivity depends on the geometry of the pore structure, on the characteristics of the raw materials, and on the exposure conditions as either contamination of salts or carbonation. The electrical conductivity of the most used aggregates, such as e.g. silica sand or granite, is extremely low and is negligible when compared with the conductivity of the cement paste (Wee, Suryavanshi and Tin 1999). The cement paste is formed by different hydration products of cement, mainly tobermorite gel and porlandite, and by a porosity network full of different ions. In the same way as the aggregates, the hydration products can be considered as insulators, and consequently, the overall conductivity of concrete is related to the flow of ions over the porosity formed in the cement paste, which provide the paths of least resistance for electrolytic conduction.

For ordinary Portland cement, sulphate resistant, slag, silica fume, and fly ash cements the dominating cations in the pore solutions are Na^+ and K^+ (Andersson *et al.* 1989). A fresh concrete, just a few hours after mixing, presents several concentrations of Na^+, Ca^{2+}, K^+, OH^- and SO_4^{2-} coming either from the cement compounds or from the mixing water. After hardening, the Ca^{2+} and SO_4^{2-} are consumed in a high proportion leaving within the pores a solution composed essentially of alkali hydroxides (Shi 2004a). In concrete free of carbonation the concentration of hydroxyl ions is in the range 0.1 M to 0.9 M, because of the presence of NaOH and KOH (Bertolini *et al.* 2004).

The use of mineral and chemical admixtures changes the composition of the pore solution of concrete. Different studies have shown how the use of silica fume, ground blast furnace slag, metakaoline, fly ash (Page and Vennesland 1983, Glasser, Luke and Angus 1988) and corrosion inhibitors or accelerators (Corbo and Farzam 1989) have a strong effect on the chemical composition and conductivity of the pore solution. The addition of supplementary cement materials results in a moderate reduction of ionic concentration and of the pH.

Shi (2004a) studied the effect of some mineral admixtures on the chemical composition of the pore solution. Slag, for example, if it is at levels of 60 to 70 % reduces the concentration of OH^- in the pore solution. The concentration of Na^+ increases and the concentration of K^+ decreases. The effect of fly ash is strongly dependent upon the type of ash and composition of alkali, calcium and silica. It can either increase or decrease the Na^+ and K^+ in the pore solution depending on whether low-CaO or high-CaO fly ash is used respectively (Shehata, Thomas and Bleszynski 1999). Silica fume in low amounts of replacement, for instance 5 %, can reduce the amount of hydroxides and is responsible for the depletion of the alkali compounds. Increasing the percentages of silica fume further causes a decrease in the alkalinity of the pore solution (Page and Vennesland 1983).

Bertolini *et al.* (2004) has published a summary of the ionic concentrations measured in the pore solution extracted mechanically from cement pastes, mortars and concretes of ordinary Portland cement, and mineral admixtures. In table 5.1 are shown the experimental results reported. This table is very important because for different mixes, it gives an initial idea about the principal ions contained in the pore solution and their respective concentrations.

Cement	Chloride added (by mass of cement)	Water / binder	Age (days)	Sample	OH⁻ [mol/m³]	Na⁺ [mol/m³]	K⁺ [mol/m³]	Ca⁺⁺ [mol/m³]	Cl⁻ [mol/m³]	SO4⁼ [mol/m³]
OPC	no	0.45	28	paste	470	130	380	1	0.2	n.a.
OPC	no	0.5	28	mortar	391	90	288	<1	3	<0.3
OPC	no	0.5	28	paste	834	271	629	1	n.a.	31
OPC	no	0.5	192	mortar	251	38	241	<1	n.a.	8
OPC	no	0.5	---	paste	288	85	228	n.a.	1	n.a.
OPC[a]	no	0.5	84	paste	589	n.a.	n.a.	n.a.	2	n.a.
OPC[b]	no	0.5	84	paste	479	n.a.	n.a.	n.a.	3	n.a.
80% GGBS	no	0.5	28	mortar	170	61	66	<1	8	15
70% GGBS	no	<0.55	84	concrete	95	89	42	n.a.	5	8
65% GGBS	no	0.5	84	paste	355	n.a.	n.a.	n.a.	5	n.a.
25% PFA	no	0.5	28	mortar	331	75	259	<1	<1	18
30% PFA	no	0.5	84	paste	339	n.a.	n.a.	n.a.	2	n.a.
10% SF	no	0.5	28	paste	266	110	209	1	n.a.	32
20% SF	no	0.5	28	paste	91	59	109	1	n.a.	33
20% SF	no	0.45	28	paste	98	36	53	1	n.a.	n.a.
30% SF	no	0.5	28	paste	26	35	53	2	n.a.	35
OPC[a]	0.4% (NaCl)	0.5	84	paste	741	n.a.	n.a.	n.a.	84	n.a.
OPC[b]	0.4% (NaCl)	0.5	84	paste	661	n.a.	n.a.	n.a.	42	n.a.
OPC	0.4% (CaCl₂)	0.5	28	mortar	62	90	161	<1	104	5
OPC	0.4% (NaCl)	0.5	35	paste	835	546	630	2	146	41
OPC	1% (NaCl)	0.5	---	paste	458	580	208	n.a.	227	n.a.
65% GGBS	0.4% (NaCl)	0.5	84	paste	457	n.a.	n.a.	n.a.	28	n.a.
80% GGBS	0.4% (NaCl)	0.5	28	mortar	138	41	299	<1	67	21
25% PFA	0.4% (CaCl₂)	0.5	28	mortar	257	157	307	<1	85	28
30% PFA	1% (NaCl)	0.5	28	mortar	457	n.a.	n.a.	n.a.	39	n.a.
10% SF	0.4% (NaCl)	0.5	35	paste	192	264	256	1	216	37
10% SF	1% (NaCl)	0.5	35	paste	158	614	345	2	615	n.a.
OPC	no	0.5	---	carbonated paste	3×10^{-4} – 2.8	10-23	4-20	31	8-16	n.a.
OPC	1% (NaCl)	0.5	---	carbonated paste	6×10^{-5} – 2.8	330-369	20-31	21	533-651	n.a.

Low C3A content (7.7%)
High C3A content (14.1%)
Interval of values from pastes exposed to environment with different CO3 concentration
n.a.=Concentration no available

Table 5-1 Chemical composition of the pore solution of various concrete materials (Bertolini *et al.* 2004)

5.3.5 Transient current in a migration test

Despite many criticisms (Feldman *et al.* 1994), the ASTM C1202-RCPT is one of the world leading tests for assessing permeability of concrete. In the RCPT the total charge is related to the movement of all ions in the pores rather than the flux of chlorides, and for concrete containing mineral admixtures, the test has been proposed for measuring just the conductivity rather than the permeability (Wee, Suryavanshi and Tin 2000). All the doubts surrounding the migration test are related to a failure to understand the physical and chemical phenomena during the test: transient current, electric field, conductivity, diffusion, adsorption, etc.

The ASTM C1202-RCPT is a test designed for solving the problem of quality assessment of concrete in the construction industry, where a rapid and easy test is

necessary. One of the principal contributions of the test developed by Whiting (1981) is the use of current, a parameter that can be easily measured for ranking different concretes. In the same way, different researchers have proposed using current in a migration test for estimating the diffusion of chloride coefficients (Yang, Chiang and Wang 2007, Yang, Cho and Huang 2002).

Although in a migration test the total current is related to all the ions available in the system (equation 5.21), it is related also to the chloride flux across the sample. This can be shown using the Nernst-Einstein equation and the chloride transport number (Lu 1997). In the same way, the chloride migration rate, k_{cl} [mol/L/h] can be found from the charge. The total charge Q_T can be obtained as the area under the current-time graph.

$$Q_T = \int i_T dt \quad (5.26)$$

According to Faraday's law (Yang 2003), the charge passed carried by chloride ions (Q_{cl}) is related to the number of moles of chloride that pass through the sample.

$$Q_{cl} = |z|Fn_{cl} \quad (5.27)$$

Where n_{cl} is the number of moles of chloride in the anode. Using equations 5.24, 5.26 and 5.27 the chloride transference number can be found.

$$t_{cl} = \frac{i_{cl}}{i_T} = \frac{dQ_{cl}/dt}{i_T} = \frac{|z|F(dn_{cl}/dt)}{i_T} \quad (5.28)$$

The chloride migration rate can be defined by equation 5.29, where V is the volume of solution in the anode.

$$k_{cl} = \frac{dn_{cl}}{Vdt} = \frac{t_{cl}}{V|z|F}i_T \quad (5.29)$$

This equation, as well as the Nernst-Planck and Nernst-Einstein equations shows that from a theoretical point of view the transient current can be used to assess the chloride transport properties of concrete. However, in practice t_{Cl} is not known, and changes during the test.

5.4 DIFFUSION TESTS

The Salt ponding test (AASHTO 1997) and Bulk diffusion test (NTBuild-443 1995) are examples of non-steady state chloride diffusion tests. Steady state chloride diffusion tests are more time consuming and the coefficient of diffusion is calculated using Fick's First Law of diffusion (Glass and Buenfeld 1998). They are carried out in a traditional diffusion cell setup where the upstream compartment is the chloride source and the downstream compartment must be chloride free at the start of the test. The chloride flux is calculated measuring the rate of change of chloride concentration in one of the compartments after the steady state is reached. More on the testing of the diffusion can be found in Hooton, Thomas and Stanish (2001).

5.5 MIGRATION TESTS

As one of the main objectives of this research was to develop a migration test to obtain more information about chloride penetration and improve our understanding of the ionic transport mechanisms in concrete, migration tests are discussed in detail. Those are summarised in this section, where the main part of the information is from reference sources. In table 5.2 the test methods that have been reviewed are summarised.

The principle of electromigration tests is to apply a constant potential difference across a fully saturated sample. These tests are usually performed in two chamber cells with the concrete in the middle and each cell full of a defined solution. As chloride is the ion of interest and the pore solution of concrete contains sodium, potassium and hydroxyls, these species are the most commonly used to fill the cells. The size of the concrete sample is usually a cylinder of 100 mm diameter and length of about 15 to 50 mm. The duration of the test is a function of the thickness of the cylinder. It is necessary to have a sufficient length in order to avoid the influence of aggregate interfaces.

Test	References
"Rapid chloride permeability test (RCPT)".	Whiting (1981) AASHTO T277 ASTM C 1202-05
Nordtest method NT335 *"Chloride diffusion coefficient from migration cell experiments"*	NTBuild-335 (1997)

Nordtest method NT492: *"chloride migration coefficient from non-steady-state migration experiments".*	NTBuild-492 (1999)
AASHTO-TP-64-03: *"Test for predicting chloride penetration of concrete by rapid migration procedure."*	AASHTO-Tp-64 (2003)
JSCE-G571-2003: *"Test method for effective diffusion coefficient of chloride ion in concrete by migration"*	JSCE-G571 (2003)
Migration chloride Test	Dhir *et al.* (1990)
CTH migration test	Luping and Nilsson (1992)
Rapid chloride conduction test	Streicher and Alexander (1995)
Conductivity concrete test	Lu (1997)
Steady state chloride migration test	Delagrave, Marchand and Samson (1996)
Steady state chloride migration test	Mcgrath and Hooton (1996)
Electromigration test	Otsuki *et al.* (1999)
Concrete tube - migration test.	Prince, Perami and Espagne (1999)
Non-steady state migration test - "ponding test".	Castellote, Andrade and Alonso (2000)
LMDC - concrete migration test.	Truc, Ollivier and Carcasses (2000)
Accelerated chloride migration test (ACMT).	Yang and Cho (2003)
CTH migration test modified with sodium iodide (NaI) ion.	(Lay *et al.* 2004)
In-situ rapid chloride permeability test.	Whiting (1984)
PERMIT in situ ion migration test.	Basheer *et al.* (2005)

Table 5-2 Summary of the test chloride migration methods reviewed

5.5.1 Non-steady state migration tests

The first non-steady state test was developed by Whiting (1981), and is known as the *"rapid chloride permeability test (RCPT)".* The test is used extensively in the concrete industry for assessing concrete quality and is included in concrete specification documents (Bentz 2007). The standards are AASHTO T277 (2007) and ASTM C 1202. These two standards are described in detail in sections 5.5.1.1 and 5.5.1.2.

Another non-steady state migration test is the Nordtest Method NT-492 (1999) approved as a standard in Finland in 1999. It was first developed by Tang and Nilsson (1992) at Chalmers University, Sweden, and called CTH (Chalmers Tekniska Högskola). The standard has some modifications from the original test in accordance with recommendations from a Nordic seminar (Luping 1997). The test can be used either for steady state or non-steady state migration tests. Tang provided the mathematical theory for calculating the migration coefficient and the set-up of his CTH test is almost the same as in the standard.

In 2003 AASHTO proposed the standard TP64 (ASSHTO 2003) based on Nordtest NT 492. The rapid migration test is a provisional AASHTO standard (Obla and Lobo 2005).

Castellote, Andrade and Alonso (2000) and Andrade *et al.* (1999b) developed a non-steady state migration test using a device similar to the "ponding test". It is shown in figure 5.5. The cathode was a stainless steel mesh which was filled with a 0.5 M NaCl solution. The anode was a steel plate and a damp sponge was placed between the electrode and the concrete sample. The voltage applied was 12 V. The duration of the test was variable according to the thickness of the sample, ranging from 7 to 28 days.
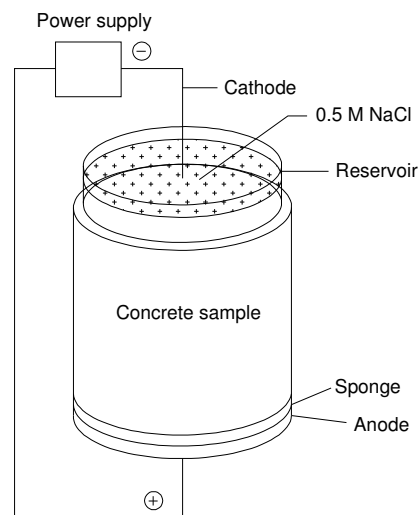
Figure 5-5 Non-steady state migration test proposed by Andrade *et al.* (1999b)

In other research, Castellote, Andrade and Alonso (2002) investigated the chloride threshold value for depassivation of the steel embedded in concrete and the simultaneous determination of the non-steady state diffusion coefficient. They used an accelerated method similar to that used by Andrade *et al.* (1999b), but a reinforced steel bar was embedded in the concrete samples.

Lay *et al.* (2004) proposed a method for measuring the migration coefficient of chloride-contaminated concrete for existing structures exposed to an environment containing chlorides or concrete produced with chlorides in the mixing materials. Lay stated that contaminated concrete cannot be tested with a conventional non-steady state test (CTH) because the chlorides interfere with the common colorimetric indicator used. Similarly, the carbonation may also interfere with the penetration depth reading. The proposed test substitutes chlorides in the CTH migration test with

sodium iodide (NaI), a different ion, but with similar properties. The indicator proposed was a solution of potassium dissolved in acetic acid.

5.5.1.1 Concrete's Ability to Resist Chloride Ion Penetration ASTM C1202-05

In this test a slice of concrete 50 mm thick and of 100 mm diameter is placed between two electrodes and 60 volts D.C. are applied. One of the cells is filled with a 0.30 N NaOH solution and the other cell is filled with a 3.0% NaCl solution. The curved surface of the specimens is coated with epoxy; and the conditioning of specimens prior the test is to vacuum the samples for 3 h under a pressure of 6650 Pa. De-aerated water is added to immerse the specimen and the vacuum level is maintained for another hour. The specimens are soaked in water for the next 18 h before testing. Figure 5.6.
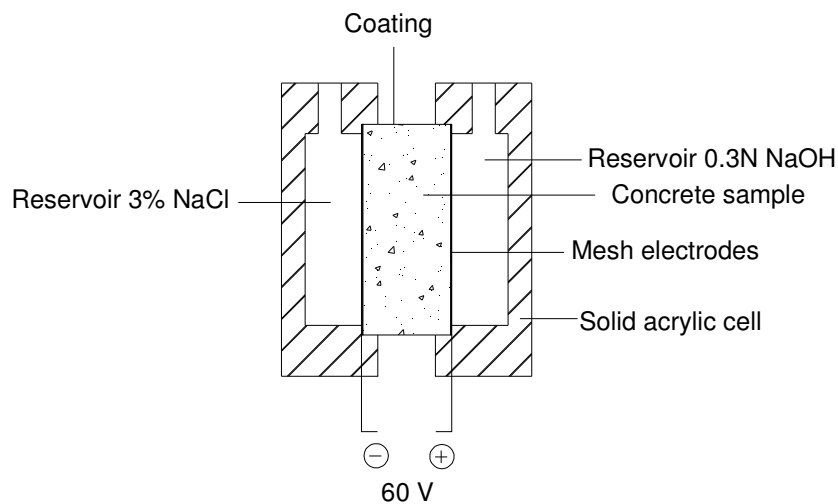
Figure 5-6 Rapid Chloride Permeability Test

During the test the main parameter measured is the flow current through the sample for a period of 6 h. The total charge passed (coulombs) is determined by calculating the area under the plot of current (A) vs. time (S). For this reason the test is known as the Coulomb Test and is used for ranking different concretes according to Table 5.3.

Charge Passed (coulombs)	Chloride Ion Penetrability
>4,000	High
2,000 - 4,000	Moderate
1,000 – 2,000	Low
100 – 1,000	Very low
<100	Negligible

Table 5-3 Chloride ion penetrability based on charge passed (ASTM C1202)

The *RCPT* has been used as an indirect measurement of the chloride ion diffusion and comparison with results from other methods and tests have been used to establish relationships with other physical features of concrete (Andrade and Whiting 1995, Wee, Suryavanshi and Tin 2000). In the first research by Whiting (1981) he found that the charge passed through the concrete corresponded well with results using the ponding test. However, Patrick, Mcgrath and Hooton (1999) found a poor correlation between the results of RCPT and those of the ponding test.

Since the introduction of the test as a standard, it has suffered some criticisms about its usefulness to determine the chloride diffusion (Feldman *et al.* 1994). The total charge is related to the movement of all ions in the pores rather than the flux of chlorides, and at the start of the test there are actually no chlorides in the samples. Also, because of the voltage applied (60 V) the measurement conditions are severe. For low-quality or young concretes, the temperature in the system can be increased, changing the physical and chemical conditions of the sample (Zhang and Gjorv 1991, Roy 1989, Mccarter, Starrs and Chrisp 2000). Since electrical conductivity is sensitive to temperature, heating will result in different measured coulomb values (Julio-Betancourt and Hooton 2004, Stanish, Hooton and Thomas 2000).

For concrete containing mineral admixtures, the RCPT can be used to measure its conductivity rather than its permeability (Wee, Suryavanshi and Tin 2000). Some researchers such Shane *et al.* (1999) discuss the validity of the test for assessing concrete containing mineral admixtures such as silica fume, fly ash and slag, which may have reduced OH^- concentration. Wee, Suryavanshi and Tin (1999) state that the information measured during the test reflects the resistivity properties of concrete rather than the chloride ion penetrability.

5.5.1.2 Chloride Non-Steady State Migration Experiment, NT BUILD 492-1999.

This test method requires cylindrical specimens of 100 mm diameter and a thickness of 50 mm. Three specimens should be used in each test. An external electrical potential is applied across the sample in order to force the chloride ions to migrate into the concrete. After the test, the sample is split and a silver nitrate solution sprayed on to one of the sections. The penetration depth is measured from the chloride precipitation, and the migration coefficient can be calculated using equations given in the standard.

The preconditioning of the samples before the test is almost the same as that in the ASTM standard; however, the fluid used for soaking the samples is a saturated $Ca(OH)_2$ solution. In the same way, the solutions used in the cathode and anode are a 10% NaCl and a 0.3 N NaOH respectively. Figure 5.7 shows the arrangement of the migration set up.

The voltage and the time used in the test depend on the electrical properties of the concrete sample. First, an initial current I_{30V} is obtained from an initial voltage of 30 V. With this current, the voltage to be applied in the test, U, is found from the standard. Finally, once the voltage U is applied, the test duration in hours is obtained from the standard using the possible new initial current I_0.
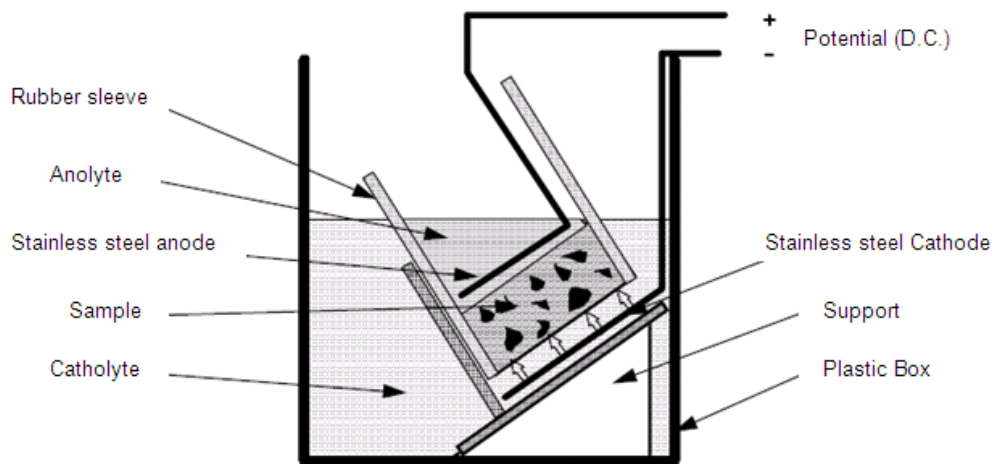
Figure 5-7 Arrangement of the migration test NTBuild-492

Figure 5.8 shows the graphical method to find the voltage and the time according to the Nordtest.
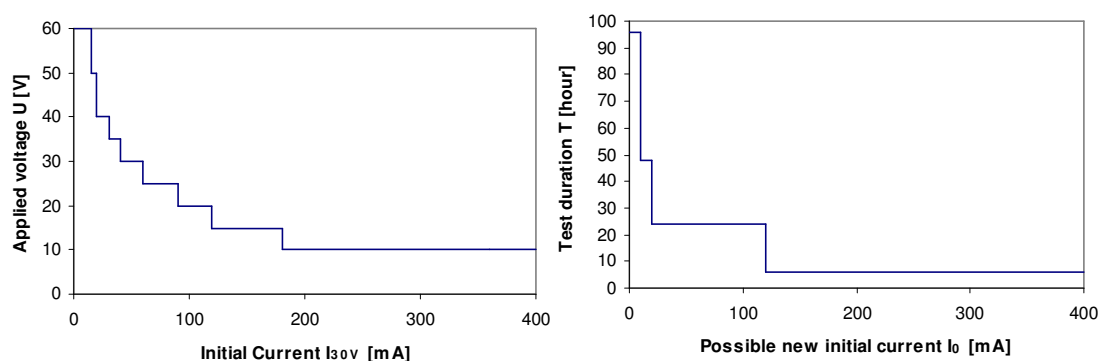
Figure 5-8 Determination of the voltage and time used in the NTBuild-492

According to the standard the non-steady state migration coefficient can be found from equation 5.30.

$$Dnssm = \frac{RT}{zFE} \frac{x_d - \alpha\sqrt{x_d}}{t}$$ (5.30)

$$E_f = \frac{U - 2}{L}$$

$$\alpha = 2\sqrt{\frac{RT}{zFE}} erf^{-1}\left(1 - \frac{2c_d}{c_0}\right)$$

where D_{nssm} is the non-steady state migration coefficient, [m^2/s], z the absolute value of ion valence, for chloride $z = 1$, U the absolute value of the applied voltage [V], T the average value of the initial and final temperatures in the anolyte solution [ºK], L the thickness of the specimen [m], x_d the average value of the penetration depths [m], t the test duration [S], erf^{-1} the inverse of error function, c_d the chloride concentration at which the colour changes ≈0.07N for OPC, c_0 the chloride concentration in the catholyte solution and E_f the electric field applied [V/m].

In the same way as the ASTM C1202, the NORDTEST 492 has suffered some criticism concerning temperature rise, movement of all ionic species in the concrete pore solution, mineral admixtures, and chemical admixtures such as calcium nitrite. Notwithstanding this, the test has been used extensively for finding the non-steady state migration coefficient for chloride.

5.5.2 Steady state migration tests

The literature survey carried out in the field of chloride migration tests shows that almost any migration test developed in the last few years is based on the set-up proposed either by Whiting (1981) or Luping and Nilsson (1992). The main differences between testing methods are the voltage that is applied, the thickness of the concrete sample, the duration of the test, the volume of each cell, and the chemical composition of each solution used in the cells.

Usually, in a steady state migration test, the concentration of chlorides is measured when the flux of chloride ions passing through the sample has reached the steady

state condition. In a saturated sample once the flux of chlorides is known, it is possible to calculate the migration coefficient according to the Nernst-Planck or the Nernst-Einstein equations.

The Nordic standard NT BUILD 355 - Steady state migration test - (NTBuild-335 1997) was developed in the early 1980's and revised in the mid 1990's. In this test the sample is located between two migration cells that are filled with 5% NaCl and 0.3 N NaOH solutions. The curved surface of the concrete sample is coated and the specimen is saturated by immersion in lime water. An external potential of 12 V DC is applied and the anode chamber is checked for chlorides using a solution 1 M AgNO3 until precipitates are observed. When the chloride contents are determined the chloride flux is calculated.

Figure 5.9 shows the chloride migration apparatus utilized by Mcgrath and Hooton (1996). The volume of the anode and cathode chambers were 0.6 and 1.5 L, and the solutions were 0.3 mol/L NaOH and 0.5 mol/L NaCl plus 0.3 mol/L NaOH respectively. Stainless steel was used as electrodes and an Ag/AgCl reference electrode assembly was used in order to adjust the desired driving potential for the test set up. A gap of 50 mm was left between the specimen face and the stainless steel electrodes in order to allow the insertion of the reference electrode. During the test the diffusion coefficient was found by monitoring the chloride concentration of the anode chamber.
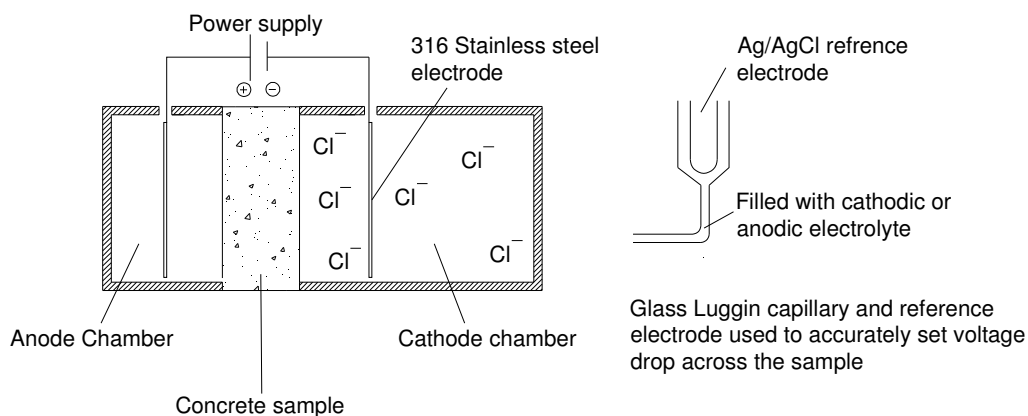
Figure 5-9 Chloride migration cell proposed by Mcgrath and Hooton (1996)

Delagrave, Marchand and Samson (1996) carried out tests for determining the steady state chloride ion migration coefficient of several different concrete mixes. Each sample was 95 mm in diameter and 1.5 mm thick and was saturated prior to

testing. In this test, the compartments of the cells were equipped with an agitating device in order to maintain the homogeneity of the solutions, and ruthenium-coated titanium electrodes were used. The cathode chamber compartment was filled with a 0.3 M sodium hydroxide plus a 0.5 M sodium chloride solution. The anode chamber compartment was filled with a 0.3M sodium hydroxide solution. A voltage of 10 V was applied and the experiments lasted approximately 3 weeks.

Streicher and Alexander (1995) proposed a rapid chloride conduction test which involved saturating a concrete sample in a 5 M NaCl solution before measuring its conductivity. They state that a concrete sample saturated in a highly conductive solution has the same pore water conductivity as the solution. Thus, the conductivity differences found in various concrete samples are due to the differences in their pore structure.

The apparatus consists of two cells of 0.5 L and each cell contains a 5 M NaCl solution. Two copper/copper sulphate half cells were used to measure the potential difference across the sample. Samples of 68 mm diameter and thicknesses between 5 and 40 mm were used. Before saturating each sample, they were dried in an oven at 50 °C for 7 days to remove moisture from the concrete pores. Then, the samples were vacuum saturated in a 5 M NaCl solution for 5 hours and left to soak for 18 hours. The set up used is shown in Figure 5.10; the voltage applied was 10 V. Finally, the current was measured in order to obtain the conduction of each concrete sample, and the transport properties of the sample were calculated using the Nernst-Einstein equation.
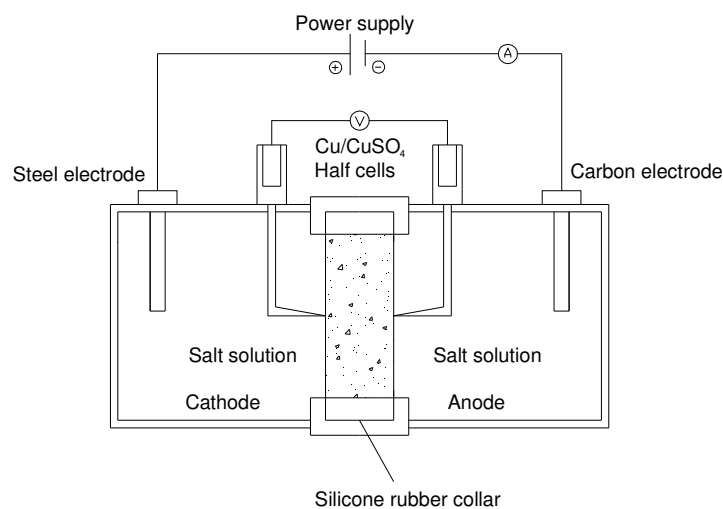
Figure 5-10 Conduction test arrangement of Streicher and Alexander (1995)

Lu (1997) proposed the Nernst-Einstein equation and used a similar test than Streicher and Alexander (1995) in order to validate his model. He supported the use of a conductivity test and proposed that the chloride diffusivity in concrete can be measured through the conductivity when the Nernst-Einstein equation is used. A low voltage applied eliminated the problem of temperature. The data measured during the test were related only with the free chloride ions, because the chloride binding can be ignored when concrete was saturated with salt. The time consumed in the test was very short.

In a research carried out by Otsuki *et al.* (1999), the diffusion coefficient of chloride ion in mortar was investigated through an electromigration test. The concept of mobility was adapted to the Nernst-Einstein equation. The test used is basically the same as proposed by the ASTM C1202 standard with some minor differences. A 30 mm thick concrete disk was adhered to a rubber attachment using epoxy resin, as shown in figure 5.11. A saturated $Ca(OH)_2$ solution was added to the anode and a 5% NaCl solution was added to the cathode. Finally, an electrical potential difference was applied to the solutions using titanium electrodes until a specific electric current density was reached.
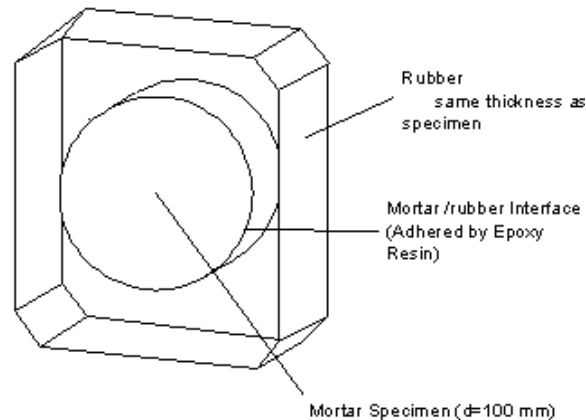
Figure 5-11 disk-type specimen of Otsuki *et al.* (1999)

In a work published in 1999, Prince, Perami and Espagne (1999) presented a novel device that allows continuous determination of the main physical parameters in a concrete migration test. Figure 5.12 shows a diagram of the set-up developed. The diffusion cell is a cylindrical PVC tank covered with a lid. The concrete sample is a cylinder of 100 mm diameter and 100 mm height in which a secondary drilling produced a central cavity of 40 mm diameter.

The "concrete tube" is fixed firmly in the cell and separates two compartments filled with different solutions. The external compartment contains about 1.2 L of 0.1N NaCl and is stirred periodically. A stainless steel electrode is used in this chamber and is connected to the negative of the power supply. The internal compartment contains about 0.2 L of 0.1N NaOH continuously stirred. A carbon electrode is used in this chamber and is connected to the positive of the power supply. Finally, the amount of chloride that diffuses through the concrete, the conductivity, and the pH are monitored. In this test the voltage applied across the two electrodes is limited to 30 V and it runs for several days.
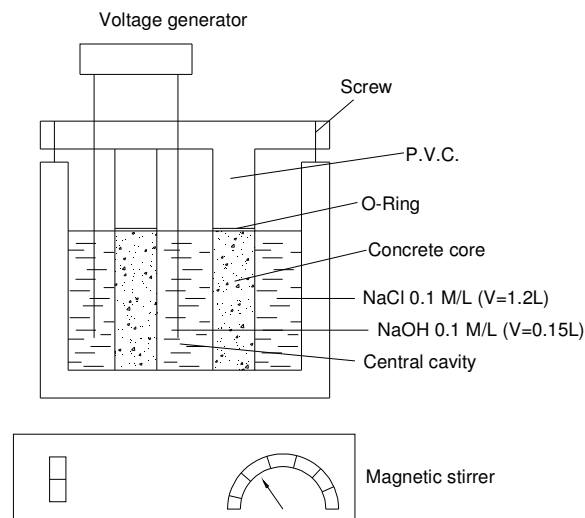
Figure 5-12 Chloride migration device developed by Prince, Perami and Espagne (1999)

Truc, Ollivier and Carcasses (2000) presented a method called LMDC (Laboratoire Metériaux et Durabilité des Constructions) that permits the determination of the effective diffusion coefficient by measuring the drop in chloride concentration in the upstream cell (cathode) and using the Nernst-Planck equation. The set up for the test developed by Truc, Ollivier and Carcasses (2000) is shown in figure 5.13. The upstream chamber was filled with 0.5 L of chloride salts (NaOH, KOH, and NaCl) and the downstream chamber was filled with 2.5 L of a hydroxide solution (NaOH+KOH). The samples used were cylinders of 110 mm diameter and 30 mm thickness and were vacuum saturated with an alkaline solution before the test. The solutions were replaced frequently during the test and 12 V were applied between the sides of the sample. Stainless steel electrodes were used.
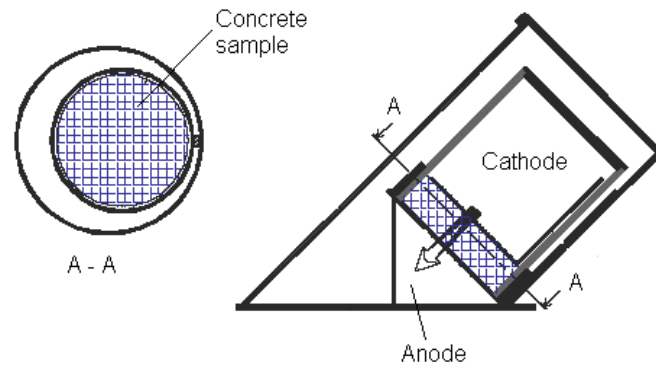
Figure 5-13 Arrangement of the LMDC chloride test developed by Truc (2000)

Yang, Cho and Huang (2002) carried out some tests with a modified device of the ASTM C1202 method. The relationships between the current, the chloride concentration and temperature were measured for several concrete mixes. In this test proposed by Yang et al. the difference from that of the ASTM standard was that the solution volume in each reservoir was 4750 ml instead of 250 ml. They suggest that by increasing the volume of the cells, the Joule effect can be eliminated. With the same accelerated chloride migration test (ACMT), but in another paper, Yang and Cho (2003) presented some results about the relationship between charge passed and chloride-ion concentration, and the relationship between stable current and the chloride migration coefficient.

In other research, Yang (2003) used an accelerated chloride migration test (ACMT) with two compartments of 4.5 L in each cell. Discs 30 mm thick and of 100 mm diameter were prepared, including vacuum saturation and setting up under the ASTM C 1202 standard. One of the cells was filled with 0.30 N NaOH solution and the other cell with 3.0% NaCl solution. The system was connected to a 24 V power supply. The electrical current in the sample and the quantity of chloride ions in the anode and cathode cells were monitored frequently throughout the 25 days that each test lasted.

A standard was developed in 2003 by the Japan Society of Civil Engineers in order to obtain the effective diffusion coefficient of chloride ions in concrete from migration tests. The JSCE-G571 (2003) standard specifies a test method in a steady state condition. In this experiment, a concrete sample of 50 mm is placed between two acrylic cells and a constant voltage is applied. The solutions used to fill the cells are 0.5 mol/L of NaCl in the cathode and 0.3 mol/L of NaOH in the anode. The volume of each cell is not strictly specified.

The conditioning of the concrete samples consists of coating the circumference of each specimen with epoxy resin and storing the specimens under standard conditions for at least 4 days. After this time, the samples are vacuumed in a desiccator for 3 hours with an inside pressure less than 150 Pa. With the vacuum pump still running, the desiccator is filled with distilled water, and the sample should be left for at least a day in the desiccator.

With the sample mounted into the cells, a potential of 15 V is applied. During the test, the solution of the cells can be renewed appropriately in order to hold the chloride concentration below 0.05 mol/L in the anode and no lower than 0.45 mol/L in the cathode. The test runs until the rate of chloride ion in the anode becomes constant.

The flux of chloride ions in the steady state is calculated from the rate of increase of ion concentration in the anode cell, and the effective diffusion coefficient of chloride is calculated from the Nernst-Planck equation. In addition to the last coefficient, the standard provides a method of calculating the apparent diffusion coefficient from the effective diffusion coefficient.

$$D_{app} = k_1 k_2 D_e \qquad (5.31)$$

where D_{app} is the apparent diffusion coefficient [cm^2/year], D_{eff} the effective diffusion coefficient [cm^2/year], k_1 the coefficient of equilibrium concentration of chloride ion on the cathode cell and that at the concrete surface, and k_2 the coefficient reflecting the effect of immobilization of chloride ions in the hydrated cement system.

5.5.3 In situ migration tests

The first in-situ version of the rapid chloride permeability test was proposed by Whiting (1984). In this test the surface of the concrete is vacuum saturated with an alkaline solution and is allowed to cure overnight; a solution of 1.5 litre of 3% (0.5 M) sodium chloride is poured into a container attached to the concrete surface and a voltage of 80 V is applied between a copper mesh electrode in the container and the reinforcement. The current is measured for a period of 6 hours. The interpretation of the data is the same as that used in the RCPT test (Basheer 2001).

A recent in situ chloride migration test was developed by Basheer *et al.* (2005) in order to assess the chloride transport resistance of concrete without extracting cores

from the structure. The test is known as PERMIT ion migration test. The device consists of two concentrical cylinders placed on the concrete surface forming two compartments (cells). The inner cell contains a chloride solution and the outer cell, contains a neutral distilled water solution. The inner cell contains a stainless steel electrode (cathode) and the outer cell contains a steel electrode (anode). An electric potential difference applied between the electrodes produces migration of chloride ions from the inner cell to the outer cell through the concrete. The chloride ion concentration in the outer cell is monitored regularly with a chloride ion selective electrode used in conjunction with a reference electrode. A representation of the PERMIT device is showed in figure 5.14 (Basheer *et al.* 2005).
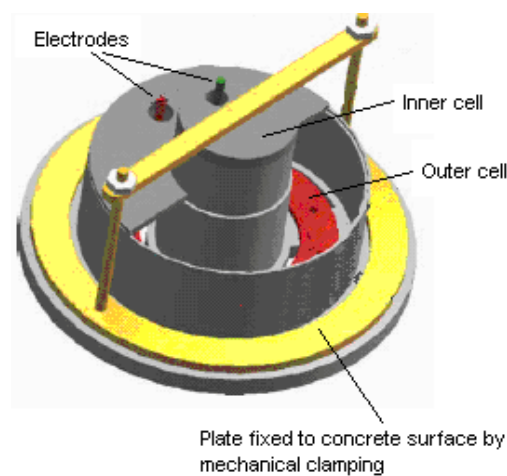
Figure 5-14 PERMIT ion migration test proposed by Basheer *et al.* (2005)

5.6   CHLORIDE MODELLING

Most of the concrete diffusion models found in the literature or available commercially are based around the analytical solution of the Fick's Second Law (equation 5.11). The main differences are the assumptions on the apparent chloride diffusion coefficient and the surface chloride content. Examples of models based on Fick's Laws of diffusion are **ClinConc** developed initially by Tang and Nilsson in 1994 (Luping 2008) and **Life-365** developed by Bentz and Thomas, which can be downloaded from the address http://www.silicafume.org/ specifiers-lifecycle.html.

Different approaches have been proposed in order to simulate the penetration of chloride into the concrete accounting all the species related or an external electrical driving force. Truc, Ollivier and Nilsson (2000) proposed a numerical model based on a finite difference method for the flux of several species with the Poisson - Nernst -

Planck equations. Sugiyama, Ritthichauy and Tsuji (2003) presented a method for numerically calculating the concentration profiles of chloride ions (Cl^-) in concrete; the method is based on the generalized form of Fick's First Law suggested by Onsager. Narsilio *et al.* (2007) simulated electromigration tests solving the Nernst–Planck equation coupled with the electroneutrality condition using the finite element method. Khitab, Lorente and Ollivier (2005) developed a numerical model to predict the chloride penetration solving the Nernst–Planck equation coupled with the current laws. A numerical model was developed by Claisse and Beresford (1997) using the Nernst – Planck equation and maintaining charge neutrality by modelling changes to the voltage distribution. Lorente *et al.* (2007) showed a model based on a second-order finite difference procedure that solves the law of mass conservation equation for each species and an electrical field equation for the overall system. Samson, Marchand and Snyder (2003) presented a model to solve the transport of ions in saturated materials during a migration test using a finite element method. More recently, Krabbenhoft and Krabbenhoft (2008) solved the Poisson - Nernst - Planck equations analytically and derived an expression for the diffusion; they propose a non-linear finite element procedure.

All the last references use the Nernst – Planck equation to find the flux of ions and the transport properties of chlorides in concrete. Some of them use it coupled with a conservation equation. In the same way, the distribution and evolution of the electrical field is considered by some researches in order to keep the electroneutrality of all the species considered.

The limitations of the assumption that the electrical field remains constant under a migration test have been pointed out by many researchers (Narsilio *et al.* 2007) and standards (JSCE-G571 2003, NTBuild-492 1999); however, the electrical field can be accounted for in a macroscopic way from equation 5.23 (Khitab, Lorente and Ollivier 2005, Lorente *et al.* 2007). A more complex expression can be found for the electrical field, if the Nernst – Planck equation is used with a chemical activity coefficient (γ) (Truc 2000); however, it has been showed that the activity term does not increase the accuracy of the results in a simulation of a migration test (Samson, Marchand and Snyder 2003, Tang 1999).

In a migration test the species that are present both in the boundary and in the pore solution of the sample (Na^+, K^+, Ca^+, OH^-, and Cl^-) flow as indicated by the Nernst-Planck equation, where an increase of concentrations at specific points in the sample

can lead to a variation in the electric field. In the same way, a variation in the electric field can lead to a variation in the flux of each ion. The concentration and chemical composition of the pore structure of concrete at the start of the test is a very important factor that needs to be taken into consideration in order to comprehend the different phenomenon associated with the test. Truc, Ollivier and Nilsson (2000) found considerable differences in the migration of chlorides when the composition of the pore solution is included in the model.

From a microscopic point of view, normal diffusion of chlorides can be reduced because of the effect of ionic interaction with other ions present into the pore solution and the effect of the known electrical double layer (Zhang and Gjorv 1996). For a diluted solution, the ion - ion interaction produces a change in the chemical potential. This has been adequately explained with the *Debye Huckel theory* (Bockris and Reddy 1998) that can be used as a qualitative tool in order to understand the phenomenon. The effect of the electrical double layer during diffusion is the generation of an additional electrical voltage at the interface between the pore wall and the pore solution (Friedmann *et al.* 2004). Castellote *et al.* (2001) found that during a migration test the effect of the electrical double layer does not seem to change the electrostatic interactions between the surface of the pores and the ions under migration.

From a macroscopic and engineering point of view, in normal diffusion the effects of the ionic interaction and the electrical double layer affect the mobility of chlorides, generating a membrane electrical potential opposed to the chemical potential. As was pointed out by Lorente *et al.* (2007) the Nernst-Planck equation must be used in natural diffusion instead of Fick's laws in order not to neglect the effect of the membrane potential.

5.7   COVENTRY UNIVERSITY MODEL

The numerical model used in this research was developed in the Construction Materials Applied Research Group of Coventry University (Claisse and Beresford 1997, Claisse, Elsayad and Ganjian 2009). This simulates a sample of concrete under conditions similar to the Rapid Chloride Permeability Test. The numerical code works by repeated application of the Nernst – Planck equation through time and space, but the flux resulting from the diffusion and migration conditions is balanced

and affected by an additional electrical field (membrane potential) if the charge neutrality condition is not satisfied.

The model was proposed for four ions in the pore solution, but can be easily changed to any number of ions. The concentration of each ion was defined in two ways: C_l represents the concentration of free ions per unit volume of liquid in the pores [free ions/V_{pores}] and C_s is the total concentration (free + adsorbed ions) per unit volume of the solid [total ions/Vsolid]. The ratio of the two concentrations is the capacity factor (α).

$$\alpha = \frac{C_s}{C_l} \qquad (5.32)$$

In the same way, the intrinsic coefficient (D_{int}) defines the transport of matter when the flux is calculated per unit cross-sectional area of the pores and the concentration in the free liquid. In contrast, the apparent diffusion coefficient (D_{app}) defines the transport of any ion when the flux is calculated per unit area of the porous material and the average concentration in the material. The reason why both coefficients are used is because the computer model calculates the intrinsic coefficient, but, the apparent coefficients are normally used to predict the service life of concrete structures. By integrating the definitions given above it is possible to prove that the ratio of chloride intrinsic diffusion to apparent diffusion coefficient is equal to the ratio of binding factor capacity to porosity (ε).

$$\frac{\alpha}{\varepsilon} = \frac{D_{int}}{D_{app}} \qquad (5.33)$$

5.7.1 Inputs and outputs of the model

Three types of inputs are required to feed the model.

1. The concrete properties such as the porosity (ε), the geometry: area (A) and length (L), the binding capacity factor for each ion simulated according to equation 5.32 (with no adsorption the capacity factor is equal to the porosity), the initial concentration of the pore solution at the start of the test, the concrete heat loss factor, and the intrinsic diffusion coefficients of the species

involved: normally sodium, potassium and hydroxides found in the concrete pore solution and chloride penetrating from the exterior.

2. The conditions in which the test is conducted, such as the duration, the external electrical field, the chemical concentrations and volume of the external solutions in contact with the sample, and the room temperature.

3. The numerical increments required to run the model such as the space (ΔX) and time (ΔT) steps.

The outputs of the model are the following.

1. The transient evolution of the total current carried for the sample, and the relative currents carried for each ion in any time.
2. The non-linear membrane potential for any time and position
3. The evolution of the concentration for each ion for any time and position
4. The evolution of the temperature according to 5.7.4

5.7.2 Diffusion and migration Fluxes

To calculate the ionic flux the model split the sample in time and space grids. A total of $n+1$ space steps of equal length, and initial and final cells which are half of the others are generated.
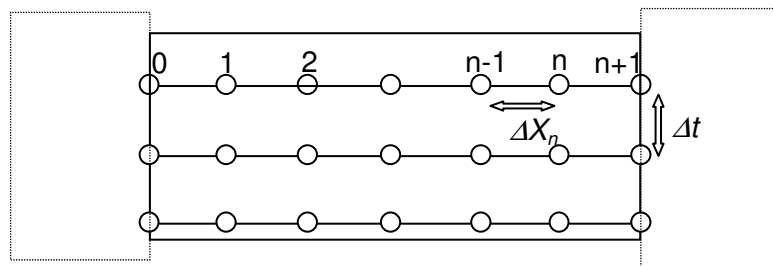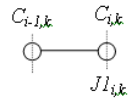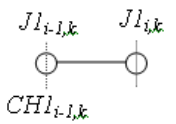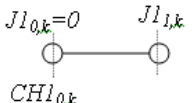
Figure 5-15 Time and space distribution of the computer model used

The flux due to diffusion $J1(x,t)$ and the concentration $C_i(x,t)$ of each ion for each node of the network are calculated through the Nernst-Planck equation. Table 5.4 shows the numerical expressions used to calculate ($J1$). The subscript i indicates the node where it is applied the flux equation, the subscript k refers to the ion being calculated, and the subscript t indicates the time step. In the same way, for each ion, the amount of matter transported ($CH1$) is obtained with the equation of continuity (5.34). Notice that the borders of the sample are treated as special cases.
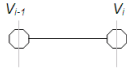
$$\frac{\partial c}{\partial t} = -\frac{\partial J}{\partial x} \qquad (5.34)$$

At the beginning of the test the driving forces that generate diffusion are the initial concentrations of the ions contained in the external cells; a time step later the ions, which are distributed uniformly, start to diffuse into the pore solution.

Diffusion	Numerical formulation	Node Analysis	Physical Eq.
Flux	$J1_{i,k}^{t} = -D_k * \varepsilon * \dfrac{(c_{i-1,k}^{t} - c_{i,k}^{t})}{\Delta X_i}$	$C_{i-1,k}$ $C_{i,k}$ $J1_{i,k}$	$J1 = -D_k * \varepsilon * \dfrac{\partial C}{\partial x}$
Change of concentration	$CH1_{i-1,k}^{t} = \dfrac{(J1_{i-1,k}^{t} - J1_{i,k}^{t}) * A * \Delta t}{Vol_{i-1}} * \dfrac{1}{\alpha}$	$J1_{i-1,k}$ $J1_{i,k}$ $CH1_{i-1,k}$	$\dfrac{\partial C}{\partial t} = -\dfrac{\partial J}{\partial x}$ $C_l = \dfrac{C_s}{\alpha}$
	$CH1_{0,k}^{t} = \dfrac{-J1_{1,k}^{t} * A * \Delta t}{Vol_0}$	$J1_{0,k}=0$ $J1_{1,k}$ $CH1_{0,k}$	$\dfrac{\partial C}{\partial t} = -\dfrac{\partial J}{\partial x}$
	$CH1_{n+1,k}^{t} = \dfrac{J1_{n+1,k}^{t} * A * \Delta t}{Vol_{n+1}}$	$J1_{n,k}$ $J1_{n+1,k}$ $J1_{n+2,k}$ $CH1_{n+1,k}$	

Table 5-4 Diffusion numerical formulation of the Coventry model

The driving force to generate migration is the external electrical field applied. At the beginning of the test this is distributed linearly in all cells in accordance with table 5.5. After one time step it starts to be adjusted and the electrical field ceases to be linear as will be shown in section 5.7.3.

V_{i-1} V_i	$V_i = V_{applied}\left[\dfrac{\Delta X}{L}\right] \qquad V_{i-1} = 0$

Table 5-5 Initial voltage distribution in each cell of the model

Table 5.6 shows the numerical formulation for calculating the migration flux (*J2*) and the concentration change (*CH2*). It is important to notice that the direction of this flux is dependent on the charge of each ion and the voltage across the cell. The charge

(z) carried by any ion times the voltage (V) determines in which direction the ion will flow, i.e. Ions charged positive tend to move toward the negative side.
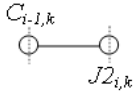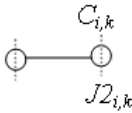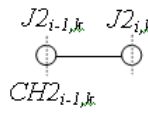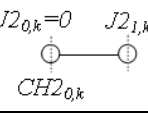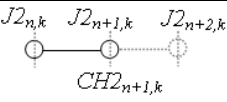
Migration	Numerical formulation	Node Analysis	Physical Eq.
Flux $z_k * V_i \leq 0$	$J2_{i,k}^t = \dfrac{-D_k * z_k * F * V_i * C_{i-1,k}^t}{R * T * \Delta X_i}$		$J2 = \dfrac{-F}{RT} DC \dfrac{\partial V}{\partial x}$
Flux $z_k * V_i > 0$	$J2_{i,k}^t = \dfrac{-D_k * z_k * F * V_i * C_{i,k}^t}{R * T * \Delta X_i}$		
Change of concentration	$CH2_{i-1,k}^t = \dfrac{(J2_{i-1,k}^t - J2_{i,k}^t) * A * \Delta t}{Vol_{i-1}} * \dfrac{1}{\alpha}$		$\dfrac{\partial C}{\partial t} = -\dfrac{\partial J}{\partial x}$ $C_l = \dfrac{C_s}{\alpha}$
	$CH2_{0,k}^t = \dfrac{-J2_{1,k}^t * A * \Delta t}{Vol_0}$		$\dfrac{\partial C}{\partial t} = -\dfrac{\partial J}{\partial x}$
	$CH2_{n+1,k}^t = \dfrac{J2_{n+1,k}^t * A * \Delta t}{Vol_{n+1}}$		

Table 5-6 Migration numerical formulation of the Coventry model

5.7.3 Charge balance and voltage correction

Once the fluxes and the changes of concentration are calculated the model ensures that charge neutrality is maintained throughout the sample at all times for all the ions together. If there is any charge build-up the model corrects the actual migration flux until the charge balance is within a specified range (< 10^{-12} Coulumbs). Macroscopically, the procedure to maintain the charge balance is according to Kirchoff's law: "...*the current density into any point will equal the current out of it*". That means that for any time the total current in node *i* is equal to the current in node *i+1*.

$$\sum_k i_{i,k}^t = \sum_k i_{i+1,k}^t \qquad (5.35)$$

In a migration test, the charge build-up generated by the differences of mobility of the ions in the pore solution is dissipated by the distortion of the electrical field. Those effects of voltage changing are applied in the model by distorting the voltage in each

space step removing any build-up of charge. In that way, only a multi-species system can be physically possible because if there is only one ion the charge neutrality never is reached.

In the model the charge surplus (*csurp*) is calculated using the numerical expressions showed in table 5.7. Notice that *csurp* is evaluated using C_s rather than C_l.

Total concentration	$cb_{i,k}^t = c_{i,k}^t + CH1_{i,k}^t + CH2_{i,k}^t$	Actual c_l
Charge surplus	$csurp_i = \sum_{i=1}^{n} z_k (cb_{i,k}^t * \alpha_k) * Vol_i * F$	$csurp = F \sum_{i=1}^{n} z * c$ [Coulombs]

Table 5-7 Numerical formulation to determine the charge surplus in the model

If at any time the charge surplus is bigger than 10^{-12} Coulombs, the electrical field for any cell is varied in a specific proportion and a loop is done to re-calculate the migration flux until the charge criteria is satisfied. If the concentration changes by more than 10% during any time step, to avoid discontinuities in the results the time step is reduced. Figure 5.16 shows a scheme of the voltage correction.

$$\text{If } Abs(CH1_{i,k}^t + CH2_{i,k}^t) > \frac{c_{i,k}^t}{10} \text{ then (decrease the time step)}$$
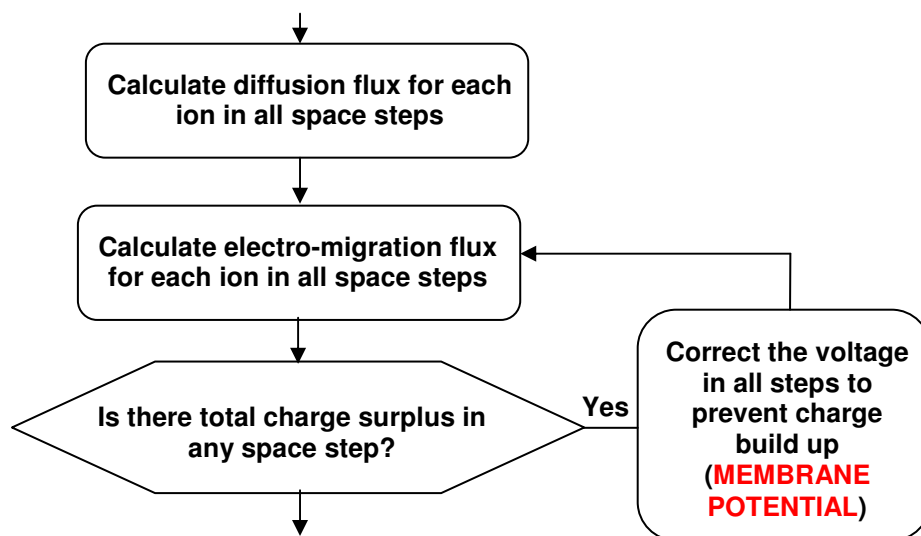
Figure 5-16 Loop condition to avoid charge surplus in the model

Ion generation and removal at the electrodes is represented in the model by assuming that the ions being generated and removed are always hydroxyl ions. The model includes provision for the depletion on the reservoirs at either side of the sample. A more detailed conceptual diagram of the model is shown in figure 5.17.
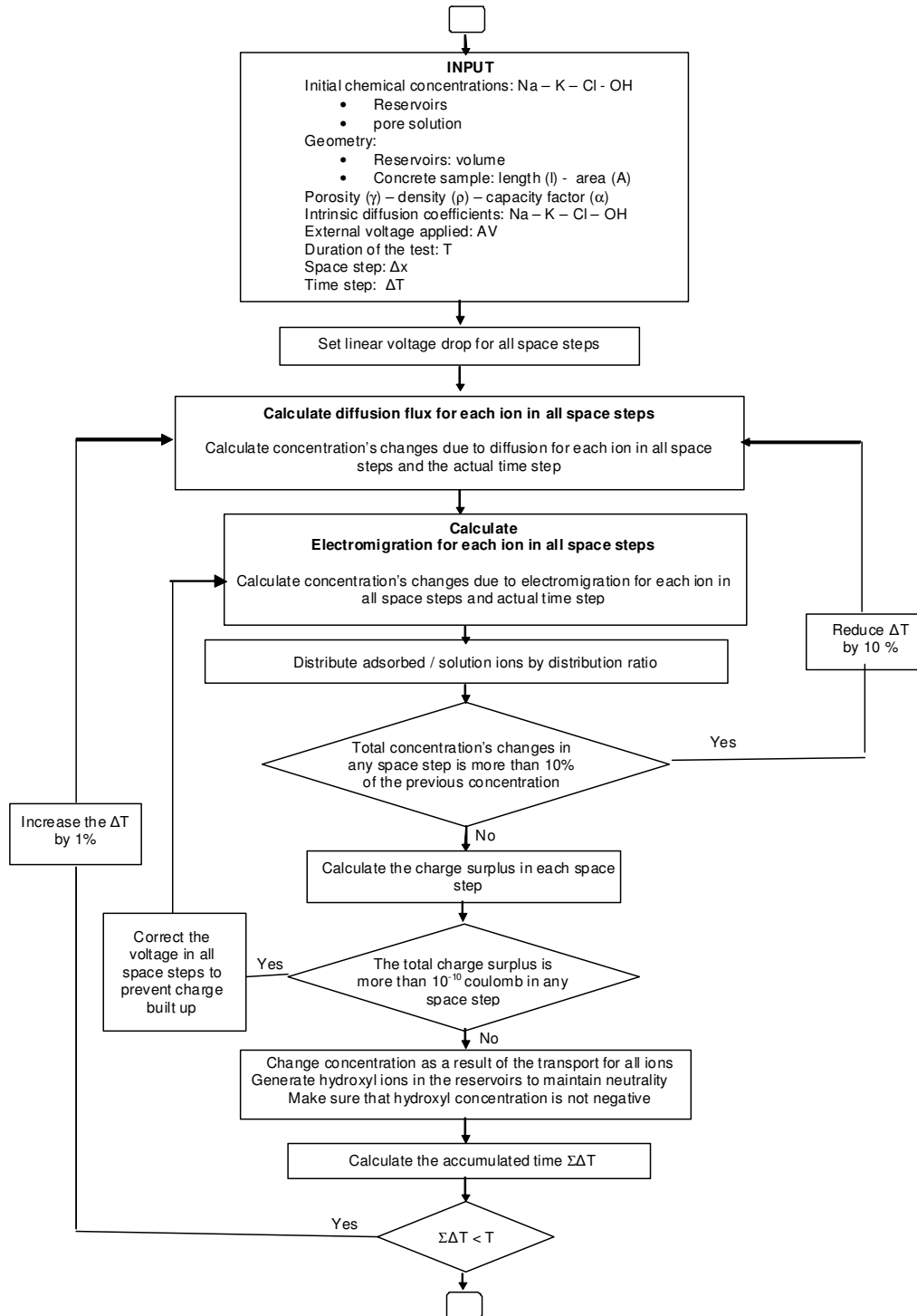
Figure 5-17 Coventry electro-diffusion computer model

5.7.4 Temperature Calculation

Conductivity of the free pore fluid increases with an increase in the temperature, and a high applied electrical potential can heat up the concrete affecting the transport properties of the sample (Mccarter, Starrs and Chrisp 2000). In a migration test, the flow of current will cause ohmic heating of the sample, a situation that is regularly observed during experiments. A detailed study of the effect of temperature on a migration tests has been carried out by Julio-Betancourt and Hooton (2004).

The rate at which a sample in a migration test loses heat is approximately proportional to the temperature difference between the sample and the room temperature. The Coventry model includes this proportionality using an experimental heat loss factor [J/K]. The thermal capacitance or heat capacity for the system sample-reservoirs is given in equation 5.36.

$$Cth = A \cdot L \cdot \rho_{con} \cdot cp_{con} + (V_{res}) \cdot \rho_w \cdot cp_w \qquad (5.36)$$

Cth is the heat capacity [J/K]; *A* and *L* are the area and length of the sample; V_{res} are the volume of reservoirs; ρ_{con} and ρ_w are the densities of concrete and water; and cp_{con} and cp_w are the specific heat capacities (measured in J/(kg·K) at constant pressure). For any time step the increase of temperature is due to the temperature generate by the sample (Joule effect) minus the heat lost (equation 5.37).

$$\Delta T^t = \frac{Ch^t \cdot AV}{Cth} - \frac{(T^t - RTP) \cdot F_{HL}}{Cth} \qquad (5.37)$$

ΔT^t is the temperature increment for the time step t [K]; Ch^t is the total charge carried in that time step [C]; *AV* is the external applied voltage [V]; T^t is the actual temperature [K]; *RTP* is the room temperature [K]; and F_{HL} is the heat loss factor [J/K]

5.8   CONCLUSIONS

20. In this chapter, the principal equations applicable to chloride penetration in concrete were discussed. Fick's laws and the Nernst-Planck and Nernst-Einstein equations were presented; however, more emphasis was dedicated to the Nernst-Planck equation which is the theoretical basis of the model selected as a tool during this research. It was concluded from the literature

survey carried out that Nernst-Planck equation coupled with the Kirchoff's Law establishes the physical conditions as ions move through porous media.

21. Since ions are charge particles, Fick's Laws do not provide a complete description of diffusion (migration). If the Nernst-Planck equation takes account of the interaction of chlorides with other species, it is necessary to establish a multi-species system to simulate the phenomenon.

22. As chlorides are accompanied by other ions, the more important aspects of the pore solution were summarised. The principal species present in the pore solution are OH^-, Na^+, and K^+, and the concentration of each one depends on many factors, such as the cement type and concentration, the presence of mineral and chemical admixtures, the age, curing conditions, and the water to binder ratio.

23. An important aspect of ionic transport is the interaction between ions and the solid phase. Some of the free ions are caught and adsorb on the cement matrix in complex and not well understood physical and chemical reactions. For chlorides the most frequent relationships between free and bound ions are presented in this chapter as isotherms.

24. From the review carried out, it is concluded that there is a lack of research on the topic of adsorption of metal alkalis and hydroxides.

25. According to equation 5.20 the voltage drop in a migration test is not linear. This non-linearity is due to the membrane potential resulting from the differences in mobility of the species involved in the test. This can be modelled with equation 5.23 or numerically with the Coventry electro-diffusion model.

26. The Coventry model was written to simulate a RCPT migration test and gives the ionic concentration, the total and partial currents, the membrane potential and the transient temperature during a simulated migration experiment.

6 DEFINITION OF VOLTAGE AND CURRENT CONTROL APPROACHES AND EXPERIMENTAL METHODS

In this chapter two ideal physical states that define the possible conditions under which chlorides will move through concrete are presented. Those conditions were developed in this thesis with the aim of contributing to a better understanding of the chloride penetration in concrete. Additionally, this chapter reports on the experimental methods used in this research to investigate the phenomenon of penetration of chlorides in cement- based materials.

6.1 INTRODUCTION

Named as voltage control and current control, these conditions make reference to the way as the electro-diffusion experiments are setup and are defined by the external electrical conditions of the concrete subjected to an environment containing chlorides. The electrochemical tests developed to obtain the voltage and current control conditions, and a new experiment to measure the voltage drop during any migration test are presented in this section. Additionally, the procedures for the characterization of the basic properties (compressive strength and open porosity), the procedures to measure the resistivity, and the methodology to measure the chloride concentration and penetration are summarized.

6.2 VOLTAGE AND CURRENT CONTROL APPROACHES

The first condition called "voltage control" is defined by a concrete sample placed between two electrodes that apply a constant potential difference between them. Under this condition a migration test like the ASTM C1202 or NT-492 can be simulated. The flow of any species present in the pore solution or in any external cells is defined according to the Nernst-Planck equation and simulated numerically according to the Coventry electro-diffusion model presented in section 5.7.

The second condition is called "current control"; it makes reference to a condition similar to voltage control, but the sample between two electrodes is subject to constant electrical current. For this condition, when the current is zero, the phenomenon of normal diffusion with no applied potential can be simulated. It is of note that when chloride ions are permitted to diffuse through concrete the system acts like a dry-cell battery and a voltage is developed. Some previous authors have

modelled chloride diffusion by simply integrating Fick's Law and using a diffusion coefficient for chloride ions. The true situation in normal diffusion is, however, far more complex because the voltage that is developed will inhibit further transport unless it is dissipated by further ionic transport. This further transport may be negative ions (such as OH-) moving in the opposite direction to the Cl- or positive ions (such as Na+) moving with them and may be the determining factor for the rate of transport of the Cl-. This cannot be modelled with a voltage control algorithm set to zero applied voltage because this implies that the two ends of the sample are short-circuited. Figure 6.1 shows this condition for a typical sample in an ASTM C1202 test and it may be seen that current flows (Lizarazo-Marriaga and Claisse 2009). Thus a new algorithm is presented in section 9 in which the system is controlled by a constant current.

If the new algorithm is used with a non-zero current the phenomena of either cathodic protection or electrochemical chloride removal can be modelled. For this condition the physical equations used are the same used previously; however, in this approach, in addition to keeping the charge neutrality throughout the sample at all times for all the ions together, it is necessary to keep the current density constant during whole duration of the test. That new condition makes the procedure to calculate the membrane potential slightly different from the one presented previously. This is discussed in section 9.5.1. Figure 6.1 shows a schematic representation of the electrical conditions.
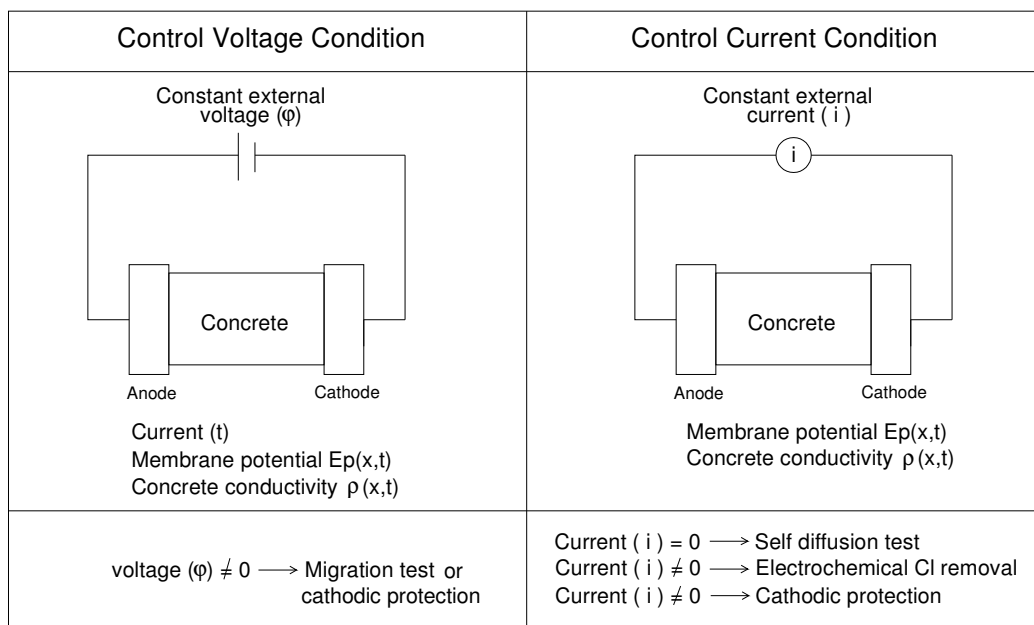
Figure 6-1 Electrical voltage and current conditions proposed

6.3   CHLORIDE MIGRTION TESTS

6.3.1 Equipment setup

The test setup used for measuring the profile of electrical properties (voltage or current) during a migration test was implemented as part of this research project, and was assembled at Coventry University. All the measurements were logged by a data acquisition device. The main part of the setup was a data logger with an analogue input resolution of 12-bits (0-2.4 V SE or +/- 2.4 V Diff) and 16 analogue inputs available. This device was accompanied by data logging software used to collect the information from the tests. A programmable DC power supply was used, capable of holding either constant voltage or constant current between 0–70 V over the entire range of currents between 0 and 3 amps. Figure 6.2 shows the equipment used.

Figure 6-2 Migration tests experimental setup used

The chamber cells or external reservoirs were made of Polymethyl methacrylate (PMMA). The design used is shown in figures 6.3a and 6.3b. The volume of each chamber assembled with the concrete sample ready for the tests was about 200ml. Each cell had two vertical holes, a small one to make the electrical connections to the electrode and a large one to facilitate release the gases generated during the test and to take measurements of the temperature into the solutions. The apparatus met the requirements of ASTM C1202.
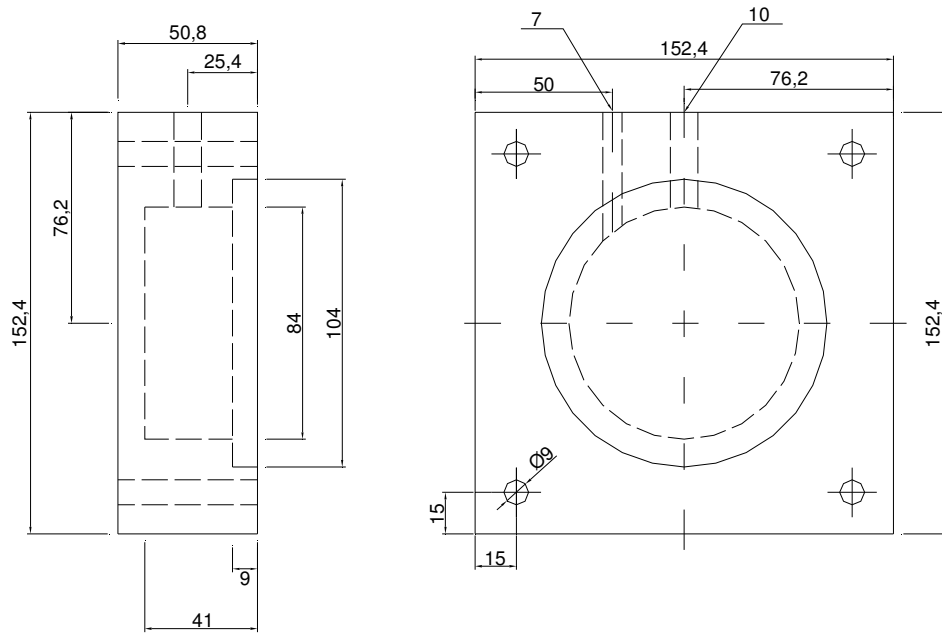
Figure 6-3a Drawing of the cell used
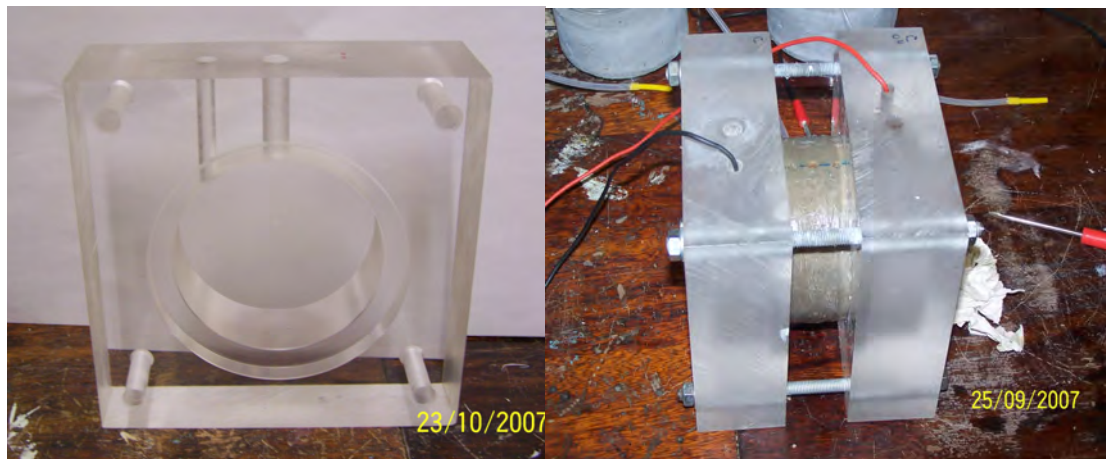
Figure 6.3b Cell isolated and cell assembled with a concrete sample

The logging of the data from the tests was carried out with the software for data acquisition that was supplied with the data logger. Figure 6.4 shows a screen of the software used to collect the data. The figure on the upper-left shows the transient current across a sample, on the lower-left it shows the transient temperature on the anode solution, and on the right it shows the variation of the voltage into the sample.

131
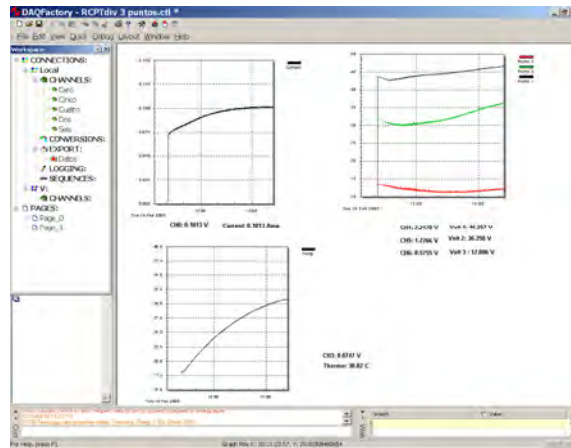
Figure 6-4 Software used to collect the data

6.3.2 Voltage control migration tests

During the voltage control migration tests a steady external voltage was applied and the transient current across the sample was measured taking the difference of potential through a small resistor wired in series with the sample. Due to Kirchoff's law, the current through the concrete sample and the resistor should be the same; consequently, the data logger measures the voltage directly through the shunt, which is converted to current using Ohm's Law. In order to get a reliable measure of current a 0.1 Ω resistor was used, with low tolerance ($\pm$0.1 %) and care was taken to establish very low resistance connections. The electric diagram used is shown in figure 6.5.
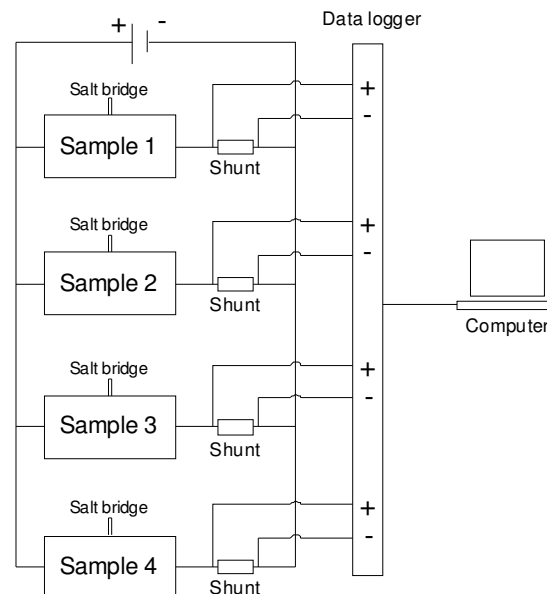
Figure 6-5 Electric diagram used during the voltage control tests

6.3.3 Membrane potential tests

The nonlinear behaviour of the electrical field during migration tests has been recently reported by some researchers: Lorente *et al.* (2007), Truc, Olliviera and Nilsson (2000), Narsilio, Li, Pivonka *et al.* (2007), Khitab, Lorente and Ollivier (2005), and Krabbenhoft and Krabbenhoft (2008); however, no complete experimental evidence has been published yet. With the aim of understanding the voltage dropping in a migration test and in order to investigate the influence of the non-linear membrane potential in the diffusion of ionic species, a new electrochemical experiment has been developed.

The arrangement developed in this research to experimentally measure the membrane potential in a migration test was based on the migration system presented in section 6.3.2; however, salt bridges were added in the concrete to check the voltage distribution across the sample (Fig. 6.6).
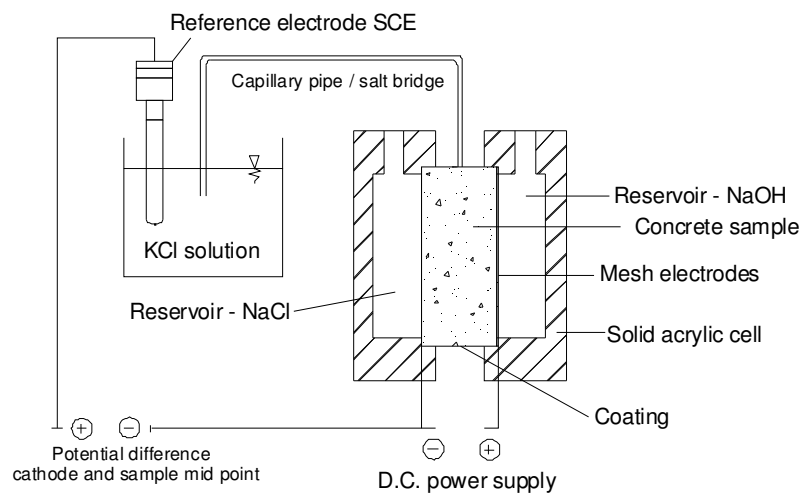
Figure 6-6 Drawing of the salt bridge used to measure the membrane potential

4-mm diameter holes were drilled in each sample 5–8mm deep. The salt bridge pipes were 4.5 mm diameter and were inserted into each hole. The salt bridges used a solution of 0.1M of potassium chloride (KCl) because both ions in it have similar mobility so no significant voltage would be set up at the interface of the salt solution and the concrete pore solution. In research by Zhang and Buenfeld (1997) and Zhang, Li and Buenfeld (2002) the membrane potential across OPC mortar specimens was measured. For this, reference electrodes and salt bridges in the external cells were used. They found that for different simulated pore solutions the total junction potentials formed between the measurement devices and the simulated

pore solution were in the range −0.8 to −6 mV. Those values were relatively low compared with the membrane potential measured during the migration tests, so, the liquid junction potential formed between the salt bridge and the pore solution concrete sample was not taken account in this test.

The voltage was measured relative to the cathode using a saturated calomel electrode (SCE) connected to the salt bridge. Due to the high voltage values found it was necessary to use a voltage divider in order to keep the readings within the range of operation of the data logger (0 − 2.44 V). Initially, a voltage divider was designed to create an output signal proportional to any input according to equation 6.1 (Witte 2002). This equation shows the relationship between $R1$ and $R2$ (resistors shown in figure 6.7), and V_{out} and V_{in} (output and input voltages).

$$V_{out} = \frac{R_2}{R_1 + R_2} V_{in}$$
(6.1)
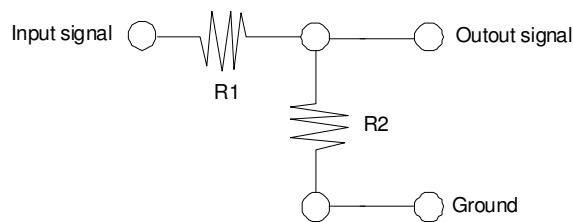
Figure 6-7 Initial voltage divider used to follow the membrane potential

Due to the load of the signal very high input impedance was required in order to ensure that the measuring process did not change the voltage readings. The internal resistance of the data logger had to be significantly greater than the resistance of the concrete during the test, because, when measuring voltages, the resistance of the equipment itself has an effect on the voltage of the circuit. To achieve the required analog input performance of the data logger, the initial voltage divider was followed by an operational amplifier configured as a voltage follower. Figure 6.8 shows the final configuration of the divider used.
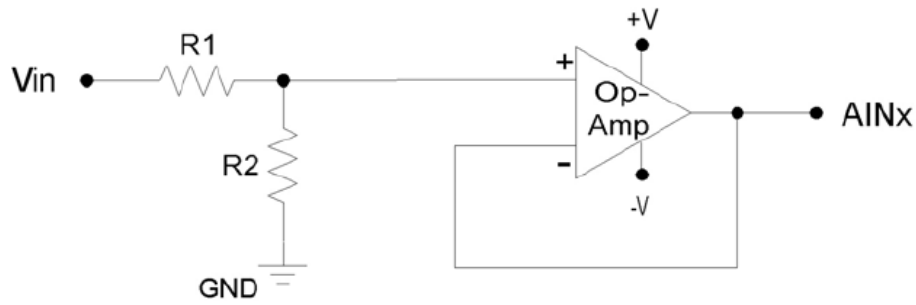
Figure 6-8 Final operational amplifier circuit used to follow the membrane potential

For each test, the current across the concrete and the voltage at different points in the sample was measured continuously. The tests were carried out in a temperature-controlled room at 21±2 ◦C, and temperature was measured continuously in the anodic reservoir. Fig. 6.9 shows a cell with three salt bridges.
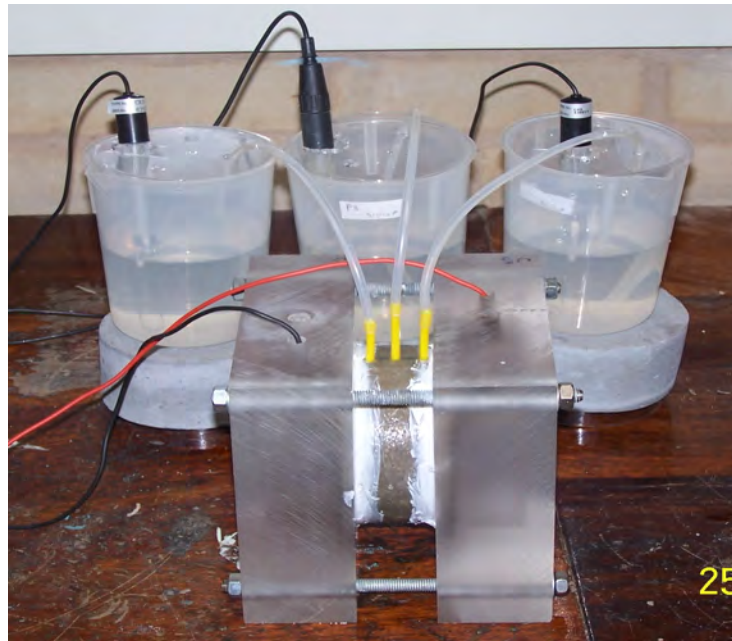
Figure 6-9 Cell assembled using three salt bridges

6.3.4 Current control migration tests

In the tests done under this condition, the current was set to a specific value different from zero and kept constant throughout the test. As a result, the voltage between the electrodes changed continuously. Taking into account that the values of voltage were higher than the range of operation of the data logger (0 – 2.44 V), it was necessary to use the voltage divider shown in figure 6.8. A diagram of the electrical configuration for this experiment is shown in figure 6.10.
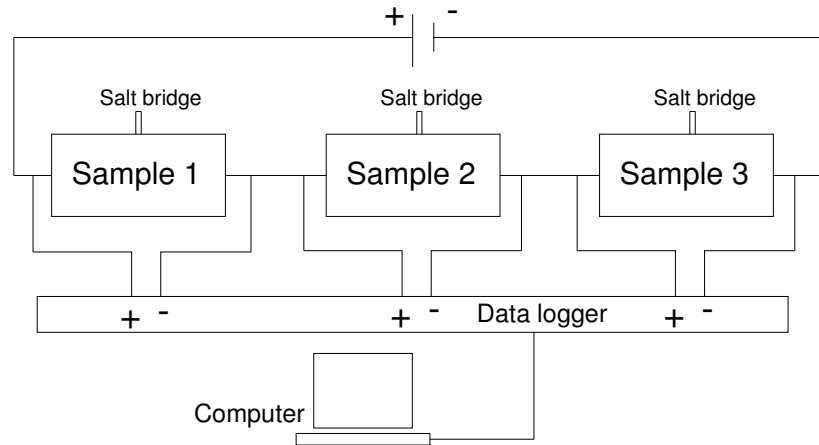
Figure 6-10 Experimental current control (non-zero) electrical diagram used

6.3.5 Behaviour of the electrodes

In order to distribute the current uniformly over the sample, copper meshes were used as electrodes. The diameter of the meshes was the same size as diameter of the the concrete specimens and they were welded to a brass ring as specified in ASTM C1202. In addition to the ionic reactions that occur across the concrete sample, during a migration test there are some electrochemical processes in the reservoir cells that it is important to point out. Evolution of gases and metal dissolution are the main processes and they were summarised by Andrade (1993).

The evolution of gases is due to the electrolysis of water. This reaction is in both anodic and cathodic cells, and generates O_2 an H_2. A small amount of bubbling was observed in the cells during some tests and the amount of gas liberated depended on the charge passed through the sample. The principal reactions in a migration test with the same solutions used in the ASTM C1202 are presented below.

$$\text{Anode: } 2H_2O \rightarrow 2O_2 + 4H^+ + 4e^- \qquad (6.2)$$
$$\text{Cathode: } 2H_2O + 4e^- \rightarrow H_2 + 2OH^- \qquad (6.3)$$
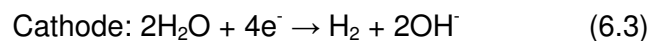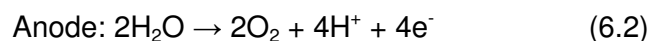
It has been reported by Prince, Perami and Espagne (1999) that the pH decreases in the anodic cell because some of the hydroxide ions migrate toward the anode, where they are oxidise, figure 6.11. In contrast, in the cathodic cell the pH increases as can be seen in figure 6.12.

$$\text{Anode: } 2OH^- \rightarrow \tfrac{1}{2}O_2 + H_2O + 2e^- \qquad (6.4)$$
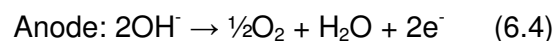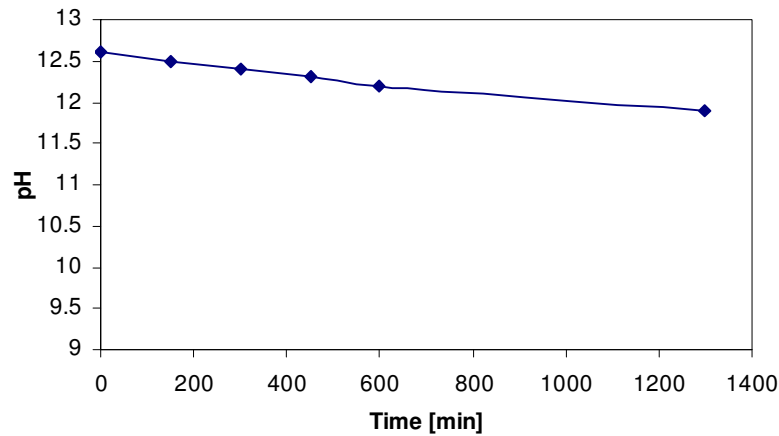
Figure 6-11 pH evolution in the anode during a standard RCPT migration test (Prince, Perami and Espagne 1999)
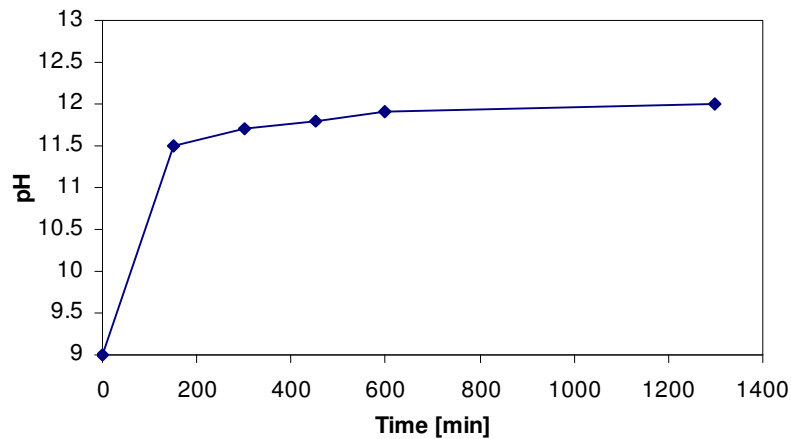
Figure 6-12 pH evolution in the cathode a standard RCPT migration test (Prince, Perami and Espagne 1999)

When the test conditions are extremely hard there can be in addition to electrolysis, oxidation of the chloride ions in the anode cells to produce chlorine (Cl_2) evolution. Under a high pH solution chlorine reacts rapidly with hydroxides to form hypochlorite and chloride as is shown in equations 6.5 and 6.6.

$$\text{Anode: } 2Cl^- \rightarrow Cl_2 + 2e^- \qquad (6.5)$$
$$\text{Anode: } Cl_2 + OH^- \rightarrow Cl^- + ClO^- + H_2O \qquad (6.6)$$
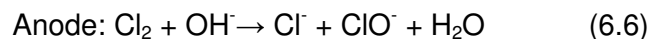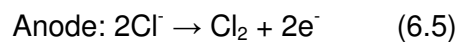
It is stated by Prince, Perami and Espagne (1999) that the hypochloride ions are unstable for two reasons: (a) the hypochloride ions can be broken by light and temperature, releasing oxygen and chloride, and (b) in acidic conditions during the electrolysis hypochloride reacts with chloride and gives chlorine. In the same way, It is advised by Prince, Perami and Espagne (1999) that care should be taken when

the amount of chlorides in the anodic cell is measured because the amount of Cl⁻ measured by potentiometric titration can be different from the amount of chlorides emerged from the concrete sample during the test.

$$\text{Cathode: } 2O_2 + H_2O + 4e^- \rightarrow 4OH^- \quad (6.7)$$
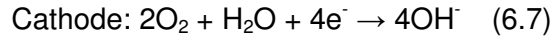
The evolution of the conductivity of the solutions of the cells during a ASTM C1202 test is shown in figure 6.13. In the cathodic solution the conductivity increases during the test due to the release of hydroxide ions by electrolysis and due to the arrival of other ions from the concrete sample. On the anode, it decreases because of the important consumption of hydroxide ions.
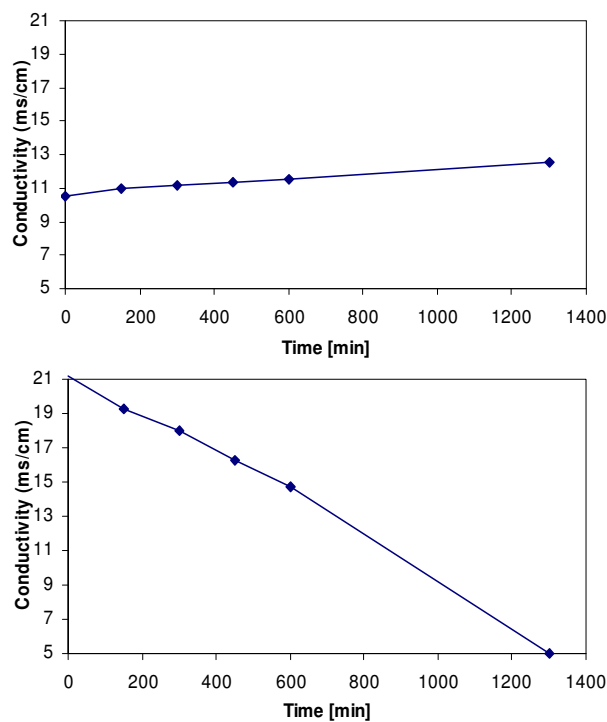
Figure 6-13 Evolution of the conductivity during a standard ASTM C1202 migration test, up: cathode / down: anode (Prince, Perami and Espagne 1999)

Corrosion of the copper metallic electrodes is another important reaction present in a migration test; it happens especially in the anode and depends on the amount of charge carried during the experiment. Figure 6.14 shows some copper electrodes. In the middle a new copper mesh is shown and on the left and right the final condition of the electrodes after an extremely strong test is shown. The cathodic electrode (left) turned black, showing little evidence of deterioration. In contrast, the anode electrode presents a significant deterioration with a green colour, typical of the copper corrosion.

Figure 6-14 Cupper electrodes used in migration tests; Left: cathode - centre: new mesh - right: anode

As the electrical potential gradient across the sample was applied from the power supply by copper electrodes into the cell solutions, there was a potential drop between the electrodes and the surface of the concrete. This was reported by Mcgrath and Hooton (1996), who carried out some experiments to investigate this potential drop. In order to determine the relationship between the difference of voltage applied in the copper electrodes and the difference of voltage across the concrete sample for the setup used in this research, an experiment was carried out using two reference electrodes put into the same electrolyte solution of the cells, one in the cathodic cell and the other one in the anodic cell. The reading of voltage for the electrodes (V_{ap}) was taken and plotted in figure 6.15 against the voltage delivered by the power supply (V_{ps}). Using linear regression this relationship was found. For this, the correlation coefficient R^2 was 0.9998.
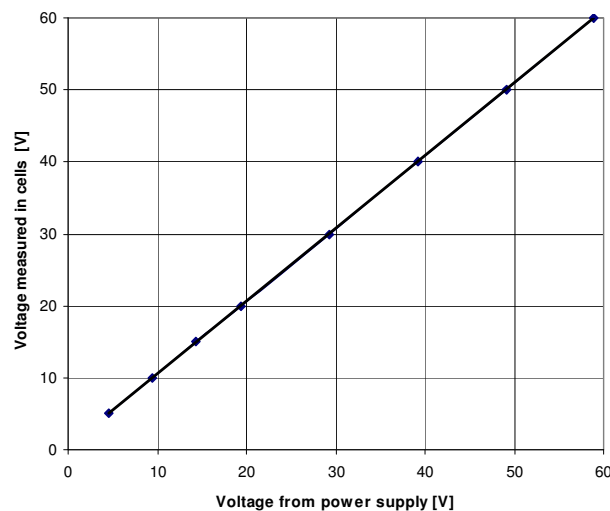
Figure 6-15 Relationship between the voltage applied by the power supply vs. the voltage measured in the cells during a migration test

$$V_{ap} = 0.9885 * V_{ps} - 0.4106 \quad \text{(6.8)}$$

6.3.6 Sample preparation

As numerous migration tests were carried out at different stages during the research, the specific conditions of concrete curing for each group of tests will be discussed later for each particular case. However, in all cases, the cylinders cast (100 mm diameter and 200 mm high) were reduced to a specific thickness with a special cutting machine for concrete samples with a tolerance of ±1.5 mm (figure 6.16). The specimens were taken from the middle part of the cylinder.

Figure 6-16 Machine used to cut concrete discs to be used in migration tests or porosity

Before any migration test, the samples were fully saturated with distilled water and the curved surface edges of all specimens were coated with a silicone impermeable coating. The procedure followed to guarantee the first condition was taken from the standard ASTM C1202 and it is summarized below. Figure 6.17 shows the equipment used to saturate the samples.

- Prior to saturation the distilled water was vigorously boiled to remove the air.
- The specimen already surface coated was placed in a vacuum desiccator and the air vacuumed for 2 h.
- With the vacuum pump still running, sufficient distilled water was drained into the desiccator to cover the specimen.
- The vacuum pump was allowed to run for one additional hour.
- After the vacuum saturation the specimen was soaked under water for 18 hours.

140

Figure 6-17 Vacuum pump and desiccator used to saturate concrete specimens

6.4   COMPRESSIVE STRENGTH

The compressive strength for paste or mortar samples was obtained with the procedure summarized in section 3.2.2.3. For concrete the recommendations of the European Standard EN 12390-3:2001: "Testing hardened concrete, Part 3: Compressive strength of test specimens" were followed. All the concrete specimens were cubic and had 100 mm size. Concrete tests were done in an Avery Denison machine coupled with a servo-controller and data acquisition unit powered hydraulically. The loading rate for the tests was set to 5 KN/S. The compressive strength is given by the equation:

$$f_c = \frac{F}{A_c}$$

(6.9)

Where f_c is the compressive strength, in Mega-Pascal (Newton per square millimetre), F is the maximum load at failure, in Newton, and A_c is the cross-sectional area of the specimen on which the compressive force acts. Figure 6.18 shows the test machine used.

Figure 6-18 Cube crusher used to measure the compressive strength

6.5   OPEN POROSITY

The open porosity accessible by water (P) was measured using the simple method of water displacement. The central part of a cylinder (30 mm thickness) was vacuum saturated until constant weight and weighed in water (W_w) and air (W_a). It was then dried in an oven at 105°C until constant weight and weighed again (W_d). The porosity was found with equation 6.10. Three replicates were tested for each mix.

$$P = \frac{W_a - W_{od}}{W_a - W_w} \qquad (6.10)$$

6.6   RESISTIVITY

There is an agreement in the engineering community about the physical meaning of the Rapid Chloride Permeability Test (ASTM C1202). It is accepted that in the way as the test has been proposed it cannot give precise and exact information about the permeability of chlorides of concrete (Andrade 1993). In contrast, the results of the test are strongly correlated with the electrical conductivity of the material. Different researchers have proposed measuring the initial conductivity either from the initial value of the RCPT (Feldman *et al.* 1994, Feldman, Prudencio and Chan 1999) or from the reading at 1 min (Julio-Betancourt and Hooton 2004). In a research developed for the Virginia Transportation Research Council (Lane 2005), the correlation was established between the electrical conductivity and the RCPT results for a large amount of data (>800 samples). Figure 6.19 shows the relationship between the charge at 6 hours and the conductivity measured at 10 min. In the figure, the 95% confidence limits and the limits of ranking charge according to the standard are shown.
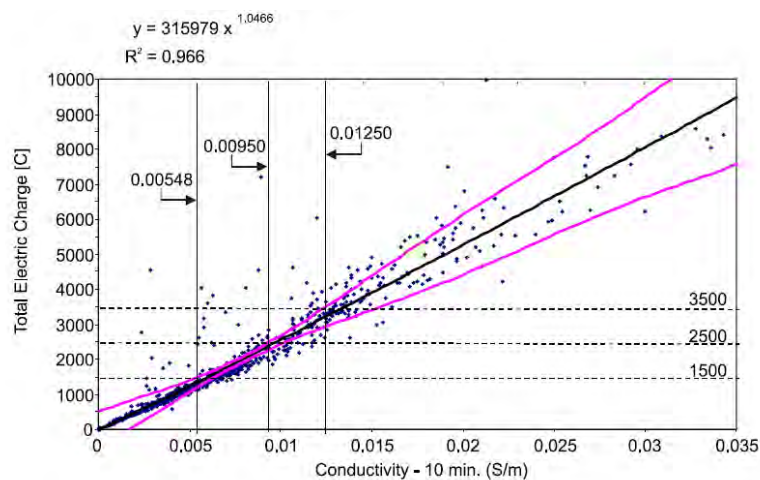
Figure 6-19 Relationship charge passed (RCPT) and electrical conductivity (Lane 2005)

Although there are no doubts about the good correlation between the charge measured in the RCPT and its initial conductivity, there is a lack of understanding of the physical and chemical phenomena in a migration test or rapid conductivity test. It is known that the electrical properties of concrete are transient in space and time during the test due to the mobility of the different ions, and it is accepted that although chlorides are the main concern, they cannot be investigated isolated of all the ions involved. The conductivity σ of a water solution containing different ions can be expressed as

$$\sigma = \sigma_{water} + \sum C_i (\lambda_{i,0} - A\sqrt{C_i})/1000$$ (6.11) (Shi, Stegemann and Caldwell 1998)

σ_{water} is the specific conductivity of water, C_i the equivalent concentration of the ion i, $\lambda_{i,o}$ is the equivalent conductivity at infinite dilution, and A_i is a experimental constant. Table 6.1 shows the values of $\lambda_{i,o}$ for some ions (Shi, Stegemann and Caldwell 1998).

Ion	Na^+	K^+	OH^-	Cl^-	Ca^{2+}	$SO4^{2-}$
equivalent conductivity $\lambda_{i,o}$ [m2equiv^{-1}ohm^{-1}]	0.00501	0.00735	0.0198	0.00763	0.00595	0.00798

Table 6-1 Equivalent conductivity at infinite concentration for various ionic species

In a research carried out by Tong and Gjorv (2001), they measured the current and the conductivity during a migration test. The conductivity was calculated from the electrical resistance measured under 1-KHz frequency. For samples of 6 months old they found that the conductivity was first reduced until the chlorides reach the anode cell. Later on, the conductivity started to increase. In the same way, Feldman *et al.* (1994) found important changes in the resistivity during the experiment for a RCPT test.

One of the effects that a transient non-linear electric field produces inside a sample is the variation of the conductivity for any time and position. If it is supposed that Ohm's Law is valid during the test, it is possible to determine the resistivity (ρ), and consequently, the conductivity σ of the sample. The electrical conductivity is defined as the inverse of the electrical resistivity and is defined using equations 6.12 and 6.13.

$$\rho = \frac{1}{\sigma} = \frac{RA}{L} = \frac{E_{ij}}{i} \frac{A}{L}$$

(6.12)

$$\sigma(t) = \frac{i(t)}{E_{ij}(t,x)} \frac{L_{ij}}{A}$$

(6.13)

Where σ is conductivity [S-m^{-1}], ρ is the electrical resistivity [Ω-m], R is the electrical resistance [Ω], i is the electrical current [A], E_{ij} is the electrical potential difference between the point i and j [V], L_{ij} is the distance between the point i and j [m], and A is the transversal area of the sample [m^2].

In electrolytic materials such as concrete, the measurement of resistivity with direct current (D.C.) causes current flow resulting in ion migration and polarization. In order to avoid those effects, alternating current (A.C.) is used. The measurement of the resistivity of concrete with AC has been reported extensively in the literature (Whiting and Nagi 2003, Wilsont, Whittington and Fordes 1983, Polder 2001, Polder *et al.* 2000), usually with a sinusoidal current and a frequency between 50 and 2000 Hz.

During the experimental program developed in this research, in addition to the D.C. resistivity (or conductivity) taken from the migration test, the A.C. resistivity was measured using an electrical A.C. signal generator (Figure 6.20) and a calibrated resistance. The electrodes used were the same cells employed during the migration test including the same solutions of the reservoirs. The voltage used was between 6 and 8 Volts.

Figure 6-20 A.C. Signal generator used to measure resistivity

In this research the resistivity tests carried out consisted of two probes or electrodes; however, there are alternative tests like the four-probe method (Wenner test), which is widely used for field measurements. Although there is a direct correlation between the two and four-probe techniques, it has been stated by Whiting and Nagi (2003)

that there are several factors which influence the resistivity measurement when the four-probe technique is used, such as the geometrical constraints, the surface contact, or the humidity content.

The influence of the frequency on the concrete's A.C. resistivity for an ordinary Portland sample is shown in the Figure 6.21-left. Initially, with an increase of the frequency the resistivity trends to go down, between 55 and 70 KHz the curve becomes stable, and for frequencies bigger than 70 KHz the resistivity starts to go up again. It is reported in the literature that values of frequency between 50 and 2000 Hz do not produce undesirable effects during the measuring, in this research a frequency of 500 Hz was selected to make all the resistivity measurements. The difference in resistivity between measurements made using 500 Hz and 50 KHz is around 11 %. In figure 6.21-right in a semi-log scale, the difference in percentage between the resistivity at any frequency (R_i) and the resistivity measured at a frequency of 500 Hz (R_{500}) is plotted. Values of resistivity measured with frequencies smaller than 5 KHz had a difference lower than 2%.
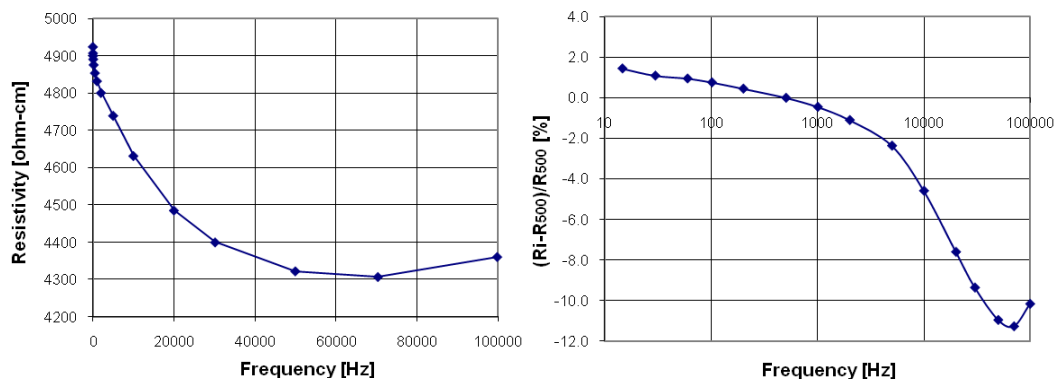
Figure 6-21 Influence of the frequency on the resistivity in OPC based samples

6.7   CURRENT CONTROL TEST (ZERO CURRENT)

Electrically this experiment corresponds to an open circuit: there is no electrical contact between both electrodes. Figure 6.22 shows a schematic representation of the circuit, where the total current through the sample is zero but the membrane potential and the concrete conductivity are not zero and are transient in time. This zero current condition makes reference to the total current of the system, and it does not imply that individual mobile species does not carry some current. The law of charge neutrality ensures that the ionic partial currents would be neutralized by themselves.
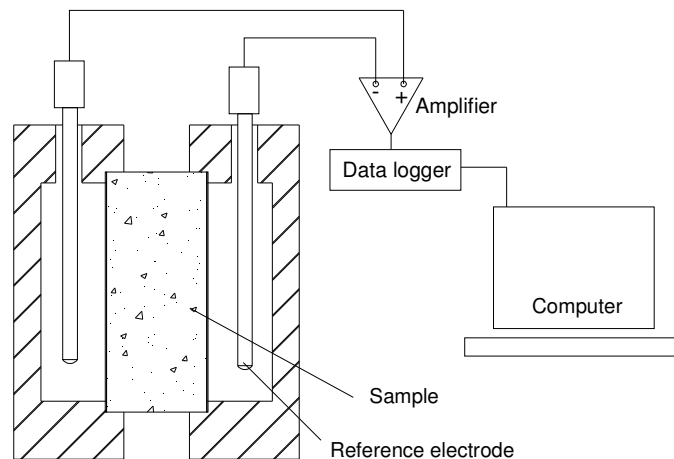
Figure 6-22 Current control test for the zero-current condition

Two identical reference electrodes were used as shown in figure 6.22 and an amplifier was used before the data-logger to buffer any current from the measuring device. The buffer impedance was 10^9 Ω. Before each test the samples were surface covered in the same way as migration tests and were vacuum saturated according to section 6.3.6. The volume of the reservoirs cells were the same shown in figure 6.3, i.e. about 200 ml, and the thickness of the samples was 10 mm.

6.8   SELF DIFFUSION CHLORIDE TESTS

Chloride immersion tests were carried out with the aim of measuring the chloride profile in the samples after a normal diffusion process. For all tests, the cylinders cast (100 mm diameter and 200 mm high) were split in two halves and the sawn surface (100 mm diameter and 100 mm high) was placed in contact with a solution of sodium chloride. To prepare the samples, the curved surface of each cylinder was covered with a silicone rubber coating in order to avoid moisture exchange and carbonation during the test. After the samples were coated, the surface that would be in contact with chlorides was placed in contact with a solution of 0.5 g/l of CaOH for one week to avoid any initial sorption effects when the chloride solution was introduced. Figure 6.23 shows the test. The external concentration of chloride was 7% NaCl prepared with distilled water and it was renewed periodically in order to conserve the boundary conditions (every two or three weeks). During the test, the solution was agitated from time to time.

At the end of the immersion period (which will be discussed later for each particular case) the concrete specimens were removed and the chloride profile and the

penetration were measured with two different techniques. The profile was obtained measuring the acid-soluble chloride profiles and the chloride penetration depth was measured using the colorimetric method (Meck and Sirivivatnanon 2003)
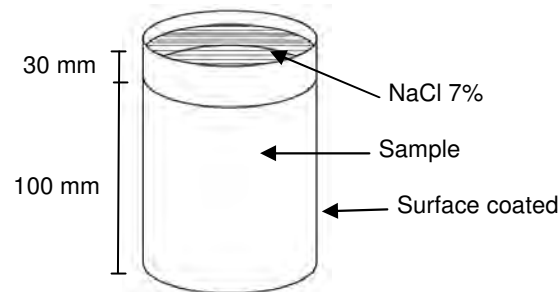
Figure 6-23 Experimental chloride self diffusion test

6.8.1 Total chloride content

The total chloride concentration was measured using the RILEM TC-178-TMC (2002) recommendation: "Analysis of total chloride content in concrete". The method uses the Volhard method of analysis (extraction and quantification) of total chloride content in hardened concrete.

In order to obtain the concentration of total chloride at different depths, the specimens were removed from the immersion test and were drilled in increasing depth intervals from the exposure surface. The powder was carefully collected and analyzed using the chemical method. Figure 6.24 shows the powder collection process. The procedures of extraction are shown in figures 6.25A and 6.25B, and the silver nitrate titration is shown in figure 6.25C.

Figure 6-24 Vertical driller used for powder collection during a concrete chloride content analysis
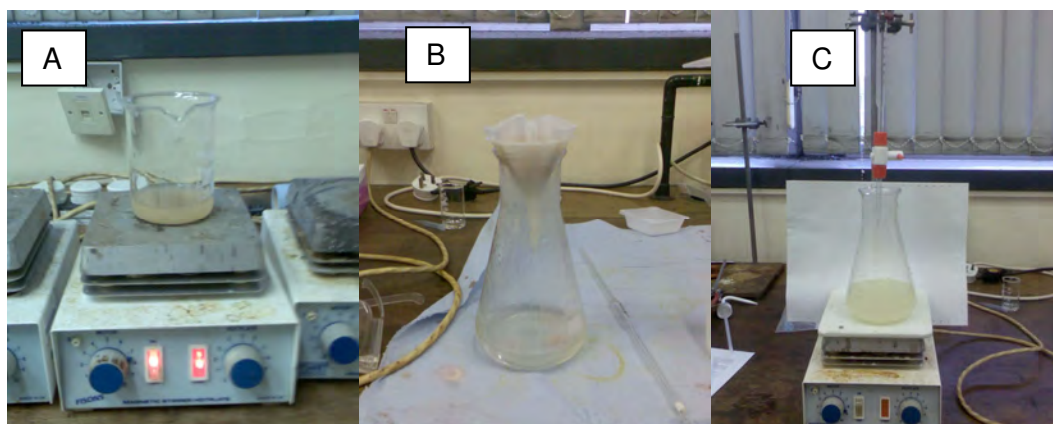
Figure 6-25 Procedure to obtain the chloride concentration according to the RILEM TC-178-TMC (2002)

6.8.2 Chloride penetration

A simple method to measure the penetration of chlorides in concrete exposed to these environments was published by Otsuki, Nagataki and Nakashita (1992) and Collepardi, Marcialis and Turriziani (1970) some time ago. The procedure known as the colorimetric method consists of spraying a solution of 1 N $AgNO_3$ on a split sample. In addition to the silver nitrate solution, there are combinations of other chemical compounds reported in the literature. For example, a combination of a 0.1 N $AgNO_3$ solution with 5% of K_2CrO_4 is known as the Maultzsch method, and the combination of 0.1 N $AgNO_3$ with fluoresceine is known as the Collepardi method (Baroghel-Bouny *et al.* 2007). In this research a solution of silver nitrate only was used, which showed the chloride contaminated area of the sample with a grey coloration, whereas the uncontaminated area presented a dark coloration. Depending of the cementitious components of the mixes evaluated the coloration was more evident in some of them, especially in those that did not include basic oxygen slag. Figure 6.26 shows a typical chloride penetration depth.

After the silver nitrate solution was sprayed a white silver chloride precipitation on the split surface was visible and the average penetration depth was obtained. The recommendation of the NTBUILT-492 was followed: "*measure with the help of a slide calliper and a suitable ruler, from the centre to both edges at intervals of 10 mm to obtain seven depths. Measure the depth to an accuracy of 0.1 mm*"
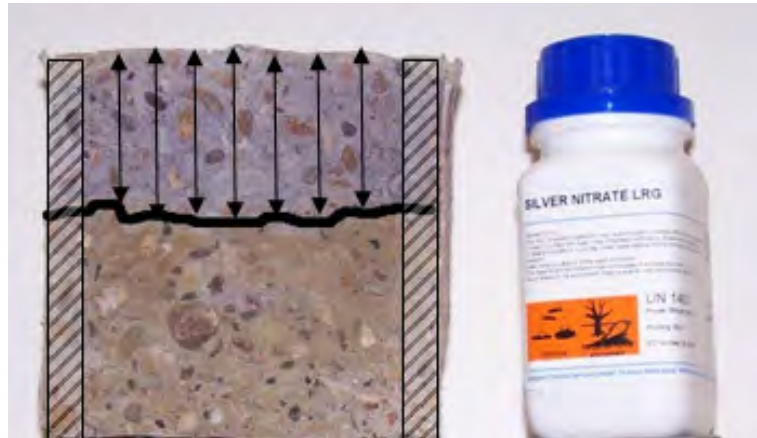
Figure 6-26 Typical chloride penetration depths after applying 0.1 N silver nitrate in a chloride contaminated concrete sample

The difference of colour in both areas is due to the reaction of the silver ions with the free chlorides to form a grey precipitate, and the reaction of silver ions with hydroxide ions form a brown precipitate. Because the boundary of those regions is a well defined line, the concentration of free chlorides in this boundary (c_d) has been studied intensively by many researchers. Big differences have been found among the values reported in the literature. That variability can be the result of the differences in the methods employed by the different researchers to evaluate the chloride penetration (x_d), the difficulties in measuring the free chloride concentration at the boundary, and the influence of other ions such as hydroxides.

Baroghel-Bouny *et al.* 2007 carried out an extensive experimental program to investigate the feasibility of using the colorimetric techniques. In that study many mixes including a broad range of mineral and chemical admixtures tested under self diffusion had an average c_d value of 0.03 ± 0.016% of free chlorides by unit mass of dry concrete, and of 0.21 ± 0.11% of free chlorides by unit mass of blended cement. The first number corresponds to the mean value and the second value corresponds to the standard deviation. In the same way, a range between 0.36 and 0.8% by unit mass of cement has been reported by Otsuki, Nagataki and Nakashita (1992). Collepardi (1996) found a value of 0.01% by unit mass of cement for the free chloride concentration. Andrade *et al.* (1999a) found values of total chlorides of 0.18 ± 0.2% by unit mass of concrete using a migration test. Finally, the standard NTBUILT-492 assumes that the concentration of free chlorides c_d at the colorimetric depth x_d (where the colour changes) is equal to 0.07 N (70 mol/m^3) for ordinary Portland cement concrete.

Experimentally the concentration of chlorides in concrete is measured as a percentage of the dry mass of concrete; however, the free chlorides can be expressed as mass per unit volume of the pore solution. It is important to notice that in order to transform the values of concentration of free chlorides stated above from percentage of dry density to mol per cubic meter it is necessary to know the density and the porosity of the concrete.

6.8.2.1   Chloride diffusion assessment with the colorimetric method

It has been shown by Baroghel-Bouny *et al.* (2007) that there is a linear relationship between the chloride penetration depth (x_d) and the square root of time. The standard diffusion process can be described with enough accuracy using only one point of the colorimetric penetration at any desired time. Using an important range of different concretes submitted to the same immersion test, Baroghel-Bouny *et al.* (2007) found a good agreement between the colorimetric method and the chloride profile, it was pointed out that the large variability of the chloride concentration in the boundary (c_d) induces only small variations in the penetration depth.

In that study (Baroghel-Bouny *et al.* 2007), it is concluded that the silver nitrate colorimetric technique gives good results when it is necessary to investigate the behaviour of a group of concretes exposed to the same external chloride concentration. It is possible to quantify, compare, and rank mixtures according to the coefficient *k* of the next equation.

$$x_d = k\sqrt{t} \qquad (6.14)$$

6.9   CONCLUSIONS

27. Voltage and current control are possible conditions proposed for an electro–diffusion test depending on the electrical circuit. These conditions, in addition to defining the experimental electrical features give the physical considerations to simulate chloride penetration in cement based materials. For each one of those conditions experiments were presented in detail.

28. The experimental methods required in this second part of the thesis have been described. They were chosen because they can be used as inputs for outputs of the model or are related with the hypothesis established in this research. The traditional tests such as open porosity, resistivity, and chloride

immersion tests have been described briefly and are documented in reference sources. In contrast, the development of the new electrochemical test proposed to measure the membrane potential has been detailed.

7 EXPERIMENTAL MEASUREMENT OF THE MEMBRANE POTENTIAL

This chapter presents the results of the experimental investigation carried out about the membrane potential on a migration test. This has the purpose to establish the guidelines and the methodology to measure the membrane potential during a migration test.

7.1 INTRODUCTION

Different approaches have been used to model the ionic penetration of chlorides through concrete. In order to understand this phenomenon, this chapter summarises an experimental investigation of the membrane potential on a migration test. To achieve this, the new test summarized in section 6.3.3 was carried out on paste and mortar samples. Results for slag blended concrete mixtures will be presented in the third part of this thesis

7.2 EXPERIMENTAL PROGRAMME

As was shown in section 6.3.5, during a migration test between the copper electrodes and the concrete sample there is a linear drop of the electrical potential at both electrodes. In the same way, across the concrete sample the electrical field is non-linear as is shown in figure 7.1; only during the initial time step at the start of the test can the electrical field be considered linear.
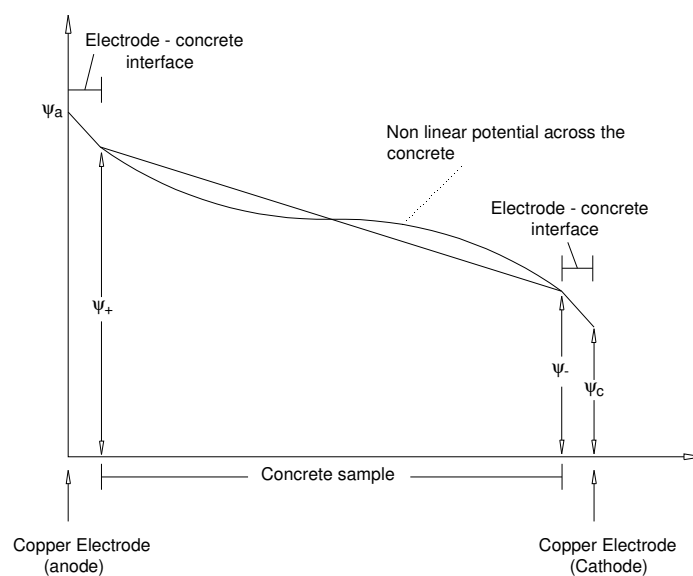
Figure 7-1 Non-linear voltage distributions in a migration test

Experimentally, the gradient or difference between the measured voltage at any time and the linear condition can be calculated. This value corresponds to the membrane potential and is calculated by subtracting the value of the voltage measured from the initial value at the start of the test for each time and position.

$$\Delta V = V_{Ti} - V_0 \qquad (7.1)$$

ΔV corresponds to the membrane potential, V_{Ti} is the voltage measured at time t, and V_0 is the voltage at the start of the test.

7.2.1 Migration tests on cement paste

This first experimental stage was proposed in order to setup and calibrate the experiment presented in sections 6.3.2 and 6.3.3. It consisted of mixes of cement paste using a Portland limestone cement CEM II/B-LL with a water binder relationship of 0.28. The specimens were cured under controlled humidity and temperature and all the voltage control migration tests were made at an age of paste samples between 28 and 35 days old. The samples were 100 mm diameter and 50 mm length and were conditioned according to 6.3.6. The test was run twice and the result shown is the average of both results. The reservoirs of the diffusion cells were filled with a 0.30 N NaOH and a 3.0% NaCl solution respectively, voltages of 15, 30 and 60 volts were kept for 16.5 hours. The current in the paste samples was monitored continuously as well as the potential difference between the mid point of the sample and the negative electrode of the system.

One of the aims of this research stage was to establish the behaviour of the electric field in a voltage control migration test, from a theoretical and experimental point of view. It was also necessary to monitor the temperature. Although the ASTM C1202 standard suggests that the temperature of the solutions should not be more than 90 °C, in order to compare the experimental results with the analytical model large gradients were not allowed in this experimental program. It is supposed that an increase in temperature will generate a change in the behaviour of each ion in the pore solution, which will raise the total current flow (Julio-Betancourt and Hooton 2004). Because of high temperatures, some changes in the physical and chemical conditions of the sample can be expected (Zhang and Gjorv 1991, Roy 1989, Mccarter, Starrs and Chrisp 2000). In addition, the electrical conductivity is sensitive to temperature; heating will result in higher measured Coulomb values.

7.2.2 Migration tests on mortar samples

It has been reported that in a concrete sample a higher cement content increases the electrical conductivity (El-Enein *et al.* 1995), and it regularly decreases on increasing the aggregate content (Princigallo, Van Breugel and Levita 2003). These effects are explained because the conductivity of the aggregate is much lower than that of the cement paste. In the same way, Wee, Suryavanshi and Tin (1999) showed that the total charge passed in a RCPT test for a higher aggregate content sample is lower compared with one of lower aggregate content. Due to the high amount of charge and temperature in the first stage for 60 volt migration tests, in a second stage mortar samples were used with the aim of decreasing the overall conductivity of the samples.

Mixes of mortar with water to cement ratio of 0.49 and 0.65 were cast. Ordinary Portland cement CEM I without mineral or chemical admixtures was used. The ratio sand to binder was 2.75 for all mixes. For each mix five cylinders of 100 mm diameter and 200 mm height were cast to be used in porosity and voltage control migration tests. In addition, three cubes of 50 mm for each mix were cast in order to know the concrete strength. Particle size analysis of the sand was carried out and is shown in figure 7.2.
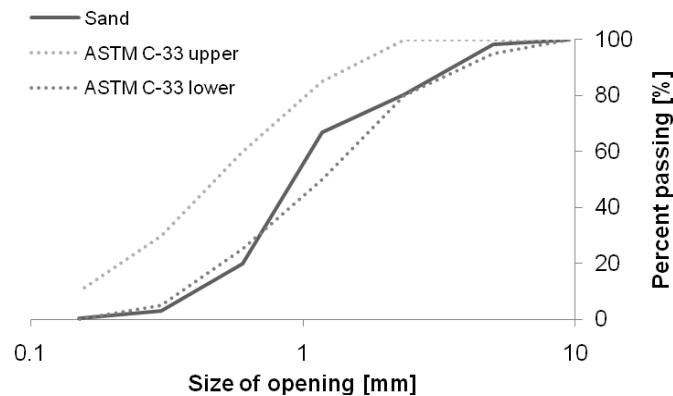
Figure 7-2 Fine aggregate size distribution and ASTM C-33 limits

The recommended ASTM C33 (2008) limits are included in figure 7.2. The curve shows that although the size of the sand is between the recommended limits, it is close to the lower limit being a coarser sand. The calculated fineness modulus was of 3.3 confirming the previous statement. The Dry density of the sand was 2660 kg/m^3. The average specific gravity for the cement used was 3.04.

The specimens were cured under controlled humidity and temperature and the mortar samples were tested at 28 days for concrete strength and open porosity. The migration tests were carried out with samples between 30 and 38 days old. Migration tests were made in mortar samples of 100 mm diameter and 50 mm length, conditioned according to 6.3.6. The concentration of sodium chloride in the cathode, the nominal external electrical potential difference applied and the water to binder ratio of the samples were different for each test according to Table 7.1. Each test was made in duplicate.

| # test | Water / binder | Δ Voltage [V] | Saturation | Concentrations | | test time [hours] |
				Anolyte (NaOH)	Catholyte (NaCl)	
1-M	0.49	60	Distilled water	0.3 N	3%	6.0
2-M	0.49	30	Distilled water	0.3 N	6%	21.6
3-M	0.49	30	Distilled water	0.3 N	3%	21.6
4-M	0.49	30	Distilled water	0.3 N	0%	21.6
5-M	0.65	30	Distilled water	0.3 N	3%	21.6
6-M	0.49	15	Distilled water	0.3 N	3%	21.6
7-M	0.65	15	Distilled water	0.3 N	3%	21.6

Table 7-1 Initial migration tests carried out on mortar samples

In addition to the electrical current the membrane potential was measured at different points. The distance between those points and the edge of the sample in contact with the negative electrode (cathode) is shown in figure 7.3. The location of the salt bridges defines four zones in the concrete sample where the conductivity can be calculated. Those zones are named as Z1, Z2, Z3 and Z4 and for each one the electric potential difference across itself was calculated.
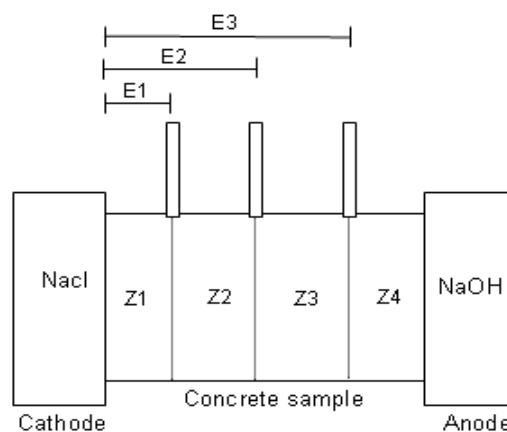
Figure 7-3 Schematic average localization of the points where the membrane potential was measured

7.3   EXPERIMENTAL OUTCOMES AND DISCUSSION

7.3.1 Tests on cement paste

The average results of the concrete strength and porosity are shown in table 7.2. The tests that ran at 15 volts did not show changes of temperature - it remained at 24 °C after 16.5 hours. The ones that ran at 30 volts showed a maximum temperature of 42 °C after 16.5 hours, and the ones that ran at 60 volts showed 100 °C after 5 hours. Because of the high temperature all the information from paste samples that ran under 60 volts was not analyzed. In the same way Shi (2004a) reported that the electric current through cement pastes of OPC is too high to complete the RCPT test (60 V). Results of the measurement of current, temperature and voltage are presented in table 7.3, and plotted in figure 7.4.

Mix	Concrete strength (28 days) [MPA]	Open porosity [%]
Paste OPC-LL	63	30.3

Table 7-2 Results of compressive strength and porosity of paste samples

Mix	Time of test [hours]	Nominal Voltage applied [V]	Initial current [mA]	Final current [mA]	Current's Change [%]	Initial Voltage Mid point [V]	Final Voltage Mid point [V]	Voltage's Change [%]	Final temperature [°C]
Paste OPC-LL	16.5	15	70.9	73.6	3.8	6.99	7.36	5.3	24
Paste OPC-LL	16.5	30	162.3	257.2	58.7	14.18	14.77	4.1	42

Table 7-3 Electrical results for paste samples

In general, results show that differences between initial (room temperature) and final temperatures and currents are greater when a higher voltage is applied. In the test run at 15 volts the Joule effect was negligible. For the test run at 30 volts, the maximum temperature reached a difference of 19 °C with respect to room temperature.
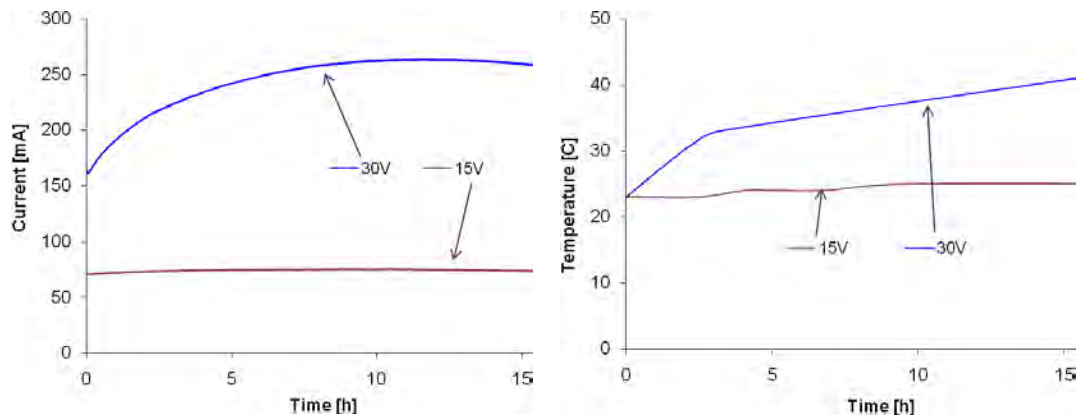
Figure 7-4 Transient current and temperature evolution for paste samples

The initial current for the test run under 30 V was 162.3 mA. There was an increase in the current for the first 12 hours, where it reached a maximum value of 260 mA. After this point, the current started to reduce; the final current at 16.5 hours was 1.59 times the initial value. In contrast, the test that ran at 15 volts shows a little variation in the total current, the initial and final values were 70.9 and 73.6 respectively, with a difference of 3.8%.

The mid-point voltage for both tests showed a rise from its initial value. However, the 30 volts test shows an initial decrease during the first 2.5 hours. Figure 7.5 (left) shows the transient voltage measured experimentally and figure 7.5 (right) shows the membrane potential change calculated from equation 7.1. For both experiments an approximate variation of 5 percent at 16.5 hours was obtained.
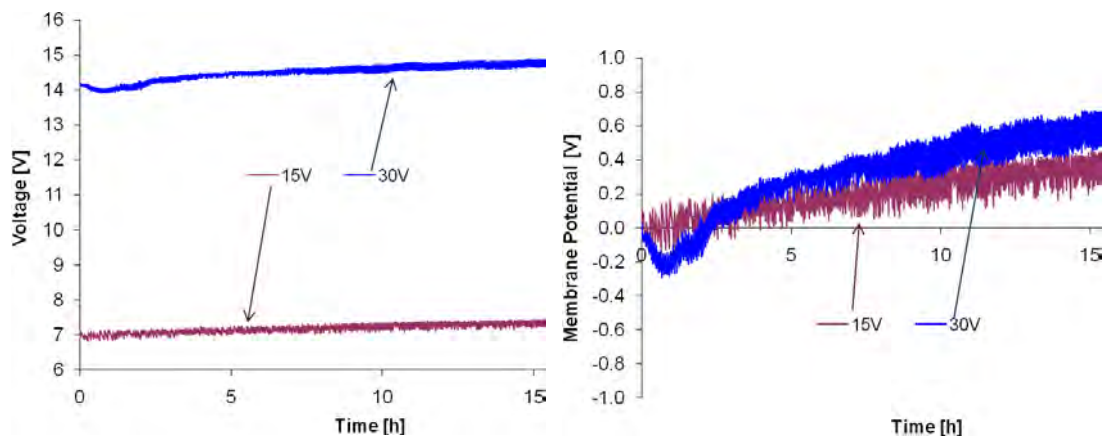
Figure 7-5 Transient voltages and membrane potential in the mid-point for paste samples

7.3.2 Tests on Mortar Samples

Results of strength and porosity are shown in table 7.4.

Mix	Concrete strength (28 days) [MPA]	Open porosity [%]
Mortar w/b=0.49	36.59	18.5
Mortar w/b=0.65	31.48	25.4

Table 7-4 Results of compressive strength and porosity for initial paste samples

It is recognized that migration tests have a significant variability. ASTM C1202-05 for instance, suggests that the results of two correctly carried out tests by the same person on samples from the same batch and the same diameter should not diverge by more than 42%. In order to confirm that the tests made are between valid ranges and the results are reliable enough to be analyzed, the maximum difference in percentage of current between two replicas of the same test was found. In table 7.5 the maximum difference in the current for each couple of samples is shown. Test 1-M does not show any difference because of the high temperature during the experiment; it was necessary to terminate it, and just one complete test was run. The results confirm that the currents for each pair are close enough to be treated as an average.

# test	Variation %
1-M	***
2-M	18.9
3-M	7.2
4-M	13.8
5-M	21.2
6-M	11.9
7-M	19.5

Table 7-5 Maximum difference of current between mortar samples of the same mix

7.3.2.1 Temperature measured in mortar tests

In addition to the variability of the test, some results can be affected by increasing the temperature. In table 7.6 the maximum values of temperature measured in the anode

solution are shown and in figure 7.6 the average transient temperature for each experiment is plotted.

# test	Δ Voltage [V]	W / b	Anode solution Max temp.[C]
1-M	60	0.49	99
2-M	30	0.49	34
3-M	30	0.49	35
4-M	30	0.49	36.5
5-M	30	0.65	38.5
6-M	15	0.49	23.5
7-M	15	0.65	24

Table 7-6 Maximum temperature measured in the anode during migration tests for initial mortar samples
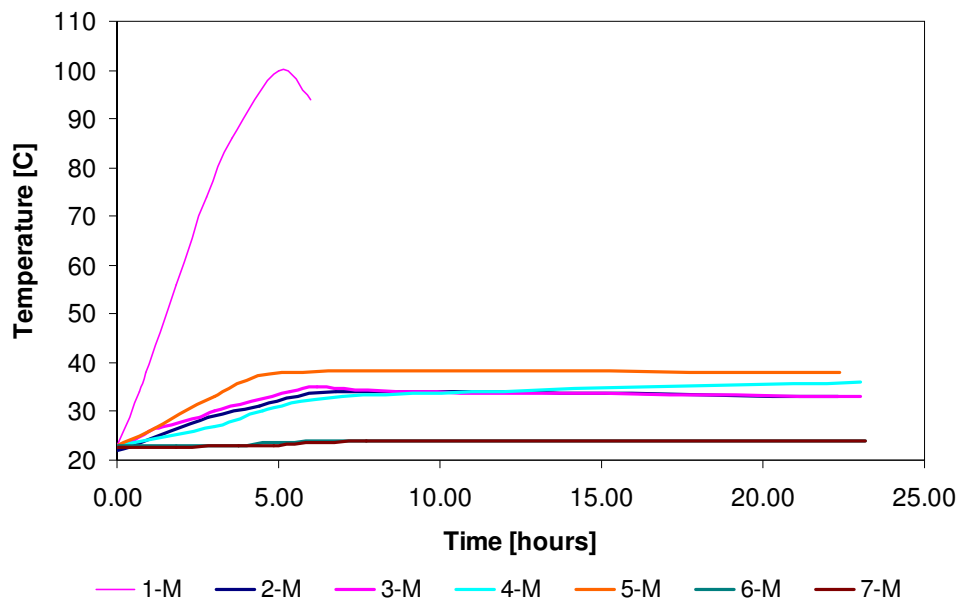
Figure 7-6 Temperature evolution measured in the anode during migration tests for initial mortar samples

The results show that the temperature for the test that ran at 60 V reached 100 °C after 5 hours. All the tests that ran at 30 V showed a similar transient increase of temperature, within a range of 34 and 39 °C. The sample of water binder ratio of 0.65 reached the highest value of this group. The tests that ran under 15 volts showed a similar increase of temperature; where there were no major differences respect the water binder ratio. For the mortar samples measured the increase of temperature was more dependant of the external voltage applied than the water binder ratio of the

material, and the relationships between temperature, external voltage, and water binder ratio are not linear.

It was found that around 5 hours after the initiation of the experiment all the samples reached at least the 90% of the maximum temperature, regardless of the solutions used in the reservoirs or the voltage applied. With the aim of estimating the influence of the voltage on the temperature, the values of external voltage vs. temperature at 5 hours for tests 1-M, 3-M and 6-M that correspond to the mortar samples with water binder ratio of 0.49 and the same solutions in the reservoirs are plotted in figure 7.7. In addition, a general equation was found using commercial curve fitting software.

$$T = 13.45e^{-0.0468V} + 9.587e^{0.0.894V}$$ (7.2)

T is the temperature in the anode solution [°C] and V is the external nominal voltage applied [V]. This equation is valid only for the mix tested and can not be generalized to all concrete or mortar mixes; however, it proves that the relationship between the voltage applied and the maximum temperature behaves in a non-linear way. In chapter 9 the relationship between voltage and temperature will be simulated and discussed according to the Coventry model results.
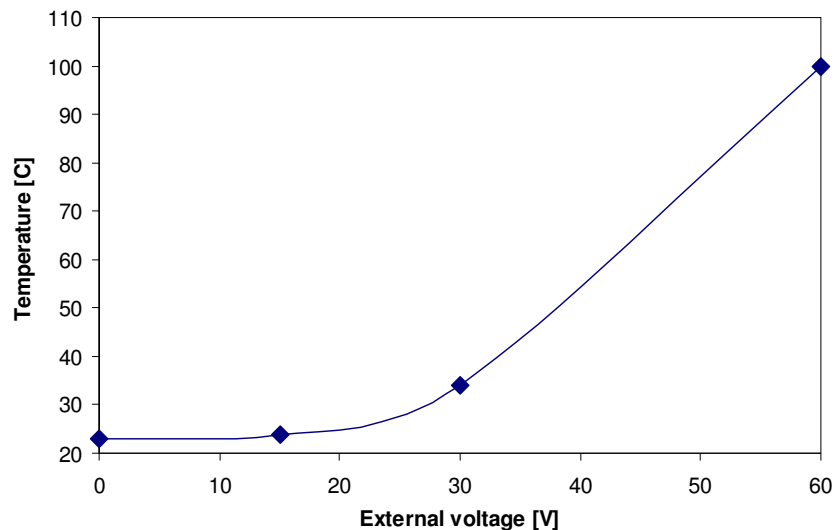
Figure 7-7 Relationship between the maximum temperature measured in the anodic cell and the external voltage applied in mortar samples

In a previous work, Julio-Betancourt and Hooton (2004) proposed a general experimental equation to account the Joule effect in an ASTM C1202-RCPT test.

This equation gives the corrected total charge value of a concrete specimen as if the temperature during the experiment were kept constant at 23±2 °C. It is known that the total charge increases with increasing the temperature, and according to Betancourt's equation, in a RCPT test a gradient of 14°C (found for the most of the 30 V tests made) yields an increase of the value of the measured charge of 25%. It has been proved previously that a 30 V test produces a lower joule effect than a 60 V test. From figure 7.7 can be seen that if the voltage is reduced to a ratio of 0.5 from 60V to 30V, the temperature is reduced as well but with an approximated ratio of 0.3. As the Betancourt's equation is valid only for RCPT tests with 60 volts and in agreement with the analysis presented above can be concluded that for the mortar migration test ran in this research with 30V the joule effect produces approximately a reduction around 8.5% (25/3). This value is lower than the average error for all the tests (15%). On the other hand, the graph of the first derivate of the equation 7.2 (figure 7.8) shows the change of the temperature caused by the change of the voltage and that represents in some way the Joule effect as well. The value of the first derivate for 30 volts is 3.5 times lower that for 60 volts. That shows how the temperature and the voltage have a strong non-linear relationship.
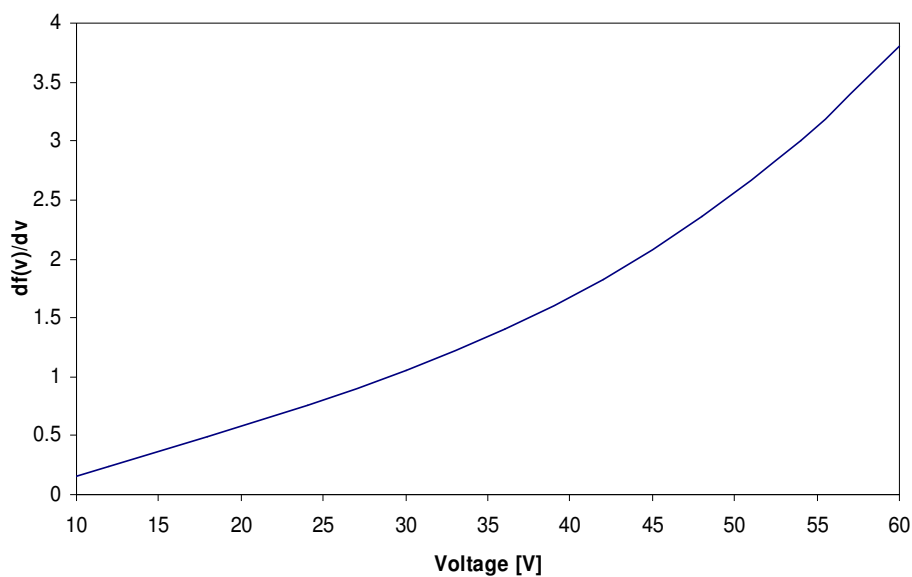
Figure 7-8 Relationship between the maximum temperature measured in the anodic cell and the first derivate of the relationship temperature-external voltage

7.3.2.2 Current measured in mortar tests

Table 7.7 shows the results of initial and final current, the difference in percentage between those values during the test, and the total charge calculated.

Mix	Δ Voltage [V]	W / b	Initial current [mA]	Final current [mA]	Current change [%]	Charge [C]
1-M	60	0.49	305.8	977.2	219.6	16140
2-M	30	0.49	147.2	141.6	4.7	13035
3-M	30	0.49	163.5	150.8	7.8	13797
4-M	30	0.49	124.5	243.1	96.7	15922
5-M	30	0.65	215.5	278.9	29.5	21539
6-M	15	0.49	80.3	72.3	9.8	6146
7-M	15	0.65	88.8	89.1	3.5	7383

Table 7-7 Summary of the electrical results for the mortar samples

For all the tests the transient current measured is plotted against time, each figure represents the average of two samples (except sample 1-M). Figure 7.9 shows the current for the test 1-M. During the first four hours of the test there was a significant increase of current, with a significant heating of the system.
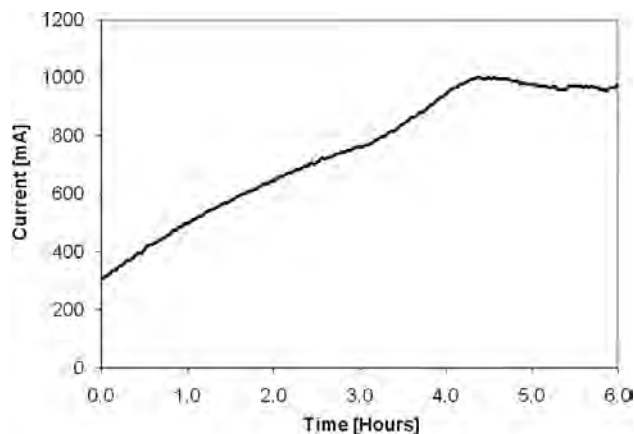
Figure 7-9 Evolution of the transient current sample 1-M; External voltage = 60 V, water to binder ratio = 0.49

Figure 7.10 shows the tests run at 30 volts. Samples 3-M and 5-M were carried out with the same electrode solutions but the water binder ratios of the samples were 0.49 and 0.65 respectively. It is confirmed that the current increases with increasing the w/b ratio, because more pores and diffusing paths may form as the w/b ratio increases. The same results have been found by Lane (2005). It has been reported by Yang, Chiang and Wang (2007) that in a test lasting long enough to allow chloride ions to migrate across the sample and reach the anodic cell, the transient current will increase at the start of the experiment reaching a maximum value before starting to decline. After a period of time the current tends to become stable with a new slight increment. Sample 5-M shows a similar behaviour to that reported by Yang, Chiang and Wang (2007), initially the current increases in the first few hours, and then

decreases for a period of time. After this period, the current become stable with a new small increase. A similar trend in the current was reported by Beresford (2002). Results of the current evolution for some experiments will be compared with the results of the Coventry model in chapter 9.
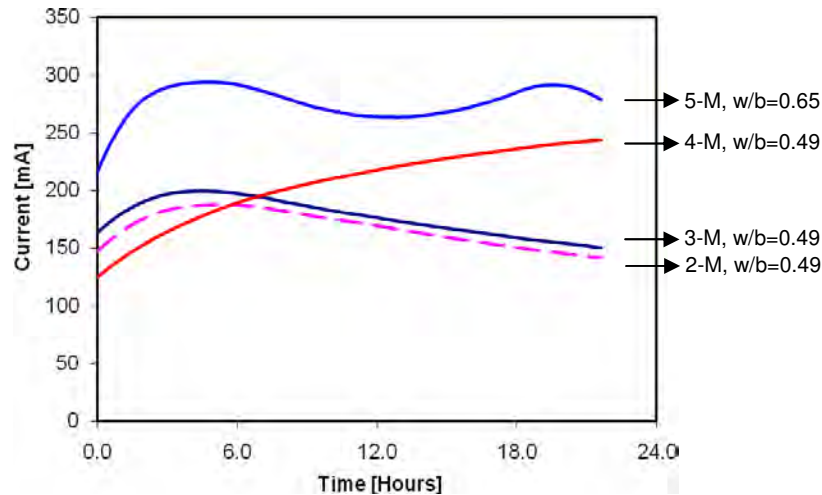
Figure 7-10 T Evolution of the transient current samples 2-M, 3-M, 4-M and 5-M; External voltage = 30 V

The transient current measured is a function of the properties of the concrete (microstructure and chemical pore solution) as well as the conditions of the test (voltage applied and solutions used in the cells). For samples 2-M, 3M and 4-M where a solution of 0.3 N NaOH was used in the anode and in the cathode solutions of 6% NaCl, 3%NaCl and distilled water were respectively used, the transient current exhibits some differences. There are small differences in the current values and in the trend of the current for samples 2-M and 3-M, both samples reached their maximum after 5 hours, and declined in current towards the end. In contrast, sample 4-M showed a continuous increase in the current during the test. Although the initial current is similar for all three tests (values can be seen in table 7.7) the final current of sample 4-M differs noticeably to the others. Yang, Chiang and Wang (2007) attribute the decrease of the current after a maximum due to a replacement of OH⁻ by Cl⁻. The graph shows that effectively, in the absence of some ions in the cathode (sample 4-M) the current continues rising up until the end of the test. The increasing current can not be attributed only to the chloride ions because if different solutions are used such as sodium hydroxide or calcium hydroxide similar trends can be found (Feldman *et al.* 1994).

Samples 6-M and 7-M were tested at 15 volts and the transient current is shown in the figure 7.11. For both samples the trend is similar, but the values of current for sample 7-M are greater than those for the sample 6-M, this is due to the higher water binder ratio. Although for those samples the current begins to decrease after 4.5 hours, it can be seen from the graph that the rate of decrease is nevertheless slight.
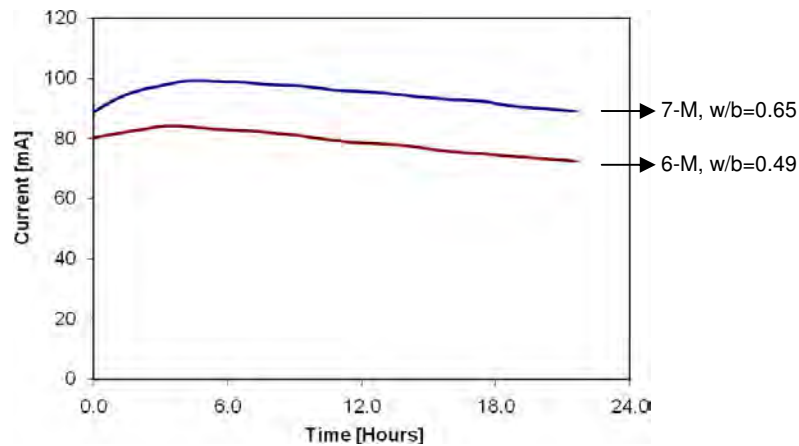
Figure 7-11 Transient current samples 6-M and 7-M; external voltage 15 V

The charge passed vs. time is shown in figure 7.12. An increase in the external applied voltage produces an increase in the charge passed. In the same way, an increase in the water binder ratio produces an increase in the charge passed. However, the charge passed seems to be more affected by the external potential voltage than by the water binder ratio. Even thought samples 2-M, 3-M, and 4-M have different concentrations of chlorides in the cathode at the start of the test, they have similar charge passed. That is very important because it proves that the passing of charge is not dependent exclusively on chloride ions. It was stated by Feldman *et al.* (1994) that chlorides are not needed in the ASTM C1202 test, which means that even if chloride ions are not present during the test, there is a profile for the current passed with a corresponding value of total charge. Nevertheless, the amount of chlorides is function of the charge as was shown previously in equation 5.29.
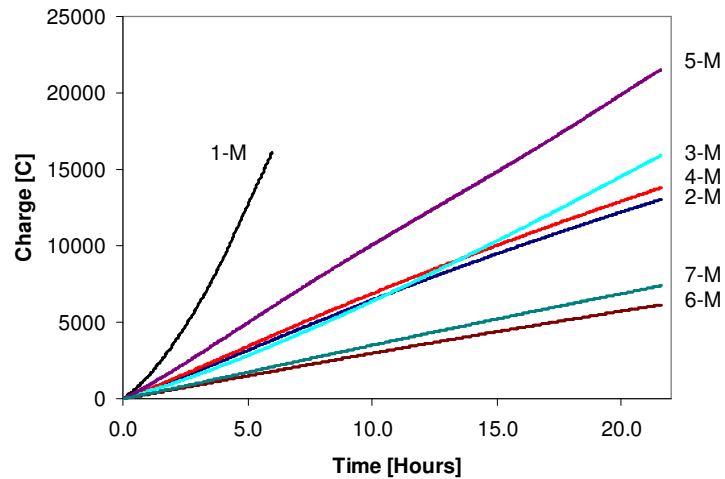
Figure 7-12 Charge passed vs. time in mortar samples

7.3.2.3 Membrane potential measured in mortar tests

For all the mortar mixes the voltages were measured in three different positions. The ideal location of those points was the mid-point and the quarters of each sample. As the drilling of the holes in order to insert the salt bridges was made mechanically with a hammer drill, some differences were found between the ideal and the actual location of each point. In order to find the position of the potential readings was assumed that at the start of the test the electrical field across the concrete sample is linear. Consequently, as the length, the total potential applied, and the potential in each point are known, the real position of each reading was calculated. Figure 7.3 shows the ideal location of the points and table 7.8 shows the average location of the points where the voltage was measured.

# test	Sample A			Sample B			Average		
	E1 [mm]	E2 [mm]	E3 [mm]	E1 [mm]	E2 [mm]	E3 [mm]	E1 [mm]	E2 [mm]	E3 [mm]
1-M	12.4	23.3	35.5	**	**	**	**	**	**
2-M	15.0	24.7	32.9	15.5	24.5	35.2	15.3	24.6	34.0
3-M	14.8	24.6	35.4	13.6	22.0	35.0	14.2	23.3	35.2
4-M	20.2	28.0	35.1	19.5	27.7	35.4	19.9	27.8	35.2
5-M	18.4	25.5	33.6	15.0	24.3	31.8	16.7	24.9	32.7
6-M	16.2	25.7	33.5	18.8	28.4	38.5	17.5	27.1	36.0
7-M	20.6	25.9	35.1	18.4	24.5	32.7	19.5	25.2	33.9

Table 7-8 Average localization of the points where was measured the membrane potential during the migration tests

The voltage across the sample was measured according to the test introduced in 6.3.3. Table 7.9 shows the average of the initial and final values of the voltage measured across the sample and their respective variation.

Mix	Initial Voltage 1/4 point [V]	Final Voltage 1/4 point [V]	Change [%]	Initial Voltage Mid point [V]	Final Voltage Mid point [V]	Change [%]	Initial Voltage 3/4 point [V]	Final Voltage 3/4 point [V]	Change [%]
1-M	14.63	14.57	0.4	27.42	31.61	15.3	41.80	45.38	8.6
2-M	8.9	8.9	0.5	14.4	16.0	11.0	19.9	22.9	14.8
3-M	8.3	8.1	2.7	13.6	14.0	2.7	20.6	22.7	10.1
4-M	11.6	9.0	22.3	16.3	16.1	2.2	20.6	22.2	7.7
5-M	9.7	10.4	7.5	14.6	16.4	12.9	19.1	21.2	11.1
6-M	5.1	5.7	13.9	7.8	8.6	10.7	10.4	11.3	9.0
7-M	5.6	5.7	2.2	7.3	7.9	8.7	9.8	11.0	12.8

Table 7-9 Summary of the membrane potential results for mortar samples

Figure 7.13 shows the variation of the voltage across the sample for all the tests made, with the exception of mix 1-M, which did not have results due to the high temperature reached during the experiment. Although for all samples there was a noise in the voltage logged, there is a good defined trend. It was found that this noise was substantially reduced by slightly increasing the depths of the drilled holes for the salt bridges. This observation indicates that the noise was caused by the random distribution of aggregate limiting the contact between the salt bridges and the pore volume. In the figure are presented two replicates for each test, those were named with the letters "a" and "b".

The profile for the replicates in each mix was very similar. It was confirmed experimentally that the voltage in the sample is not linear during the test and the profile is related with the features of the sample and also with the conditions of the test. In order to filter the noise found experimentally during the logging of the tests a commercial curve fitting software (The Mathworks 2001) has been used. As the transient voltage data collected experimentally was noisy, it was necessary to apply a smoothing algorithm to find its features. In those algorithms, it was assumed that the relationship between the voltage data and the time data is in reality smooth, and the smoothing process results in a better approximation of the real value because the stochastic noise has been eliminated. The methods used for smoothing the data were filtering (averaging) and local regression.
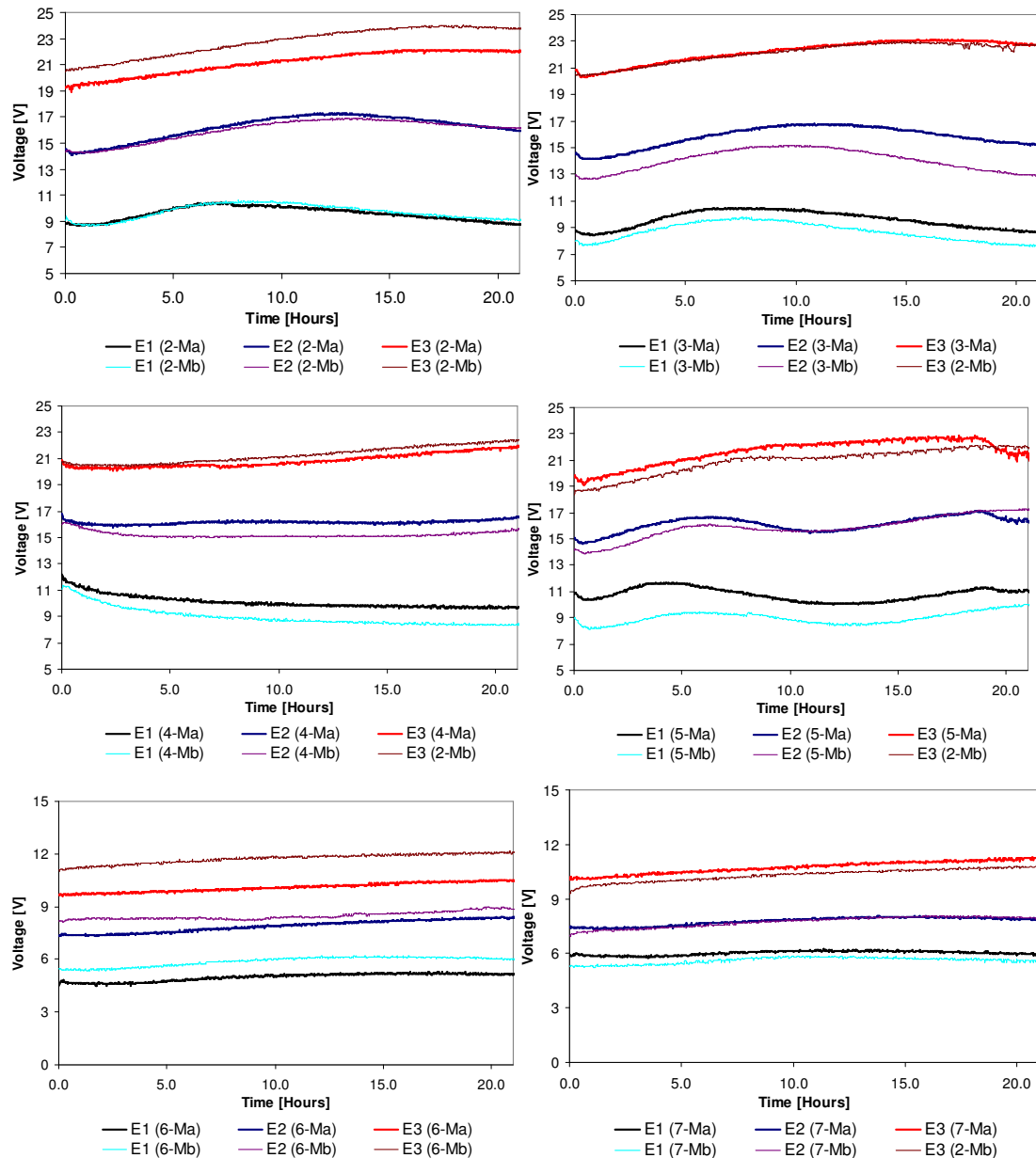
Figure 7-13 Difference of electrical potential across the sample measured during the mortar migration tests and respect to the cathode electrode

A summary of the procedure used in order to determine the transient membrane potential is presented below and an example is shown in figure 7.14 for mix 7-M.

1. For each mix the voltage was logged in three different points of the concrete sample.

2. The membrane potential was calculated for each replica of each mix from the equation 7.1.

3. The data from the experiment were filtered with a commercial curve fitting software to smoothen the graphs out and to avoid the noise effects.

4. The transient voltage was calculated as the average of the filtered voltages of the replicas.

The behaviour of this membrane potential across the sample during the test is shown in the figures 4.15 to 4.20 as contour graphs. The value of the membrane potential at the edges of the sample was assumed to be zero because those points correspond to the electrodes into the solutions.
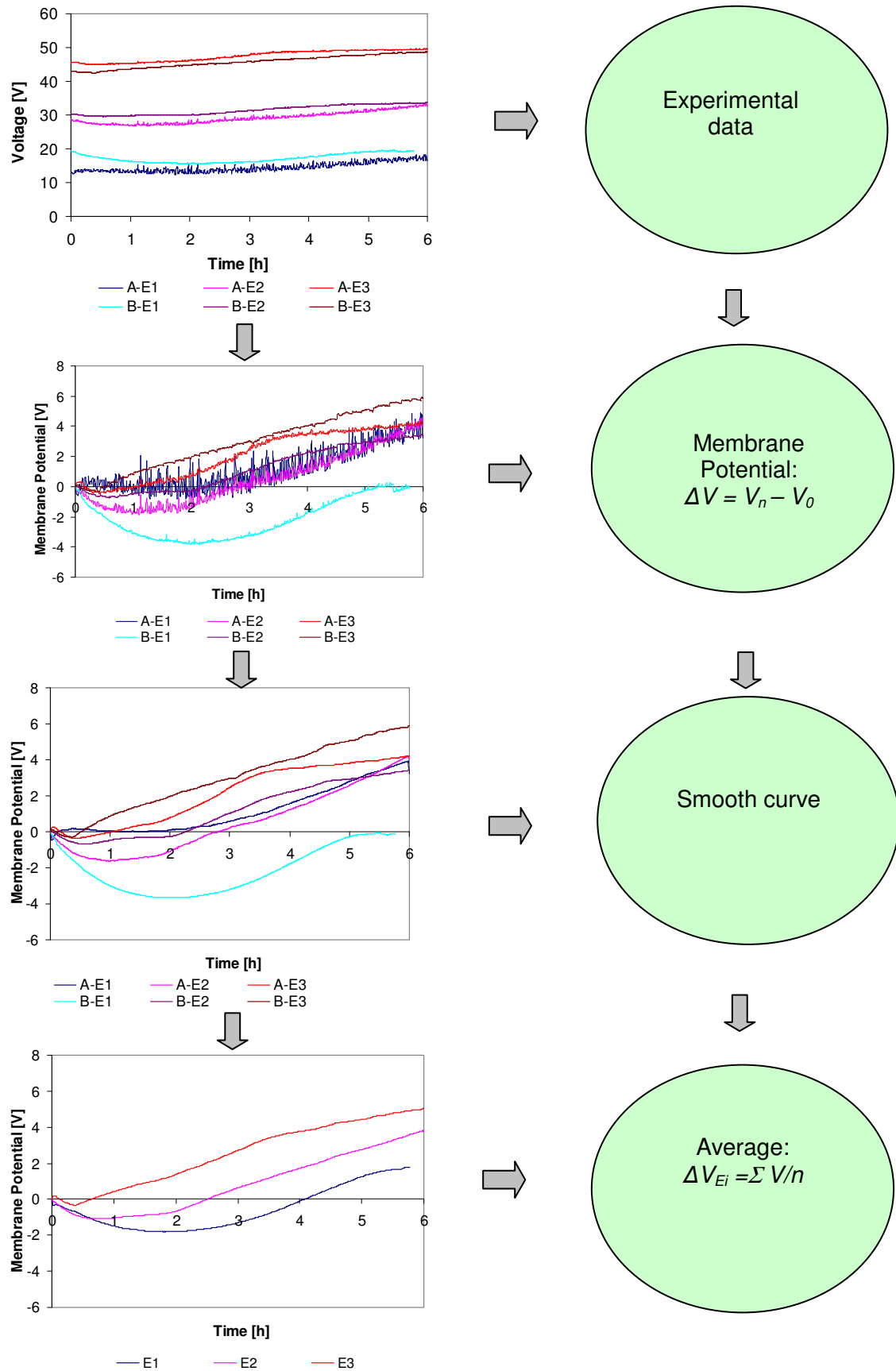
Figure 7-14 Algorithm proposed to calculate the membrane potential during a voltage control migration test
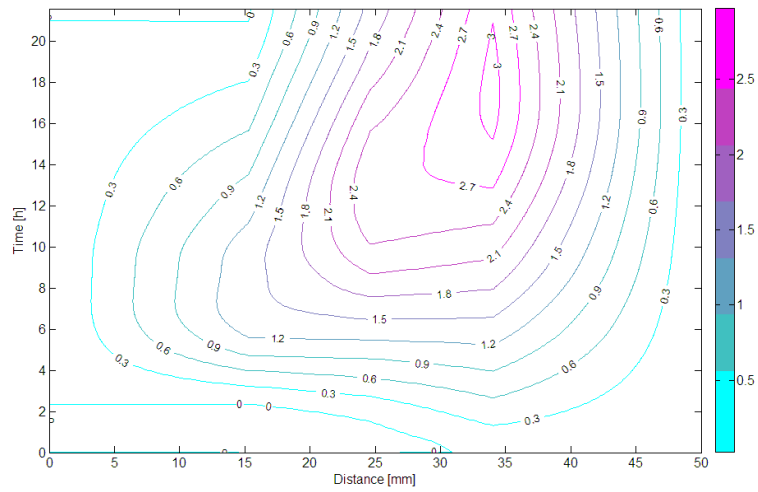
Figure 7-15 Average membrane potential mix 2-M, w/b=0.49, external voltage = 30V
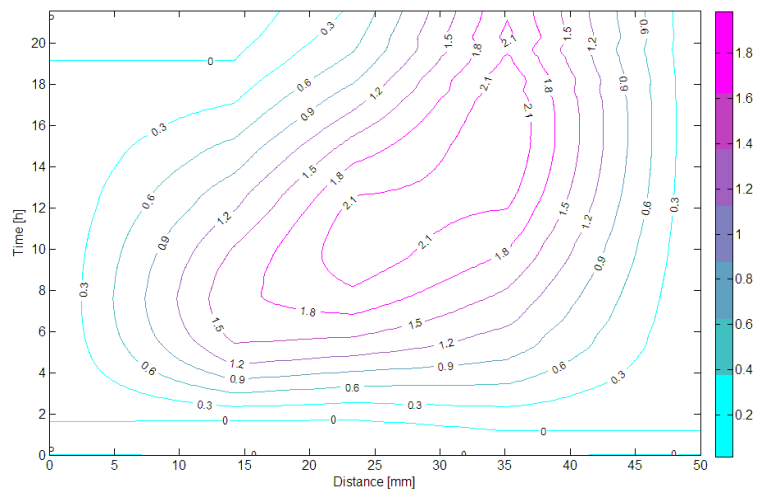
Figure 7-16 Average membrane potential mix 3-M, w/b=0.49, external voltage = 30V

Figure 7-17 Average membrane potential mix 4-M, w/b=0.49, external voltage = 30V
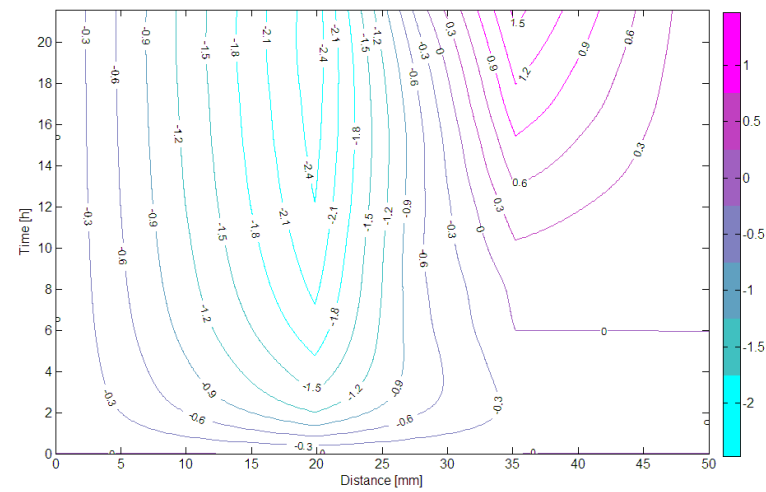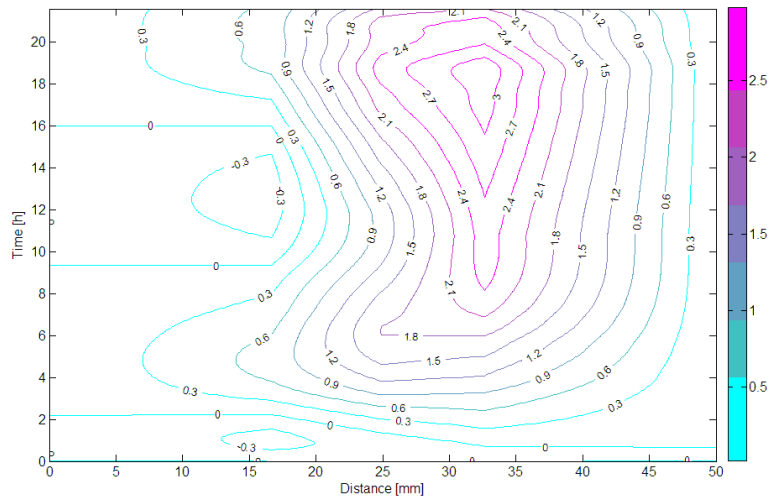
Figure 7-18 Average membrane potential mix 5-M, w/b=0.65, external voltage = 30V
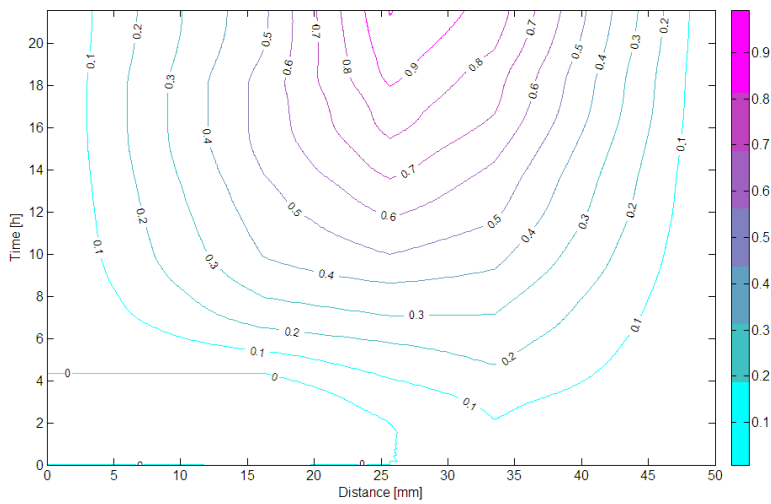
Figure 7-19 Membrane potential mix 6-Ma, w/b=0.49, external voltage = 15V
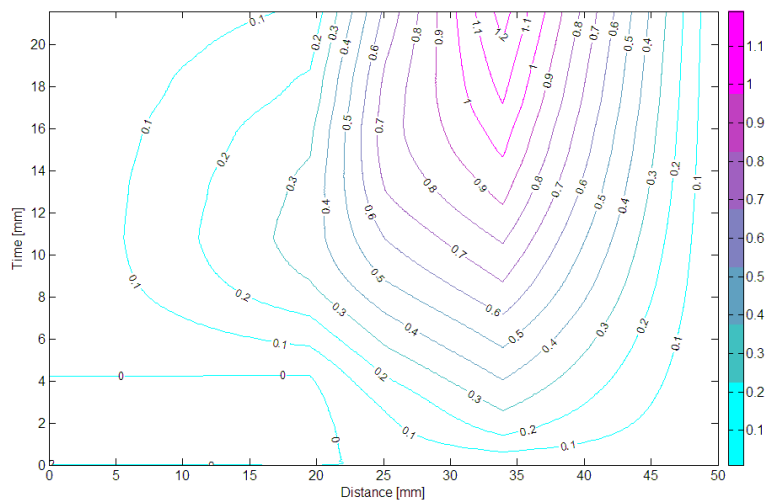
Figure 7-20 Average membrane potential mix 7-M, w/b=0.65, external voltage = 15V

171

All the mixes tested with solutions of NaCl in the cathode and NaOH in the anode showed a similar distribution of membrane potential. There was an increase of voltage in the area that was near to the alkaline solution. Mixes 2-M, 3-M and 5-M reached a maximum value of voltage with a subsequent reduction. For those samples, in the area near to the cathode the membrane potential either tends to be constant throughout the test or presented a smooth negative variation. Although the samples run with 15 V showed an equivalent profile to the ones run at 30 V, the profile had a lower potential and there was not enough time to reach a maximum value. The sample tested with distilled water in the cathode presented a different profile; there was a negative peak, but this time it was located near the chloride solution.

The behaviour of the voltage during a migration test shown in figures 7.15 to 7.20 represent a unique feature of the material under specific conditions of electro-migration. The similarities found show that it follows a physical pattern and can be used in order to try to explain the complex phenomena during electro-migration of ions through concrete.

From the contour plots the membrane potential for any point and duration of the test can be examined, it has either an academic or scientific value. However, those tests are expensive and not easy to complete. As an alternative, it has been proposed to study just the behaviour of the mid-point (located in the centre of the sample) as a source of additional information in a practical situation. The implementation of the test for qualifying or assessing concretes mixes can be suitable with the information of the membrane potential in the mid-point.

The electric membrane potential in the mid-point for each mix is shown in figure 7.21. Both samples run with 15 V (6-M and 7-M) showed from the start a sustained increase in the membrane potential, although mix 7-M, with water binder ratio 0.65, reached a maximum value at 15 hours and then began to fall. In contrast, sample 6-M did not reach a maximum during the test. Mixes 2-M, 3-M, and 5M showed from the start of the test a slightly negative membrane potential during the first hour of the experiment. After this time, those samples start to increase the voltage. Mixes 2-M and 3-M reached a maximum positive value of membrane potential at 13 and 10 hours respectively. Mix 5-M showed an initial maximum value of potential at 5 hours, a steady decreasing between 5 and 10 hours, followed by a local minimum at 12 hours, and a second maximum value at twenty hours. Sample 4-M without chlorides

in the cathodic solution showed a different trend from the other samples. For this mix the membrane potential was negative from the start of the test.
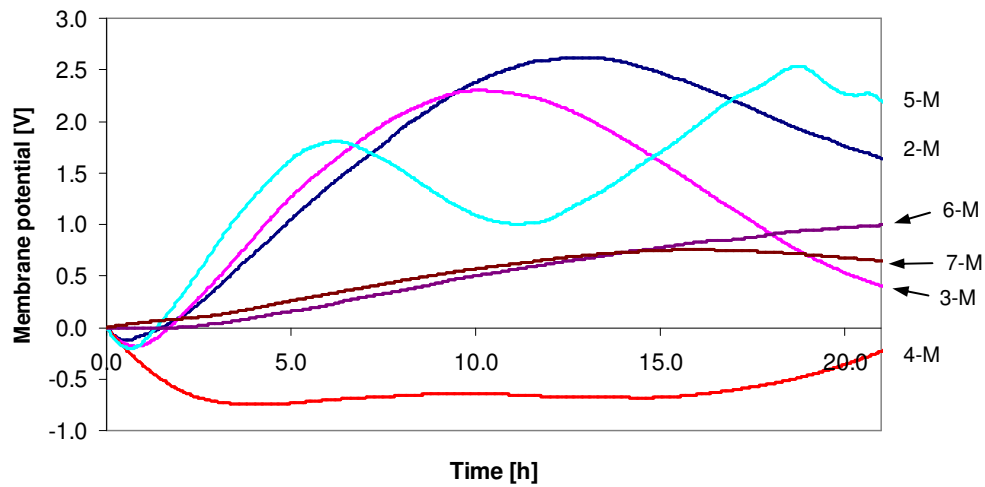
Figure 7-21 Membrane potential of mortar samples measured in the mid-point

7.3.2.4 Conductivity in mortar samples

In order to see the variation of the conductivity during the test, the electrical potential difference was calculated across the segments where the voltage was measured (zones Z1 - Z2 - Z3 - Z4 figure 7.3) and the conductivity was calculated using the equation 6.13 defined in chapter 6.

$$\sigma(t) = \frac{i(t)}{E_{ij}(t,x)} \frac{L_{ij}}{A}$$

(6.13)

If the electric field is constant along the sample it is expected that the behaviour of the conductivity has the same trend as the current. However, as the voltage varies across the sample, the calculated conductivity across the sample has a different value. The electrical properties of a mortar sample during a migration test are transient in time and position due to the movements of ions into the pore solution. The change in the conductivity of the samples can not be attributed to any gradient of temperature as was discussed earlier. Figures 7.22 to 7.24 show the variation of the conductivity for the four zones where the potential was measured.

The conductivity for tests 2-M and 3-M are similar, that is due to the nature of the experiment. The movement of ions is due principally to electrical migration and the contribution of the diffusion is negligible. All the zones had the same pattern: the conductivity increased from the start of the test, reached a maximum value and starts

to decrease steadily. Zone 1 got its maximum value at 2 hours, the zone 2 got its maximum value at 6 hours, the zone 3 got its maximum at 8 hours, and finally, the zone 4 got its maximum at 15 hours. The variation of the conductivity of the sample 4-M showed a different trend than the previous mixes, that is explained by the absence of ions in the cathodic reservoir.
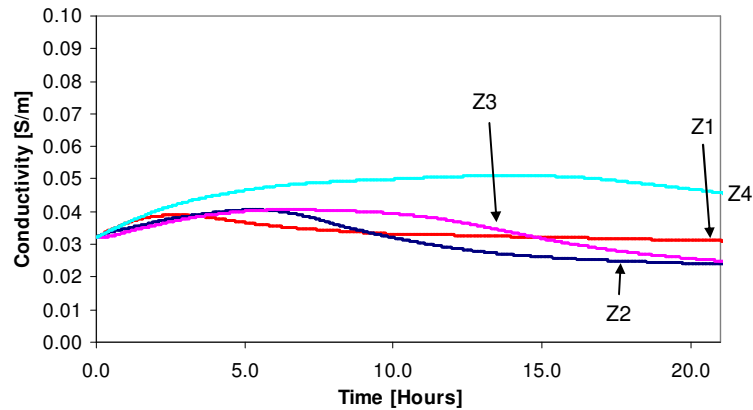
Figure 7-22 Average conductivity variation during the test mix 2-M
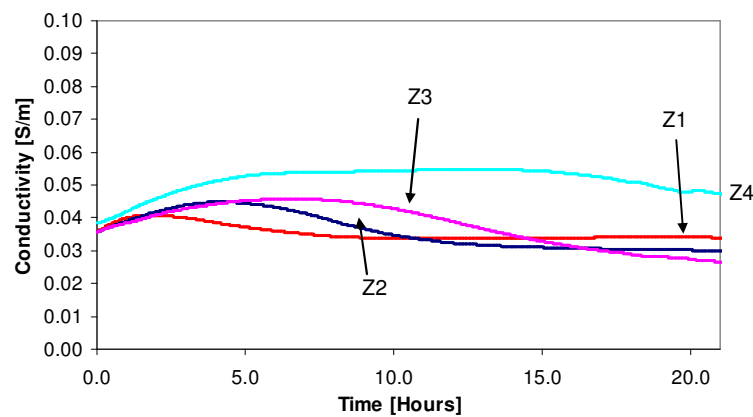
Figure 7-23 Average conductivity variation during the test mix 3-M
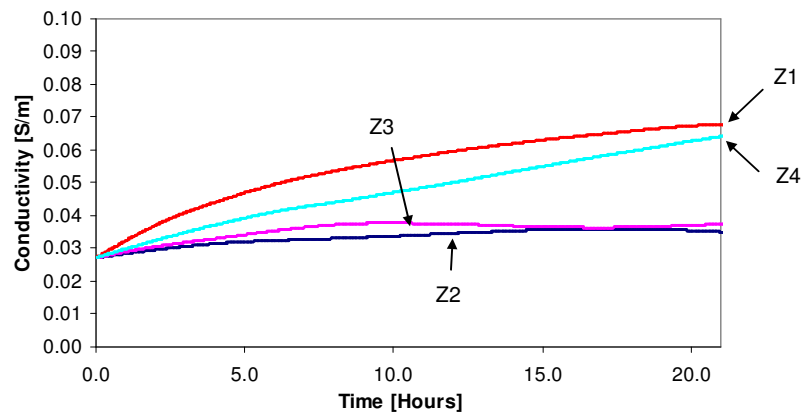
Figure 7-24 Average conductivity variation during the test mix 4-M

7.4   CONCLUSIONS

29. The electrical field is not linear in a migration test; it varies in time in position according to the development of the membrane potential.

30. From a macroscopic point of view, the local maximum or any feature of the mid-point membrane potential can be explained as a result of the variation of the conductivity of the pore solution due to the migrations of all ions involved.

31. The transient conductivity is defined by the relationship between the transient voltage and the transient current at any point. The evolution of the mid-point membrane potential can be measured experimentally and can give additional information in a migration test.

32. From the experimental program carried out and from the simulations made, it has been proven that the voltage during either normal diffusion or migration is not linear. The test proposed to measure the membrane potential has given encouraging results and the simulations confirm that under controlled conditions, changes in the parameters of the test and in the properties of the material affect the membrane potential.

33. A methodology to measure the membrane potential has been developed. This can be used in cement based materials subjected to a standard RCPT migration test.

8 OPTIMIZATION OF THE VOLTAGE CONTROL CONDITION

8.1 INTRODUCTION

Almost all numerical models used to simulate the ionic penetration into porous media give, as outputs, the evolution of the ionic concentration as a function of the exposure conditions, and some material transport related properties. The exposure conditions can be natural or laboratory controlled and can be established with a good level of accuracy, especially for the former. In contrast, the transport related properties represent a major problem because of the difficulties in measurement. Although the diffusion coefficient and the binding capacity factor of chlorides can be measured experimentally, for other species involved in a diffusion or migration process (OH^-, K^+, Na^+) they represent a highly complex problem. In the same way, the chemical composition of the pore solution is a test not easy to perform because it requires special equipment.

In addition, regardless of the experimental method used to find the chloride coefficient of diffusion, there are some difficulties with each procedure. For example, in addition to the problem of the duration of the tests, the determination of chloride concentrations either in solutions or in concrete requires special equipment and the laboratory work is time consuming. Additionally, all the procedures assume no depletion of chlorides in the source reservoirs, a situation which requires the continuous replacement of the solutions or, at least, the monitoring of the concentration, even if large quantities of initial solution are used. In addition, the effect of other ionic species and their interaction with chlorides is neglected.

As was explained in section 5.7, the Coventry electro-diffusion model gives as outputs the ionic concentration, the transient current and the mid-point membrane potential during a migration test. The programme uses the physical transport properties and the test conditions as input data. However, as during a migration test the physical transport properties are unknown, an optimization technique was proposed in this research. With this, some of the transport properties of any specific mortar or concrete mix are determined using the Coventry model and the optimization technique together. This was achieved by running the model a number of times and using the results as a database in order to obtain the input data from known output.

The optimization technique used was an artificial neural network algorithm (ANN). It was trained to optimize the principal related physical properties involved during a standard migration test. This new method consists of the experimental determination of the electrical current and the electrical membrane potential during the ASTM C1202 test, and then obtaining the chloride transport related properties with the integrated physical-neural network model.

In a first part of this chapter some theoretical aspects of the artificial neural network systems are introduced. It is important to note that the theory of ANN reported here is general and does not follow a rigorous mathematical approach; this is given by Gurney (1997). In a second part of the chapter the assumptions made on the physical problem of migration are presented, in a third part the development of the neural network is presented. Finally, the optimization neural network was applied to some concrete mixes and based on the experimental results and the simulations, the intrinsic diffusion coefficients of chloride, hydroxide, sodium and potassium were obtained. Also, the initial hydroxide composition of the pore solution, the porosity, and the chloride binding capacity were obtained.

8.2   ARTIFICIAL NEURAL NETWORKS

An Artificial Neural Network (ANN) is one of the artificial intelligence techniques used as information processing systems, capable of learning complex cause and effect relationships between input and output data (Demuth, Beale and Hagan 2008). They are highly non-linear, and can capture complex interactions among input and output variables. Like in human beings, in an ANN a neuron is connected to other neurons through links that produce a stimulus to the entry and exit as a response, in addition, they have the ability to communicate among them. A neural network has a finite number of neurons distributed in the input layer, which represents the input data, an output layer, which computes the neural networks outputs, and one or more intermediary layers called hidden layers, which generate the relationships between layers of entry and exit.

A neural network is trained to develop a particular task or function adjusting the intensity with which the neurons are interconnected. The back-propagation algorithm is one of the most commonly used in civil engineering applications. Initially in each connection between neurons is assigned a weight, a value that is fitted during the back propagation learning process. Commonly a neural network is trained or

adjusted in a way that the input variables correspond with an expected output. This situation is shown in Figure 8.1; the network is trained by adjusting the weights through the comparison between the outputs (values predicted by the model) and the target values.
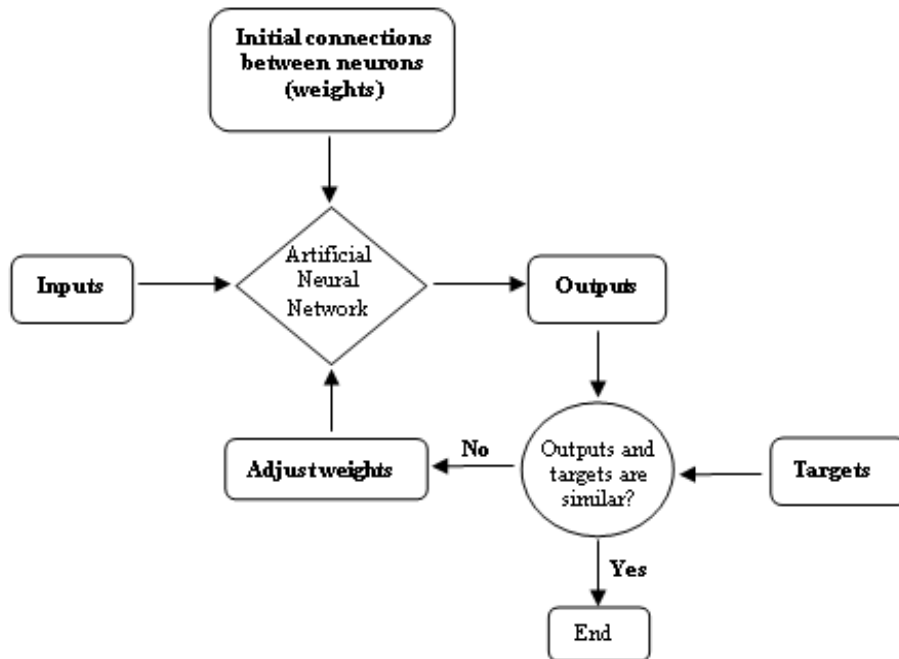
Figure 8-1 Training back-propagation algorithm of the neural network method

Usually within a network, the entrance to a neuron is a numeric value defined as a scalar *p*, which in turn is multiplied by a weight *w* in order to generate a product *wp*, scalar as well. In order to generate a scalar output in a neuron, it is necessary to evaluate a function known as transfer function *f*, which may sometimes be influenced by a bias defined by a scalar *b*. The transfer function *f*, usually corresponds to a step, linear or sinusoidal function, which uses *n* as an argument and generates a scalar output. When a neuron contains multiple entries, defined by a vector as shown in Figure 8.2, the value of *n* or argument of the transfer function is defined as:

$$n = w_{1,1} p_1 + w_{1,2} p_2 + ... + w_{1,R} p_R + b \qquad (8.1)$$

where R is the number of elements in the vector of entry.

$$a=f(Wp+b)$$
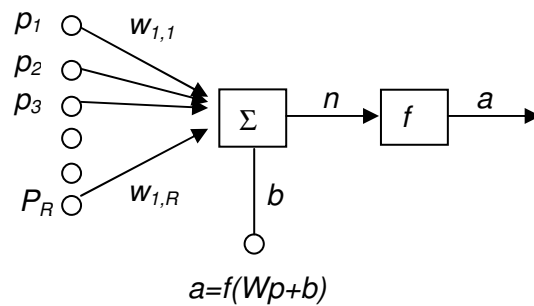
Figure 8-2 Neuron with multiples entries (Demuth, Beale and Hagan 2008)

8.3   GENERAL ASSUMPTIONS

The computational simulation of any physical system needs some assumptions in order to decrease the problem complexity. In that way, the next suppositions were established in the optimization model developed in this research.

In a migration test the profile and evolution of the membrane potential and the current is associated either with:

• Factors related with the test, such as the electrical external potential, the volume of the reservoirs, and the chemistry of the external solutions,

or

• Factors related with the features of the sample, such as the concentration of species in the pore solution, the tortuosity of the pore network, the porosity of concrete, the intrinsic properties of diffusion for each ion present and the binding capacity or adsorption of each ion.

If in any chloride migration experiment all the conditions related to the test are carefully controlled, it can be argued that the differences in the current and the mid-point membrane potential among different mixes are due to the differences in the transport characteristics of the material. With measuring the transient current by itself it is not possible to determine a unique numerical value for all the concrete transport properties because there are too many unknowns and not enough relationships to solve the system. However, with the simultaneous measurement of the current and

the mid-point membrane potential it is possible to determine an unique combination of the transport properties by using the neural network and making the following assumptions:

1. The chloride apparent diffusion coefficients were determined from the intrinsic diffusion coefficient, the porosity of the material, and the binding capacity factor using equation 5.33.

2. Although it is well known that chloride, hydroxide, sodium, and potassium have complex reactions with the cement hydration products, chlorides were the only ions permitted in the model to have adsorption or binding with the cement matrix. The reason for adopting this assumption was to limit the number of variables to optimize. In addition, although it has been demonstrated experimentally that non-linear isotherms better reflect the ionic adsorption, the model uses an average linear isotherm that closely approximates the average adsorption of chlorides.

3. At the start of the test the chemical pore solution is composed of ions OH^-, K^+ and Na^+, and in order to keep electroneutrality, it was assumed that the concentration of hydroxyl ions is equilibrated with a proportion of 33% of sodium and 66% of potassium. This assumption was based on published results (Bertolini *et al.* 2004).

4. The external experimental conditions are as in ASTM C1202, i.e. voltage applied, duration of the test, concentration of the external solutions, size of the sample, etc.

8.4   OPTIMIZATION MODEL

The integrated computational model developed was composed of two main techniques; the Coventry electro-diffusion model (already presented in section 5.7), and an artificial neural network. The latter had a back-propagation algorithm with a multilayer architecture. An input layer of 6 neurons, a hidden layer of 3 neurons and an output layer of 7 neurons (figure 8.3) were used.
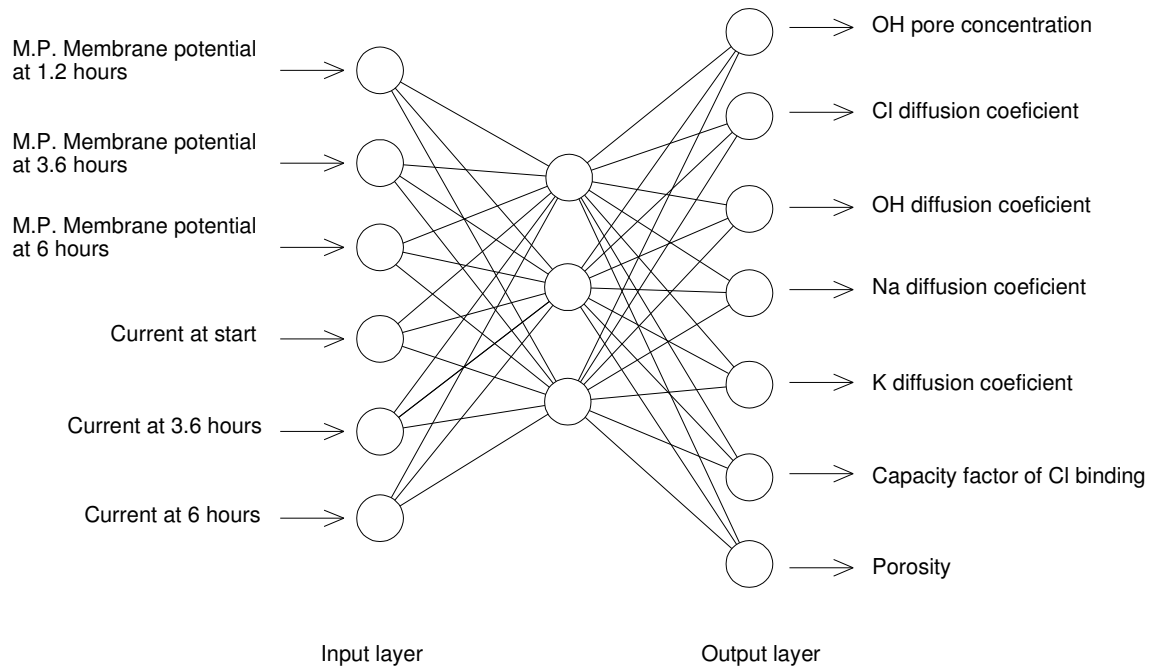
Figure 8-3 Inputs and outputs of the neural network model proposed

The 6 Input neurons correspond to the experimental values of current and the mid-point membrane potential through the sample at different times. The output neurons correspond to the intrinsic diffusion coefficients of Cl^-, OH^-, Na^+ and K^+, the porosity, the hydroxide composition into the pore solution at the start of the test, and the binding capacity factor for chloride ions. The transfer function used was a hyperbolic tangent sigmoid one, which was limited to be between -1 and +1, and the Levenberg-Marquardt training algorithm was used, figure 8.4.
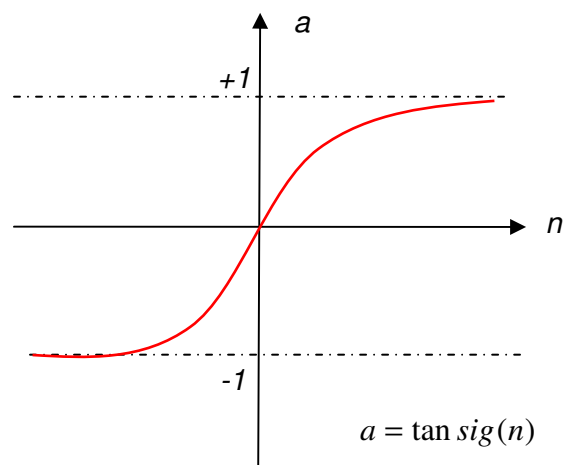
Figure 8-4 Tan-Sigmoid Transfer Function

The neural network model was constructed and trained using the neural network tool box of Matlab®. To train the network the numerical physical model was run several times in order to obtain enough input vectors and the corresponding target vectors. Figure 8.5 shows a conceptual diagram of the training process.
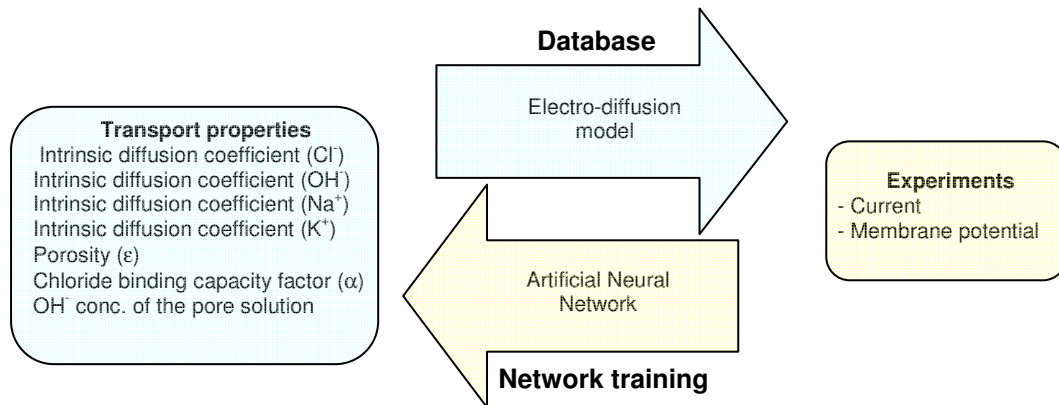
Figure 8-5 Conceptual diagram integrated model: Coventry model-neural network

During the training, all the inputs and outputs were normalized between -1 and +1 in order to avoid the influence of the scale of the physical quantities. In the same way, to feed the neural network it is necessary to normalize the data. A linear relationship was used to find the equivalence between the real coordinate system and the natural system (-1 to +1), as is shown in figure 8.6 and equation 8.2.
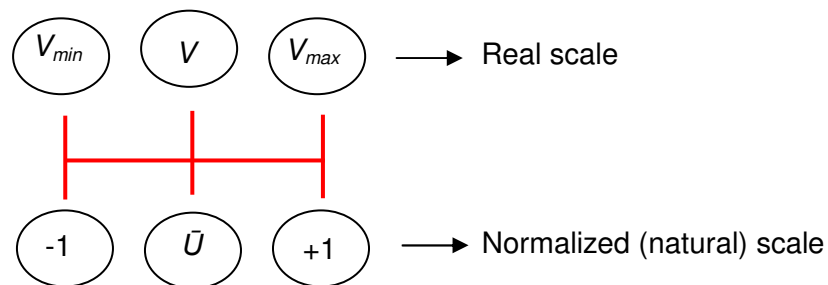
Figure 8-6 Relationship between real and normalized scales

$$\bar{u} = \frac{2(V_i - V_{avg})}{V_{max} - V_{min}} \qquad (8.2)$$

V_i corresponds to the physical parameter i, and $\bar{u}$ correspond to the same parameter but in the natural scale. The corresponding constants to normalize the input experimental data are:

	Voltage MP [V]			Current [mA]		
Time [h]	1.2	3.6	6.0	0.0	3.6	6.0
V_{max}	2.20	6.48	7.56	298.40	552.34	512.24
V_{min}	-4.99	-9.79	-11.26	1.22	1.20	1.09
V_{avg}	-1.40	-1.66	-1.85	149.81	276.77	256.67
L	7.19	16.28	18.82	297.18	551.14	511.15

Table 8-1 Transformation input matrix: real to natural scale

In the same way, the properties obtained with the network are normalized between 1 and -1. Each property is converted to its real scale with the following equation and transformation matrix.

$$V = \frac{\bar{U}(\bar{U}_{max} - \bar{U}_{min})}{2} + \bar{U}_{avg}$$

(8.3)

	OH conc	D_{Cl}	D_{OH}	D_{Na}	D_k	Cap Cl	porosity
$\bar{U}_{max}$	550	9.E-10	9.E-10	8.E-10	4.E-10	2	0.30
$\bar{U}_{min}$	30	7.E-12	3.E-12	2.E-12	2.E-12	0.16	0.05
$\bar{U}_{avg}$	290	4.54E-10	4.52E-10	4.01E-10	2.01E-10	0.896	0.18
L	520	8.93E-10	8.97E-10	7.99E-10	3.98E-10	1.47	0.25

Table 8-2 Transformation output matrix: natural to real scale

From the Coventry model more than 2000 combinations of transport properties and the transient electrical properties were obtained. Of those, a selection was made limiting the current and membrane potential to the maximum and minimum values of table 8.1. As a result, a total of 989 combinations were used for training the neural network. From the total data, 959 combinations were used to train the network and 30 combinations were used to validate the behaviour of the network during the training process. The matrices used in the learning process are:

Total data: $[Inputs]_{6x989} \Rightarrow [Outputs]_{7x989}$, training data: $[Inputs]_{6x959} \Rightarrow [Outputs]_{7x959}$, and validating data: $[Inputs]_{6x30} \Rightarrow [Outputs]_{7x30}$. The first subscript of each matrix relates to the current and membrane potential at different times for the inputs, and the transport properties for the outputs. The second subscript refers to the number of combinations available. Figure 8.7 shows the network learning process carried out with the Matlab neural network tool box.
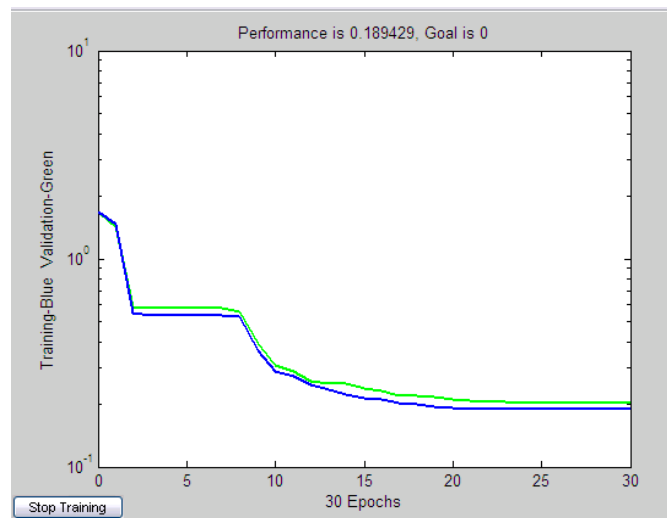
Figure 8-7 Output of the Matlab learning process

At the end of the training process, the neural network consisted of 3 layers (figure 8.3), two weight matrices [$w_{i,j}$] and two bias vectors [b_i]. Matrix W_1 contains the weights establish between the input layer and the hidden layer. For each element $w_{i,j}$ the subscript i refers to the hidden layer and subscript j refers to the input layer, so its dimension is [3x6]. Matrix W_2 contains the weights establish between the output layer and the hidden layer, so, its dimension is [7x3]. The vector b_1 contains the bias for the hidden layer, so, its dimension is [3]; and the vector b_2 contains the bias for the output layer, so, its dimension is [7]. The matrices and vectors which define the optimization model are presented below.

$$W_1 = \begin{bmatrix} 0.037168 & 0.0015873 & 0.016917 & -0.032529 & 0.12886 & -0.16357 \\ -0.11184 & 0.033282 & -0.051304 & 0.073564 & -0.33367 & 0.38711 \\ -0.9246 & 0.47213 & 1.0308 & -0.32507 & -0.87958 & -0.088945 \end{bmatrix}$$

$$W_2 = \begin{bmatrix} -67.7942 & -132.8252 & 44.3873 \\ -0.91499 & 5.5639 & 2.125 \\ 0.74141 & 0.7888 & 1.6033 \\ -4.9404 & 4.8932 & -0.84265 \\ -3.1335 & 22.9354 & -26.6329 \\ 2.7039 & 0.52601 & -4.4843 \\ -2.1563 & 0.53275 & -4.7481 \end{bmatrix}$$

$$b_1 = \begin{bmatrix} -0.42898 \\ 1.5532 \\ 2.7834 \end{bmatrix} \qquad b_2 = \begin{bmatrix} 49.7906 \\ -8.1677 \\ -3.224 \\ -7.2992 \\ 2.0746 \\ 4.1633 \\ 3.4127 \end{bmatrix}$$

8.5   EXPERIMENTAL PROGRAMME

In order to investigate the validity of the optimization model an experimental program was carried out on different concrete samples without admixtures. The results of the experiments were used as inputs of the neural network and the transport properties obtained. In appendix 4 the steps required to use the neural network are detailed.

8.5.1 Materials

Samples of type I ordinary Portland cement (OPC) with different water to cement ratios were mixed. Table 8.3 shows the mix designs and the nomenclature used in this study. All the tests were made on samples around 180 days old which were cured in controlled conditions of humidity and temperature. All mixes were compacted mechanically with a vibrating table. The moulds were filled with concrete in three layers and compacted to remove the air and reach the maximum density.

Mix	w/b	OPC [Kg/m^3]	Fine agg. [Kg/m^3]	Coarse agg. [Kg/m^3]	Water [Kg/m^3]
OPC 4	0.4	400	705	1058	160
OPC 5	0.5	400	664	995	200
OPC 6	0.6	400	622	933	240

Table 8-3 Concrete mix proportions of samples used to validate the optimization model

8.5.2 Tests

The tests carried out are summarized below.

Open porosity: three replicates were tested for each mixture (according to section 6.5).

Chloride migration: The current in a voltage control (ASTM C1202) test and the mid-point membrane potential tests were measured (according to 6.3). Two replicates were tested for each mixture.

Chloride penetration in a self-diffusion test: For this, the external concentration of chloride was 7% NaCl and it was renewed every 3 weeks. After 12 weeks of diffusion, the chloride penetration depth was measured using the colorimetric method (according to section 6.8.2). The coefficient k of equation 6.14 was calculated for each mix.

8.6   EXPERIMENTAL OUTCOMES

8.6.1 Transient current

The average current measured for each mix in the migration test is shown in figure 8.8. As was expected, an increase in the water cement ratio gave an increase in the current passed, and a corresponding increase in the temperature of the sample. The measured maximum value of temperature in the anode solution was of 63, 44, and 36 °C for samples of water cement ratio of 0.6, 0.5 and 0.4 respectively. The values of charge calculated as the area under the graph of current versus time were 9580, 6863 and 4149 coulombs for samples of water cement ratio of 0.6, 0.5 and 0.4 respectively.
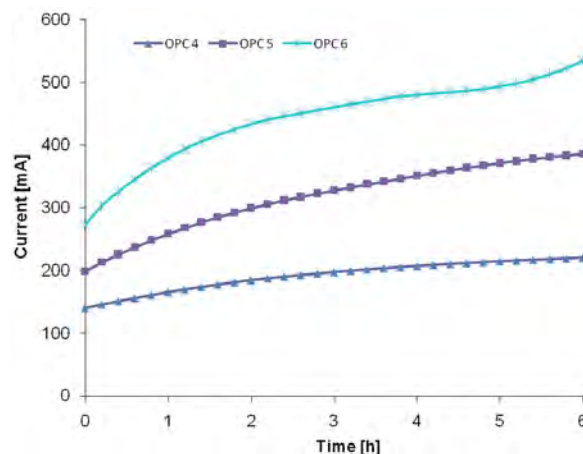
Figure 8-8 Current measured experimentally on samples used to validate the optimization model

8.6.2 Mid-point membrane potential

The membrane potential measured is shown in figure 8.9a. For some samples, there was signal noise which may have been caused by the random distribution of

aggregate limiting the contact between the salt bridges and the pore volume. The experimental results were filtered with commercial curve-fitting software in order to find the best trend of the results and this can be seen in figure 8.9b. The average membrane potential for each mix is shown in figure 8.9c. It can be seen that for all mixes the membrane potential showed a rise from its initial value, however, mix OPC-6 showed an initial decrease during the first 2 hours.
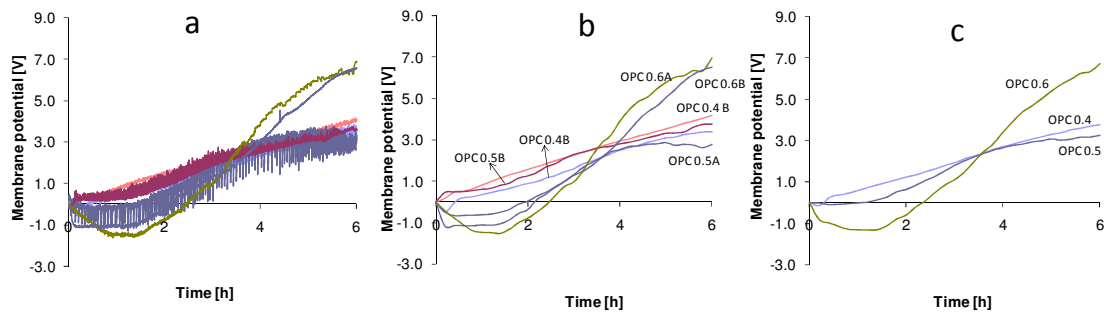
Figure 8-9 Mid-point membrane potential measured

8.6.3 Chloride penetration

The chloride penetration coefficients k obtained from the gravity diffusion test and equation 6.16 are shown in figure 8.10. As was expected, an increase in the water cement ratio yielded an increase in the chloride penetration coefficient.
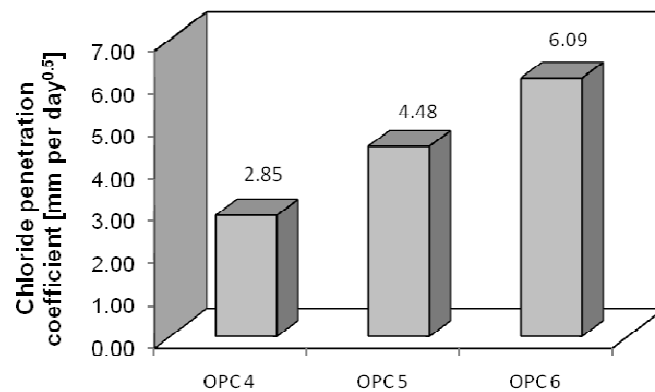
Figure 8-10 Chloride penetration coefficients k on samples used to validate the optimization model

8.7   PREDICTION OF CHLORIDE RELATED PROPERTIES

The experimental values of the transient current and the mid point voltage obtained from the migration test (table 8.4) were normalized and the artificial neural network was run. The outputs of the model are the calculated chloride transport related

properties. As a measure of the reliability of the network, the transport properties obtained were used to run the electro-diffusion model in order to obtain a simulated transient current and mid point membrane potential. The comparison of these curves is shown in figure 8.11. It can be seen that for the current the simulations are in agreement with the experiments, and for the membrane potential although there are some small differences there is a well defined trend.

	Voltage MP [V]			Current [mA]		
Time [s]	1.2	3.6	6.0	0.0	3.6	6.0
OPC 4	0.7215	2.4105	3.7850	140.4	203.9	220.5
OPC 5	0.0365	2.3885	3.2730	199.4	342.2	386.1
OPC 6	-1.3135	2.4760	6.7320	272.5	474.5	535.4

Table 8-4 Experimental data obtained from the current and membrane potential experiments and used as inputs of the neural network
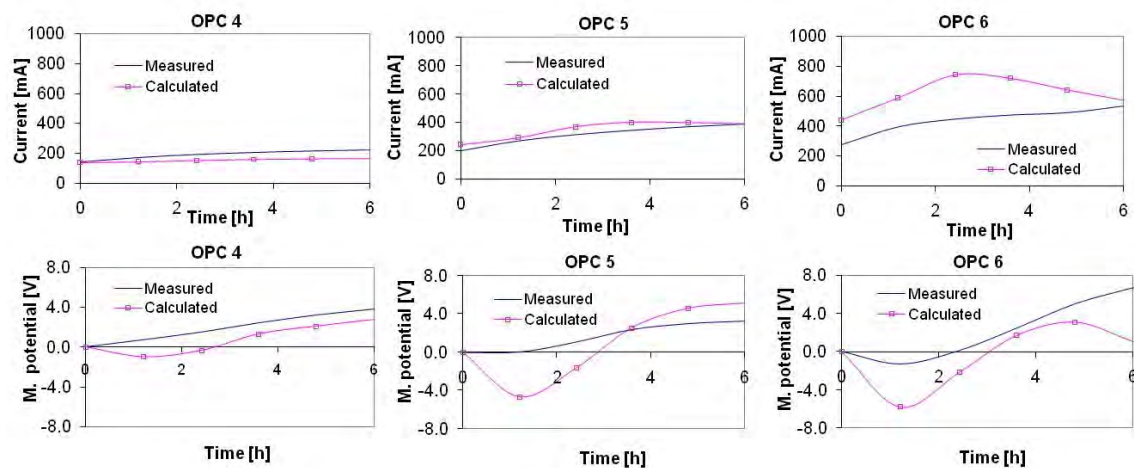
Figure 8-11 Transient mid-point membrane potential and current simulated and measured

The differences between the measured and simulated membrane potential can be explained by factors related to the accuracy of the measurement device used during the experiment, the heating of the material under an electrical field and the variability of the test. However, it may be seen that the neural network is able to give a good fit to the profile of the membrane potential, given that the number of possible combinations of properties that yield a given current and membrane potential is almost infinite.

The calculated transport properties include the porosity, the binding capacity factor and the initial hydroxide composition at the start of the test. As was expected, the

porosity increases with an increase of the water binder ratio (figure 8.12). In the figure it can be seen that the trend of the measured porosity is similar to that calculated; however some differences arise from errors in both the numerical and experimental methods.
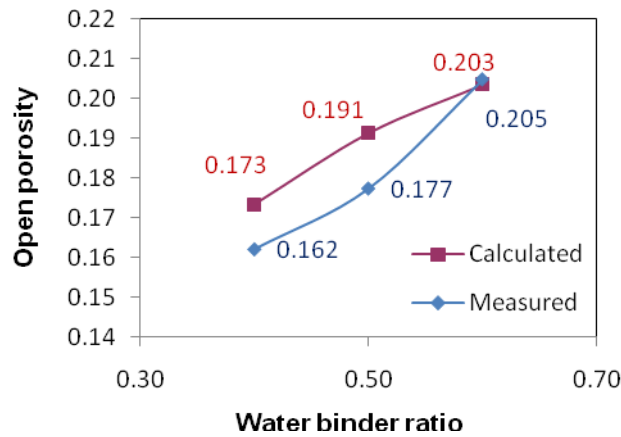
Figure 8-12 Porosity measured experimentally and simulated with the optimization model

According to the simulations the binding capacity factor decreases as the water binder ratio increases, presumably due to the refining of the hydration compounds enabling them to physically bind more free chloride ions (figure 8.13). A different trend was reported by Dhir, El-Mohr and Dyer (1997). In this, is stated that there is an increase in the chloride binding capacity for OPC cement pastes with an increasing in the water to binder ratio. However, no physical explanation for this is provided. It is possible that the differences between the results reported on the former reference and the results obtained with the neural model arise because were used paste and concrete samples respectively.
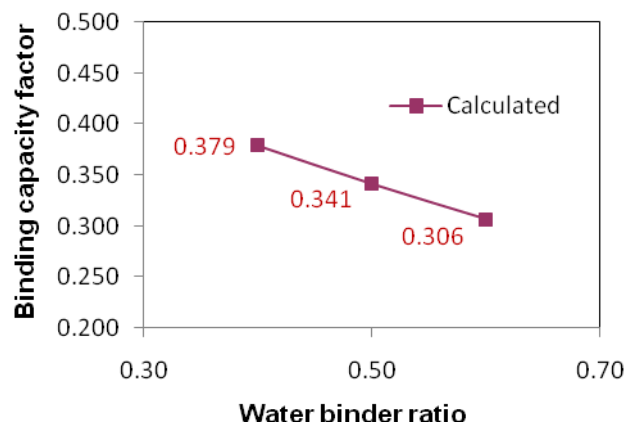
Figure 8-13 Binding capacity factor (α) calculated with the optimization model

Figure 8.14 shows that the calculated initial chemical content of the pore solution increases with an increase in the water binder ratio. This can be attributed to the higher amount of water, which causes a diminution in the ability of the hydration products to fix alkali metals.
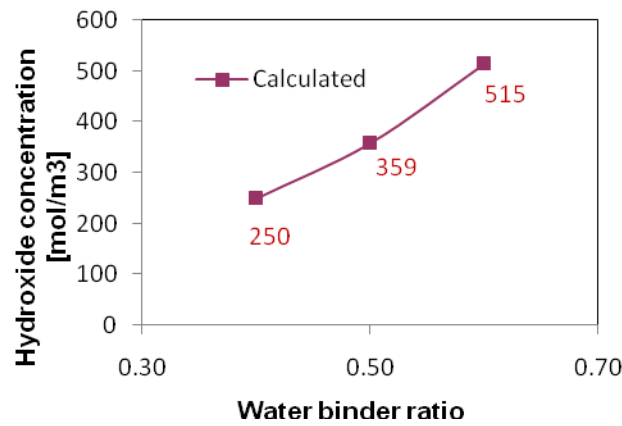
Figure 8-14 Hydroxide concentration calculated with the optimization model

The calculated intrinsic diffusion coefficients for all the species involved in the simulation (Cl^-, OH^-, Na^+, K^+) are shown in figure 8.15. As was stated by Andrade (1993), cations had a smaller diffusion coefficient than chlorides and hydroxides, except in the case of mix 6, in which hydroxide and sodium have a similar diffusivity. As was expected, the calculated numerical values of the intrinsic coefficients for all the species are, for all the cases, smaller than the coefficients of diffusion in infinite diluted solutions, as can be seen in any electrochemistry textbook. The values obtained are physically possible and are in acceptable ranges.
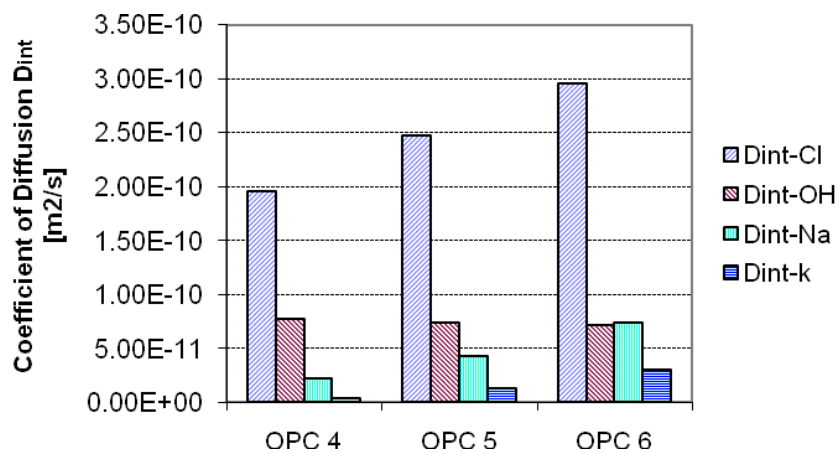
Figure 8-15 Intrinsic diffusion coefficients calculated with the optimization model

In the same way that the measured chloride penetration coefficient increases its value with the increase of the water binder ratio, the calculated chloride intrinsic coefficient also increases. The relationship between the chloride coefficients obtained from the diffusion test (using equation 6.14) and the migration test (using the integrated model) is shown in figure 8.16. The correlation coefficient R^2 was 1, indicating a strong relationship between the coefficients.
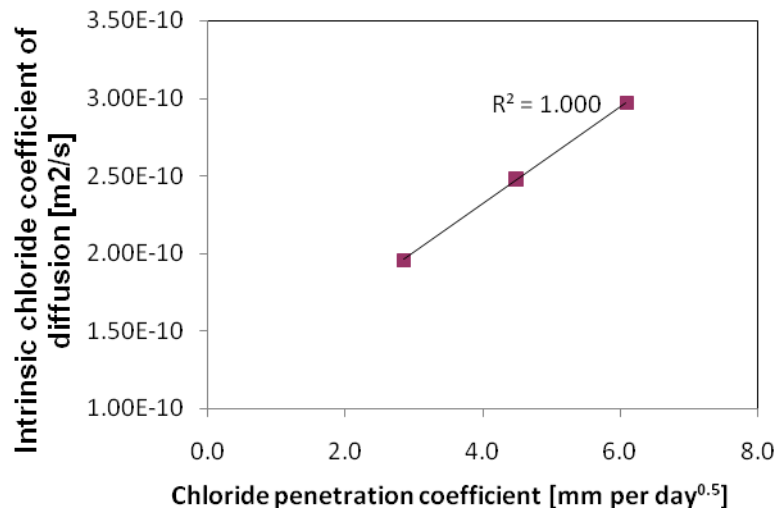
Figure 8-16 Relationship Intrinsic diffusion coefficients calculated and chloride penetration coefficients measured

It should be noticed that the number of points to establish the relationship shown in figure 8.16 is limited; however, it was presented to show the development of the neural network model. In part three of this thesis, additional data will be presented to make that relationship more representative.

8.8 CONCLUSIONS

34. From the work done in this chapter it can be concluded that the limitations of a simple or complex chloride penetration model are the inputs required. Between those, the external environment conditions and the transport material properties are the most important factors. The external conditions can be evaluated "*easily*", while for the former, "*expensive*" tests are required. Many experimental procedures have been developed for chloride ions in the last 30 years and new methodologies about this topic are frequently published. This is a clear indication that not all the problems have been solved and there remains a considerable amount of research still to do.

35. The standard determination of the chloride diffusion coefficients is time and resource consuming, in addition to the uncertainties of the methods and theories used.

36. From the technical literature in this chapter, it can be demonstrated that neural networks are a reliable technique to optimize a physical phenomenon. In that way, the optimization technique proposed in this research is an alternative that can yield to the accurate calculation of the concrete diffusivity with a short an inexpensive test.

37. The neural network model trained on numerical simulations of the migration tests yields viable results for the fundamental properties of concrete. The initial hydroxide composition of the pore solution, the chloride binding capacity, the open porosity and the intrinsic diffusion coefficients of chloride, hydroxide, sodium, and potassium were all estimated with acceptable results.

38. The properties optimized by the neural network model were in acceptable and physically possible ranges.

9 MODELLING VOLTAGE AND CURRENT CONTROL CONDITIONS

In this chapter the results of a programme dedicated to the study of the voltage and current control conditions, introduced in section 6.2, are presented. This has been done in order to validate numerically and experimentally the hypothesis behind those conditions.

9.1   INTRODUCTION

The ability of the Coventry University model to simulate adequately a voltage control test was assessed both numerically and experimentally. Great attention was given to the effect of the numerical process, the evolution of the electrical properties and the ionic concentrations. As current control tests and self-diffusion tests describe well-established mechanisms of chloride penetration into concrete, modifications to the Coventry model were introduced to mathematically simulate the effect of such conditions, and these findings were also validated experimentally. All experiments were carried out using the same mortar material, cast with the particular objective of obtaining the correct inputs needed for the computer models.

In addition to the two tests described above, two new electrical conditions, known as power control and variable voltage control respectively, were established and simulated. Again the general Coventry model was adjusted to meet the requirements of constant power and changing voltage simulations. For those conditions, no experimental work was carried out; rather, such simulations might form the basis upon which extensive future modelling and experimental research could be carried out.

The tasks undertaken in this stage of the research can be summarised as follows:

- First, based on the transient current and the membrane potential measured, the transport related properties were obtained using a neural network algorithm.

- Second, the voltage control ASTM C1202 test was simulated. The numerical process used, along with the results of the electrical properties and the ionic concentrations, were discussed. Additionally, the voltage control NT-492

migration test was simulated and the theoretical assumptions of the standard were discussed.

- Third, for the current control (non-zero current) condition, the most important theoretical aspects of the computer model were introduced. Basically, the Coventry model was slightly modified and the changes highlighted. Using this new computational code, the current control experiments were simulated and the validity of the model was assessed.

- Fourth, two additional computational models for migration tests under conditions of constant power and under variable voltage control were developed. Using these models, the response of the total current, the external voltage, the power and the temperature were able to be investigated.

- Finally, the computer code to simulate a current control condition (zero current) was introduced. Using this variant of the model, diffusion experiments were simulated.

9.2 EXPERIMENTAL PROGRAMME

9.2.1 Materials

A single mortar mix having a water to cement ratio of 0.36, and a sand to binder ratio of 3 was cast. Ordinary Portland cement CEM I without mineral or chemical admixtures was used. Nine cylinders of 100 mm diameter and 200 mm height were cast for use in open porosity, diffusion, and migration tests. In addition, three cubes of 50 mm were cast for the purpose of ascertaining the concrete strength. The specimens were cured under lime water at 21 ±2 °C prior to testing.

Table 9.1 shows the proportions of the materials used. The particle size analysis of the sand was already shown in figure 7.2. Because of the low water to cement ratio the mix had a poor workability, and so it was compacted manually using prolonged tamping in order to reach its maximum density.

	kg/m^3		
W/B	OPC	Sand	Water
0.36	650	1950	234

Table 9-1 Mortar mix design used in the voltage and current control experiments

9.2.2 Test

9.2.2.1   Compressive strength and open porosity tests

Compressive strength and porosity tests were carried out according to sections 6.4 and 6.5 once the samples had reached an age of 90 days. Three replicates were tested for each test.

9.2.2.2   Voltage control tests

The electrical current and the membrane potential were measured in a voltage control migration test, (ASTM C1202 – section 6.3.2), in samples of 90 days old. Three replicates were tested.

9.2.2.3   Current control (current ≠ 0) tests

The voltage drop was measured in a current control migration test (section 6.3.4) during a 6-hour experiment. The set up of the test was similar to the one recommended in ASTM C1202. But, instead of using a constant external voltage, a constant external current was being applied. The experiments were conducted in two stages. First, an initial experiment was carried out using a current of 50 mA. However, due to the low voltage generated, it was decided that the three specimens should best be tested under a current of 100 mA. All the samples used in this test were older than 100 days at the time of the experiment.

9.2.2.4   Current control (zero current) tests

The membrane potential was measured across the mortar specimens under a current control test with zero current (section 6.7). 10 mm thick samples were fitted between the reservoirs of the diffusion cell and potassium chloride was used in both external solutions. Concentrations of 1 M and 0.1 M KCl were used in the cathode and anode respectively. In order to monitor the potential difference across the sample, which corresponds to the membrane potential, calomel reference electrodes were used. No salt bridges were used for this test. The duration of the test was 12 days and two samples were tested.

In this test, solutions of KCl were used in the external reservoirs in order to avoid any junction potential developing due to the taking of experimental measurements. As was mentioned before, the diffusivity of potassium and chloride are similar, so no

significant electric potential was likely to develop between the reference electrodes and the solutions. At the time of testing, all the samples were older than 180 days.

9.2.2.5 Chloride penetration in self diffusion – "immersion" tests

Self diffusion chloride tests were carried out for a period of 72 days on samples of mortar according to section 6.8. The external concentration of chloride was 7% NaCl and this was renewed every 3 weeks. After the exposition period, the total chloride concentration was measured at different depths using the RILEM-TC-178-TMC recommendation. The experiments were started 100 days after casting the mortar specimens and two replicates were tested.

9.3 OPTIMIZATION OF PROPERTIES

Results of current and mid point membrane potential from the experimental voltage control migration tests are shown in table 9.2. Note that the values of membrane potential were previously filtered and adjusted according to the algorithm presented in figure 7.14. For both electrical parameters measured, the standard deviation is given in order to show the variability of the experiments.

	Inputs											
	Mid-point membrane potential [V]						Current [mA]					
Time [s]	0.00	1.21	2.42	3.60	4.81	6.00	0.00	1.21	2.42	3.60	4.81	6.00
measured	0.00	0.93	2.16	3.44	4.37	5.05	135.69	157.67	179.26	194.64	205.44	211.43
Stan dev	0.00	0.75	1.20	1.50	1.55	1.33	29.13	32.01	35.34	35.27	34.09	32.34

Table 9-2 Mid-point membrane potential and electrical current from the voltage control experiments (inputs of the optimization model)

Using the experimental results of table 9.2 and the neural network optimization model (section 8.4), the transport related properties for the mortar mix under test were calculated. Figure 9.1-A shows the intrinsic diffusion coefficients obtained. A discussion of the numerical values and the ratios among the diffusion coefficients is given in chapter 12. Figure 9.1-B shows the porosity measured experimentally and simulated with the numerical model. The simulated hydroxyl concentration of the pore solution before the tests was 240 mol/m^3 and the simulated linear chloride binding capacity factor was 0.38.
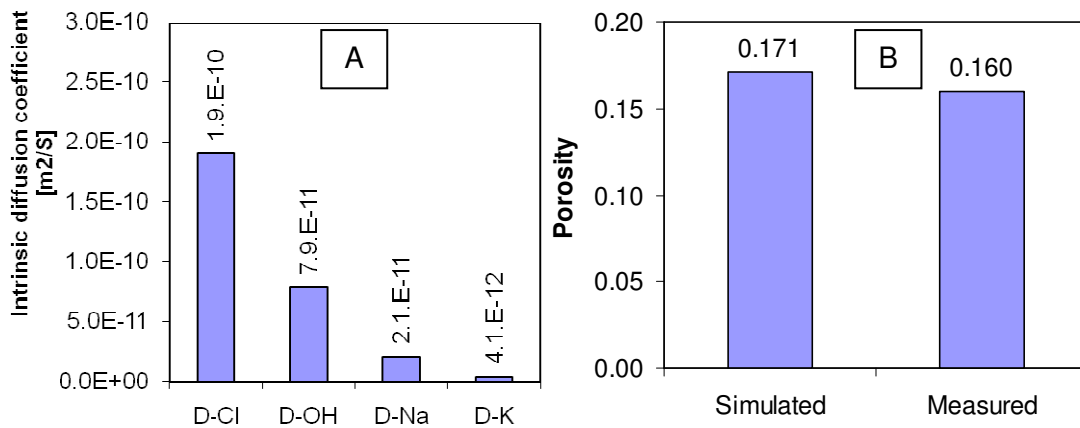
Figure 9-1 (A) Simulated intrinsic diffusion coefficients, and (B) simulated and measured porosity

The properties obtained using the neural network were used to feed the Coventry model in order to obtain the corresponding simulated transient current and mid point membrane potential. Figure 9.2 shows the evolution of the measured and simulated membrane potential. Figure 9.3 shows the current profile of the simulated and measured electrical current. An additional simulated profile included in this figure shows the results obtained when the model is run without the voltage correction (and taking no account of the effect of the membrane potential).
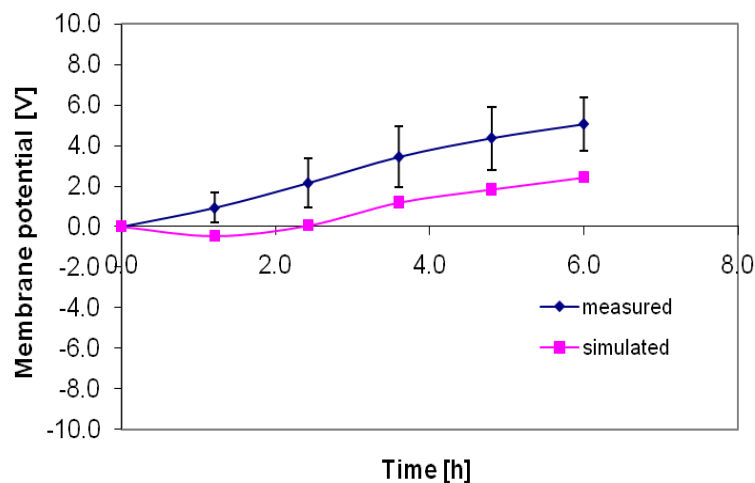
Figure 9-2 Measured experimentally and simulated mid-point membrane potential

The average compressive strength measured was 48.6 MPa.
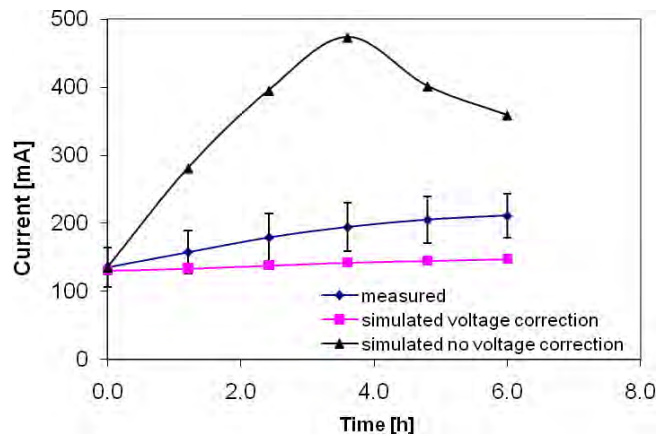
Figure 9-3 Evolution of the measured and simulated electrical current during the test

The temperature measured during the test was compared with the simulated temperature obtained when running the voltage control model with the transport properties optimized. The room temperature used was 295°K and the heat loss factor was 0.30 J/°K. (The latter was established from a calibration carried out at the initial stage of the research). As was expected, the simulated and measured temperatures are in very good agreement. The evolution of the temperature is a function of the evolution of the charge, and it was shown in figure 9.3 that the simulated and measured currents are similar.
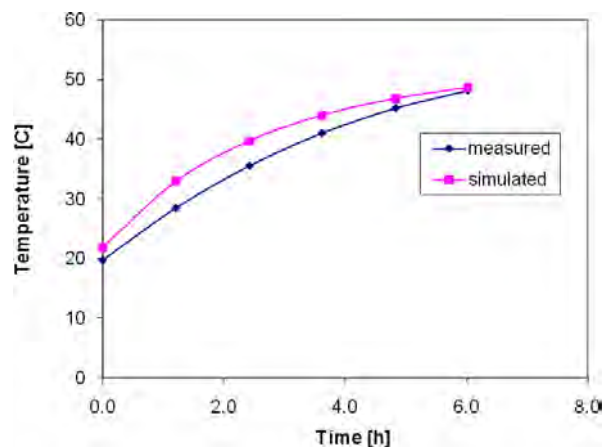
Figure 9-4 Evolution of the measured and simulated temperature during the voltage control test

9.4   SIMULATING VOLTAGE CONTROL

In this section, using the optimized transport properties, the voltage control model was run and its principal outcomes are presented and discussed. Table 9.3 shows the input parameters used in order to set up the ASTM C1202 test computationally.

	Valence Z	Intrinsic Diffusion D m^2/s	Concentration [mol/m^3] (in liquid)			Capacity factor
			negative	in sample	positive	
hydroxyl	-1	7.877E-11	0	239.973	300	0.171
chloride	-1	1.904E-10	530	0.00E+00	0	0.383
sodium	1	2.061E-11	530	7.92E+01	300	0.171
potassium	1	4.099E-12	0	1.61E+02	0	0.171

No of cells:	100
Voltage correction?	**YES**
Time step [s]:	2
Run time [hours]:	6
Porosity:	0.171
Applied voltage [V]:	60

Sample length [m]	0.05
Sample radius [m]	0.05
Room temperature [K]	295
Cell volumes [m^3]:	2.00E-04
Heat loss factor [J/K]:	0.30

Table 9-3 Input Parameters used - voltage control model

9.4.1 Effect of the numerical process

The numerical formulation of the Coventry model used to solve the diffusion and migration terms, of the Nernst-Planck equation presented in tables 5.4 and 5.6, corresponds to a finite differences scheme. Although this gives a good approximation of the solution of the physical phenomenon, it is numerically affected by the size of the steps of time and position. If the time and position steps tend to zero, the model prediction is more similar to the real solution. However, an excessive decrease in the time and length steps generates significant increases in the execution times. In order to verify the influence of the size of these steps in the results, a sensitivity analysis as a function of the total charge passed was performed.

The influence of the number of cells on the total charge is shown in figure 9.5-A. For the mortar sample simulated under conditions similar to the ASTM test there was an important effect on the charge when the number of cells was less than 100. By contrast, there were relatively small differences in charge, when more than 100 cells were used. According to this result, equation 9.1 can be used to define the relationship between the length of the sample L [mm] and the number of cells

$$\frac{L}{\#cells} \leq 0.5 \quad (9.1)$$

Figure 9.5-B shows the influence of the time step on the total charge passed. For a time step equal to 2 s, a difference of 0.2% on the charge, respect to the charge calculated with 0.5 s was obtained. According to figure 9.5, the steps presented in table 9.2 are sufficient to keep the numerical error within acceptable limits.
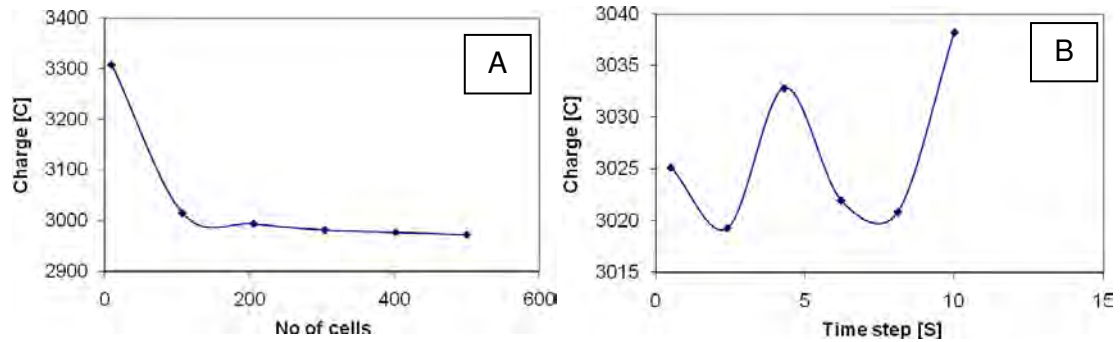
Figure 9-5 Influence of the number of cells and the time step on the total charge passed

9.4.2 Membrane potential and current evolution

The simulated membrane potential for the mortar mix is shown in figure 9.6 as a colour contour map. A similar profile was obtained in chapter 7 for tests and materials of similar characteristics. In the same way as mentioned earlier, the membrane potential is non-linear in time and position, allowing the sample to maintain its charge neutrality throughout the experiment and at all points within the sample. If the model is run without the voltage correction, (i.e. no charge neutrality), the membrane potential would have a value of zero for each time and position, in contrast to the experimental findings.
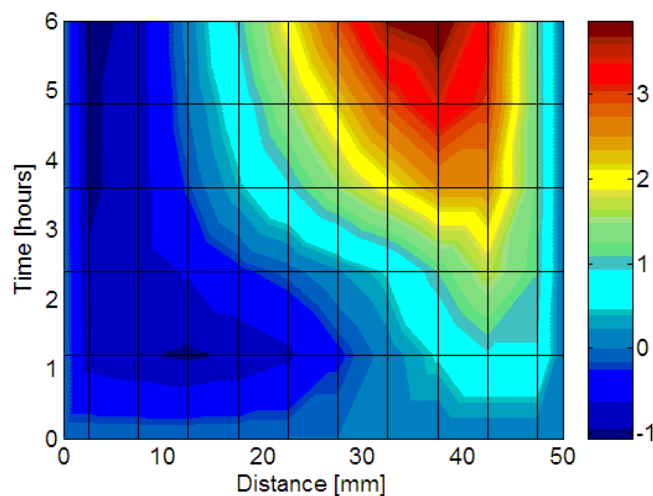
Figure 9-6 Simulated membrane potential [V] for the mortar mix

Figure 9.7 and 9.8 shows the ionic current for anion and cations included in the simulation. Although the total current at any point within the sample is constant for a specific time, the currents passed by individual ions do not follow this rule and are typically non-zero. From the figure it can be observed that the hydroxide and chloride ions are responsible for most of the total current passed. At the beginning of the test hydroxyl ions predominate; however, a couple of hours later, chlorides, which are now penetrating massively into the sample, have begun to control the current being passed. By the end of the test, the chloride ions were responsible for about 80% of the total current.

The role of cations is less important than that of anions; however, they are essential for establishing the necessary conditions of neutrality within the system. Although chloride and hydroxide are much more mobile species, without sodium and potassium the neutrality condition would never be successfully achieved.
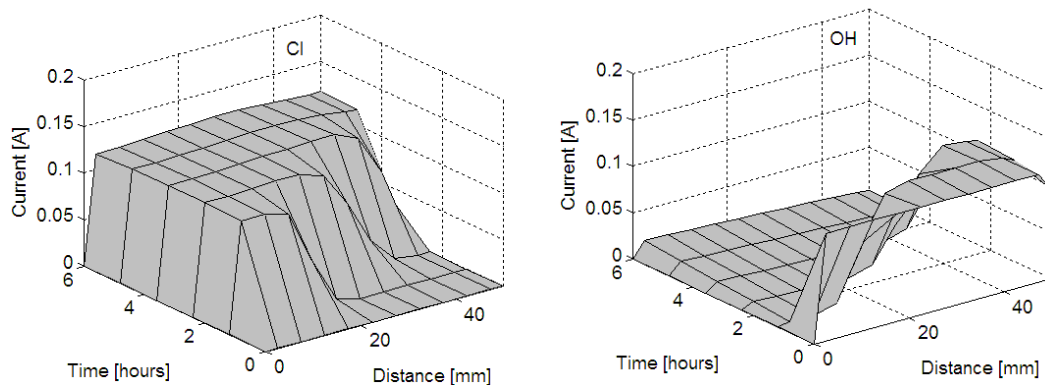
Figure 9-7 Ionic current during the ASTM C1202 test: chloride and hydroxyl ions
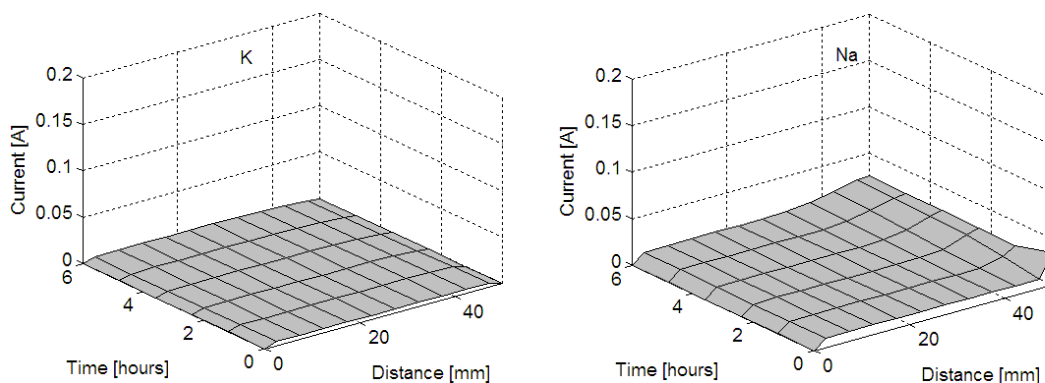
Figure 9-8 Ionic current during the ASTM C1202 test: potassium and sodium

The transport number was defined in equation 5.24 as the ratio of the current passed by any ion to the total current passed by all the ions. Figure 9.9 shows in bars chart

the simulated current passed for each ion and the total current for three different times. Figure A shows the condition where no voltage correction is taken into account in the model, and figure B shows the results using the voltage correction presented in section 5.7.3. From the figures it can be observed that the transport number is non-linear in both time and position; however, if a steady state condition is reached during the test, the transport number is likely to become a constant.
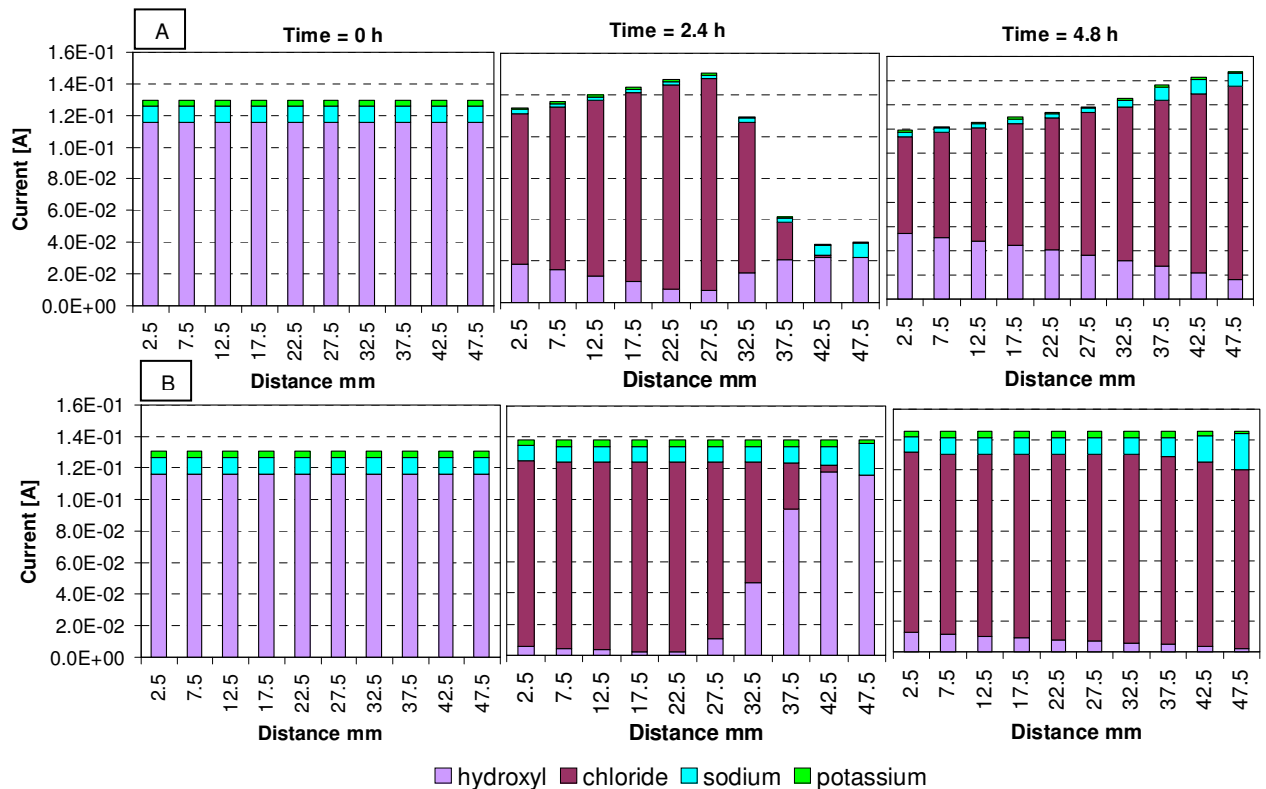
Figure 9-9 Ionic current in a ASTM C1202 test (A) no voltage correction (no ionic interaction) (B) voltage correction (ionic interaction)

9.4.3 Ionic concentrations

For the mortar sample simulated, the ionic concentrations of OH^-, Cl^-, Na^+ and K^+ are shown in figure 9.10 as colour contour maps. At the beginning of the test, chlorides were present only in the cathode external reservoir; however, as the test progressed, chlorides penetrated the specimen and reached the other external cell (anode).
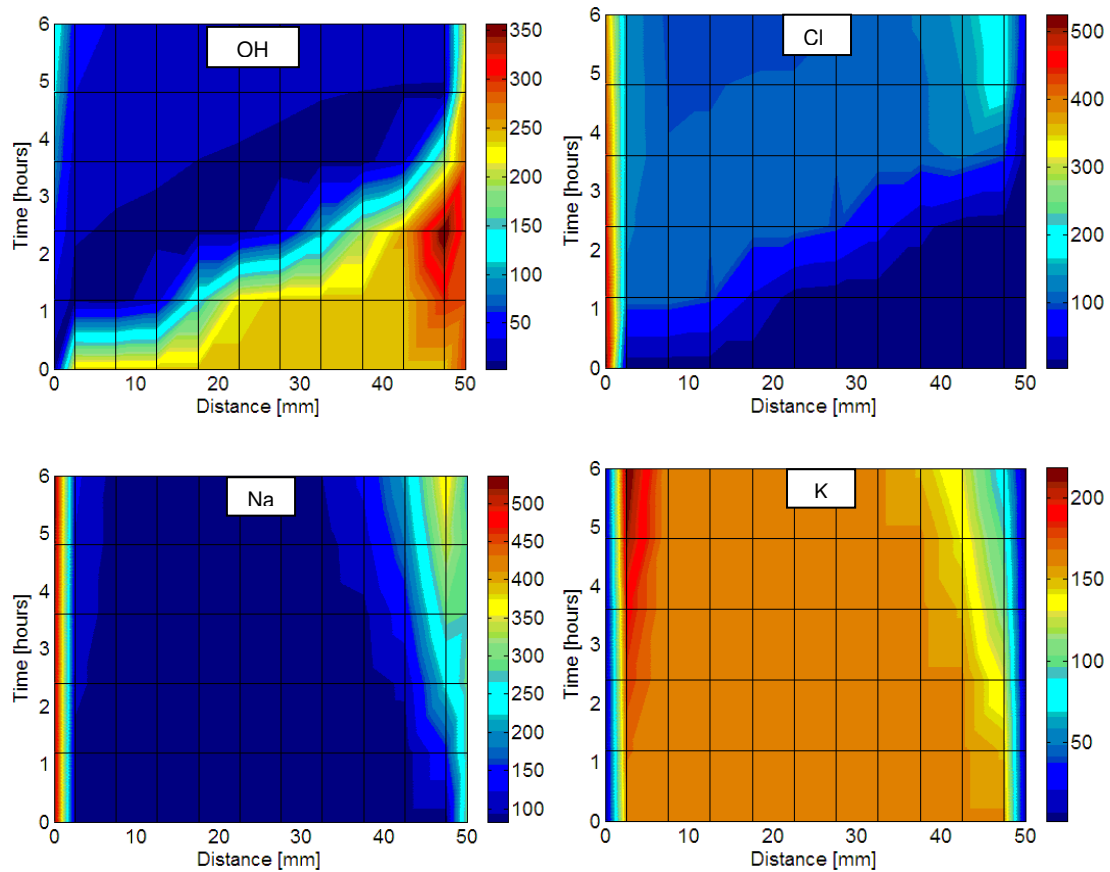
Figure 9-10 ASTM C-1202 simulated concentrations for hydroxyl, chloride, sodium and potassium [mol/m³]

From the results of concentrations it can be seen that prior to the start of the test, the hydroxyls ions were uniformly distributed in the pore solution and in the anode external cell. However, as is clear from figure 9.11, the concentration of those ions increase in the cathode while decreasing in the anode.

This behaviour is considered realistic because in an actual test the hydroxyl ions will migrate towards the anode where they are oxidized, releasing electrons. Simultaneously, at the cathode, hydroxyl ions and oxygen are released from water molecules, as a result of electrolysis. The results in figure 9.11 accord well with the findings of Prince, Perami and Espagne (1999).

The balance equations for anode and cathode are:

$$\text{Cathode: } 2H_2O + 4e^- \rightarrow H_2 + 2OH^- \qquad (6.3)$$

$$\text{Anode: } 2OH^- \rightarrow \tfrac{1}{2}O_2 + H_2O + 2e^- \qquad (6.4)$$
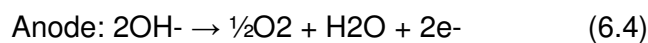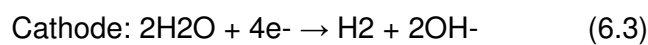
In modelling the migration process, due to charge neutrality requirements, hydroxyl ions that are generated at the cathode are transported through the concrete to the anode where they are subsequently destroyed.
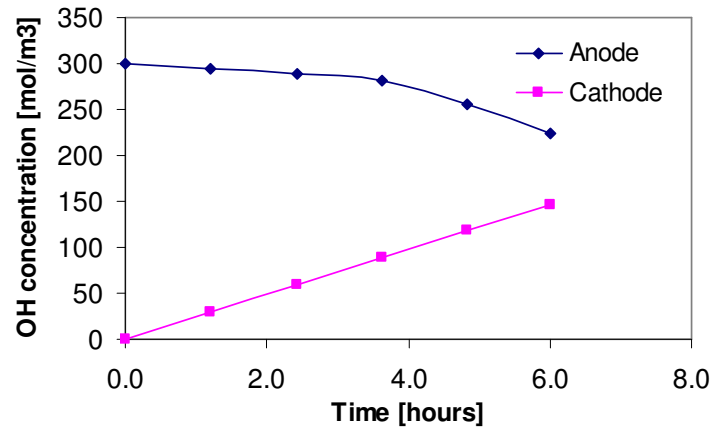
Figure 9-11 Simulated concentration of OH⁻ in the external reservoirs during a voltage control migration test

9.4.4 Influence of different parameters on the charge in a ASTM C1202 test

In this section, the influence of a number of both material and experimental parameters upon the total charge obtained during a standard RCPT test is presented. The relationships between the parameters being evaluated and the charge were simulated using the input data tabulated in table 9.3 above. Figure 9.12 shows the simulated relationships.

material-related parameters:
the effect of the intrinsic chloride diffusion coefficient,
the OH⁻ initial concentration of the pore solution,
the binding capacity factor,
the capillary porosity.

experiment related parameters:
the length and diameter of the specimen,
the volume and chloride concentration of the external reservoirs cells,
the external voltage applied.
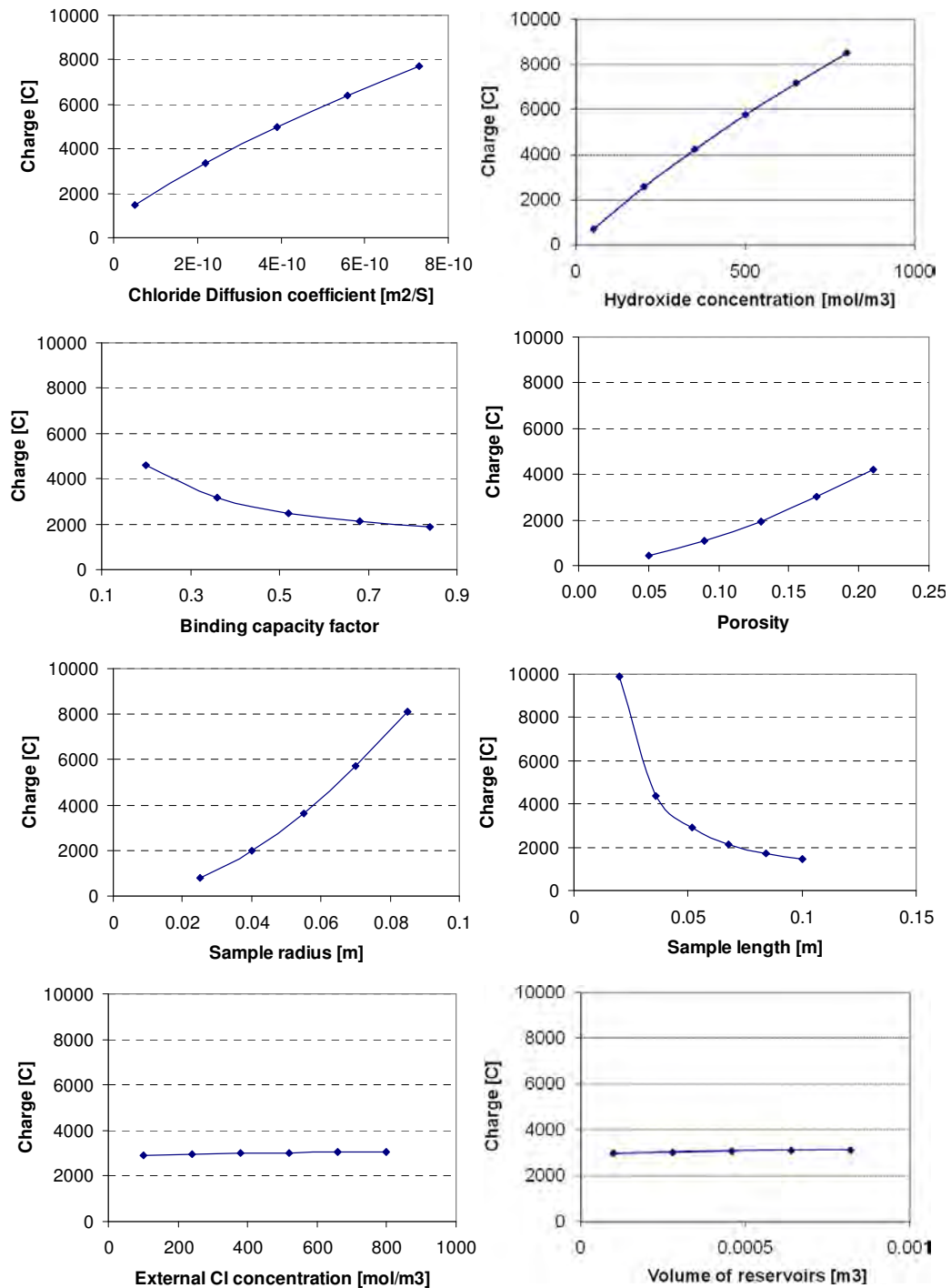
Figure 9-12 Effect of the sample and materials properties on the charge passing during a standard ASTM C-1202 test

As was expected, the material parameter that most affects the charge passed in an RCPT test is the chloride diffusion coefficient. However, the hydroxyl concentration is also highly relevant, particularly since the mineral admixtures that are typically used, (especially silica fume, fly ash, and GGBS), all have a significant effect upon the pore solution. In chapter 12 of this thesis, the effect of the pore solution on the reliability of

the charge passed as a measure of chloride transport in mixtures containing GGBS is presented. With respect to the parameters used in setting up an experiment, the geometry of the sample is extremely important, and significantly affects the charge as well as the external voltage. However, it is possible to standardize all the external conditions.

9.4.5 Nordtest method NT- 492

The migration Nordtest NT492 has been used extensively to find the non-steady-state migration coefficient. It uses the mathematical solution for the Nernst-Planck equation for a chloride mono-ion system assuming a semi-infinite homogeneous medium (Luping and Nilsson 1992).

$$c(x,t) = \frac{c_s}{2}\left[e^{ax}\,ercf\left(\frac{x+aDt}{2\sqrt{Dt}}\right) + ercf\left(\frac{x-aDt}{2\sqrt{Dt}}\right)\right] \qquad (9.2)$$

where $c(x,t)$ is the concentration of chloride after a time t at a distance x form the surface of the sample, $ercf$ is the complement of the error function erf, c_s is the steady chloride concentration at the surface, and a is a constant related with the external voltage applied, defined by equation 9.3.

$$a = \frac{zF\varphi}{RT} \qquad (9.3)$$

Under special conditions, the numerical results obtained from the Coventry model are similar to those found using equation 9.2. Those conditions refer to the following assumptions.

- There is no ion interaction between different species (No voltage correction: no membrane potential is generated).
- There is no binding of any species (Capacity factor (α)/porosity (ε) =1).
- There is no depletion of the chloride concentration in the cathode during the test.
- There is no pore solution in the sample.

In order to illustrate the theoretical concentration profiles of equation 9.2, the Coventry model was run using the inputs shown in table 9.4. The numerical values were established according the suggestions of the standard and the physical conditions stated above. Figure 9.13 shows the calculated chloride profiles for

different times, which behave in a similar way to that described by Luping and Nilsson (1992). Under the influence of an electrical field, chlorides move by migration at a constant speed and therefore induce a front of penetration. The steady state is reached when the chloride concentration inside the sample do not change.

| | Valence z | Intrinsic Diffusion D m²/s | Concentration [mol/m³] (in liquid) | | | Capacity factor |
			negative	in sample	positive	
Chloride	-1	1.90 x10^{-10}	1900	0.00E+00	0	1

No of cells:	500		Sample length [m]	0.05
Voltage correction?	**NO**		Sample radius [m]	0.05
Time step [s]:	1		Room temp [K]	295
Run time [hours]:	8		Cell volumes [m³]:	1
Porosity:	1		Heat loss fact [J/K]:	0.3
Applied voltage [V]:	8			

Table 9-4 Input data simulation Nordtest NT-492 (mono-ion system)
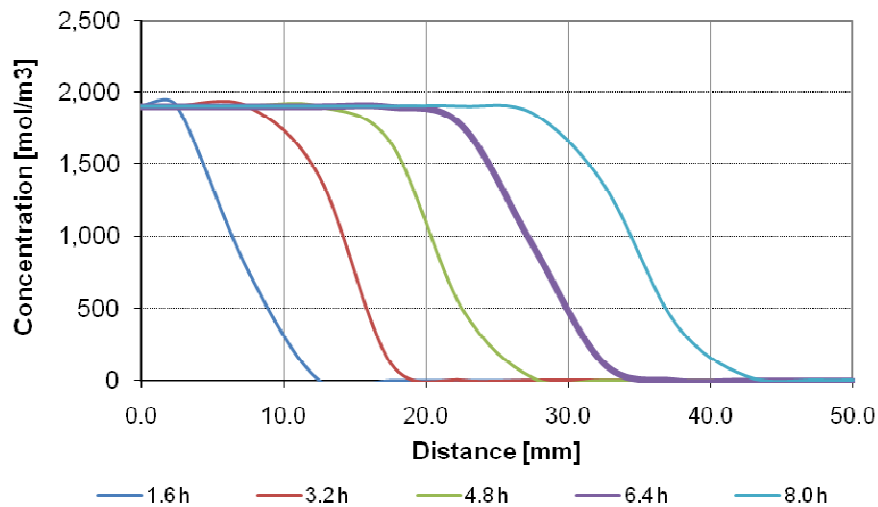
Figure 9-13 Theoretical concentration profiles for different times [hours] (obtained from the Coventry model with no voltage corrections)

In order to compare the theoretical chloride profiles from equation (9.2) with the profiles simulated by the Coventry model (including ionic interaction, chloride binding, and the real volume reservoirs) a new simulation was carried out. The input data is shown in table 9.5, including the diffusion coefficients and the initial concentration of the species incorporated. Results of the model are shown in figure 9.14, which shows the evolution of chlorides for different times.

Using the concentration profiles obtained from the "virtual" migration test shown in figure 9.14, the non-steady state migration coefficient was determined (D_{nssm}) following the procedure suggested by the NT492. (The approximate equations given by the standard to obtain the coefficient were already presented in section 5.5.1.2). The chloride profile at 6.4 hours had a penetration of 9.3 mm when the concentration was 70 mol/m^3. That specific concentration was used because it is the concentration of free chlorides in the boundary when the colorimetric method is used.

	Valence Z	Intrinsic Diffusion D m^2/s	Concentration [mol/m^3] (in liquid)			Capacity factor
			negative	in sample	positive	
hydroxyl	-1	7.877E-11	0	239.973	300	0.171
chloride	-1	1.904E-10	1900	0.00E+00	0	0.383
sodium	1	2.061E-11	1900	7.92E+01	300	0.171
potassium	1	4.099E-12	0	1.61E+02	0	0.171

No of cells:	500	Sample length [m]	0.05
Voltage correction?	**YES**	Sample radius [m]	0.05
Time step [s]:	1	Room temperature [K]	295
Run time [hours]:	8	Cell volumes [m^3]:	0.03
Porosity:	0.171	Heat loss factor [J/K]:	0.30
Applied voltage [V]:	8		

Table 9-5 Input data to simulate the Nordtest NT-492 (including ionic interaction)

Figure 9-14 Coventry model concentration profiles for different times [hours]

The chloride diffusion coefficient (D_{nssm}) obtained from the concentration profile at 6.4 hours of figure 9.14, according to the standard, was 5.23x10^{-11} m^2/s. This diffusion coefficient, which acts as a proportional parameter in equation 9.2, forces the profile to have an approximate concentration of free chlorides of 70 mol/m^3 at 9.3 mm.

Figure 9.15 shows the chloride evolution at 6.4 hours when the NT-493 migration test is simulated using three different approaches.

(1) The analytical equation 9.2, which assumes a mono-ion system (only chlorides) without binding. For this, the chloride diffusion coefficient used was the value obtained from the neural network model: $D=1.9 \times 10^{-10}$ m^2/s.

(2) The voltage control model presented in section 5.7. This includes ionic interaction and binding. For this were used all the transport properties optimized in section 9.3.

(3) The analytical equation 9.2, which assumes a mono-ion system (only chlorides) without binding. For this, the chloride diffusion coefficient used was the value obtained from the "virtual" NT-493 standard: $D_{nssm} = 5.23 \times 10^{-11}$ m^2/s.
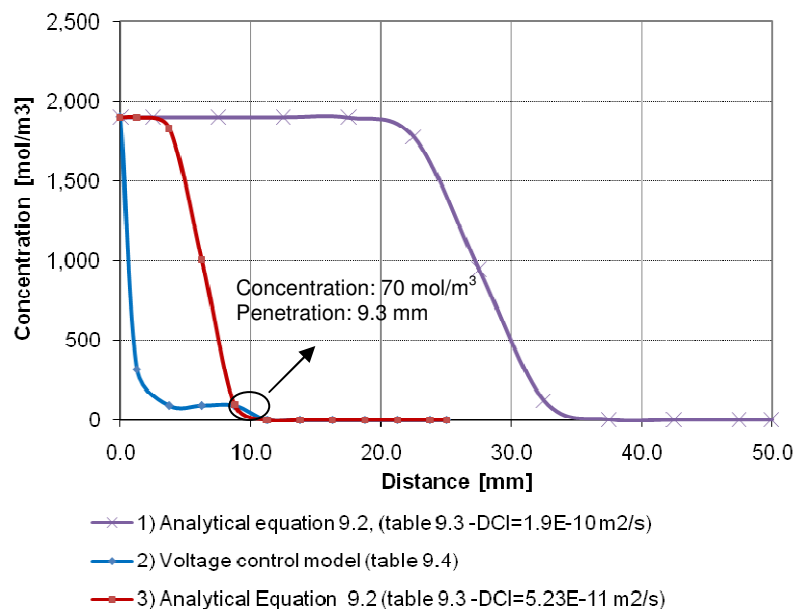
Figure 9-15 Results of chloride concentration profiles in a NT-493 test at 6.4 hours using different approaches

Although approaches (2) and (3) had the same value of concentration (70 mol/m^3) for a penetration of 9.3 mm, the profiles were very different. From figure 9.15 it can be seen that although in the Nordtest the diffusion coefficients were found from a known value of penetration and concentration, the profile obtained is very different to that calculated using ionic interaction and binding. The penetration fronts described by Luping and Nilsson (1992) were obtained, using in their model, a single ion condition; in reality, of course, the situation is much more complex. Indeed, when the Nernst-Planck equation, adapted to account for ionic interactions, is used, the penetration front does not behave in the way reported by Luping and Nilsson (1992).

9.4.6 "Apparent" good chloride resistance due to the pore solution

As was mentioned before, the ASTM C1202 test has been criticized due to the possibility of obtaining low charge results reflecting low penetrability when in fact concrete could in reality have high chloride penetrability. That situation could occur in samples with a high chloride diffusion coefficient but with a depleted pore solution hydroxyl ion concentration like in some kind of pozzolans which deplete that hydroxyl ion concentration. Also in a number of different concrete admixtures including calcium nitrite, calcium nitrate, calcium chloride and sodium thiocyanate which affect the current measured but do not adversely affect the durability. In order to illustrate this situation, figure 9.16 shows the electrical current for a concrete sample simulated under different inputs.
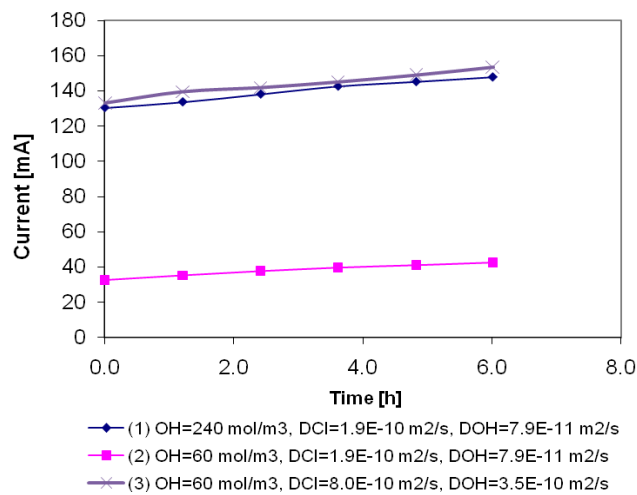
Figure 9-16 Current evolution of different samples using different OH⁻ concentration and chloride diffusion coefficient

In the figure, Sample (1) corresponds to the mortar cast, using as inputs the optimized properties shown in table 9.3. Sample (2) uses similar values to that of sample (1), with the exception of the hydroxide ion concentration of pore solution, which was decreased from 240 mol/m^3 to 60 mol/m^3. Sample (3) uses similar properties to that of Sample (1), but here the hydroxyl ion concentration of pore solution was 60 mol/m^3, and the intrinsic diffusion coefficients of chloride and hydroxyl were increased by a factor of 4 approximately.

Although the total charge for samples (1) and (3) is very similar, the chloride diffusivity is very different. In that way, the applicability of the RCPT test and the resistivity as tools to evaluate the chloride penetrability for slag mixes is investigated and discussed in detail in chapter 12.

9.5   CURRENT CONTROL (non-zero current)

In this section the theoretical and experimental aspects of a migration test under a current control condition are presented. First, the basic elements of the model proposed are summarised: the computational diagram flow of the model is shown, emphasizing on the changes respect to the voltage control condition. Second, experimental results of voltage are compared with numerical results; and finally, the chloride and voltage evolution in the sample is simulated and discussed.

9.5.1 Current Control Model (non-zero current)

Under a current control condition a concrete sample is subjected to a steady known electrical current. The current density must be constant in time and position during the test. In consequence, the corresponding external voltage applied to the sample does not remain constant over time. This situation makes for some slight modifications to the computer code, as shown in section 5.7 for the Coventry voltage control model.

Although the external electrical field in the current control is not an input, it can be calculated numerically. At the beginning of the test an approximate voltage is approximated according to the Nernst-Einstein equation, the resitivity, and Ohm's Law:

Numerical formulation	Physical Equation
$$\sigma^{t=0} = \sum_{i,k} \sigma_{i,k} = \sum_{i,k} \frac{z_k^2 F^2 C_{i,k}}{RT} \varepsilon D_k$$	Nernst-Einstein (5.6) $$D_i = \frac{RT\sigma_i}{z_i^2 F^2 C_i}$$
Resistivity (6.14) $\rho = \dfrac{1}{\sigma} = \dfrac{RA}{L}$; Ohm's Law $V = RI_{app}$	

Table 9-6 Equations used to find the Initial voltage in the current control model

Using the initial estimated voltage, the model calculates the diffusion and migration fluxes and avoids the excess of charge in the same fashion as the voltage control model. However, a new routine has been introduced in order to check whether the total current passed through the sample (I_{total}) is similar to the external current applied (I_{app}). If this condition is not met in full, the external voltage is rectified and the diffusion and migration fluxes are recalculated iteratively until this condition is

satisfied. Once the above condition is met, a next time step is adopted. Figure 9.17 shows a detail of the routine.

$$Error = \frac{I_{app} - I_{total}}{I_{total}}$$

$$|Error| < 0.0001$$

No

$$V_i^{new} = V_i + V_i(Error)$$

Yes
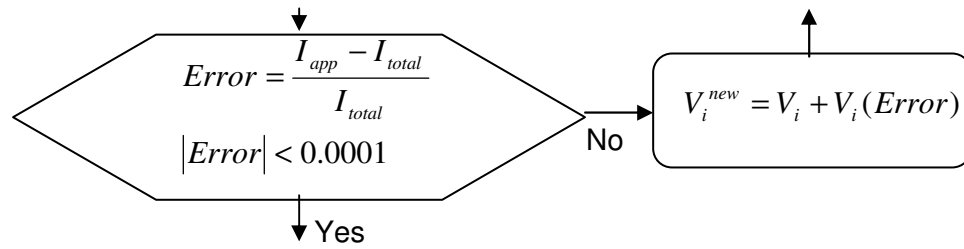
Figure 9-17 Current control routine to check and correct the voltage applied in each time

Figure 9.18 shows the flow chart of the model, highlighting the modifications with respect to the voltage control condition.

INPUTS

Approximate initial voltage (Table 9.5)

Calculate diffusion flux for each ion in all space steps

Calculate Electro-migration for each ion in all space steps

Distribute adsorbed / solution ions by distribution ratio

Total concentration's changes in any space step is more than 10% of the previous concentration — Yes → Reduce ΔT by 10 %

No

Calculate the charge surplus in each space step

Correct the voltage in all space steps

Correct the voltage in all space steps to prevent charge built up — Yes ← The total charge surplus is more than 10⁻¹⁰ coulomb in any space step

No

Is the current Error <0.0001? — No

Yes

Change concentrations

Calculate the accumulated time ΣΔT

Increase the time step by 1%

ΣΔT < T — Yes

Figure 9-18 Flow diagram for the current control model

212

9.5.2 Results and discussion of current control (non-zero current)

For the voltage control condition the membrane potential was calculated according to equation 7.1, as the difference between the total voltage measured and the voltage applied. As for that condition the external voltage applied is constant, the excess in voltage measured experimentally was attributed to the ionic contribution. Likewise, for the current control condition the total voltage measured is composed of a corresponding external voltage and an internal membrane potential. Unfortunately, as this external voltage is transient in time, it is not possible calculate the membrane potential using equation 7.1. So, the results for this experiment are shown as total voltage measured and not as membrane potential.

The experimental and simulated difference of potential through the whole complete sample, and between the cathode and the centre of the specimen (mid point) are shown in figure 9.19. The single test run under a steady current of 50 mV is shown in figure A. Figure B shows the results for the sample run under 100 mA. As three replicates were run experimentally for this last current, the variability of the experiments is given as error bars with amplitude equal to the standard deviation. From the figure can be seen that the simulations are in very good agreement with the experiments. The higher error found in the mid-point can mainly be attributed to the effect of the position of the hole drilled to insert the salt bridge.
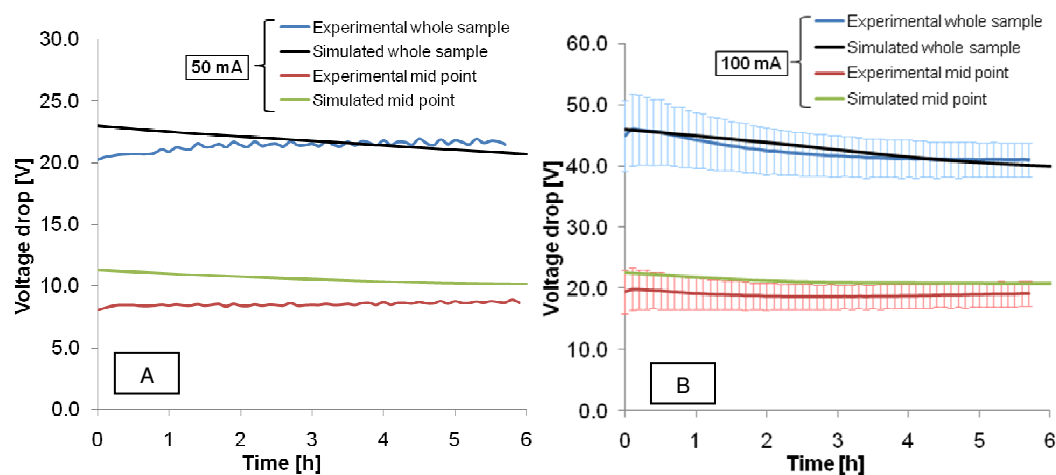
Figure 9-19 Evolution of the voltage between the whole sample (electrodes) and between the mid point and the cathode during a current control test

Figure 9.20 shows the results of temperature evolution for samples run under 50 and 100 mA.
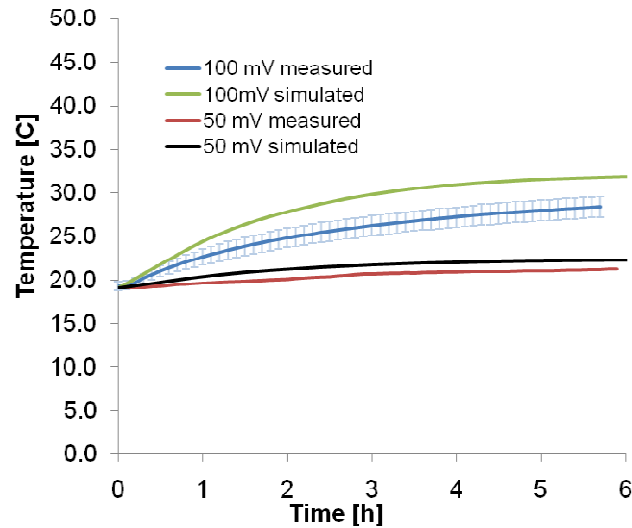
Figure 9-20 Measured and simulated evolution of the temperature during the current control experiments

The simulated voltage generated at different times, under a constant 100 mA, is shown in figure 9.21. At the beginning of the test, the voltage evolution was linear through the sample; however, voltage deviations were necessary to keep the total current constant. Simulations of ionic current for each ion included in this simulation showed a similar behaviour to that obtained in figure 9.7, Chloride and hydroxyl ions are responsible for the majority of the current carried, while sodium and potassium together carry only a minor amount of the overall current.
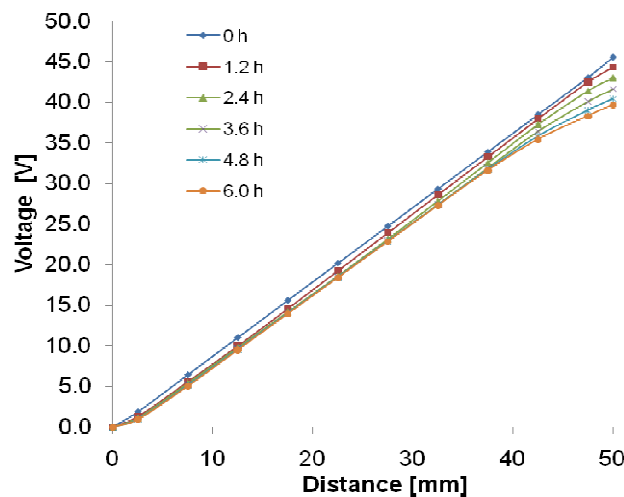
Figure 9-21 Simulated voltage adjustments at different times (100 mA) during the current control condition

The free chloride concentration profile for the 100 mA current control test simulated at different times is shown in figure 9.22. This test is regarded as in a non-steady

condition, the source reservoir is depleting over time and the chloride ions are just beginning to reach the anode reservoir.
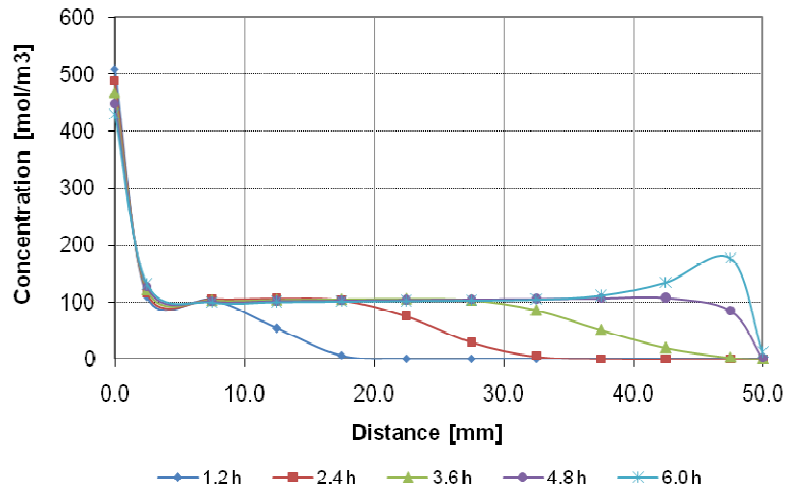
Figure 9-22 Simulated chloride profile at different times (100 mA) during the current control condition

9.6 PRELIMINARY MODELLING TO PROPOSED FUTURE WORK

As was mentioned earlier, one of the main criticisms of the ASTM test is the high temperature obtained, so new alternative tests are being proposed worldwide to decrease the impact of heating upon the chloride penetration results. The main response of ASTM to these problems has been the development of the "5 minute test". This is the same RCPT test but run for a greatly reduced time, giving a rapid indication of concrete quality.

Another key problem of the standard RCPT test is that it measures the electrical conductivity. At the beginning of the test, the main electrical contributors are hydroxyl ions; so, a mix may be formulated with low conductivity (e.g. by using pozzolans to depleted the hydroxyl ion concentrations) to pass the test while having relatively poor durability (section 9.4.6). Also a number of different concrete admixtures including: calcium nitrite, calcium nitrate, calcium chloride and sodium thiocyanate will increase the measured current but do not adversely affect the durability.

Simulations and experimental results of voltage and current control migration tests were already presented in sections 9.4 and 9.5. In order to contribute to the understanding of additional testing possibilities, this section reports briefly on some preliminary modelling that has been carried out using other modifications to the Coventry University model. The computer code has been adjusted to address certain specific electrical conditions; in particular, the numerical results of some "virtual"

migration tests controlled by power and changing voltage conditions are presented. Simulations were conducted in order to ascertain the response of voltage, current, power, and temperature. However, no experimental work has been carried out to substantiate any of these results. The main objective then of these simulations of the different migration tests controlled under different parameters (current, variable voltage and power) has been to provide a preliminary assessment of the feasibility of modelling tests. It is expected that the results might serve as basis for conducting new researches.

9.6.1 Power control model

Power is defined as the amount of energy used during a test across a specific unit of time. This is influenced by the external conditions of the experiment (external voltage) and also by the internal characteristics of the concrete sample (its resistivity). The condition of power control is reached when a specimen of concrete is subjected to a constant power by varying the driven voltage. Nowadays, DC power supplies can be voltage, current, or power controlled; this new electrical condition then is not a difficult one to set up.

The computer model for power control was developed in the same way as for the current control model. However the main condition to be achieved in this instance was constant power. At the beginning of the test an approximate voltage is calculated according to Nernst-Einstein equation, the resitivity, and equation 9.4, which relates electrical resistance and power.

$$Power(t) = Current(t) x Voltage(t) = \frac{[voltage(t)]^2}{resis \tan ce(t)} \quad (9.4)$$

As in the current control model, using this estimated initial voltage, the model then calculates the diffusion and migration fluxes and avoids any charge surplus; here, however, the constant power condition is guaranteed using the routine shown in figure 9.23. The power generated (P_{gen}, calculated by equation 9.4) is compared with the power desired (P_{app}), and if the difference is higher than a specific limit (0.1%) the external voltage is adjusted and the diffusion and migration fluxes are recalculated iteratively until this condition is fulfilled. Once the above condition is met, a new time step is started.

$$Error = \frac{P_{app} - P_{gen}}{P_{gen}}$$

$$|Error| < 0.001$$

No

$$V_i^{nuevo} = V_i + V_i(Error)$$

Yes
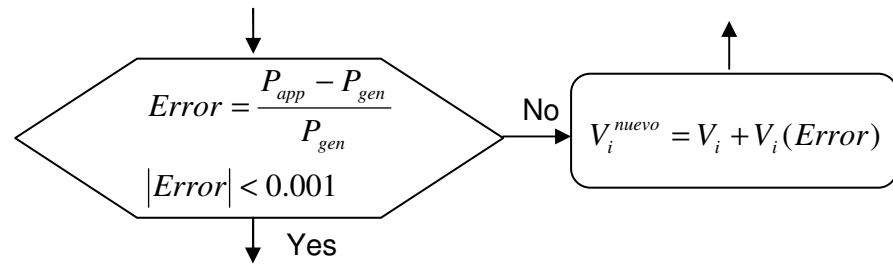
Figure 9-23 Power control routine to correct the voltage

9.6.2 Transient voltage control model

The transient voltage control consists of a migration test in which the external voltage is not constant over time. It changes linearly as can be seen in figure 9.24 and requires as inputs an initial voltage (V_0), the final voltage (V_f) and the duration of the test (t_f). Basically, the computational model is the same routine as for the voltage control model; however, a new condition was introduced in order to set the actual voltage at any particular moment in time.

$$V(t) = V_0 + \frac{t}{t_f}(V_f - V_0) \qquad (9.5)$$
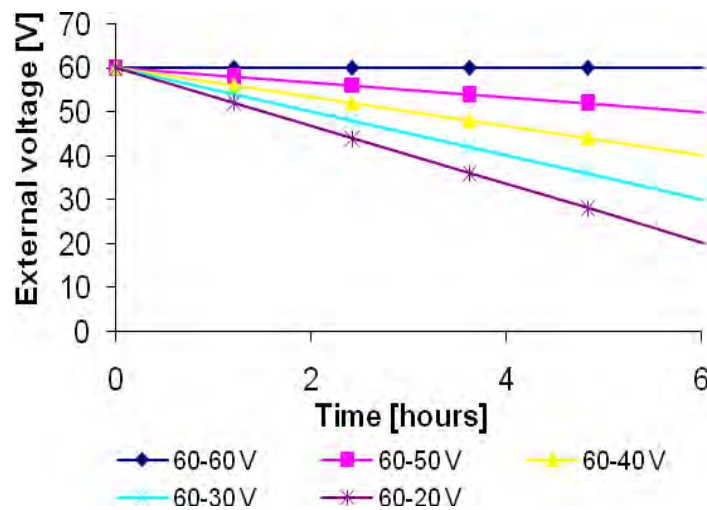
Figure 9-24 Transient external voltages

9.6.3 Response of migration tests under different conditions

In figures 9.25 to 9.28 are shown the electrical response of the electrical conditions developed in this research. The simulations were carried out for the material optimized in section 9.3 and conditioned as is advised by the standard ASTM C1202. Figure 9.25 shows the current, power and temperature simulated from a voltage

control test under different applied external voltages. Figure 9.26 shows the external voltage generated, the power and the temperature simulated in current control tests under different applied external currents. Figure 9.27 shows the external voltage, the current and the temperature generated when the test is run under different power settings. Figure 9.28 shows the current, the power and the temperature generated in a variable voltage migration test under different external input voltages.
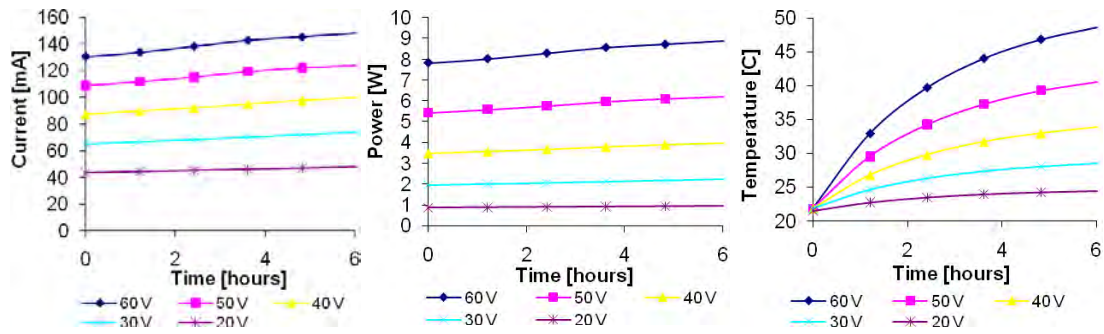
Figure 9-25 Evolution of different parameters for the voltage control condition
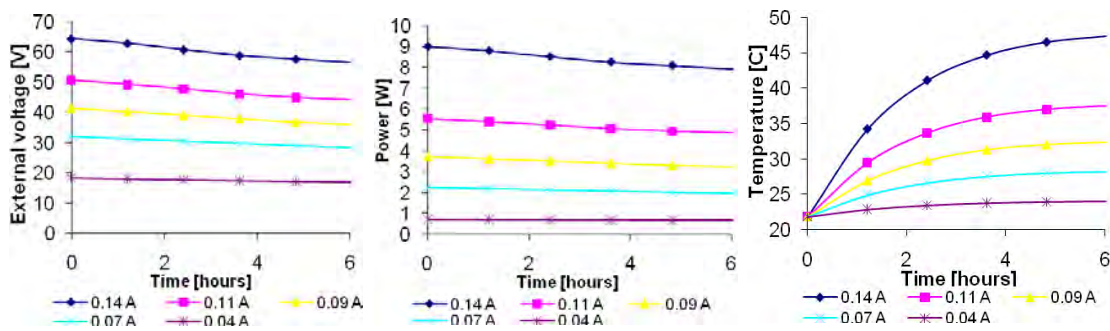
Figure 9-26 Evolution of different parameters for the current control condition
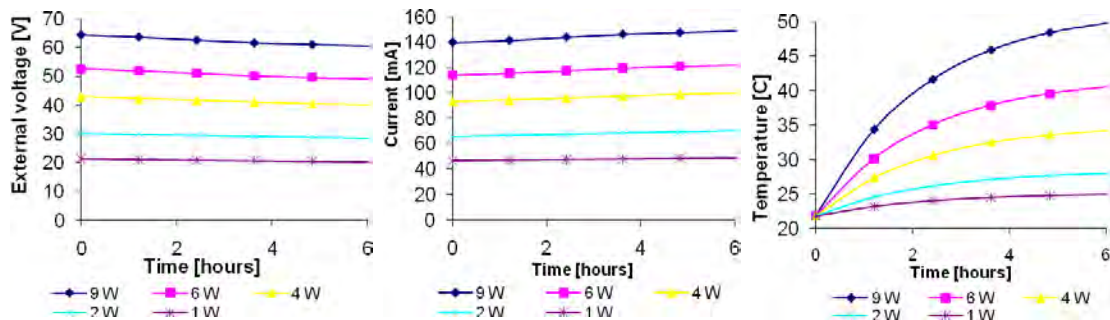
Figure 9-27 Evolution of different parameters for the power control condition
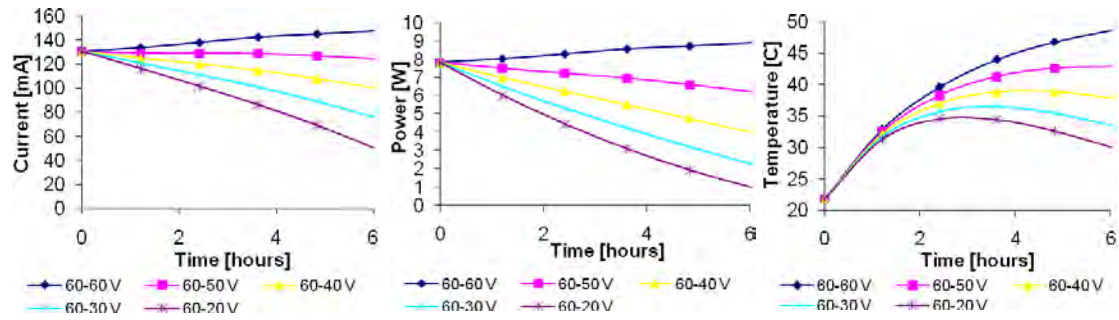
Figure 9-28 Evolution of different parameters for the transient voltage control condition

The Ohmic heating is a significant problem in the standard ASTM test because "low quality" samples can overheat if run at 60 Volts. The theoretical evaluation of the temperature in a migration test was introduced in section 5.7.4, where it was calculated using equation 5.37.

$$\Delta T^t = \frac{Ch^t \cdot AV}{Cth} - \frac{(T^t - RTP) \cdot F_{HL}}{Cth} = \frac{Power^t \cdot \Delta time}{Cth} - TDis \qquad (5.37)$$

where *TDis* is the part of the temperature dissipated. From equation 5.37 it can be seen that if a constant power is used as input, all the samples will reach the same temperature. If it is assumed that the heat capacity (*Cth*) and the heat loss factor (*F_{HL}*) are constant for all types of concrete, the temperature developed for any mix will be a function of the test conditions and not of the concrete quality. A test of this nature would be perfectly practical for commercial work; indeed most new electronic power supplies have serial ports which enable voltage-change sequences to be applied.

Figure 9.29 shows the numerical results of the simulation of 5 different samples under conditions of power control (6 watts). Sample variation was achieved using different transport properties (Cl diffusion coefficients and pore solution). As was expected, in all the samples the same value of temperature was obtained, although the total current passed and voltage were transient in time.
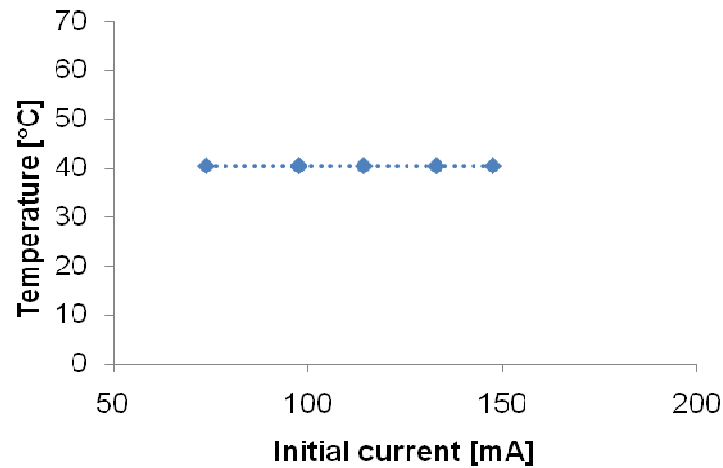
Figure 9-29 Relationship temperature vs. initial current for different samples (different Cl diffusion coefficients and pore solution) under simulations of the power control condition

9.7 CURRENT CONTROL (zero current)

In this section the theoretical and experimental aspects of the current control (zero current) condition are presented.

9.7.1 Current Control Model (zero current)

Under this condition a concrete sample is subjected to a constant current, which in this particular case has a value of zero. Although the computational routine developed in section 9.5 for the current control model (non-zero current) is the basis of this model, some slight changes were introduced. During a test of this nature, no external voltage or current is applied; this being the case, the driving forces to produce ionic flux are therefore only the gradients of concentration and the membrane potential generated due to ionic interaction. The principal requirement of the model is to ensure that the total current density is equal to zero for each time and position.

In the model, the initial membrane potential is approximated to zero in order to calculate the initial flux, using only the concentration term of the Nernst-Planck equation (Fick's Law). Then, the charge neutrality is maintained in the same way as explained in section 5.7.3, and an additional "*zero current*" routine was included. In this, the current calculated due to the flux is limited to 1×10^{-8} A. If this condition is not met in full, the membrane potential is adjusted and the diffusion and migration fluxes are recalculated iteratively until this condition is fulfilled. Once that condition is achieved, the routine moves on to a subsequent time step.

As outputs of the model, the transient current and concentration of each ion, the membrane potential and the temperature of the system sample-cells can be calculated.

9.7.2 Results and discussion of current control (zero current)

Using the transport related properties of the optimized mortar (section 9.3), the diffusion current control test was simulated. Figure 9.30 shows the voltage membrane potential results across the entire sample obtained from the experiments and from the numerical models. For all the experiments carried out the profile of the membrane potential was similar. First, an initial negative voltage (between -30 and -40 mV) gradually was reduced until a specific point, where the voltage started to increase. After around a week, the profile of membrane potential tended to become steady. A very similar behaviour was already reported by Zhang and Buenfeld (1997), although the numerical values reported in that reference are different because of the differences between the materials used.

The simulated membrane potential results between both external electrodes shown in figure 9.30 were obtained from two approaches: a) the voltage control model presented in section 5.7 using as input an external voltage equal to zero (VC), and b) the current control model developed in section 9.7.1 using the condition of zero current (CC).

In the voltage control model, the membrane potential across the sample for any time was equal to zero (between anode and cathode). This was expected because that was the condition stated by the model. In contrast, the current control model showed values of membrane potential across the sample that were different to zero for any time. They were of the same order of magnitude as those from the experiments, and were in very good agreement with them. The large differences found in the initial value of membrane potential for the simulated CC model was due to the numerical procedure to calculate this; basically, whereas in the model the calculation of the voltage is adjusted iteratively, at the start of the test the error has not yet been corrected by the model.

The evolution of the membrane potential for any point with respect to the cathode in any time is shown in figure 9.31-A, when the voltage control model was used, and in figure 9.31-B when the current control model was used. Values of membrane

potential at the start of the simulations were excluded from the figures for the reasons stated above. Significant differences were observed in the evolution of the membrane potential according to whether the phenomenon was simulated using voltage control, or current control models. It is believed that the condition of current control is physically much closer to reality
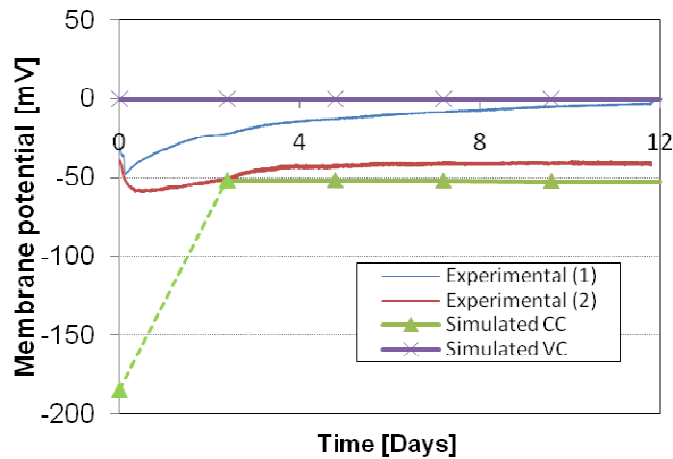
Figure 9-30 Evolution of the membrane potential across the whole sample
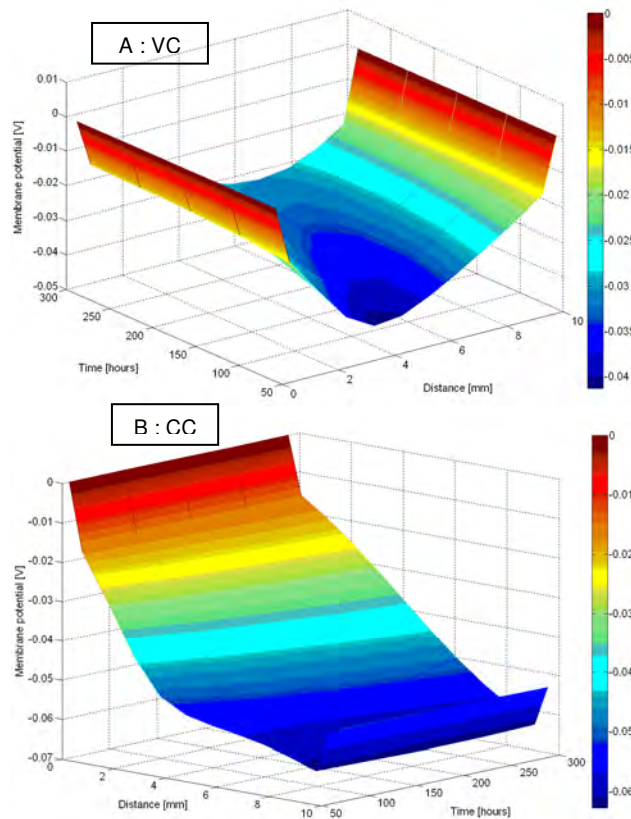
Figure 9-31 Membrane potential simulated (respect to the cathode) A: voltage control model; B: current control model

As was expected, using the current control model the current simulated at different positions at the end of the test (12 days) was always equal to zero. In contrast, for the voltage control model, a small total current was developed (0.0007 A). It is important to notice that in both models the charge neutrality condition was fulfilled. The simulated chloride profile for the voltage and current control conditions at 12 days is shown in figure 9.32. Although the membrane potential and the current obtained from both models were different, no important differences were found between the concentration chloride profiles - the concentration for both models at that specific time was very similar.

It was stated by Zhang and Buenfeld (1997) that the membrane potential has a strong effect on the ionic chloride diffusion in a diffusion cell similar to the one simulated in this research. Certainly the ionic flux is function of the membrane potential according to the Nernst-Planck equation; however, the membrane potential is the result of the ionic interactions due to a physical current condition – that of charge neutrality. It is believed that the behaviour of the current is the key factor during diffusion, and that the membrane potential is purely an effect, as might be the ionic concentration and the temperature.
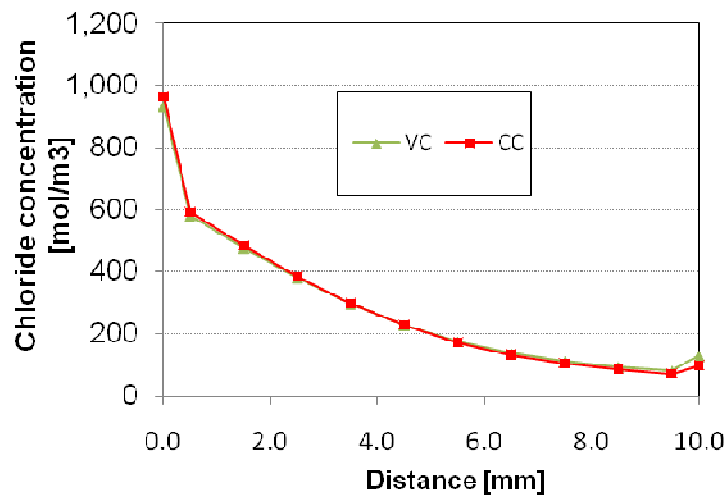
Figure 9-32 Simulated chloride concentration profiles after 12 days; VC: voltage control model; CC: current control model

The similarities of the chloride concentration results for both models can be explained by the fact that the current developed by the sample in a voltage control model is too low to produce any significant differences in the concentration. However, the current control model represents a much more accurate and realistic conceptual model.

9.8   SELF DIFFUSION – "IMMERSION" TESTS

9.8.1 Measured and simulated total chloride profile

In this section, the total chloride concentrations at different depths measured after the self diffusion tests were used to obtain the apparent diffusion coefficient $D_{app-Fick}$. This coefficient was already defined in section 5.3.2 according to the complementary error function solution of the Fick's Second Law. Using the measured concentrations of total chloride, expressed as mol per cubic meter of concrete volume, the chloride concentration at the surface C_{s-Fick} and $D_{app-Fick}$ were found by iteration to produce the best fit by least squares. In the same way, using the optimized transport properties obtained with the neural network algorithm and the corresponding geometrical and external conditions of the self diffusion test, the chloride concentration profile at different distances was simulated from the external NaCl. For this, the current control computer model was used.

Table 9.7 shows the values of $D_{app-Fick}$ and C_{s-Fick} calculated adjusting the experimental data to the error function, and the simulated C_s and D_{app} obtained from the numerical model. The relationships between the total and free chloride concentrations and the intrinsic and apparent coefficients were defined previously by equations 5.31 and 5.32 respectively.

	D_{app} [m^2/s]	C_s [mol/m^3]
Measured experimental (Fick)	1.25×10^{-11}	530
Optimized numerically (model)	8.50×10^{-11}	459

Table 9-7 Apparent diffusion coefficient D_{app} and chloride surface concentration C_s [Total chloride per concrete volume]

Figure 9.33 shows the experimental chloride concentration data for both experimental samples tested (S1 and S2), the best profile obtained fitting the error function to the experimental data, and the result of the current control model using the optimized data. In the figure the chloride concentration refers to the total chloride concentration (free + adsorbed ions) per cubic meter of the whole sample.
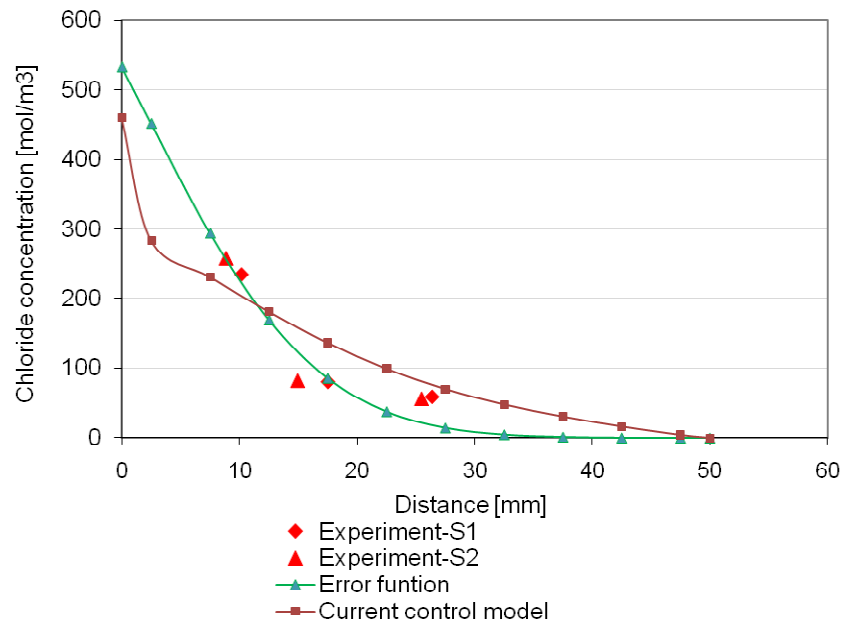
Figure 9-33 Total chloride concentration profiles [mol per unit volume of solid] using the error function to adjust the experimental data and the current control model

9.8.2 Chloride concentration profile in a binary system

If in a concrete sample in contact with a solution of sodium chloride it is assumed that there are no binding reactions and there is no ionic pore solution, the effect of the membrane potential on the free chloride and sodium concentration, (expressed as mol per cubic meter of pore solution), is shown in figure 9.34. In this, two different situations are displayed:

a) When the flux is simulated taking no membrane potential into account, the profile was different for both ions. Chlorides showed a bigger profile because its diffusion coefficient is bigger. It was expected that chloride ions move more quickly than sodium ions.

b) When the membrane potential is accounted for in the model, both ions move at the same velocity and the profile is similar, so, the profiles overlap each other. The interactions between chloride and sodium result in an electrical field (membrane potential), which moderates the speed of the ions, always maintaining charge neutrality. For a normal concrete, which includes more ions in the pore solution and binding capabilities, the effect of the membrane potential is far more complex.
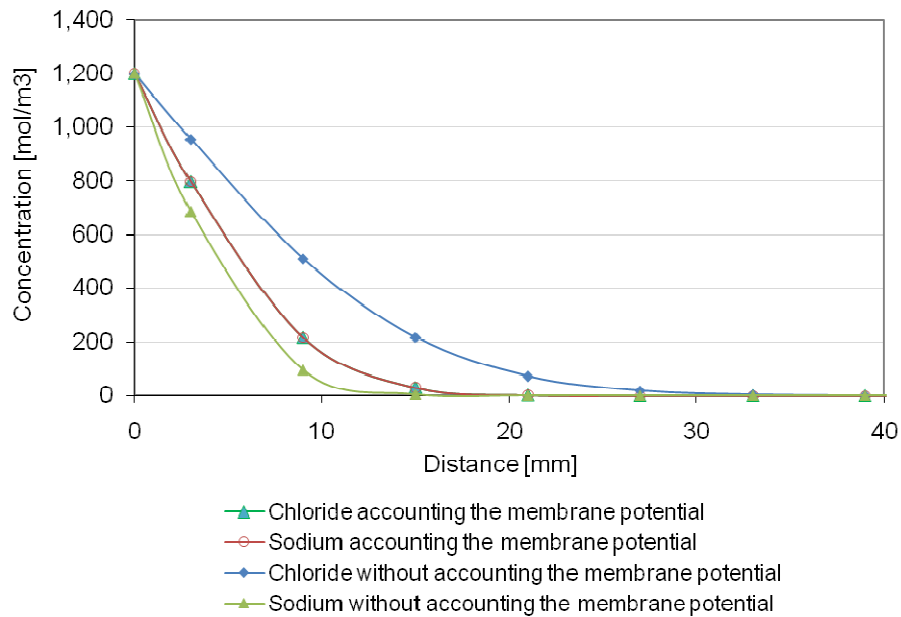
Figure 9-34 Chloride concentration profiles in real and ideal binary systems

9.8.3 Measured and simulated chloride concentration profiles

With the aim of studying the chloride concentration profile at different distances from the external NaCl, the gravity chloride diffusion test (section 6.8) was simulated using different approaches. The time selected to show the evolution of the concentration was 72 days because this was the duration of the self diffusion experiments and measured profiles were available for that time. As acid soluble analysis was used to determine the total chloride concentration of ions per unit volume of concrete, the coefficient obtained was "apparent" $D_{app-Fick}$. However, as the computer model gives results in terms of the concentration of free ions per unit volume of liquid in the pores, it was necessary to convert $D_{app-Fick}$ to the corresponding intrinsic coefficient $D_{int-Fick}$. For this, equation 5.32 was used assuming that the porosity and the capacity factor of the material were 0.171 and 0.383 respectively. The resulting $D_{int-Fick}$ was $2.81.25 \times 10^{-11}$ m^2/s.

Figure 9.35 shows the profile when the phenomenon was simulated using approaches directly related to Fick's law.

(1) The Analytical equation 9.2, which without an external applied voltage becomes equation 5.11 (Fick's law). The intrinsic chloride diffusion coefficient calculated from the experiments, $D_{int-Fick} = 2.81 \times 10^{-11}$ m^2/s was used.

(2) The Coventry model under a condition of external voltage equal to zero, with no voltage correction or binding capacity. Only chlorides were included in the system so there was no pore solution. The intrinsic chloride diffusion coefficient calculated from the experiments, $D_{int\text{-}Fick}$ =2.81x10^{-11} m^2/s was used.

(3) The Coventry model under a condition of external voltage equal to zero, with no voltage correction, but including a binding capacity factor (α) of 0.383. No pore solution was included in the modelling. The intrinsic chloride diffusion coefficient used was $D_{int\text{-}Fick}$ =2.81x10^{-11} m^2/s.

(4) The current control model using all the transport related properties optimized.

(5) The Coventry model under a condition of external voltage equal to zero, no voltage correction, and no pore solution. The intrinsic chloride diffusion coefficient used was the optimized D_{int} =1.9x10^{-11} m^2/s.
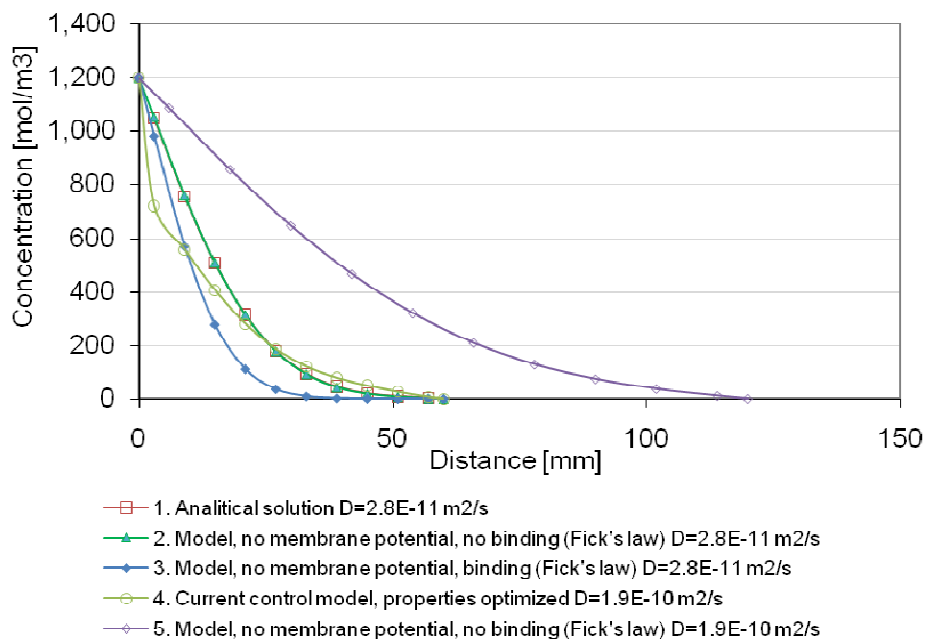
Figure 9-35 Free chloride concentration profiles [mol per unit volume of liquid in pores] for different approaches

Approaches (1) and (2), as was expected, had the same profile and overlap each other; the chloride concentration was the same for both conditions. This provides a check that, for a simplified condition, the computer simulation gave the correct solution. Approach (3) corresponds to the numerical solution of Fick's Law including chloride binding properties. It shows the strong effect of this property upon the

chloride concentration. Approach (4) is the numerical model developed in this research using all the optimized transport properties. The result was in good agreement with approaches (1) and (2), demonstrating the reliability of the optimization method. Approach (5) is the numerical solution of Fick's Law using the chloride diffusion coefficient optimized.

Most of the chloride profiles plotted in figure 9.35 do not include membrane potential and binding. Chloride profiles from approaches including ionic interaction (membrane potential) are shown separately in figure 9.36. *(There is no technical reason for presenting two graphs; for clarity it was decided to present the results in two graphs because of the large amount of data.)*
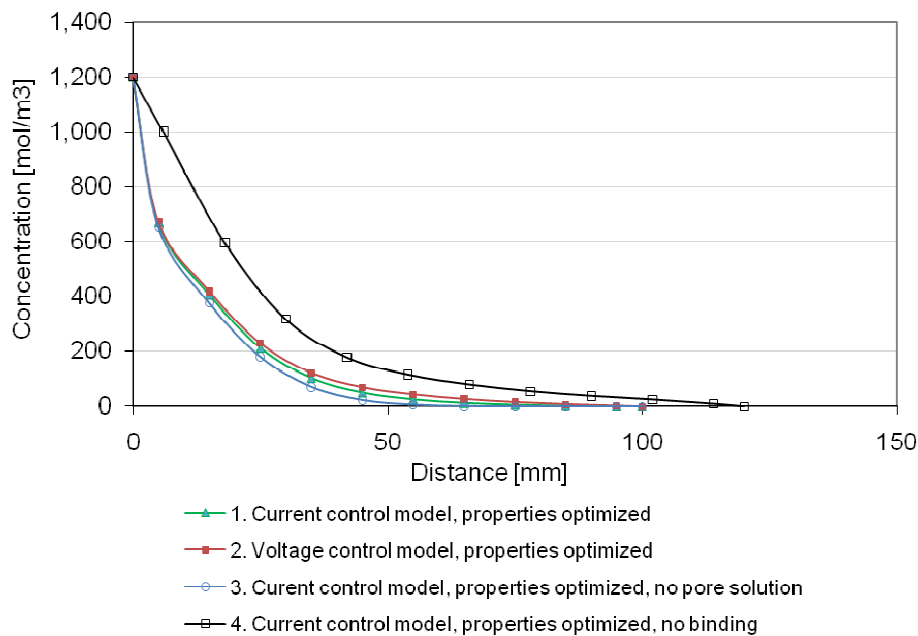
Figure 9-36 Free chloride concentration profiles [mol per unit volume of liquid in pores] for different approaches

From the figure can be seen that the voltage and current control models gave a similar trend. The concentration at short distances from the external solution for both models was in very good agreement; however, the difference between the models increases with distance. As was mentioned in section 9.7.2, the chloride concentration in a diffusion test simulated by the voltage and current models is similar and for practical purposes the concentration of chloride can be considered the same. However, the physical description of the current model is the most appropriate.

The effect of the pore solution is also shown in figure 9.36. When the pore solution was included in the simulation, the concentration of chlorides was increased due to the effects of the interaction between the ionic species. In that figure, the simulation of the test can also be seen without accounting for the chloride binding capacity of the material. Important differences in the concentration profiles were found due to the binding, it produces an important effect that must not be neglected.

Figure 9.37 shows the chloride concentration profile simulated for the experiment at different times.
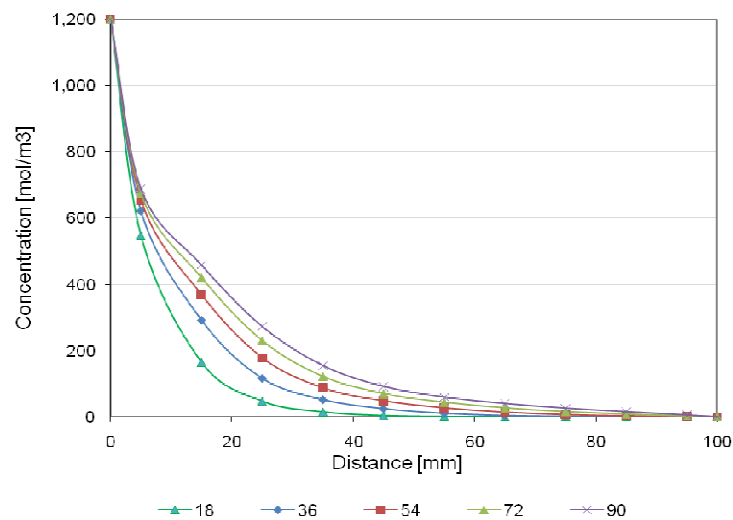
Figure 9-37 Simulated free chloride concentration profiles at different times using the current control model

9.8.4 Current evolution

From Faraday's Law and equations 5.3, 9.2 and 9.3, the total current for a chloride mono ion system, can be expressed as equation 9.6 (Luping and Nilsson 1992).

$$i = AFD_{cl}c_s \left[\frac{1}{\sqrt{\pi D_{cl}t}} e^{\frac{(x-aD_{cl}t)^2}{4D_{cl}t}} + \frac{a}{2} erfc\left(\frac{x - aD_{cl}t}{2\sqrt{Dt}} \right) \right] \tag{9.6}$$

Using various approaches the total current, developed during the diffusion test, was simulated. Results for current control, voltage control and the theoretical model described in equation 9.6 were compared in figure 9.38. The time selected to show the evolution of the current was 72 days. The approaches used to simulate the total current were as follows.

(1) The electro-diffusion current control model. As was expected, the total current was equal to zero at any point of the sample. The current density generated by each ion was annulled by the current density generated by the remaining ions. When any species diffused through the sample a charge surplus was avoided through the generation of a membrane potential. The author suggests that this simulation represents the best physical description of the behaviour of the sample.

(2) The electro-diffusion voltage control model. The total current was constant across the whole sample. The value of current simulated was 0.1 mA.

(3) The electro-diffusion model with no voltage correction. In this, in resolving of the Nernst-Planck equation there was no membrane potential generation. As a result, the Nernst-Planck equation was resolved using Fick's First Law for each ion. The total current had a value of 0.5 mA near the surface. Further away from the surface the current decreases. The total current for any point was the result of the sum of the current driven for all ions, according to their charge and diffusion direction.

(4) The theoretical equation 9. In this, it was supposed that the only specie involved was chloride. The total current profile obtained was similar to the previous condition but the total current near to the surface was recorded as 2.8 mA.
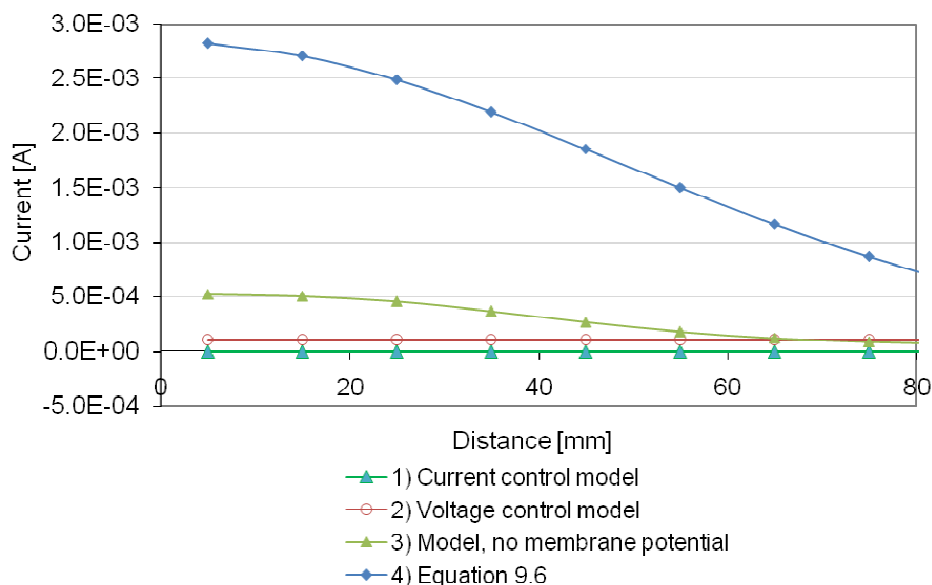
Figure 9-38 Total current calculated at 72 days using different approaches

9.9   CONCLUSIONS

39. The application of the Nernst-Planck equation to the simulation of diffusion or migration of any ionic species through a saturated porous medium using the non-linear voltage membrane potential include all the microscopic interactions in a macroscopic way.

40. The straightforward application of Fick's law to simulate chloride diffusion in concrete which has been used by many authors in the past can be significantly improved by using a numerical simulation which includes the effects of the other ions in the system.

41. The diffusion coefficients obtained through the neural network model cannot be compared with others reported elsewhere unless they are obtained through the same hypothesis.

42. The differences in the numerical values of the chloride diffusion coefficients obtained in this research and reported in the literature are explained in the theoretical assumptions adopted during their experimental determination.

PART 3: TRANSPORT RELATED PROPERTIES IN SLAG CONCRETE

In this third part of the dissertation the most important transport related properties of slag blended concretes were investigated experimentally and computationally. Several transport tests were carried out on the final mixes developed in the first part of the research and on mixes of Portland cement and ground blast furnace slag with different proportions. Additionally, on certain mixes, numerical simulations using the optimization model introduced in chapter 8 were carried out.

10 "OTHER" EXPERIMENTAL METHODS

This chapter deals with the theoretical aspects of some of the experimental methods used to measure the transport related properties of slag concrete mixes, in addition to the experimental procedures shown in chapter 6.

10.1 INTRODUCTION

Different experiments are included in this section. Firstly, the methods used to measure the rheology are presented. Secondly, the measurement techniques for carbonation, rate of water absorption, and water permeability are summarized. Finally, the principal aspects of corrosion measurements on steel in concrete are presented. As the chloride related experimental methods were already presented in the second part of this document, these will not be discussed here.

10.2 WORKABILITY OF CONCRETE MIXES

Workability is one of the most important properties of concrete, mortar, or paste mixes in fresh condition, and is closely related to both compressive strength and durability. The American Concrete Institute defines workability as "*the property of freshly mixed concrete or mortar that determines the ease with it can be mixed, placed, consolidated, and finished to a homogenous condition*". Because of the generality and ambiguity of this definition, for more than a century various techniques and tools for measuring the workability of concrete have been proposed. Today there are three main classes of measurement methods (Table 10.1).

Qualitative methods	Qualitative empirical methods	Quantitative fundamental methods
To be used only in general descriptive way without any attempt to quantify	To be used as a simple quantitative statement of behaviour in a particular set of circumstances	To be used strictly in conformance with standard definitions

Table 10-1 Classes and methods of workability measurement (ACI-238 2008)

Another classification of the tests and techniques for measuring workability is based on the concept of a rheological flow curve, which establishes the relationship between the shear stress and the rate of deformation of a fresh concrete mixture. Depending on whether a test yields one point or multiple points in this curve, this will

be known as simple or multipoint. The qualitative and quantitative empirical methods define a single point within the curve, while the quantitative fundamental tests draw a entire curve with their complete physical parameters. In the ACI 238 (2008) about 33 different single point and about 19 multipoint tests are reported.

Newton's law of viscosity ($\tau = \eta\dot{\gamma}$) states that, for a Newtonian fluid, the shear stress applied (τ) in one direction is directly proportional to the rate of deformation ($\dot{\gamma}$), and the constant of proportionality is equal to the viscosity (η). According to the ACI 238 the fresh concrete behaves as a viscoplastic material. That means that when the shear values are smaller than a critical shear stress (τ_o) concrete behaves like a solid, but when that critical shear stress is exceeded the material flows like a viscous fluid. The shear stress is usually modelled by the Bingham equation ($\tau = \tau_o + \eta\dot{\gamma}$), which establishes a linear relationship similar to Newton's Law, but, there is a critical shear stress known as yield stress (τ_0). The Bingham plastic model can be classified as ideal or non-ideal, according to whether the viscosity is treated as a constant, or rather as a function of the rate of deformation. Figure 10.1 shows the definitions given above.
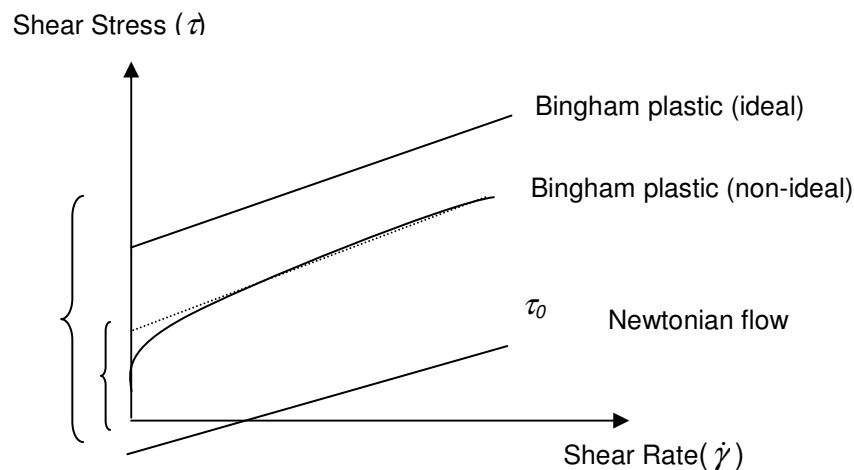
Figure 10-1 Theoretical flow curves

Technologically, the most advanced and reliable tools for measuring the rheological properties of a mixture are rotational rheometers; they apply a shear force to a fresh concrete sample by means of different levels of stress. By measuring the torque and the rotational speed, the physical properties such as yield stress (τ_0) and viscosity (η) are determined. Nowadays 16 rotational rheometers are reported, all having different characteristics, but sharing the same essential purpose (ACI-238 2008).

With the aim of studying the flow properties of the slag concrete mixes developed in this research, the rotational rheometer proposed by the International Centre for Aggregates Research (ICAR) was used (Koehler 2004). This instrument is commonly used in the research and development of new blends and in quality control applications. The range of this equipment is from slumps of 7 cm to super fluid concrete. Figure 10.2 shows the instrument used.

Figure 10-2 ICAR rheometer used in this research

Another test used to measure the flow of the concrete mixes was the slump test. This was carried out according to part II of BS1881.

Figure 10-3 Slump test equipment

10.3 CARBONATION DEPTH

Carbonation is the reaction of calcium-silicate-hydrates and calcium hydroxide with carbon dioxide to form calcium carbonate. It is a source of major concern in concrete

structures because it causes a reduction of the hydroxide concentration of the concrete pore solution to pH values smaller than 9. As the pH in the pore solution is reduced, the passive film of the reinforcement steel can become broken and corrosion may occur. In a reinforced concrete structure, a passive thin protective layer of γ-Fe_2O_3, with a thickness between 20 and 60 Å is formed on the surface of the reinforcing steel bars. The high alkaline environment around the steel supports the generation of this protective layer, which is dense and stable so long as the pH is greater than 11.5, but breaks down with carbonation (Hewlett 2004).

Although the transport mechanism of carbonation is quite different from that which occurs with chlorides, both are intimately related. When coupled with chloride ingress, carbonation reduces the durability of concrete further, because it affects the relationship between the free and bound chlorides (the capacity factor), accelerating the deterioration process.

The chemical changes in the composition of a concrete matrix due to carbonation are summarized by the following (Sulapha 2003):

$$Ca(OH)_2 \rightarrow Ca^{+2}(aq) + 2OH^-(aq) \qquad (10.1)$$

$$Ca^{+2}(aq) + 2OH^-(aq) + CO_2 \rightarrow CaCO_3 + H_2O \qquad (10.2)$$

$$3CaO \cdot 2SiO_2 \cdot 3H_2O + 3CO_2 \rightarrow 3CaCO_3 \cdot 2SiO_2 \cdot H_2O \qquad (10.3)$$

$$3CaO \cdot SiO_2 + 3CO_2 + \mu H_2O \rightarrow SiO_2 \cdot \mu H_2O + 3CaCO_3 \qquad (10.4)$$

$$2CaO \cdot SiO_2 + 2CO_2 + \mu H_2O \rightarrow SiO_2 \cdot \mu H_2O + 2CaCO_3 \qquad (10.5)$$
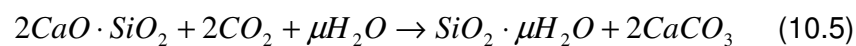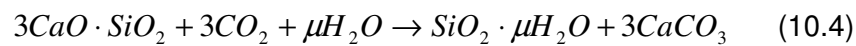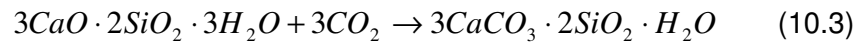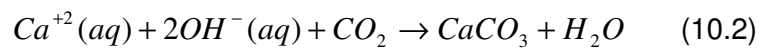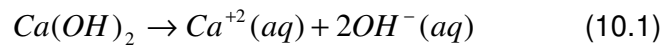
As the penetration of CO_2 in concrete takes place through the pore system, the principal mechanism of transport is diffusion. In this, the concentration gradient of CO_2 in the environment acts as the driving force. Although Fick's First Law of diffusion can be used to model the carbonation depth, the Square Root Theory has been used successfully by Al-Khayat, Haque and Fattuhi (2002). In this, the carbonation depth x_c is related to the exposure time t, through a carbonation coefficient k_c. Although the coefficient k_c does not have a clear physical meaning, it can be used to rank or compare concrete mixes diffusing under the same conditions of exposure.

$$x_c = k_c \sqrt{t} \qquad (10.6)$$

The method of measuring carbonation depth was the phenolphthalein method recommended by RILEM-TC56 (1988). A solution of 1% phenolphthalein in 70% ethyl alcohol is sprayed to a freshly broken surface. In the non-carbonated part of the specimen a purple colour is obtained after a few minutes, signifying that the concrete still has a high alkalinity. In contrast, in the carbonated part there is no coloration. The depth of carbonation x_c of a concrete cube sample is the average of 6 readings taken in the sample according to figure 10.4.

$$x_c = \frac{A_1 + A_2 + B_1 + B_2 + C_1 + C_2}{6} \quad (10.7)$$
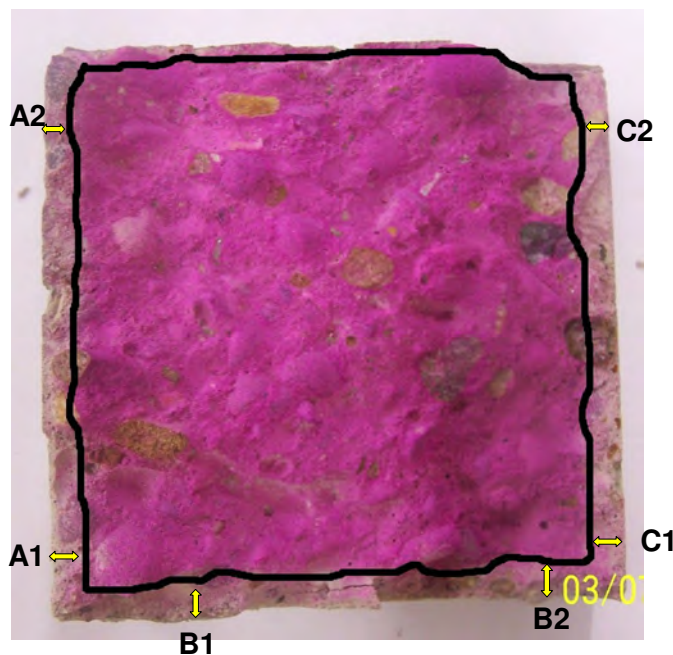
Figure 10-4 Carbonation depth concrete sample

It is important to note that this method only provides a qualitative indication of the presence of carbonation. No indication of the degree of carbonation or the real pH of the concrete is obtained.

10.4 WATER SORPTIVITY

According to Hall (1989), sorptivity is "….*the property which characterizes the tendency of a porous material to absorb and transmit water by capillary suction*". In a non-saturated concrete or mortar sample, the rate of fluid penetration or sorptivity is mainly controlled by absorption due to capillary rise (with no applied pressure); so, this property can be an indirect measure of the potential durability of the material. It is

known that most of the processes of deterioration in cement based materials are initiated by water.

The test method employed to measure the sorptivity is described in ASTM C-1585 (2004) and is based on the work of Hall (1989). Here, the increase in mass or the penetration resulting from absorption of water is measured when just one surface of the sample is placed in contact with the fluid. It is stated by Basheer (2001) that the cumulative absorbed volume per unit area of the inflow surface (m^3/m^2), increases as a function of the square root of the time ($s^{0.5}$)

$$i = S\sqrt{t} + A \quad (10.8)$$

where S is the sorptivity of the material ($m^3/m^2/ s^{0.5}$) and A is a constant that is needed to adjust the experimental data. A has a physical explanation; the open porosity of the inflow surface allows pores to fill with water instantly at the beginning of the test. In figure 10.5 a typical result of the test is shown as an example.
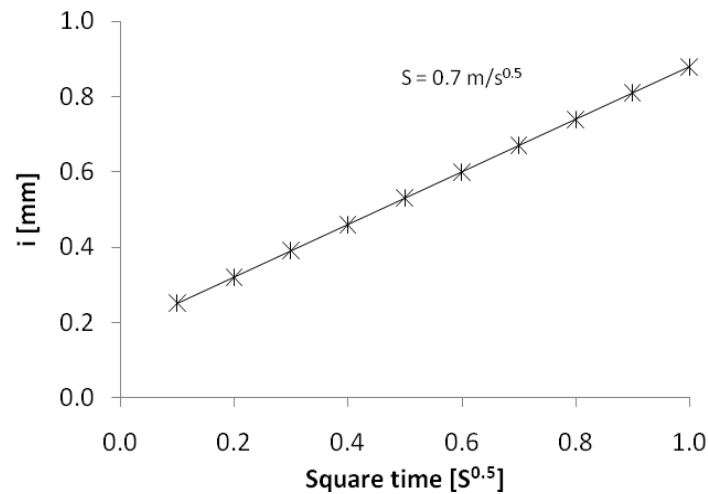
Figure 10-5 Typical result of sorptivity for a normal concrete

In order to conduct the test, one of the surfaces of the sample is left in contact with water and the increase in weight observed is measured at specific times. After obtaining enough number of points the graph of the figure 10.5 is plotted. Figure 10.6 shows the set-up used in this research.
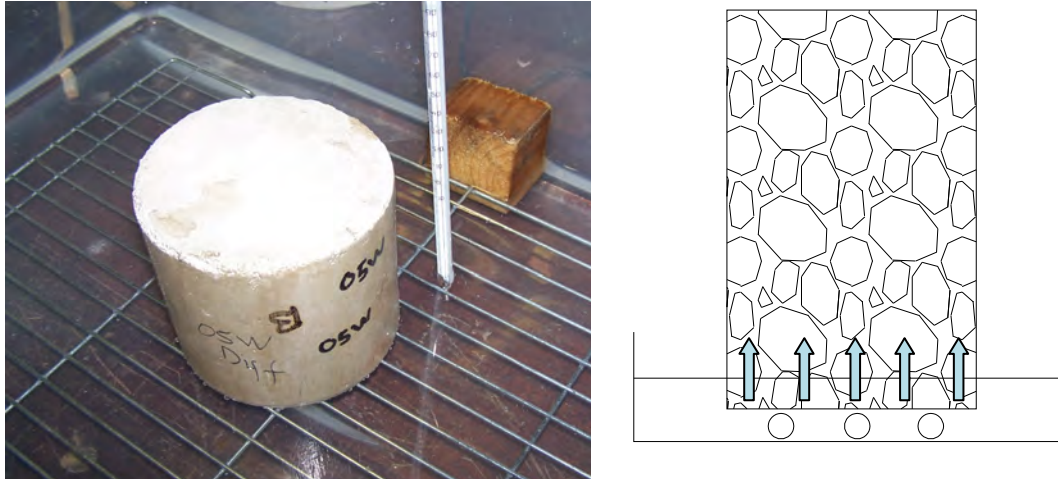
Figure 10-6 Sorptivity test - picture and schematic diagram

Sorptivity is influenced by many factors (ASTM-C1585 2004), such as the type, quality and composition of the raw materials, the placement and finishing, the type and curing time, the degree of hydration or age, and especially, the water content of the material. In order to maintain the same humidity conditions for all the samples tested, a procedure of conditioning was established. After each period of curing the samples were left to dry at 80 °C in an oven for 5 days. It was assumed that any higher drying temperature might adversely affect the capillary system of the external layers of the samples; so, it was decided to use this "low" temperature and the time of drying was extended. After drying, all the surfaces of the specimens, except the one that was in contact with water, were covered with an epoxy or rubber emulsion.

10.5 WATER PERMEABILITY

Water permeability is defined as the rate at which a fluid will flow through a sample when there is a pressure difference. The experimental measurement of this property has some difficulties because in order to test mortar or concrete, high pressures (usually between 20 and 120 Bars) and triaxial cells are required. It is assumed that the flow due to a high pressure head across the pore system of a sample is governed by Darcy's Law. This states that a laminar flow in steady state condition moving through a porous system is proportional to the intrinsic permeability (Basheer 2001).

$$V = \frac{Q}{A} = \frac{k_p}{\mu} \frac{\partial p}{\partial l} \qquad (10.9)$$

where Q is the volume rate flow [m³/s], A is the area of cross section [m²], ∂p [Pa] is the pressure loss over the flow path of length ∂l [m], μ is the viscosity of the fluid [Ns/m²], and k is the intrinsic permeability of the material [m²]. The intrinsic permeability k_p is a property of the material and is independent of the properties of the fluid. It is related to the coefficient of permeability , which defines the actual fluid used.

$$K_p = \frac{\rho g}{\mu} k_p \quad (10.10)$$

K_p is the coefficient of permeability [m/s], ρ is the density of fluid [kg/m³], and g is the acceleration of the gravity [m/s²]. Basically, the test consists of applying a vertical water pressure gradient to a concrete or mortar cylindrical sample until the steady state flow condition is reached. To achieve this, the specimen is housed in a triaxial cell, like the one shown in figures 10.7 and 10.8, and a radial oil confining pressure is maintained around the specimen. The water effluent is collected and the flow rate is determined.
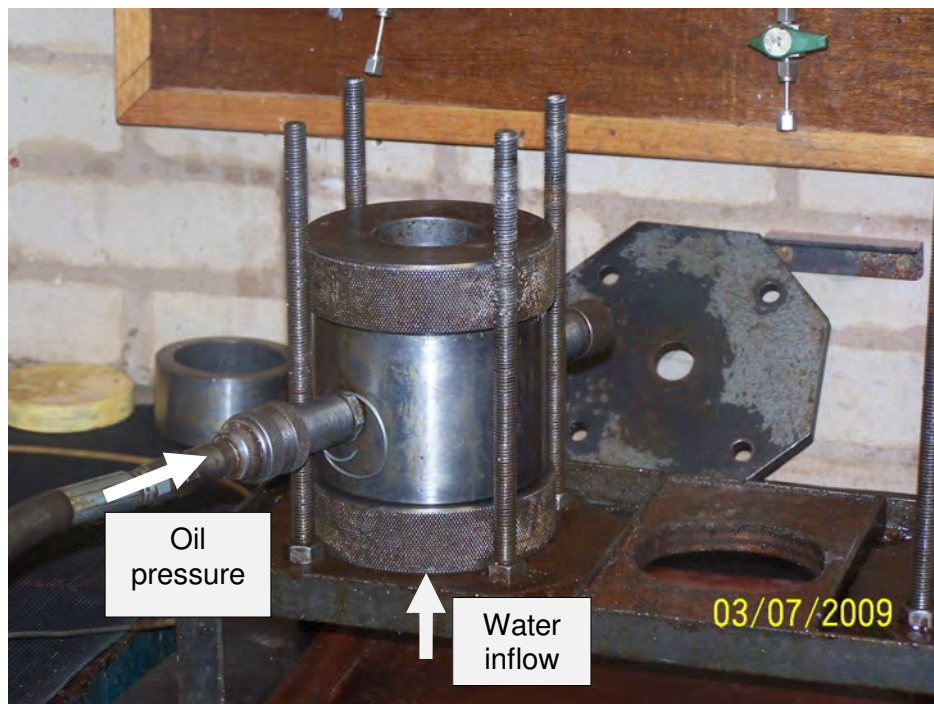
Figure 10-7 Cell used to measure the water permeability of concrete
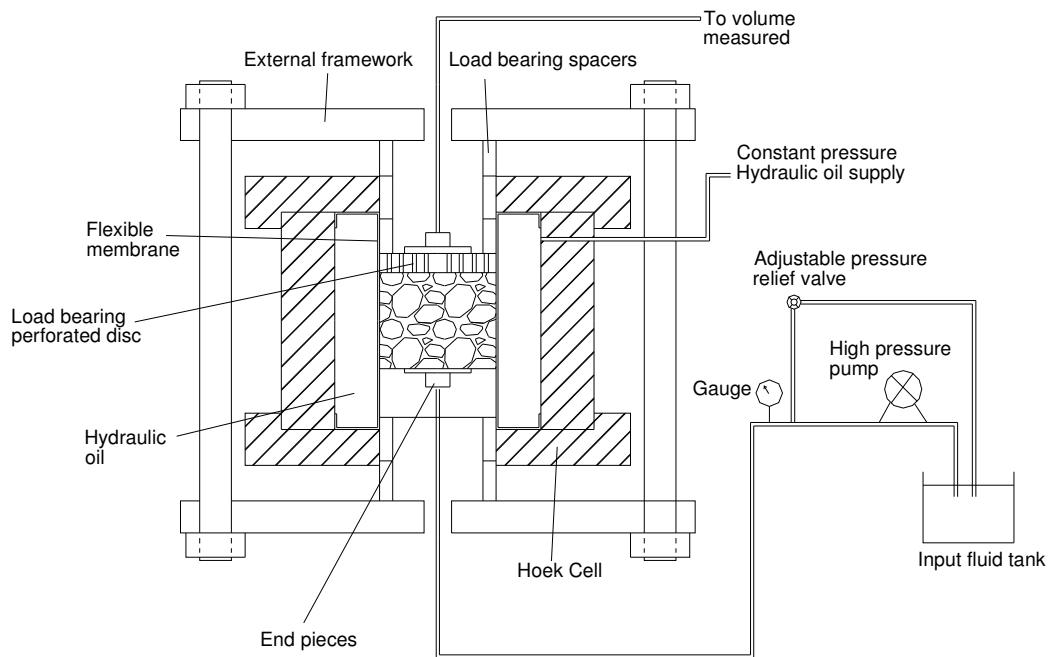
Figure 10-8 High pressure water permeability system

10.6 CORROSION

In the corrosion process of metals there are always two simultaneous reactions. A anodic reaction of oxidation in which the metal increases its valence liberating electrons, and a cathodic reaction of reduction, in which there is consumption of electrons. In neutral solutions or in acidic water, iron shows the following reactions (Jones 1996):

$$\text{Anodic Reaction:} \qquad Fe \rightarrow Fe^{2+} + 2e^- \qquad (10.11)$$

$$\text{Cathodic Reaction:} \quad 2H_2O + 2e^- \rightarrow H_2 + 2OH^- \quad (10.12a)$$

$$2H^+ + 2e^- \rightarrow H_2 \qquad (10.12b)$$
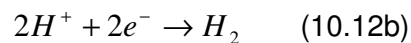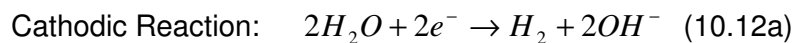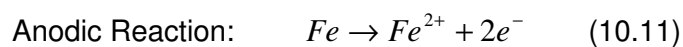
As there is a transfer of electrons in each half cell electrochemical reaction, the anodic and cathodic half cells will tend to reach a rest potential E_{corr}. That corresponds to equilibrium in terms of electrical current between metal dissolution and the associated reduction reaction. The rest potential is a function of the ability with which the electrons can be exchanged. Polarisation is defined as the potential change from the equilibrium half cell electrode potential. In cathodic polarisation there is a surplus in the electrons supplied to the metal. The application of a negative

potential (cathodic over-voltage) in order to supply an excess of electrons, decreases the corrosion rate and is known as cathodic protection. In anodic polarisation, where electrons are separate from the metal, a deficiency of electrons results in a positive potential change, and dissolution of the metal.

Corrosion is an electrochemical process which always involves an exchange of electrons. This flow of electrons is proportional to the velocity of the reactions and is measured as current. The relationship between current and mass of metal reacted in a corrosion process is stated by equation 10.13, where m is the mass reacted, F is the Faraday constant, I is the current, z is the electrical charge of the metal, a is the atomic weight, and t the time (Jones 1996).

$$m = \frac{Ita}{zF} \qquad (10.13)$$

If equation 10.13 is divided by time t and by the area A, it is possible to find the corrosion rate r as a linear function of the current density i [$\mu A/cm^2$].

$$r = \frac{m}{tA} = (\frac{a}{zF})i \qquad (10.14)$$

The relationship between polarization and current density according to Jones (1996) is presented in equations 10.15 and 10.16.

Anodic polarization $\qquad \eta_a = \beta_a \log \frac{i_a}{i_o} \qquad (10.15)$

Cathodic polarization $\qquad \eta_c = \beta_c \log \frac{i_c}{i_o} \qquad (10.16)$

η_a and η_c are the anodic and cathodic polarization over-potentials, β_a and β_c are known as the Tafel constants, i_a and i_c are the anodic and cathodic current densities, and i_o corresponds to the exchange current density at equilibrium. The theoretical derivation of equations 10.15 and 10.16 is out of the scope of this document, however, it can be found in Jones (1996).

Although both of the half cell reactions shown in equations 10.11 and 10.12 occur simultaneously and each one has its own half cell potential and exchange current density, the half cell electrode potentials $e_{Fe/Fe^{2+}}$ and e_{H^+/H_2} in the anode and cathode are not isolated, so, they must polarize to a common intermediate equilibrium value. This can be seen in figure 10.9.
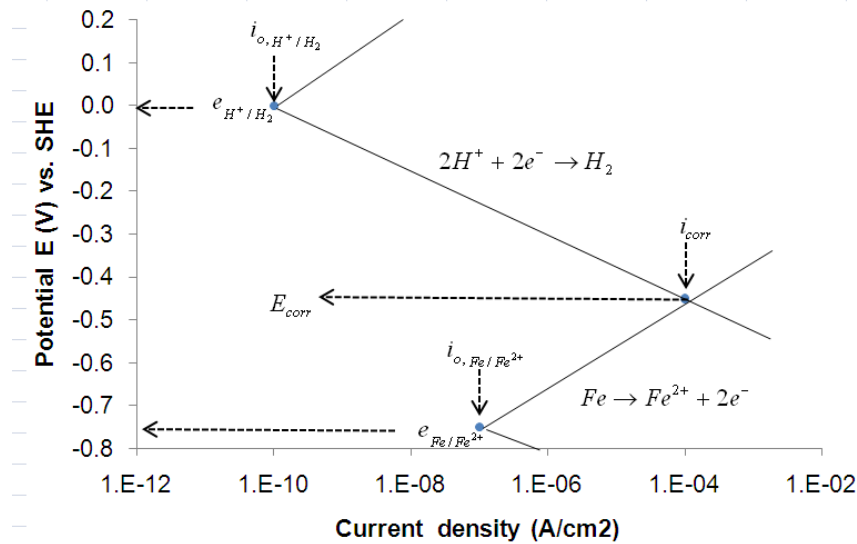
Figure 10-9 Polarization of anodic and cathodic half cell reactions (Jones 1996)

If the system is subjected to an external excess of electrons, through the application of a negative voltage or current, the electrode potential will change from E_{corr} to E. So, the surplus of electrons decreases the rate of the anodic reaction and increases the cathodic reaction according to the principle of charge conservation.

$$i_{applied} = i_c - i_a \qquad (10.17)$$

Typical cathodic and anodic polarization curves of potential versus the logarithm of the current applied are shown in figure 10.10. It can be seen that when the over-potential is close to zero, the curves are asymptotic to E_{corr}. However, when there is a higher over-potential, the relation *Potential vs. log($i_{applied}$)* is linear. That linear part of the graph is known as Tafel behaviour, and their slopes correspond to the Tafel constants included in equations 10.15 and 10.16.

Another approach known as equivalent circuit can be used to understand the relationships between polarization curves and current in a metallic corrosion process (Claisse 1988).
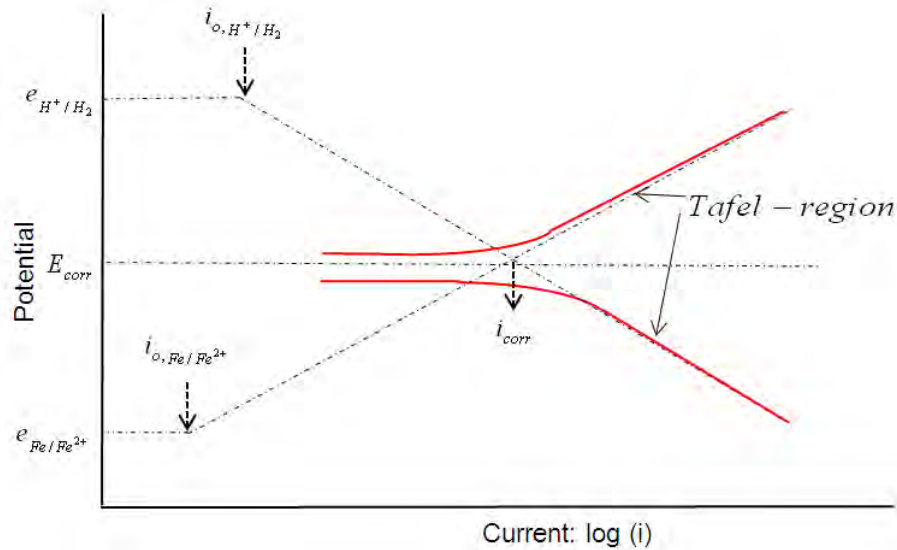
Figure 10-10 Experimental polarization curves and Tafel constants (Jones 1996)

10.6.1 Linear Polarization

Jones (1996) states that experimentally it is observed that the degree of polarization for a given applied current is greater for a lower corrosion rate. In the same way, there is an apparent linearity close to the origin of the polarization curve for over-voltages of up to a few millivolts. The slope of this linear curve is inversely proportional to the corrosion rate. These conditions form the basis a the method of linear polarization, used experimentally for measuring the rate of corrosion of a metal under aggressive conditions.

If in equations 10.15 and 10.16 i_{corr} is used instead of i_o and the polarization is made from the rest potential voltage E_{corr}, the cathodic (ε_c) and anodic (ε_a) over-voltages are a function of the Tafel constants and of the corrosion rate i_{corr}. It is important to notice that the over-voltage is $\varepsilon_{c/a} = E_{c/a} - E_{corr}$. Figure 10.11 shows a schematic experimental polarization curve (arbitrary units were used), where an over-voltage equal to zero corresponds to the rest potential.

$$\varepsilon_a = \beta_a \log \frac{i_a}{i_{corr}} \qquad (10.18)$$

$$\varepsilon_c = \beta_c \log \frac{i_c}{i_{corr}} \qquad (10.19)$$
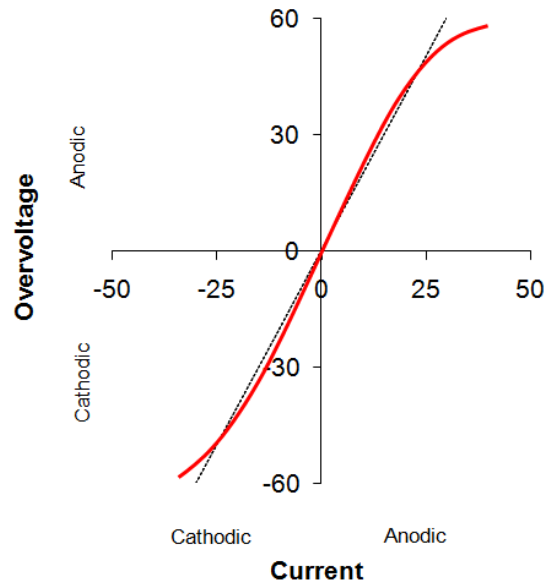
Figure 10-11 Hypothetical anodic and cathodic polarization curves in linear coordinates

The polarization resistance (*Rp*) is defined for a given electrochemical system as a function of the over-potential and the current density applied.

$$R_p = \left[\frac{d\varepsilon}{di_{applied}} \right]_{\varepsilon \to 0} \quad (10.20)$$

In addition, it has been shown by Claisse (1988) and Jones (1996) that if equations 10.18 and 10.19 are converted to their exponential form, and substituting them to equation 10.17, the polarisation resistance can be defined as a function of the Tafel constants, the over-voltage and the rate of corrosion.

$$R_p = \frac{\beta_a \beta_c}{2.3 i_{corr}(\beta_a + \beta_c)} = \frac{B}{i_{corr}} \quad (10.21)$$

The measurement of the corrosion rate in this project was carried out using a potentiostat. A controlled over-voltage was impressed in a corroding reinforced bar. The generated current $i_{applied}$ was proportional to the corrosion rate. The potentiostat works by adjusting an applied polarizing current to control the voltage between the working and reference electrodes. Equation 10.22 was used to determine the polarization resistance. The potentiostat used was a HI -TEK DT2101 as is shown in figure 10.12.

245

$$R_p = \frac{\Delta\varepsilon}{\Delta i_{applied}} = \frac{B}{i_{corr}} \quad (10.22)$$

Figure 10-12 Potentiostat used to measure the polarization resistance in reinforced concrete samples

A diagram of the experimental set up used to measure corrosion of steel in concrete is shown in figure 10.13.
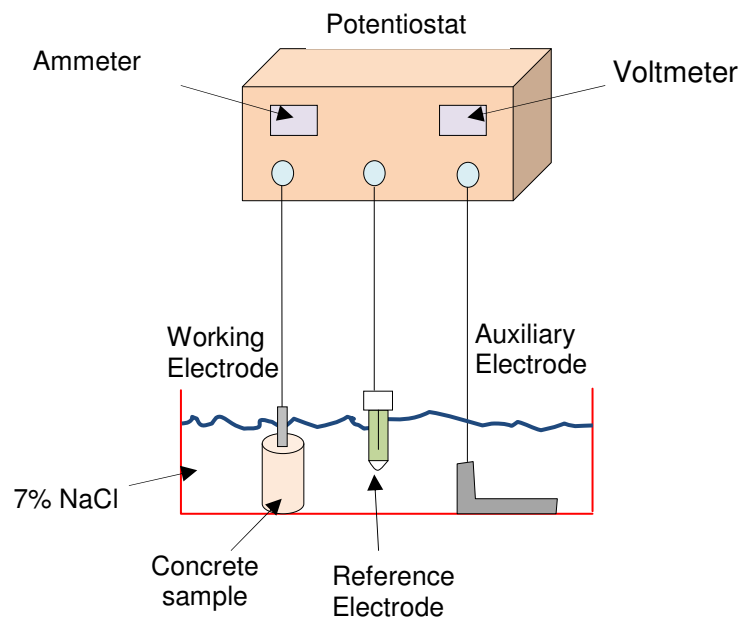
Figure 10-13 Corrosion experiment circuit set up

The reference electrode was a Calomel reference electrode, the auxiliary electrode was a 10 mm thick steel sheet, and the working electrodes were steel bars cast in each of the concrete final mixes investigated in this research. The concrete samples were cylinders of 100 mm of diameter, cast with a 7.5 mm round bar in them. Figure 10.14-right shows a diagram of a typical sample. The samples were placed in a plastic tank containing a solution of 7% sodium chloride. With the aim of accelerating the corrosion process, between each polarization resistance reading, a constant positive voltage of 100 mV was applied to the samples. To do this, the specimens

were connected in parallel and the voltage was supplied by the potentiostat as shown in figure 10.12-left. The disconnected samples were left for 1 day before tests.

φ=7.5 mm

30 mm

100 mm
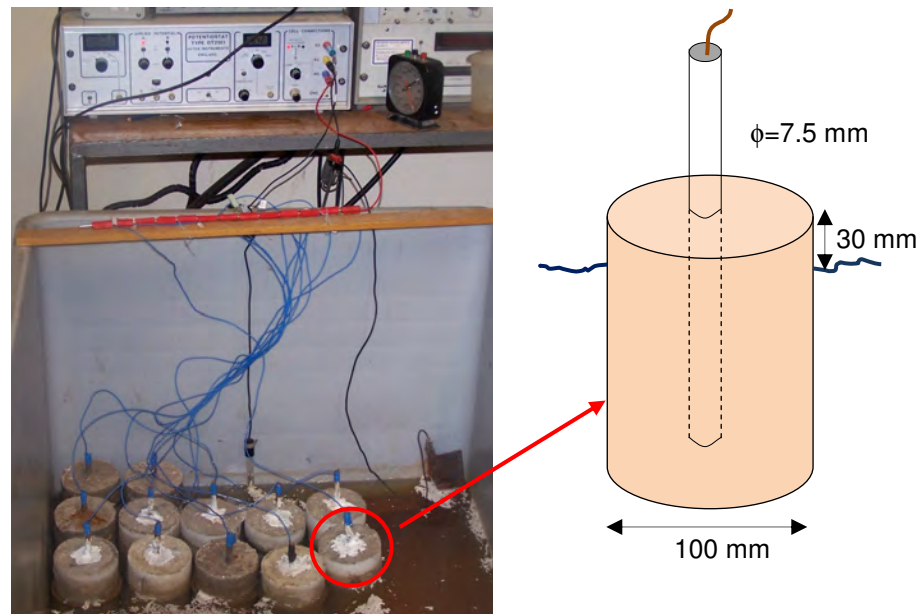
Figure 10-14 (left) Set up of the experiment, (right) corrosion reinforced concrete sample

During the measurement of corrosion rates the total electrical current through the circuit shown in figure 10.11 is equal to the sum of the polarisation resistance R_p, the internal resistance of the potentiostat, and the resistance of the electrolytic medium. Although the electrical resistance of the potentiost and the sodium chloride solution are negligible, the electrical resistance of concrete R_c surrounding the steel electrode does have an important effect. That is, the total resistance R measured is actually the sum of R_p and R_c. The determination of the concrete resistance (R_c) was made according to section 6.5.

In addition to the effects of the electrical concrete resistance on the total current measured, the concrete double layer capacitance C_{dl} can introduce some errors in the measurement of R_p (Claisse 1988). In order to compensate for the effect of C_{dl} in this research a time delay of 30 seconds was introduced between the application of the external voltage and the measurement of current.

As was shown in equation 10.21, the constant B is function of the anodic and cathodic Tafel constants. However, for practical applications it is common practice when the conditions of the corrosion process are known to use experimental values as reported in the literature. It has been suggested by Broomfield (2007)

in reinforced concrete structures values of 26 mV for reinforced steel actively corroding, and 52 mV if the steel is considered passive. In this research, as an external anodic voltage of 100 mV was applied continually to the samples, the value of the constant B assumed was 26 mV.

10.6.2 Half-Cell Potentials

The rest or equilibrium potential of steel (E_0) is correlated with the severity of corrosion in reinforced concrete structures. The ASTM C-876 (1991) provides general guidelines for evaluating corrosion in concrete as outlined in Table 10.2. Note that the potentials are in respect to a saturated calomel electrode.

Half-cell potential reading vs. SCE	Corrosion activity
less negative than -0.200 V	90% probability of no corrosion
between -0.200 V and -0.350 V	an uncertain probability of corrosion
more negative than -0.350 V	90% probability of corrosion

Table 10-2 Probability of corrosion according to half-cell readings (ASTM C-876)

11 CHLORIDE TRANSPORT RELATED PROPERTIES

In this chapter an experimental programme was designed in order to measure and simulate computationally some of the most important transport related properties in concrete mixes containing the two types of slag used in this research.

11.1 INTRODUCTION

In an initial stage, the final slag binders developed in the first part of this dissertation were investigated. For each of these, the following tests were carried out: workability, compressive strength, open porosity, initial water absorption capacity (sorptivity), carbonation, chloride migration and self diffusion, electrical resistivity, water permeability, and corrosion.

Because some of the final binders investigated are new, little is known about their chloride related properties, and there was no prior knowledge about the influence upon their durability of either the water to binder ratio or the conditions of curing. In order to contribute to a better understanding, the water binder ratio and the curing conditions were also included as variables within this part of the research.

In a second stage of this part of the research, mixes of ordinary Portland cement and ground granulated blast furnace slag at different proportions were investigated. Chloride related tests were carried out on different combinations of OPC and GGBS in order to establish the influence of the proportion of slag on the transport properties of this popular mixture. The tests carried out were compressive strength, open porosity, chloride migration and self diffusion, and electrical resistivity.

In addition to the experimental programme carried out, the chloride transport related properties of 20 different mixtures were obtained from the tests of current and mid point membrane potential, using the optimization model presented in chapter 8. Based on the experimental results and the simulations, the intrinsic diffusion coefficients of chloride, hydroxide, sodium and potassium were obtained. Also, the initial hydroxide composition of the pore solution, the porosity, and the chloride binding capacity were determined.

11.2 EXPERIMENTS ON FINAL BINDERS

11.2.1 Materials

The final binders developed in the first part of the research were investigated in this chapter on concrete samples. The cementitious materials are shown in table 3.2.

Binder	Materials	Binder name
1	100% OPC (reference)	O
2	40% OPC + 60% GGBS	OG
3	70% OPC + 30% BOS	OB
4	40% OPC + 30% GGBS + 30% BOS	OGB
5	10% BPD + 54% GGBS + 36% BOS	BGB
6	5%PG + 60% GGBS + 35% BOS	PGB

Table 3.2 Final slag mixes selected

The properties of the sand used were already described in Chapter 7.1.2. Coarse aggregate from a quarry with a mixed surface texture of both rounded smooth and angular rough particles was used (5-13 mm). Figure 11.1 shows the size distribution of particles, using the ASTM C33 (2008) recommended limits. The material was between the limits of size number 7 according to the standard. The dry density of the sand was 2650 kg/m^3.
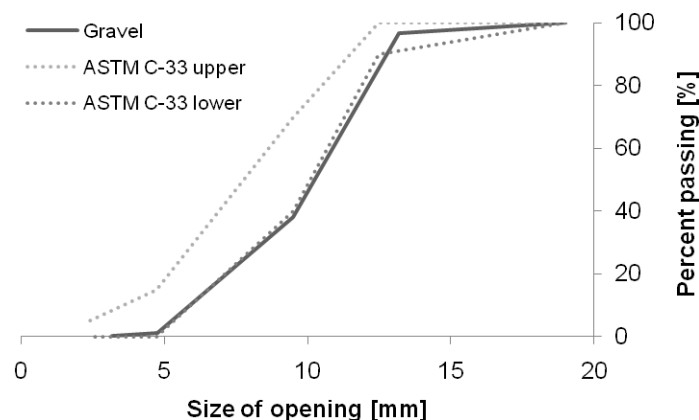
Figure 11-1 Coarse aggregate size distribution and ASTM C-33 limits

The water used as part of the mix was obtained from the tap and no chemical admixtures or similar materials were used.

11.2.2 Mix design, casting and curing

In the design of the concrete mixes some variables were fixed and controlled to make the results comparable. The main parameters taken into account in obtaining the proportions of the mixtures were the following:

- Water to binder ratios of 0.40 and 0.50 were used for each mixture.
- The total amount of cementitious materials used for all the mixes was 400 kg/m^3.
- The ratio between coarse aggregate and sand was fixed at 1.23.

The procedure to obtain the proportions of the materials in weight was to determine for each material the absolute volume for a cubic meter of concrete. For this, the densities of the materials were used. Table 11.1 shows the weights calculated for each material.

A mechanical horizontal pan mixer of 50 litres of capacity was used to mix the different materials (figure 11.2). First, the dry materials (binders, sand, and gravel) were mixed for 1 minute, and with the pan still rotating, 1/4 of the water was added and mixed for a further minute. After that, the mixer was stopped for 1 minute to allow the aggregate pores to fill with water and the mixture scraped off the sides of the pan. Finally, the remaining water was added and mixed continuously for 2 minutes more.

#	Mix	W/B	Binder [kg/m^3]						Water Kg/m^3	Sand Kg/m^3	Gravel Kg/m^3
			OPC	GGBS	BOS	BPD	PG	Total			
1	O-4	0.40	400	0	0	0	0	400	160	795	972
2	O-5	0.50	400	0	0	0	0	400	200	747	913
3	OG-4	0.40	160	240	0	0	0	400	160	805	984
4	OG-5	0.50	160	240	0	0	0	400	200	757	925
5	OB-4	0.40	280	0	120	0	0	400	160	792	968
6	OB-5	0.50	280	0	120	0	0	400	200	744	910
7	OGB-4	0.40	160	120	120	0	0	400	160	797	974
8	OGB-5	0.50	160	120	120	0	0	400	200	749	916
9	BGB-4	0.40	0	216	144	40	0	400	160	799	976
10	BGB-5	0.50	0	216	144	40	0	400	200	751	917
11	PGB-4	0.40	0	240	140	0	20	400	160	800	978
12	PGB-5	0.50	0	240	140	0	20	400	200	752	919

Table 11-1 Proportions of the slag concrete mixes cast

Figure 11-2 Horizontal 50 litre mixer

Because of the large number of experiments and the variety of sample sizes and forms, different types of casting moulds were required (figure 11.3). All the concrete was cast in standard pre-oiled moulds and the samples were covered after casting with a polyethylene sheet until the next day. For each mix, the tests were carried out on concrete samples subjected to two different curing conditions. Wet (water) curing and dry (air) curing conditions were used. In the first one, the specimens were submerged in lime water and kept at 20±2 °C. In contrast, under the dry curing condition the specimens were left in the laboratory environment at 20±4 °C and 40-60% in direct contact with the air.

Figure 11-3 Pre-oiled moulds before casting

11.2.3 Design of experiments

Table 11.2 shows a summary of the experiments carried out, in which 12 mixes under the two different curing conditions were assessed. A total of 24 different types of specimens were investigated. The samples were named according to the binder materials of table 3.2, the water binder used (0.4 or 0.5), and the curing condition (wet or air). For example, the sample OGB4W corresponds to the mix 40% OPC + 30% GGBS+ 30%BOS with a water to binder ratio of 0.4 and subjected to a wet curing condition. Samples "W" were kept in water meanwhile samples "A" were left to cure in air.

The following tests were carried out.

Workability: Before casting the specimens, the slump was measured for all mixes according to Part II of BS1881. Additionally, the flow properties of the mixes were measured using the ICAR rheometer. However, because of the low slump of the mixtures with water to binder ratio of 0.4, it was not possible to use this machine on those mixtures.

Compressive strength: The compressive strength was measured on 100 mm cube specimens at ages of 3, 28, and 90 days. The specimens were cured according to the conditions specified prior to the tests, and three replicates were tested for each mixture.

Open porosity: This test was carried out according to the method presented in section 6.5. The tests were carried out on samples at an age of 90 days, and three replicates were tested for each mixture. The specimens were cured according to the specified conditions.

Initial Sorptivity: This test was carried out according to the method presented in section 10.4. The tests were carried out on samples at an age of 90 days, and two replicates were tested for each mixture. The specimens were cured according to the specified conditions prior to the tests.

Electrical resistivity: A.C. resistivity was measured on the same samples used in the chloride migration tests at 90 days. Three replicates were tested for each mixture. The procedure followed is presented in section 6.6.

Chloride penetration in self diffusion tests: The chloride penetration was measured from diffusion tests on cylindrical specimens. The experiments were started 90 days after casting and lasted for another 90 days. The specimens were cured according to the specified conditions before beginning the tests, and three replicates were tested for each mixture. The procedure followed was presented in section 6.8.

Chloride migration: Voltage control (ASTM C1202) and membrane potential tests were carried out on 50 mm cylindrical specimens at the age of 90 days. The specimens were cured according to the specified conditions prior to the tests, and three replicates were tested for each mixture.

Carbonation: The carbonation depth was measured on 100 mm cube specimens at the age of 1 year after casting. During the first 28 days the samples were allow to cure according to the specified curing conditions. After this initial period of time all the samples were removed from their curing environment and were left on the roof of the John Laing building at Coventry University until the test. The environment around the samples was that found in the City of Coventry-UK. The samples were cast in the summer of 2008 and three replicates were tested for each mixture.

Water permeability: Cylindrical Samples of 55 mm of diameter and 30 mm thickness were tested. The specimens were cured according to the standard conditions prior the tests, and two replicates were tested for each mixture.

Corrosion: Cylinders with an embedded 7.5 mild steel bar were used to assess the protection given to the reinforcement by the concrete. After demoulding, the samples were kept in tap water (pH≅7.3) as shown in figure 10.12-right for 150 days, and the rest potentials at regular intervals measured. At the end of this period, the samples were immersed in a 7% NaCl solution, where a constant voltage of +100mV was applied. This external voltage was driven by the potentiostat in order to polarize the samples at +100mV. The polarization resistance was measured over a further 182 days and two replicates for each test were used.

#	Proportions	Water/ Binder	Curing	Name	Comp. strength	Carb.	Cl penet	Cl Mig	Resistivity	Open Porosity	Water sorptivity	Corrosion	Water permeability
1	100% OPC (reference)	0.40	wet	O4W	3	3	3	3	3	3	2	2	2
2	100% OPC (reference)	0.40	air	O4A	3	3	3	3	3	3	2	0	0
3	100% OPC (reference)	0.50	wet	O5W	3	3	3	3	3	3	2	0	0
4	100% OPC (reference)	0.50	air	O5A	3	3	0	0	0	0	0	0	0
5	40%OPC+ 60%GGBS	0.40	wet	OG4W	3	3	3	3	3	3	2	2	2
6	40%OPC+ 60%GGBS	0.40	air	OG4A	3	3	3	3	3	3	2	0	0
7	40%OPC+ 60%GGBS	0.50	wet	OG5W	3	3	3	3	3	3	2	0	0
8	40%OPC+ 60%GGBS	0.50	air	OG5A	3	3	0	0	0	0	0	0	0
9	70%OPC+ 30%BOS	0.40	wet	OB4W	3	3	3	3	3	3	2	2	2
10	70%OPC+ 30%BOS	0.40	air	OB4A	3	3	3	3	3	3	2	0	0
11	70%OPC+30%BOS	0.50	wet	OB5W	3	3	3	3	3	3	2	0	0
12	70%OPC+30%BOS	0.50	air	OB5A	3	3	0	0	0	0	0	0	0
13	40%OPC+30%GGBS+30%BOS	0.40	wet	OGB4W	3	3	3	3	3	3	2	2	2
14	40%OPC+30%GGBS + 30%BOS	0.40	air	OGB4A	3	3	3	3	3	3	2	0	0
15	40%OPC+30%GGBS + 30%BOS	0.50	wet	OGB5W	3	3	3	3	3	3	2	0	0
16	40%OPC+30%GGBS + 30%BOS	0.50	air	OGB5A	3	3	0	0	0	0	0	0	0
17	10%BPD+54%GGBS + 36%BOS	0.40	wet	BGB4W	3	3	3	3	3	3	2	2	2
18	10%BPD+54%GGBS + 36%BOS	0.40	air	BGB4A	3	3	3	3	3	3	2	0	0
19	10%BPD+54%GGBS + 36%BOS	0.50	wet	BGB5W	3	3	3	3	3	3	2	0	0
20	10%BPD+54%GGBS + 36%BOS	0.50	air	BGB5A	3	3	0	0	0	0	0	0	0
21	5%PG+60%GGBS + 35%BOS	0.40	wet	PGB4W	3	3	3	3	3	3	2	2	2
22	5%PG+60%GGBS + 35%BOS	0.40	air	PGB4A	3	3	3	3	3	3	2	0	0
23	5%PG 60%GGBS + 35%BOS	0.50	wet	PGB5W	3	3	3	3	3	3	2	0	0
24	5%PG+60%GGBS + 35%BOS	0.50	air	PGB5A	3	3	0	0	0	0	0	0	0

Table 11-2 Summary of the concrete slag experiments carried out

11.2.4 Experimental outcomes and discussion

11.2.4.1 Workability of fresh mixes

Although the relationship between workability and the transport properties was not studied, results of workability are presented in order to characterize the fresh properties the novel slag mixes developed. Results of slump are shown in figure 11.4. As was expected, significant differences between mixtures of different water content were found. As was reported by ACI-238 (2008), the blended slag binders improved the slump of the OPC for both water contents. Although for slag mixes with water/binder 0.5 the increase in the slump was between 30 and 50 mm higher than the slump of pure OPC samples, those mixtures still showed an adequate cohesion, and aggregate segregation was not detected. For mixtures containing BOS, bleeding was observed; this was attributed to the high specific gravity of the steel slag.
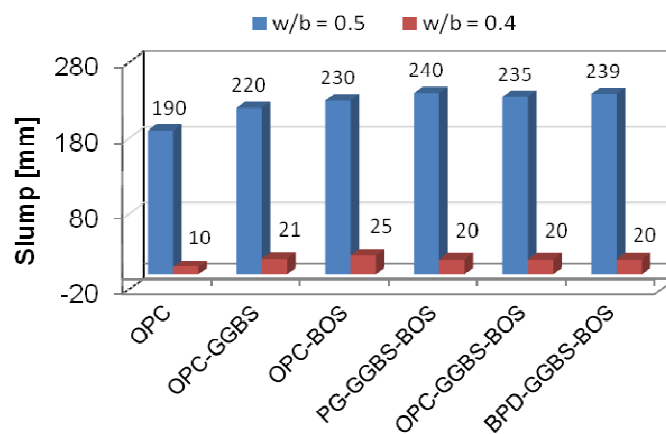
Figure 11-4 Concrete slag mixtures' slump

The experimental flow curves for the mixtures tested are shown in figure 11.5.
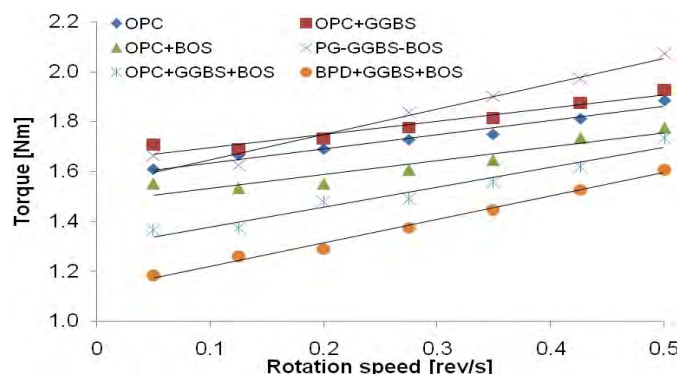
Figure 11-5 Measured flow curves (w/b=0.5) of concrete slag mixes

From the experimental flow curves the physical parameters were determined. The yield stress [Pa] and viscosity [Pa*s] obtained are shown in Figure 11.6. It is noted that the plastic viscosity and the yield stress are strongly influenced by the presence of the binary mixture GGBS-BOS and that the presence of OPC generates a decrease in those properties.
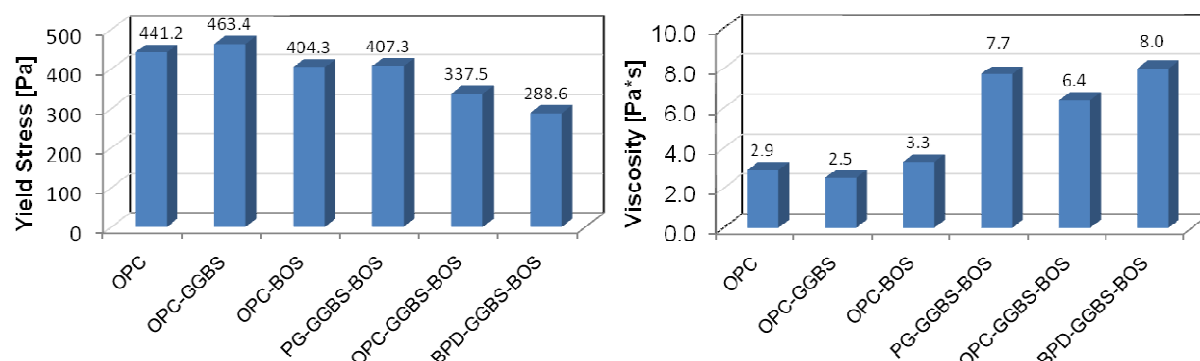
Figure 11-6 Yield stress and viscosity of final slag concrete mixes

As was reported by Wallevik (2006), a low correlation between the slump and the measured parameters was obtained. Figure 11.7 shows the relationships between the slump and the yield stress and viscosity.
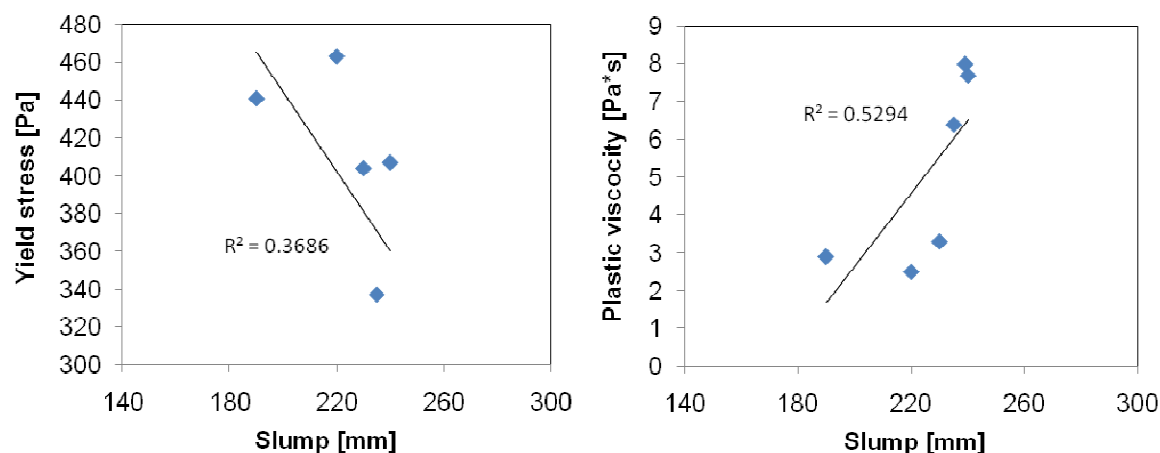
Figure 11-7 Relationships between yield stress and viscosity – slump for final slag concrete mixes

11.2.4.2 Compressive strength

Figure 11.8 shows the results of compressive strength for all the mixes evaluated. The variability of the test is shown through error bars with amplitude equal to twice the standard deviation. Although the mechanical properties of OPC and GGBS blended concretes are well reported in the literature, for the other mixtures the availability of data is limited. The following conditions were observed for all the binders: an increase in the age of curing produces an

increase in the strength, the samples cured in water showed more strength than their air-cured equivalents, and a decrease in the water to binder ratio produced an increase in the compressive strength.
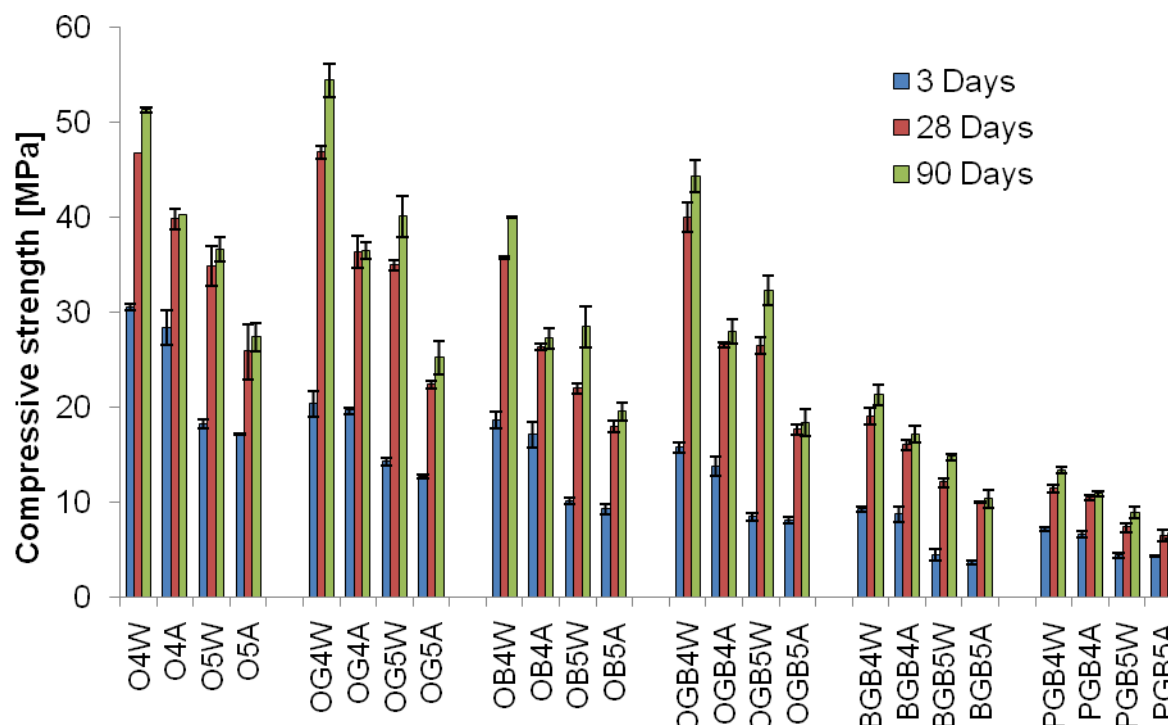
Figure 11-8 Compressive strength of blended concrete samples

Strength development:

The strength at 90 days will be called here final strength; however, it does not mean that at later ages could no be more strength increase. The O4W mixture (OPC, w/b=0.4, curing=water) at 3 days developed 60% and at 28 days developed 91% of its final strength. Mixture OG4W showed at early age a delay in the rate of strength development, this mix developed 37% at 3 days and developed at 28 days 86% of its final strength. Mixtures OGB4W and BGB4W behaved similarly to OG4W, showing a significant delay in the rate of compressive strength development. Mixtures OB4W and PGB4W did not show delay in the rate of compressive strength development.

For blended mixtures the compressive strength evolution depends on the amount and the type of slag replacement. In OPC combinations, GGBS produces a delay at early ages because the slag glassy compounds react slowly with water and it takes time to develop hydration products. However, at later ages, it can produce higher compressive strength than simple OPC. In the same way, BOS produces a delay in the development of the compressive

strength, but, at 90 days this material gains little in compressive strength. In ternary mixes OPC-GGBS-BOS there is a situation that lies between the conditions mentioned before.

Curing influence:

For all air cured mixtures, the percentage of compressive strength developed for any mix at 28 days, with respect to the value of strength of the same mix at 90 days was much higher than when samples were water cured. This observation is important because it means that when the samples are not properly cured (i.e. in air), they did not show further increase in strength at later ages (after 28 days). The values of strength observed at 28 days and 90 days were relatively similar.

Reductions of compressive strength due to differences in curing were obtained for all mixes. For example, mix O4 had a reduction of 4% at 3 days, 15% at 28 days and 21.5% at 90 days when it was air cured. In the same way, mix O5 had a reduction of 5.5% at 3 days, 25.7% at 28 days and of 25.2% at 90 days. For all the mixes at early ages (3 days) it was observed that the air curing did not affect the compressive strength significantly. This could be because the water necessary for hydrating the mixes exists in the specimens at least during the first days. In contrast, the reduction of strength for samples air cured after 3 days is significant, being more important for mixes containing OPC and GGBS in combination and with higher water to binder ratios. The differences in curing conditions resulted in a reduction of the compressive strength; at 90 days for example that reduction can be observed in table 11.3

Mixture	O4	O5	OG4	OG5	OB4	OB5	OGB4	OGB5	BGB4	BGB5	PGB4	PGB5
Reduction [%]	21.5	25.2	33.0	37.0	32.0	32.3	36.9	43.0	19.4	30.1	18.9	25.0

Table 11-3 Reduction of compressive strength at 90 days because of curing for blended concrete samples

Water to binder ratio influence:

For OPC mixtures at 90 days, an increase in the water to binder ratio has a greater impact on strength than does the curing method. In contrast, OPC-GGBS, OPC-BOS and OPC-GGBS-BOS mixtures are more susceptible to the curing type than to the water to binder ratio. The two non-Portland mixtures behaved similarly to OPC. In all cases, samples with water to binder ratio of 0.5 and cured in air showed the greatest loss of strength because the dual detrimental factors worked simultaneously.

The effect of the water binder ratio on the compressive strength as calculated by the difference between samples with the same binder and curing conditions, was analyzed. For any age and type of curing, the reduction of compressive strength due to changes in the water to binder ratio was important, being higher for early ages. In all binders, the reduction of strength due to changes in the water binder is higher for samples cured in air. For all mixes, table 11.4 shows the reduction in compressive strength at 90 days due to an increase in the water to binder ratio.

Mixture	OW	OA	OGW	OGA	OBW	OBA	OGBW	OGBA	BGBW	BGBA	PGBW	PGBA
Reduction [%]	28.5	31.9	26.2	30.7	28.8	28.2	27.1	34.1	36.6	39.8	33.5	38.6

Table 11-4 Reduction in compressive strength at 90 days due to the water to binder ratio for blended concrete samples

Materials influence:

At early age (3 days), regardless of the curing or water to binder ratio, for all slag binders the measured compressive strength was lower than the OPC reference. At 90 days, the compressive strength of OPC-GGBS samples cured under water was higher than the reference - an increase of 6 and 9.5% was obtained for samples with 0.4 and 0.5 water binder ratio respectively. It shows that if this mix is adequately water cured it can be expected to have a strength superior to one of 100% ordinary Portland cement. For the same binder when cured in air, it was a reduction of 9.3 and 7.8% with respect to the OPC reference that was obtained for samples with 0.4 and 0.5 of water binder ratio respectively.

As was reported by Tasdemir (2003), Mineral additives with coarse particles cause a reduction in the strength of concrete. In that way, the blended mixture OPC-BOS had a reduction of compressive strength at 90 days (with respect to the OPC sample with the same water to binder ratio and curing conditions) of 22% for samples cured in water and a reduction about 30% for samples cured in air. These values can be considered consistent with expectations, taking into account the poor cementitious properties of steel slag. However, the reduction of strength at 90 days found in the first stage of the research for a paste mix with 30% BOS and 70% OPC was around 7%. It is believed that the greater reduction in strength in concrete samples is due to failure of the cement paste-aggregate interfaces. This was concluded from visual observations of the specimens after testing.

The ternary mixture OPC-GGBS-BOS under conditions of water curing showed more compressive strength at 90 days than the similar OPC-BOS. For that ternary mix the reduction of compressive strength with respect to the OPC reference was of 13.6 and 11.8% for samples with water binder ratio of 0.4 and 0.5 respectively. That makes this novel mix attractive from the standpoint of its mechanical properties because it contains only 40% of ordinary Portland cement. As was pointed out before, samples cured in air were affected considerably; for this mix, the reduction of compressive strength due to the curing conditions was of 30.5 and 32.7% for samples with water binder ratio of 0.4 and 0.5 respectively.

The results of compressive strength for the mixtures with 100% waste were not as good as expected, especially for the mix including plasterboard gypsum. Although in the first part of the research a compressive strength of paste samples for both mixes (PG and BPD activated) of around 32 MPa was obtained, the maximum strength obtained for the BGB and PGB mixes were 21.4 and 13.5 MPa respectively. The reduction of strength with respect to the OPC reference for the mixes of 0.4 water to binder ratio and cured in water was of 58.4 and 73.8% for BGB and PGB respectively. In the same way as in than OB mixes, some problems of adhesion between the cement paste and the aggregate were detected.

11.2.4.3 Open Porosity

Capillarity porosity was determined using 30 mm thick slices of concrete cylinders after 90 days of curing. Capillary pores are defined as pores with a diameter bigger than 10 nm, as opposed to gel pores, which have a small diameter (Midness and Young 1981). In theory, permeability is related only to capillarity porosity because the water adsorbed on the cement matrix is practically immobile. Powers (1958) found the permeability of the "gel" to be approximately 2×10^{-17}m/s. It should be noticed that the open porosity test only gives an indication of the total water accessible porosity and some problems are reported in the experimental procedure (Nokken 2004):

- 100% saturation is not easy to obtain in concretes with closed microstructure.

- Errors can be introduced in the determination of saturated surface dry mass (i.e., more surface area)

Figure 11.9 shows the porosity measured for the final concrete mixes. The results vary due to the binders, water binder ratio and curing condition.
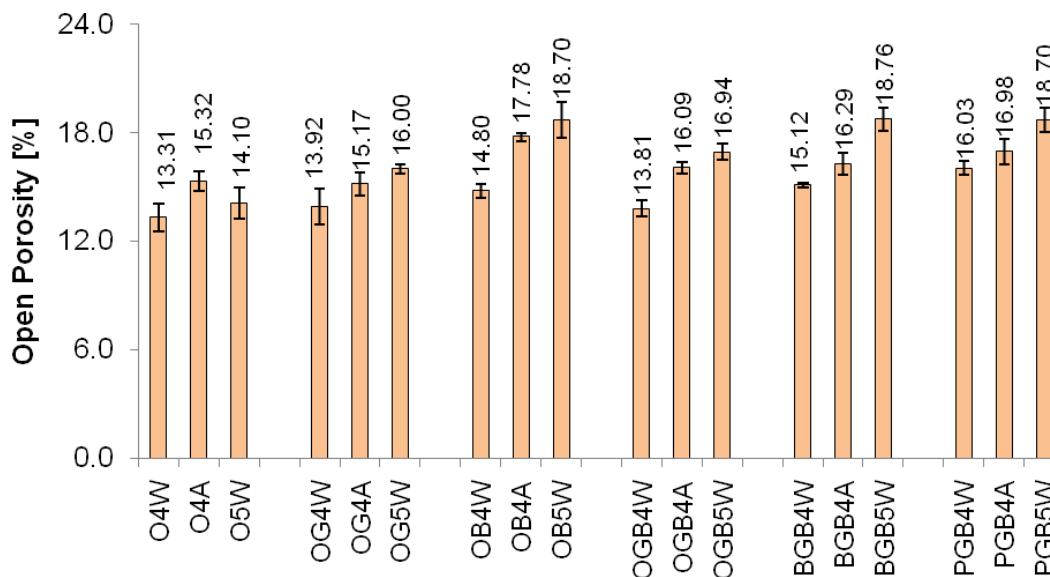
Figure 11-9 Open porosity measured on blended concrete samples

11.2.4.4 Water absorption - Sorptivity

Water absorption measurements were taken every minute for 25 minutes. Figures 11.10 to 11.12 show the change in mass with square root of time. The initial water absorption was calculated according to ASTM C1585, equation 10.8: "*the absorption i is the change in mass divided by the product of the cross-sectional of the test specimen and the density of water [mm]; the initial rate of water absorption [mm/min$^{1/2}$] is defined at the slope of the line that is the best fit to i plotted against the square root of time [min$^{1/2}$]*".

The slope of the curve *S* (sorptivity) and the constant *A* were obtained using least-squares linear regression analysis. For this, the points from 1 to 25 minutes were used, but times after the plot showed an important change of slope were excluded.
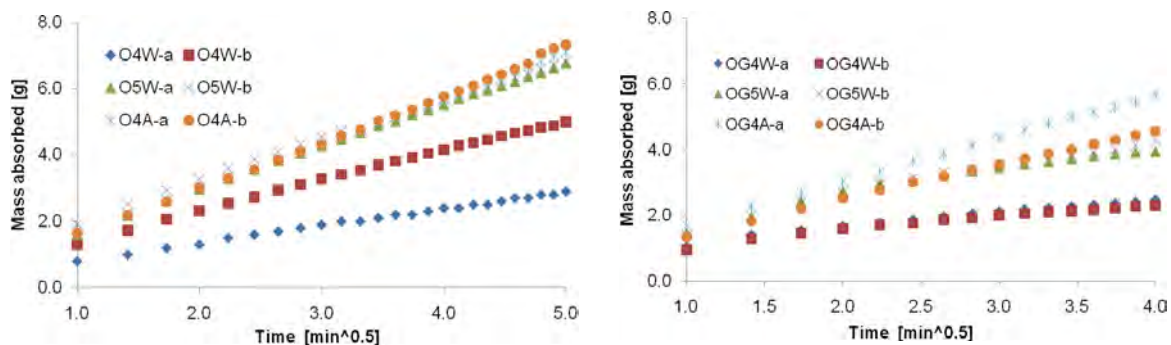
Figure 11-10 Mass absorbed on concrete samples; left: OPC and right: OPC-GGBS
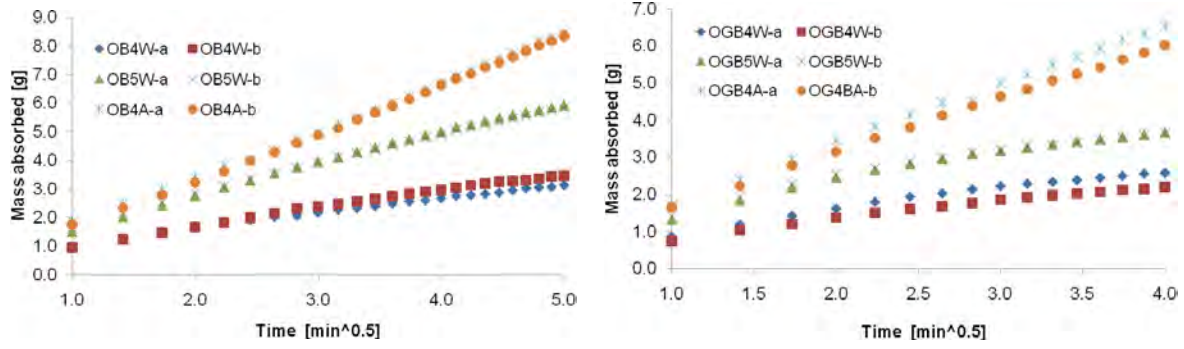
Figure 11-11 Mass absorbed on concrete samples; left: OPC-BOS and right: OPC-GGBS-BOS
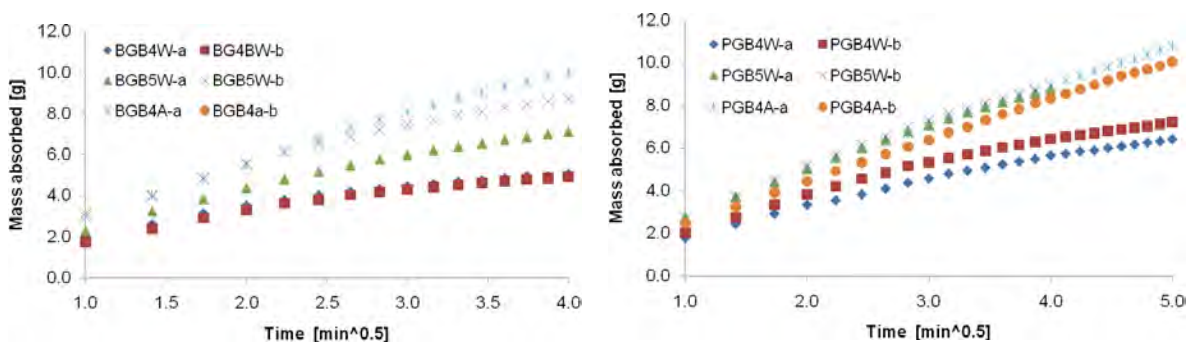
Figure 11-12 Mass absorbed on concrete samples; left BPD-GGBS-BOS and right: PG-GGBS-BOS

The initial rate of water absorption for each mix is given in appendix 5 and the sorptivity for all the mixes are shown in figure 11.13.
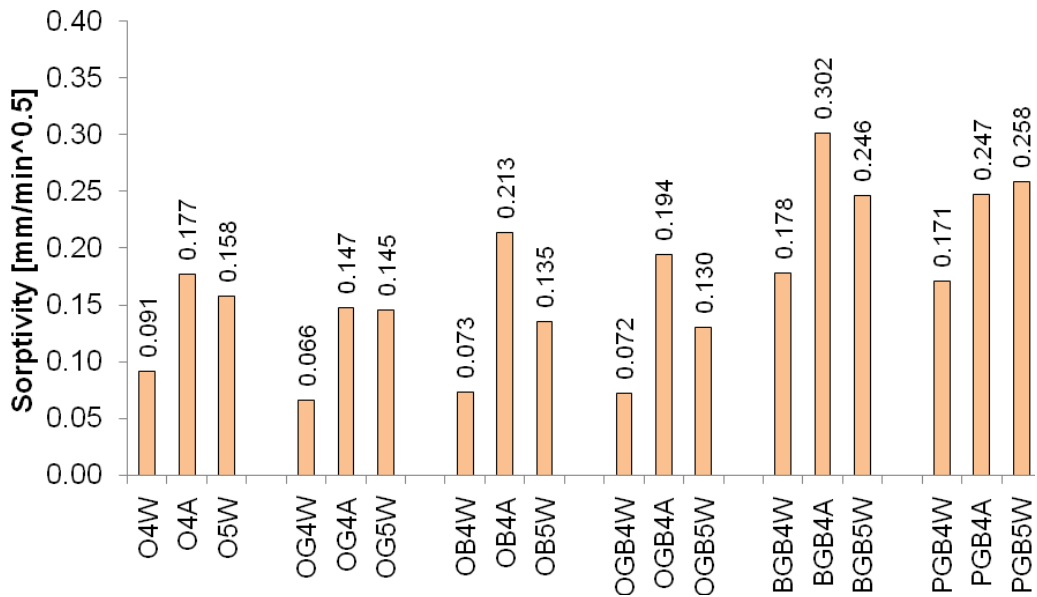
Figure 11-13 Initial sorptivity measured on concrete blended samples

For all binders, as expected, the sorptivity of the specimens cured in water was higher than the specimens cured in air because of better hydration. The binder most vulnerable to the curing conditions was the combination OB, which had a sorptivity increase of 293%, followed by the mix OGB which had an increase of 269%. The sample OG had an increase of 224% and the OPC reference of 194%. The sorptivity in non-Portland binders was less vulnerable to air curing with an increase of 169% and 151% for BGB and PG mixes respectively. For all mixes, an increment in the water to binder ratio produced an increase in sorptivity, however, it was less important than the effect of the air curing.

It is shown that either the GGBS or BOS when blended with OPC and cured adequately produce a reduction in capillary absorption with respect to the OPC reference. For the GGBS blended mixes this can be explained by the slag being finer than OPC filling the capillary pores, and also the pozzolanic properties of the slag improving the pore structure as was stated by ACI-233 (2003). In contrast, for the BOS blended mix it is believed that the material behaves as a filler, which blocks the capillary pathways and reduces the capillary absorption.

Hall (1989) published sorptivity data for ordinary Portland cement based materials. He showed that sorptivity varies with water binder ratio and with different degrees of compaction. The numerical values of capillary absorption showed in that research for concrete with prolonged tamping (well compacted), with water to binder ratio 0.4 and 0.5, are 0.094 and 0.12 $mm/min^{1/2}$ respectively. The results obtained in this research for similar mixtures are in very good agreement with the results reported by Hall, the numerical values obtained here were 0.091 and 0.158 $mm/min^{1/2}$ respectively.

The sorptivity measured for water cured non-Portland mixes was about twice the value obtained for the OPC reference. However, the reduction of strength with respect to the reference was about 2.5 and 4 times for BPD and PG blended mixtures respectively. The lack of proportionality can be attributed to the very fine particle sizes of the mineral admixtures. Similar results were reported by Al-Harthy, Taha and Al-Maamary (2003).

11.2.4.5 Electrical Resistivity

The AC electrical resistance was measured on the water saturated cylinder samples just before carrying out the voltage control migration tests. The corresponding resistivity calculated with equation 6.14 in ohm-m is shown in figure 11.14.
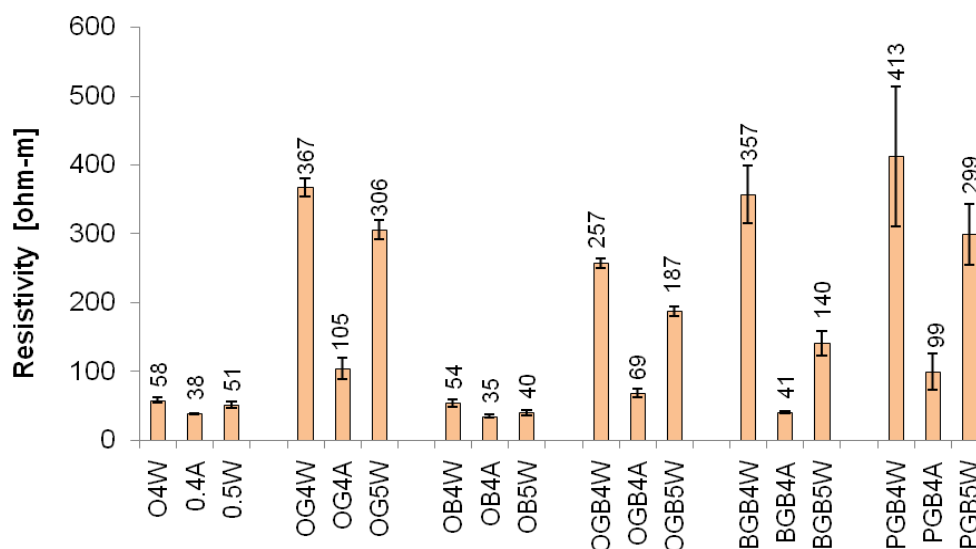
Figure 11-14 Initial resistivity measured on concrete blended samples

Mixtures with GGBS developed higher resistivity compared to the specimens without it, showing huge differences between the results of different curing conditions. In the same way, it was observed for all mixes that resistivity decreases with an increase of the water to binder ratio. For water cured OPC-GGBS samples, an increase of resistivity due to the addition of GGBS of about 6 times the reference's value can be seen. This could be mainly due to the refinement of the porous matrix and the depletion of the OH⁻ concentration of the pore solution as was explained in section 6.6. Samples OPC-BOS show a decrease in resistivity, but their value was quite similar to that of the reference. The samples containing GGBS and BOS had resistivity values of more than 4 times the OPC reference. The non-Portland cement mixes showed higher values of resistivity with respect to the OPC samples. For those mixes with water binder ratio 0.4 and cured in water, there was an increase in the resistivity of 600 and 700% for the BPD and PG mixes respectively.

The diffusivity of any species is linearly related to the electrical conductivity of that species according to the Nernst-Einstein equation (5.6). However, the experimental test carried out gives information about the total conductivity resulting from all the ions together in the pore solution, rather than the single ionic conductivity. In that sense, the questions about the use of the resistivity test for a transport property are because there could be two possibilities: (i) samples which have low resistivity values due to low diffusivity and (ii) those where the low value of resistivity has been caused mainly by ion depletion in a pozzolanic reaction.

As in the previous properties measured, the curing has a significant effect on resistivity, especially for those GGBS. The average resistivity reduction obtained due to air curing for

GGBS mixes was around 70%. For the reference mix and the OPC-BOS mix the reduction from air curing was just 35%

11.2.4.6 Chloride diffusion tests

Results of chloride penetration after 90 days of diffusion are shown in figure 11.15. All the results are presented with error bars for the standard deviation obtained from the experiments. Figure 11.16 shows the chloride penetration coefficient (k) calculated from equation 6.14 [mm/days$^{0.5}$].
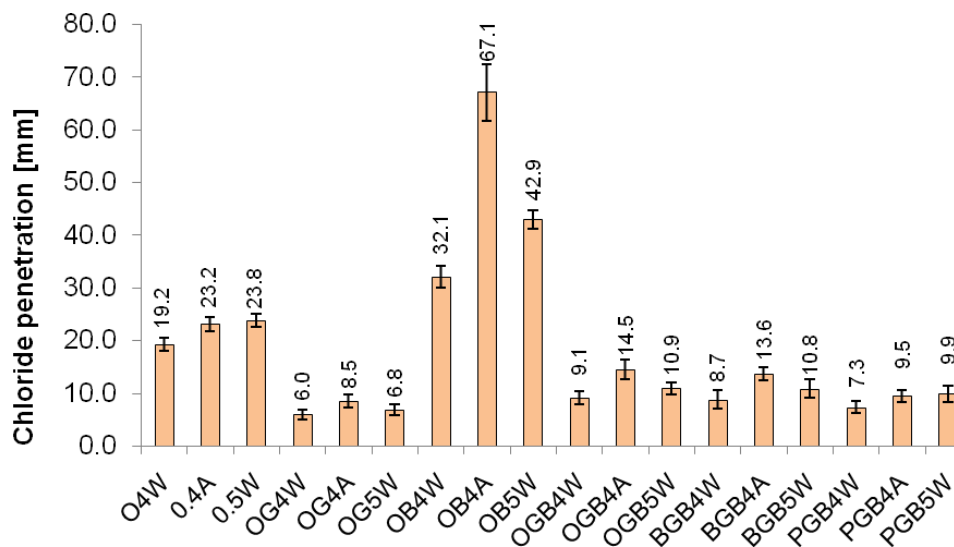
Figure 11-15 Experimental chloride penetration after 90 days of self-diffusion measured on concrete blended samples
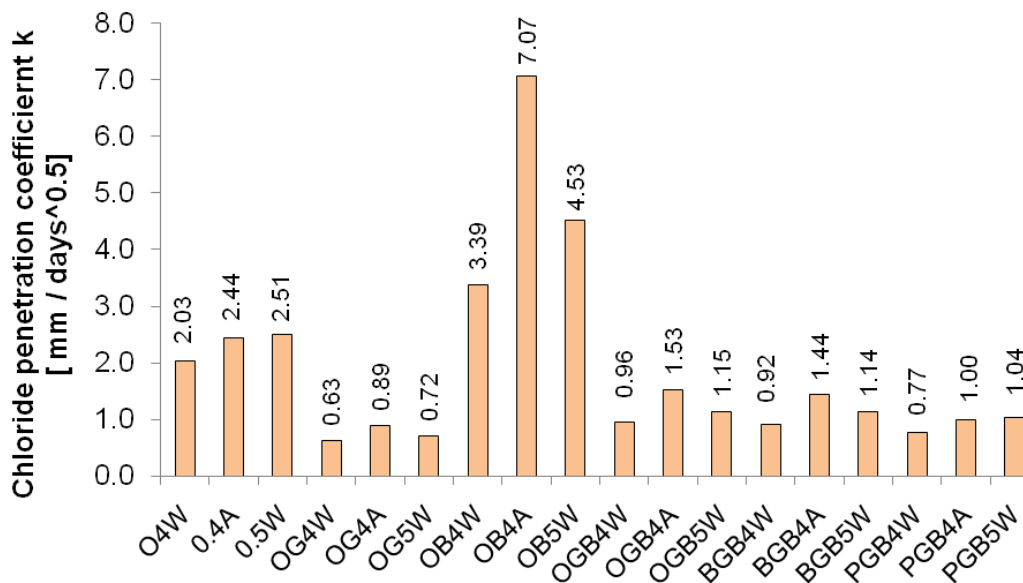
Figure 11-16 Chloride penetration coefficients *k* calculated using equation 6.16

From the previous figures it may be observed that for the mixtures studied the most important factor is the presence of GGBS. Samples containing GGBS showed lower values of k than samples without this mineral admixture. The water to binder ratio and the curing conditions also influenced the chloride penetration. For all mixtures, the air curing resulted in an increase of the coefficient $k,$ which might be expected due to the reduced level of hydration in the surface layers of the air-cured concrete. The most serious effects of this type of curing were in mixture OPC-BOS, followed by OPC-GGBS-BOS, BPD-GGBS-BOS, OPC-GGBS, PG-GGBS-BOS and finally and least affected, OPC

. The benefits of GGBS on the chloride penetration are well known and have been reported in many publications. For example, in a research carried out by Thomas *et al.* (2008), it was found that the addition of blast furnace slag at a proportion of 65% (concrete water binder ratio of 0.4) decreases the apparent diffusion coefficient by a ratio of 18 with respect to a sample without slag.

Samples OPC-GGBS and OPC-GGBS-BOS water cured showed a reduction in the chloride coefficient of penetration k of 70 and 52% with respect to the OPC reference. However, the OPC-BOS mix showed an increment of about 70% with respect to the reference. It may be seen that the chloride penetration measured for non-Portland mixtures was always lower than the OPC references. Although previous results of compressive strength, open porosity and sorptivity indicate that those materials should have some chloride related durability problems, their chloride penetration resistance was higher than the references. It is believed that this good behaviour in terms of chloride penetration is due to the ability of those mixes to bind chlorides. As was stated before in 5.3.1, GGBS increases the chemical chloride binding capacity because the C_3A reacts with free chlorides forming insoluble calcium chloroaluminate hydrates (Friedel's salt).

It is also indicated that the effect of sulphates on the binding capacity of GGBS-BOS mixes is different from normal OPC mixes. Luo *et al.* (2003) states that in a normal OPC mix the C_3A has a preferential reaction with sulphates and less C_3A can bind chloride to form Friedel's salt. That situation seems not to happen in the PG-GGBS-BOS mix, as it has a high chloride penetration resistance, attributable mainly to its ability to fix chlorides.

11.2.4.7 Chloride migration tests

The current and the membrane potential were obtained from the voltage control tests. Figure 11.17 shows the profile of the values measured experimentally and error bars for the standard deviation obtained for OPC blended samples. From the evolution of the current the

charge passed was calculated and analyzed as a related transport property, and from the combination of the current and the membrane potential, the related properties were simulated according to the optimization technique develop in chapter 8. This will be shown in section 11.4.
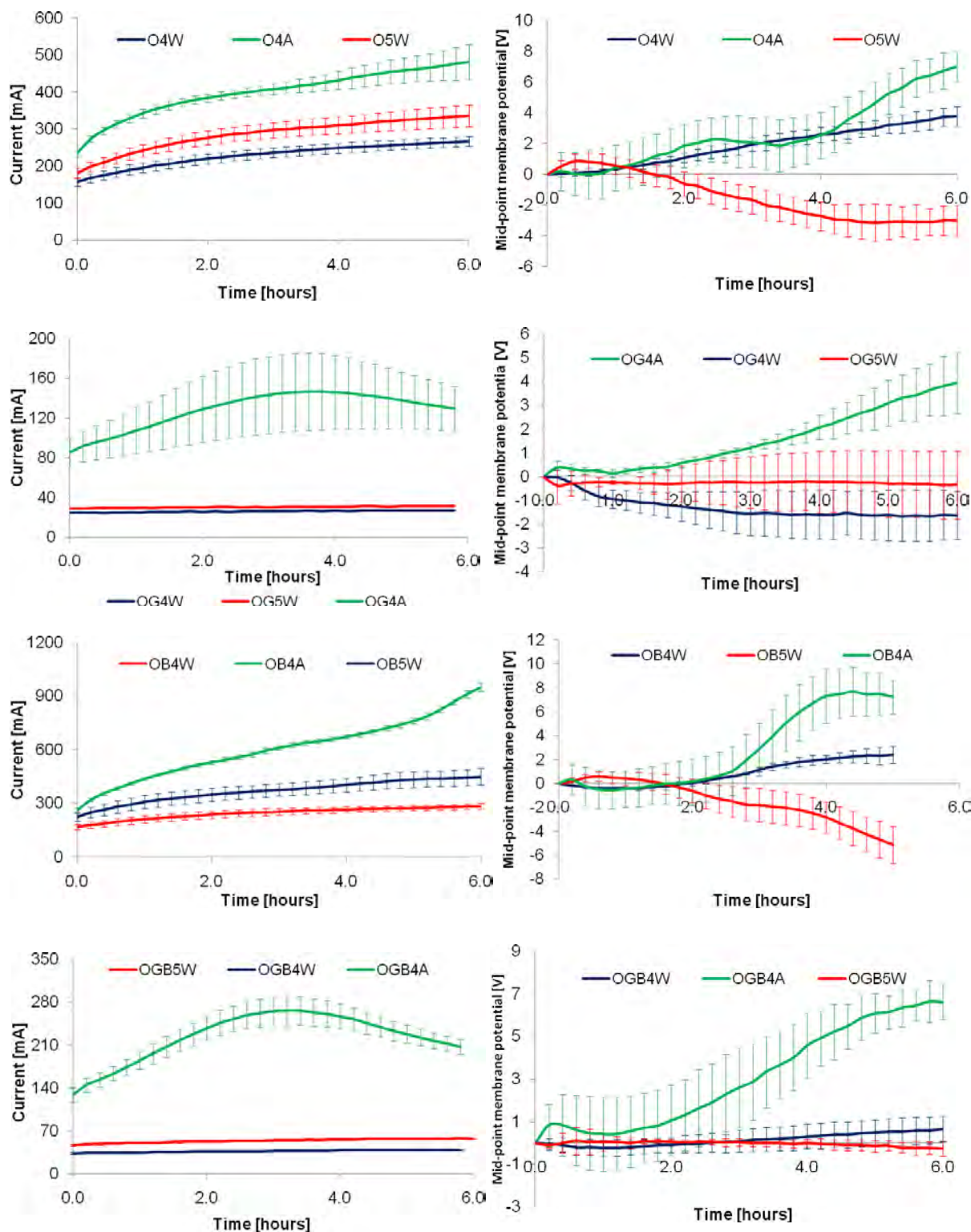
Figure 11-17 Current and membrane potential on blended OPC samples

It may be observed from the last figure that the current is influenced by the water binder ratio and the curing conditions. It is more sensitive in all cases to the air curing. In the same way, the profile of the current is very different for different types of binders.

For the non-Portland cement mixes it was not possible to measure the membrane potential. During the sample preparation it was necessary to drill a 4 mm hole in order to insert the salt bridge used to follow the voltage distribution during the test. Unfortunately, due to the low compressive strength, the samples were damaged during the drilling. Figure 11.18 shows the crack pattern produced.

Figure 11-18 BPD sample cracked during drilling

Figure 11.19 shows the evolution of the current for both non-Portland samples.
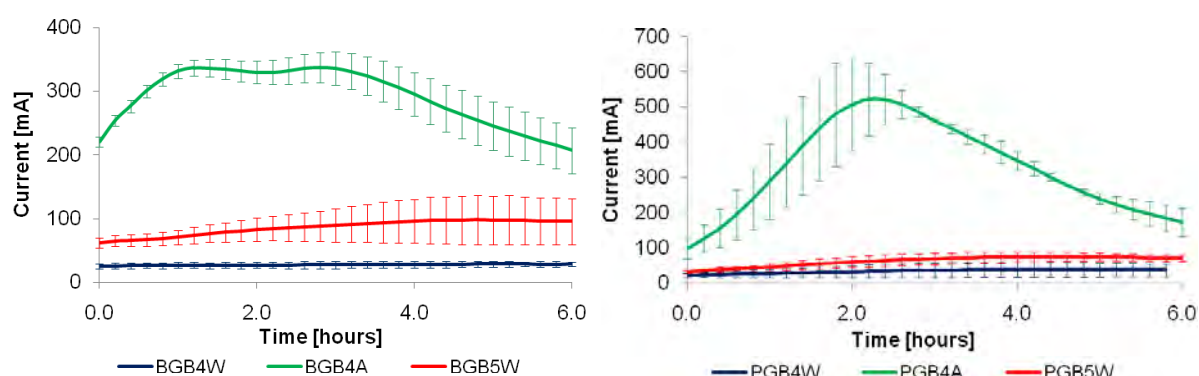
Figure 11-19 Current measured on non-Portland samples

11.2.4.7.1   Charge passed

The charge passed was calculated as the area under the curve of current vs. time as specified in ASTM C1202. Figure 11.20-A shows the evolution of charge for samples of water to binder ratio 0.4 and cured in water. Two groups are clearly defined, GGBS blended mixes and mixes without GGBS. Figure 11.20-B shows mixes of water binder 0.4 but cured in air. And figure 11.20-C shows the mixes of water to binder ratio of 0.5.
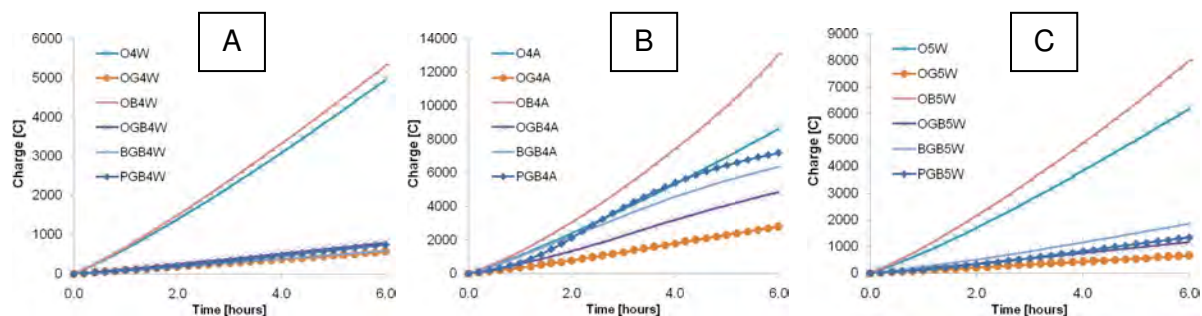
Figure 11-20 Evolution of the charge passed on concrete blended samples

Figure 11.21 shows the charge passed for each mix after 6 hours of the test, which includes the limits of chloride penetrability presented in table 5.3 (ASTM C1202). As for the chloride penetration and resistivity tests, samples with GGBS showed low values. In GGBS samples adequately cured and with low water binder ratio, values of charge corresponding to low chloride penetrability were measured. In contrast, for similar samples, but without GGBS, the charge passed corresponded to high chloride penetrability. This test is very sensitive to the air curing condition; especially for non-Portland samples which increased the charge passed by a factor of 10 when they were cured in air.
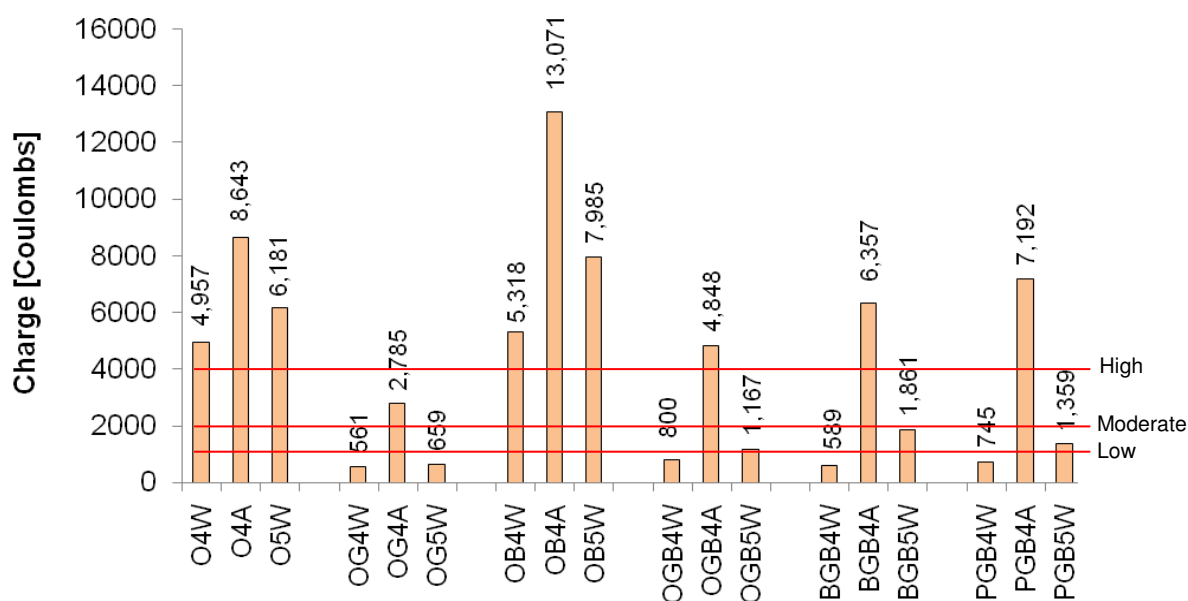
Figure 11-21 Charge passed after 6 hours during the ASTM C1202 test on blended samples

The Maximum temperatures obtained during the ASTM C1202 tests are shown in table 11.5.

Sample	O4W	O4A	O5W	OG4W	OG4A	OG5W	OB4W	OB4A	OB5W
Max temp [c]	47.0	63.0	51.8	24.0	34.2	25.6	47.6	85.6	60.7
Sample	**OGB4W**	**OGB4A**	**OGB5W**	**BGB4W**	**BGB4A**	**BGB5W**	**PGB4W**	**PGB4A**	**PGB5W**
Max temp [c]	25.6	46.4	27.8	24.0	48.0	30.3	27.7	66.6	43.8

Table 11-5 Maximum temperature measured during the RCPT test

11.2.4.8 Carbonation

One year after casting, the cubes were split with a compression machine and a solution of phenolphthalein was sprayed on the fresh surface. For all the cubes tested, including the non-Portland samples, after a couple of minutes a well defined boundary emerged, indicating 2 distinct areas having markedly different values of pH. Figure 11.22 shows the carbonation front for the sample BGB5W.

Figure 11-22 Carbonation depth in sample BPD-GGBS-BOS (w/b=0.5, water cured)

The results for the carbonation depth calculated with equation 10.7 are shown in figure 11.23. It was observed that this depth is principally a function of the type of binder, additionally by the curing regime, and finally, but also importantly, the water to binder ratio. As is stated by Basheer (2001), carbonation is related with the material intrinsic carbon dioxide diffusion coefficient and with the material calcium hydroxide reserve, which acts as

buffer against the carbon dioxide, preventing it from penetrating further. Non-Portland mixes showed the higher carbonation depth, this can be explained because of the high porosity of those mixes, but, especially because of the mineralogical composition of the products of hydration formed in them. In Part 1 of this thesis it was shown that during the hydration of BGB and PGB there was no portlandite observed. It is believed that the pH boundary shown by the phenolphthalein indicator results from the dissolution of the calcium silicate hydrates, and the pink coloration observed during the test was due to the alkalinity of the calcium hydrates.

For OPC-GGBS and OPC-GGBS-BOS the carbonation depth is much less than for non-Portland mixes, but is higher than for OPC-BOS mixtures. During OPC-GGBS hydration it is well know that GGBS does not consume calcium hydroxide, so, a small amount of portlandite produced by the OPC hydration remains as a buffer. This protection, together with the refined microstructure, results in an adequate carbonation resistance. For the OPC-GGBS-BOS mix portlandite can be available; however, a decrease in the quality of the pore structure is expected and a higher carbonation was measured. In OPC-BOS mixtures there is enough calcium hydroxide available to keep the carbonation depth low, despite the expected reduction of the quality of the pore structure.
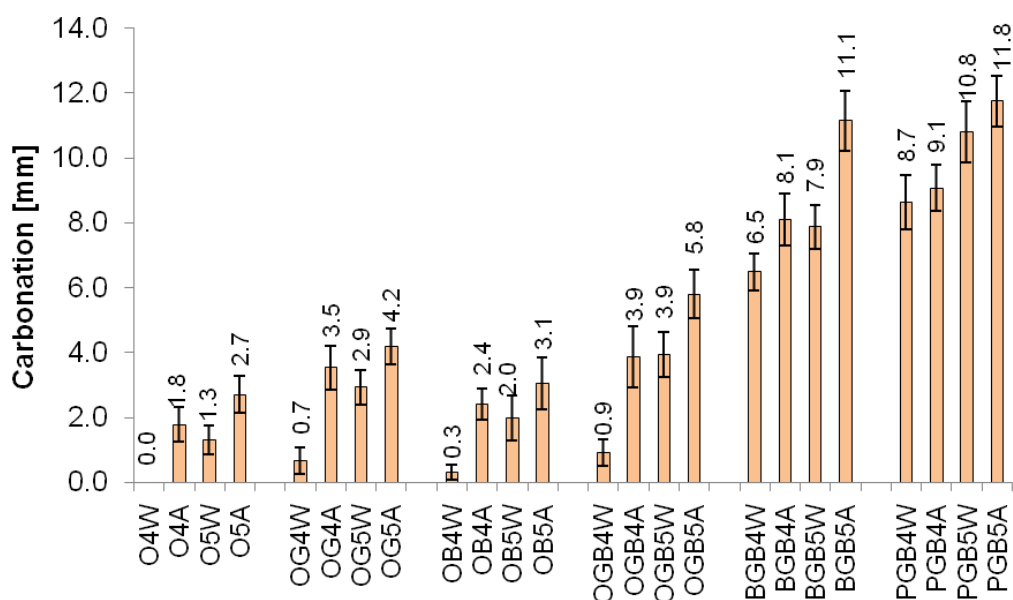
Figure 11-23 Carbonation penetration after 1 year of exposition

Results of the carbonation coefficient k_c (equation 10.6) are shown in figure 11.24. It can be seen that air cured samples showed an increase in the coefficient for all mixtures.
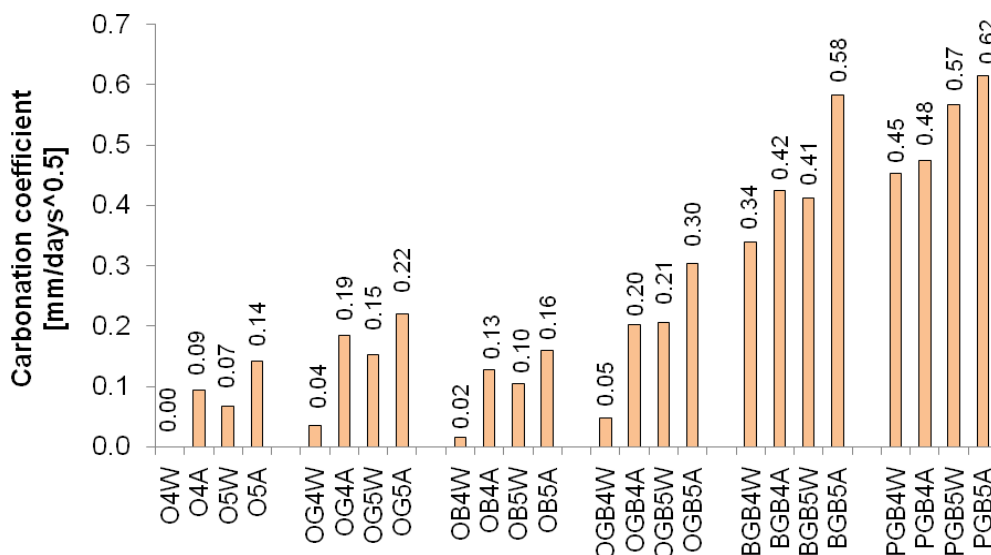
Figure 11-24 Carbonation coefficient of penetration k_c [mm/day$^{0.5}$]

11.2.4.9 Water permeability

Figure 11.25 shows the steady state water permeability results for the slag concretes tested. The coefficient of water permeability K_p was calculated from the experimental results using equation 10.10. In the figure are shown for each mix both samples tested and the numerical value of the average. Results obtained for OPC samples are in agreement with values reported by Basheer (2001) for a sample with water binder 0.4. OPC samples blended with GGBS and BOS showed results of permeability in the range of 10^{-13} m/s, in contrast, non-Portland mixes showed a significant increase of the water coefficient of permeability with values in the order of 10^{-11} m/s.
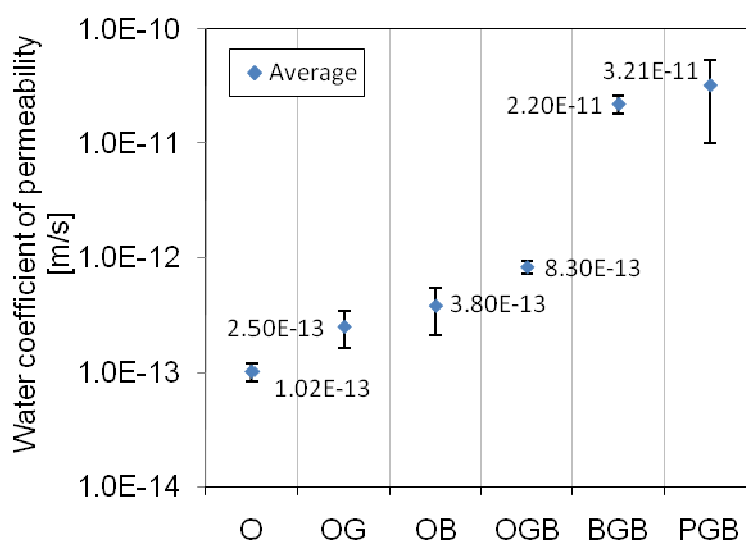
Figure 11-25 Water coefficient permeability for concrete blended samples

11.2.4.10   Corrosion Tests

After casting the corrosion samples (w/b = 0.4), the specimens were cured in tap water continuously for more than 150 days. Using a saturated calomel electrode (SCE) the half cell potentials were recorded to asses the electrochemical activity of the reinforcement in this "neutral" environment. Figure 11.26 shows the results of potential for this period, two replicates being tested for each mix.

Throughout the 150 days period, samples containing OPC invariably showed potentials more positive than -200 mV. That means, according to ASTM C876 (1991), that there is a "*90 % probability that no reinforcing steel corrosion is occurring*". As was expected, OPC and blended GGBS - BOS mixtures develop enough protection to keep the steel passivity. For non-Portland mixtures two periods can be distinguish. In an initial stage after casting, the samples showed very negative potentials (<-450 mV), presumably due to the presence of aggressive ions in the pore solution such as sulphates in the case of PG, and chlorides in the case of BPD. After a few days of curing, the materials developed a matrix of hydration products, where those aggressive ions could precipitate, and the potentials increased rapidly and became steady. In this final stage, the mix PG-GGBS-BOS showed a potential more positive than -200 mV with no sign of corrosion. However, the mix BPD-GGBS-BPD increased its potential, but it became steady in the region -200 to -350 mV, indicating uncertainty about corrosion.
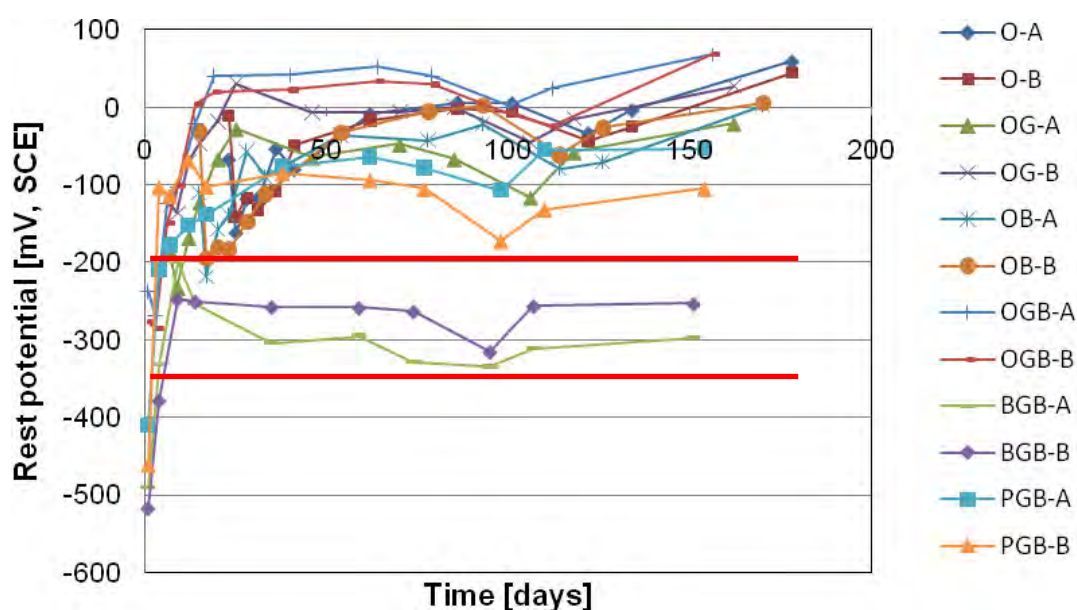
Figure 11-26 Rest potential measured during the curing period (150 days)

After the curing period the samples were exposed to a 7% sodium chloride solution and to an external potential voltage of +100 mV for 182 days. Results of the AC electrical resistance measured between the steel bar and the secondary electrode are shown in figure 11.27. Samples without GGBS showed the lowest values of resistance. The results were in agreement with the resistivity outcomes of section 11.2.4.5. For blended Portland mixes the electrical resistance was steady during the entire period of testing. In contrast, the non-Portland cement showed a decrease in resistivity caused presumably by chloride penetration. The PG-GGBS-BOS had at the beginning of the test an extraordinarily high electrical resistance that started to decrease noticeably after 30 days. The BPD mix, as well as the PG mix, decrease in resistance but in a moderate way.
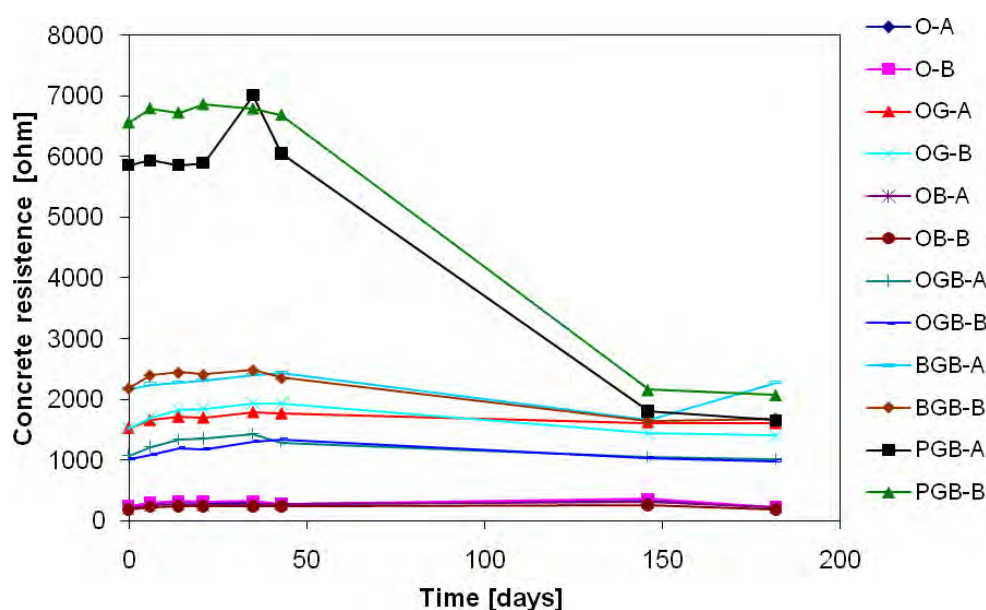
Figure 11-27 Electrical resistance during the induced corrosion period

In addition to the resistivity and the polarization resistance, the corrosion potential (rest potential) was used to investigate qualitatively the electrochemical activity of the bars embedded in the different mixtures. The evolution of the rest potential is shown in figure 11.28. All the mixtures containing Portland cement showed values of potential more positive than -200 mV at the beginning of the test, where no corrosion was detected. Although at 180 days all the samples decrease E_{corr}, those values were very close to the ASTM limit of -200 mV. It was not possible through this technique to distinguish which samples behaved better. For non-Portland samples more E_{corr} activity than in Portland samples was detected from the beginning. Both mixtures showed high probability of corrosion at 180 days.
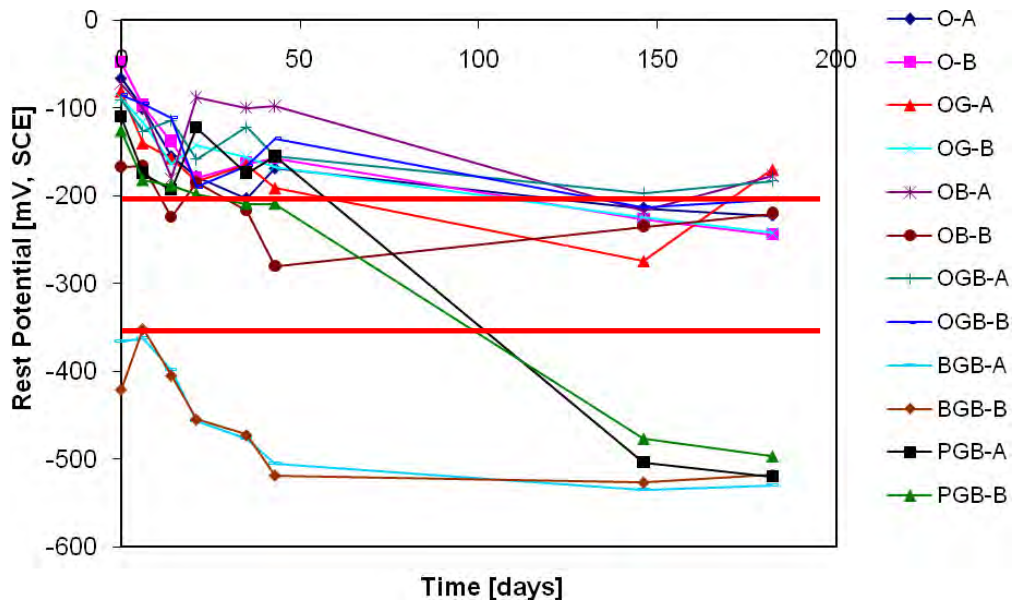
Figure 11-28 Rest potential during the induced corrosion period

The results of current density calculated with the polarization resistance technique are shown in figure 11.29, where some corrosion levels are defined according to table 11.6 (Aperador, Mejía de Gutiérrez and Bastidas 2009). Slag-Portland cement mixtures showed low values of current density with low levels of corrosion during all the period of testing. For those mixes it can be stated that the material gave enough protection to the steel to remain passive or with very low corrosion activity. In contrast, samples of non-Portland mixes showed very high levels of corrosion after 180 days of testing. It was found that those mixes are very vulnerable to corrosion when they are in an aggressive chloride environment.
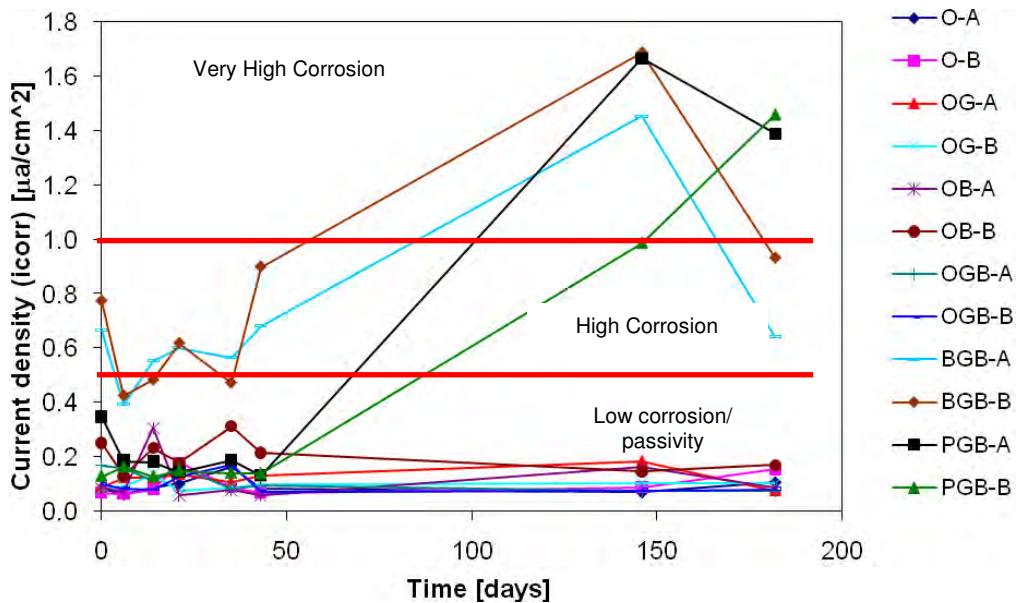
Figure 11-29 Current density I_{corr}, during the induced corrosion period

i_{corr} [µA/cm^2]	Level of corrosion
<0.1	passivity
0.1<i_{corr}< 0.5	Low corrosion
0.5<i_{corr}< 1	High corrosion
>1	Very high corrosion

Table 11-6 Corrosion levels proposed by Aperador, Mejía de Gutiérrez and Bastidas (2009)

The current density results are in good agreement and correlate "relatively" well with the logarithm of I_{corr}. Figure 11.30 shows the relationship between the logarithm of I_{corr} vs. E_{corr} for data taken at 182 and 146 days. Two groups of data are seen in the figure, samples with and without OPC. A similar relationship between I_{corr} vs. E_{corr} was reported by Jones (1996).
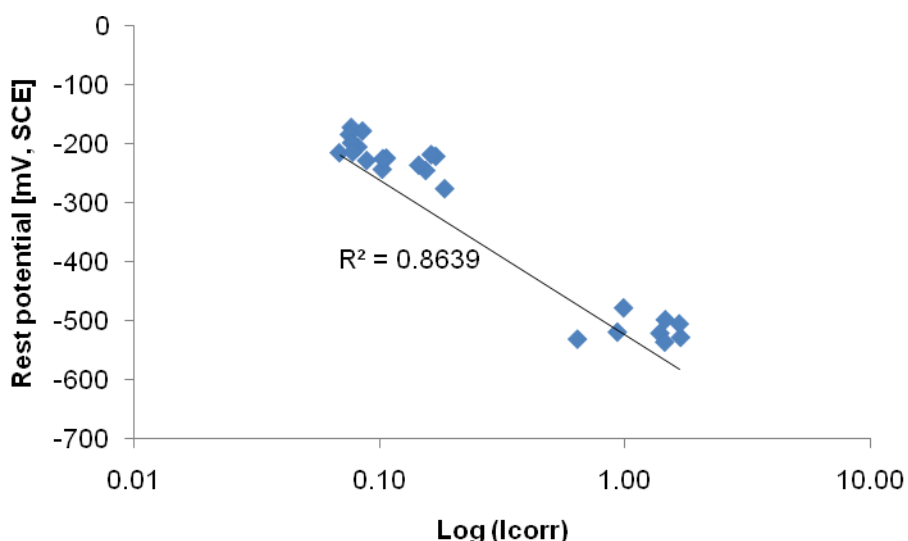
Figure 11-30 Relationship Log(I_{corr}) vs. E_{corr}

From equation 10.14 the equivalence for iron between the current density and the corrosion rate in mils (0.001 in) per year [mpy] is $1\mu A/cm^2 = 0.46 mpy$. Figure 11.31 shows the corrosion rate, calculated with the formula shown above, for all the samples at 180 days of testing. All the slag-OPC blended mixtures behaved similarly to the OPC reference. Figure 11.32 shows the condition of the steel bars after the tests. The bars were cleaned after removal from the cylinders for a reliable visual inspection. The visual inspection was consistent with the results obtained from the polarization resistance, low corrosion on OPC-slag samples and very high signs of corrosion in non-Portland mixes.
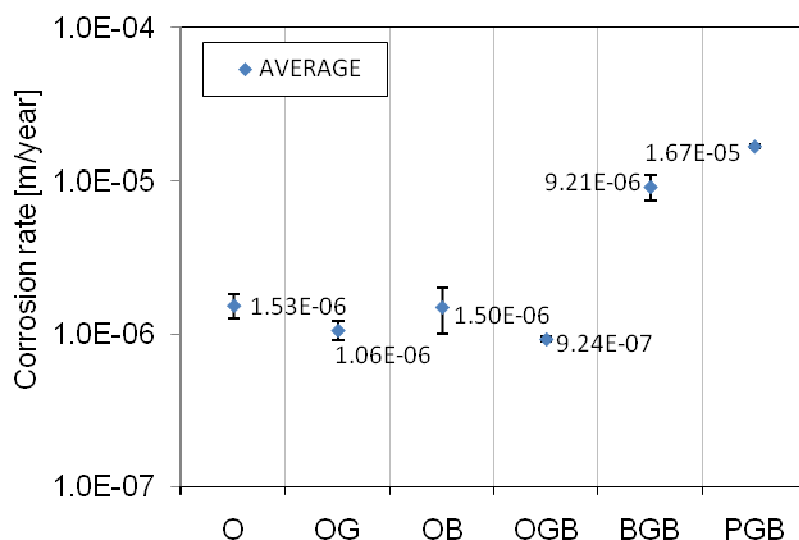
Figure 11-31 Corrosion rate measured at 182 days
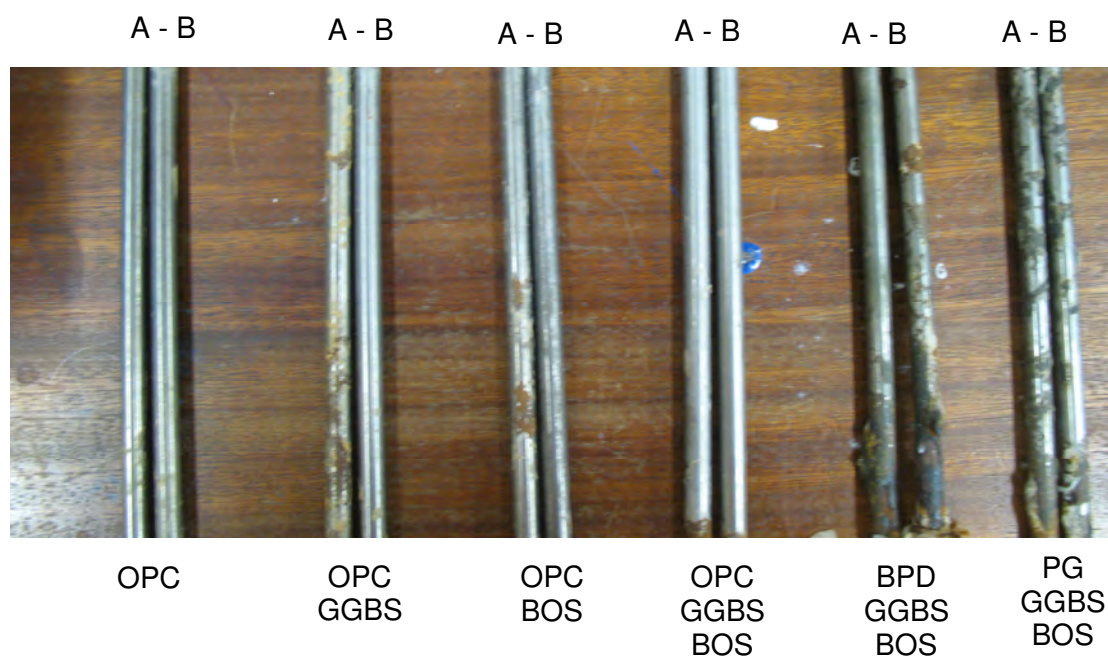
Figure 11-32 Reinforced bars after 182 days of testing

Figure 11.33A shows a detail of the PG-GGBS-BOS cylinder after 182 days of testing. A build up dark residue could be seen to have accumulated on the top of the samples showing high signs of corrosion. Figure 11.33B shows a detail of the bars for this mix.
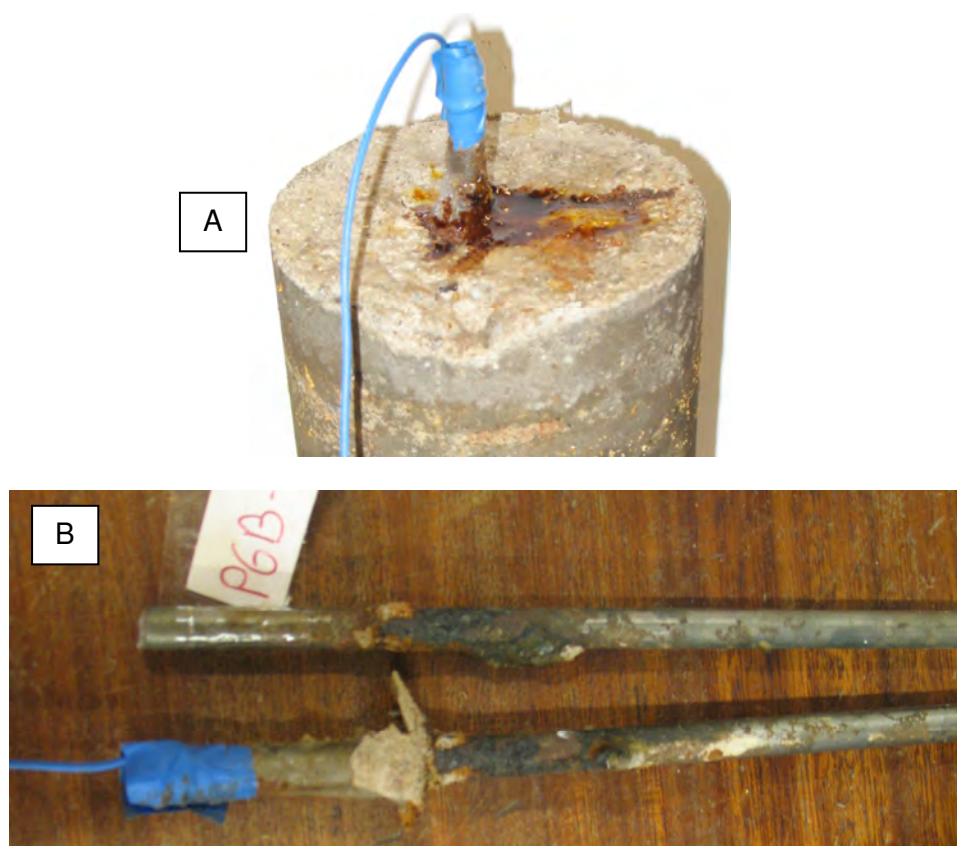
Figure 11-33 PG-GGBS-BOS cylinder and bar detail after 180 days of testing

11.3 EXPERIMENTS ON OPC - GGBS MIXES

In this section some experiments were carried out to investigate the influence of the replacement of GGBS on some transport chloride related properties. For this, just mixtures of OPC and GGBS with different proportions of replacement were cast and the properties experimentally determined. *This set of experiments is shown in a separate section in order to help the reader to understand the progress of the research*. The outcomes will be discussed in detail in chapter 12 along with the results obtained from the neural network optimization model presented in section 11.4.

11.3.1 Materials

The blast furnace slag used was that presented in the first part of this thesis and the OPC used was of type I according to ASTM. The sand and gravel were the same shown in figures 7.2 and 11.1 respectively. The water was obtained from the tap.

11.3.2 Mix design, casting and curing

The procedures of casting and curing were similar to those presented in section 11.2.2, but the samples were water-cured only under controlled conditions, no air curing was carried out

for this stage. The concrete mixes cast had different levels of slag replacement and water to binder ratio.

In order to provide as much information and make a more reliable analysis of the data, the mixes cast at different stages of the research are presented in table 11.7. They are classified according to the length of the curing time before testing. Group C1 was cured in standard conditions for more than 100 days, C2 was cured in the standard conditions for 180 days and samples of Group C3 were cured for 120 days. Additionally, the mixes were divided into groups "A" and "B" because different commercial brands of the Portland cement were being used (group A: Hanson cement, group B: Castle Cement).

It is well known that the chloride diffusion coefficient and most of the transport related properties are time dependent. In research carried out by Khitab (2005), the following equation was proposed to evaluate the transient effective diffusion coefficient.

$$D_{eff} = 8.10^{-13}(70/t)^{0.5} \qquad (11.1)$$

where D_{eff} is the effective diffusion coefficient [m^2/s] and t is the curing time [days]. Equation 11.1 indicates that the diffusion coefficient is not strongly affected after 70 days. So, it is assumed in this research that the curing time given to the different OPC-GGBS mixtures is enough to avoid the effect of the time dependent variability of the transport properties.

Group	#	Mix	Prop.	W/B	Binder [%] OPC	Binder [%] GGBS	Binder [kg/m^3] OPC	Binder [kg/m^3] GGBS	Binder [kg/m^3] Total	Water Kg/m^3	Sand Kg/m^3	Gravel Kg/m^3
C 1-A	25	O5-A	100%OPC	0.49	100	0	394	0	394	193	692	988
	26	OG5-10-A	90%OPC+ 10%GGBS	0.49	90	10	355	39	394	193	691	987
	27	OG5-30-A	70%OPC+ 30%GGBS	0.49	70	30	276	118	394	193	690	986
	28	OG5-50-A	50%OPC+ 50%GGBS	0.49	50	50	197	197	394	193	690	985
C 2-B	29	O4-B	100%OPC	0.40	100	0	400	0	400	160	705	1058
	30	O5-B	100%OPC	0.50	100	0	400	0	400	200	664	995
C 3-B	31	OG4-30-B	70%OPC+ 30%GGBS	0.40	70	30	280	120	400	160	704	1055
	32	OG4-50-B	50%OPC+ 50%GGBS	0.40	50	50	200	200	400	160	702	1054
	33	OG5-30-B	70%OPC+ 30%GGBS	0.50	70	30	280	120	400	200	662	993
	34	OG5-50-B	50%OPC+ 50%GGBS	0.50	50	50	200	200	400	200	661	991

Table 11-7 Proportions of the OPC-GGBS mixes cast

11.3.3 Design of experiments

The following tests were carried out in accordance with the procedures summarized in previous sections. Two replicates were used, except for compressive strength where three replicas were tested. Table 11.8 shows a summary of the experiments.

(i) Compressive strength (on 100 mm cubes) and open porosity.

(ii) Chloride migration (current and mid point membrane potential).

(iii) Chloride diffusion (90 days of exposure on a 7% NaCl solution).

(iv) A.C. electrical resistivity.

Mix	W/B	C. Strength	Cl Diffusion	Cl Migration	Porosity	Resistivity
O5-A	0.49	Yes	No	Yes	Yes	Yes
OG5-10-A	0.49	Yes	No	Yes	Yes	Yes
OG5-30-A	0.49	Yes	No	Yes	Yes	Yes
OG5-50-A	0.49	Yes	No	Yes	Yes	Yes
O4-B	0.40	Yes	Yes	Yes	Yes	Yes
O5-B	0.50	Yes	Yes	Yes	Yes	Yes
OG4-30-B	0.40	Yes	Yes	Yes	Yes	Yes
OG4-50-B	0.50	Yes	Yes	Yes	Yes	Yes
OG5-30-B	0.40	Yes	Yes	Yes	Yes	Yes
OG5-50-B	0.5	Yes	Yes	Yes	Yes	Yes

Table 11-8 Tests carried out on OPC-GGBS mixes

11.3.4 Results

Results of compressive strength are shown in table 11.9.

Mix	Compressive strength [Mpa]			Average
	A	B	C	[Mpa]
O5-A	37.3	36.6	36.9	36.9
OG5-10-A	33.7	33.5	33.6	33.6
OG5-30-A	32.8	32.9	33.2	33.0
OG5-50-A	33.1	33.7	33.4	33.4
O4-B	62.3	66.6	No	64.4
O5-B	44.6	46.4	No	45.5
OG4-30-B	66.7	63.9	No	65.3
OG4-50-B	56.9	54.3	No	55.6
OG5-30-B	51.3	48.3	No	49.8
OG5-50-B	47.9	45.4	No	46.7

Table 11-9 Compressive strength of OPC-GGBS mixes

From the migration tests the current and the mid point membrane potential were determined. With the algorithm presented in figure 7.14 the graphs of membrane potential were smoothed and filtered to reduce the experimental noise. Figure 11.34 shows the evolution of the total current and the membrane potential for samples of group "A"; figure 11.35 shows the results for samples of group "B" with water to binder ratio of 0.50; and figure 11.36 shows the results for samples of group "B" but with water to binder ratio of 0.40.
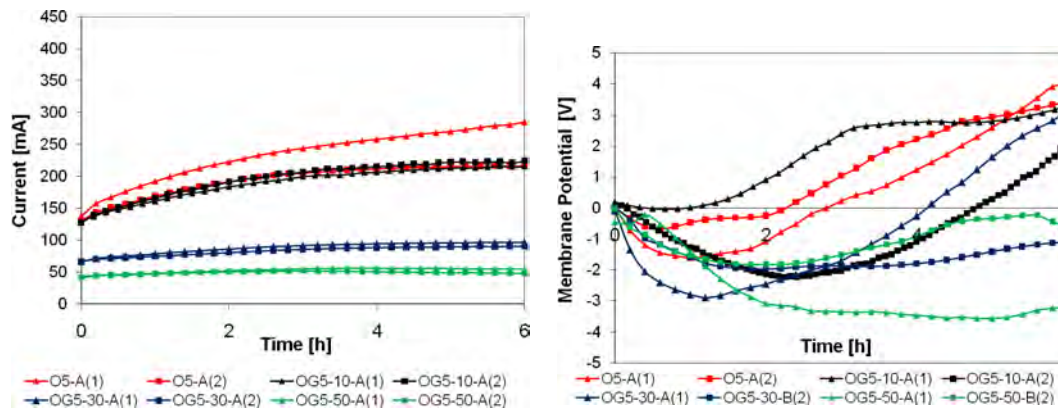
Figure 11-34 Current and membrane potential evolution samples "A"
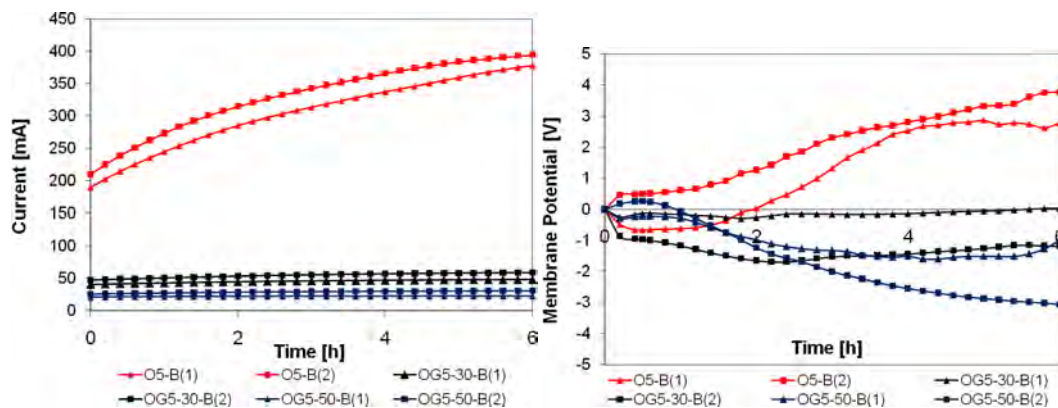
Figure 11-35 Current and membrane potential evolution samples "B", w/b=0.5
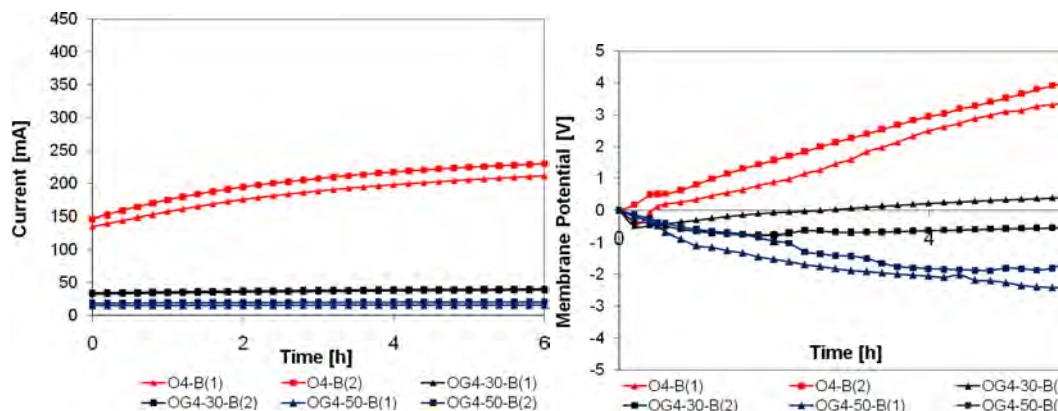
Figure 11-36 Current and membrane potential evolution samples "B", w/b=0.4

In figures 11.34 to 11.36 the individual results measured experimentally for each sample are shown graphically. The variability of the experiments is not shown in terms of the standard deviation as was done in figures 11.17 and 11.19 because just two samples were available and it was considered more appropriate to present the range. The average maximum temperature value obtained during the 6 hours of the test is shown in table 11.10.

Mix	O5-A	OG5-10-A	OG5-30-A	OG5-50-A	O4-B	O5-B	OG4-30-B	OG4-50-B	OG5-30-B	OG5-50-B
Max Temp. [C]	42.3	40	31.3	26.7	36	44	25.7	23.8	27	24.6

Table 11-10 Maximum temperature of OPC-GGBS mixes

The results for A.C. resistivity, charge, porosity and chloride coefficient of penetration are shown in table 11.11. In the same way as in figures 11.34 to 11.36, and for the same reason, the individual results and the average for each test are presented.

Mix	W/B	Proportions	Sample	Resistivity [ohm-m]	Charge [C]	Porosity	Cl coefficient k [mm/day$^{0.5}$]
O5-A	0.49	100%OPC	A	65.07	5066.41	15.04	No
O5-A	0.49	100%OPC	B	66.68	4220.75	16.05	No
O5-A	0.49	100%OPC	Average	65.88	4643.58	15.55	No
OG5-10-A	0.49	90%OPC+10%GGBS	A	70.16	4252.03	16.50	No
OG5-10-A	0.49	90%OPC+10%GGBS	B	70.55	4151.87	15.60	No
OG5-10-A	0.49	90%OPC+10%GGBS	Average	70.35	4201.95	16.05	No
OG5-30-A	0.49	70%OPC+30%GGBS	A	131.90	1902.17	17.00	No
OG5-30-A	0.49	70%OPC+30%GGBS	B	128.96	1794.30	17.90	No
OG5-30-A	0.49	70%OPC+30%GGBS	Average	130.43	1848.24	17.45	No
OG5-50-A	0.49	50%OPC+50%GGBS	A	202.05	1136.34	17.90	No
OG5-50-A	0.49	50%OPC+50%GGBS	B	211.85	1056.73	17.35	No
OG5-50-A	0.49	50%OPC+50%GGBS	Average	206.95	1096.54	17.63	No
O4-B	0.40	100%OPC	A	72.08	3950.12	16.00	2.86
O4-B	0.40	100%OPC	B	68.89	4348.78	16.42	2.85
O4-B	0.40	100%OPC	Average	70.48	4149.45	16.21	2.85
O5-B	0.50	100%OPC	A	50.59	6575.54	17.00	4.48
O5-B	0.50	100%OPC	B	50.82	7151.25	18.46	4.47
O5-B	0.50	100%OPC	Average	50.70	6863.39	17.73	4.48
OG4-30-B	0.40	70%OPC+30%GGBS	A	286.14	778.38	14.60	0.96
OG4-30-B	0.40	70%OPC+30%GGBS	B	267.48	813.23	16.31	0.96
OG4-30-B	0.40	70%OPC+30%GGBS	Average	276.81	795.80	15.45	0.96
OG4-50-B	0.40	50%OPC+50%GGBS	A	603.97	332.23	15.30	0.70
OG4-50-B	0.40	50%OPC+50%GGBS	B	499.14	426.26	16.39	0.60

OG4-50-B	0.40	50%OPC+50%GGBS	Average	551.55	379.25	15.85	0.65
OG5-30-B	0.50	70%OPC+30%GGBS	A	227.16	977.00	17.20	1.07
OG5-30-B	0.50	70%OPC+30%GGBS	B	195.29	1180.34	17.52	1.08
OG5-30-B	0.50	70%OPC+30%GGBS	Average	211.23	1078.67	17.36	1.08
OG5-50-B	0.50	50%OPC+50%GGBS	A	445.86	473.78	17.63	0.98
OG5-50-B	0.50	50%OPC+50%GGBS	B	366.89	614.46	18.16	1.06
OG5-50-B	0.50	50%OPC+50%GGBS	Average	406.37	544.12	17.89	1.02

Table 11-11 GGBS-OPC experimental results

11.4 SIMULATION OF TRANSPORT PROPERTIES

The transport related properties of a total of 20 mixtures were obtained through the neural network optimization model. The inputs of the network, as is shown in figure 8.3 correspond for each mix to the experimental values of the mid point membrane potential at 1.2, 3.6 and 6 hours, and the current at the start, 3.6 and 6 hours of the test. The numerical values used as inputs are shown in appendix 6.

Some of the final binder mixes shown in section 11.2, OPC, OPC-GGBS, OPC-BOS and OPC-GGBS-BOS samples, were simulated. Mixtures with BPD and PG were not simulated because it was not possible to measure the mid point membrane potential. In the same way, samples OB4A and OB5W are not included because in an initial simulation were obtained results that were not physically possible. For OPC-GGBS mixes all the samples of groups "A" and "B" are included.

Following the procedure detailed in section 8.4, with the numerical values of the inputs and the optimization model the chloride related properties were determined. In order to assess the general performance of the neural network, the Coventry University electro-diffusion model was run with the obtained transport properties to obtain the simulated values of total current and mid point voltage. Those results are plotted in figures 11.37 and 11.38 which show the relationship between the current and voltage measured and simulated for all the mixtures. The red line represents the ideal condition of zero error, where the predictions match the measured data perfectly.
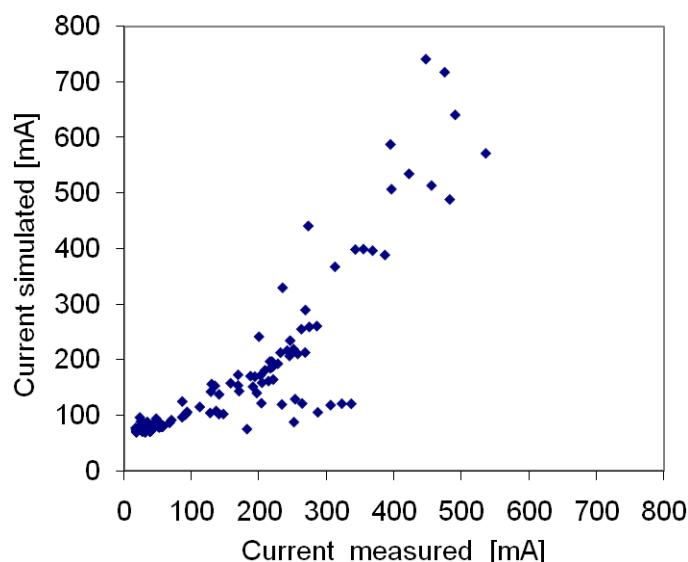
Figure 11-37 Current measured experimentally and calculated using the optimization model
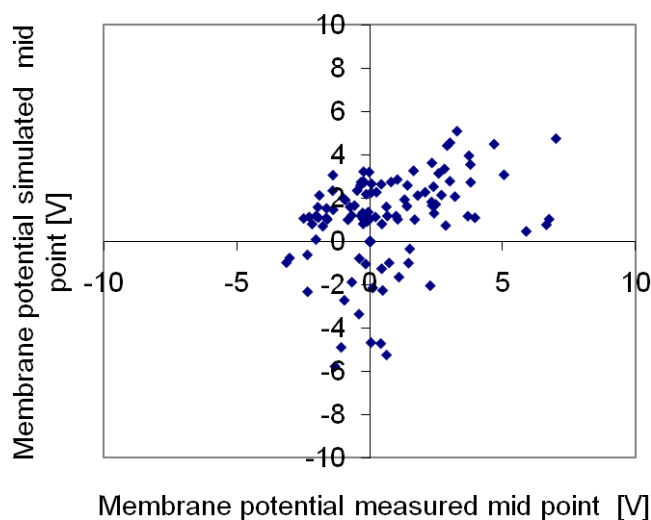
Figure 11-38 Mid-point membrane potential measured and calculated using the optimization model

Some very important observations can be made related with figures 11.37 and 11.38.

1. The procedure applied to find the transport properties of a concrete mix contains, as expected, errors. These can be either from the collection of the experimental data or a product of the process of the numerical model.

2. The ability of any model to predict an event lies in its capability to adapt to different inputs. In that way, the figures show the results from very different mixes (different binders and curing regimen) demonstrating the ability of the neural network to generalize the phenomenon.

3. The simulations for current are better than those for the mid point voltage, as was found and commented on in chapter 8.

The ability of the network to simulate the membrane potential and the current was discussed above; however, it is necessary to evaluate the reliability of the properties obtained, especially the chloride diffusion coefficient. For this purpose, the relationship between the calculated chloride intrinsic diffusion coefficients and the measured chloride penetration coefficient for mixtures cured in a saturated condition is shown in figure 11.39. Mixtures which were air cured were not included in this relationship, because of the big influence that curing has on the transport properties; this topic deserves to be investigated separately.

Figure 11.39 shows the regression that fits the best straight line to the data, and shows the numerical coefficient of determination R^2, which indicates the amount of variability. The value of correlation was of r=0.95, and shows that the chloride intrinsic diffusion coefficient obtained through the Integrated numerical - neural network model is in good agreement with the measured penetration regardless of the mineral admixtures used. From the same figure it is argued, that for any sample of concrete, the data of current obtained from the traditional ASTM C1202 test and the membrane potential obtained from the electrochemical test presented in this thesis together define the transport properties of the material.

From figure 11.39 should be noted that the correlation between the intrinsic chloride coefficient and the chloride penetration is valid only for the materials used over the range shown in the figure. It is believed that the trend obtained does not cross the origin because in too small diffusion coefficients physically there is not transport of matter, so, the measured penetration coefficient always be zero until a certain diffusion coefficient is reached; however, using the limited data obtained in this research does not confirm this postulate.
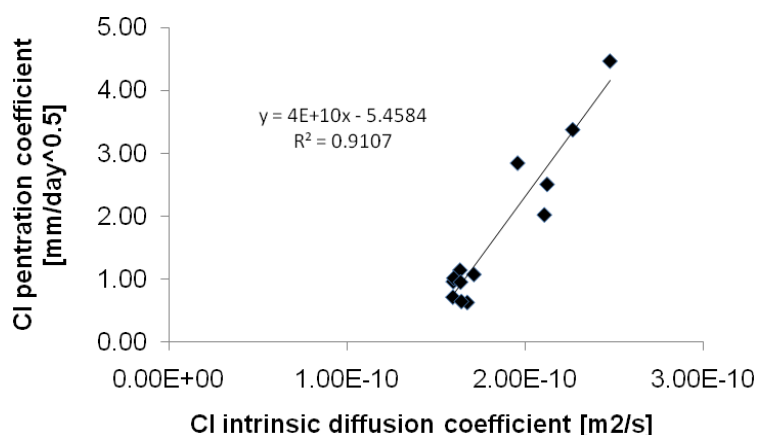
Figure 11-39 Relationship between the calculated intrinsic diffusion coefficients and the chloride penetration coefficients *k* for concrete blended mixes

11.4.1 Results of the simulations

The transport related properties obtained with the optimization technique are shown in table 11.12. Those results will be discussed in detail in chapter 12 of this thesis.

			Outputs				
Mix	OH conc [mol/m^3]	$D_{int\text{-}Cl}$ [m^2/s]	$D_{int\text{-}OH}$ [m^2/s]	$D_{int\text{-}Na}$ [m^2/s]	$D_{int\text{-}K}$ [m^2/s]	Capacity Cl	Porosity
O4W	274.001	2.11E-10	7.73E-11	2.71E-11	5.93E-12	0.367	0.178
O4A	455.249	2.58E-10	7.30E-11	5.19E-11	1.87E-11	0.331	0.197
O5W	90.429	2.12E-10	6.82E-11	4.04E-11	4.62E-11	0.400	0.207
OG4W	159.114	1.68E-10	8.06E-11	1.48E-11	3.04E-12	0.408	0.163
OG4A	247.959	1.61E-10	8.03E-11	1.41E-11	2.87E-12	0.410	0.162
OG5W	173.329	1.60E-10	8.09E-11	1.34E-11	2.82E-12	0.416	0.160
OB4W	285.849	2.27E-10	7.67E-11	3.25E-11	7.73E-12	0.355	0.182
OGB4W	176.423	1.60E-10	8.09E-11	1.34E-11	2.81E-12	0.415	0.160
OGB4A	313.712	1.55E-10	8.01E-11	1.33E-11	2.73E-12	0.413	0.161
OGB5W	186.305	1.64E-10	8.04E-11	1.42E-11	2.95E-12	0.411	0.162
O5-A	262.014	2.19E-10	7.76E-11	2.89E-11	6.25E-12	0.360	0.179
OG5-10-A	251.562	2.07E-10	7.80E-11	2.54E-11	5.29E-12	0.369	0.176
OG5-30-A	158.957	1.96E-10	7.94E-11	2.12E-11	4.28E-12	0.382	0.171
OG5-50-A	154.751	1.81E-10	7.99E-11	1.77E-11	3.56E-12	0.395	0.167
O4-B	249.994	1.96E-10	7.83E-11	2.23E-11	4.55E-12	0.379	0.173
O5-B	359.048	2.48E-10	7.45E-11	4.35E-11	1.37E-11	0.341	0.191
OG5-50-B	192.014	1.60E-10	8.06E-11	1.36E-11	2.86E-12	0.414	0.161
OG5-30-B	167.574	1.71E-10	8.03E-11	1.56E-11	3.17E-12	0.404	0.164
OG4-50-B	151.433	1.70E-10	8.05E-11	1.52E-11	3.11E-12	0.407	0.163
OG4-30-B	167.160	1.64E-10	8.07E-11	1.41E-11	2.93E-12	0.411	0.162

Table 11-12 Chloride transport related properties optimized

11.5 CONCLUSIONS

43. The addition of GGBS and BOS improve the workability of concrete mixtures. However, due to the large size of the BOS grains used in this research, some bleeding was detected during mixing.

44. No correlation was found between the flow properties measured with the rheometer and the slump measured with Abram's cone.

45. All slag mixes showed a compressive strength development similar to the standard OPC reference mixes: ageing produced an increase; air curing produced a decrease;

and an increase in the water binder ratio also produced a decrease in the compressive strength.

46. The reduction of compressive strength because of curing deficiencies was more significant for mixtures containing OPC-GGBS. In the same way, samples OPC-GGBS adequately cured showed better strengths than OPC references at 90 days.

47. Non-Portland mixes did not develop the compressive strength expected according to the preliminary results of part 1. However, those 0% ordinary Portland cement mixtures are suitable in concrete applications requiring low values of compressive strength. In contrast, mixes OPC-BOS and OPC-GGBS-BOS showed interesting and encouraging results of compressive strength, which suggest their possible application in industrial purposes.

48. During the sorptivity tests it was found that effectively, the initial water absorbed by capillary suction increases as the square root of the elapsed time. Air curing and an increase of the water binder ratio produced a significant rise in sorptivity for all mixtures.

49. Non-Portland samples showed to have high values of sorptivity and to be very vulnerable to poor curing. Binary or ternary OPC blended mixes including blast furnace slag or/and steel slag showed a very good performance in relation to this property when properly cured.

50. The electrical resistivity is a very promising durability parameter because it is easy to measure, tests do not take too long, and the laboratory equipment requirements are relatively low.

51. GGBS decreases the resistivity of concrete mixtures notably producing changes in the pore microstructure and composition of the pore solution. Adequately cured GGBS mixes have a resistivity two or three times greater than OPC; however, if no adequate curing is carried out, the resistivity can be of the same order of magnitude as OPC.

52. Mixtures containing GGBS are highly resistant to chloride penetration. Portland and non-Portland GGBS samples showed that the use of blast furnace slag notably decreases the chloride diffusivity in concrete.

53. Samples of OPC-BOS were found particularly vulnerable to chloride diffusion, especially when poor curing conditions were applied.

54. The low chloride penetration in GGBS blended mixtures is attributed to many factors; however, it is believed that the binding capacity factor is the predominant one.

55. The evolution of the mid point membrane potential was measured successfully in OPC-slag mixes. In contrast, in non-Portland mixes it was not possible measure it. The current profile was measured successfully in the same way in all the final mixes and the charge calculated.

56. The use of GGBS significantly reduces the charge passed in Portland and non-Portland blended mixes. For all samples, poor curing, as in the resistivity test, has a very important effect; it increases the total charge passed significantly.

57. Due to their alkaline reserve, the carbonation profile of OPC and OPC-BOS samples was very low. Samples of GGBS showed more carbonation than OPC and are very vulnerable to poor curing. Non-Portland mixes showed high levels of carbonation, probably influenced by the lack of calcium hydroxide as a hydration product.

58. OPC samples showed the lowest water coefficient of permeability, followed by OPC-GGBS, OPC-BOS and OPC-GGBS-BOS. Non-Portland mixes shoed a significant increase of the water coefficient of permeability with respect to the OPC reference.

59. From the Corrosion tests it was concluded that all the slag-Portland mixes had an acceptable behaviour during the experiments. For them, no big differences were found with respect to the OPC reference; their corrosion resistance can be stated as being similar to the OPC samples. In contrast, non-Portland mixes showed high corrosion levels.

60. Using the results of the current and membrane potential profiles twenty slag-mixes were modelled. As a result, the transport properties were successfully obtained. The diffusion coefficients of chloride, hydroxide, potassium and sodium, the chloride linear binding capacity factor, the hydroxide concentration at the beginning of the test, and the capillary porosity were determined.

12 DISCUSSION OF RESULTS ON CHLORIDE TRANSPORT PROPERTIES

In this chapter the experimental and numerical results obtained in chapter eleven "Chloride transport related properties" are discussed. The tests carried out were correlated with the others in order to identify the dependency of the different variables and mechanisms. Similarly, the transport properties obtained with the computation model were analyzed, and the principal results discussed. Special emphasis was given to OPC-GGBS mixtures which are in common use in industrial applications.

12.1 INTRODUCTION

As was stated in chapter 5, chloride penetration in concrete can lead to steel corrosion. Thus, it is important know the level of protection that a specific concrete mix offers to the reinforcement and the relationships between different transport properties. Although there are an important number of durability tests available, their dependency with the chloride transport properties some times is not well understood in blended concretes. So, the relationship between the most used experimental tests and the fundamental transport properties is analyzed for slag blended mixes.

12.2 CORRELATIONS BETWEEN EXPERIMENTAL PARAMETERS

The results of the seven experimental tests carried out on chapter 11 (chloride penetration, charge passed, electrical resistivity, sorptivity, compressive strength, porosity and carbonation) were correlated to estimate the relationships among all of them. Table 12.1 shows the correlation matrix obtained where the coefficient of determination R^2 was found using least squares regression analysis for the best type of equation that fit the data. Two sets of data were analyzed, first, "*all samples*" including results of final binders (section 11.2) and experiments on OPC-GGBS mixes (section 11.3); the other set of data analyzed were "*OPC-GGBS well cured*" that included data from section 11.3 and samples O4W, O5W, OG4W, and OG5W from section 11.2. The results are discussed in the next sections giving more emphasis on tests that showed better correlation.

| | Cl penetration k | | Carbonation kc | | Porosity | | Compressive strength | | Sorptivity | | Charge | |
	All samples	OPC-GGBS well cured	All samples	OPC-GGBS well cured	All samples	OPC-GGBS well cured	All samples	OPC-GGBS well cured	All samples	OPC-GGBS well cured	All samples	OPC-GGBS well cured
Electrical Resistivity	R^2=0.7215 Power	R^2=0.88 Power	R^2=0.096 Linear	R^2=0.0164 Linear	R^2=0.261 Linear	R^2=0.0091 Linear	R^2=0.018 Linear	R^2=0.114 Linear	R^2=0.03 Linear	R^2=0.1357 Linear	R^2=0.8112 Power	R^2=0.9971 Power
Charge	R^2=0.785 Linear	R^2=0.846 Linear	R^2=0.1916 Linear	R^2=0.0025 Linear	R^2=0.028 Linear	R^2=0.051 Linear	R^2=0.092 Linear	R^2=0.047 Linear	R^2=0.143 Linear	R^2=0.131 Linear	----	----
Sorptivity	R^2=0 Linear	R^2=0.161 Linear	R^2=0.656 Linear	R^2=0.462 Linear	R^2=0.421 Linear	R^2=0.314 Linear	R^2=0.708 Linear	R^2=0.98 Linear	----	----	----	----
Compressive strength	R^2=0 Linear	R^2=0.022 Linear	R^2=0.857 Linear	R^2=0.461 Linear	R^2=0.178 Linear	R^2=0.063 Linear	----	----	----	----	----	----
Porosity	R^2=0.07 Linear	R^2=0.031 Linear	R^2=0.37 Linear	R^2=0.9 Linear	----	----	----	----	----	----	----	----
Carbonation kc	R^2=0.14 Linear	R^2=0.16 Linear	----	----	----	----	----	----	----	----	----	----

Table 12-1 Statistical relationships between tets carried out

Note: Values of R^2 are only relevant where there is a scientific or engineering reason for it.

Measurement of concrete resistivity (or conductivity) is a method which has great acceptance due to the known relationship between the electrical conductivity of the pore solution and the microstructure of the concrete. Recent publications show great progress in the understanding of the resistivity as an indicator of the durability (Sengul and Gjorv 2009, Sengul and Gjorv 2008, Mccarter *et al.* 2009), and efforts are being made to establish a new ASTM standard: "Test Method for Indication of Concrete's Ionic Conductivity", of just 5-minutes in duration, in contrast to the 6-hour ASTM C1202. The results obtained in chapter 11 are analyzed and discussed in order to complement the understanding on the resistivity of blended slag mixtures.

The relationship between the A.C. resistivity and the chloride ion penetration expressed by the coefficient *k* is shown in figure 12.1. The graph includes all the mixes tested in the previous chapter. A well-defined plot emerges, forming a "L" shape. Two regions are easily recognized, the samples of OPC, OPC-BOS and air cured GGBS mixes are in region "A", and the remaining high resistivity GGBS mixtures are in region "B". In zone "A", for small changes in the resistivity big changes in the chloride penetration coefficient are expected, while in zone "B" big changes in resistivity correspond only to small changes in the chloride penetration coefficient. That big difference in the slope *Δk/Δresistivity* suggests that if the resistivity (or conductivity) should be used as a general index to rank mixes or assess the chloride penetration of slag blended concretes, then the non-linearity needs to be taken into account. In the figure 12.1 is shown as well the relationship between the conductivity (calculated as the inverse of resistivity) and the chloride penetration; it is shown that the use of conductivity also offers a direct relationship with the penetration, however the resistivity is used as parameter because it is frequently more used in concrete assessment.
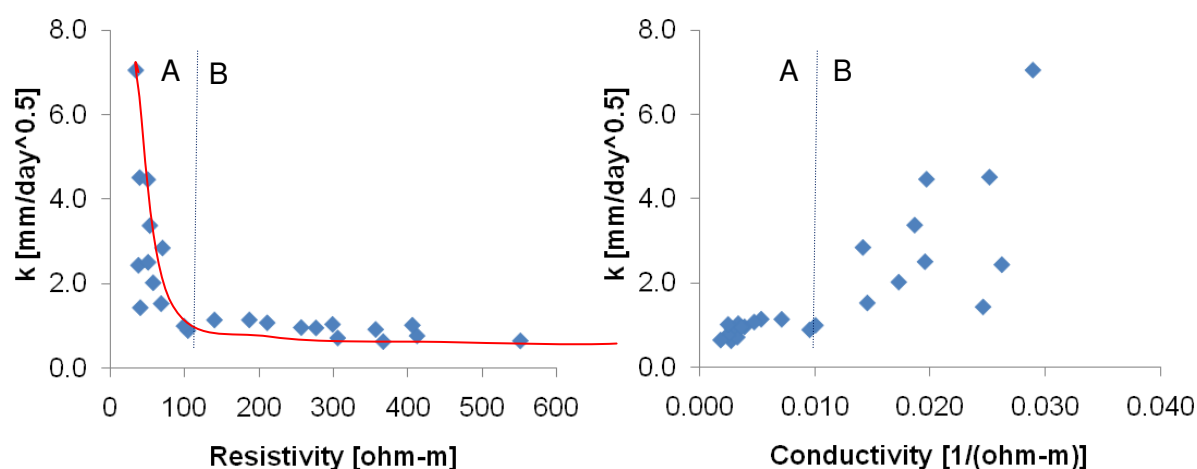
Figure 12-1 Relationship between the measured chloride penetration coefficient *k* and the measured resistivity/conductivity (all samples)

Figure 12.1 shows the resistivity (conductivity)-chloride penetration behaviour of general slag mixtures; however, for industrial applications adequately cured mixes of just GGBS and OPC have a more extensive use. The relationship between the measured resistivity and the chloride penetration coefficient *k* for those mixtures is shown in figure 12.2. Equation 12.1 is the best fit to the data.
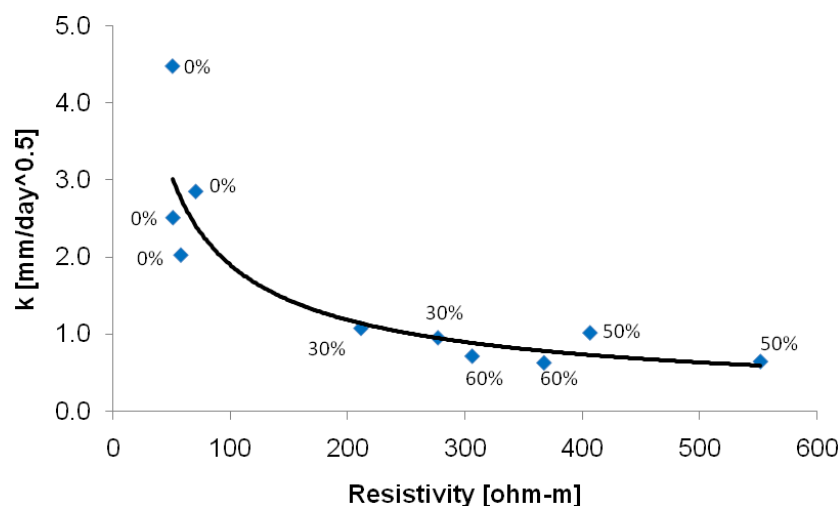
Figure 12-2 Relationship between the measured chloride penetration coefficient *k* and the measured resistivity (OPC-GGBS samples well cured)

$$k\left[\frac{mm}{day^{0.5}}\right] = 43.42\left(\mathrm{Re}\,sistivity[ohm-m]\right)^{-0.679} \qquad (12.1)$$

Equation 12.1 is a good indicator of the chloride penetrability for GGBS-OPC blended concretes; however, it is important to note that the resistivity has been measured with the samples fully saturated before any chloride contamination, according to the procedure shown in section 6.3.6. In other research, Basheer *et al.* (2002) investigated experimentally the correlations between the electrical resistance and the chloride diffusion coefficient for blended mixtures. They found that the resistivity is time dependant and is affected by the chloride penetration. Additionally, they found a non-linear relationship governed by a power equation.

The correlation index obtained between the electrical resistivity and coefficient of carbonation was very low as is shown in table 12.1. This value means that for the mixtures investigated no dependency was found between the carbonation measured after one year of natural carbonation exposure and the saturated resistivity at 90 days. Again, it is important to clarify that although carbonation and curing induce changes in the resistivity of concrete, as was shown by Luco (2008) and Whiting and Nagi (2003), no clear dependency was found between those two properties.

In a paper published by Hossain (2005) it was shown that the electrical resistivity decreased with an increase of the total porosity measured with mercury intrusion porosimetry. There was a strong dependency between those parameters; however, the results obtained in this research do not show any dependency. It is believed that the lack of correlation obtained in this investigation was a result of the way the porosity was measured. It seems that in the open porosity measured by vacuum, water does not penetrate the small capillary pores of some specimens introducing an error in the results. That is more notorious for samples OPC-GGBS which gave a coefficient of determination R^2 much lower than the other samples which presumably were better saturated. In other research Shane *et al.* (2000) showed that the electrical conductivity does not have a very strong relationship with the porosity.

In the same way than as with porosity, no direct relationship between compressive strength and resistivity was observed.

Electrical measurements (conductivity or resistivity) have been used successfully to study the durability of the concrete cover, and a direct relationship with the capillary absorption has been reported by Chrisp *et al.* (2002). Normally, the resistivity used to asses the "skin" of concrete is the known "*Four-Probe Resistivity Measurement Technique*" (Whiting and Nagi 2003) which allows to measure the resistivity in the field. As was mention above, sorptivity is a transport mechanism related principally with the concrete cover; so, as the resistivity measured in this research corresponds to the average resistivity of the overall sample the correlation obtained between these two parameters was very poor.

Figure 12.3 shows the relationship between the AC resistivity measured and the charge calculated after 6 hours of the RCPT for all the mixes tested in chapter 11. For all the data excluding the PG samples, the equation (12.2) was found using least squares regression analysis. The correlation coefficient R^2 obtained was 0.992.

$$ch \arg e[C] = 724048 \left(\mathrm{Re}\, sistivity[ohm - m] \right)^{-1.212} \qquad (12.2)$$

In figure 12.3 can be seen that samples containing PG showed a defined linear trend, influenced presumably by the presence of gypsum. However, due to the small number of data is not possible to have a good reliability about this relationship. Additionally, the relationship between conductivity and charge is also shown in this figure; however the main analysis has been done in function of the resistivity due that this parameter is most used in concrete technology.
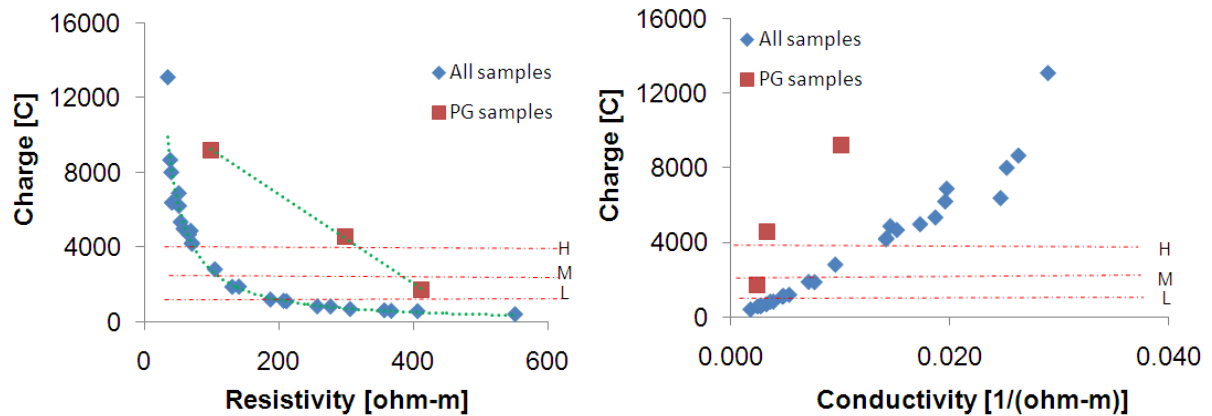
Figure 12-3 Relationship between the measured resistivity/conductivity and the charge passed

The data shown in figure 12.3 includes samples with different binders, curing regimes, and water to binder ratios; however, if the same relationship is established using only mixes OPC-GGBS cured in saturated conditions a similar correlation is obtained. For this new relationship (equation 12.3) the determination coefficient R^2 obtained was 0.997. Figure 12.4 shows the relationship between AC resistivity and charge for those mixtures. The proportions of mineral admixture are marked in the same figure.

$$ch\arg e[C] = 695166\left(\mathrm{Re}\,sistivity[ohm-m]\right)^{-1.203} \qquad (12.3)$$
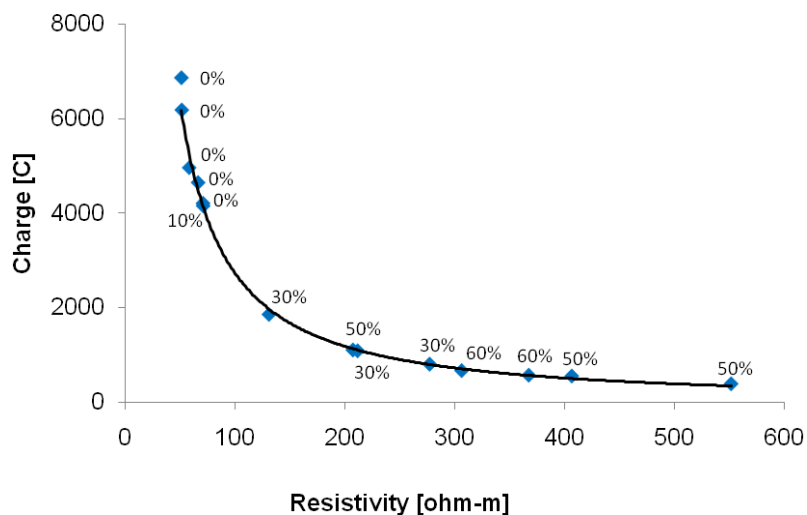
Figure 12-4 Relationship between the measured resistivity and the measured charge passed (OPC-GGBS samples well cured)

The non-linearity of the resistivity-charge relationship can be explained if the graph of the evolution of the current during an RCPT is analyzed. For any mix at the beginning of the test the instantaneous DC resitivity (calculated with the initial current i_o) and the AC resitivity are

equivalent; however, as was observed during the experiments, mixes with low chloride ion penetrability, i.e. concrete with high volume of GGBS (>30%) and low water to binder ratio, usually show a constant evolution of the current as is shown in figure 12.5. The total charge calculated for those kinds of mixes (shown as Area1) is always a function of the initial current i_o. For mixes with high chloride ion penetrability the evolution of the current is not constant during the experiment and a new Area2 is developed. Although the total charge for these mixtures is related with the Area1, the Area2 introduces a non-linearity as shown in figure 12.4
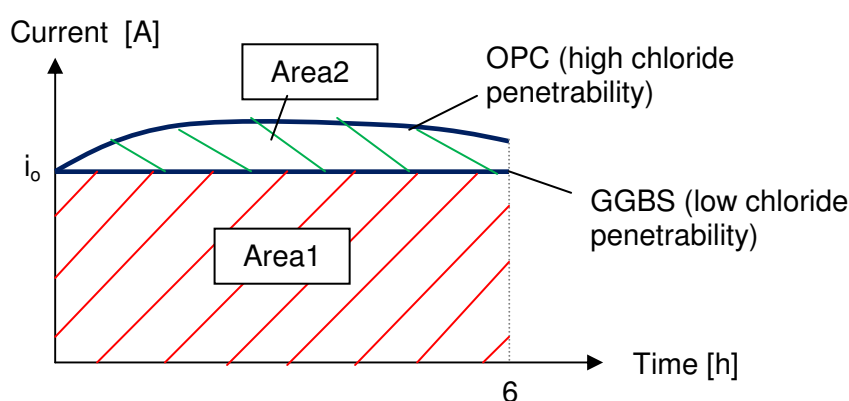
Figure 12-5 Evolution of the electrical current during the ASTM C1202 test

The total charge measured after 6 hours of the RCPT test showed a good correlation with the chloride penetration coefficient. Figure 12.6 shows that relationship and includes the linear trend obtained by least square regression analysis for both sets of data analyzed. This is why the RCPT is so popular with industry.
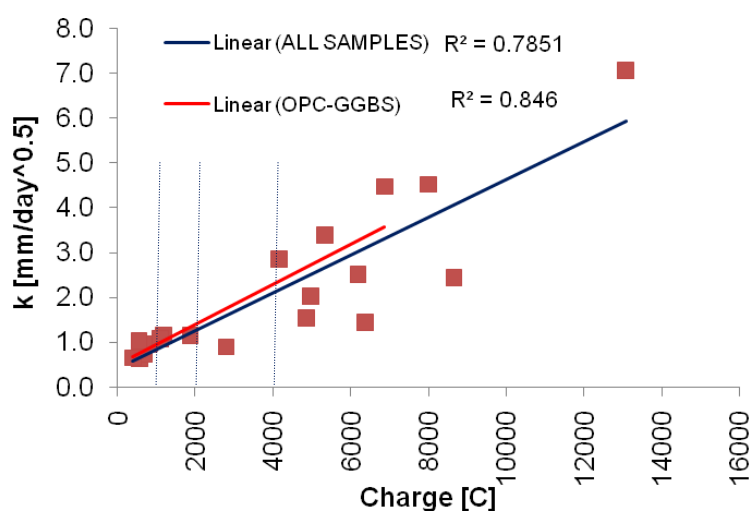
Figure 12-6 Relationship electrical charge and chloride coefficient of penetration *k*

The coefficient of determination for the correlation of the total charge with the carbonation, porosity, compressive strength and sorptivity presented in table 12.1 shows that for the data analyzed there is no direct dependency between those variables. The charge only seems to be strongly related with the chloride penetration.

No relationship was found between the sorptivity and the chloride penetrability. This result was expected because during the chloride self-penetration tests the only mechanism of transport allowed was diffusion. Before the samples were in contact with the salt solution they were in contact with an alkaline solution to avoid any sorption.

It has been stated by Dias (2000) that in air-dried OPC concrete there is an increase in weight and reduction in sorptivity due to carbonation of the surface zone. It was stated that concrete surfaces with poorer quality or bad curing show greater reductions in sorptivity as a result carbonation. The relationship between sorptivity and carbonation is shown in figure 12.7.
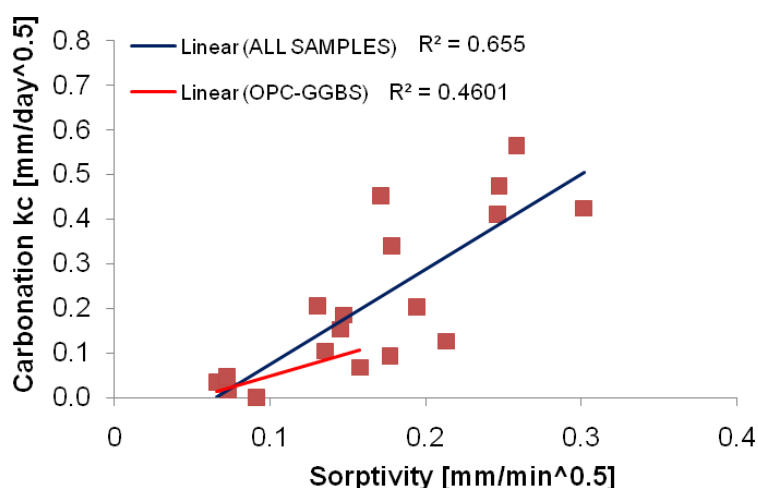
Figure 12-7 Relationship sorptivity and carbonation coefficient k_c

The relationship found between sorptivity and porosity is shown in figure 12.8, where a slight dependence between these two variables can be seen. This relationship emerges as a result of the similarities in both tests. In the test of porosity, water is forced to enter the sample by vacuum suction filling in the capillary pores. Similarly, in the sorptivity test, water is imbibed by the sample filling in the surface capillary pores.
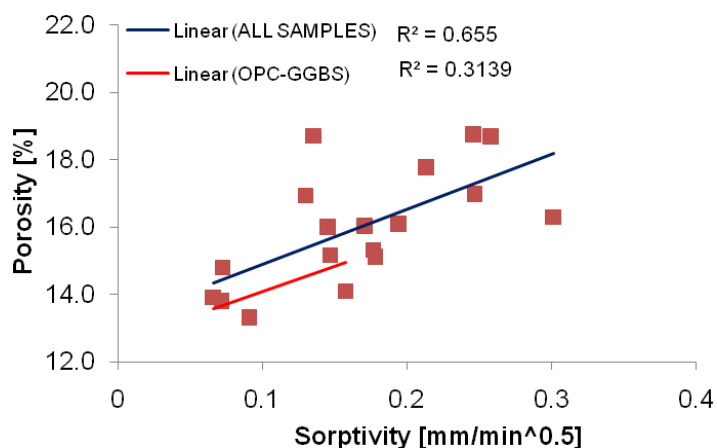
Figure 12-8 Relationship between sorptivity and open porosity

The relationship between sorptivity and compressive strength is shown in figure 12.9. A similar trend was reported by Hewlett (2004), but a better correlation was found using a power equation. For OPC-GGBS mixes a very good correlation was found. In table 12.1 a value of R^2=0.98 was shown. However, this good relationship must be taken with caution because just 4 points were available. In addition, all the results showed very low values of sorptivity and high values of compressive strength.
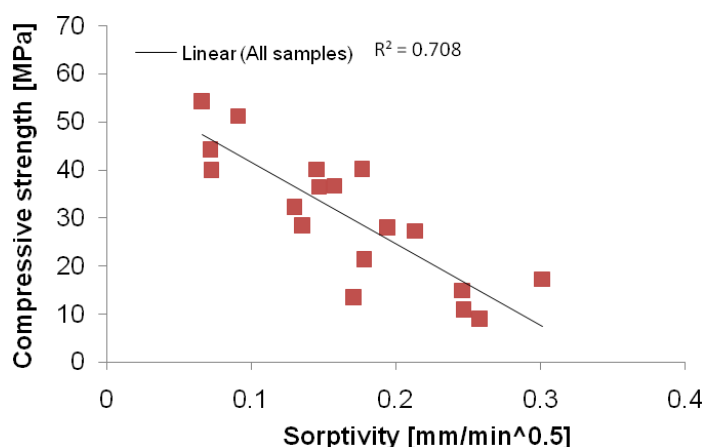
Figure 12-9 Relationship between sorptivity and compressive strength (all samples)

No correlation was found between compressive strength and chloride penetration. This result is of special interest because it is normally assumed that the compressive strength is intimately correlated with the chloride penetration in concrete; so, the cube test is sufficient to measured durability. Additionally, no correlation was found between the compressive strength and the open porosity. In contrast, a well defined trend was found between compressive strength and carbonation for all mixes, figure 12.10. A similar relationship was reported by Hewlett (2004).
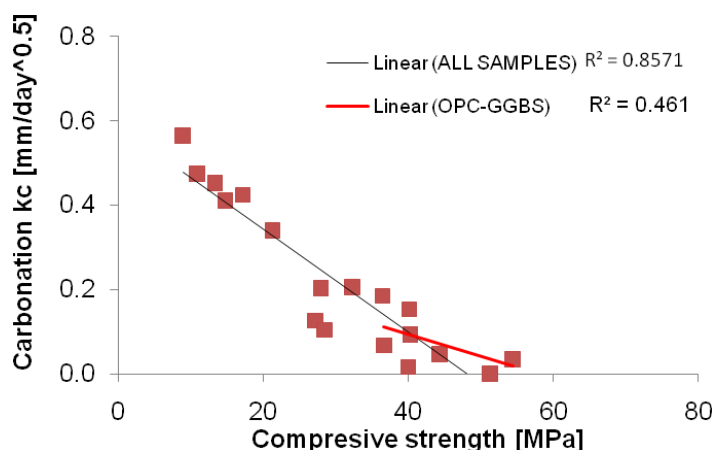
Figure 12-10 Relationship between sorptivity and compressive strength

12.3 EFFECT OF SLAG REPLACEMENT ON MEASURED CHARGE AND RESISTIVITY IN GGBS - OPC MIXES

From table 12.1 it can be argued that the electrical tests, resistivity and charge passed are good indicators of the chloride penetration. However, as was stated in section 6.6, the electrical properties of concrete are related, in addition to their transport properties, to the pore solution composition. In that way, using GGBS as mineral admixture to replace OPC produces changes in the electrical properties of the material, and those changes can be related with variations on the chemical composition of the pore solution rather than with the concrete resistance to chloride penetration.

The effect of GGBS replacement on the charge passed and resisistivity is shown in figures 12.11 and 12.12 respectively. In figures "A" the relationships for samples of different water binder ratio are shown, and in figures "B" a general relation obtained using all the data available are shown. The equations that best fit the experimental results are shown in the figures.
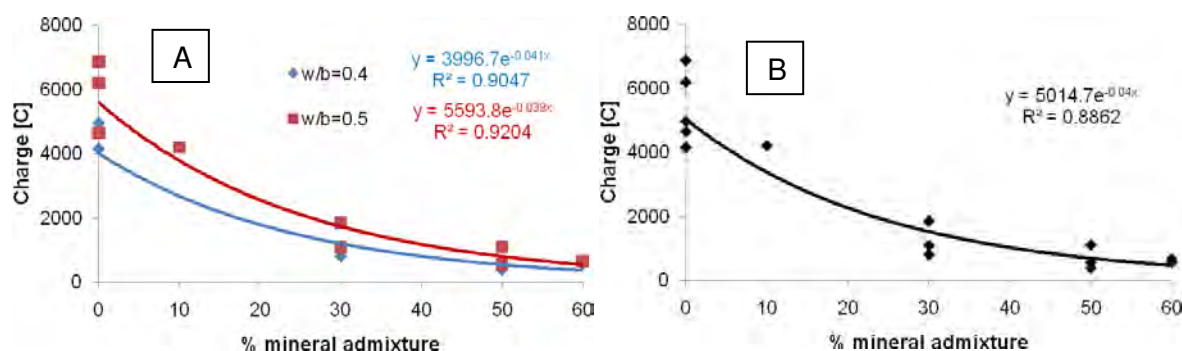
Figure 12-11 Effect of GGBS replacement on the charge passed (OPC-GGBS samples well cured)
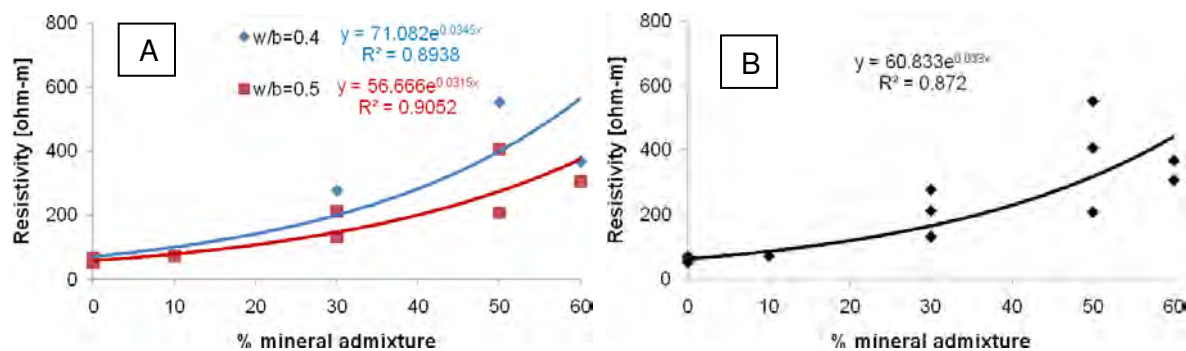
Figure 12-12 Effect of GGBS replacements on the resistivity (OPC-GGBS samples well cured)

12.4 SIMULATION OF TRANSPORT RELATED PROPERTIES

All the migration tests had non-steady state conditions because of the characteristics of the experiments, in which there were small volume external cells, a high external voltage, and a short duration. Although in some mixes it was possible that the chlorides reached the anode (thus giving a uniform condition through the sample), the depletion of the external cells ensured that a steady state condition was never achieved. Therefore, the estimated intrinsic diffusion coefficients were for non steady state conditions.

Figure 12.13 shows the calculated intrinsic coefficients of diffusion. The sodium and potassium coefficients were significantly smaller than the values for chlorides and hydroxides, as observed previously by Andrade (1993). These results confirm that the mobility of cations in a porous media are less than the mobility of anions. However, they are responsible for part of the total charge passed and are absolutely necessary in the simulation. Either in a self diffusion test or in the presence of an applied voltage gradient across the specimen, the charge electroneutrality is maintained in the Coventry model by adjusting the membrane potential at all times. Small changes in the diffusion of cations produce large changes in the mid point membrane potential. As was expected, the calculated numerical values of the intrinsic coefficients for all the species are, for all the cases, smaller than the coefficients of diffusion in infinite diluted solutions, as can be seen in any electrochemistry textbook (Bockris and Reddy 1998). The values obtained are possible and are within acceptable ranges.

The diffusion coefficients obtained for sodium (D_{int-Na}) were greater than for potassium (D_{int-K}). The ratio D_{int-Na}/D_{int-K} was different depending on the amount and type of admixture. It was found that if there was an increase in the amount of mineral admixture, the ratio D_{int-Na}/D_{int-K} tended to decrease. Although the coefficient of diffusion for potassium is greater than for sodium in an infinite dilute solution (Bockris and Reddy, 1998), the results of the model

showed that for the samples tested this is not always the case. This may be because differences in the matrix (immobile ions) and the ionic exchange in the pore solution. The ratio D_{int-Na}/D_{int-K} varies for each concrete sample according to all its transport properties including the composition of its pore solution at the start of the test.

The migration diffusion coefficients obtained for chlorides and hydroxides showed that both ions have a high mobility and are responsible for most of the transport of charge. However, in contrast with the conclusions of Feldman *et al.* (1994), the results of the simulations indicated that the diffusion coefficients of chlorides were greater than the hydroxide coefficients. The numerical values of the apparent chloride coefficients were between 10 and 60% greater than the hydroxides, depending on the level of mineral admixture replacement. With an increase in the amount of either mineral admixture, the ratio D_{app-Cl}/D_{OH} tends to decrease. It is believed that the ratio between the diffusivity of chlorides and hydroxides depends on all the external conditions of the test and all the internal transport properties and features of the concrete, and it is not a rule that it is always less than one.
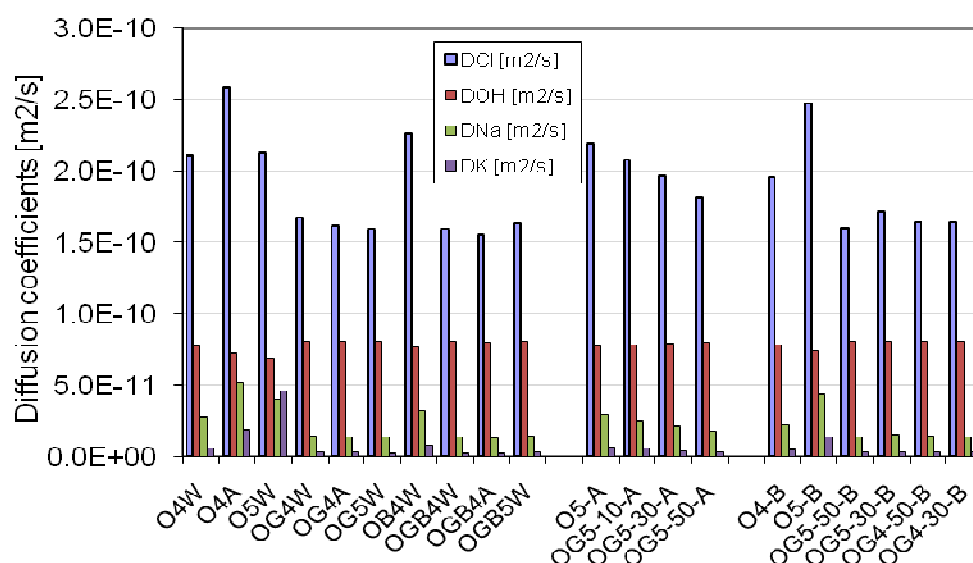
Figure 12-13 simulated intrinsic diffusion coefficients

Due to the lack of availability of experimental data, many researchers (Truc 2000, Khitab 2005) assumed that the ratio of the intrinsic coefficient of diffusion of any ion in concrete (D_{int-i}) to the intrinsic coefficient of diffusion of chloride in concrete (D_{int-Cl}) is equal to the ratio of the coefficient of diffusion of any ion in a solution at infinite dilution (D_i^0) to the coefficient of diffusion of chloride in a solution at infinite dilution(D_{cl}^0). This relationship is shown in equation 12.4.

$$\frac{D_{\text{int}-i}}{D_{\text{int}-Cl}} = \frac{D_i^0}{D_{Cl}^0} \qquad (12.4)$$

From the simulations it was concluded that the intrinsic diffusion coefficients of OH⁻, Na⁺, and K⁺ do not necessarily follow a linear correlation with the Cl diffusion coefficient, and they are not always directly proportional to the ratio between the diffusion coefficients at infinite dilution as is stated by equation 12.4. Figure 12.14 shows the relationship between the simulated Cl diffusion coefficients and the diffusion coefficients of other ions.
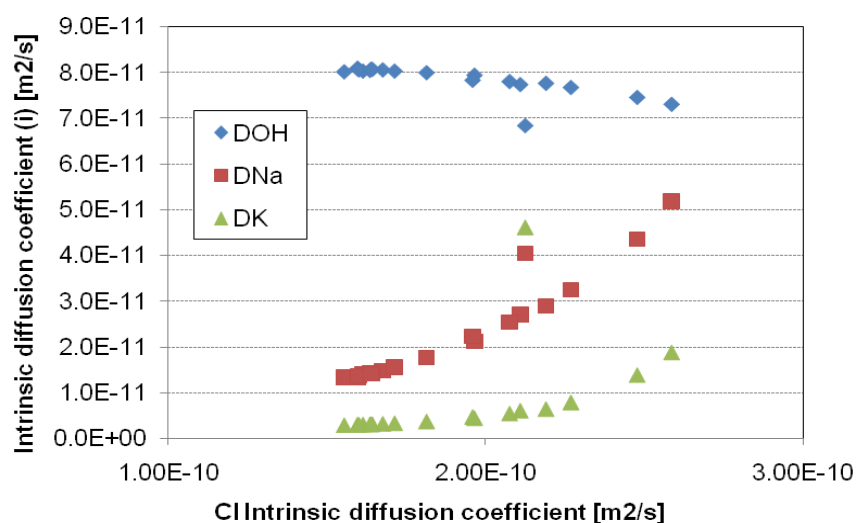
Figure 12-14 Relationship intrinsic diffusion coefficients of Cl⁻ and OH⁻, Na⁺ and K⁺

The data shown in figure 12.14 was analyzed statistically and the best correlation was obtained using regression analysis (notice that the data of mix O5W was excluded from the analysis, because it is clearly out of trend). Table 12.2 shows an equation to determine the intrinsic diffusion coefficient from the intrinsic chloride diffusion coefficient for each ion. It is believed that for slag mixtures table 12.2 represents a better approximation than equation 12.4.

Ion	Equation	R^2
OH⁻	$D_{OH}^{conc} = -0.0689 D_{Cl}^{conc} + 9 \cdot 10^{-11}$	0.9438
Na⁺	$D_{Na}^{conc} = 3 \cdot 10^9 (D_{Cl}^{conc})^2 - 0.7426 D_{Cl}^{conc} + 6 \cdot 10^{-11}$	0.9978
K⁺	$D_{K}^{conc} = 2 \cdot 10^9 (D_{Cl}^{conc})^2 - 0.6922 D_{Cl}^{conc} + 6 \cdot 10^{-11}$	0.9851

Table 12-2 Relations intrinsic diffusion coefficients of OH⁻, Na⁺ and K⁺ as a function of Cl⁻

Results for the simulated initial hydroxide concentration for the final binders at the beginning of the test are shown in figure 12.15. It is observed that the addition of slag produces a decrease in the initial OH^- concentration. However, for mixture O5W this is not necessarily the case, it is believed that for that particular mix the simulated results of hydroxide concentration show some inconsistency and are considered atypical.

According to the results of the model, air curing has a strong influence on the initial OH^- concentration. For mixtures OPC, OPC-GGBS and OPC-GGBS-BOS an increase of around 40% in the hydroxide concentration was obtained when the mixes were air cured. This result is consistent with the results of resistivity, which were strongly affected by the air curing condition. Presumably, two reasons may influence the higher OH concentration found in air cured samples: (a) the un-hydrated particles of OPC give to the concrete an excess of alkalinity, and (b) The OH diffuse out in the tanks during the curing period when the samples are water curing.
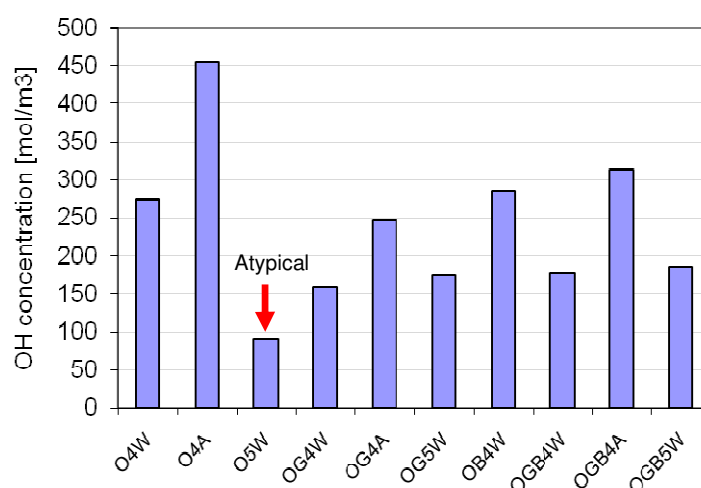
Figure 12-15 Simulated OH$^-$ concentrations in the pore solution at the beginning of the test

The simulated results for open porosity and binding capacity factor are shown in figure 12.16. As was expected, the porosity tends to increase with an increase of the water binder ratio and with the adition of GGBS (figure 12.16A). The binding capacity factor increases with the adition of GGBS (figure 12.16B).
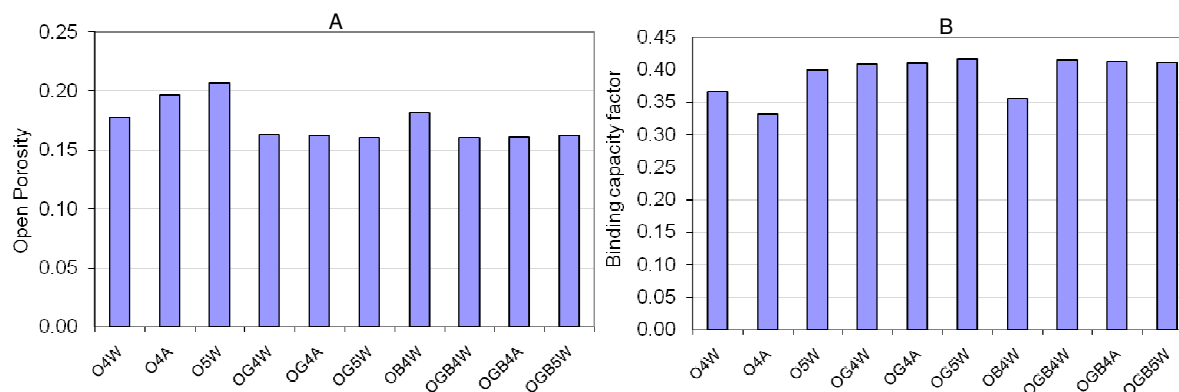
Figure 12-16 Simulated (A) open porosity and (B) binding capacity factor

12.4.1 Simulation of transport properties of OPC-GGBS mixes

Due to the wide application of blast furnace slag in binary OPC-GGBS mixtures, the most important results of this combination are discussed in this section. Figure 12.17 shows the influence of the proportion of GGBS on the simulated OH⁻ concentration at the beginning of the test. As individual points are shown the data obtained from the model (blue points) and as continuous line (line red) shows the resulting average for each proportion. Notice that the value of OH⁻ concentration for mixture O5W was not included for the reasons given above.

For the OPC samples an average value of 286 mol/m^3 was obtained for hydroxide. This corresponds, according to section 8.3, to 97 mol/m^3 of sodium and 189 mol/m^3 of potassium in order to maintain the initial electro-neutrality of the system (units in mol per cubic meter of pore solution). With the increase of the amount of the mineral admixture, a reduction was found in the initial hydroxide composition of the pore solution, as was expected. It was previously reported by Page and Vennesland (1983). The calculated hydroxide reduction of the solution into the pores for the 30% GGBS blended concrete was around 40% with respect to the OPC. Above 30% of replacement, there was no further reduction in the hydroxide ion concentration

The calculated chloride binding capacity factor is shown in figure 12.18. It was found that it tends to increase with an increase in the amount of mineral admixture. The greatest chloride capacity factor was found in mixes of 60% of GGBS. Similar results were found by Dhir, El-Mohr and Dyer (1996).

From the integrated model, the calculated porosity was also found. There was a reduction in the porosity with an increase in the amount of admixture, and the beneficial effect of GGBS

and PFA was greatest with 50% of GGBS. Figure 12.19 shows the variation of the calculated open porosity for different percentages of admixture.
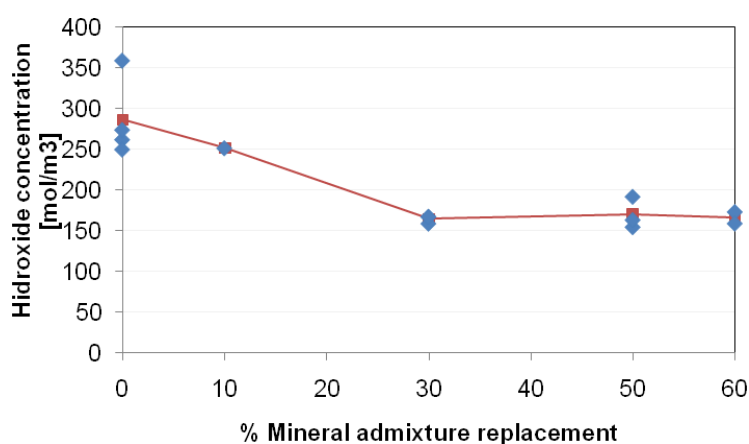
Figure 12-17 Simulated effects of GGBS replacements on hydroxide composition
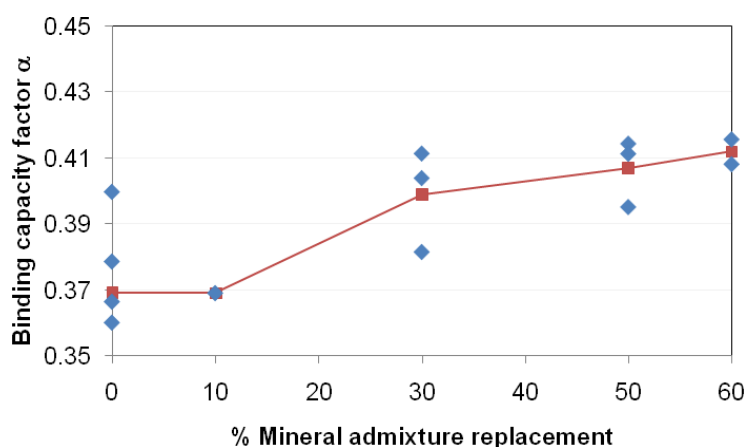
Figure 12-18 Simulated effects of GGBS on the chloride binding capacity
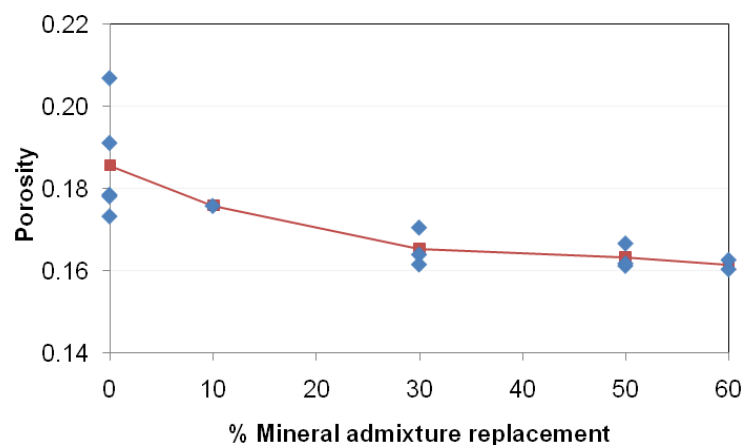
Figure 12-19 Simulated effects of GGBS on the porosity

For the OPC-GGBS mixes the apparent chloride diffusion coefficients were found using equation 5.32, which establishes the relationship between the apparent and intrinsic chloride diffusion coefficients. Figure 12.20 shows the simulated effects of GGBS on the apparent Cl diffusion coefficient. An increase in GGBS produces a reduction in the diffusion coefficient. The calculated apparent diffusion coefficients obtained were relatively high compared with some reported in the literature. Usually, for a concrete of good quality, a chloride diffusion coefficient in the order of 10^{-12} m^2/s is expected. However, these differences can be explained by the fact that the diffusion coefficients obtained in this research apply to a multi-species system coupled through the membrane potential, rather tnan of those obtained in experiments reported in literature where ions are physically affected by the ionic exchange among species, but the coefficients are calculated with equations that account for only single chloride diffusion and no ionic interaction.
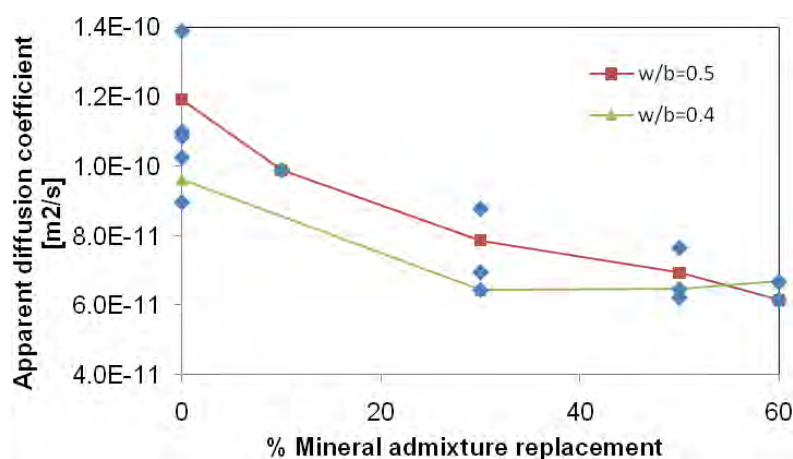
Figure 12-20 Simulated effects of GGBS on the Cl apparent diffusion coefficient

12.4.1.1 Correlation of the estimated properties with the charge and resistivity

The effects of the resistivity and charge passed on the alkalinity of the pore solution, defined as the OH^- initial concentration, and the chloride capacity factor are shown in figure 12.21. As was expected, a good correlation was found between both electrical tests and the hydroxide concentration calculated with the computational model (figures A and C).The conductivity of a concrete sample is strongly related with the conductivity of the pore solution as was pointed out by Shi, Stegemann and Caldwell (1998). In the same way, a good relationship was found between the measured electrical properties and the chloride capacity factor simulated (figures B and D). This last observation has great importance because as was concluded in chapter 10, for samples of OPC-GGBS the capacity factor is the key factor which dominates the penetration of chlorides. If the electrical tests are, at the same time,

dependent on the pore solution concentration and the chloride capacity factor, it can be argued that when the tests are applied to OPC-GGBS mixes, the conductivity of pore solution is measured, but equally the penetration of chlorides is measured.
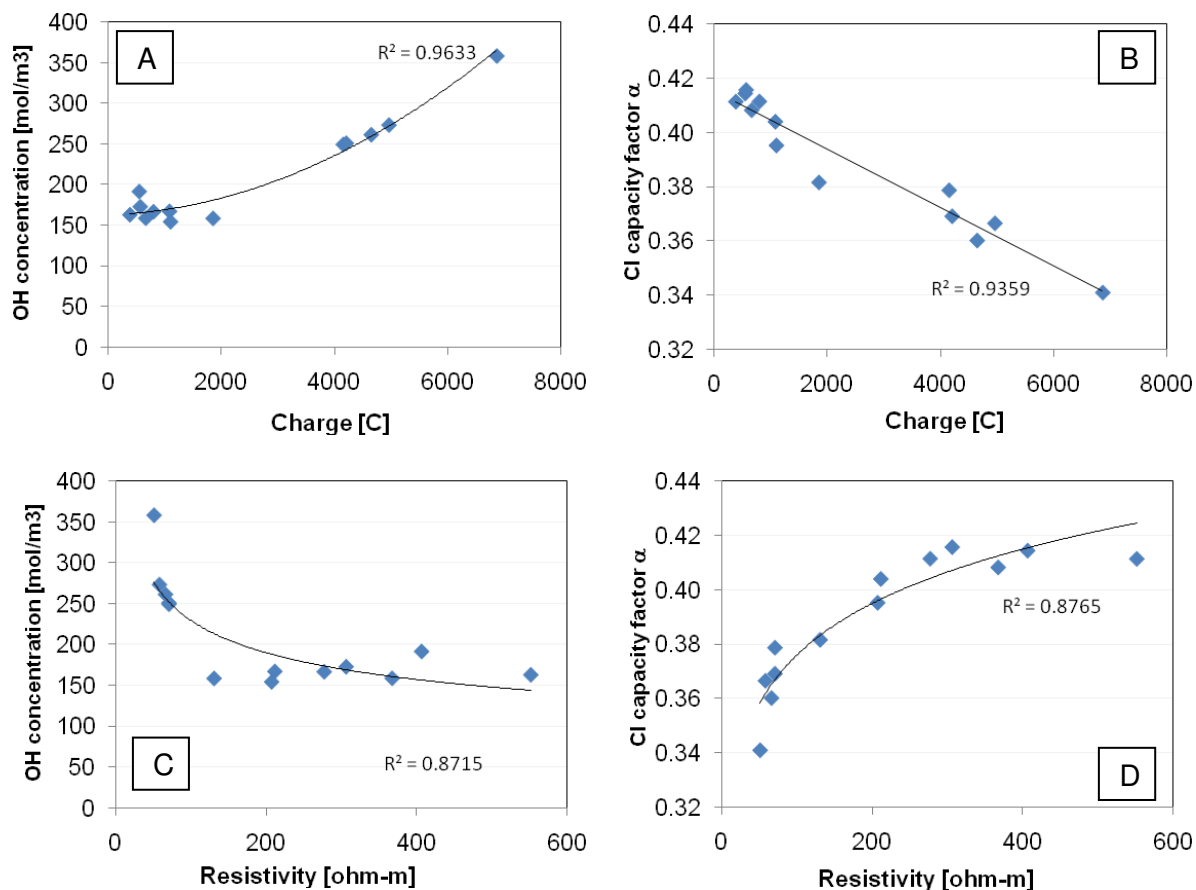
Figure 12-21 Effects of charge and resistivity on the chloride capacity factor and initial alkalinity for OPC-GGBS samples

The relationship between the charge in Coulombs obtained from the standard ASTM C1202 test and the calculated chloride diffusion coefficients is shown in figure 12.22. The correlation between the charge and the intrinsic (left) and apparent (right) coefficients is shown. The link between both coefficients was defined by equation 5.32. The intrinsic coefficient defines the transport of matter when the flux is calculated per unit cross-sectional area of the pores and the concentration in the free liquid. In contrast, the apparent coefficient defines the transport of any ion when the flux is calculated per unit area of the porous material and the average concentration in the material. The reason why both coefficients are presented is because the computer model calculates the intrinsic coefficient, but the apparent coefficients are normally used to predict the service life of concrete structures. From the figures can be seen that the charge-chloride diffusion coefficient relationship for GGBS had an acceptable correlation with determination coefficients of R^2=0.895 and 0.919. According to this, the equations that define

that relationship can be used as a tool to estimate the diffusion coefficients in [m^2/s] from the measured value of charge [in Coulombs] for GGBS mixes with levels of GGBS replacement between 0 and 60 percent.

$$D_{int-GGBS} = 1x10^{-14} \times Ch \arg e + 2x10^{-10} \qquad (12.5)$$

$$D_{app-GGBS} = 1x10^{-14} \times Ch \arg e + 6x10^{-11} \qquad (12.6)$$
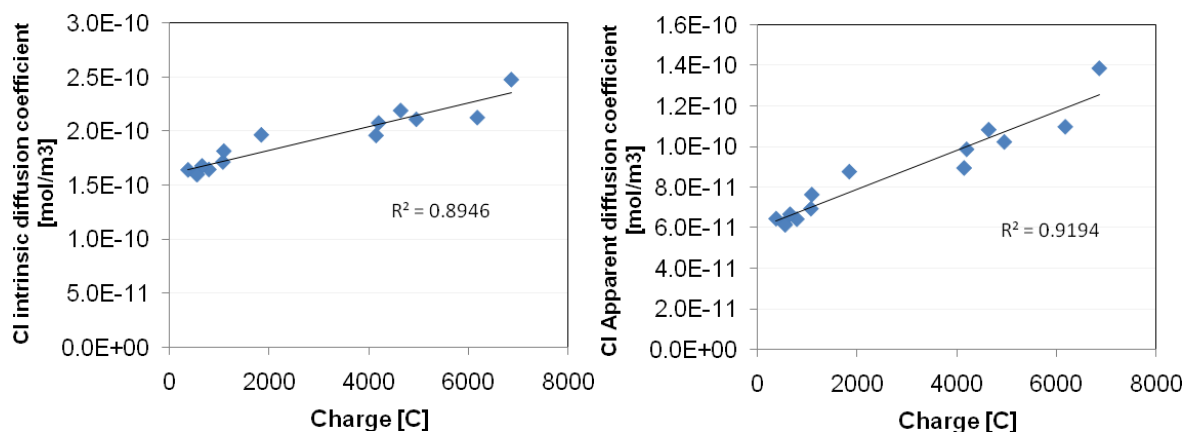
Figure 12-22 Simulated effects of GGBS on the Cl diffusion coefficients

The relationships between the electrical resistivity and the calculated chloride diffusion coefficients are shown in figure 12.23 and equation 12.27 and 12.28.
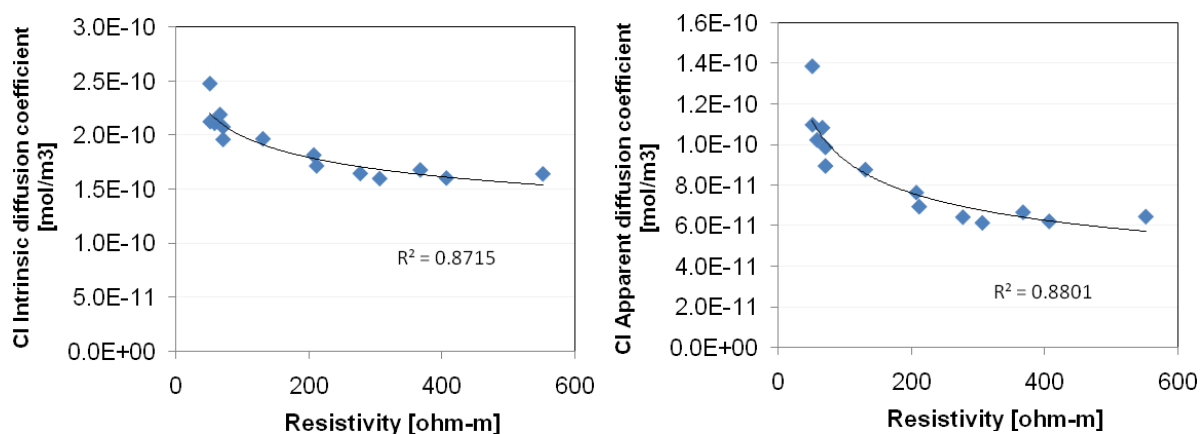
Figure 12-23 Simulated effects of GGBS on the Cl diffusion coefficients

$$D_{int-GGBS} = 4x10^{-10} \times \mathrm{Re}\, sistivity^{-0.151} \quad (12.7)$$

$$D_{int-GGBS} = 3x10^{-10} \times \mathrm{Re}\, sistivity^{-0.283} \quad (12.8)$$

12.5 CONCLUSIONS

61. The statistical relationships between the tests carried out in chapter 11 was determined and presented in table 12.1. The experimental tests showed that the most related variables to the chloride penetration were the resistivity and the charge passed. The sorptivity, compressive strength, and porosity did not show strong relationships with the chloride penetration coefficient.

62. The proportion of slag used in OPC-GGBS mixes affects the measured charge and resistivity. Those relationships are non-linear, an increase in the mineral admixture corresponding to an increase in the resistivity and a decrease in the total charge passed.

63. Using Artificial Neural Networks trained on numerical simulations of the migration test yields viable results for the fundamental properties of concrete. The initial hydroxide composition of the pore solution, the chloride binding capacity, the porosity, and the diffusion coefficients for all the species involved were estimated with good results.

64. Results obtained show that the ratios between sodium and potassium, and chlorides and hydroxides in a migration test do not follow the behaviour of single species in a dilute solution. In the same way, the calculated values of chloride diffusion coefficient were larger than those usually reported in the literature; however, they are in good agreement with the measured chloride penetration.

65. The use of the resistivity and the total electric charge passed as indirect measures of the chloride penetration is suitable in OPC-GGBS mixes. The low values of resistivity are related with the conductivity of the pore solution, but are intimately linked as well to the binding capacity and the diffusivity of chlorides. Some equations are given to correlate the diffusion coefficients with the charge and resistivity.

FINAL REMARKS

13 FINAL REMARKS

13.1 INTRODUCTION

The main intention of this thesis was to investigate the chloride transport related properties of slag concrete using traditional experimental methods and computational methods. With that general aim in mind, during the progress of the research, all the proposed objectives were achieved and several findings emerged, bringing with them new ideas about the complex, but fascinating "world" of ionic transport in concrete.

In an initial part of this last chapter, the main thesis contributions are summarized. In a second part, the principal limitations and constrains about the theory or experiments used are stated, this serves no purpose other than to make clear the scope and limitations of the research. Finally, taking into account the findings and limitations presented, several aspects could serve as a basis for future investigations. Those suggestions are given for possible further studies.

13.2 SCIENTIFIC CONTRIBUTIONS OF THE THESIS

As two main themes, slag based concrete materials and chloride penetration in concrete, were proposed at the beginning of this project as a mater of study, the thesis was divided in parts. First and second parts made direct reference to the general topics of study, and the third part involved the elements developed in the previous two parts. Using this last part, the main objective of the research was fulfilled.

It is important to note that in this section specific conclusions about the research are not presented, here the principal achievements reached through the progress of the research program are summarized. Specific conclusions were listed at the end of each chapter. The key findings and scientific contributions of the thesis are presented below

Development and characterization of slag cement-based materials

1. A complete literature survey was carried out about the raw materials used in this research. This is summarised and presented in chapter 2.

2. Several combinations of iron slag (GGBS) and weathered steel slag (BOS) where mixed to produce suitable cementing binders. Paste mixes of 60% GGBS and 40% BOS showed the optimum value of strength at 90 days. The development of strength was attributed to the GGBS activation because of the alkaline (lime) contribution of BOS. A new model was proposed to explain this hydration process which was investigated using analytical data obtained from X-ray diffraction and other complementary tests. This mix was the base of the final slag binders developed in this research.

3. Five final binders containing principally GGBS and BOS, activated using OPC, BPD, and PG were optimized to obtain the best combination that produced the highest compressive strength. Those binders were investigated in detail to characterize their setting and hydration processes.

Binder	Materials
1	100% OPC (reference)
2	40% OPC + 60% GGBS
3	70% OPC + 30% BOS
4	40% OPC + 30% GGBS + 30% BOS
5	10% BPD + 54% GGBS + 36% BOS
6	5%PG + 60% GGBS + 35% BOS

Table 13.1 Final mixes selected

Multi-species ionic transport in concrete

4. In this research, the ionic transport in concrete has been investigated. For this, a computer model initially developed to simulate a standard RCPT migration test was used. The theoretical bases of that model were investigated in detail from an extensive literature review. Consistent with the model, it was found that Nernst-Planck equation, solved using a multi-species approach coupled with the charge neutrality and a binding isotherm, is a very good theoretical representation of the physical phenomena that occur in a migration test. The principal hypothesis of the computer model was the condition of charge neutrality of the different ionic species. This was achieved in the model through the generation of an additional membrane potential produced by the differences in mobility of the species involved.

5. From the theoretical review carried out about "*electro-diffusion*", it was concluded that the Nernst-Planck equation coupled with the charge neutrality should be always used

in order to describe the ionic transport in concrete. However, the electrical conditions of the physical-real system should be taken into account. As a result, ideal conditions of voltage control, current control (non-zero current) and current control (zero current) were introduced for the first time. Using those, modelling of migration tests, cathodic protection or self-diffusion tests must be carried out. The reliability of voltage control and current control models were evaluated against experimental tests. The results showed that the simulations were in accordance with the experiments, showing the accuracy of the theoretical assumptions.

6. A new electrochemical test for measuring the evolution of the electrical field through a concrete sample in a standard migration test was developed in this research. This proved that the electrical field is non-linear in time and position. In the same way, a methodology developed to calculate the mid-point membrane potential was proposed, obtaining more information from a voltage control migration.

7. A novel and new methodology proposed to obtain the transport related properties of concrete was developed. In this, the observed current and membrane potential obtained from the new electrochemical migration tests are optimised using an artificial neural network (ANN) to obtain the intrinsic diffusion coefficients of the species involved (Cl^-, OH^-, Na^+ and K^+), the initial hydroxide composition of the pore solution, and the open porosity of the sample. Numerical results from this methodology were assessed experimentally obtaining encouraging results.

8. Additionally to the voltage and current control conditions given above, two new models of electrical conditions named power and variable voltage control were developed. Those are alternatives to manage the temperature problem of poor quality concrete samples in the standard RCPT.

Transport related properties and chloride resistance of slag cement-based materials

9. Traditional chloride transport related tests were carried out on the final slag binders developed in the initial stage of the research. The influence of the water to binder ratio and the curing regimen on those tests was evaluated, analysed and discussed. The behaviour of slag based concrete mixes under workability, compressive strength, open porosity, initial water absorption capacity (sorptivity), carbonation, chloride migration and self diffusion, electrical resistivity, water permeability, and corrosion was investigated.

10. The transport related properties of several slag based mixtures were simulated using the optimization neural network model. Those properties were correlated with the experimental tests to investigate the effect of the slag on the transport.

13.3 THE THESIS CONSTRAINTS

The work carried out in this research needs to be circumscribed within a context in which its limitations are clearly identified. These limitations make reference to specific features of the materials, of the experimental process, and of the theoretical or numerical aspects of the research.

The materials

1. All the results, discussion and conclusions where obtained using materials with specific characteristics and properties as is detailed in section 3.2.1. Specially the steel slag (BOS) which was in a weathered condition.

The experimental process

2. The heating of the samples during the experiments was a parameter that has en affect on the transport mechanisms. In order to avoid any influence of the temperature this always was kept to a minimum. A complete discussion about it was given in section 7.2.

3. The reaction of the metallic electrodes due to electrolysis induces an additional potential in the cells in a migration test. This situation was investigated and discussed in detail in section 6.3.5, where it was concluded that the over-potential generated does not decrease the actual voltage applied in more than 1.2%.

4. All the experimental work carried out in this thesis is limited to samples controlled under specific conditions. Results obtained from samples cast *in situ* must be interpreted with precaution.

5. The conditioning of the samples used in order to determine experimentally the membrane potential requires a lot of work and not always is possible prepare adequately the samples, especially in concrete with low compressive strength.

The theoretical assumptions

6. In the Nernst-Planck equation, used to calculate the ionic flux, the ionic strength was considered negligible. Although the pore solution of a concrete sample is far from being an ideal solution, research carried out by Truc, Olliviera and Nilsson (2000) showed that the error does not increase substantially if the activity of the solution is not taken into account during the simulation of a migration test.

7. All the equations of transport included in the model were related with ionic transport. No water osmosis was allowed in the model. Theoretically, due to different ionic osmotic potentials in the electrolytes, water could tend to move generating an additional transport mechanism. This mechanism was considerate negligible with respect to the magnitude of ionic transport due to the electrical field or even the concentration gradient of any species.

13.4 FUTURE WORK

The following are indications about possible work in the research field addressed in this investigation.

1. Mixes of GGBS and weathered BOS showed themselves to be novel concrete mixes which are very resistant to chloride penetration. Further study is recommended to assess the application of this kind of controlled low strength materials (CLSM) to immobilize other kind of ions, such as wastes in the nuclear industry.

2. The experimental determination of transport properties, such as diffusion coefficients and binding capacity, for species other than chlorides must be the object of further study

3. A linear binding isotherm was used in the model. This has the advantage that it gives a direct relationship between the intrinsic and apparent diffusion coefficients, and between bound and free chlorides. In a new version of the Coventry model the possibility of including a chloride non-linear binding isotherm must be evaluated.

4. In the current control model, variable voltage control model, and power control model introduced in chapter 9, the initial calculation of the corresponding external voltage is

carried out iteratively adjusting parameters by loop conditions. In the way those have been programmed, the computer model requires prolonged times (several minutes) to give results. A rigorous professional computer programming is advised for all models, maintaining the Coventry University source code, but looking after the technical and specific computing aspects.

5. The experimental measurement of the membrane potential has an incalculable scientific value; however, it is difficult to implement industrially due to difficulties in the conditioning and preparation of the samples. Further study should be carried out trying to obtain the information which has been obtained by using a salt bridge by altering the supply voltage during the test or some other technique.

6. It has been demonstrated in chapter 9 that the power control is an efficient way to keep temperature controlled in a migration test. Research is advised to establish all the related parameters of this test and new values of charge to rank chloride penetrability in concrete.

REFERENCES

AASHTO-277 (2007) *Electrical Indication of Concrete's Ability to Resist Chloride Ion Penetration (Rapid Chloride Permeability Test).* Washington: American Association of State Highway and Transportation Officials

AASHTO-TP-64 (2003) *Test for Predicting Chloride Penetration of Concrete by Rapid Migration Procedure.* Washington: American Association of State Highway and Transportation Officials

AASHTO T259 (1997) *Standard Method of Test for Resistance of Concrete to Chloride Ion Penetration,* Washington: American Association of State Highway and Transportation Officials

American Concrete Institute ACI (2003) *Slag Cement in Concrete and Mortar.* ACI-233r-03. Farmington Hills, MI 48331 U.S.A: American Concrete Institute

American Concrete Institute ACI (2008) *Report on Measurements of Workability and Rheology of Fresh Concrete.* ACI-238.1r-08. Farmington Hills, MI 48331 U.S.A: American Concrete Institute

Akin-Altun, I. and Yilmaz, I. (2002) 'Study on Steel Furnace Slags with High MgO as Additive in Portland Cement'. *Cement and Concrete Research* 32, (8) 1247-1249

Al-Harthy, A. S., Taha, R. and Al-Maamary, F. (2003) 'Effect of Cement Kiln Dust (Ckd) on Mortar and Concrete Mixtures.' *Construction and Building Materials* 17, (5) 353-360

Al-Khayat, H., Haque, M. N. and Fattuhi, N. I. (2002) 'Concrete Carbonation in Arid Climate ' *Materials and Structures* 35, (7) 421-426

Andersson, K., Allard, B., Bengtsson, M. and Magnusson, B. (1989) 'Chemical Composition of Cement Pore Solutions.' *Cement and Concrete Research* 19, (3) 327-332

Andrade, C. (1993) 'Calculation of Chloride Diffusion Coefficients in Concrete from Ionic Migration Measurements.' *Cement and Concrete Research* 23, (3) 724-742

Andrade, C., Castellote, M., Alonso, C. and Gonzalez, C. (1999a) 'Relation between Colorimetric Chloride Penetration Depth and Charge Passed in Migration Tests of the Type of Standard ASTM C1202-91.' *Cement and Concrete Research* 29, (3) 417-421

Andrade, C., Castellote, M., Alonso, C. and González, C. (1999b) 'Non-Steady-State Chloride Diffusion Coefficients Obtained from Migration and Natural Diffusion Tests. Part I: Comparison between Several Methods of Calculation ' *Materials and Structures* 33, (1) 21-28

Andrade, C. and Whiting, D. (1995) 'Comparison of AASHTO T-277 (Electrical) and AASHTO T-259 (90 Day Ponding) Results'. in L.-O. Nilsson and J.-P. Ollivier (ed) *Proceedings: Chloride Penetration into Concrete.* Saint-Rémy-lès-Chevreuse, France

Aperador, W., Mejía De Gutiérrez, R. and Bastidas, D. (2009) 'Steel Corrosion Behaviour in Carbonated Alkali-Activated Slag Concrete.' *Corrosion Science* 51, (9) 2027-2033

American Society for Testing and Materials C33 (2008) *Standard Specification for Concrete Aggregates*. ASTM-C33-2008. ASTM International West Conshohocken, Pennsylvania

American Society for Testing and Materials C109 (2008) *Standard Test Method for Compressive Strength of Hydraulic Cement Mortars (Using 2-in or 50-mm cube specimens)*. ASTM-C109-2008. ASTM International West Conshohocken, Pennsylvania

American Society for Testing and Materials C125 (2007) *Standard Terminology Relating to Concrete and Concrete Aggregates*. ASTM-C125-2007. ASTM International West Conshohocken, Pennsylvania

American Society for Testing and Materials C150 (2007) *Standard Specification for Portland Cement*. ASTM-C150-2007. ASTM International West Conshohocken, Pennsylvania

American Society for Testing and Materials C187 (2004) *Standard Test Method for Normal Consistency of Hydraulic Cement*. ASTM-C187-2004. ASTM International West Conshohocken, Pennsylvania

American Society for Testing and Materials C191 (2008) *Standard Test Methods for Time of Setting of Hydraulic Cement by Vicat Needle*. ASTM-C191-2008. ASTM International West Conshohocken, Pennsylvania

American Society for Testing and Materials C490 (1997) *Standard Practice for Use of Apparatus for the Determination of Length Change of Hardened Cement Paste*. ASTM-C490-1997. ASTM International West Conshohocken, Pennsylvania

American Society for Testing and Materials C595 (2008) *Standard Specification for Blended Hydraulic Cements*. ASTM-C595-2008. ASTM International West Conshohocken, Pennsylvania

American Society for Testing and Materials C876 (1991) *Standard Test Method for Half-Cell Potentials of Uncoated Reinforcing Steel in Concrete*. ASTM-C876-1991. ASTM International West Conshohocken, Pennsylvania

American Society for Testing and Materials C1152 (2004) *Standard Test Method for Acid-Soluble Chloride in Mortar and Concrete*. ASTM-C1152-2004. ASTM International West Conshohocken, Pennsylvania

American Society for Testing and Materials C1202 (2005) *Standard Test Method for Electrical Indication of Concrete's Ability to Resist Chloride Ion Penetration*. ASTM-C1202-2005. ASTM International West Conshohocken, Pennsylvania

American Society for Testing and Materials C1218 (2008) *Standard Test Method for Water-Soluble Chloride in Mortar and Concrete*. ASTM-C1218-2008. ASTM International West Conshohocken, Pennsylvania

American Society for Testing and Materials C1585 (2004) *Standard Test Method for Measurement of Rate of Absorption of Water by Hydraulic-Cement Concretes*. ASTM-C1585-2004. ASTM International West Conshohocken, Pennsylvania

American Society for Testing and Materials D5106 (2008) *Standard Specification for Steel Slag Aggregates for Bituminous Paving Mixtures. ASTM-C1585-2004*. ASTM International West Conshohocken, Pennsylvania

Atkinson, A., Claisse, P. A., Ganjian, E. and Tyrer, M. (1998-2005) *Novel Composite Landfill Liners.* An ENTRUST project jointly undertaken by Imperial College and Coventry University

Atkinson, A. and Nickerson, A. K. (1984) 'The Diffusion of Ions through Water-Saturated Cement ' *Journal of Materials Science* 19, (9) 3068-3078

Bakharev, T., Sanjayan, J. G. and Cheng, Y. B. (2001) 'Resistance of Alkali-Activated Slag Concrete to Carbonation.' *Cement and Concrete Research* 31, (9) 1277-1283

Barneyback Jr, R. S. and Diamond, S. (1981) 'Expression and Analysis of Pore Fluids from Hardened Cement Pastes and Mortars.' *Cement and Concrete Research* 11, (2) 279-285

Baroghel-Bouny, V., Belin, P., Maultzsch, M. and Henry, D. (2007) '$AgNO_3$ Spray Tests: Advantages, Weaknesses, and Various Applications to Quantify Chloride Ingress into Concrete. Part 1: Non-Steady-State Diffusion Tests and Exposure to Natural Conditions.' *Materials and Structures* 40, (8) 759-781

Basheer, P. A. M. (2001) 'Permeation Analysis'. in *Handbook of Analytical Techniques in Concrete Science and Technology.* ed. by Ramachandran, V. S. and Beaudoin, J. J.: NOYES PUBLICATIONS

Basheer, P. A. M., Andrews, R. J., Robinson, D. J. and Long, A. E. (2005) '"Permit" Ion Migration Test for Measuring the Chloride Ion Transport of Concrete on Site.' *NDT & E International* 38, (3) 219-229

Basheer, P. A. M., Gilleece, P. R. V., Long, A. E. and Mc Carter, W. J. (2002) 'Monitoring Electrical Resistance of Concretes Containing Alternative Cementitious Materials to Assess their Resistance to Chloride Penetration.' *Cement and Concrete Composites* 24, (5) 437-449

Bentz, D. P. (2007) 'A Virtual Rapid Chloride Permeability Test.' *Cement and Concrete Composites* 29 (10)*, 723-731

Beresford, T. (2002) *Chloride Transport in Concrete* Unpublished Master of Philosophy thesis, Coventry: Coventry University

Bertolini, L., (Editor), B. Elsener, Pedeferri, P. and Polder, R. B. (2004) *Corrosion of Steel in Concrete: Prevention, Diagnosis, Repair London:* Wiley

Bin, Q., Wu, X. and Tang, M. (1992) *High Strength Alkali Steel–Iron Slag Binder.* Proc., 9th Int. Congress on the Chemistry of Cement. New Delhi, India

Bockris, J. and Reddy, A. (1998) *Modern Electrchemistry 1 Ionics.* New York: Plenum Press

Broomfield, J. P. (2007) *Corrosion of Steel in Concrete: Understanding, Investigation, and Repair.* London: Taylor & Francis

British Standards Institution (1974) *Specification for Supersulphated Cement. BS 4248:1974.* London: British Standards Institution

Cann, G. M., Claisse, P. A. and Lorimer, J. P. (2007) 'Production of Gypsum Products from Waste Battery Acid'. *Proceedings of the International Conference on Sustainable Construction Materials and Technologies*. Held 11-13 June 2007 at Coventry University: London Taylor and Francis,

Castellote, M., Alonso, C., Andrade, C., Chadbourn, G. A. and Page, C. L. (2001) 'Oxygen and Chloride Diffusion in Cement Pastes as a Validation of Chloride Diffusion Coefficients Obtained by Steady-State Migration Tests.' *Cement and Concrete Research* 31, (4) 621-625

Castellote, M., Andrade, C. and Alonso, C. (1999a) 'Chloride-Binding Isotherms in Concrete Submitted to Non-Steady-State Migration Experiments.' *Cement and Concrete Research* 29, (11) 1799-1806

Castellote, M., Andrade, C. and Alonso, C. (1999b) 'Modelling of the Processes During Steady-State Migration Tests: Quantification of Transference Numbers ' *Materials and Structures* 32, (3) 180-186

Castellote, M., Andrade, C. and Alonso, C. (2000) 'Phenomenological Mass-Balance-Based Model of Migration Tests in Stationary Conditions Application to Non-Steady-State Tests.' *Cement and Concrete Research* 30, (12) 1885-1893

Castellote, M., Andrade, C. and Alonso, C. (2002) 'Accelerated Simultaneous Determination of the Chloride Depassivation Threshold and of the Non-Stationary Diffusion Coefficient Values.' *Corrosion Science* 44, (11) 2409-2424

Chatterjee, A. K. (2001) 'X-Ray Diffraction.' In *Handbook of Analytical Techniques in Concrete Science and Technology.* ed. by Ramachandran, V. S. and Beaudoin, J. J.: NOYES PUBLICATIONS

Chrisp, T. M., Mccarter, W. J., Starrs, G., Basheer, P. A. M. and Blewett, J. (2002) 'Depth-Related Variation in Conductivity to Study Cover-Zone Concrete During Wetting and Drying.' *Cement and Concrete Composites* 24, (5) 415-426

Claisse, P. (2006) 'A New Way of Looking at the Rapid Chloride Permeability Test.' American Concrete Institute Convention Held at Charlotte NC USA: Farmington Hills, U.S.A

Claisse, P. A. (1988) *The Properties and Performance of High Strength Silica Fume Concrete.* Unpublished PhD thesis, Leeds University

Claisse, P. A. (2005) 'Transport Properties of Concrete.' *Concrete International* 27, (1) 43-48

Claisse, P. A. and Beresford, T. W. (1997) 'Obtaining More from the Electrical Chloride Test.' *ACI - SP170-57* 170,

Claisse P.A., Elsayad H. and Ganjian E. (2009) 'Modelling the rapid chloride permeability test.' Cement and Concrete Research. doi:10.1016/j.cemconres.2009. 10.004

Collepardi, M. (1996) 'Quick Method to Determine Free and Bound Chlorides in Concrete.' In Nilsson, L.-O. and Ollivier, J.-P. (ed.) *RILEM International Workshop on Chloride Penetration into Concrete*. RILEM Publications SARL

Collepardi, M., Marcialis, A. and Turriziani, R. (1970) 'The Kinetics of Penetration of Chloride Ions into the Concrete (in Italian) ' *Il Cemento* 157–164

Corbo, J. and Farzam, H. (1989) 'Influence of Three Commonly Used Inorganic Compounds on Pore Solution Chemistry and Their Possible Implications to the Corrosion of Steel in Concrete.' *ACI materials journal* 86, (5) 498-502

Crank, J. (1976) *The Mathematics of Diffusion* second. Oxford: University Press

Czernin, W. (1980) *Cement Chemistry and Physics for Civil* Engineers. Lockwood (London)

De Schutter, G. (1999) 'Hydration and Temperature Development of Concrete Made with Blast-Furnace Slag Cement.' *Cement and Concrete Research* 29, (1) 143-149

Delagrave, A., Marchand, J. and Samson, E. (1996) 'Prediction of Diffusion Coefficients in Cement-Based Materials on the Basis of Migration Experiments.' *Cement and Concrete Research* 26, (12) 1831-1842

Delagrave, A., Bigas, J. P., Ollivier, J. P., Marchand, J. and Pigeon, M. (1997) 'Influence of the Interfacial Zone on the Chloride Diffusivity of Mortars.' Advanced Cement Based Materials 5, (3-4) 86-92

Demuth, H., Beale, M. and Hagan, M. (2008) *Neural Network Toolbox™ 6 User's Guide.*

Detwiler, R., Bhatty, J. and Bhattacharja, S. (1996) *Supplementary Cementing Materials for Use in Blended Cements* PCA-RD112

Dhir, R. K., El-Mohr, M. A. K. and Dyer, T. D. (1996) 'Chloride Binding in Ggbs Concrete.' *Cement and Concrete Research* 26, (12) 1767-1773

Dhir, R. K., El-Mohr, M. A. K. and Dyer, T. D. (1997) 'Developing Chloride Resisting Concrete Using Pfa.' *Cement and Concrete Research* 27, (11) 1633-1639

Dhir, R. K., Jones, M. R., Ahmed, H. E. H. and Seneviratne, A. M. G. (1990) 'Rapid Estimation of Chloride Diffusion Coefficient in Concrete.' *Magazine of Concrete Research* 42, (152) 177-185

Dias, W. P. S. (2000) 'Reduction of Concrete Sorptivity with Age through Carbonation.' *Cement and Concrete Research* 30, (8) 1255-1261

Dongxue, L., Xinhua, F., Xuequan, W. and Mingshu, T. (1997) 'Durability Study of Steel Slag Cement.' *Cement and Concrete Research* 27, (7) 983-987

El-Enein, S. A. A., Kotkata, M. F., Hanna, G. B., Saad, M. and El Razek, M. M. A. (1995) 'Electrical Conductivity of Concrete Containing Silica Fume.' *Cement and Concrete Research* 25, (8) 1615-1620

Feldman, R., Prudencio, L. R. and Chan, G. (1999) 'Rapid Chloride Permeability Test on Blended Cement and Other Concretes: Correlations between Charge, Initial Current and Conductivity ' *Construction and Building Materials* 13, (3) 149-154

Feldman, R. F., Chan, G. W., Brousseau, R. J. and Tumidajski, P. J. (1994) 'Investigation of the Rapid Chloride Permeability Test.' *ACI materials journal* 91, (2) 246-255

Friedmann, H., Amiri, O., Ait-Mokhtar, A. and Dumargue, P. (2004) 'A Direct Method for Determining Chloride Diffusion Coefficient by Using Migration Test.' *Cement and Concrete Research* 34, (11) 1967-1973

Glass G.K. and Buenfeld, N. R. (1998) 'Theoretical Assessment of the Steady State Diffusion Cell Test.' *Journal of materials science* 33, (21) 5111-5118

Ganjian, E., Claisse, P. and Pouya, H. (2007) *The Use of Plasterboard and Gypsum Waste in Road Bases, Sub-Bases and Stabilised Sub-Grades.* Coventry, UK: Coventry University

Geiseler, J. (1996) 'Use of Steelworks Slag in Europe.' *Waste Management* 16, (1-3) 59-63

Geiseler, J., Kollo, H. and Lang, E. (1992) 'Influence of Blast Furnace Cements on Durability of Concrete Structures.' *Materials Journal - ACI* 92, (3) 252-257

Glasser, Fredrik, Luke and Angus (1988) 'Modification of Cement Pore Fluid Compositions by Pozzolanic Additives ' *Cement and Concrete Research* 18, (2) 165-178

Gruskovnjak, A., Lothenbach, B., Winnefeld, F., Figi, R., Ko, S. C., Adler, M. and Mäder, U. (2008) 'Hydration Mechanisms of Super Sulphated Slag Cement.' *Cement and Concrete Research* 38, (7) 983-992

Gurney, K. (1997) *An Introduction to Neural Networks.* London: CRC Press

Hall, C. (1989) 'Water Sorptivity of Mortars and Concretes: A Review.' *Magazine of Concrete Research,* 41, (147) 51-61

Hamann, C. H., Hamnett, A. and Vielstich, W. (2007) *Electrochemistry.* Wiley

Hewlett, P. (2004) *Lea's Chemistry of Cement and Concrete. Elsevier Butterworth-Heinemann Publishers*

Hogan, F. J. and Meusel, J. W. (1981) 'The Evaluation of Durability and Strength Development of a Ground Granulated Blastfurnace Sl.' *Cement, Concrete, Aggregates* 3, (1)

Hooton, R. D.,Thomas M.D. and Stanish, K. (2001) *Prediction of Chloride Penetration in Concrete.* University of Toronto, Department of Civil Engineering

Hossain, K. M. A. (2005) 'Correlations between Porosity, Chloride Diffusivity and Electrical Resistivity in Volcanic Pumice-Based Blended Cement Pastes.' *Advances in Cement Research* 17, (1) 29-37

Jones, D. A. (1996) *Principles and Prevention of Corrosion.* Upper Saddle iver, NJ 07458: Prentice Hall

JSCE-G571 (2003) *Test Method for Effective Diffusion Coefficient of Chloride Ion in Concrete by Migration.*: Japan Society of Civil Engineers

Julio-Betancourt, G. A. and Hooton, R. D. (2004) 'Study of the Joule Effect on Rapid Chloride Permeability Values and Evaluation of Related Electrical Properties of Concretes.' *Cement and Concrete Research* 34, (6) 1007-1015

Karami, S. (2008) *Using by-Product Industrial Materials to Replace All Cement in Construction Products.* Unpublished PhD thesis, Coventry University

Khitab, A. (2005) *Modélisation Des Transferts Ioniques Dans Les Milieux Poreux Saturés: Application À La Pénétration Des Chlorures À Travers Les Matériaux Cimentaires.* Unpublished PhD thesis, Paul Sabatier University

Khitab, A., Lorente, S. and Ollivier, J. P. (2005) 'Predictive Model for Chloride Penetration through Concrete.' Magazine of Concrete Research 57, (9) 511-520

Koehler, E. P. (2004) *Development of a Portable Rheometer for Fresh Portland Cement Concrete.* Unpublished MS thesis, University of Texas at Austin

Konsta-Gdoutos, M. S. and Shah, S. P. (2003) 'Hydration and Properties of Novel Blended Cements Based on Cement Kiln Dust and Blast Furnace Slag.' *Cement and Concrete Research* 33, (8) 1269-1276

Kourounis, S., Tsivilis, S., Tsakiridis, P. E., Papadimitriou, G. D. and Tsibouki, Z. (2007) 'Properties and Hydration of Blended Cements with Steelmaking Slag.' *Cement and Concrete Research* 37, (6) 815-822

Krabbenhoft, K. and Krabbenhoft, J. (2008) 'Application of the Poisson-Nernst-Planck Equations to the Migration Test.' *Cement and Concrete Research* 38, (1) 77-88

Lane, D. S. (2005) *Supplanting the Rapid Chloride Permeability Test with a Quick Measurement of Concrete Conductivity.* VTRC Report Details

Larsen, C. K. (1998) *Chloride Binding in Concrete, Effect of Surrounding Environment and Concrete Composition.* Unpublished PhD thesis thesis, Norwegian University of Science and Technology

Lay, S., Liebl, S., Hilbig, H. and Schiel, P. (2004) 'New Method to Measure the Rapid Chloride Migration Coefficient of Chloride-Contaminated Concrete.' *Cement and Concrete Research* 34, (3) 421-427

Leng, F., Feng, N. and Lu, X. (2000) 'An Experimental Study on the Properties of Resistance to Diffusion of Chloride Ions of Fly Ash and Blast Furnace Slag Concrete ' *Cement and Concrete Research* 30, (6) 989-992

Lizarazo-Marriaga, J. and Claisse, P. (2009) 'Determination of the Chloride Transport Properties of Blended Concretes from a New Electric Migration Test.' In Alexander, M. G. and Bertron, A. (ed.) *Concrete in aggressive aqueous environments - Performance, Testing, and Modeling.* RILEM Publications SARL

Lorente, S., Voinitchi, D., Bégué-Escaffit, P. and Bourbon, X. (2007) 'The Single-Valued Diffusion Coefficient for Ionic Diffusion through Porous Media.' *J. Appl. Phys* 101, (024907)

Lu, X. (1997) 'Application of the Nernst-Einstein Equation to Concrete.' *Cement and Concrete Research* 27, (2) 293-302

Luco, F. (2008) *Phd Thesis.* Unpublished thesis, University of Alicante

Luo, R., Cai, Y., Wang, C. and Huang, X. (2003) 'Study of Chloride Binding and Diffusion in Ggbs Concrete.' *Cement and Concrete Research* 33, (1) 1-7

Luping, T. (1997) *Chloride Diffusion Coefficient of Concrete and Relevant Test Methods - the State of the Art and Suggestions for Future Work.* Borfis, Sweden: Swedish National Testing and Research Institute

Luping, T. (2008) 'Engineering Expression of the Clinconc Model for Prediction of Free and Total Chloride Ingress in Submerged Marine Concrete.' *Cement and Concrete Research* 38, (8-9) 1092-1097

Luping, T. and Nilsson, L.-O. (1992) 'Rapid Determination of the Chloride Diffusivity in Concrete by Applying an Electric Field.' *ACI materials journal* 89, (1) 49-53

Mahieux, P. Y., Aubert, J. E. and Escadeillas, G. (2009) 'Utilization of Weathered Basic Oxygen Furnace Slag in the Production of Hydraulic Road Binders.' *Construction and Building Materials* 23, (2) 742-747

Matschei, T., Bellmann, F. and Stark, J. (2005) 'Hydration Behaviour of Sulphate-Activated Slag Cements.' *Advances in Cement Research* 17, (4)

Mccarter, W. J., Starrs, G. and Chrisp, T. M. (2000) 'Electrical Conductivity, Diffusion, and Permeability of Portland Cement-Based Mortars.' *Cement and Concrete Research* 30, (9) 1395-1400

Mccarter, W. J., Starrs, G., Kandasami, S., Jones, R. and Chrisp, M. (2009) 'Electrode Configurations for Resistivity Measurements on Concrete.' *ACI materials journal* 106, (3)

Mcgrath, P. F. and Hooton, R. D. (1996) 'Influence of Voltage on Chloride Diffusion Coefficients from Chloride Migration Tests.' *Cement and Concrete Research* 26, (8) 1239-1244

Meck, E. and Sirivivatnanon, V. (2003) 'Field Indicator of Chloride Penetration Depth.' *Cement and Concrete Research* 33, (8) 1113-1117

Mehta, K. and Monteiro, P. (1992) *Concrete: Structure, Properties, and Materials* Prentice Hall College Div

Meusel, J. W. and Rose, J. H. (1983) 'Production of Granulated Blast Furnace Slag at Sparrows Point, and the Workability and Strength Potential of Concrete Incorporating the Slag.' *ACI SP-79*

Midness, S. and Young, J. F. (1981) *Concrete.* Englewood Cliffs, N.J.: Prentice-Hall, Inc.

Mohammed, T. U. and Hamada, H. (2003) 'Relationship between Free Chloride and Total Chloride Contents in Concrete.' *Cement and Concrete Research* 33, (9) 1487-1490

Monshi, A. and Asgarani, M. K. (1999) 'Producing Portland Cement from Iron and Steel Slags and Limestone.' *Cement and Concrete Research* 29, (9) 1373-1377

Muller, H. (1977) *What Is Dust? Characterization of Classification of Kiln Dust.* Holderbank Management and Consulting Limited

Naik, T. R. (2007) *Sustainability of the Cement and Concrete Industries.* Proc. Int. Conf: Sustainable construction materials and technologies. Coventry.: Taylor and Francis, London

Narsilio, G. A., Li, R., Pivonka, P. and Smith, D. W. (2007) 'Comparative Study of Methods Used to Estimate Ionic Diffusion Coefficients Using Migration Tests.' *Cement and Concrete Research* 37, (8) 1152-1163

Nilsson, L.-O. (1996) *Chloride Penetration into Concrete, State-of-the-Art. Transport Processes, Corrosion Initiation, Test Methods and Prediction Models.* Copenhagen: Road Directorate

Nokken, M., Boddy, A., Hooton, R. D. and Thomas, M. D. A. (2006) 'Time Dependent Diffusion in Concrete--Three Laboratory Studies.' *Cement and Concrete Research* 36, (1) 200-207

Nokken, M. R. (2004) *Development of Capillary Discontinuity in Concrete and Its Influence on Durability.* Unpublished PhD thesis, University of Toronto

NT-Build 335 (1997) *Concrete, Mortar and Cement-Based Repair Materials: Chloride Diffusion Coefficient from Migration Cell Experiments.* Nordtest, Esbo, Finland

NT-Build 443 (1995) *Concrete Hardened: Accelerated Chloride Penetration.* Nordtest, Esbo, Finland

NT-Build 492 (1999) *Nordtest Method: Concrete, Mortar and Cement-Based Repair Materials: Chloride Migration Coefficient from Non-Steady-State Migration Experiments.*

O'rourke, B., Mcnally, C. and Richardson, M. G. (2009) 'Development of Calcium Sulfate-Ggbs-Portland Cement Binders.' *Construction and Building Materials* 23, (1) 340-346

Obla, K. and Lobo, C. (2005) 'Laboratory Demonstration of Advantages of Performance Specifications.' *The Indian Concrete Journal* December, 22-26

Oss, H. G. V. (2003) 'Slag Iron and Steel, U.S. Geological Survey Minerals Yearbook.'

Otsuki, N., Hisada, M., Otani, T. and Maruyama, T. (1999) 'Theoretical Evaluation of Diffusion Coefficient of Chloride Ion in Mortar from Mobility.' *ACI materials journal* 96, (6) 627-633

Otsuki, N., Nagataki, S. and Nakashita, K. (1992) 'Evaluation of Agno 3 Solution Spray Method for Measurement of Chloride Penetration into Hardened Cementitious Matrix Materials.' *Materials Journal* 89, (6) 587-592

Page, C. L. and Vennesland, O. (1983) 'Pore Solution Composition and Chloride Binding Capacity of Silica-Fume Cement Pastes.' *Materials and Structures* 16, (1) 19-25

Pal, S. C., Mukherjee, A. and Pathak, S. R. (2002) 'Corrosion Behaviour of Reinforcement in Slag Concrete.' *Materials Journal* 99, (6)

Pandey, S. P. and Sharma, R. L. (2000) 'The Influence of Mineral Additives on the Strength and Porosity of Opc Mortar.' *Cement and Concrete Research* 30, (1) 19-23

Patrick, F., Mcgrath, P. F. and Hooton, R. D. (1999) 'Re-Evaluation of the Aashto T259 90-Day Salt Ponding Test - an Evaluation of Chloride Penetration Testing Methods ' *Cement and Concrete Research* 29, (8) 1239-1248

Polder, R., Andrade, C., Elsener, B., Vennesland, O., Gulikers, J., Weidert, R. and Raupach, M. (2000) 'Rilem Tc 154-Emc: Electrochemical Techniques for Measuring Metallic Corrosion: Test Methods for on Site Measurement of Resistivity of Concrete.' *Materials and Structures/Mat6riaux et Constructions* 33, 603-611

Polder, R. B. (2001) 'Test Methods for on Site Measurement of Resistivity of Concrete — a Rilem Tc-154 Technical Recommendation ' *Construction and Building Materials* 15, (2-3) 125-131

Popovics, S. (1992) *Concrete Materials - Properties, Specifications and Testing* 2nd Edition edn.: Noyes Publications

Powers, T. C. (1958) 'The Physical Structure and Engineering Properties of Concrete.' *Portland Cement Association* Bulletin 90

Prince, W., Perami, R. and Espagne, M. (1999) 'Mechanisms Involved in the Accelerated Test of Chloride Permeability.' *Cement and Concrete Research* 29, (5) 687-694

Princigallo, A., Van Breugel, K. and Levita, G. (2003) 'Influence of the Aggregate on the Electrical Conductivity of Portland Cement Concretes.' *Cement and Concrete Research* 33, (11) 1755-1763

Qasrawi, H., Shalabi, F. and Asi, I. (2009) 'Use of Low Cao Unprocessed Steel Slag in Concrete as Fine Aggregate.' *Construction and Building Materials* 23, (2) 1118-1125

Rai, A., Prabakar, J., Raju, C. B. and Morchalle, R. K. (2002) 'Metallurgical Slag as a Component in Blended Cement.' *Construction and Building Materials* 16, (8) 489-494

Revil, A. (1999) 'Ionic Diffusivity, Electrical Conductivity, Membrane and Thermoelectric Potentials in Colloids and Granular Porous Media: A Unified Model.' *Journal of Colloid and Interface Science* 212, (2) 503-522

Rilem-Tc-178-Tmc (2002) 'Recommendations of Rilem Tc 178-Tmc: 'Testing and Modelling Chloride Penetration in Concrete' Analysis of Total Chloride Content in Concrete.' *Materials and Structures* 35, (253)

Roszczynialski, W., Gawlicki, M. and Wczelik, W. N. (1997) 'Production and Use of by-Product Gypsum in the Construction Industry.' In *Waste Materials Used in Concrete Manufacturing.* ed. by Chandra, S.

Roy, D. M. (1989) 'Hydration, Microstructure and Chloride Diffusion of Chloride Ions in Hardened Cement Pastes.' *ACI SP-114* 2, 1265-1281

Roy, D. M. and Ldorn, G. M. (1982) 'Hydration, Structure, and Properties of Blast Furnace Slag Cements, Mortars, and Concrete.' *ACI -Journal Proceedings* 79, (6)

Roy, D. M. and Parker, K. M. (1983) 'Microstructure and Properties of Granulated Slag-Portland Cement Blends at Normal and Elevated Temperatures.' *ACI SP-79*

Rubin, J. (1983) 'Transport of Reacting Solutes in Porous Media: Relation between Mathematical Nature of Problem Formulation and Chemical Nature of Reactions.' *Water Resources Research* 19, 1231-1252

Sajkata, Ayano and Fujii (2007) *Steel Making Slag Concrete as Sustainable Construction Materials*. Sustainable construction materials and technologies June 11 – June 13 Coventry, UK

Samson, E., Marchand, J. and Snyder, K. A. (2003) 'Calculation of Ionic Diffusion Coefficients on the Basis of Migration Test Results ' *Materials and Structures* 36, (3) 156-165

Sengul, O. and Gjorv, O. E. (2008) 'Electrical Resistivity Measurements for Quality Control During Concrete Construction.' *ACI Materials Journal* 105, (6)

Sengul, O. and Gjorv, O. E. (2009) 'Effect of Embedded Steel on Electrical Resistivity Measurements on Concrete Structures.' *ACI materials journal* 106, (1)

Shane, J. D., Aldea, C. D., Bouxsein, N. F., Mason, T. O., Jennings, H. M. and Shah, S. P. (1999) 'Microstructural and Pore Solution Changes Induced by the Rapid Chloride Permeability Test Measured by Impedance Spectroscopy.' *Concrete Science and Engineering* 1, (2) 110 - 119

Shehata, M. H., Thomas, M. D. A. and Bleszynski, R. F. (1999) 'The Effects of Fly Ash Composition on the Chemistry of Pore Solution in Hydrated Cement Pastes.' *Cement and Concrete Research* 29, (12) 1915-1920

Shi, C. (2004a) 'Effect of Mixing Proportions of Concrete on Its Electrical Conductivity and the Rapid Chloride Permeability Test (Astm C1202 or Asshto T277) Results.' *Cement and Concrete Research* 34, (3) 537-545

Shi, C. (2004b) 'Steel Slag—Its Production, Processing, Characteristics, and Cementitious Properties.' *J. Mat. in Civ. Engrg* 16, (3) 230-236

Shi, C. and Day, R. L. (1995) 'A Calorimetric Study of Early Hydration of Alkali-Slag Cements.' *Cement and Concrete Research* 25, (6) 1333-1346

Shi, C. and Qian, J. (2000) 'High Performance Cementing Materials from Industrial Slags -- a Review.' *Resources, Conservation and Recycling* 29, (3) 195-207

Shi, C., Stegemann, J. A. and Caldwell, R. J. (1998) 'Effect of Supplementary Cementing Materials on the Specific Conductivity of Pore Solution and Its Implications on the Rapid Chloride Permeability Test (Aashto T277 and Astm C1202) Results.' *Materials Journal* 95, (4) 389-394

Shoaib, M. M., Balaha, M. M. and Abdel-Rahman, A. G. (2000) 'Influence of Cement Kiln Dust Substitution on the Mechanical Properties of Concrete.' *Cement and Concrete Research* 30, (3) 371-377

Singh, M. and Garg, M. (2002) 'Calcium Sulfate Hemihydrate Activated Low Heat Sulfate Resistant Cement.' *Construction and Building Materials* 16, (3) 181-186

Song, S. and Jennings, H. M. (1999) 'Pore Solution Chemistry of Alkali-Activated Ground Granulated Blast-Furnace Slag.' *Cement and Concrete Research* 29, (2) 159-170

Stanish, K. D., Hooton, R. D. and Thomas, M. D. A. (2000) *Testing the Chloride Penetration Resistance of Concrete: A Literature Review.* FHWA Contract Dtfh61-97-R-00022. Toronto, Ontario, Canada: University of Toronto

Streicher, P. E. and Alexander, M. G. (1995) 'A Chloride Conduction Test for Concrete.' *Cement and Concrete Research* 25, (6) 1284-1294

Stutzman, P. (1996) *Guide for X-Ray Powder Diffraction Analysis of Portland Cement and Clinker.* National Institute of Standards and Technology

Sugiyama, T., Ritthichauy, W. and Tsuji, Y. (2003) 'Simultaneous Transport of Chloride and Calcium Ions in Hydrated Cement Systems.' *Journal of Advanced Concrete Technology* 1, (2) 127-138

Sulapha, P., Wong, S. F., Wee, T. H. and Swaddiwudhipong, S. (2003) 'Carbonation of Concrete Containing Mineral Admixtures.' *Journal of Materials in Civil Engineering* 15, (2) 134-143

Suryavanshi, A. K., Scantlebury, J. D. and Lyon, S. B. (1998) 'Corrosion of Reinforcement Steel Embedded in High Water-Cement Ratio Concrete Contaminated with Chloride.' *Cement and Concrete Composites* 20, (4) 263-281

Tailing, B. and Krivenko, P. (1997) 'Blast Furnace Slag – the Ultimate Binder.' In *Waste Materials Used in Concrete Manufacturing.* ed. by Chandra, S.

Tang, L. (1999) 'Concentration Dependence of Diffusion and Migration of Chloride Ions: Part 2. Experimental Evaluations.' *Cement and Concrete Research* 29, (9) 1469-1474

Tang, L. and Nilsson, L. O. (1993) 'Chloride Binding Capacity and Binding Isotherms of Opc Pastes and Mortars.' *Cement and Concrete Research* 23, (2) 247-253

Tasdemir, C. (2003) 'Combined Effects of Mineral Admixtures and Curing Conditions on the Sorptivity Coefficient of Concrete.' *Cement and Concrete Research* 33, (10) 1637-1642

Taylor, H. F. W. (1990) *Cement Chemistry*. Academic Press

RILEM-TC56 (1988) 'Cpc-18 Measurement of Hardened Concrete Carbonation Depth ' *Materials and Structures* 21, (6)

The Mathworks (2001) *Curve Fitting Toolbox - for Use with Matlab.* Matworls

Thomas, M. D. A., Scott, A., Bremner, T., Bilodeau, A. and Day, D. (2008) 'Performance of Slag Concrete in Marine Environment.' *ACI materials journal* 105, (6) 628-634

Todres, H., Mishulovich, A. and Ahmed, J. (1992) *Cement Kiln Dust Management: Permeability*. vol. RD103T: PCA

Tong, L. and Gjorv, O. E. (2001) 'Chloride Diffusivity Based on Migration Testing.' *Cement and Concrete Research* 31, (7) 973-982

Tossavainen, M., Engstrom, F., Yang, Q., Menad, N., Lidstrom Larsson, M. and Bjorkman, B. (2007) 'Characteristics of Steel Slag under Different Cooling Conditions.' *Waste Management* 27, (10) 1335-1344

Truc, O. (2000) *Prediction of Chloride Penetration into Saturated Concrete - Multi - Species - Approach*. Unpublished Ph.D. thesis, Chalmers University

Truc, O., Ollivier, J.-P. and Nilsson, L.-O. (2000) 'Numerical Simulation of Multi-Species Transport through Saturated Concrete During a Migration Test -- Msdiff Code.' *Cement and Concrete Research* 30, (10) 1581-1592

Truc, O., Ollivier, J. P. and Carcasses, M. (1998) 'Comparaison Cth Rapid Method / Essai De Migration En Régime Stationnaire.' *Sci. Mater. et Durabilités des Bétons*.

Truc, O., Ollivier, J. P. and Carcasses, M. (2000) 'A New Way for Determining the Chloride Diffusion Coefficient in Concrete from Steady State Migration Test.' *Cement and Concrete Research* 30, (2) 217-226

Truc, O., Olliviera, J.-P. and Nilsson, L.-O. (2000) 'Numerical Simulation of Multi-Species Transport through Saturated Concrete During a Migration Test - Msdiff Code.' *Cement and Concrete Research* 30, (10) 1581-1592

Tsakiridis, P. E., Papadimitriou, G. D., Tsivilis, S. and Koroneos, C. (2008) 'Utilization of Steel Slag for Portland Cement Clinker Production.' *Journal of Hazardous Materials* 152, (2) 805-811

Uomoto, T. and Kobayashi, K. (1983) 'Strength and Durability of Slag-Gypsum Cement Concrete.' *ACI SP-79*

Wallevik, J. E. (2006) 'Relationship between the Bingham Parameters and Slump.' *Cement and Concrete Research* 36, (7) 1214-1221

Wee, T. H., Suryavanshi, A. K. and Tin, S. S. (1999) 'Influence of Aggregate Fraction in the Mix on the Reliability of the Rapid Chloride Permeability Test.' *Cement and Concrete Composites* 21, (1) 59-72

Wee, T. H., Suryavanshi, A. K. and Tin, S. S. (2000) 'Evaluation of Rapid Chloride Permeability Test (Rcpt) Results for Concrete Containing Mineral Admixtures.' *ACI materials journal* 97, (2) 221-232

Whiting, D. (1981) *Rapid Determination of the Chloride Permeability of Concrete.* FHWA/RD-81/119.

Whiting, D. (1984) 'In-Situ Measurement of the Permeability of Concrete to Chloride Ions, Sp 82, in-Situ/Non-Destructive Testing of Concrete.' *SP 82. CANMET, ACI* 501–524

Whiting, D. A. and Nagi, M. A. (2003) *Electrical Resistivity of Concrete - a Literature Review.* Portland Cement Association 2003

Wilsont, Whittington and Fordes (1983) 'Microprocessor-Based System for Automatic Measurement of Concrete Resistivity.' *J. Phys. E: sci. Instrum* 16,

Witte, R. A. (2002) *Electronic Test Instruments.* Prentice Hall

Xuequan, W., Hong, Z., Xinkai, H. and Husen, L. (1999) 'Study on Steel Slag and Fly Ash Composite Portland Cement.' *Cement and Concrete Research* 29, (7) 1103-1106

Yang, C. C. (2003) 'The Relationship between Charge Passed and the Chloride Concentrations in Anode and Cathode Cells Using the Accelerated Chloride Migration Test.' *Materials and Structures* 36, 678-684

Yang, C. C. (2006) 'On the Relationship between Pore Structure and Chloride Diffusivity from Accelerated Chloride Migration Test in Cement-Based Materials.' *Cement and Concrete Research* 36, (7) 1304-1311

Yang, C. C., Chiang, S. C. and Wang, L. C. (2007) 'Estimation of the Chloride Diffusion from Migration Test Using Electrical Current.' *Construction and Building Materials* 21, (7) 1560-1567

Yang, C. C. and Cho, S. W. (2003) 'An Electrochemical Method for Accelerated Chloride Migration Test of Diffusion Coefficient in Cement-Based Materials.' *Materials Chemistry and Physics* 81, (1) 116-125

Yang, C. C., Cho, S. W. and Huang, R. (2002) 'The Relationship between Charge Passed and the Chloride-Ion Concentration in Concrete Using Steady-State Chloride Migration Test.' *Cement and Concrete Research* 32, (2) 217-222

Yang, C. C. and Wang, L. C. (2004) 'The Diffusion Characteristic of Concrete with Mineral Admixtures between Salt Ponding Test and Accelerated Chloride Migration Test.' *Materials Chemistry and Physics* 85, (2-3) 266-272

Yb/T022-92 (1992) 'Steel Slag Used in Cement.'

Yuan, Q., Shi, C., De Schutter, G., Audenaert, K. and Deng, D. (2009) 'Chloride Binding of Cement-Based Materials Subjected to External Chloride Environment - a Review.' *Construction and Building Materials* 23, (1) 1-13

Zhang, J. Z. and Buenfeld, N. R. (1997) 'Presence and Possible Implications of a Membrane Potential in Concrete Exposed to Chloride Solution.' *Cement and Concrete Research* 27, (6) 853-859

Zhang, J. Z., Li, J. and Buenfeld, N. R. (2002) 'Measurement and Modelling of Membrane Potentials across Opc Mortar Specimens between 0.5 M Nacl and Simulated Pore Solutions.' *Cement and Concrete Composites* 24, (5) 451-455

Zhang, M. H. and Gjorv, O. E. (1991) 'Permeability of High Strength Lightweight Concrete.' *ACI materials journal* 88, (5) 463-469

Zhang, T. and Gjorv, O. E. (1996) 'Diffusion Behavior of Chloride Ions in Concrete.' *Cement and Concrete Research* 26, (6) 907-917

APPENDICES

APPENDIX 1: Binder mixes investigated

OPC–GGBS–BOS paste mixes

Name	Material Proportions [%]		
	OPC	GGBS	BOS
O100	100	---	---
G100	---	100	---
B100	---	---	100
O20B80	20	---	80
O40B60	40	---	60
O60B40	60	---	40
O80B20	80	---	20
G20B80	---	20	80
G40B60	---	40	60
G60B40	---	60	40
G80B20	---	80	20
O20G80	20	80	---
O40G60	40	60	---
O60G40	60	40	---
O80G20	80	20	---
O10G40B50	10	40	50
O10G50B40	10	50	40
O20G20B60	20	20	60
O20G40B40	20	40	40
O20G60B20	20	60	20
O30G10B60	30	10	60
O30G30B40	30	30	40
O30G50B20	30	50	20
O40G20B40	40	20	40
O40G30B30	40	30	30
O40G40B20	40	40	20
O50G10B40	50	10	40
O50G30B20	50	30	20

BPD–GGBS-BOS paste mixes

Name	Material Proportions [%]		
	BPD	GGBS	BOS
BPD05G57B38	5	57	38
BPD10G54B36	10	54	36
BPD15G51B34	15	51	34

PG–GGBS-BOS paste mixes

Name	Material Proportions [%]		
	PG	GGBS	BOS
G20B80	---	20	80
G40B60	---	40	60
G60B40	---	60	40
G80B20	---	80	20
P05G95	5	95	---
P10G90	10	90	---
P15G85	15	85	---
P20G80	20	80	---
P30G70	30	70	---
P10B90	10	---	90
P20B80	20	---	80
P30B70	30	---	70
P05G40B55	5	40	55
P05G50B45	5	50	45
P05G60B35	5	60	35
P10G30B60	10	30	60
P10G40B50	10	40	50
P10G50G40	10	50	40
P10G60B30	10	60	30
P15G35B50	15	35	50
P15G50B35	15	50	35
P15G60B25	15	60	25
P20G40B40	20	40	40
P20G50B30	20	50	30
P20G60B20	20	60	20
P30G40B30	30	40	30
P40G35B25	40	35	25

APPENDIX 2: Fick's Second Law of diffusion

In the parallelepiped shown in figure A3.1, of unit area and length *dx,* ions are diffusing. The concentration in faces 1 and 2 are define according the following relationships

$$C_1 = C \qquad (A1.1)$$

$$C_2 = C + \frac{dC}{dx} dx \qquad (A1.2)$$
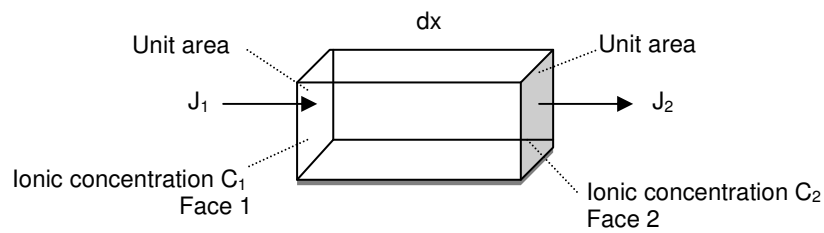
Figure A1.1

In the same way, using the Fick's First Law, the fluxes into and out of the parallelepiped are:

$$J_1 = -D\frac{dC}{dx} \qquad (A1.3)$$

$$J_2 = -D\frac{d}{dx}\left[C + \frac{dC}{dx} dx\right] = -D\frac{dC}{dx} - \frac{d^2C}{dx^2} dx \qquad (A1.4)$$

The net outflow of material from the parallelepiped of volume *dx* is

$$dJ = D\frac{d^2C}{dx^2} dx \qquad (A1.5)$$

So, the net outflow of ions per unit volume per unit time is the variation of the concentration with time.

$$\frac{dJ}{dx} = \frac{dC}{dt} = D\frac{d^2C}{dx^2} \qquad (A1.6)$$

APPENDIX 3: Nernst-Einstein equation

From the electrochemistry the total current can be expressed as equation A2.1

$$i = zFJA \qquad \text{(A2.1)}$$

The Ohm's law states that

$$R = \frac{E}{i} \qquad \text{(A2.2)}$$

If the electric field (E_d) is linear it can be defined as equation A2.3

$$E_d = \frac{E}{x} = \frac{iR}{x} = \frac{zFJAR}{x} \qquad \text{(A2.3)}$$

The resistance (R) can be related with the overall conductivity (σ) by the resistivity (ρ).

$$R = \frac{\rho x}{A}$$

$$\sigma = \frac{1}{\rho}$$

$$R = \frac{x}{\sigma A} \qquad \text{(A2.4)}$$

The electric field can be expressed as a function of the conductivity.

$$E_d = \frac{zFJA}{x}\frac{x}{\sigma A} = \frac{zFJ}{\sigma} \qquad \text{(A2.5)}$$

The Nernst-Planck equation states

$$J_i = \frac{z_i F}{RT} D_i c_i E_d \qquad \text{(A2.6)}$$

Replacing the electric field (equation A2.5) into the Nernst-Planck equation can be found the Nearest-Einstein equation (equation A2.7).

$$D_i = \frac{RT\sigma_i}{z_i^2 F^2 c_i} \qquad \text{(A2.7)}$$

APPENDIX 4: Procedure to run the Concrete Transport Properties neural network *"ANNcoventry v2.0"*

With the aim to give the possibility to all the concrete research community of using a novel technique to optimize the chloride related properties of a concrete sample is presented in this paper as a source open, a summary of the procedure necessary to run the model and the network file built under Matlab®. The method used to optimize the transport related properties of a concrete sample during a 6 hours ASTM C1202 migration test is a back propagation artificial neural network (ANN), where as inputs are necessary experimental observations of current and membrane potential under the conditions of the standard test.

1. Artificial Neural Network

The Artificial Neural Network uses a multilayer architecture: Six neurons define the input layer, corresponding to values of the current and the mid-point membrane potential at different times. A middle hidden layer has 3 neurons, and the output layer output has 7 neurons corresponding to the intrinsic diffusion coefficients of Cl^-, OH^-, Na^+ and K^+, the porosity, the hydroxide composition in the pore solution at the start of the test, and the binding capacity factor for chloride ions.

Figure A3.1 Multilayer neural architecture used

2. Input layer

From the standard ASTM-C1202 experiment the transient current and the mid point membrane potential are obtained. Below is shown a detailed procedure to obtain the inputs of the network with the materials presented in chapter 8.

a) Measure experimentally the physical current and the midpoint membrane potential.
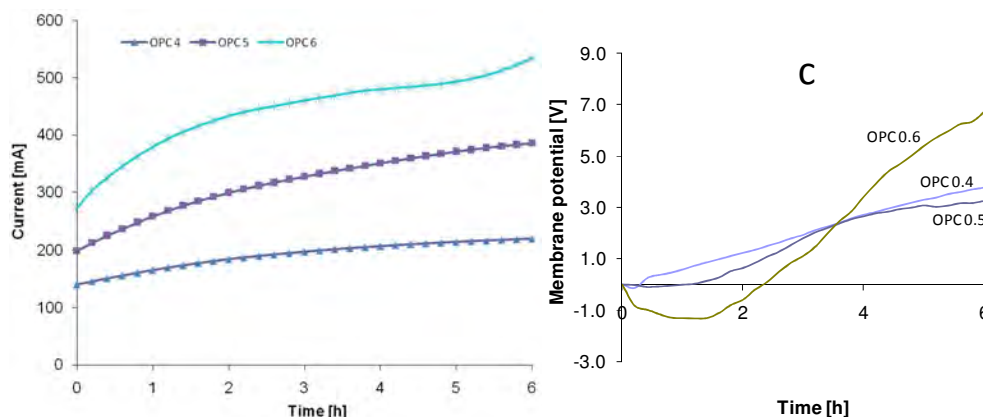
Figure A3.2 Membrane potential and current measured

b) Obtain values of membrane potential at 1.2, 3.6, and 6 hours, and current at 0, 3.6, and 6 hours.

	Voltaje MP [V]			Current [mA]		
Time [s]	1.2	3.6	6.0	0.0	3.6	6.0
OPC 4	0.7215	2.4105	3.7850	140.4	203.9	220.5
OPC 5	0.0365	2.3885	3.2730	199.4	342.2	386.1
OPC 6	-1.3135	2.4760	6.7320	272.5	474.5	535.4

Table A3.1 Values of current and membrane potential at specific times

c) To feed the neural network it is necessary normalize the data between -1 and +1 in order to avoid the influence of the scale of the physical quantities. A linear relationship is used to find the equivalence between the real coordinate systems and the natural systems (-1 to +1).
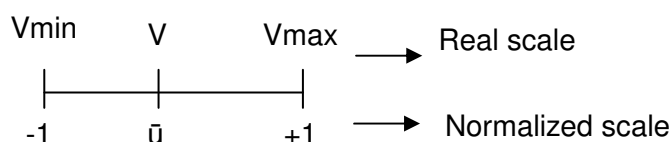
$$\overline{u} = \frac{2(V - V_{avg})}{V_{max} - V_{min}}$$

The corresponding constants to normalize the input experimental data are:

Time [s]	Voltage MP [V]			Current [mA]		
	1.2	3.6	6.0	0.0	3.6	6.0
V_{max}	2.20	6.48	7.56	298.40	552.34	512.24
V_{min}	-4.99	-9.79	-11.26	1.22	1.20	1.09
V_{avg}	-1.40	-1.66	-1.85	149.81	276.77	256.67
L	7.19	16.28	18.82	297.18	551.14	511.15

Table A3.2 Transformation matrix used to normalize the input data

The corresponding normalized values of membrane potential and electrical current are shown in table A3.3.

Time [s]	Membrane Potential			Current		
	1.2	3.6	6.0	0.0	3.6	6.0
OPC 4	0.589	0.500	0.599	-0.064	-0.264	-0.142
OPC 5	0.399	0.497	0.544	0.333	0.237	0.506
OPC 6	0.023	0.508	0.912	0.826	0.718	1.090

Table A3.3 Values of current and membrane potential normalized

3. Obtaining the transport related properties

d) Open Matlab® and type "*nntool*" to use the graphic interface of the neural network toolbox.
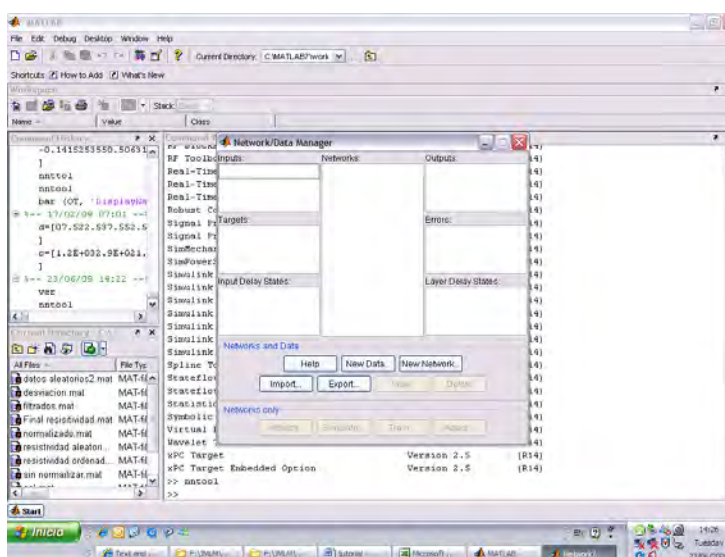
Figure A3.3 Screen of the Matlab® Neural Network tool box

e) Load the network file "**ANNcoventry V2.0**" to the Matlab® workspace and import that file to the network/Data manager. Create a matrix in the workspace with the inputs values and import it to the network/Data manager. Notice that the input data needs to be entered as matrix of dimension m_xn; m is always 6 (6 input neurons) and n is the number of mixes optimized (in this example 3). In this example the input matrix correspond to table A3.3 transposed.
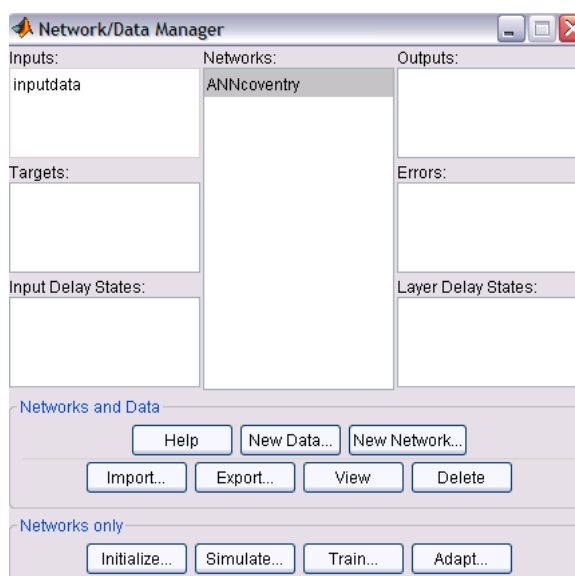
Figure A3.4 Screen of the network/Data manager

f) Open the window Simulate of the network and select as input the matrix "inputdata". To run click on simulate network. The outputs are saved in the network/Data manager and should be exported to the Matlab workspace.
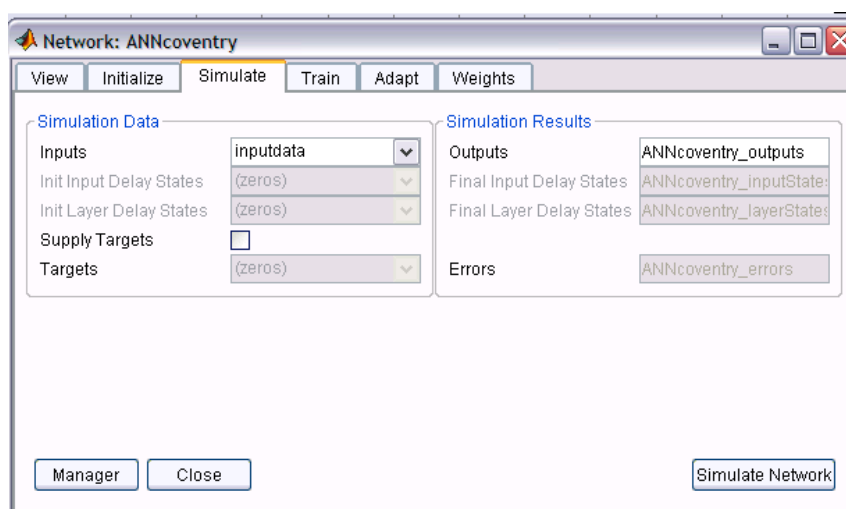
Figure A3.5 Simulation of the data

g) From Matlab® the output matrix has a dimension $m_x n$; m is always equal to 7 because in the output layer there are 7 neurons and n is equal to the number of mixes analyzed (in this case 3). Notice that the data is normalized, and then it is necessary to transform it to its real scale.

	Mix 0.4	Mix 0.5	Mix 0.6
OH Concentration	-0.15387	0.26557	0.86461
Cl Diffusion Coef.	-0.57714	-0.46121	-0.35184
OH Diffusion Coef.	-0.83219	-0.84062	-0.84619
Na Diffusion Coef.	-0.9479	-0.8947	-0.8162
K Diffusion Coef.	-0.98718	-0.94098	-0.85541
CL Capacity factor	-0.70277	-0.75393	-0.80106
Porosity	-0.01296	0.12976	0.22695

Table A3.4 Outputs of the network (normalized)

h) Each property is converted to its real scale with the following equation and transformation matrix.

$$V = \frac{\bar{U}(\bar{U}_{max} - \bar{U}_{min})}{2} + \bar{U}_{avg}$$

	OH conc	D_{Cl}	D_{OH}	D_{Na}	D_k	Cap Cl	porosity
$\bar{U}_{max}$	550	9.E-10	9.E-10	8.E-10	4.E-10	2	0.30
$\bar{U}_{min}$	30	7.E-12	3.E-12	2.E-12	2.E-12	0.16	0.05
$\bar{U}_{avg}$	290	4.54E-10	4.52E-10	4.01E-10	2.01E-10	0.896	0.18
L	520	8.93E-10	8.97E-10	7.99E-10	3.98E-10	1.47	0.25

Table A3.5 Transformation matrix used to find the real data

Finally, the optimized transport related properties are computed:

	OH conc [mol/m3]	D_{Cl} [m2/s]	D_{OH} [m2/s]	D_{Na} [m2/s]	D_k [m2/s]	Cap Cl	porosity
OPC 4	249.994	1.96E-10	7.83E-11	2.23E-11	4.55E-12	0.379	0.173
OPC 5	359.048	2.48E-10	7.45E-11	4.35E-11	1.37E-11	0.341	0.191
OPC 6	514.799	2.96E-10	7.20E-11	7.49E-11	3.08E-11	0.306	0.203

Table A3.6 Final transport related properties

APPENDIX 5: Results of capillary absorption

Mix	Capillary absorption equation	Correlation coefficient
O4W	i = 0.0911(t^0.5) + 0.0506	R^2 = 0.9986
O4A	i = 0.177(t^0.5) + 0.0244	R^2 = 0.9993
O5W	i = 0.1577(t^0.5) + 0.0803	R^2 = 0.9992
OG4W	i = 0.0659(t^0.5) + 0.0719	R^2 = 0.9806
OG4A	i= 0.1473(t^0.5) + 0.0583	R^2 = 0.9992
OG5W	i = 0.1453(t^0.5) + 0.0444	R^2 = 0.9871
OB4W	i = 0.0729(t^0.5) + 0.0668	R^2 = 0.9948
OB4A	i = 0.2133(t^0.5)- 0.0033	R^2 = 0.999
OB5w	i = 0.1354(t^0.5) + 0.0872	R^2 = 0.9971
OGB4W	i = 0.0722(t^0.5) + 0.0417	R^2 = 0.9874
OGB4A	i= 0.1943(t^0.5) + 0.0271	R^2 = 0.9992
OGB5W	I = 0.1303(t^0.5) + 0.0524	R^2 = 0.9895
BGB4W	i = 0.1783(t^0.5) + 0.0663	R^2 = 0.99
BGB4A	i = 0.3015(t^0.5) + 0.1034	R^2 = 0.9953
BGB5W	i = 0.246(t^0.5) + 0.124	R^2 = 0.9901
PGB4W	i= 0.1709(t^0.5) + 0.1031	R^2 = 0.99
PGB4A	i = 0.247(t^0.5) + 0.1043	R^2 = 0.9991
PGB5W	i= 0.2583(t^0.5) + 0.1243	R^2 = 0.9937

APPENDIX 6: Input data of the Neural Network algorithm

	Time [s]											
	Voltage Membrane Potential [V]						Total Current [mA]					
Mat	0.0	1.2	2.4	3.6	4.8	6.0	0.0	1.2	2.4	3.6	4.8	6.0
O4W	0.00	0.48	1.45	2.34	3.01	3.77	157	202	227	245	257	268
O4A	0.00	0.62	2.27	2.07	4.67	6.99	234	354	396	422	455	482
O5W	0.00	0.41	-1.08	-2.34	-3.14	-3.02	182	251	287	306	322	336
OG4W	0.00	-1.00	-1.40	-1.60	-1.64	-1.63	25	25	26	27	27	27
OG4A	0.00	0.24	0.79	1.68	2.85	3.95	86	112	136	147	140	127
OG5W	0.00	-0.26	-0.24	-0.23	-0.26	-0.34	29	30	31	31	31	31
OB4W	0.00	-0.41	0.44	1.79	2.33	2.90	168	219	246	262	274	285
OGB4W	0.00	-0.21	-0.03	0.21	0.45	0.66	34	35	37	38	39	39
OGB4A	0.00	0.42	1.64	3.68	5.87	6.63	129	196	253	263	233	203
OGB5W	0.00	0.05	0.06	-0.02	-0.11	-0.27	47	51	54	56	57	58
O5-A	0.00	-0.96	-0.16	1.30	2.58	3.72	134	187	216	231	241	251
OG5-10-A	0.00	-0.68	-0.40	0.62	1.41	2.80	128	168	193	208	216	220
OG5-30-A	0.00	-2.35	-2.03	-1.38	-0.14	1.03	67	70	86	90	92	93
OG5-50-A	0.00	-1.77	-2.49	-2.28	-1.96	-1.90	42	49	52	54	53	51
O4-B	0.00	0.72	1.50	2.41	3.19	3.79	140	170	190	204	214	220
O5-B	0.00	0.04	1.09	2.39	3.01	3.27	199	268	312	342	368	386
OG5-50-B	0.00	-0.36	-1.39	-1.94	-2.17	-2.03	23	24	25	26	26	26
OG5-30-B	0.00	-0.75	-0.93	-0.83	-0.69	-0.58	44	47	50	51	53	53
OG4-50-B	0.00	-1.34	-1.92	-2.31	-2.47	-2.52	17	17	18	18	18	18
OG4-30-B	0.00	-0.48	-0.34	-0.26	-0.14	-0.06	33	35	37	38	39	39

APPENDIX 7: Papers published

Effect of the non-linear membrane potential on the migration of ionic species in concrete

Juan Lizarazo Marriaga [a,*], Peter Claisse [b]

[a] Departamento de Ingeniería Civil, Universidad Nacional, Bogotá-Colombia
[b] Construction Materials Applied Research Group, Coventry University CV1 5FB, UK

ARTICLE INFO

ABSTRACT

In a concrete migration test the ionic species are present either in the boundary layer or in the pore solution and they flow as is indicated by the Nernst–Planck equation. This equation supposes that the flux of each ion is independent of every other one. However, due to ion–ion interactions there are ionic fields that affect the final flux producing an additional voltage known as the membrane potential. In order to understand this phenomenon, this paper describes a theoretical and experimental investigation of the implications of the membrane potential on the migration of chlorides in concrete. A new electrochemical test has been carried out and its results were compared with a numerical simulation. From the results it has been proved that the voltage drop during a migration test is not linear and changes during the test. Thus the Nernst–Planck equation may be applied to the simulation of migration of any ionic species through a saturated porous medium by using the non-linear voltage to represent all the microscopic interactions in a macroscopic way. The results may be used to improve the reliability of the ASTM C1202 chloride migration test.

1. Introduction

The rate at which chloride ions can diffuse through concrete is strongly related to the corrosion of reinforcement in structures. If chloride ions reach the vicinity of the rebar, the passive film around the steel bar can be broken and the process of corrosion can start. The mechanisms that control the penetration of chloride into saturated concrete are complex and understanding them is essential for the design assessment of durable reinforced concrete. When the ions move, their negative charge creates an electrostatic field which causes them to interact with other ions in the area. The other ions may be more chloride or other mobile species such as hydroxyl, sodium, or potassium. These processes will affect the transport of ions with or without an applied electric field.

Pure diffusion tests take long time; however, engineering and construction times are shorter. To solve this problem, pure diffusion can be accelerated by the application of an electrical potential gradient (migration tests). Under the influence of an electric field ions experience a force directing them toward the electrode that has the opposite charge to the ion [1]. The time needed to perform a pure diffusion test may be months; but, a migration test can be done in just days or hours. Thus there is a need to provide a better

understanding of migration tests so the results may be interpreted more accurately.

The migration of ions into concrete is controlled by the following factors:

- the chemical potential of the ion (concentration gradient),
- the applied electrical potential (if it exists),
- the charge of the ion,
- the concentration of each species in the pore solution,
- the porosity and tortuosity of the pore network,
- the chemical reactions between the ions present in the porous and the cement hydration products. These reactions can either be of dissolution, decalcification or binding [2,3].

The particular concern when testing concrete is that a durable concrete in which chlorides do not penetrate the cover layer will have low porosity, high tortuosity and high binding capacity. When a pozzolanic admixture is added it will react with the free lime and reduce the hydroxyl ion concentration. This will reduce the measured migration current but will not necessarily make the concrete more durable because the porosity, tortuosity and binding may be unaffected.

Different approaches have been used in recent years to model the ionic penetration of chlorides through concrete. In order to understand this phenomenon, this paper reports on a theoretical and experimental investigation to give a better explanation for the

* Corresponding author. Tel.: +571 3165000.
E-mail address: jmlizarazom@unal.edu.co (J.L. Marriaga).

movement of chloride ions and any other species in concrete under the influence of an applied electric field. The principal research was to determine the voltage within a sample during the ASTM C1202 rapid chloride test by simulating the movement of ions. The results of the experimental program were compared with these numerical simulations. The non-linear behaviour of the electrical field during normal diffusion and migration has been reported previously by some researchers [4–6], however, the authors are not aware of any experimental evidence for it. The only reference found for this was the work made by Zhang et al. [7,8] who measured the total membrane potential across a sample of concrete in a diffusion test.

1.1. Research objectives

In summary, the objectives of this work are as follows:

(1) To develop a theoretical explanation for the movements of chloride ions in concrete under the influence of an applied electric field.
(2) To use the theory to calculate the evolution of the voltage within a sample during the ASTM C1202 rapid chloride test.
(3) To provide an experimental validation of the theory when applied to the ASTM C1202 test.
(4) To enable the problem with the ASTM C1202 test to be overcome. This problem gives misleadingly low results if pozzolanic admixtures such as pulverised fuel ash or silica fume are added to concrete.

The method to be validated in (3) calculates the mid-point voltage at different times from the known properties of the sample, particularly the chloride diffusion coefficient. To achieve the final objective (4) it is necessary to calculate the properties from observations of the voltage. This may be achieved by running the model a number of times and using the results as a database in order to obtain the input data from known output. This may, for example, be achieved with an Artificial Neural Network which is trained using output from the model.

2. Theory

2.1. Modelling the migration test

In a fully saturated concrete sample there may be a difference in the concentration of ions in different regions. If a constant electric potential is applied, as in the ASTM C1202 (RCPT) test [9] or NT-492 [10], the total flux J_i for each species in the system must be the sum of the migration flux $(J_M)_i$ and the diffusion flux $(J_D)_i$.

$$J_i = (J_M)_i + (J_D)_i \tag{1}$$

The diffusional flux due to a concentration gradient in a solution has been known empirically since 1855 as Fick's first law [11]:

$$(J_D)_i = -D_i \frac{\partial c_i}{\partial x} \tag{2}$$

where J_i is the flux of species i (mol/(m^2 s)), D_i is the diffusion coefficient of species i (m^2/s), c_i is the ionic concentration of species i in the pore fluid (mol/m^3), and x is the distance (m).

In an ideal solution the driving force for diffusion can be considered in terms of the chemical potential of the particular species. In the same way, the driving force for migration is proportional to the external electric field. In an electrolytic system under a difference of potential, the transport of charge is ionic transport. The migration flux of species i is defined in the following equation [12]:

$$(J_M)_i = -u_i z_i F_i c_i \frac{\partial E}{\partial x} \tag{3}$$

where u_i is the mobility of species i in the pore fluid (m^2 s^{-1} V^{-1}), z_i is the electrical charge of species i, F is the Faraday constant (9.65×10^4 C/mol), and E is the electrical potential (V). In the same way, the diffusion coefficient is proportional to the mobility of each ion [1]:

$$D_i = RTu_i \tag{4}$$

The general law governing the ionic movements in concrete is considered to be due to the chemical and electrical potential [13], and is known as the Nernst–Planck equation:

$$J_i = -D_i \frac{\partial c_i}{\partial x} - \frac{z_i F}{RT} D_i c_i \frac{\partial E}{\partial x} \tag{5}$$

where R is the gas constant (8.31 J/(mol K) and T is the absolute temperature (K). The Nernst–Planck equation supposes that the flux of each ion is independent of every other one; however, due to ion–ion interactions there are ionic fields that affect the final flux. The drift of a species i is affected by the flows of other species present. The law of electroneutrality ensures that no excess of charge is introduced [1]. Under a concrete migration test, the current density into any point will equal the current out of it (Kirchoff's law):

$$0 = F \sum_i z_i J_i \tag{6}$$

Faraday's law states the equivalence of the current density (i_i) and the ionic flux:

$$i_i = -z_i F J_i \tag{7}$$

In an electrolyte solution in which concentration gradients of the ionic species and an electrical field are present, the total current density (i_T) is equal to the sum of the current density produced by the diffusion and the migration conditions:

$$i_T = -\sum_i z_i F(J_D + J_M)_i \tag{8}$$

The total current can be given by a combination of Eqs. (2)–(4):

$$i_T = \sum_i z_i FRT u_i \frac{\partial c_i}{\partial x} + \sum_i z_i^2 F^2 u_i c_i \frac{\partial E}{\partial x} \tag{9}$$

The electric potential gradient is given by two terms: a linear or ohmic potential and a non-linear or membrane potential:

$$\frac{\partial E}{\partial x} = \underbrace{\frac{i_T}{\left(\sum_i z_i^2 F^2 u_i c\right)}}_{\text{ohmic potential}} - \underbrace{\frac{\sum_i z_i FRT u_i (\partial c_i/\partial x)}{\left(\sum_i z_i^2 F^2 u_i c\right)}}_{\text{membrane potential}} \tag{10}$$

The first term is related to the ohmic potential when an external voltage is applied and is characteristic for charge transfer accounting exclusively the migration driving forces. The second term of Eq. (10) is that for the membrane potential gradient $\partial E_p/\partial x$, formed when various charged species have different mobility. In a concrete migration test the non-linearity of the electric field is due to the membrane potential gradient and it is equivalent to the liquid junction potential [4]:

$$\frac{\partial E_p}{\partial x} = -\frac{RT}{F} \frac{\sum_i z_i u_i (\partial c_i/\partial x)}{\sum_i z_i^2 u_i c_i} \tag{11}$$

Likewise, the electric field due to the diffusion potential can be expressed in terms of the transference number (t_i) [3]:

$$\frac{\partial E_p}{\partial x} = \frac{RT}{F} \sum_i \frac{t_i}{z_i} \frac{\partial \ln c_i}{\partial x} \tag{12}$$

The non-linearity of the electric field in a migration test can be explained from a physical point of view. At the start of the test the field is uniform across the concrete, however, when the different

ions start to migrate they cannot move freely, they are charged particles and interact with species of opposite signs. The membrane potential affects the electric field across the concrete and its effect over the sample can be explained in term of resistances. Each point into the concrete sample has a changing resistivity as the free and adsorbed ionic concentrations in it change during the test.

2.2. Review of modelling of the chloride diffusion–migration

Different approaches have been proposed in order to simulate the penetration of chloride into the concrete taking into account all the different species and an external electrical driving force. Truc et al. [14] proposed a numerical model based on a finite difference method for the flux of several species with the Poisson–Nernst–Planck equations. Sugiyama et al. [2] presented a method for numerically calculating the concentration profiles of chloride ions (Cl^-) in concrete; the method is based on the generalized form of Fick's First Law suggested by Onsager. Narsilio et al. [15] simulated electromigration tests solving the Nernst–Planck equation coupled with the electroneutrality condition using a finite element method. Khitab et al. [5] developed a numerical model to predict the chloride penetration solving the Nernst–Planck equation coupled with the current laws. A numerical model was developed by Claisse and Beresford [16] using the Nernst–Planck equation and maintaining charge neutrality by modelling changes to the voltage distribution. Lorente et al. [4] showed a model based on a second-order finite difference procedure that solves the law of mass conservation equation for each species and an electrical field equation for the overall system. Samson et al. [17] presented a model to solve the transport of ions in saturated materials during a migration test using a finite element method. More recently, Krabbenhoft and Krabbenhoft [6] solved the Poisson–Nernst–Planck equations analytically and derived an expression for the diffusion using a non-linear finite element procedure.

The assumption that the electrical field remains constant under a migration test has been pointed out by many researchers [15] and standards [10,18]. However, the electrical field can be accounted for a macroscopic way from Eq. (11) [4,5]. A more complex expression can be found for the electrical field, if the Nernst–Planck includes a chemical activity coefficient (γ) [19], however, it has been showed that the activity term does not increase the accuracy of the results in a concrete migration test [17,20].

In a migration test the species present either in the boundary layer or in the pore solution of the sample (Na^+, K^+, Ca^+, OH^-, and Cl^-) flow as is indicated by the Nernst–Planck equation. An increase in concentrations at specific points in the sample leads to variations in the electric field and the variation in the electric fields lead to variations in the flux of each ion. In the same way, the concentration and chemical composition of the pore structure of concrete at the start of the test are very important factors that need to be considered during the simulation. Truc et al. [14] found big differences in the migration of chlorides when the composition of the pore solution is included in the model.

From a microscopic point of view, the diffusion of chlorides can be affected by the effect of ionic interaction with other ions present into the pore solution and the effect of the known electrical double layer [21]. For a diluted solution, the ion–ion interaction produces a change in the chemical potential. The *Debye Huckel theory* [1] can be used as a qualitative tool in order to understand the phenomenon. The effect of the electrical double layer during diffusion is the generation of an additional electrical voltage at the interface between the pore wall and the pore solution [22]. Castelote et al. [23] found that during a migration test the effect of the electrical double layer does not seem to change the electrostatic interactions between the surface of the pores and the ions under migration.

From a macroscopic and engineering point of view, in normal diffusion the effects of the ionic interaction and the electrical double layer affect the mobility of chlorides generating a membrane electrical potential which may be opposed to the chemical potential. As was pointed out by Lorente et al. [4], the Nernst–Planck equation must be used in natural diffusion (i.e. with no applied voltage) instead of Fick's laws in order not to neglect the effect of the membrane potential.

The numerical model used in this research was developed in the Construction Materials Applied Research Group of Coventry University [16]. It works by repeated application of the Nernst–Planck equation through time and space. To avoid discontinuities in the results the time step is reduced so the concentration does not change by more than 10% during any time step. The model was proposed for four ions in the pore solution, but can be easily changed to each number of ions. The transport processes into the concrete were restricted by binding with linear isotherms. A linear isotherm defines a linear relationship between free and the bound ions over a range of concentration at a given temperature.

The effects of voltage changes in a migration test are applied in the model by distorting the voltage in each space step and checked by ensuring that charge neutrality is maintained throughout the sample at all times for all the ions together. At each time step adjustments are made to ensure that the total voltage across the sample is correct. Ion generation and removal at the electrodes is represented in the model by assuming that the ions being generated and removed are always hydroxyl ions. The model includes provision for the depletion on the reservoirs at either side of the sample. A conceptual diagram of the model is shown in Fig. 1.

3. Experimental

3.1. New experiments

An experimental program has been carried out to understand the voltage drop in a migration test and in order to investigate the influence of the non-linear membrane potential in the diffusion of ionic species. The experimental results were used to validate and calibrate the numerical model used in this paper.

The apparatus used in this research was similar to ASTM C1202, but salt bridges were added in the concrete to check the voltage distribution across the sample (Fig. 2). 4-mm diameter holes were drilled in each sample 5–8 mm deep. The salt bridge pipes were 4.5 mm diameter and were inserted into each hole. The salt bridges used a solution of 0.1 M of potassium chloride (KCL) because both ions in it have similar mobility so no significant voltage would be set up at the interface of the salt solution and the concrete pore solution. In a previous research, Zhang et al. [8] measured the membrane potential across OPC mortar specimens during a diffusion test using reference electrodes and salt bridges in external cells. They found that for different simulated pore solutions the total junction potentials formed between the measurement devices and the simulated pore solution were in the range of −0.8 to −6 mV. Those values were relatively low compared with the membrane potential measured during the migration tests, so, the liquid junction potential formed between the salt bridge and the pore solution concrete sample was not taken account in the research reported in this paper.

The voltage was measured relative to the cathode using a saturated calomel electrode (SCE) connected to the salt bridge. For each test, the current across the concrete and the voltage at different points in the sample were measured continuously with a data logger. The tests were carried out in a temperature controlled room at $21 \pm 2\,°C$. During the tests the temperature was measured continuously in the anodic reservoir. Fig. 2 shows the cell and
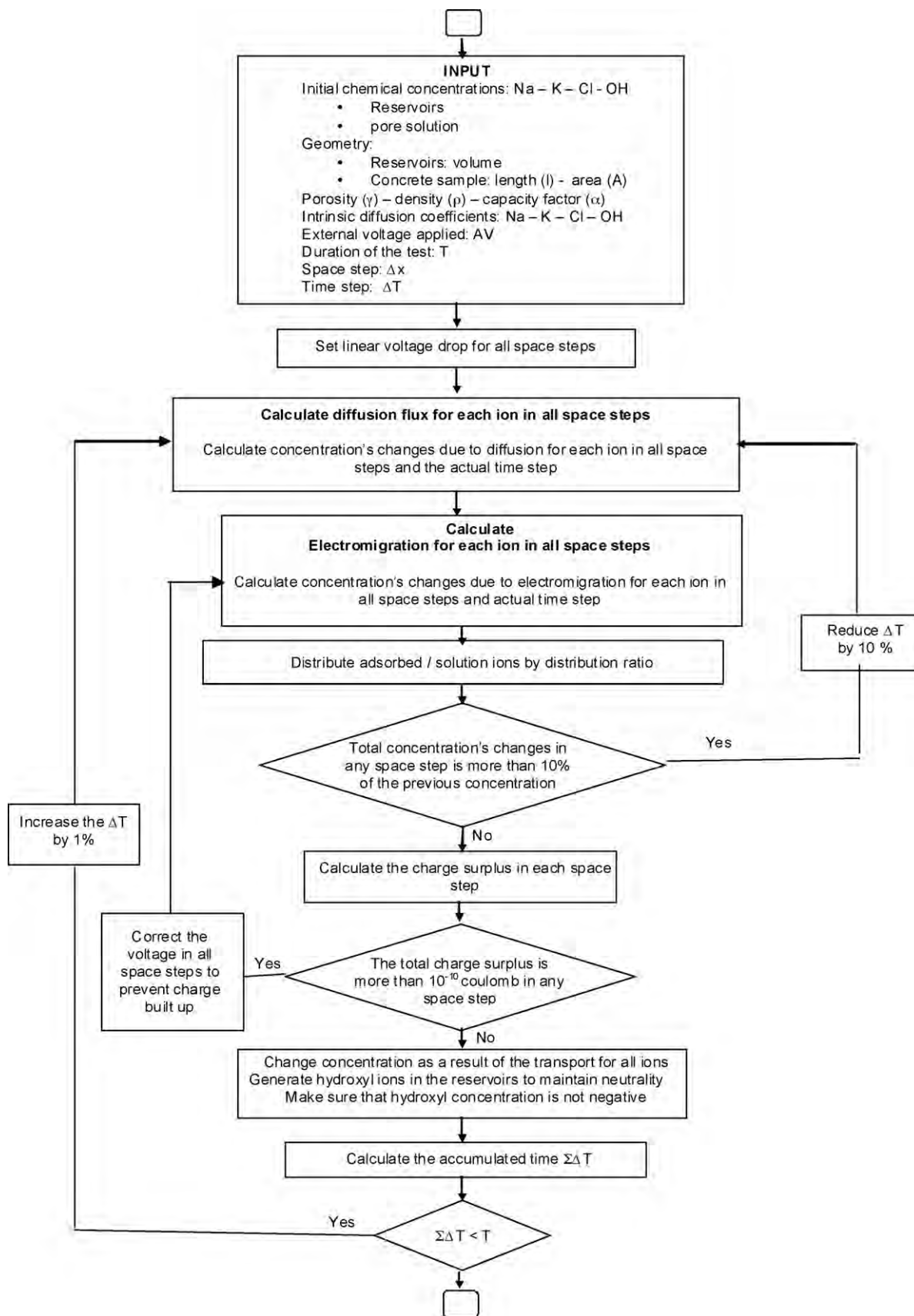
Fig. 1. Computer model used in this research.
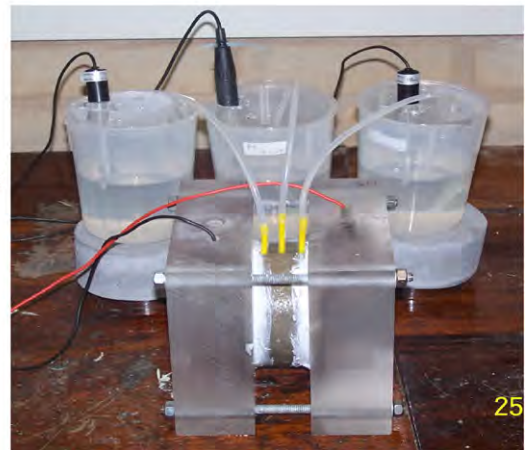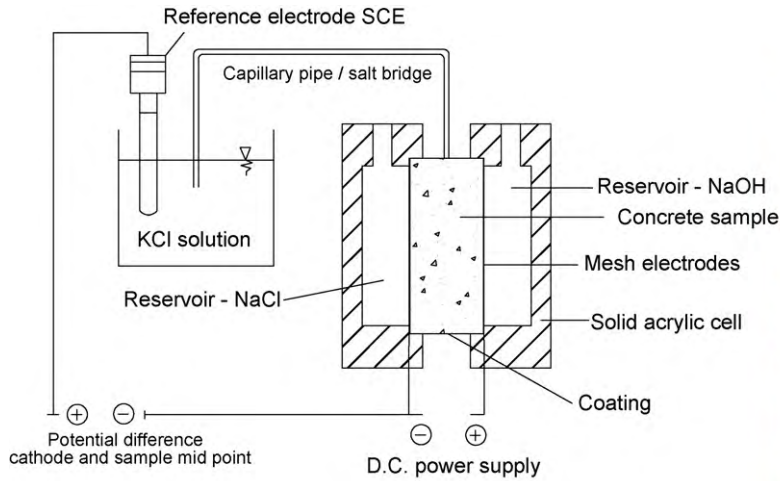
Fig. 2. Cell and salt bridge.
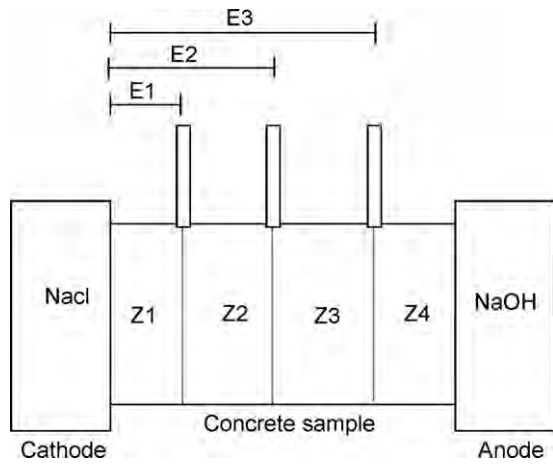
Fig. 3. Locations where the voltage was measured.

the salt bridge. The volume of the anode and cathode chambers with the concrete sample ready for the tests was approximately 200 ml.

A 3 A, 70 V programmable DC power supply was used. The data logger had 16 analogue inputs with 12-bit resolution (0–2.4 V SE or ±2.4 V diff.). A very high input impedance was required in order to ensure that the measuring process did not change the voltage readings. The internal resistance of the data logger had to be significantly greater than the resistance of the concrete during the test, because when measuring voltages the resistance of the equipment itself has an effect on the voltage of the circuit. To achieve the required analog input performance of the data logger, it had a high resistance voltage divider followed by an operational amplifier configured as a voltage follower.

3.2. Material and test procedures

Mixes of mortar with water to cement ratio of 0.49 (mix 1) and 0.65 (mix 2) were cast. Ordinary Portland cement CEM I without mineral or chemical admixtures was used. The ratio binder/sand was 2.75 for all mixes. For each mix five cylinders of 100 mm diameter and 200 mm height were made to be used in porosity and migration tests. The open porosity accessible by water (P) was measured using the simple method of water displacement. The central part of each cylinder (30 mm thickness) was vacuum saturated until constant weight and weighed in water (W_w) and air (W_a). They were then dried in an oven at 105 °C until constant weight and weighed again (W_d). The porosity was found with Eq. (13). Three replicates were tested for each mix. In addition, three 50 mm cubes for each
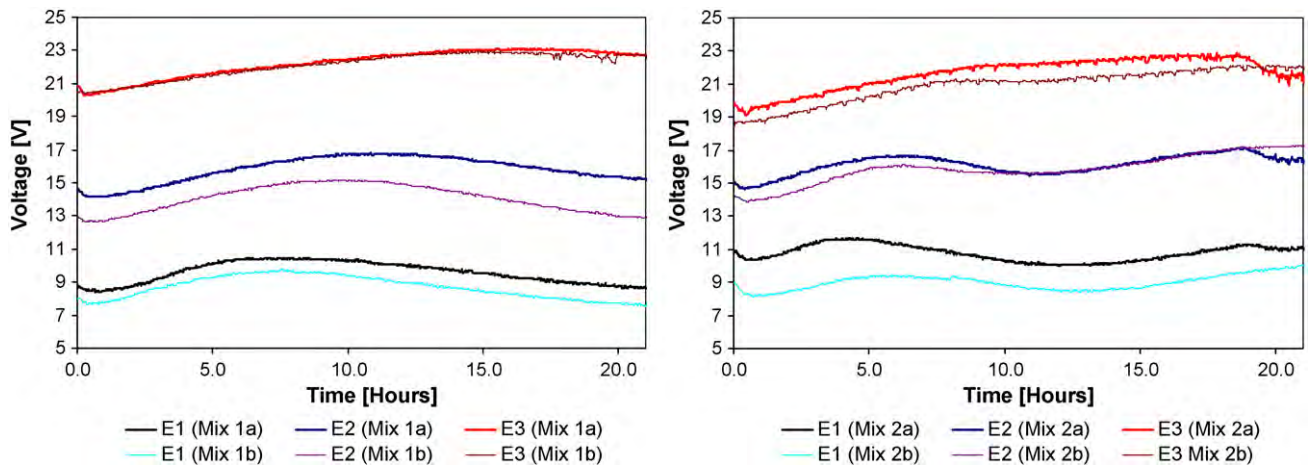
Fig. 4. Difference of potential across the sample.

Table 1
Results of compressive strength and porosity.

Mix	Water/binder	Concrete strength (28 days) (MPa)	Open porosity (%)
1	0.49	36.59	18.5
2	0.65	31.48	25.4

mix were cast in order to measure the mortar strength:

$$P = \frac{W_a - W_d}{W_a - W_w} \tag{13}$$

The specimens were cured under controlled humidity and temperature and all the migration tests were made at ages between 28 and 38 days. The mortar cylinders cast (100 mm diameter and 200 mm high) were cut to 50 mm thick and 100 mm diameter. Two samples were taken of each cylinder, being taken from its central part. The test was run on two replicate samples and the reported result is the average of both results. The anode and cathode reservoir cells were filled with a 0.30N NaOH and a 3.0% NaCl solution, respectively (as specified in ASTM C1202), and a DC voltage of 30 V were applied for 21 h. This voltage was lower than the specified in the ASTM standard because 60 V caused unacceptable heating. The current was monitored every 2 min as well as the potential difference between the salt bridges in the sample and the negative electrode of the system.

For both mixes the voltages were measured at three different positions. The target location of those points was the mid point and the quarters of each sample. The distance between the points where the potential was measured and the edge of the sample in contact with the negative electrode (cathode) is shown in Fig. 3. The locations of the salt bridges define four zones named as Z1, Z2, Z3 and Z4 and the electric potential difference across each one was measured.

As at the start of the test the electric field is linear across the sample. The gradient or difference between the measured voltage at any time and the linear condition can be calculated. This value corresponds to the membrane potential and is calculated by subtracting the value of the voltage measured from the initial value measured at the start of the test for each time and position:

$$\Delta V = V_{ti} - V_0 \tag{14}$$

ΔV corresponds to the membrane potential, V_{Ti} is the voltage measured at time t, and V_0 is the voltage at the start of the test. In order to avoid the noise found experimentally during the logging of the tests a commercial curve fitting software was used. It was found that this noise was substantially reduced by slightly increasing the depths of the drilled holes for the salt bridges. This observation indicates that the noise was caused by the random distribution of aggregate limiting the contact between the salt bridges and the pore volume.

4. Results and discussion

4.1. Experimental results

The results of strength and porosity are shown in Table 1. Fig. 4 shows the variation of the voltage across the sample in the mixes tested. Points E1, E2, and E3 are the points where the voltage was measured at the quarters and the mid point of the sample. Although for all the samples there was noise in the voltage, there is a good defined trend and the profile for the replicates in each mix were very similar. The voltage for each sample was not linear with respect to time and position during the test and the profile was related with the features of the sample and the conditions of the test.

The behaviour of the membrane potential across the sample during the test is shown in Figs. 5 and 6 as contour graphs, each graph represents the average of two samples. The value for the mem-
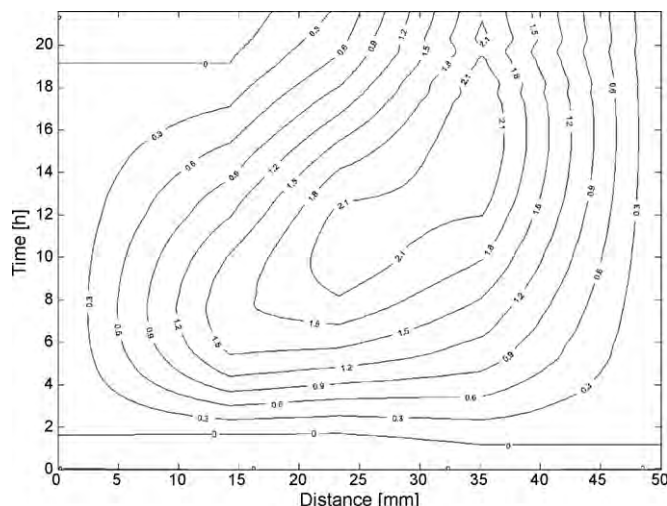
Fig. 5. Average membrane potential (V), mix 1 : $w/b = 0.49$.

brane potential at the edges of the sample was assumed as zero because those points correspond to the electrodes in the solutions. Both mixes showed a similar distribution of the membrane potential. There was an increase of voltage in the area that was near to the alkaline solution (positive electrode) and both mixes reached a maximum value of voltage with a subsequent reduction. In the area near to the cathode, the membrane potential either tended to be constant during the test or presented a smooth negative variation.

From the contour plots all the membrane potentials at any point throughout the duration of the test can be seen. However tests of this type are expensive and not easy to complete. As alternative, it has been proposed to study just the behaviour of the mid point as a source of additional information in a practical situation. It is expected that the mid-point voltage would provide sufficient information for most practical purposes.

4.2. Simulation of the migration tests

In order to validate the numerical model both migration tests were simulated. The test for mix 1 ($w/b = 0.49$) was selected as initial comparison and in the simulation of mix 2 ($w/b = 0.65$) the value of the porosity was adjusted to obtain the value measured experimentally. The characteristics of the system sample/cells are
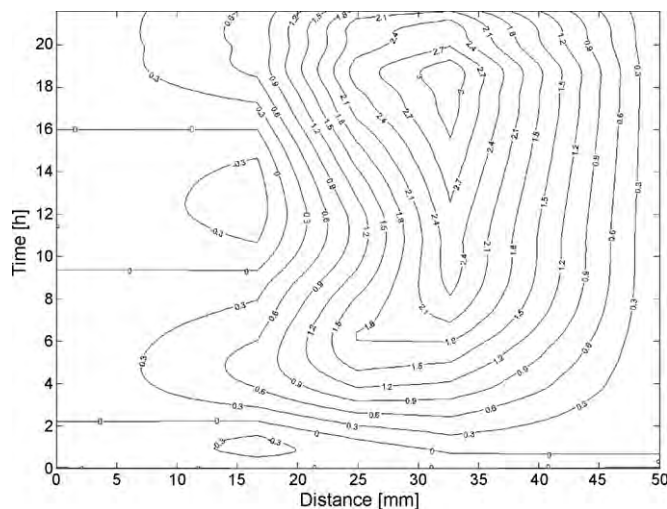
Fig. 6. Average membrane potential (V), mix 2 : $w/b = 0.65$.

Table 2
Input parameters at the start of the test.

	Intrinsic diffusion D (m^2/s)	Concentration (mol/m^3) upstream (negative)	Concentration (mol/m^3) pore solution	Concentration (mol/m^3) downstream (positive)
Hydroxyl	1.60E−10	0	240	300
Chloride	3.00E−10	529	0.0	0
Sodium	4.00E−11	529	79	300
Potassium	9.00E−12	0	161	0
Sample length/radius (m)		0.05/0.05	Run time (h)	21
Ext. voltage (V)		30	Porosity	0.19
Cell volumes (m^3)		0.0002	Cl capacity factor	0.3

shown in Table 2. For this particular simulation, the initial pore solution concentration was based on published results [24]. The intrinsic diffusion coefficients for all the ions were obtained applying for the mix 1 an optimization process. The computer program was run enough times to find the best combination of coefficients to fit the experimental values of current and membrane potential in the mid point of the sample.

The intrinsic diffusion coefficients for sodium and potassium found were significantly lower than the values for chlorides and hydroxides as observed previously by other researchers [8,13]. Those results confirm that the mobility of cations in porous media has a different behaviour than when they diffuse in an ideal solution. In the same way, the observed intrinsic diffusion coefficients for chlorides and hydroxides show that both ions are responsible for the most transport of charge, however, small changes in the diffusion of cations produce large changes in the mid-point membrane potential. Although the ratio of the intrinsic diffusion coefficients of chloride and hydroxide was greater than one, it is apparent that the high mobility of chlorides is reduced in the computer model through the interactions between the ions and the hydration products of concrete using a linear isotherm.

The total electrical current through the samples is shown in Fig. 7 where the experimental results are presented with the simulations for mixes 1 and 2. For mix 1—the current modelled was presented both with the membrane potential and without any voltage correction. The experimental results and the simulation with the membrane potential were in good agreement, being better for initial times than for long times; the difference between them at the end of the tests was around 35%. In contrast, the profile of the current without including the membrane potential showed big differences respect to the experimental results. Although the initial current was similar, there was a maximum value of current three times greater than when was the voltage corrected. The current passed by mix 2 presented a similar profile for the experimental results and the simulations with the membrane potential correc-
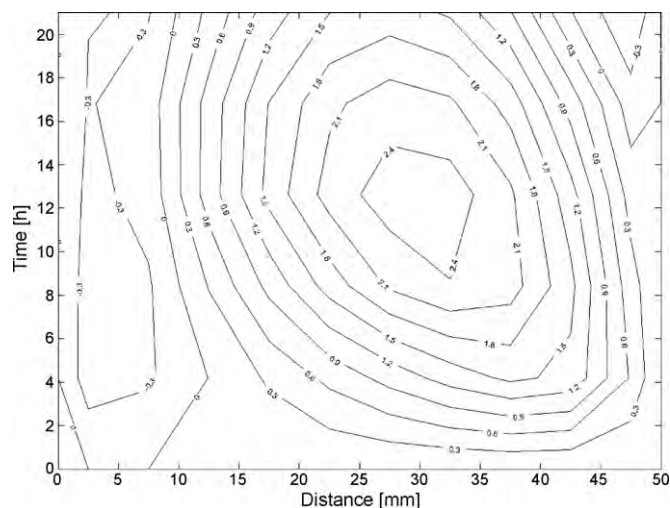
Fig. 8. Simulated membrane potential (V), (mix 1 : $w/b = 0.49$).

tions. As was expected, the last mix showed higher values of current because of its higher water cement ratio.

The behaviour of the simulated membrane potential of mix 1 across the sample and during the test is shown in Fig. 8 as a contour graph. The numerical values were taken from the numerical program and plotted with the contour function of Matlab®. The simulated membrane potential behaves in the same way as the corresponding experiment (Fig. 5). The voltage was negative in the first half of the sample during all the experiment; in contrast, the second half of the sample had positive values of membrane potential. The simulated and measured mid-point membrane potential is shown in Fig. 9 for mix 1. Although the measured profile showed some initial negative values and reached a local maximum membrane
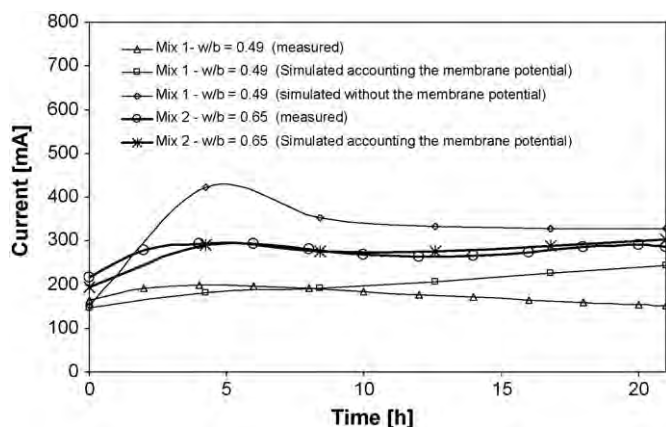
Fig. 7. Current variations during the experiments.
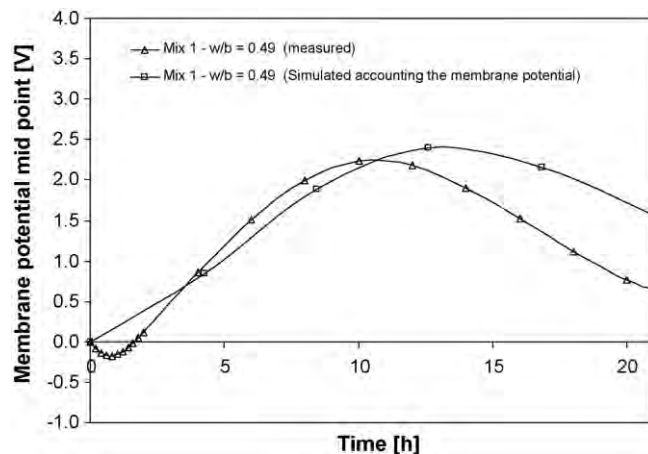
Fig. 9. Simulated membrane potential (V), mid-point mix 1 : $w/b = 0$.
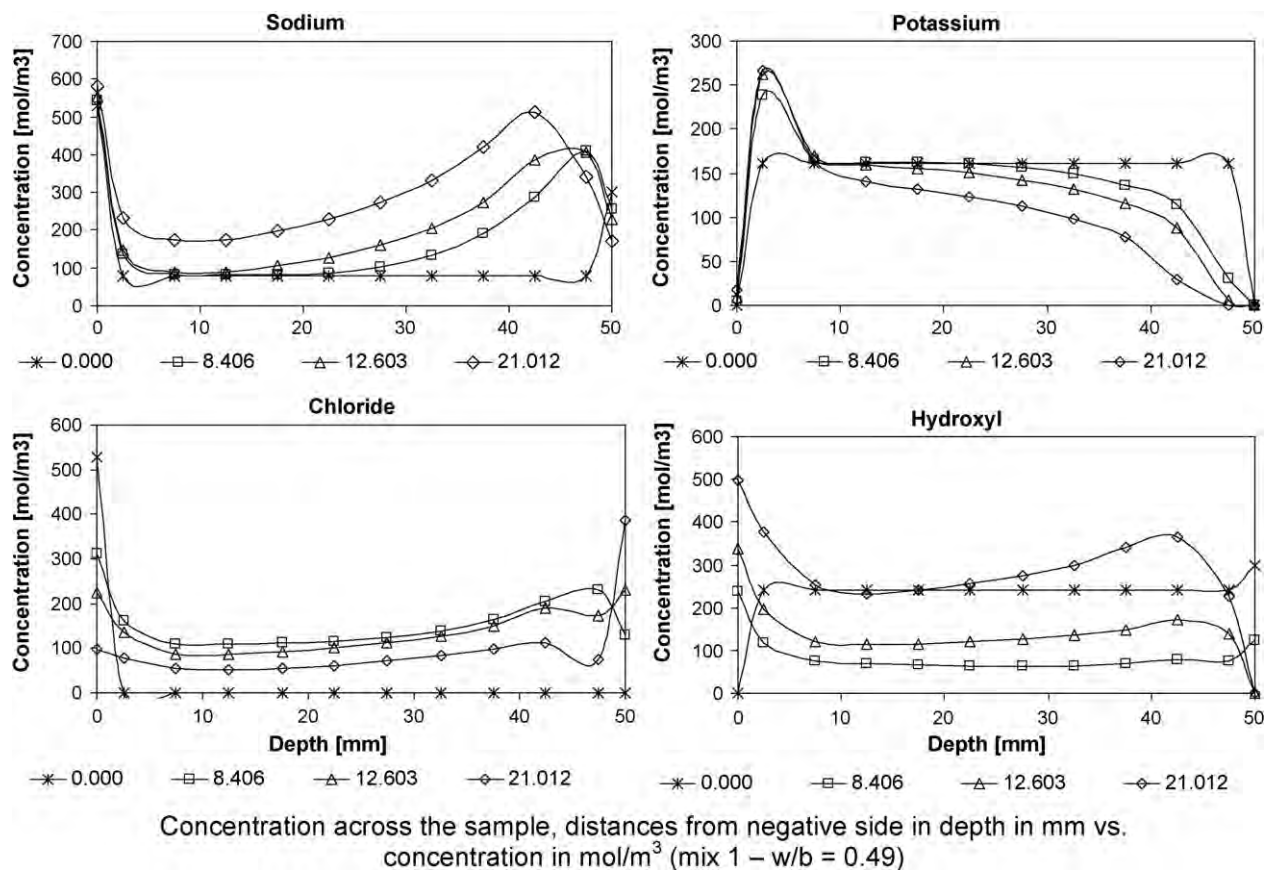
Fig. 10. Concentration across the sample, distances from negative side in depth in mm vs. concentration in mol/m^3 (mix 1 : $w/b = 0.49$).

potential voltage before the simulations, both graphs showed similar behaviour and have same profile. From a macroscopic point of view, the local maximum or any feature of the mid-point membrane potential can be explained as a result of the variation of the conductivity of the pore solution due to the migrations of all ions involved. The transient conductivity is defined by the relationship between the transient voltage and the transient current at any point.

The transport properties of any specific mortar or concrete mix can be determined accurately using together with the model any optimization technique. This may be achieved by running the model a number of times and using the results as a database in order to obtain the input data from known output. This may, for example, be achieved with an Artificial Neural Network which is trained using output from the model, so that a transient current and a transient membrane potential measured experimentally can be used to calculate the diffusion coefficients for all the ions involved during the test.

Although the principal aim of the computer model is simulate the chloride penetration, the profile of the other ions is calculated as result of the interaction between them. The relationship between the transport properties of the chlorides and the hydroxide ion has been recognised for long time ago, however, the transport of potassium and sodium in concrete is not extensively studied in the literature. Fig. 10 shows the profiles of concentration for the four ions used during the simulation of mix 1.

5. Conclusions

· From the experimental program carried out and from the simulations made, the membrane potential was simulated and it has been proved that the voltage drop in concrete or mortar samples during a migration test is not linear with respect to time

and position. The application of the Nernst–Planck equation to the simulation of migration of any ionic species through a saturated porous medium accounting for the non-linear voltage allows models to include all the microscopic interactions in a macroscopic way.

· All the ions (sodium, potassium, hydroxide and chlorides) present in a migration test, either in the pore solution or coming from the external cells, need to be included in the simulation in order to account the non-linear effects caused by differences of mobility. The computer model proposed predicts in a proper way the transient current and the membrane potential during the experiments.

· This model may be used to solve the problem with the ASTM C1202 procedure which occurs when it is used to test concrete or mortar with pozzolanic admixtures.

Acknowledgements

References

[1] J. Bockris, A. Reddy, Modern Electrochemistry 1 Ionics, Plenum Press, 1998.
[2] T. Sugiyama, W. Ritthichauy, Y. Tsuji, J. Adv. Concrete Technol. 1 (2003) 127.
[3] C. Yang, Cement Concrete Res. 36 (2006) 1304.
[4] S. Lorente, D. Voinitchi, P. Bégué-Escaffit, X. Bourbon, J. Appl. Phys. 101 (2007) 024907.
[5] A. Khitab, S. Lorente, J.P. Ollivier, Mag. Concrete Res. 57 (2005) 511.
[6] K. Krabbenhoft, J. Krabbenhoft, Cement Concrete Res. 38 (2008) 77.
[7] J.Z. Zhang, N.R. Buenfeld, Cement Concrete Res. 27 (1997) 853.
[8] J.Z. Zhang, J. Li, N.R. Buenfeld, Cement Concrete Comp. 24 (2002) 451.

[9] ASTM C 1202, Standard Test Method for Electrical Indication of Concrete's Ability to Resist Chloride Ion Penetration, 2005.

[10] NTBUILD 492, Nordtest method: concrete, mortar and cement-based repair materials: chloride migration coefficient from non-steady state migration experiments, 1999.

[11] P.A.M. Basheer, in: V.S. Ramachandran, J.J. Beaudoin (Eds.), Handbook of Analytical Techniques in Concrete Science and Technology, Noyes Publications, 2001, p. 16.

[12] C.H. Hamann, A. Hamnett, W. Vielstich, Electrochemistry, 2nd ed., Wiley, 2007.

[13] C. Andrade, Cement Concrete Res. 23 (1993) 724.

[14] O. Truc, J.P. Ollivier, L.O. Nilsson, Cement Concrete Res. 30 (2000) 1581.

[15] G. Narsilio, R. Li, P. Pivonka, D.W. Smith, Cement Concrete Res. 37 (2007) 1152.

[16] P. Claisse, T.W. Beresford, Proceedings of the Fourth CANMET/ACI International Conference on Durability of Concrete, vol. 170, Australia, 1997, p. 1119, ACI-SP.

[17] E. Samson, J. Marchand, K.A. Snyder, Mater. Struct. 36 (2003) 156.

[18] JSCE-G571, Test Method for Effective Diffusion Coefficient of Chloride Ion in Concrete by Migration, Japan Society of Civil Engineers, 2003.

[19] O. Truc, Prediction of chloride penetration into saturated concrete—multi-species-approach, Ph.D Thesis, Chalmers University, Goteborg, Sweden, 2000.

[20] L. Tang, Cement Concrete Res. 29 (1999) 1469.

[21] T. Zhang, O.E. Gjørv, Cement Concrete Res. 26 (1996) 907.

[22] H. Friedmann, O. Amiri, A. Aït-Mokhtar, P. Dumargue, Cement Concrete Res. 34 (2004) 1967.

[23] M. Castellote, C. Alonso, C. Andrade, G.A. Chadbourn, C.L. Page, Cement Concrete Res. 31 (2001) 621.

[24] P. Pedeferri, R.B. Polder, in: L. Bertolini, B. Elsener (Eds.), Corrosion of Steel in Concrete: Prevention, Diagnosis, Repair, Wiley, 2004.
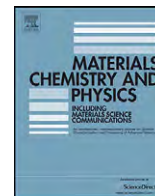
Determination of the concrete chloride diffusion coefficient based on an electrochemical test and an optimization model

Juan Lizarazo-Marriaga [a,*], Peter Claisse [b]

[a] *Departamento de Ingeniería Civil, Universidad Nacional, Bogotá, Colombia*
[b] *Materials Applied Research Group, Coventry University COV 5FB, UK*

ARTICLE INFO

ABSTRACT

The chloride diffusion coefficient is an indication of the capacity of any type of concrete to resist chloride penetration and is used to predict the service life of reinforced concrete structures. Its determination has been subject of intense study in the last 50 years and today there is no complete agreement in the methodologies used. In addition, its experimental determination is time and recourse consuming. As alternative, this article presents a new methodology to find the fundamental properties of concrete including the diffusion coefficients. From the measurement of the electrical properties of concrete during a migration test and using and integrated physical–neural network model the chloride related properties can be found. Results of experiments of normal diffusion were compared with the results of the new methodology and gave encouraging results.

© 2009 Elsevier B.V. All rights reserved.

1. Introduction

Corrosion of reinforcing steel is the major cause of deterioration of reinforced concrete structures. Carbon dioxide and especially chlorides are the main causes of corrosion. The chloride diffusion coefficient defines the capacity of any specific concrete to resist chloride penetration and is used to predict the service life of reinforced concrete structures. Usually it is measured experimentally with self (gravity) diffusion or migration tests, but differences can be found in the numerical values of the coefficients depending on the methodology used [1]. Either diffusion or migration tests can be done under steady state or non-steady state conditions. Pure diffusion tests take a long time but migration tests are performed in relatively short time.

Salt ponding [2] and Bulk diffusion [3] are examples of non-steady state chloride diffusion tests where the apparent diffusion coefficient is determined by fitting profiles of the acid soluble chloride concentration to Fick's second law of diffusion [4]. Steady state chloride diffusion tests are more time consuming and are calculated using the Fick's first law of diffusion [5]. They are made in a traditional diffusion cell setup where the upstream compartment is the chloride source and the downstream compartment must be chloride free at the start of the test. The chloride flux is calculated measuring the rate of change of chloride concentration in one of the compartments after the steady state is reached.

Migration (otherwise known as electromigration) tests differ from diffusion tests because a constant electrical potential difference is applied across the concrete, so that the calculation of the diffusion coefficient is based on the Nernst–Planck equation [6] rather than on Fick's law. The Nordtest Method NT 492 [7] is an example of non-steady state migration tests. It was developed by Luping and Nilsson [8] who provided the mathematical theory for calculating the effective diffusion coefficient. The Nordtest Method NT 355 standard [9], and the Japanese JSCE-G571-2003 [10] specify test methods in a steady state condition. For those the flux is calculated according to the measured change of concentration of chlorides when the ions passing through the sample have reached a steady state. The migration coefficient is calculated using the Nernst–Planck or the Nernst–Einstein [11] equations.

Regardless of the experimental method used to find the coefficient of diffusion there are some difficulties with each procedure. For example, in addition to the problem of the duration of the tests the determination of chloride concentrations either in solutions or in concrete requires special equipment and the laboratory work is time consuming. Additionally, all the procedures assume no depletion of chlorides in the source reservoirs, a situation which requires the continuous replacement of the solutions or, at least, the monitoring of the concentration, even if large quantities of initial solution are used. In addition, the effect of other ionic species and their interaction with chlorides is neglected. Finally, if the chloride penetration determined with the colorimetric

* Corresponding author at: Coventry University, Research room JL 118, Priory Street, Coventry CV1 5FB, UK. Tel.: +571 3165000; fax: +44 024 7688 8881.

E-mail addresses: jmlizarazom@unal.edu.co (J. Lizarazo-Marriaga), P.Claisse@coventry.ac.uk (P. Claisse).

method [12], it is not easy to measure and has a high variability.

In order to offer an alternative to the standard methods for calculating the chloride coefficient of diffusion for concrete, this article presents a new procedure consisting of a new electrochemical test and a computational method. The principal aim of the article is to present the theoretical basis of a new method. This new method consists of the experimental determination of the electrical current and the electrical membrane potential during a migration test similar to that proposed by ASTM C1202 [13]. The chloride transport related properties are determined with an integrated physical–neural network model. The computational model proposed uses the Nernst–Planck equation and accounts for the interaction of all the species involved by changing the membrane potential voltage in order to avoid any charge surplus inside the concrete sample. In addition, the model uses an artificial neural network to optimize the experimental results to calculate the chloride related properties. The validity of the new methodology was checked by comparing the chloride coefficients obtained from it with the chloride coefficients obtained with a traditional diffusion test.

2. Theoretical aspects of the membrane potential and current during a migration test

The Nernst–Planck equation defines the ionic movements in a fully saturated concrete due to the chemical and electrical potential [6].

$$J_i = D_i \frac{\partial c_i}{\partial x} + \frac{z_i F}{RT} D_i c_i \frac{\partial E}{\partial x} \tag{1}$$

where c_i is the ionic concentration of species i in the pore fluid; x the distance; z_i the electrical charge of species I; F the Faraday constant; E the electrical potential; $\partial E/\partial x$ the electrical field; J_i the flux of specie i; D_i the diffusion coefficient of species i; R the gas constant; and T the absolute temperature.

In a concrete migration test, in addition to the external electrical field applied there is an internal electrical field produced because of the interactions among all the ions involved in the test (Cl^-, OH^-, Na^+ and K^+). As a result, the electrical field contained in the term for the migration flux of Eq. (1) does not depend only on the constant external electrical potential applied; it is also related with the electrical membrane potential, which is the additional voltage generated due to the requirements of charge neutrality. Different ions have different mobility [14] and diffuse or migrate at different speeds, so an excess of charge builds up this membrane potential in order to compensate the flux of the species and keep the electroneutrality of the system. Eq. (2) shows the total electrical field formed by the external voltage and the membrane potential, where φ is the external electrical voltage applied and E_p is the membrane potential. A more complex expression can be found if the Nernst–Planck equation includes a chemical activity coefficient (γ) [15], however, it has been proved that the activity term does not increase the accuracy of the results in a migration concrete test [16,17].

$$\frac{\partial E}{\partial x} = \frac{f(\varphi)}{x} - \frac{\partial E_p}{\partial x} = \frac{f(\varphi)}{x} - \frac{RT}{F} \frac{\sum_i z_i D_i (\partial c_i / \partial x)}{\sum_i z_i^2 D_i c_i} \tag{2}$$

Lu [11] stated that if concrete is considered a solid electrolyte, the diffusivity of charged species i is related to its partial conductivity σ_i, and this relationship is known as the Nernst–Einstein equation. If the partial conductivity and the concentration are known, the diffusion coefficient of a species can be found from Eq. (3).

$$D_i = \frac{RT\sigma_i}{z_i^2 F^2 c_i} \tag{3}$$

The overall conductivity of concrete (σ) can be related with the partial conductivity of one specie (σ_i)

$$\sigma_i = t_i \sigma \tag{4}$$

where t_i is the transference number of species i, which is defined as

$$t_i = \frac{Q_i}{Q} = \frac{i_i}{i} \tag{5}$$

where Q_i is the charge contribution of specie i and Q the total charge passed through the sample. The total charge can be expressed as a function of the coefficient of diffusion for specie i (Eq. (6)). Eqs. (2) and (6) show that the diffusion coefficient is strongly related to the charge (area under the graph of current versus time) and the membrane potential.

$$Q = \frac{RT\sigma Q_i}{z_i^2 F^2 c_i D_i} \tag{6}$$

In a chloride mono-ion system, defined as a system where chlorides are isolated of any interaction with other ions, the mathematical solution for the Nernst–Planck equation for a semi-infinite homogeneous medium is [8]:

$$c(x, t) = \frac{c_s}{2} \left[e^{ax} \mathrm{ercf} \left(\frac{x + aDt}{2\sqrt{Dt}} \right) + \mathrm{ercf} \left(\frac{x - aDt}{2\sqrt{Dt}} \right) \right] \tag{7}$$

where $c(x, t)$ is the concentration of chloride after a time t at a distance x form the surface of the sample; ercf the complementary error function erf; c_s the steady chloride concentration at the surface; and a is a constant related with the external voltage applied and is defined by Eq. (8).

$$a = \frac{zF\varphi}{RT} \tag{8}$$

From Faraday's Law, $i_i = -z_i F J_i A$, and from Eqs. (1) and (7), the total current for a chloride mono-ion system, can be expressed as Eq. (9), where A is the area of the cross-section of the sample.

$$i = AFD_{Cl}c_s \left[\frac{1}{\sqrt{\pi D_{Cl}t}} e^{((x-aD_{Cl}t)^2/4D_{Cl}t)} + \frac{a}{2}\mathrm{erfc}\left(\frac{x - aD_{Cl}t}{2\sqrt{Dt}} \right) \right] \tag{9}$$

3. Experiments

3.1. Test details

The tests carried out as part of this research are summarised in the following section. Each test was run twice and the result shown is the average of both results.

3.1.1. Current and membrane potential in the ASTM C1202 test

The procedure used to measure the electrical current was according to ASTM C1202. In this, a steady external electrical potential of 60 V D.C. was applied to a sample of concrete of 50 mm thick and 100 mm diameter for 6 h. The anode and cathode were filled with 0.30N sodium hydroxide and 3.0% sodium chloride solutions, respectively. The samples were prepared before the test in conformity with the standard.

In addition to the standard test, a salt bridge was added in the middle of the sample to check the voltage distribution. A hole of 4 mm diameter and 6–9 mm deep was drilled at the mid-point. The salt bridge used was a solution of 0.1 M potassium chloride (KCl) in order to avoid any junction potential at the interface of the salt solution and the pore solution. The voltage was measured using a saturated calomel electrode (SCE) relative to the cathode cell. The current through the concrete and the voltage at the mid-point were measured continuously every 10 s with a data logger. The membrane potential was calculated by subtracting the value of the voltage measured from the initial value measured at the start of the test. The value of voltage measured at any time in the mid-point position is given in Eq. (10).

$$\Delta V = V_{Ti} - V_0 \tag{10}$$

ΔV corresponds to the membrane potential; V_{Ti} is the voltage measured at time t; and V_0 the voltage at the start of the test. More detail of the experiment can be found in Ref. [14]. Fig. 1 shows the test. The results were analysed using the computer model described in Section 4 of this article.

Table 1
Concrete mix design.

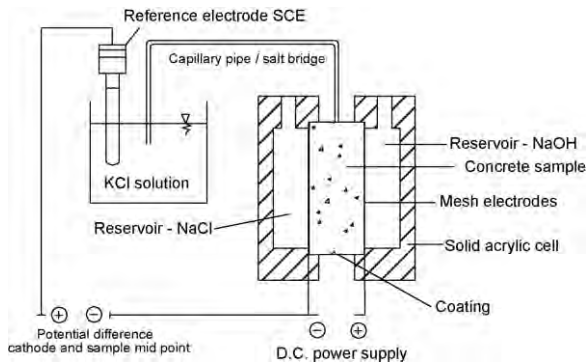| Mix	w/b	OPC (kg m^{-3})	Fine aggregate (kg m^{-3})	Coarse aggregate (kg m^{-3})	Water (kg m^{-3})
OPC 4	0.4	400	705	1058	160
OPC 5	0.5	400	664	995	200
OPC 6	0.6	400	622	933	240

Fig. 1. Cell and salt bridge [14].

3.1.2. Chloride diffusion test

The sawn surface of 100 mm diameter and 100 mm high concrete cylinders were placed in contact with a solution of sodium chloride. To prepare the samples, the curved surface of each cylinder was covered with a rubber coating in order to avoid moisture exchange and carbonation during the test. After the samples were coated, the surface that would be in contact with chlorides was in placed contact with a solution of 0.5 g l^{-1} of CaOH for 1 week to avoid any initial sorption effect when the chloride solution was introduced. Fig. 2 shows the test.

The external concentration of chloride was 7% NaCl and it was renewed every 3 weeks. After 12 weeks of diffusion, the chloride penetration depth was measured using the colorimetric method [18]. Each sample was split axially and sprayed with a solution of 0.1 M silver nitrate. After 15 min a white silver chloride precipitation on the split surface was visible and the penetration depth was measured. It was assumed that the free chloride concentration at which the color changes is around 0.07N for ordinary Portland cement concrete [7].

The solution of the Nernst–Planck equation presented in Eq. (7) for the condition of zero external voltage gives Eq. (11) and corresponds to the solution of Fick's second law presented by Crank [19].

$$c(x, t) - c_0 = (c_s - c_0)\left(\mathrm{erfc}\left(\frac{x}{\sqrt{4tD}}\right)\right) \tag{11}$$

where c_0 is the initial concentration of chlorides. In this study it was assumed that at the start of the test the initial concentration of chlorides inside the sample was zero ($c_0 = 0$) The free chloride concentration, the depth of penetration, the chloride surface concentration (c_s), and the time of the diffusion test were known so the diffusion coefficient could be calculated using Eq. (11).

3.1.3. Open porosity

The open porosity accessible by water (P) was measured using the simple method of water displacement. The central part of each cylinder (30 mm thickness) was vacuum saturated until constant weight and weighed in water (W_w) and air (W_a). They were then dried in an oven at 105 °C until constant weight and weighed again (W_d). The porosity was found with Eq. (12). Three replicates were tested for each mix.

$$P = \frac{W_a - W_d}{W_a - W_w} \tag{12}$$
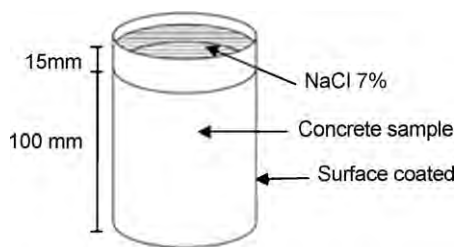
Fig. 2. Experimental diffusion test.

3.2. Concrete mixes

Samples of type I ordinary Portland cement (OPC) with different water cement ratios were mixed. Table 1 shows the mix designs and the nomenclature used in this study. All the tests were made on samples around 6 months old which were kept in a controlled humidity and temperature room until each test was started. During the mixing, depending on the water content, the mixes had different flow properties. In order to avoid affecting the strength because of the differences in the mix compaction, all the mixes were therefore compacted mechanically with a vibrating table. The moulds were filled with concrete in three layers and compacted to remove the air and reach the maximum density.

4. Computer model

The computational model used two main techniques. An electro-diffusion numerical routine was used for calculating the transient current and the mid-point membrane potential during migration and diffusion tests. This programme uses the physical transport properties as input data and gives as outputs the transient current and the electrical membrane potential. However, as in reality the physical transport properties are unknown, a neural network algorithm was trained to optimize those physical properties. As a result of combining both techniques, the transport properties of a concrete sample could be determined from experimental observations of mid-point membrane potential and current measured simultaneously during a migration test.

4.1. Numerical electro-diffusion model

The numerical model used in this research works by repeated application of the Nernst–Planck equation through microscopic time and space steps for various ions simultaneously. The ions considered were potassium found in the initial pore solution of the sample, sodium and hydroxide found in the pore solution and in the external cells, and chloride found in the external cells. The effects of the membrane potential are applied by distorting the voltage in each space step and checked by ensuring that charge neutrality is maintained throughout the sample at all times for all the ions together. At each time step adjustments are made to the voltage to ensure that there is not charge surplus inside the sample.

In the model the concentration of ions is defined in two ways: the free ions per unit volume of liquid (C_l) and the total ions per unit volume of solid (C_s). The ratio of those concentrations is named the binding capacity factor (α). In the same way, the intrinsic coefficient (D_{int}) defines the transport of matter when the flux is calculated per unit cross-sectional area of the pores and the concentration in the free liquid. In contrast, the apparent diffusion coefficient (D_{app}) defines the transport of any ion when the flux is calculated per unit area of the porous material and the average concentration in the material. The reason why both coefficients are presented is because the computer model calculates the intrinsic coefficient, but the apparent coefficients are normally used to predict the service life of concrete structures.

The model can be set under two conditions; first, a migration test with an applied steady external voltage ($\varphi \neq 0$) can be modelled under a condition called voltage control in this article. In this, for any time step, although the current density into any point is equal to the current out of it (Kirchoff's law), the total current is transient and changes with time (but not with position). The second condition called current control, allows the model to simulate a self-diffusion
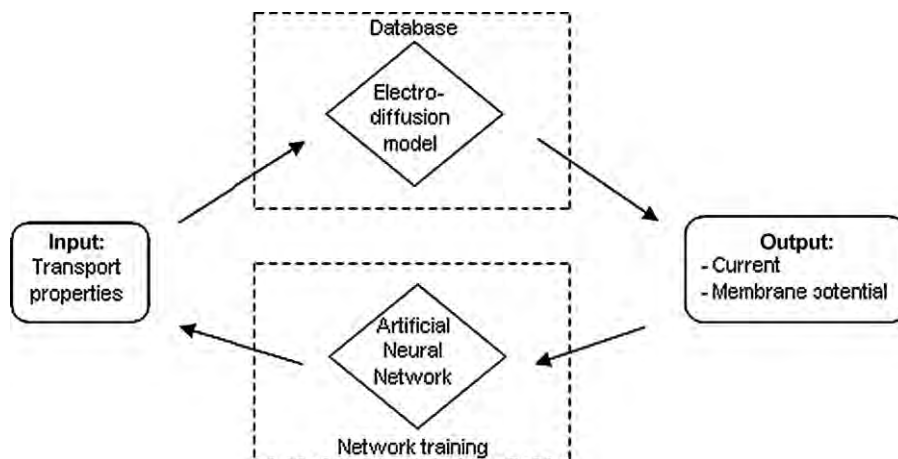
Fig. 3. Conceptual diagram integrated model.

test under no external field applied ($\varphi = 0$). In this, in addition to the voltage correction necessary to prevent a charge surplus, the programme keeps the total current equal to a pre-set value (zero for this test).

As outputs in both conditions the model calculates the transient current caused by each ion, the concentrations, the voltage variation and the membrane potential at all times during the test and in each position [20]. The model was written in visual basic and run as a macro in Microsoft Excel.

4.2. Neural network optimization model

To train the network the numerical electro-diffusional model was run many times in order to obtain a database of the input and the corresponding target vectors. During the training the outputs of the model were used as inputs for the neural network and all the data were normalized between −1 and +1 in order to avoid the influence of the scale of the physical quantities. In the same way, a tangential transfer function was limited to be between −1 and +1. The Levenberg–Marquardt training algorithm was used. Fig. 3 shows a conceptual diagram of the integrated model.

The optimization model uses a feed-forward back propagation-network with a multilayer architecture. Six neurons define the

input layer, corresponding to values of the current and the mid-point membrane potential at different times. A middle hidden layer has three neurons, and the output layer output has seven neurons corresponding to the intrinsic diffusion coefficients of Cl^-, OH^-, Na^+ and K^+, the porosity, the hydroxide composition in the pore solution at the start of the test, and the binding capacity factor for chloride ions. The neural network model was constructed using the neural network tool box of Matlab®. Fig. 4 shows the input, the hidden layer and the outputs of the network.

4.3. Integrated numerical–neural network model

Obtaining the related transport chloride properties of concrete from measurements of current has been reported recently [21]; however, long durations and steady state conditions are required. In the present research, with the simultaneous measurement of the current and the mid-point membrane potential, it is possible to determine a unique combination of the transport properties by using the trained neural network. In order to simulate the transport properties of concrete and taking into account the complex variables related with the physical phenomenon some assumptions were made:
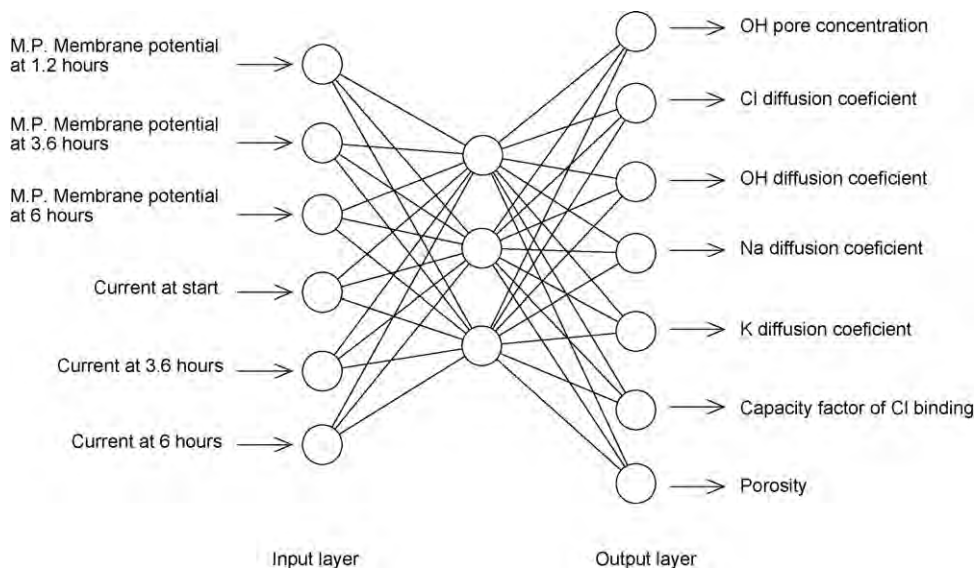
Fig. 4. Multilayer neural architecture used.

Fig. 5. Current measured experimentally.

(1) The only ions that interact with the cement matrix products are chlorides and that interaction is defined with a linear binding isotherm. Although has been demonstrated experimentally [22] that non linear isotherms reflects the absorption phenomena better, the model uses an average linear isotherm that represents in a good way the average adsorption of chlorides.

(2) The relationship between chloride intrinsic diffusion ($D_{\text{int-Cl}}$) and apparent diffusion coefficients ($D_{\text{app-Cl}}$) is defined through the porosity of the material (ε) and the binding capacity factor (α). The assumption of a linear isotherm means that α is a constant for each ion. It is important to notice again that the apparent diffusion coefficient is the ratio of the flux to the total concentration of chlorides (free and adsorbed) defined per unit volume of the medium. In contrast, the intrinsic diffusion coefficient is the ratio of the flux in the pores to the concentration of free ions in the pore solution per volume of liquid in the pores.

$$\frac{\alpha}{\varepsilon} = \frac{D_{\text{int-Cl}}}{D_{\text{app-Cl}}} \tag{13}$$

(3) At the start of the test the chemical pore solution is composed of ions OH^-, K^+, and Na^+, and, in order to keep electroneutrality, it was assumed that the concentration of hydroxyl ions is equilibrated with a proportion of 33% of sodium and 66% of potassium. This assumption was based on published results [23].

Fig. 7. Chloride coefficients of diffusion D_{Fick} ($m^2\ s^{-1}$).

5. Results and discussion

5.1. Experimental determination of the transient current, membrane potential and the diffusion coefficients

The average current measured for each mix in the migration test is shown in Fig. 5. As was expected, an increase in the water cement ratio gave an increase in the current passed, and a corresponding increase in the temperature of the sample. The measured maximum value of temperature in the anode solution was of 63, 44, and 36 °C for samples of water cement ratio of 0.6, 0.5 and 0.4, respectively, and the values of charge calculated as the area under the graph of current versus time were 9580, 6863 and 4149 C for samples of water cement ratio of 0.6, 0.5 and 0.4, respectively.

The membrane potential measured is shown in Fig. 6a. For some samples, there was signal noise which may have been caused by the random distribution of aggregate limiting the contact between the salt bridges and the pore volume. This was substantially reduced by slightly increasing the depths of the drilled holes for the salt bridges. The experimental results were filtered with commercial curve fitting software in order to find the best trend of the results and this can be seen in Fig. 6b. The average membrane potential for each mix is shown in Fig. 6c, it can be seen that for all mixes the membrane potential showed a rise from its initial value, however, mix OPC 6 showed an initial decrease during the first 2 h.

The chloride diffusion coefficients obtained from the gravity diffusion test and Eq. (11) were called D_{Fick} in this article and are shown in Fig. 7. As was expected, an increase in the water cement ratio yielded an increase in the coefficient of diffusion. The values of chloride diffusion coefficient obtained experimentally are in the normal ranges reported in the literature [24], however, the concrete tested can be ranked as high permeability because the diffusion coefficients obtained experimentally were greater than $10^{-12}\ m^2\ s^{-1}$. The
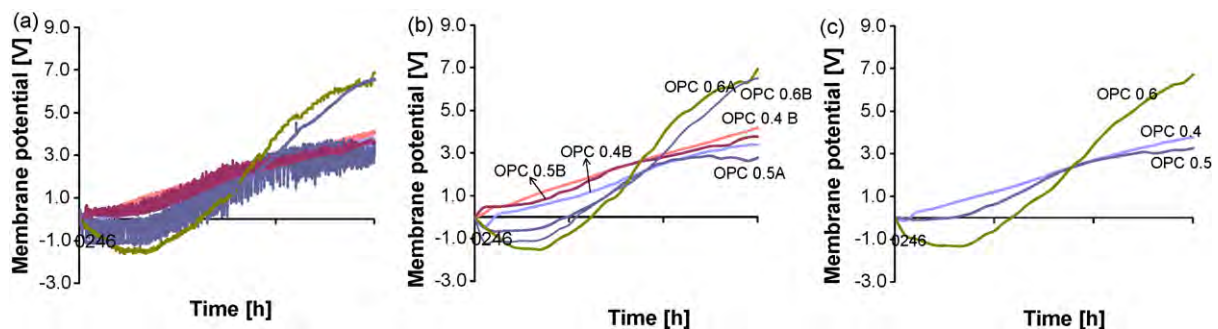
Fig. 6. Membrane potential measured.
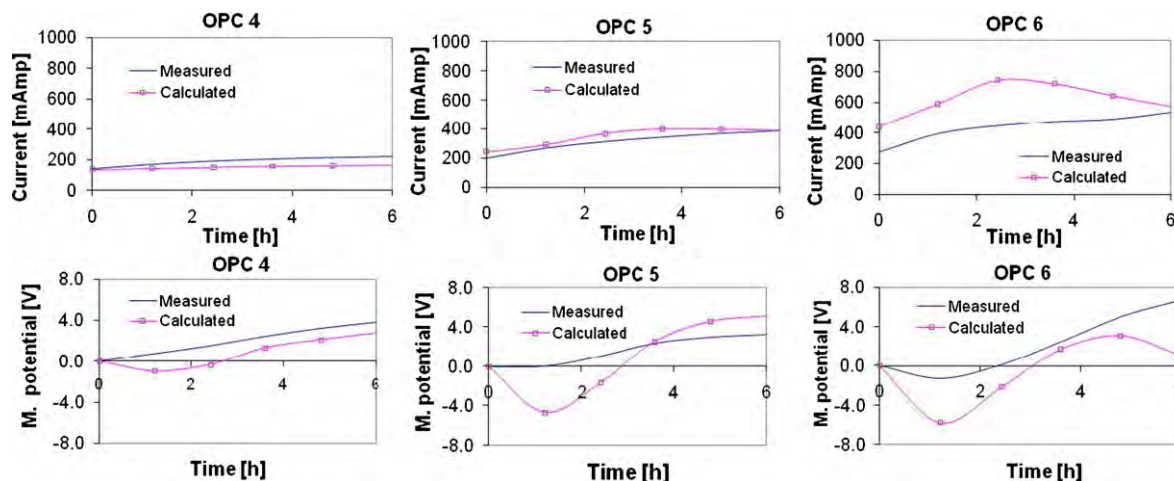
Fig. 8. Transient mid-point membrane potential and current simulated and measured.
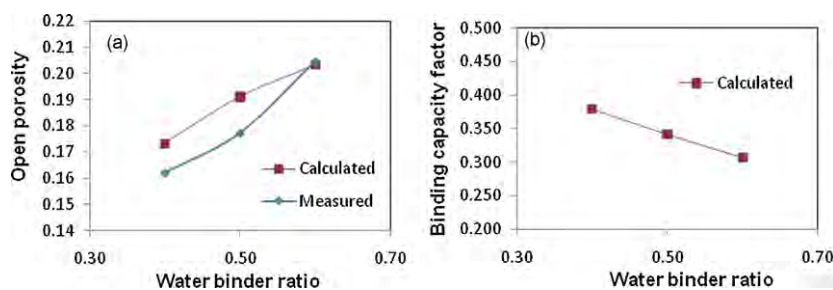
Fig. 9. Porosity and binding capacity factor.

high values of the coefficient of diffusion are in accordance with the high values of porosity measured.

5.2. Prediction of chloride related properties

The trained neural network was fed with the values for the transient current and the mid-point voltage from the migration test and the chloride transport related properties were calculated. As a measure of the reliability of the network, the transport properties obtained were used to run the electro-diffusional model in order to obtain a simulated transient current and mid-point membrane potential. The comparison of these curves is shown in Fig. 8. It can be seen that for the current the simulations are in a very good agreement with the experiments, and for the membrane potential although there are some small differences there is a well-defined trend.

The differences between the measured and simulated membrane potential can be explained by factors related with the accuracy of the measurement device used during the experiment, the heating of the material under an electrical field, or the variability of the test. However, it may be seen that the neural network is able to give a good fit to the profile of the membrane potential given that the number of possible combinations of properties that yield a given current and membrane potential is almost infinite.

The calculated transport properties include the porosity, the binding capacity factor and the initial hydroxide composition at the start of the test. As was expected, the porosity increases with an increase of the water binder ratio (Fig. 9a). In the figure it can be seen that the trend of the measured porosity is similar to that calculated; however, some differences arise from errors in either the numerical and experimental methods. The binding capacity factor decreases as the water binder ratio increases, presumably is due

to the refining of the hydration compounds enabling them to bind more free chloride ions (Fig. 9b). The calculated initial chemical content of the pore solution increases with increase in the water binder ratio. This can be attributed to the higher amount of water, which can keep more alkalis in the pore solution.

The calculated intrinsic diffusion coefficients for all the species involved in the simulation (Cl$^-$, OH$^-$, Na$^+$, K$^+$) are shown in Fig. 10. As was stated by other researchers [6], the anions had a smaller diffusion coefficient than chlorides and hydroxides, except than for mix 6, in which hydroxide and sodium have a similar diffusivity. As was expected, the calculated numerical values of the intrinsic coefficients for all the species are, for all the cases, smaller than the coefficients of diffusion in infinite diluted solutions as can be seen in any electrochemistry textbook. The values obtained are physically possible and are in acceptable ranges.

In the same way that the measured chloride diffusion coefficient increases its value with the increase of the water binder ratio, the calculated chloride intrinsic coefficient also increases. The relation-
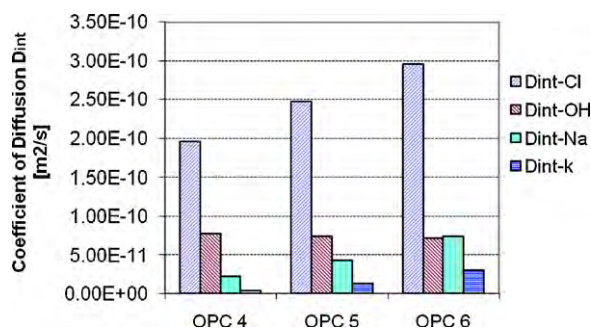
Fig. 10. Intrinsic diffusion coefficients calculated.
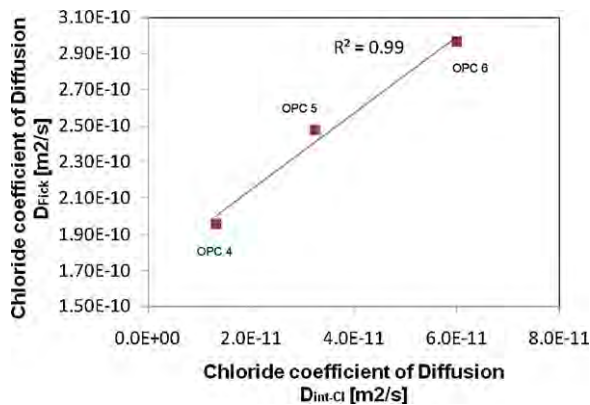
Fig. 11. Relationship between the chloride diffusion coefficients.

ship between the chloride coefficients obtained from the diffusion test (using Fick's law) and the migration test (using the integrated model) is shown in Fig. 11. The correlation coefficient R^2 was 0.99, indicating a strong relationship between the coefficients. The differences arise because of the physical equations used. Both coefficients are related but are defined in a different way. The first was obtained with Fick's law under conditions of pure diffusion and the second was obtained with the Nernst–Planck equation, including chloride adsorption and interaction among all the species involved. The differences were overcome by using the numerical model as described below.

5.3. Simulation of the current and chloride concentration

With the aim of showing the simulation of the current and the chloride concentration for mix 4, the gravity chloride diffusion test was simulated using the computer model. The time selected to show the evolution of the current was 36 days. Fig. 12 shows the profile of the current when the phenomenon was simulated using three different approaches.

(1) The electro-diffusion current control model with zero current. As was expected, the total current was equal to zero at any point of the sample. The current density generated by each ion was annulled by the current density generated by the remaining ions. When any species diffused through the sample a charge surplus was avoided through the generation of a membrane potential. The authors suggest that this simulation best represents the physical situation in the sample.
(2) The electro-diffusion model with no voltage correction. In this, in the solution of the Nernst–Planck equation there is no membrane potential generation. As a result, the Nernst–Planck
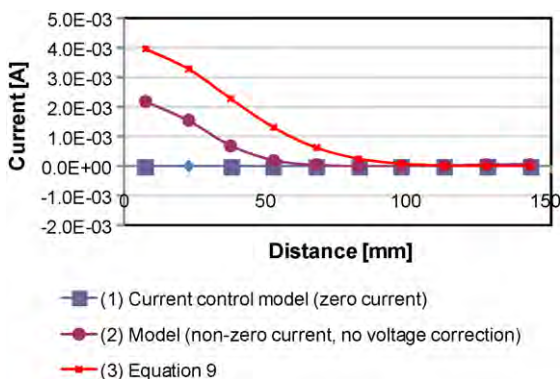
Fig. 12. Total current at 864 h (36 days).
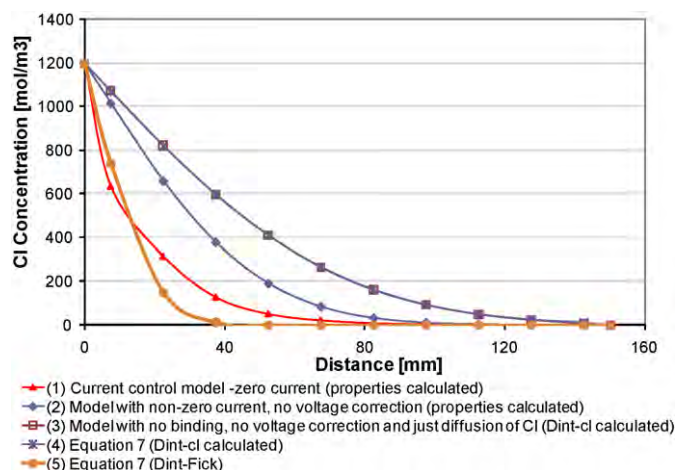
Fig. 13. Chloride profile at 90 days.

equation was solved using Fick's first law for each ion. The total current had a value of 2.1 mA near the surface because at that point the flux of chloride and sodium was high. In the same way, far away from the surface the current decreases. The total current for any point is the result of the sum of the current driven for each ion, according to its charge and diffusion direction.
(3) The theoretical Eq. (9). In this it is supposed that the only species involved are chlorides. The total current profile obtained was similar to the previous condition but the total current near to the surface was 4 mA.

The chloride concentration profile at different distaces from the external NaCl solution is shown in Fig. 13. The time selected to show the evolution of the concentration along the sample was 90 days. As for the current, different aproches were used:

(1) The electro-diffusion current control model with zero current using the transport related properties calculated with the model.
(2) The electro-diffusion model with no voltage correction using the transport related properties obtained.
(3) The model, but with only chlorides present in the system so there was no pore solution or chloride binding. The chloride diffusion coefficient used was the obtained from the neural network.
(4) Eq. (7), which without an external applied voltage becomes Eq. (11) (Fick's law), using the intrinsic chloride diffusion coefficient obtained from the neural network.
(5) Fick's law, but the concentration was obtained using the chloride coefficient of diffusion obtained with the diffusion test D_{Fick}. This represents the profile of a function that passes through two points where the concentration was measured experimentally. However, some deviations can be expected because of the variability and uncertainty in the assumption that the change of color in the colorimetric method is at $0.07 \, mol \, l^{-1}$.

Approaches (3) and (4), as was expected, had the same profile; the chloride concentration was the same for both conditions. This provides a check that, for a simplified condition, the computer simulation gave the correct solution.

It can be seen from the graph that for methods 3 and 4 that permit development of a net total current (which is not possible in reality because there is no circuit) the chloride concentration is higher. The higher the total current developed, the higher the chloride profile simulated.

Method 5 represents the real free chloride concentration (as measured in the diffusion test), and it can be seen that it has a similar trend to the one predicted with the current control model (method 1).

6. Conclusions

- The experimental–numerical procedure proposed gives viable results for the fundamental properties of concrete. The initial hydroxide composition of the pore solution, the chloride binding capacity, the porosity, and the diffusion coefficients for all the species involved were estimated with good results.
- The standard determination of the chloride diffusion coefficients is time and resource consuming, in addition to the uncertainties of the methods and theories used. The neural network methodology proposed is an alternative that can yield to the accurate calculation of the concrete diffusivity with a short and inexpensive test.
- The straightforward application of Fick's law to simulate chloride diffusion in concrete which has been used by many authors in the past can be significantly improved by using a numerical simulation which includes the effects of the other ions in the system.

Acknowledgments

References

[1] C.C. Yang, L.C. Wang, Materials Chemistry and Physics 85 (2004) 266.
[2] AASHTO, Standard Method of Test for Resistance of Concrete to Chloride ion Penetration, AASHTO T 259-80, 1997.
[3] NTBUILD-443, Concrete Hardened: Accelerated Chloride Penetration, 1995.
[4] M. Nokken, A. Boddy, R.D. Hooton, M. Thomas, Cement and Concrete Research 36 (2006) 200.
[5] G.K. Glass, N.R. Buenfeld, Journal of Materials Science 33 (1998) 5111.
[6] C. Andrade, Cement and Concrete Research 23 (1993) 724.
[7] NTBUILD-492, Concrete, Mortar and Cement-based Repair Materials: Chloride Migration Coefficient from Non-steady-state Migration Experiments, 1999.
[8] T. Luping, L. Nilsson, ACI Materials Journal 89 (1992) 49.
[9] NTBUILD-335, Concrete, Mortar and Cement-based Repair Materials: Chloride Diffusion Coefficient from Migration Cell Experiments, 1997.
[10] JSCE-G571, Test Method for Effective Diffusion Coefficient of Chloride Ion in Concrete by Migration, Japan Society of Civil Engineers, 2003.
[11] X. Lu, Cement and Concrete Research 27 (1997) 293.
[12] Q. Yuan, C. Shi, F. He, G. Schutter, K. Audenaert, K. Zheng, Cement and Concrete Research 38 (2008) 1177.
[13] ASTM-C1202, Standard Test Method for Electrical Indication of Concrete's Ability to Resist Chloride Ion Penetration, 2005.
[14] J. Lizarazo-Marriaga, P. Claisse, Electrochimica Acta 54 (2009) 2761.
[15] O. Truc, PhD thesis, Prediction of Chloride Penetration into Saturated Concrete – Multi-Species – Approach, Chalmers University, Sweden, 2000.
[16] E. Samson, J. Marchand, K. Snyder, Materials and Structures 36 (2003) 156.
[17] L. Tang, Cement and Concrete Research 29 (1999) 1469.
[18] E. Meck, V. Sirivivatnanon, Cement and Concrete Research 33 (2003) 1113.
[19] J. Crank, The Mathematics of Diffusion, second edition, Oxford University Press, 1976.
[20] P. Claisse, T.W. Beresford, Fourth CANMET/ACI International Conference on Durability of Concrete, Australia, ACI – SP 170, 1997, p. 1119.
[21] C. Yang, S. Chiang, L. Wang, Construction and Building Materials 21 (2007) 1560.
[22] A. Delagrave, J. Bigas, J. Ollivier, J. Marchand, M. Pigeon, Advanced Cement Based Materials 5 (1997) 86.
[23] P. Pedeferri, R.B. Polder, in: L. Bertolini, B. Elsener (Eds.), Corrosion of Steel in Concrete: Prevention, Diagnosis, Repair, Wiley, 2004.
[24] P.A.M. Basheer, Permeation analysis, in: V.S. Ramachandran, J.J. Beaudoin (Eds.), Handbook of Analytical Techniques in Concrete Science and Technology, Noyes Publications, 2001.

Determination of the transport properties of a blended concrete from its electrical properties measured during a migration test

J. Lizarazo-Marriaga* and P. Claisse†

Universidad Nacional, Bogotá; Coventry University

The Nernst–Planck equation describes ionic movements in saturated porous materials subject to chemical concentration gradients in the pore fluid and applied electric fields. When applied to a macroscopic system the equation supposes that the flux of each ion is independent of every other one. However, owing to the ionic exchange among different or similar species, there are ionic potentials that affect the final flux. These will distort the applied electric field and thus keep the electroneutrality of the sum of all the ionic species involved. The applied potential will fall linearly across the sample but an additional 'membrane' potential will change with position and time. This paper summarises a theoretical and experimental investigation into the application of the non-linear electric membrane potential to the simulation of the migration of chlorides in concrete. A new electrochemical test has been developed and carried out with different samples of concrete blended with pulverised fuel ash (PFA) and ground granulated blast furnace slag (GGBS). During the tests the transient current and the electrical membrane potential were measured. A numerical model developed previously using the classical equations, but including changes in the concrete membrane potential, was optimised using an artificial neural network (ANN). Based on the experimental results and the simulations, the intrinsic diffusion coefficients of chloride, hydroxide, sodium and potassium were obtained. Also, the initial hydroxide composition of the pore solution, the porosity, and the chloride binding capacity were determined. The results showed good agreement with the theory and can help to explain the complex phenomena that occur during a concrete migration test.

Introduction

Chloride penetration in reinforced concrete is a major concern because of the deterioration of the steel. The resistance to chloride transport can be determined with diffusion tests but these take a long time. The diffusion tests are accelerated by the application of an electrical potential gradient (migration tests) in order to save time. Under the influence of an electric field, ions experience a force directing them towards the electrode that is charged oppositely to the charge on the ion (Bockris and Reddy, 1998). The time needed to perform a pure diffusion test may be months; but, a migration test can be completed in just days or hours.

For fully saturated concrete samples with a difference in the concentration of ions in different regions and a constant applied electric potential as in the rapid chloride permeability test (RCPT) (ASTM, 2005) or NT-492 (NORDTEST, 1999), the total flux J_i for each species in the system must be the sum of the migration flux $(J_M)_i$ and the diffusion flux $(J_D)_i$

$$J_i = (J_M)_i + (J_D)_i \qquad (1)$$

The general law governing the ionic movements in concrete due to the chemical and electrical potential (Andrade, 1993) is known as the Nernst–Planck equation

$$J_i = D_i \frac{\partial c_i}{\partial x} + \frac{z_i F}{RT} D_i c_i \frac{\partial E}{\partial x} \qquad (2)$$

where c_i is the ionic concentration of species i in the pore fluid; x is the distance; z_i is the electrical charge

* Departamento de Ingeniería Civil, Universidad Nacional, Bogotá, Colombia
† Materials Applied Research Group, Coventry University COV 5FB, UK

1

of species i; F is the Faraday constant; E is the electrical potential; $\delta E/\delta x$ is the electrical field; J_i is the flux of species i; D_i is the diffusion coefficient of species i; R is the gas constant; and T is absolute temperature.

When applied to a macroscopic system the Nernst–Planck equation supposes that the flux of each ion is independent of every other one; however, owing to ion–ion interactions there are electrostatic fields that affect the final flux. The drift of a species i is affected by the flows of other species present. The law of electroneutrality ensures that no excess of charge is introduced to the system (Bockris and Reddy, 1998). In a concrete migration test, the current into any point will equal the current out of it (Kirchoff's law). An increase of concentrations at specific points in the sample can lead to a variation in the electric field. A variation in the electric field can lead a variation in the flux of each ion.

As a result of the ion–ion interactions, the electrical field contained in the term for the migration flux does not depend only on the constant external electrical potential applied (φ); it is also related to the electrical membrane potential which is formed when various charged species have different mobility. At the start of the test the electrical field is uniform across the concrete; however, when the different ions start to migrate owing to the external voltage applied, they cannot move freely. They are charged particles and interact with species of opposite signs. Owing to the membrane potential a few seconds after the test has started the electrical field is no longer constant. This non-linearity of the electric field is due to the membrane potential gradient and it is equivalent to the liquid junction potential (Lorente *et al*., 2007) in a concrete migration test. Equation 3 shows the ionic and the membrane potentials for the electrical field. A more complex expression can be found if the Nernst–Planck equation includes a chemical activity coefficient (γ) (Truc, 2000). However, it has been proven that the activity term does not increase the accuracy of the results in a concrete migration test (Samson *et al*., 2003; Tang, 1999).

$$\frac{\partial E}{\partial x} = \frac{\varphi}{x} - \frac{RT}{F} \frac{\sum_i z_i D_i \dfrac{\partial c_i}{\partial x}}{\sum_i z_i^2 D_i c_i} \qquad (3)$$

Different approaches have been proposed in order to simulate the penetration of chloride during a migration test accounting for all the species and an external electrical driving force. In the references (Claisse and Beresford, 1997; Khitab *et al*., 2005; Krabbenhoft and Krabbenhoft, 2008; Lorente *et al*., 2007; Narsilio *et al*., 2007; Sugiyama *et al*., 2003; Truc *et al*., 2000) the Nernst–Planck equation has been used as the way to find the flux of ions and the transport properties of

chlorides in concrete. Some researchers have used it coupled either to the conservation equation or accounting for the distribution and evolution of the electrical field.

In order to determine and understand the penetration of chlorides through concrete, a theoretical and experimental investigation has been carried out. An electrochemical migration test has been developed to determine the electrical membrane potential in laboratory concrete samples by measuring the potential within the samples (Lizarazo-Marriaga and Claisse, 2009). Ordinary Portland concrete (OPC) mixes blended with pulverised fly ash (PFA) and granulated ground blast furnace slag (GGBS) have been cast and the transient current and the electrical membrane potential were measured under controlled conditions. A numerical model developed previously (Claisse and Beresford, 1997) using the classical equations, but including changes in the concrete membrane potential distribution, was optimised using an artificial neural network (ANN) model. The new integrated computational model combines a numerical approach to solve the physical problem of electrodiffusion and an artificial intelligence approach to optimize the numerical and experimental results. The outputs of the model yielded the intrinsic diffusion coefficients of chloride, hydroxide, sodium and potassium. The hydroxide composition of the pore solution, the porosity and the chloride capacity of binding were also determined.

Experimental investigation

Test details

The tests carried out as part of this research are summarised in the following section. Each test was run twice and the result shown is the average of both results

Rapid chloride permeability test (RCPT) ASTM-C1202-05. For each test, a slice of concrete 50 mm thick and 100 mm in diameter was placed between two cells containing electrodes and 60 V direct current (d.c.) was applied. One of the cells was filled with a 0·30 N NaOH solution and the other cell was filled with a 3·0% NaCl solution. The curved surface of the specimens was coated with epoxy. Before the test the samples were vacuum saturated in conformity with the standard. The total charge in coulombs was calculated as the area under the current–time curve. The volume of each cell reservoir was approximately 200 ml. All tests were carried out in a temperature-controlled room at $21 \pm 2°C$. During the tests, the temperature was measured continuously.

New procedure for measuring the membrane potential in the ASTM C-1202 test. Salt bridges were added at different points in the concrete sample to

2

check the voltage distribution across the sample. Holes 4 mm in diameter and 6–9 mm deep were drilled at each point. The salt bridge used was a solution of 0·1 M potassium chloride (KCl) in order to avoid any junction potential at the interface of the salt solution and the pore solution. The voltage was measured using a standard calomel electrode (SCE) relative to the cathode cell. The current through the concrete and the voltage at different points inside the sample were measured continuously each second with a data logger. A high-impedance data logger (20 MΩ) was used in order to avoid drawing any current through the salt bridges. Figure 1 shows the experimental set-up.

For all the tests, the voltage was measured automatically at three different positions across each sample. The target location of these points was the mid-point and the quarter-points. As, at the start of the test, the electric field is linear across the sample, the membrane potential was calculated as the difference between the measured voltage at any time and the initial voltage. In order to avoid the noise found experimentally during the logging of the tests, a commercial curve-fitting software (The MathWorks, 2001) was used. It was found that this noise was substantially reduced by slightly increasing the depths of the drilled holes for the salt bridges. This observation indicates that the noise was caused by the random distribution of aggregate limiting the contact between the salt bridges and the pore volume.

In a previous study, Zhang *et al.* (2002) measured the membrane potential across OPC mortar specimens during a normal diffusion test using reference electrodes and salt bridges immersed in the external cells of
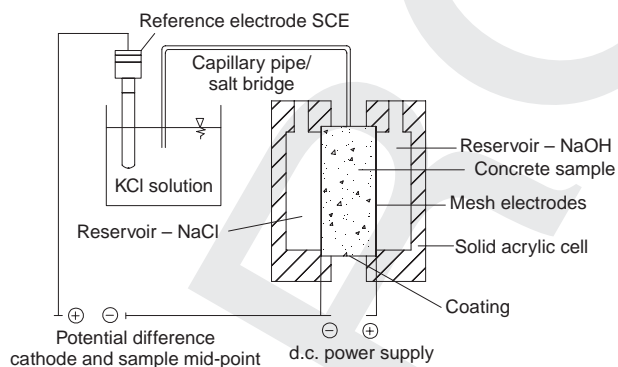
the sample. They found that for different simulated pore solutions the total junction potentials formed between the measurement devices and the simulated pore solution were in the range between -0·8 and -6 mV. Those values were relatively low compared with the membrane potential measured during the migration tests, so the liquid junction potential formed between the salt bridge and the pore solution in the concrete sample was not accounted for in the research reported in this paper.

As the external voltage across the sample was applied from the power supply by copper electrodes immersed into the cell solutions, there was a small potential drop between the electrodes and the surface of the concrete (McGrath and Hooton, 1996). The relationship between the external voltage delivered by the power supply and the voltage between both ends of the sample was measured and corrected for during the simulations.

Chloride penetration. The chloride penetration was measured after each migration test was finished. The procedure used was the colorimetric method of the Nordtest NT Build 492. Each sample was split axially and sprayed with a solution of 0·1 M silver nitrate. After 15 min, a white silver chloride precipitation on the split surface was visible and the penetration depth was measured.

Concrete mixes

Samples of OPC bended with GGBS and PFA in different proportions were prepared with a fixed water–binder ratio of 0·49. The level of replacement was 10, 30 and 50% for each mineral admixture to cement and the amount of water was kept in the range 195–200 kg/m³. The chemical compositions of the materials used were identified using X-ray fluorescence (XRF) and the specific gravity (SG) of admixtures was measured with a helium picnometer (Micromeritics AccuPyc 1330). Results for the composition of the oxides are presented in Table 1.

Table 2 shows the mix designs and the nomenclature used in this study. All the migration tests were made on samples around 100 days old, which were kept in a room with controlled humidity and temperature until the test. According to the water demand of the admixtures and the proportions used, the mixes had different flow properties. In order to avoid affecting the strength

Figure 1. Cell and salt bridge

Table 1. Chemical oxide composition of materials used (*according to the producer)

Binder	Chemical composition: %												SG: g/cm³
	SiO_2	TiO_2	Al_2O_3	Fe_2O_3	MnO	MgO	CaO	Na_2O	K_2O	P_2O_5	SO_3	LOI	
OPC*	19·7		4·9	2·4		2·1	63·3	0·2	0·6		2·7	2·7	3·04
GGBS	34·5	0·55	13·16	0·74	0·45	7·75	38·7	0·29	0·55	0·02	1·75	0·7	2·92
FA	47·2	0·96	25·35	9·27	0·05	1·71	2·33	1·52	3·43	0·23	0·48	7·6	2·35

Table 2. Concrete mix design

Mix	w/b	%			Unit content: kg/m^3					
		OPC: %	FA: %	GGBS: %	OPC: kg	PFA: kg	GGBS: kg	Fine agg.: kg	Coarse agg.: kg	Binder: kg
OPC	0·49	100	0	0	394	0	0	692	988	394
10% PFA	0·49	90	10	0	355	39	0	689	984	394
30% PFA	0·49	70	30	0	276	118	0	684	977	394
50% PFA	0·49	50	50	0	197	197	0	678	969	394
10% GGBS	0·49	90	0	10	355	0	39	691	987	394
30% GGBS	0·49	70	0	30	276	0	118	690	986	394
50% GGBS	0·49	50	0	50	197	0	197	690	985	394

because of the differences in the mix compaction, all the mixes were compacted mechanically with a vibrating table. The moulds were filled with concrete in three layers and compacted to remove the air and reach the maximum density.

Modelling

The integrated computational model developed was composed of two main techniques. An electrodiffusion numerical routine was used for calculating the transient current and the mid-point membrane potential during a migration test. This programme uses the physical transport properties as input data. However, as during the test, the physical transport properties are unknown, so a neural network algorithm was trained to optimise those physical properties. As a result of combining both techniques, the transport properties of a concrete sample could be determined when the current and the mid-point membrane potential were measured simultaneously during a migration test.

Numerical electrodiffusion model

The numerical model used in this research was developed in the construction materials applied research group of Coventry university (Claisse and Beresford, 1997). The model works by repeated application of the Nernst–Planck equation through microscopic time and space steps. The effects of the membrane potential in a migration test are applied by distorting the voltage in each space step and checked by ensuring that charge neutrality is maintained throughout the sample at all times for all the ions together. After each time step, adjustments are made to ensure that the total voltage across the sample is correct. The model was able to simulate the transient current during the test, the voltage variation and the membrane potential at each time during the test and in each position. In addition, the model was able to determine the concentration of all the ions used at each time during the test and in each position inside the sample (see Figure 2).

Neural network optimisation model

The network used in this research had a backpropagation algorithm with a multilayer architecture with an input layer of six neurons, a hidden layer of three neurons and an output layer of seven neurons (Figure 3). The six input neurons correspond to the experimental values of current and the mid-point membrane potential through the sample at different times. The output neurons correspond to the intrinsic diffusion coefficients of Cl, OH, Na and K, the porosity, the hydroxide composition into the pore solution at the start of the test, and the binding capacity factor for chloride ions. In the electrodiffusion model the concentration of ions is defined in two ways: the free ions per unit volume of liquid (C_l) and the total ions per unit volume of solid (C_s). The ratio of those concentrations is named the binding capacity factor (α) and it does not have physical units. The neural network model was constructed using the neural network tool box of Matlab$^®$.

To train the network, the numerical physical model was run computationally a number of times in order to obtain enough input vectors and the corresponding target vectors. More than 2000 combinations of logical values of transport properties were run with the physical model producing a reliable database to train the neural network. During the training, all the inputs and outputs were normalised between -1 and +1 in order to avoid the influence of the scale of the physical quantities. In the same way, a tangential transfer function was limited to be between -1 and +1. The Levenberg–Marquardt training algorithm was used.

Integrated numerical–neural network model

The profile and evolution of the membrane potential and the current is associated either with

(*a*) factors related to the test, such as the electrical external potential and the chemistry of the external reservoirs cells, or

(*b*) factors related to the features of the sample, such as the concentration of species in the pore solution,
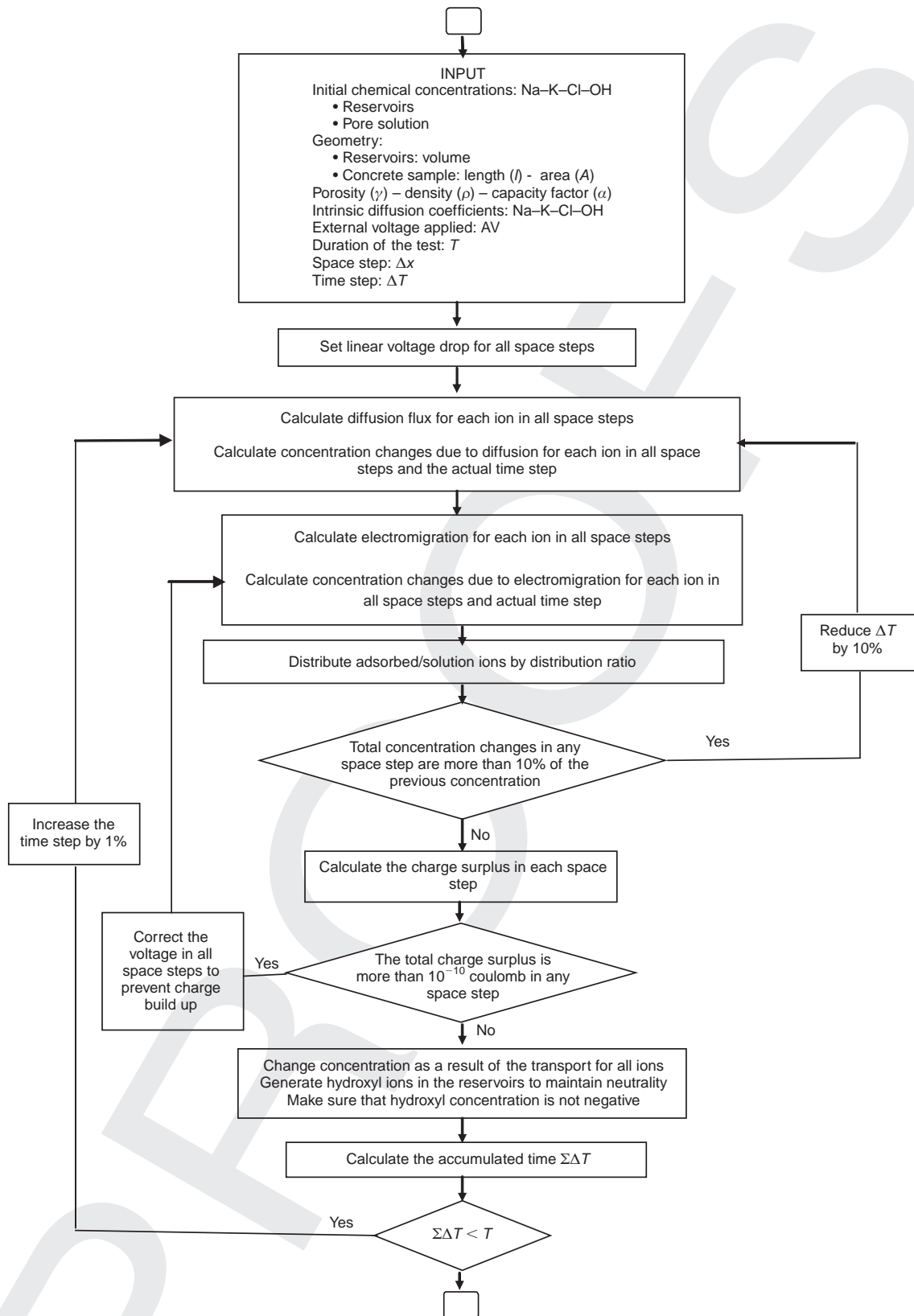
Figure 2. Computer model used in this research

the tortuosity of the pore network, the porosity of concrete, the intrinsic properties of diffusion for each ion present, and the binding capacity or adsorption for each ion.

In the experiments, all the conditions related to the test were carefully controlled and were the same for all mixes. So, it can be argued that the differences in the current and the mid-point membrane potential among
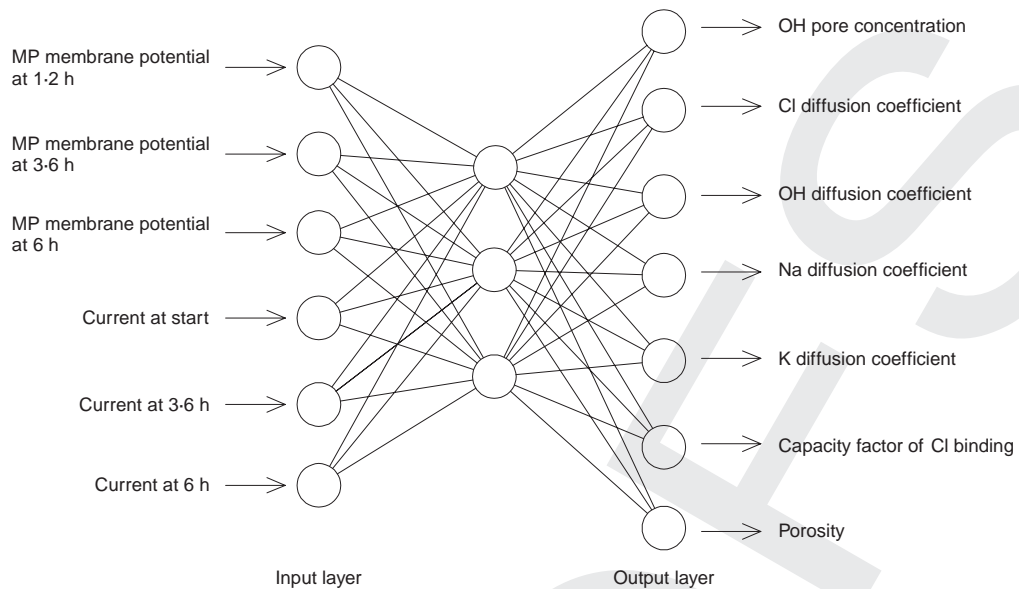
Figure 3. Neural network used

mixes were due to the differences in the transport characteristics of each mix. When measuring the transient current by itself, it is not possible to determine a unique numerical value for all the concrete transport properties because there are too many unknowns and not enough relationships to solve the system. However, with the simultaneous measurement of the current and the mid-point membrane potential it is possible to determine a unique combination of the transport properties by using the neural network and making the following assumptions.

(*a*) Although it is well known that chlorides, hydroxides, sodium and potassium have complex reactions with the cement hydration products, the only ions permitted in the model to have adsorption or binding with the cement matrix were chlorides. The reason for making this assumption was to limit the number of variables to optimise.

(*b*) The chloride apparent diffusion coefficients (D_{app-Cl}) were determined from the intrinsic diffusion coefficient (D_{Cl}), the porosity of the material (ε), and the binding capacity factor (α) using Equation 4 (Lizarazo-Marriaga and Claisse, 2009).

$$\frac{\alpha}{\varepsilon} = \frac{D_{Cl}}{D_{app-Cl}} \quad (4)$$

(*c*) As the adsorptions for hydroxides and cations were neglected, the intrinsic and apparent diffusion coefficients were equal for those ions, giving $\alpha/\varepsilon = 1$.

(*d*) The chloride transport processes into the concrete were restricted by binding with a linear isotherm. Although it has been demonstrated experimentally (Delagrave *et al.*, 1997) that non-linear isotherms better reflect the adsorption phenomena, the model uses an average linear isotherm that represents the average adsorption of chlorides well and allows the

model to have a direct relationship between intrinsic and apparent diffusion coefficients.

(*e*) The pore solution at the start of the test does not include chloride ions and the equilibrium for hydroxyl ions was assumed to be maintained at a proportion of 33% of sodium and 66% of potassium. The ratio potassium to sodium in the starting materials was always 2. This assumption was based on published results (Bertolini *et al.*, 2004).

Test results and discussion

The total electrical charge passed, the chloride penetration during the test, and the evolution of the membrane potential were measured and analysed. Using the integrated computational model, the transport properties of the mixes tested were then found.

Charge and chloride penetration

The final charge passed and the chloride penetration are shown in Table 3. The results indicate that there were great benefits using either GGBS or PFA. The best results were obtained when replacements of 30% of PFA and 50% of GGBS were used. Figure 4 shows a summary of the properties measured relative to the values corresponding to the OPC samples. The addition of either mineral admixture produces a positive effect, reducing the charge and chloride penetration.

Membrane potential

The behaviour of the membrane potential across the sample during the test is shown in Figure 5 as contour graphs for samples OPC, 10% GGBS and 10% PFA; each graph represents the average of two samples. The horizontal axis is the length of the sample: 50 mm, and the vertical axis is the duration of the experiment: 6 h.

6

Table 3. Properties measured

Mix	OPC	10% PFA	30% PFA	50% PFA	10% GGBS	30% GGBS	50% GGBS
Penetration: mm	5·00	4·20	0·62	0·68	4·45	1·02	0·66
Charge: coulombs	4644	2435	1237	1253	4202	1848	1097
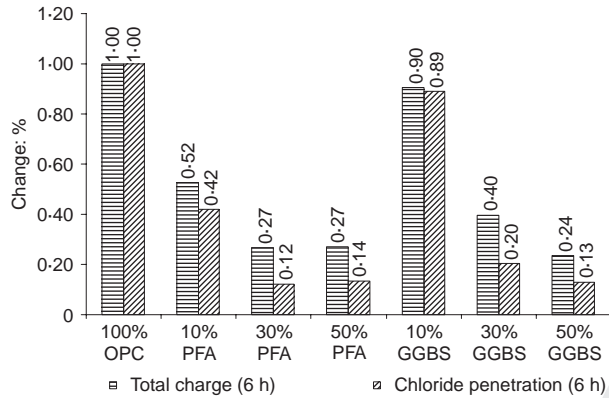
Figure 4. Total charge and chloride penetration (60 V)

The iso-response curves for the membrane potential show that the distribution of the voltage is not linear in time and space during a migration test. For all the contours there is a well-defined area with negative values of voltage (with a total voltage lower than the voltage at the start of the test) or areas with positive values (voltages bigger than the initial external applied voltage). Depending on the type and amount of mineral admixture used, the contour reached either a maximum or a minimum.

The contour plots indicate that, if the amount of admixture is increased, the voltage tends to reach more negative values, especially for the PFA mixes. If the total electric field is constant in the sample it would be expected that the behaviour of the conductivity would have the same trend as the current. However, as the voltage varies across the sample, the calculated conductivity at any point across the sample is transient in time and position owing to the effect of the membrane potential. This is very important because this effect needs to be included in the general equations of ionic transport in order to predict adequately the chloride penetration.

From the contour plots the membrane potential at any point and time during the test can be examined. This has academic and scientific value. However, such tests are expensive and not easy to complete. As an alternative, it has been proposed to use only the behaviour of the mid-point as a source of additional information. The electric membrane potential at the mid-point for each mix is shown in Figure 6. All mixes showed from the start a sustained decrease, reaching a local minimum and starting again to increase the voltage values.

Figure 5. Membrane potential measured

7

Figure 6. Membrane potential in the mid-point of the samples

Integrated numerical–neural network model

The artificial neural network (ANN) was trained using the results of the model and then used to obtain the transport properties from the experimental results. Table 4 shows the 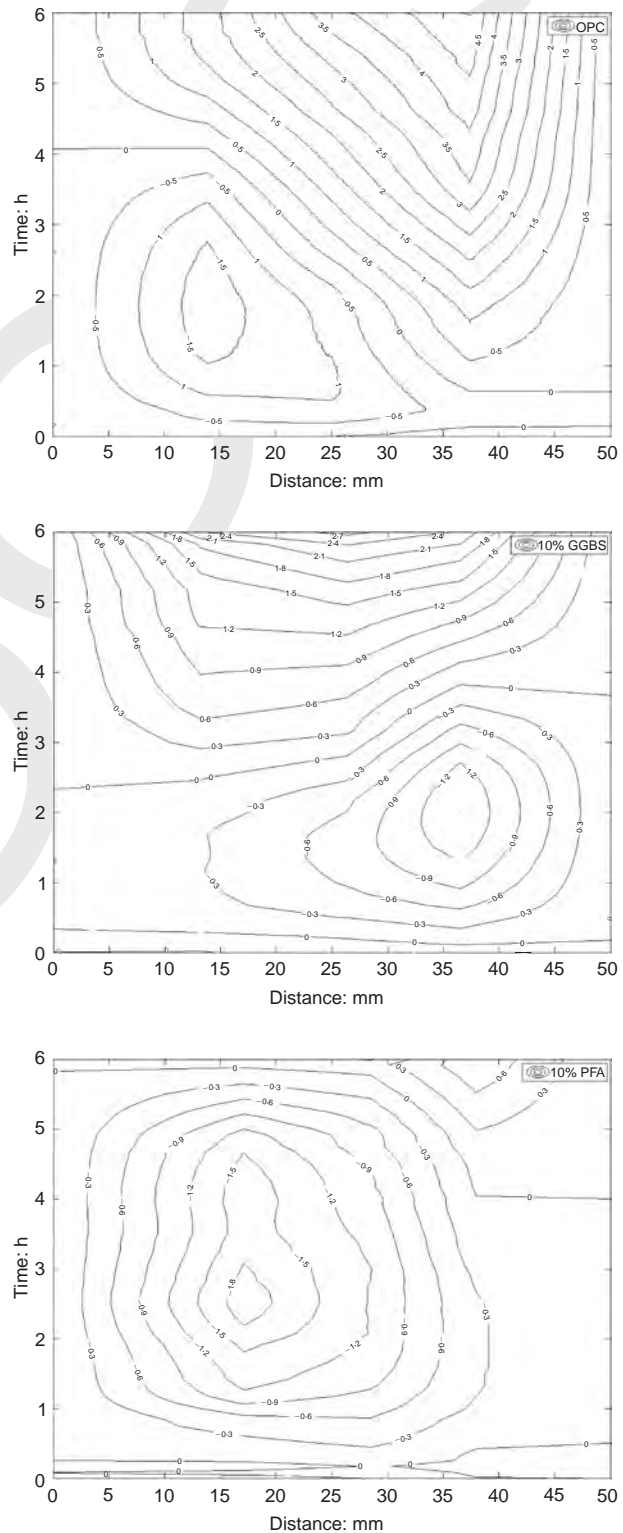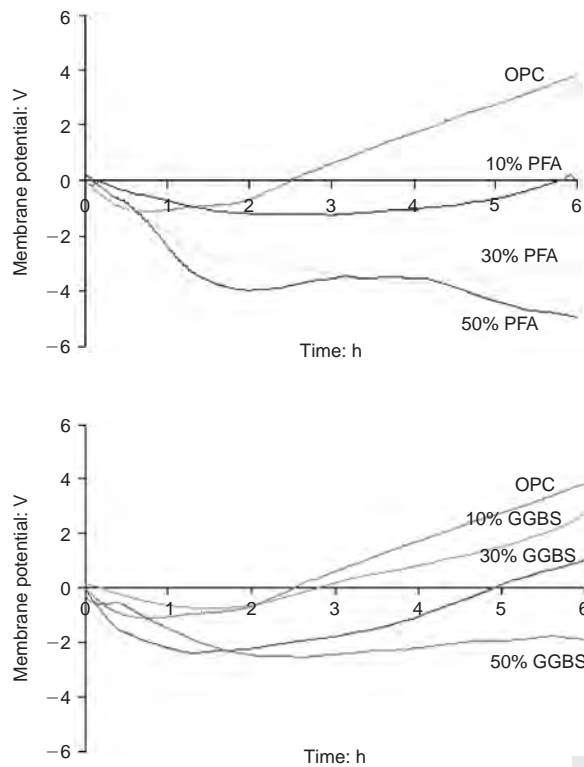numerical values of the properties obtained for all the mixes. In order to validate the results, the physical numerical model was run again for each mix using as inputs the values obtained from the neural network. As an example, Figure 7 shows the simulated and measured transient currents and mid-point membrane potentials for some of the samples used. From the graphs, it can be concluded that all the simulations are in very good agreement with the experiments, with the simulations for the current better than those for the mid-point voltage.

Transport properties

All the migration tests had non-steady-state conditions because of the characteristics of the experiments in which there were a small volume of external cells, a high external voltage, and a short duration. Although in some mixes it was possible that the chlorides reached the anode (thus giving a uniform condition through the sample), the depletion of the external cells ensured that a steady-state condition was never achieved. Therefore, the estimated Cl^- apparent diffusion coefficient and the intrinsic diffusion coefficients for the other ions in the system are for non-steady-state conditions. Figure 8 shows the calculated apparent coefficients of diffusion. The sodium and potassium coefficients were significantly smaller than the values for chlorides and hydroxides, as observed previously by other researchers (Andrade, 1993; Zhang *et al.*, 2002). These results confirm that the mobility of cations in a porous media is less than the mobility of anions. However, they are responsible for part of the total charge passed and are absolutely necessary in the simulation. Either in a self-diffusion test or in the presence of an applied voltage gradient across the specimen, the charge electroneutrality is maintained in the code by adjusting the membrane potential at all times. Small changes in the diffusion of cations produce large changes in the mid-point membrane potential. The diffusion coefficients obtained for sodium (D_{Na}) were greater than for potassium (D_K), the ratio D_{Na}/D_K was different depending on the amount and type of admixture. It was found that if there was an increase in the amount of mineral admixture, the ratio D_{Na}/D_K tended to decrease. Although the coefficient of diffusion for potassium is greater than for sodium in an infinite dilute solution (Bockris and Reddy, 1998), the results of this work showed that for the samples tested this is not always the case because of the ionic exchange among all the ions coming from the external cells and the pore solution. The ratio D_{Na}/D_K varies for each concrete sample according to all its transport properties including the composition of its pore solution at the start of the test.

The obtained migration diffusion coefficients for chlorides and hydroxides showed that both ions have a

Table 4. Transport properties calculated with the integrated model

	OH conc'n	Intrinsic coefficient, D_{Cl}: m^2/s	Intrinsic coefficient, D_{OH}: m^2/s	Intrinsic coefficient, D_{Na}: m^2/s	Intrinsic coefficient, D_k: m^2/s	Factor capacity, Cl	Capillary concrete porosity	Apparent coefficient, $D_{app/Cl}$: m^2/s
OPC	234·1	$1·94 \times 10^{-10}$	$7·81 \times 10^{-11}$	$3·52 \times 10^{-11}$	$1·07 \times 10^{-11}$	0·29	0·19	$1·25 \times 10^{-10}$
10%PFA	223·2	$1·09 \times 10^{-10}$	$3·68 \times 10^{-11}$	$2·17 \times 10^{-11}$	$8·21 \times 10^{-12}$	0·35	0·18	$5·55 \times 10^{-11}$
30%PFA	208·6	$8·17 \times 10^{-11}$	$2·56 \times 10^{-11}$	$1·59 \times 10^{-11}$	$7·23 \times 10^{-12}$	0·41	0·17	$3·37 \times 10^{-11}$
50%PFA	207·3	$1·05 \times 10^{-10}$	$2·99 \times 10^{-11}$	$1·60 \times 10^{-11}$	$8·19 \times 10^{-12}$	0·40	0·17	$4·42 \times 10^{-11}$
10%GGBS	226·0	$2·06 \times 10^{-10}$	$7·66 \times 10^{-11}$	$3·13 \times 10^{-11}$	$1·12 \times 10^{-11}$	0·30	0·18	$1·25 \times 10^{-10}$
30%GGBS	199·2	$1·00 \times 10^{-10}$	$3·80 \times 10^{-11}$	$1·92 \times 10^{-11}$	$7·71 \times 10^{-12}$	0·40	0·17	$4·27 \times 10^{-11}$
50%GGBS	199·1	$9·32 \times 10^{-11}$	$2·85 \times 10^{-11}$	$1·52 \times 10^{-11}$	$7·67 \times 10^{-12}$	0·42	0·17	$3·65 \times 10^{-11}$
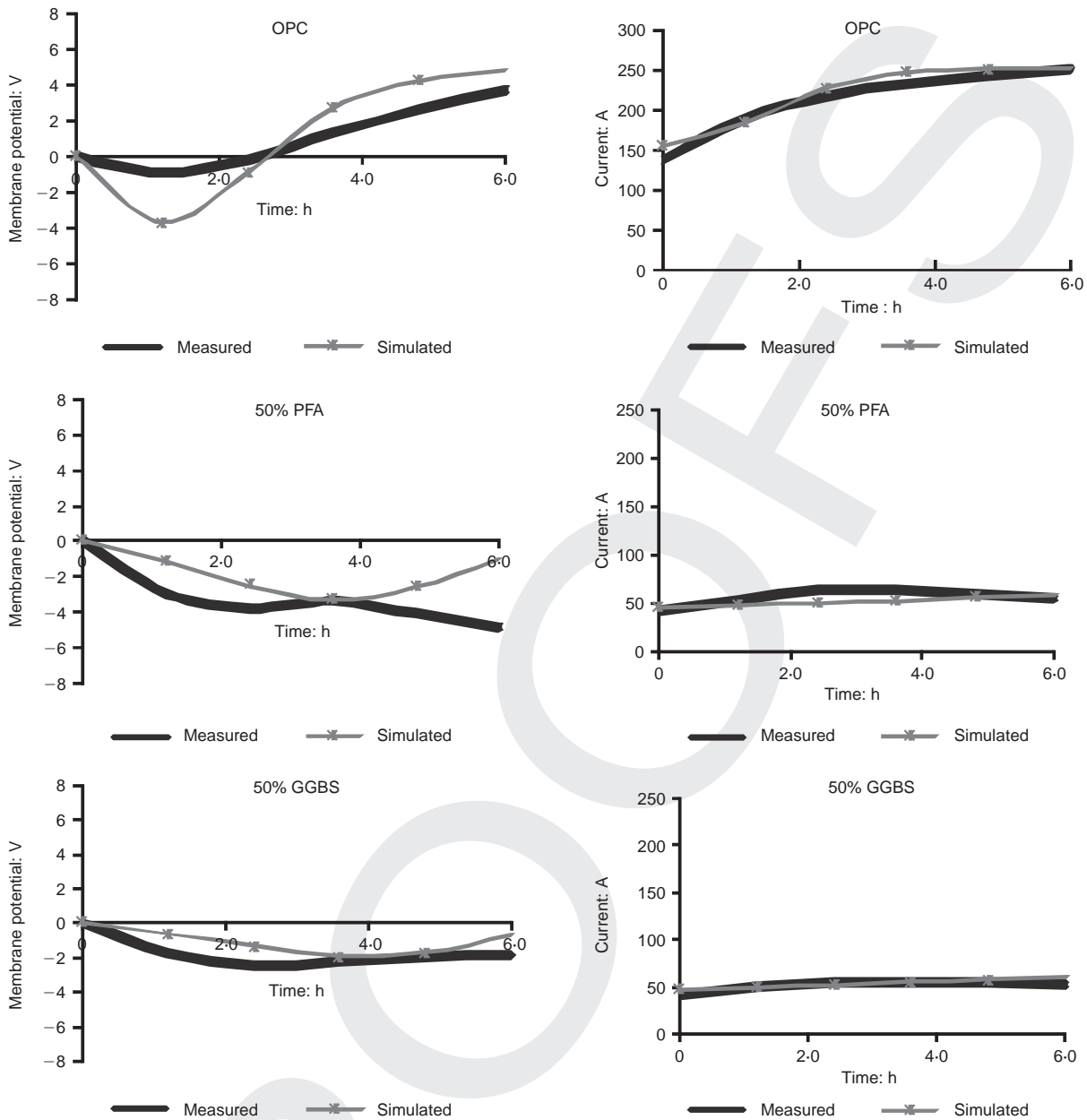
Figure 7. Transient mid-point membrane potential and current, both simulated and measured
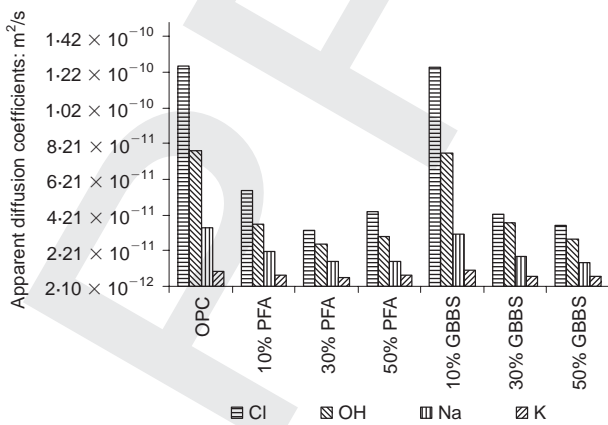
Figure 8. Calculated apparent diffusion coefficients

high mobility and are responsible for most of the transport of charge. However, in contrast with the conclusions of some researchers (Feldman *et al*., 1994; Zhang *et al*., 2002) the results of the simulations indicated that the diffusion coefficients of chlorides were greater than the hydroxide coefficients. The numerical values of the apparent chloride coefficients were between 10 and 60% greater than for the hydroxides depending on the level of mineral admixture replacement. With an increase in the amount of either mineral admixture, the ratio D_{app-Cl}/D_{OH} tends to decrease. It is believed that the ratio between the diffusivity of chlorides and hydroxides depends on all the external conditions of the test and all the internal transport properties and features of the concrete and it is not a rule that it is always less than one.

9

On the other hand, the calculated apparent diffusion coefficients obtained were relatively high compared with some reported in the literature. Usually, for a concrete of good quality, a chloride diffusion coefficient on the order of 10^{-12} m^2/s is expected. However, these differences can be explained through two reasons: first, the water binder ratio for all the mixes used was just 0·49; this means that the concrete used was not the most impermeable. Second, the diffusion coefficients obtained in this work apply to a multispecies system coupled through the membrane potential, instead of those obtained in experiments and reported in literature where ions are physically affected by the ionic exchange among species, but the coefficients are calculated through equations that account for only single chloride diffusion and no ionic interaction.

The simulated results for the initial composition of the pore solution are shown in Figure 9 as the hydroxide ion (OH⁻) concentration. For the OPC sample, for example, a numerical value of 234 mol/m^3 was obtained for hydroxide that corresponds to 78 mol/m^3 of sodium and 156 mol/m^3 of potassium in order to keep the initial electroneutrality of the system (units are mol per cubic metre of pore solution). With the increase of the amount of mineral admixture, a reduction was found in the initial hydroxide composition of the pore solution as was expected. This has been previously reported by Page and Vennesland (1983). The calculated hydroxide reduction of the solution into the pores for the 30% GGBS blended concrete was around 15% with respect to the OPC, and for the 30% PFA blended concrete was around 10% with respect to the OPC. Above 30% of replacement, there was no further reduction in the hydroxide ion concentration.

From the integrated model, the calculated porosity was found. There was a reduction in the porosity with an increase in the amount of any admixture, and the beneficial effect of GGBS and PFA was greater with mixes of 30% PFA and 50% GGBS respectively. Figure 10 shows the variation of the calculated porosity for different percentages of admixture. In the same way, the calculated chloride capacity factor of binding is

Figure 10. Calculated concrete capillary porosity against mineral admixture level of replacement

shown in Figure 11. It was found that it tends to increase with an increase in the amount of mineral admixture. The greatest chloride capacity factor was found in the mixes of 30% PFA and 50% GGBS and confirms the optimum percentages for those materials.

Correlation of the estimated chloride diffusion coefficients with the measured charge and penetration

The correlation coefficient r between the obtained chloride diffusivity and the chloride penetration after 6 h was calculated in order to find out their association and dependency. Figure 12 shows the regression that fit the best straight line to the data and shows the numer-

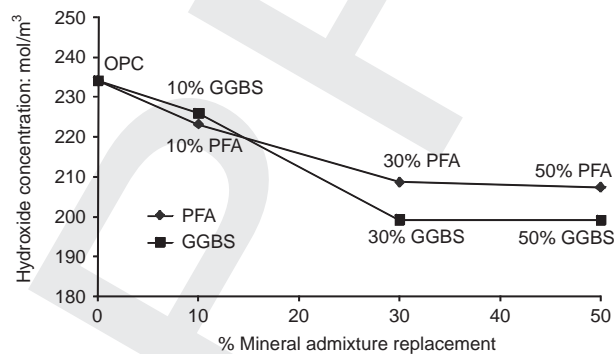*Figure 11. Calculated capacity factor plotted against level of mineral admixture replacement*

Figure 9. Calculated hydroxide concentration at the start of the test plotted against level of mineral admixture replacement
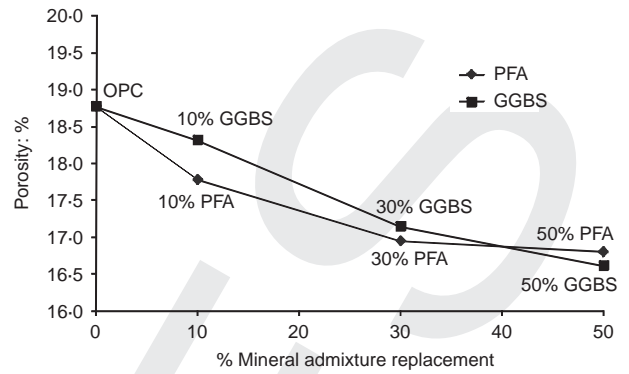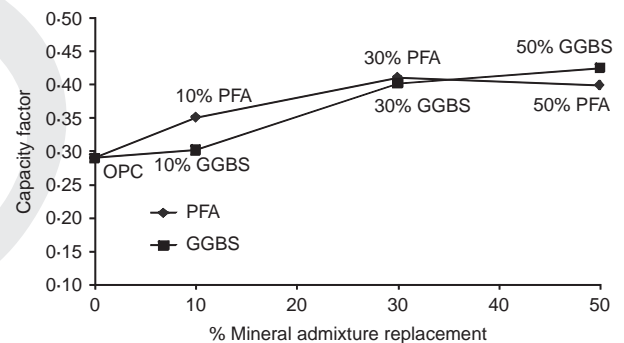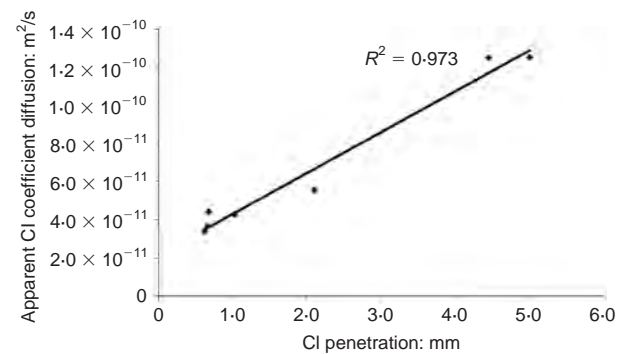

Figure 12. Correlation between the calculated Cl apparent diffusion coefficient and the Cl penetration measured during the test

ical coefficient of determination R^2, which indicates the amount of variability. The value of correlation was $r = 0.99$, and shows that the apparent chloride coefficient of diffusion obtained through the Integrated numerical–neural network model is in good agreement with the measured penetration regardless of the mineral admixtures used. From Figure 12, it is argued that for any sample of concrete the information of current obtained from the traditional ASTM C1202 test and the membrane potential obtained from the electrochemical test presented in this paper define together the transport properties of the material. In addition, the numerical values of the diffusion coefficients can be obtained from the computational model proposed.

The relationship between the charge in coulombs obtained from the standard ASTM C1202 test and the calculated chloride diffusion coefficients is shown in Figure 13. The correlation between the charge and the intrinsic (part (a)) and apparent (part (b)) coefficients is shown. The link between both coefficients was defined by Equation 4. The intrinsic coefficient defines the transport of matter when the flux is calculated per unit cross-sectional area of the pores and the concentration in the free liquid. In contrast, the apparent coefficient defines the transport of any ion when the flux is calculated per unit area of the porous material and the average concentration in the material. The reason why both coefficients are presented is because the computer model calculates the intrinsic coefficient, but the apparent coefficients are normally used to predict the service live of concrete structures. From Figure 13(b) it can be

seen that the relation charge–apparent chloride coefficient for GGBS had a very good correlation with a determination coefficient $R^2 = 0.974$. According to this, the equation that defines that relationship can be used as a tool to estimate the apparent diffusion coefficient in m^2/s from the measured value of charge in coulombs for GGBS mixes ($D_{app-GGBS}$) with any level of replacement between 0 and 50%.

$$D_{app-GGBS} = 3 \times 10^{-14} \times charge - 4 \times 10^{-13} \quad (5)$$

For PFA mixes, the charge and the apparent chloride diffusion coefficient had an acceptable correlation as shown in Figure 13(b); in general terms this shows that the ASTM C1202 test adequately predicts the chloride penetrability in a blended GGBS or PFA concrete. However, it has been reported extensively in the literature that in a migration test the flow of current and the charge passed through the mixtures with mineral admixtures, especially with PFA, is strongly related to the conductivity of the pore fluid within the concrete (Chindaprasirt *et al*. 2007; Sengul *et al*., 2005; Wee *et al*., 2000; Yang and Wang, 2004). As the percentage of any admixture replacement affects the ionic concentration and the conductivity of concrete, Figure 14 shows the correlation between the ratio of chloride diffusivity to charge plotted against percentage of admixture replacement for the intrinsic (Figure 14(a)) and apparent (Figure 14(b)) coefficients. Figure 14(a) shows that the ratio of intrinsic coefficient to charge increases linearly with the increase of the amount of mineral admixtures,
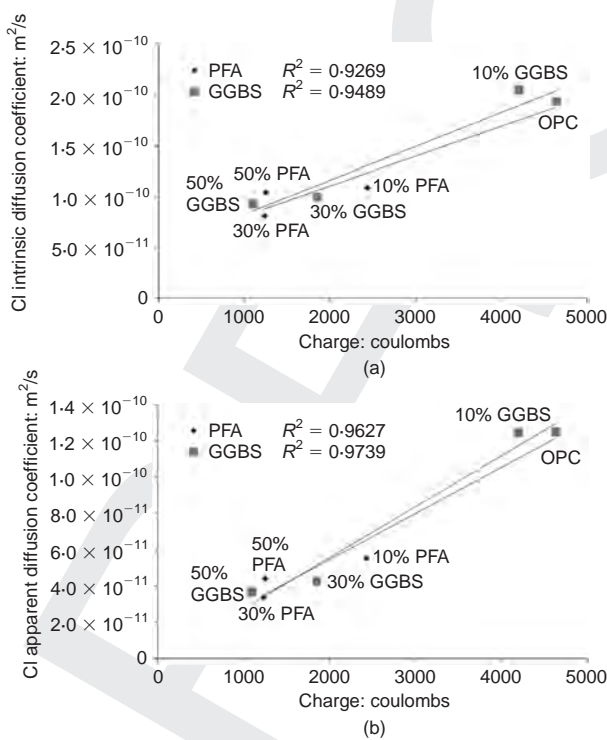

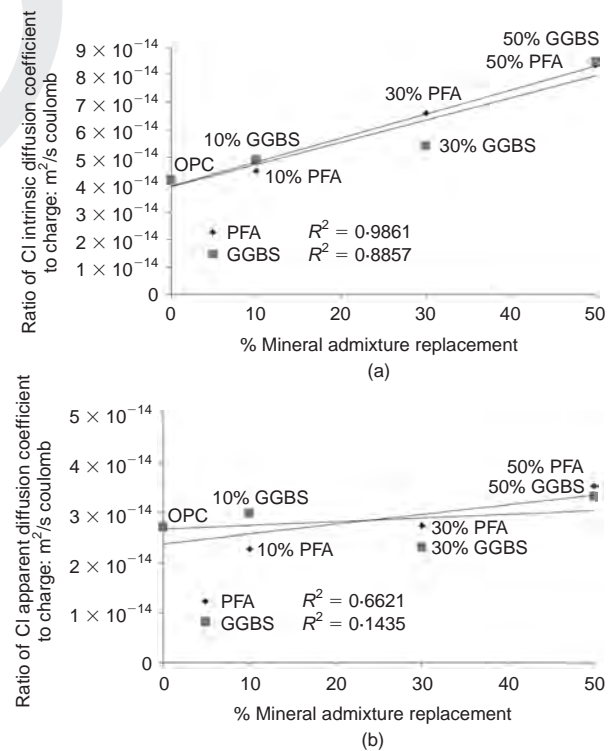*Figure 13. Correlation between diffusion coefficients and charge*

Figure 14. Correlation between diffusion coefficients and mineral admixture replacement

especially for PFA which showed a determination coefficient of $R^2 = 0 \cdot 986$. The chloride intrinsic diffusion coefficient for PFA ($D_{int\text{-}PFA}$) in m^2/s can be obtained from Equation 6 from the measured value of charge in coulombs and the level of PFA as a percentage (%PFA). The apparent coefficient can be calculated from

$$D_{int-PFA} = [9 \times 10^{-16} \times (\%PFA) + 4 \times 10^{-14}]$$
$$\times \text{Charge} \qquad (6)$$

In Figure 14(b), the ratio of apparent diffusion to charge plotted against percentage of admixture shows that there is a poor relationship between them, especially for the GGBS mixes. The very good correlation of the ratio of chloride intrinsic diffusion coefficient to charge plotted against percentage of admixture for PFA mixes shows that when this admixture is used it is necessary to correct the charge calculated during the ASTM C1202 in order to obtain more reliable results.

Conclusions

(*a*) Measuring the voltage within a sample is a powerful method to obtain more useful data from migration tests.

(*b*) Using ANNs trained on numerical simulations of the migration test yields viable results for the fundamental properties of concrete. The initial hydroxide composition of the pore solution, the chloride binding capacity, the porosity and the diffusion coefficients for all the species involved were estimated with good results.

(*c*) Results obtained show that the ratios between sodium and potassium, and chlorides and hydroxides in a migration test do not follow the behaviour of single species in a dilute solution. In the same way, the calculated values of chloride diffusion coefficient were larger than those usually reported in the literature; however, they are in good agreement with the measured chloride penetration.

(*d*) This paper presents methods to modify the ASTM C1202 test and obtain far more information about the samples and their potential durability.

Acknowledgements

References

Andrade C (1993) Calculation of chloride diffusion coefficients in concrete from ionic migration measurements. *Cement and Concrete Research* **23(3)**: 724–742.

American Society for Testing and Materials (ASTM) (2005) *Standard Test Method for Electrical Indication of Concrete's Ability to Resist Chloride Ion Penetration*. ASTM International, West Conshohocken, PA, ASTM-C1202

Bertolini LBE, Pedeferri P and Polder RB (eds) (2004) *Corrosion of Steel in Concrete: Prevention, Diagnosis, Repair*. Wiley, Chichester.

Bockris J and Reddy A (1998) *Modern Electrochemistry 1 Ionics*. Plenum Press.

Chindaprasirt P, Rukzon S and Sirivivatnanon V (2008) Resistance to chloride penetration of blended Portland cement mortar containing palm oil fuel ash, rice husk ash and fly ash. *Construction and Building Materials* **22(5)**: 932–938.

Claisse PA and Beresford TW (1997) *Obtaining More from the Electrical Chloride Test*. American Concrete Institute, Farmington Hills, MI, ACI–SP 170, 170–57.

Delagrave A, Bigas JP, Ollivier JP, Marchand J and Pigeon M (1997) Influence of the interfacial zone on the chloride diffusivity of mortars. *Advanced Cement Based Materials* **5(3)**: 86–92.

Feldman RF, Chan, GW, Brousseau RJ and Tumidajski PJ (1994) Investigation of the rapid chloride permeability test. *ACI Materials Journal* **91(2)**: 246–255.

Khitab A, Lorente S. and Ollivier JP (2005) Predictive model for chloride penetration through concrete. *Magazine of Concrete Research* **57(9)**: 511–520.

Krabbenhoft K and Krabbenhoft J (2008) Application of the Poisson–Nernst–Planck equations to the migration test. *Cement and Concrete Research* **38(1)**: 77–88.

Lizarazo-Marriaga J and Claisse P (2009) Effect of the non-linear membrane potential on the migration of ionic species in concrete. *Electrochimica Acta* **54(10)**: 2761–2769.

Lorente S, Voinitchi D, Bégué-Escaffit P and Bourbon X (2007) The single-valued diffusion coefficient for ionic diffusion through porous media. *Journal of Applied Physics* **101(2)**.

Mcgrath PF and Hooton RD (1996) Influence of voltage on chloride diffusion coefficients from chloride migration tests. *Cement and Concrete Research* **26(8)**: 1239–1244.

Narsilio GA, Li R, Pivonka P and Smith DW (2007) Comparative study of methods used to estimate ionic diffusion coefficients using migration tests. *Cement and Concrete Research* **37(8)**: 1152–1163.

NORDTEST (1999) *Concrete, Mortar and Cement-Based Repair Materials: Chloride Migration Coefficient from Non-Steady-State Migration Experiments*. NORDTEST, Esbo, Finland, NTBUILD-492 NORDTEST method.

Page CL and Vennesland O (1983) Pore solution composition and chloride binding capacity of silica-fume cement pastes. *Materials and Structures* **16(1)**: 19–25.

Samson E, Marchand J and Snyder KA (2003) Calculation of ionic diffusion coefficients on the basis of migration test results *Materials and Structures* **36(3)**: 156–165.

Sengul O, Tasdemir C and Tasdemir MA (2005) Mechanical properties and rapid chloride permeability of concretes with ground fly ash. *ACI Materials Journal* **102(6)**: 414–421.

Sugiyama T, Ritthichauy W and Tsuji Y (2003) Simultaneous transport of chloride and calcium ions in hydrated cement systems. *Journal of Advanced Concrete Technology* **1(2)**: 127–138.

Tang L (1999) Concentration dependence of diffusion and migration of chloride ions: Part 2. Experimental evaluations. *Cement and Concrete Research* **29(9)**: 1469–1474.

The Mathworks (2001) *I. Curve Fitting Toolbox – For Use With MATLAB*. The Mathworks, Inc., Natick, MA.

Truc O (2000) *Prediction of Chloride Penetration into Saturated Concrete – Multi-species Approach*. PhD thesis, Chalmers University, Goteborg, Sweden.

Truc O, Ollivier J-P and Nilsson L-O (2000) Numerical simulation of multi-species transport through saturated concrete during a migration test – MsDiff code. *Cement and Concrete Research* **30(10)**: 1581–1592.

Wee TH, Suryavanshi AK and Tin SS (2000) Evaluation of rapid chloride permeability test (RCPT) results for concrete containing mineral admixtures. *ACI Materials Journal* **97(2)**: 221–232.

Yang CC and Wang LC (2004) The diffusion characteristic of concrete with mineral admixtures between salt ponding test and accelerated chloride migration test. *Materials Chemistry and Physics* **85(2–3)**: 266–272.

Zhang JZ, Li J and Buenfeld NR (2002) Measurement and modelling of membrane potentials across OPC mortar specimens between 0·5 M NaCl and simulated pore solutions. *Cement and Concrete Composites* **24(5)**: 451–455.

Discussion contributions on this paper should reach the editor by ???

1: AQ Please note, Chindaprasirt et al. 2007 in text citation, but 2008 and reference list at end of paper. Please check ref. details and amend as necessary

2: AQ Please give location of publisher

3: AQ Details of ACI have been inserted for publisher, OK? Also, what is 170-57? Is this a page no. or some other detail of the publication?

4: AQ Please give page nos. for this journal reference

DETERMINATION OF THE CHLORIDE TRANSPORT PROPERTIES OF BLENDED CONCRETES FROM A NEW ELECTRIC TEST

Juan Lizarazo-Marriaga[1,2] and Peter Claisse[2]

(1) Departamento de Ingeniería Civil, Universidad Nacional, Bogotá-Colombia

(2) Construction Materials Applied Research Group, Coventry University CV1 5FB, UK

Abstract

This paper describes methods to measure the movement of chloride in concrete, which causes corrosion of steel reinforcement. The general law governing ionic movements in concrete due to the chemical and electrical potential is known as the Nernst-Planck equation. In an electrical migration test, because of the ion-ion interactions, there are ionic potentials that affect the flux producing a non-linearity of the electric field. These keep the electroneutrality of the species involved. This paper summarises a theoretical and experimental investigation of the application of these electric membrane potentials and the electrical current to the simulation of the migration of chlorides in concrete. A new test used to measure the membrane potentials has been developed and carried out with samples of concrete blended with pulverised fly ash (FA) and ground granulated blast furnace slag (GGBS). A numerical model using the classical equations, but including changes in the voltage distribution through the concrete was optimised using an artificial neural network (ANN) model. Based on the experimental results and the simulations, the intrinsic diffusion coefficients of all the species were numerically obtained, as well as the hydroxide composition of the pore solution, the porosity and the chloride capacity of binding.

1. INTRODUCTION

Due to very significant problems with reinforcement corrosion the penetration of chloride ions in concrete has been studied intensively for more than 40 years worldwide. As a result, physical models and experiments are well established. However, with the advent of more powerful computers, new numerical and experimental techniques are being applied to the solution of the complex problem of chloride penetration. This paper reports a research programme aimed at giving a better understanding of the phenomena involved in the chloride penetration in cement based materials. The general approach used is to solve the Nernst-Planck equation numerically for two physical ideal states that define the possible conditions under which chlorides will move through concrete. These conditions are voltage control and current control.

The first condition called "voltage control" is defined by a concrete sample placed between two electrodes that apply a constant potential difference between them. Under this condition a migration test like the ASTM C1202 [1] or NT-492 [2] can be simulated. The flow of any species present in the pore solution or in any external cells is defined according to the Nernst-Planck equation (1). In order to keep the charge neutrality throughout the sample at all times for all the ions together the term for the electrical field is distorted in each position and checked to ensure that charge neutrality is maintained.

$$J_i = D_i \frac{\partial c_i}{\partial x} + \frac{z_i F}{RT} D_i c_i \frac{\partial E}{\partial x} \qquad (1)$$

In equation 1 c_i is the ionic concentration of species i in the pore fluid; x the distance; z_i the electrical charge of species i; F the Faraday constant; E is the electrical potential; dE/dx the electrical field; J_i is the flux of specie i; D_i is the diffusion coefficient of species i; R is the gas constant; and T is absolute temperature. The electrical field dE/dx affected by the charge neutrality condition is a function of the constant external applied voltage (φ) and the internal voltage generated by the differences of mobility of the multispecies system (E_p). Although equation 2 comes from the condition under zero current, that zero current condition makes reference to the total current of the system, and it does not imply that the mobile species does not carry some current. A complete deduction of that equation is presented in reference [3], where is shown that the electrical field can be divided in an ohmic potential related with the external voltage and a membrane potential related with the mobile species.

$$\frac{\partial E}{\partial x} = ohmic.potential(\varphi) - membrane.potential(\partial E_p) \qquad (2)$$

That internal voltage is known as the membrane potential voltage [3] and physically it accounts macroscopically for all the complex phenomena involved in the pore solution (e.g. the ionic exchange and the electrical double layer). It is responsible for the non-linear behaviour of the voltage during a migration test. Microscopically the electrical field due to the membrane potential can be expressed according to the equation 3 [4].

$$\frac{\partial E_p}{\partial x} = \frac{RT}{F} \frac{\sum_i z_i D_i \frac{\partial c_i}{\partial x}}{\sum_i z_i^2 D_i c_i} \qquad (3)$$

Macroscopically the membrane potential is found with the following procedure. Faraday's law allows calculating the current passed (i_i) for each ion (equation 4); in addition, due to Kirchhoff's first law, for any time, the total current density that comes to a certain point must be equal to the current density that comes out of it. This means that the voltage needs to be adjusted in each point into the sample in order to ensure this condition [5].

$$i_i = -z_i F J_i A \qquad (4)$$

The second condition is called "current control", it makes reference to a condition similar to voltage control, but to the sample between two electrodes is subject to constant electrical current. For this condition, when the current is zero, the phenomenon of normal diffusion with no applied potential can be simulated. It is of note that when chloride ions are permitted to diffuse through concrete the system acts like a dry-cell battery and a voltage is developed. Some previous authors [6] have modelled chloride diffusion by simply integrating Fick's law and using a diffusion coefficient for chloride ions. The true situation in normal diffusion is, however, far more complex because the voltage that is developed will inhibit further transport unless it is dissipated by further ionic transport. This further transport may be negative ions (such as OH-) moving in the opposite direction to the Cl⁻ or positive ions (such as Na+) moving with them and may be the determining factor for the rate of transport of the Cl-. This cannot be modelled with a voltage control algorithm set to zero applied voltage because this implies that the two ends of the sample are short-circuited. Figure 1 shows this condition for a typical sample in an ASTM C1202 test and it may be seen that current flows. Thus a new algorithm is being developed in which the system is controlled by a constant current.

If the new algorithm is used with a non-zero current the phenomena of either cathodic protection or electrochemical chloride removal can be modelled. For this condition the physical equations used are the same used previously, however, in this approach, in addition to keep the charge neutrality throughout the sample at all times for all the ions together is necessary to keep the current density constant during all the time. That new condition makes the procedure to calculate the membrane potential slightly different to the one presented previously. Figure 1 shows a schematic representation of the conditions used.

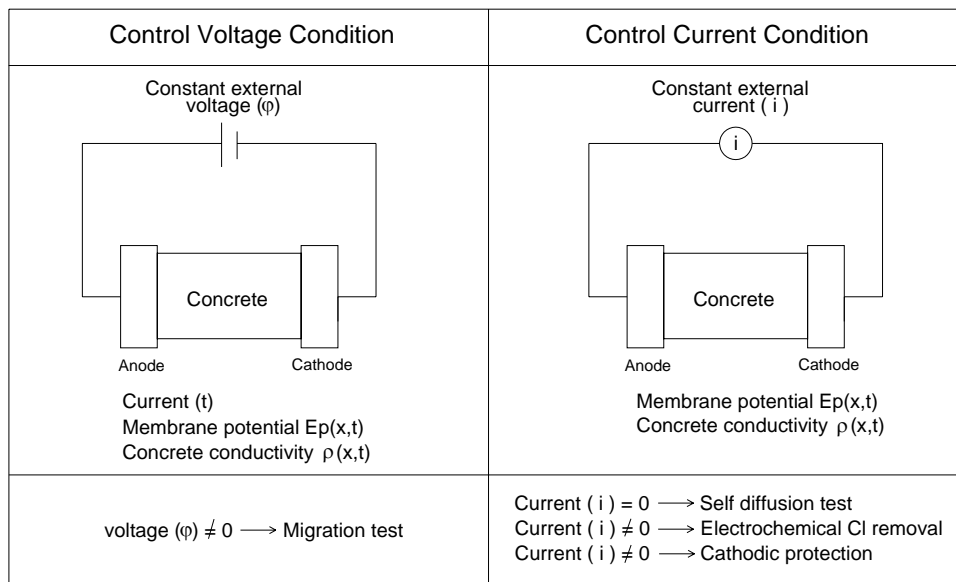Figure 1 Voltage and current conditions

The voltage control model simulates a standard electrical migration test. As result, it gives the total transient electrical current, the electrical membrane potential and the ionic concentrations. As inputs, it requires the external conditions of the test and the transport related properties. Theoretically, this approach, or any similar one, gives a better

understanding of the complex phenomena involved. But in a practical situation its application is limited because of the difficulties found in the determination of all the transport properties. The accurate determination of the transport related properties, especially the coefficients of diffusion of all the species in concrete, is not easy. However, the electrical current and the electrical membrane potential can be measured experimentally.

In order to give an alternative approach to finding the transport related properties of concrete, this paper reports on a computer model based on the optimization of the voltage controlled condition. The optimization technique used was an artificial neural network (ANN) which was trained running the model a number of times and using the results as a training database. After the training process the transient current and a new test developed to measure the transient membrane potential were used to calculate the diffusion coefficients for all the ions involved. The model was applied to blended concrete mixes of Portland cement (OPC), ground blast furnace slag (GGBS), and pulverised fuel ash (PFA), for which the electrical current and the membrane potential were obtained experimentally.

2. MODELLING

2.1. Artificial Neural Networks

Artificial Neural Networks (ANNs) are artificial intelligence techniques used as information processing systems, capable of learning complex cause and effect relationships between input and output data [7]. They are highly nonlinear, and can capture complex interactions among input and output variables. Like in human beings, in an ANN a neuron is connected to other neurons through links that produce a stimulus to the entry and exit as a response, in addition, they have the ability to communicate among them. A neural network has a finite number of neurons distributed in the input layer, which represents the input data, an output layer, which computes the neural networks output, and one or more intermediary layers called hidden layers, which generate the relationships between layers of entry and exit.

A neural network is trained to develop a particular task or function to adjust the intensity with which the neurons are interconnected. The back-propagation algorithm is the most used in civil engineering applications. Initially in each connection between neurons is assigned a weight, a value that is fitted during the back propagation learning process. Commonly a neural network is trained or adjusted in a way that the input variables correspond with an expected output. This situation is shown in Figure 2; the network is trained by adjusting the weights through the comparison between the outputs (values predicted by the model) and the target values.

2.2. Computer Model

The electro-diffusion numerical routine (voltage control model) was used for calculating the transient current passed and the mid point membrane potential during a migration test. However, as the constitutive transport properties were unknown, a neural network algorithm was trained to optimize them. As a result, with the optimization process, the transport properties of a concrete sample could be determined when the current and the mid-point membrane potential were measured during a migration test. Figure 3 shows a conceptual diagram of the model
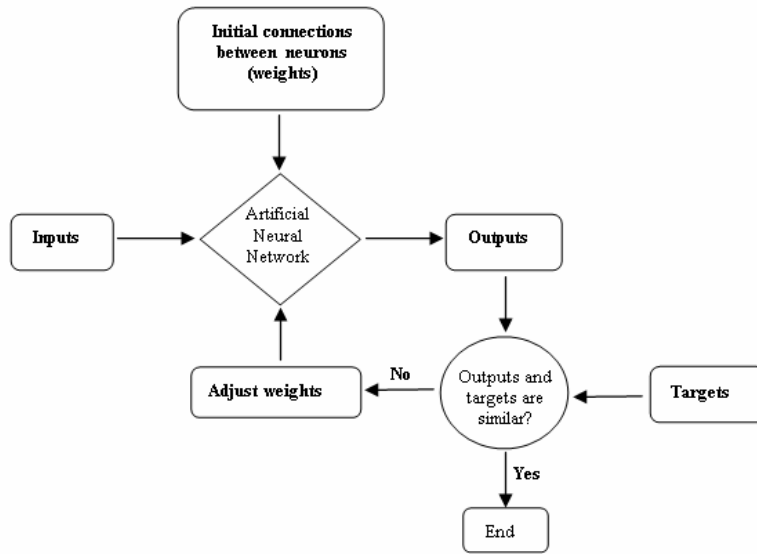
Figure 2 Back-propagation training of the neural network

The optimization model used a feed-forward back propagation-network with a multilayer architecture. Six neurons define the input layer, they correspond to values of the current and the mid point membrane potential in the sample at different times. A middle hidden layer had 3 neurons, and the output layer output had 7 neurons corresponding to the intrinsic diffusion coefficients of Cl, OH, Na and K, the porosity, the hydroxide concentration in the pore solution at the start of the test, and the binding capacity factor for chloride ions. The neural network model was constructed using the neural network tool box of Matlab^{TM} [7].
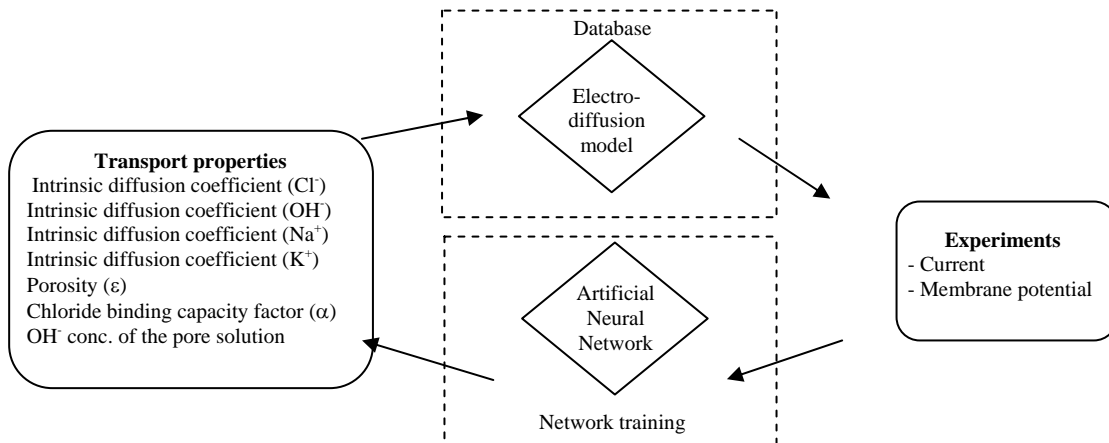

Figure 3 Conceptual diagram integrated model

In the electro-diffusion model the concentration of ions is defined in two ways: the free ions per unit volume of liquid (C_l) and the total ions per unit volume of solid (C_s). The ratio of

those concentrations is named the factor binding capacity (α). In the same way, the intrinsic coefficient (Dcl) defines the transport of matter when the flux is calculated per unit cross-sectional area of the pores and the concentration in the free liquid. In contrast, the apparent diffusion coefficient (Dapp-cl) defines the transport of any ion when the flux is calculated per unit area of the porous material and the average concentration in the material. The reason why both coefficients are presented is because the computer model calculates the intrinsic coefficient, but the apparent coefficients are normally used to predict the service live of concrete structures.

With the current and the mid point membrane experimentally measured, the transport properties were found by using the trained neural network assuming the following conditions:

(i) Although it has been proved experimentally that non-linear isotherms describes the absorption phenomena most accurately, the binding chloride capacity calculation in the model used a linear isotherm. By integrating the definitions given above it is possible to prove that the ratio chloride intrinsic diffusion to apparent diffusion coefficient is equal to the ratio binding factor capacity to porosity.

$$\frac{\alpha}{\varepsilon} = \frac{D_{Cl}}{D_{app-cl}}$$

(5)

(ii) At the start of the test the chemical pore solution was assumed to be composed of the ions OH^-, K^+, and Na^+, and in order to keep the electroneutrality it was assumed that the concentration of hydroxyl ions was equilibrated with a proportion of 33% of sodium and 66% of potassium.

(iii) Although the binding properties for OH^-, K^+, and Na^+ can be adjust in the electro-diffusion model and in the reality they have binding properties, the adsorption for those species was neglected due to the high number of variables to optimize with the neural network.

3. EXPERIMENTS

3.1. Current and membrane potential in the ASTM C1202 test

The procedure used to measure the electrical current was the standard ASTM C1202 test. In this, a steady external electrical potential of 60 volts D.C was applied to a sample of concrete of 50 mm thick and 100 mm diameter for 6 hours. The Anode and cathode were filled with 0.30 N sodium hydroxide and 3.0% sodium chloride solutions respectively. The samples were prepared for the test in conformity with the standard.

In addition to the measurements in the standard test a new electrochemical measurement was carried out. A salt bridge was added in the middle point of the sample to check the voltage distribution. A hole of 4 mm diameter and 6-9 mm deep was drilled at that point. The salt bridge used was a solution of 0.1 M potassium chloride (KCl) in order to avoid any junction potential at the interface of the salt solution and the pore solution. The voltage was measured using a saturate calomel electrode (SCE) relative to the cathode cell. The current through the concrete and the voltage in the mid point inside the sample were measured

continuously every 10 seconds with a data logger. The membrane potential was calculated by subtracting the value of the voltage measured from the initial value measured at the start of the test and the value of voltage measured at any time in the midpoint position.

$$\Delta V = V_{Ti} - V_0$$

(6)

ΔV corresponds to the membrane potential, V_{Ti} is the voltage measured at time t, and V_0 is the voltage at the start of the test. A more detailed description of the experiment can be found in reference [3].

3.2 Materials

Concrete samples of OPC blended with GGBS and PFA with a replacement proportion of 50% and 30% respectively were mixed. Table 1 shows the mix designs and the nomenclature used in this paper. All the migration tests were carried out on samples around 100 days old which were kept in a controlled humidity and temperature room at 21±1 °C and RH of 97% until testing.

Table1 Concrete mix design

| Mix | w/b | % | | | Unit content: kg/m3 | | | | | |
		OPC %	PFA %	GGBS %	OPC [Kg]	PFA [Kg]	GGBS [Kg]	Fine agg. [Kg]	Coarse agg. Kg]	Binder [Kg]
OPC	0.49	100	0	0	394	0	0	692	988	394
30%PFA	0.49	70	30	0	276	118	0	684	977	394
50%GGBS	0.49	50	0	50	197	0	197	690	985	394

4. RESULTS AND DISCUSSION

The results of the electrochemical tests for all the mixes are showed in figure 4. Each graph shows the transient current measured according the ASTM C1202 and the membrane potential at the mid point of the sample. For the graphs of membrane potential the noise found experimentally was removed with a commercial curve fitting software [8].
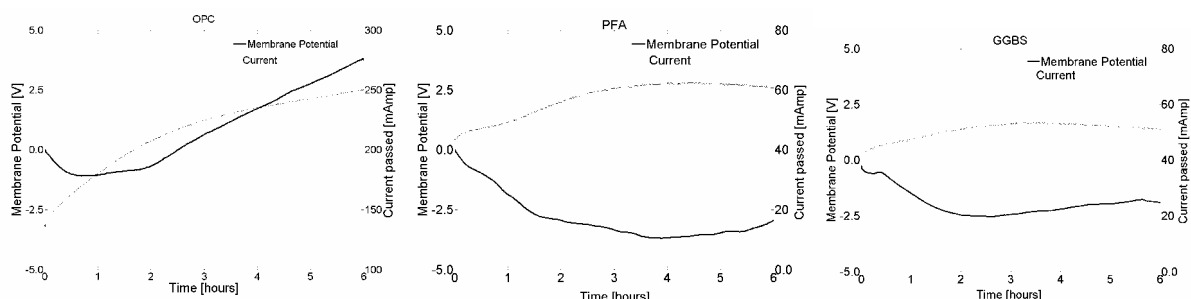

Figure 4 Membrane potential and current measured

The trained neural network was fed with the experimental measured transient current and the mid point voltage, and the transport related properties were calculated. The coefficients of diffusion obtained are shown in figure 5, for all the mixes and all the ions considered in this research. Although the effective diffusion coefficients were calculated by the model, the apparent diffusion coefficients are presented in the figure. It is important to notice, that for hydroxide, sodium, and potassium the intrinsic coefficients are equal to the apparent coefficients because the adsorption was neglected for those ions.
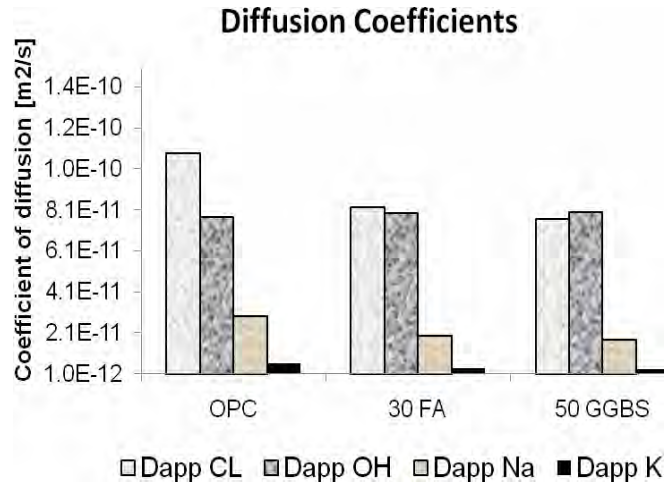

Figure 5 Coefficients of diffusion for all the species

In the same way, figure 6 shows the porosity, the chloride binding capacity, and the initial concentration of hydroxide calculated with the computer model at the start of the migration test. As was expected, the addition of mineral admixtures decreases the porosity, increases the capacity factor, and decreases the alkalinity of the pore solution. Although no experimental data is presented for those properties, the values obtained are in the ranges expected for the materials used.
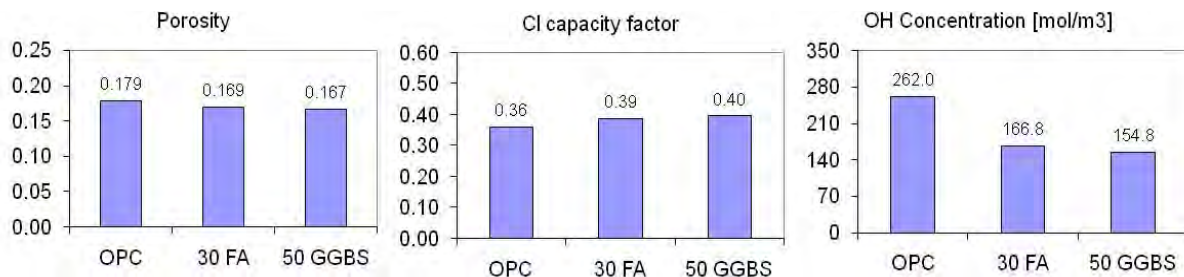

Figure 6 Porosity, capacity factor and OH$^-$ concentration estimated

5. CONCLUSIONS

- A computer modelling system has been developed by combining an electrochemical algorithm which uses the classical equations with an optimizing neural network algorithm. The model has been used successfully in combination with an electrochemical test.

- The calculated properties will be used as inputs to simulate the penetration of chloride under a self diffusion conditions using the condition known as current control (zero current)

6. ACKNOWLEDGEMENTS

The authors would like to thank the support of the Universidad Nacional de Colombia, COLFUTURO, and the Programme Alβan (Scholarship No. E06d101124CO).

7. REFERENCES

[1] American Society for Testing and Materials, ASTM-C1202, 'Standard Test Method for Electrical Indication of Concrete's Ability to Resist Chloride Ion Penetration', 2005.
[2] NTBUILD-492, 'Nordtest method: Concrete, mortar, and cement–based repair materials: Chloride migration coefficient from non-steady-state migration experiments', 1999.
[3] Lizarazo-Marriaga J., Claisse P., 'Effect of the non-linear membrane potential on the migration of ionic species in concrete', Electrochim. Acta **54** (10) (2009) 2761-2769.
[4] Lorente S., Voinitchi D., Bégué-Escaffit P., Bourbon X., 'The single-valued diffusion coefficient for ionic diffusion through porous media', J. Appl. Phys. **101**(2) (2007)
[5] Claisse P., Beresford T., 'Obtaining More From the Electrical Chloride Test', ACI – SP ACI-SP **170** (2) (1997) 1119-1132.
[6] Glass G., Buenfeld N., 'Theoretical assessment of the steady state diffusion cell test', Journal of materials science, **33** (21) 1998 5111-5118.
[7] Demuth, H., Beale M., Hagan M., 'Neural Network Toolbox™ 6 User's Guide', Ed. Matlab. 2008.
[8] The MathWorks Inc, 'Curve Fitting Toolbox - For Use with MATLAB', 2001.

Resistencia a la compresión y reología de cementantes ambientalmente amigables

Compressive strength and rheology of environmentally-friendly binders

Juan Manuel Lizarazo Marriaga[1] y Peter Claisse[2]

RESUMEN

Siendo la producción de cemento responsable de aproximadamente el 9% de la producción industrial de gases de invernadero, y en pro de generar materiales alternativos, en este artículo se presentan los resultados de una investigación encaminada a desarrollar cementantes que potencialmente representen una alternativa ambientalmente sostenible en la construcción civil. Combinaciones de escoria granulada de alto horno, escoria de acería obtenida mediante un proceso de oxígeno básico, polvo de horno de cemento y residuo de demolición de divisiones de yeso fueron usados para optimizar la resistencia a la compresión y obtener cinco mezclas de concreto con cementantes hechos parcial o totalmente con residuos industriales. Los resultados obtenidos muestran que las resistencias de las mezclas compuestas de cemento Portland y residuos industriales son adecuadas para una cantidad importante de aplicaciones en construcción civil, y aunque para las mezclas formadas completamente por residuos industriales se presentó una importante disminución en la resistencia a la compresión, los resultados obtenidos mostraron un gran potencial para determinadas aplicaciones industriales. Adicionalmente a la resistencia a la compresión, a dichas mezclas se les determinaron sus propiedades reológicas definiendo sus características de flujo y trabajabilidad.

Palabras clave: escoria granulada de alto horno, escoria básica de oxígeno, polvo del horno de cemento, yeso, reología.

ABSTRACT

Ordinary Portland cement production accounts for 9% of worldwide greenhouse gas emissions. This paper summarises the results of research aimed at developing environmentally-friendly binders which can be used as an alternative in civil construction, aimed at generating alternatives and sustainable materials. Mixes of the combination of granulated ground blast furnace slag, basic oxygen slag, cement kiln dust and plasterboard gypsum were used for optimising the binders, according to their compressive strength, to obtain 5 concrete mixtures made partially or completely with industrial waste. The results showed that the compressive strength of mixtures of Portland cement and industrial waste were suitable for different civil construction applications and, although mixtures formed entirely from industrial waste had a significant decrease in their compressive strength, the results showed great potential for specific industrial applications. In addition to compressive strength, the rheological properties of these mixtures were determined for defining flow and workability characteristics.

Keywords: granulated ground blast furnace slag, basic oxygen slag, cement kiln dust, plasterboard gypsum, rheology.

Introducción

Durante el año 2002 alrededor de 2,7 millones de metros cúbicos de concreto fueron producidos a nivel mundial (Naik, 2007); de esta producción, poco más o menos del 15% en peso corresponde al cemento Portland usado y refleja el inmenso consumo de este compuesto como material de construcción. Por cada tonelada de cemento producida aproximadamente una tonelada de CO_2 es liberada a la atmosfera; además, la producción de cemento equivale aproximadamente al 9% de la producción industrial de gases de invernadero. Estas situaciones confirman el tamaño del problema ambiental que se genera en la producción del cemento Portland y que contribuye al calentamiento global que actualmente está sufriendo el planeta Tierra. De la misma forma, el consumo de concreto y de cemento ha crecido notablemente en los últimos años y se espera que siga creciendo en el futuro, por lo que existen grandes retos ambientales que hacen necesario generar materiales cementantes alternativos que garanticen un medio ambiente más amigable pero que al mismo tiempo ofrezcan las mismas características ingenieriles del cemento Portland.

Durante ya varios años se ha vuelto práctica común el uso de adiciones minerales en forma de subproductos industriales adicionados al cemento; con estos, además de reducir la problemática ambiental se pueden obtener cementantes más baratos y con mejores propiedades ingenieriles, como lo son la resistencia y la durabilidad. Entre las adiciones minerales normalmente usadas se encuentran la ceniza volante (*FA*) (ACI-232, 2004) obtenida como subproducto de la calcinación del carbón usado en la generación eléctrica en centrales termoeléctricas, el humo de sílice (*SF*) (ACI-234, 2006) obtenido como subproducto industrial en la producción del ferrosilicio y sus derivados, y la escoria de alto horno (***GGBS***) (ACI-233, 2003) obtenida como un subproducto de la industria siderúrgica durante la fabricación del hierro. La escoria de alto horno es

[1] Ingeniero civil. M.Sc., en Estructuras, Universidad Nacional de Colombia, Bogotá. Profesor, Departamento de Ingeniería Civil y Agrícola, Universidad Nacional de Colombia, Bogotá. jmlizarazom@unal.edu.co
[2] BA and MA, in Physics, Oxford University, United Kingdom. Ph.D., in Civil Engineering, Leeds University, United Kingdom. Professor, Construction Materials, Coventry University, United Kingdom. P.Claisse@coventry.ac.uk